NASA SP-189

PROGRESS OF NASA RESEARCH RELATING TO NOISE ALLEVIATION OF LARGE SUBSONIC JET AIRCRAFT

A Conference Held at
LANGLEY RESEARCH CENTER
Hampton, Virginia
October 8-10, 1968

NATIONAL AERONAUTICS AND SPACE ADMINISTRATION

NASA SP-189

PROGRESS OF NASA RESEARCH RELATING TO NOISE ALLEVIATION OF LARGE SUBSONIC JET AIRCRAFT

A conference held at
Langley Research Center
Hampton, Virginia
October 8-10, 1968

Scientific and Technical Information Division
OFFICE OF TECHNOLOGY UTILIZATION 1968
NATIONAL AERONAUTICS AND SPACE ADMINISTRATION
Washington, D.C.

For sale by the Clearinghouse for Federal Scientific and Technical Information
Springfield, Virginia 22151 – CFSTI price $3.00

PREFACE

The papers presented at this conference contain information on the progress of research efforts of the National Aeronautics and Space Administration in the field of noise alleviation of large subsonic jet aircraft. The presentations were made according to subject matter, as follows: (1)Nacelle Acoustic Treatment Technology, (2) Nacelle Acoustic Treatment Application, (3) Noise Generation and Reduction at Source, (4) Operational and Environmental Considerations, and (5) Subjective Reaction.

Contributions were made by representatives from NASA Headquarters and Ames, Flight, Langley, Lewis, and Marshall Research Centers, as well as by representatives of The Boeing Company, Bolt Beranek and Newman, Inc., Conesco Division of Flow Corporation, Department of Transportation, IIT Research Institute, Lockheed Missiles and Space Company, McDonnell Douglas Corporation, North Carolina State University, Pratt & Whitney Aircraft, Stanford Research Institute, TRACOR, Inc., and Wyle Laboratories.

A list of attendees is included.

CONTENTS

PREFACE iii

Robert W. Boswinkle, Jr., General Chairman

1. INTRODUCTORY REMARKS. 1
Charles W. Harper

2. INTERAGENCY AIRCRAFT NOISE ABATEMENT PROGRAM 3
Charles R. Foster

3. CONFERENCE SCOPE AND NOISE CONCEPTS 7
Harvey H. Hubbard

NACELLE ACOUSTIC TREATMENT TECHNOLOGY
I. E. Garrick, Chairman

4. NONLINEAR ACOUSTIC THEORY FOR THIN POROUS SHEETS 17
William E. Zorumski and Tony L. Parrott

5. DUCT-LINING MATERIALS AND CONCEPTS. 29
R. A. Mangiarotty, Alan H. Marsh, and Ernest Feder

6. PERFORMANCE OF INLET SOUND SUPPRESSORS 53
Charles E. Feiler, Edward J. Rice, and L. Jack Smith

7. STRUCTURAL AND ENVIRONMENTAL STUDIES OF ACOUSTICAL DUCT-LININGMATERIALS. 63
H. A. Watson, Jr., J. D. Thompson, and Carl E. Rucker

NACELLE ACOUSTIC TREATMENT APPLICATION
John G. Lowry, Chairman

8. INTRODUCTORY REMARKS ON NACELLE ACOUSTIC TREATMENT APPLICATION. 103
Harry T. Norton, Jr.

9. DESIGN CONCEPTS 113
Robert E. Pendley

10. GROUND-RUNUP TESTS OF ACOUSTICALLY TREATED INLETS AND FAN DUCTS 131
Alan H. Marsh, E. L. Zwieback, and J. D. Thompson

11. FLIGHT-TEST NACELLES 163
J. S. Coxon and C. A. Henry

12. NOISE PREDICTIONS AND ECONOMIC EFFECTS OF NACELLE MODIFICATIONS TO MCDONNELL DOUGLAS DC-8 AIRPLANES 173
Robert E. Pendley and Alan H. Marsh

13. SONIC-THROAT INLETS 197
C. C. Higgins, J. N. Smith, and W. H. Wise

14. TREATED INLETS 217
George T. Drakeley and Ralph B. McCormick

15. FAN-DUCT DEVELOPMENT 227
Ralph B. McCormick

16. NOISE PREDICTIONS AND ECONOMIC EFFECTS OF BOEING NACELLE MODIFICATIONS 241
D. C. Nordstrom and D. S. Miller

17. CONCLUDING REMARKS ON NACELLE ACOUSTIC TREATMENT APPLICATION 259
John G. Lowry

NOISE GENERATION AND REDUCTION AT THE SOURCE
Newell D. Sanders, Chairman

18. QUIET ENGINE PROGRAM - PRELIMINARY ENGINE DESIGN AND AIRCRAFT INTEGRATION 263
Joseph F. McBride

19. QUIET ENGINE PROGRAM - DETAILED ENGINE DESIGNS 273
James J. Kramer

20. COMPRESSOR NOISE ANALYSIS 287
Martin V. Lowson

21. POTENTIAL OF INLET-GUIDE-VANE CONFIGURATION FOR INLET NOISE REDUCTION 307
David Chestnutt and John L. Crigler

22. A STUDY OF EXHAUST NOISE AS IT RELATES TO THE TURBOFAN ENGINE 319
Colin G. Gordon

23. OPTICAL CROSSED-BEAM INVESTIGATION OF LOCAL SOUND GENERATION IN JETS 335
Fritz R. Krause and Lennox N. Wilson

OPERATIONAL AND ENVIRONMENTAL CONSIDERATIONS
Bradford H. Wick, Chairman

24. VARIABILITY IN AIRPLANE NOISE MEASUREMENTS 359
David A. Hilton and Herbert R. Henderson

25. TWO METHODS OF EVALUATING CLIMBOUT NOISE 369
W. Latham Copeland

26. FLIGHT INVESTIGATION OF METHODS FOR IMPLEMENTING NOISE-ABATEMENT LANDING APPROACHES 377
Hervey C. Quigley, Robert C. Innis, and Emmett B. Fry

27. TECHNIQUE FOR CALCULATING OPTIMUM NOISE-ABATEMENT TAKE-OFF PROFILES 395
Heinz Erzberger, Homer Q. Lee, H. Rodney Peery, and Fred J. Drinkwater III

28. PROCEDURES FOR ESTIMATING THE EFFECTS OF DESIGN AND OPERATIONAL CHARACTERISTICS OF JET AIRCRAFT ON GROUND NOISE 411
James H. Farrell

29. PREDICTED AND MEASURED XB-70 GROUND-TO-GROUND ENGINE NOISE 423
Norman J. McLeod, Paul L. Lasagna, and Terrill W. Putnam

30. PROPAGATION OF SOUND FROM AIRPORT GROUND OPERATIONS. 435
Dwight E. Bishop and Peter A. Franken

31. METHODS OF DETERMINING THE EXCESS ATTENUATION FOR GROUND-TO-GROUND NOISE PROPAGATION. 453
Stanley H. Guest and Bert B. Adams

32. EFFECTS OF ATMOSPHERIC REFRACTION ON FAR-FIELD SOUND PROPAGATION . . . . . ,493
Orvel E. Smith

33. SYNTHESIS OF AIRCRAFT NOISE 537
Ernest G. Hinterkeuser

SUBJECTIVE REACTION
Harvey H. Hubbard, Chairman

34. PREDICTION OF EFFECTS OF NOISE ON MAN 547
Karl D. Kryter

35. STUDIES RELATING THE INDIVIDUAL CHARACTERISTICS OF PEOPLE WITH THEIR RESPONSES TO NOISE 561
Richard G. Pearson and Franklin D. Hart

36. ASSESSMENT OF THE VALIDITY OF PURE TONE CORRECTIONS TO PERCEIVED NOISE LEVEL 573
Karl S. Pearsons

37. JUDGMENT TESTS OF AIRCRAFT NOISE 587
Karl D. Kryter, Paul J. Johnson, and James R. Young

38. PERCEIVED SOUND AND THE FREQUENCY RESPONSE CHARACTERISTICS OF THE HUMAN AUDITORY SYSTEM 601
Jess H. Jones

39. HOUSE VIBRATIONS SIGNIFICANT FOR INDOOR SUBJECTIVE RESPONSE 637
William H. Mayes, Donald S. Findley, and Huey D. Carden

40. COMMUNITY REACTIONS TO AIRCRAFT NOISE – NOISE MEASUREMENTS . . . 649
William K. Connor

41. COMMUNITY REACTIONS TO AIRCRAFT NOISE – PUBLIC REACTIONS 661
William R. Hazard

LIST OF ATTENDEES 673

1. INTRODUCTORY REMARKS

By Charles W. Harper

NASA Headquarters

Speaking for NASA Headquarters, I would like to welcome you to another in the series of conferences on aeronautics research and development. NASA conducts these conferences to keep the aviation world up to date with the results of the NASA research programs in aeronautics. Each one serves to collect and summarize recent work in a particular area – this one, of course, relating to control of aircraft noise.

Although this is the first conference devoted wholly to aircraft noise, NASA, and NACA before it, has been conducting research on noise for many years. Until recently the majority of this effort was directed at understanding the fundamentals of noise generation of both propeller and turbojet aircraft with but relatively small effort directed at the application of these results. However, in the past 2 years, the NASA has extended its research to examine directly the problem of practical control of noise.

This extension is a direct result of the very rapid growth in air transportation and a corresponding growth in the level of public annoyance from noise. About 2 years ago, in view of public concern, the President established an industry-government committee, under the direction of the Office of Science and Technology, for the specific purpose of developing a national noise-alleviation program. Among the committee recommendations was the very important one, to NASA, that NASA extend its more basic research on noise to the point of determining the practicality of various possible noise-alleviation techniques. A most important objective of this program was to provide the data from which trade-off studies could be made between implementation costs and noise alleviation.

The committee recommended specifically that NASA accelerate examination of the practicality of noise alleviation along three lines. These were as follows:

(1) The potential of applying sound-suppression techniques to engines and nacelles typical of those now in use

(2) The possibility of using steeper approach angles in routine operation to remove the noise farther from the observer

(3) The possibility of developing practical engines producing significantly less noise than those now in use

In addition, NASA was asked to assist other agencies in developing a better understanding of the relations between noise and annoyance. As one consequence of accepting these responsibilities, NASA support for research programs related to noise has risen from less than $1 million per year to nearly $18 million this year, most of which is used to obtain industry support for the program.

I would like to emphasize that this conference is in the nature of a progress report. Although we consider the results obtained to date to be promising, we recognize that much remains to be done before our primary objective is achieved. One principal reason for presenting this progress report is to provide the opportunity to adjust the future activities to meet the primary objective to the maximum possible satisfaction of everyone involved. NASA is fully aware of the major economic implications of solutions to this noise problem and recognizes the need for more definitive information before any final decisions can be made.

Since this is a progress report, it is clear that various interpretations can be placed on some of the still incomplete results. In preparing this material for presentation, we have made every effort to be wholly objective. While we are generally encouraged from our analysis of the results, we do recognize that different interpretations might be less favorable. Therefore, one principal objective of this meeting is to enable frank and complete discussion either in the next $2\frac{1}{2}$ days or subsequently. We intend from these discussions that the future phases of the program will be designed to assure acquisition of all information needed to reach the most acceptable solutions to this problem.

2. INTERAGENCY AIRCRAFT NOISE ABATEMENT PROGRAM

By Charles R. Foster

Department of Transportation

I would like to express my appreciation to NASA for inviting the Department of Transportation (DOT) to attend this conference, and I also appreciate the opportunity to discuss the Interagency Aircraft Noise Abatement Program. As you are well aware, noise is one of the major contributors to the environmental pollution problem which is plaguing our society today. In our context, it is a waste product of transportation systems and, along with air and water waste, is rapidly deteriorating our environment.

The need for a national program attacking aircraft noise was first acted on by Dr. Hornig, the President's Science Advisor, who established an Ad Hoc Jet Aircraft Noise Panel in October 1965, composed of representatives from NASA, FAA, and industry. The panel developed recommendations concerning the implementation of a coordinated noise abatement program.

The President of the United States in his transportation message to the Congress on March 2, 1966, gave particular attention to aircraft noise. He directed Dr. Hornig to work with NASA, FAA, Department of Commerce, and Department of Housing & Urban Development (HUD) to frame an action program to attack this problem. Specifically, he asked these Departments and Agencies to develop noise standards and compatible uses of land near airports, to consult with local communities and industry, and to recommend needed legislative or administrative actions. On March 22, 1967, in a memorandum for Heads of Departments and Agencies, the President directed all organizations to take into explicit and due account aircraft noise whenever it is relevant to any program and to cooperate with DOT and HUD in efforts to control and reduce the problems of aircraft noise. Under Dr. Hornig's leadership, the Federal Aircraft Noise Abatement Program was subsequently organized. This program resulted in the initiation of several projects structured to carry out the recommendations reported by the Jet Aircraft Noise Panel.

With the formation of the Department of Transportation the responsibility for both the Federal Aircraft Noise Abatement Program and the Sonic Boom Coordinating Committee, which was initially under Dr. Hornig's direction to provide policy and technical direction for national studies on sonic boom, were transferred to DOT.

As recent as March 8, 1968, the President, in his message to the Congress on conservation, restated his concern with the ever-mounting volume of aircraft noise, along with other types of noise. Specifically, he directed all departments of government to take account of noise factors in choosing the location and design of buildings, highways, and

other facilities whose construction is assisted by federal funds. He also urged the Congress to take prompt action on the pending legislation to deal with aircraft noise.

Public Law 90-411, an act to amend the Federal Aviation Act of 1958 to require aircraft-noise-abatement regulations, was passed by the Congress and signed into law by the President on July 21, 1968. I think it is important to note that the House passed this bill by a vote of 312 to 0 – one of the very few times that a bill has passed unanimously. There were only 10 dissenting votes in the Senate.

The FAA now has authority to prescribe and amend such rules and regulations as may be necessary to provide for the control and abatement of aircraft noise and sonic boom. The forthcoming regulations on noise abatement and the ability of our industry to comply will be vitally influenced by the work that NASA is doing – that is, by the work that you will hear about during this conference.

Now, with this historical background, I would like to present briefly the organizational structure of the Interagency Aircraft Noise Abatement Program which was developed to discharge efficiently the overall responsibilities of the Department of Transportation and other appropriate government agencies.

The Advisory Committee is composed of the top officials of the government agencies listed. (See chart presented as fig. 1.) There is also participation from nongovernmental interests such as the National Academy of Sciences. This group provides advice and guidance to the Secretary, Department of Transportation. The detailed coordination and review of the program is concentrated in the Coordination Committee. You will note that the agencies represented on the Coordination Committee are largely the same as those represented on the Advisory Committee. You will also note from the chart that we have established eight functional panels, chaired by the agency shown. Membership on these eight panels is selected based on the best individual expertise available in each functional area.

The Noise Re'search Panel is primarily involved with the problems of quieting engines and aircraft. Here we find coordination of projects such as those that will be discussed at this conference.

The Sonic Boom Research Panel, as its name implies, is primarily concerned with the problems of sonic-boom generation and propagation.

The Land Use/Airports Panel is concerned primarily with the problems of noise exposure forecasts and their implication on communities adjacent to airports. Guidance concerning criteria for compatible land use is developed in this panel, and appropriate government programs in the areas of land use are coordinated to ensure that the noise problem is taken into consideration in the conduct of these programs.

The Operations Panel is the forum which looks at how to fly the aircraft and where to fly to create minimum noise exposure which must be consistent with overriding safety requirements. Projects such as developing optimum-noise-abatement take-off profiles, developing the capability to execute steeper approaches to landing, and developing, noise-abatement Air Traffic Control procedures are the sort of things that are being evaluated by this panel. You will learn more about these projects from subsequent papers.

The Human Response Panel is concerned primarily with the psychoacoustic aspects of aircraft noise. It is the primary group working on the development of meaningful yardsticks and units of measurement that will be used in rating and evaluating noise from the human response viewpoint. The last day of the conference will cover this area.

The Natural Environment Panel is concerned with the impact of aircraft noise, including sonic booms, on our national parks, natural artifacts, and wildlife. These are problems about which much concern has been expressed.

The Legislative/Legal Panel includes lawyers who are involved in the aircraft-noise problem. There has been a great deal of litigation concerning alleged damage incurred as a result of aircraft noise and sonic booms. This panel keeps abreast of current activities in the legal field of aircraft noise and develops and recommends legislative proposals as required.

The Structures Panel is concerned, as the title implies, with impact and effects of noise on manmade structures. Here is where we find a concentration of effort in developing sound-proofing materials and techniques that may be applied to existing as well as new structures in the vicinity of airports. Here we also find effort underway that will be useful in developing criteria to be incorporated in uniform building codes which can assist in reducing noise intrusion in homes and other structures. Papers that relate to this subject area will also be presented at this conference.

In discussing aeronautical research, Secretary Boyd, just over a week ago, before the Subcommittee on Advanced Research and Technology of the House Committee on Science and Astronautics, stated that the Federal Government has to do a tremendous amount of research and invest a great deal of money in noise. He further stressed the point that we cannot buy quiet overnight.

As this conference progresses, we will see the important role that NASA plays in the national noise-abatement effort. We feel that the outstanding contributions made in the past will be matched by even greater contributions in the future as we all endeavor to remove the noise albatross from around the neck of air transportation.

INTERAGENCY AIRCRAFT NOISE ABATEMENT PROGRAM

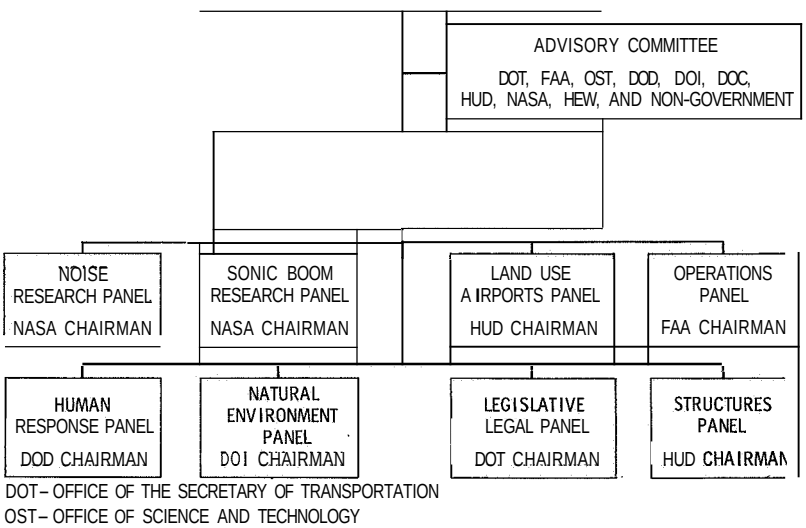

Figure 1

3. CONFERENCE SCOPE AND NOISE CONCEPTS

By Harvey H. Hubbard

NASA Langley Research Center

SUMMARY

The scope and objectives of the conference are indicated. In addition, some guidelines and definitions for the presentation of the subject matter of subsequent papers are provided.

INTRODUCTION

The scope of the conference and its objectives can be described with the aid of figure 1. The focal point for all discussions will be the airport noise problem for large commercial jet airplanes. Emphasis is on the technical aspects of the problem, rather than on the political, legal, or regulatory aspects. Attention will be given to the minimization of noise during landing approach, ground operations, and climbout. There will be no direct references to helicopters, V/STOL aircraft, military aircraft, and general aviation, although the material presented will have some obvious application to those vehicles. Likewise, no direct reference will be made to the sonic-boom problem nor to land-use planning. In addition to indicating the scope and objectives of the conference, the purpose of this paper is to provide some guidelines and definitions for the presents-tion of the subject matter of subsequent papers.

NOISE-REDUCTION METHODS

At the present time the optimum approach to noise alleviation has not been defined. However, such methods as noise reduction at the source through proper component design, operational procedures to minimize noise exposures, and the application of duct treatment technology are all known to be beneficial and will be discussed in several of the conference papers.

One of the main conclusions of the International Conference on the Reduction of Noise and Disturbance Caused by Civil Aircraft, held at Lancaster House, London, November 22-30, 1966, was that future airplanes needed to have more acceptable noise characteristics than those currently in service. The ability to control noise at the source was considered necessary not only to produce noise reductions but also to make possible predictions of noise as a basis for effective community planning.

ENGINE CONSIDERATIONS

The most significant factor in noise alleviation at the source has been the development of the fan jet or bypass engine. Two fan jet engines are illustrated in figure 2. The illustration labeled "Current" represents a type of fan jet engine that is in common commercial airplane usage and which is also involved in some of the noise-reduction studies to be described. The second illustration represents a higher bypass-ratio engine of the type being developed for large future commercial airplanes. These future engines are characterized by large-diameter fan sections and large fan exits.

The data of figure 3 illustrate the noise-reduction potential for the proposed type of engine. Relative perceived noise levels are shown as a function of bypass ratio for the current operational engines and for those proposed for future airplanes. Data are for a 200-foot sideline-observer location and for equal-rated thrust. Perceived noise level is defined more exactly subsequently; however, it is noted to be a unit of subjective noisiness and, hence, lower values are desired. The current family of turbojets constitute the reference point in this figure and, of course, for them the bypass ratio is 0. The current fan jets are represented by the middle shaded area, and the bypass ratios are noted to be relatively small. Much study and development work has led to consideration of bypass ratios of the order of 4 and above for purposes of noise reduction. The noise-reduction potential for the future engines is represented by the bottom boundary of the long shaded region and this bottom boundary is largely defined by the jet-mixing noise. Because noise from the rotating machinery and internal equipment for these high-bypass-ratio engines tends to be relatively more intense, the long shaded region has considerable depth. Much of the present-day research is aimed at reducing the levels of the interior noise components represented by this shaded region so that the full noise-reduction potential of such engines may be realized.

Two general philosophies of internal noise reduction for fan engines are illustrated by the drawings in figure 4. The fact that the inner components, such as the fan, compressor, and turbine, are significant in noise production leads to the first philosophy that proper design of such components can be effective in optimizing the noise charscteristics of the engine. The second philosophy of design, as represented by the bottom drawing, is based on the concept of minimum interference with the interior components of the engine and involves only the application of noise-reduction materials external to the engine in the vicinity of the engine nacelle.

The component-design approach is judged to be most attractive for future engine developments rather than for modification of existing engines. The concept of applying acoustic treatment in the nacelle external to the engine is attractive for retrofitting existing nacelles as well as for incorporation into new engine designs.

ENGINE NOISE SPECTRA

The characteristic noise spectra for engines of interest for commercial applications can be discussed with the aid of figure 5. This figure contains schematic representations of the two types of noise present in all engine spectra, that is, broadband noise and tones. The broadband noise, which is characterized by random-type time histories, may come from the mixing of the exhaust jets with the outside air and from the interactions of the airflows with both the stationary and rotating parts of the engine. The tones, on the other hand, have periodic time histories and are associated with only tine rotating components of the engine. It is significant that for the turbojet engine, the broadband noise dominates; for the current fan jet engines, both the broadband and the tone noises are important; and, for some future fan jet engines, the tones may dominate the noise spectrum.

Subsequent papers show the tone content of the noise to be especially significant from a subjective standpoint. Hence, the proper measurement of the significant components of the noise spectrum is important. The rest of this paper is devoted mainly to descriptions of concepts of measurement and subjective evaluation of noise and to definitions of important quantities. This review of these quantities and concepts should be helpful in understanding some of the subsequent papers.

One of the useful variables in the analyses of aircraft noise data is the characteristic bandwidth of the analysis equipment. The data of figure 6 illustrate the results that are obtained from analyses of different filter bandwidths for a relatively simple broadband spectrum with one tone. The analyses of such a spectrum with commercially available analyzers such as, for instance, 1/10-octave, 1/3-octave, and full-octave filter systems would give the spectra indicated in the figure. All the spectrum lines are representations of the same noise; that is, the overall noise level is the same for each. The full-octave band spectrum, for instance, has higher band levels than the 1/3-octave band spectrum in the region of the broadband components because of the wider filter bandwidth. The levels of the bands containing the tone are nearly the same irrespective of bandwidth since the tone is relatively strong. One of the important subjective response considerations in spectra with tones is the amount by which the tone protrudes above the broadband noise; hence, the definition of such a factor must take into account the bandwidth which has been used. Since the choice of bandwidth is a matter of judgment, various bandwidth values are used. Wider bandwidths generally lead to simplified procedures whereas narrow bandwidths lead to a more detailed physical description of the data.

Noise levels (a term used interchangeably with sound pressure levels) are expressed in decibels, referred to the conventional value of 0.0002 $dyne/cm^2$. A decibel is a logarithmic unit and represents the smallest perceptible change in amplitude of a sound. A 6-dB change represents a factor of 2 in sound pressure or a factor of 4 in sound power.

PERCEIVED-NOISINESS CONCEPTS

One of the subjective measurements of noise that has received wide acceptance and which will be referred to in several of the conference papers is that of perceived noisiness. Although this concept will be treated in detail in some of the subsequent papers, a brief discussion here of the basic concepts may be helpful in the understanding of some of the other subject matter to be presented.

Figure 7 indicates the nature of the reaction of people to noise. Shown in the figure is an example of a 1/3-octave band noise spectrum for which each of the frequency bands is judged by human subjects to be equally noisy. It can be seen that a high-frequency band having relatively low band levels is considered to be as noisy as a lower frequency band having higher band levels. The curve labeled "Equal-noisiness contour" is one of a family of curves used to define weighting functions in the calculation of perceived noise levels.

Perceived noise level is noted to be a function of the sound pressure level plus a spectrum shape factor derived from curves such as the one just described; that is -

$$\begin{matrix}\text{PERCEIVED NOISE} \\ \text{LEVEL (PNL)}\end{matrix} = \begin{matrix}\text{SOUND PRESSURE} \\ \text{LEVEL (SPL)}\end{matrix} + \begin{matrix}\text{SPECTRUM SHAPE} \\ \text{FACTOR}\end{matrix}$$

The significance of the spectrum shape factor is further illustrated by the data presented in figure 8. The two broadband noise spectra are judged to be equally noisy even though the overall noise level associated with the solid curve is 10 dB higher. The much higher noise levels of the solid-curve spectrum at low frequencies compensate for the slightly higher levels of the dashed-curve spectrum at high frequencies.

The concept of effective perceived noise level involves the modification of the perceived noise level to include both a tone weighting factor and a duration weighting factor; that is -

$$\begin{matrix}\text{EFFECTIVE} \\ \text{PERCEIVED NOISE} \\ \text{LEVEL (EPNL)}\end{matrix} = \text{PNL} + \begin{matrix}\text{TONE} \\ \text{FACTOR}\end{matrix} + \begin{matrix}\text{DURATION} \\ \text{FACTOR}\end{matrix}$$

The nature of the tone weighting factor can be represented by the spectra of figure 9. These spectra are judged to be equally noisy; that is, the solid-curve basic octave-band spectrum with a tone superposed is equivalent to the dashed-curve octave-band spectrum for which the overall noise level is 7 dB higher. This is just an example; the actual tone weighting factor varies both as a function of the tone amplitude and its frequency.

The nature of the duration weighting factor is illustrated by the sketches in figure 10. Shown schematically in the figure are two perceived-noise-level time histories of flyover noise, one of which has a duration twice that of the other as measured at levels 10 PNdB down from the peak values. Some experiments have indicated that these two flyover-noise situations would be equally acceptable if the peak perceived noise level of the longer one was 3 PNdB lower. This value of 3 PNdB may be considered as an order of magnitude of the duration correction since it may vary for different types of noises.

CONCLUDING REMARKS

The subject matter of the conference is noted to be divided into five sections:

(1) Nacelle acoustic treatment technology

(2) Nacelle acoustic treatment application

(3) Noise generation and reduction at the source

(4) Operational considerations

(5) Subjective reaction

Much of the information in the first two sections, which relate to the development of acoustic nacelle treatment technology and to its application in aircraft design, has been derived from contractual studies with The Boeing Company and McDonnell Douglas Corporation. Each section consists of a number of NASA and contractor papers and these papers represent progress reports since in most cases the research is still underway. Other contractor participants were Bolt Beranek and Newman, Inc., Conesco Division of Flow Corporation, IIT Research Institute, Lockheed Missiles and Space Company, North Carolina State University, Pratt & Whitney Aircraft, Stanford Research Institute, TRACOR, Inc., and Wyle Laboratories.

AIRPORT – **COMMUNITY NOISE**

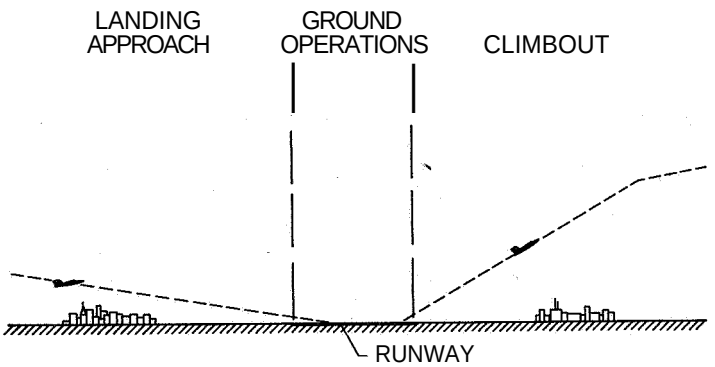

Figure **1**

BY-PASS ENGINES

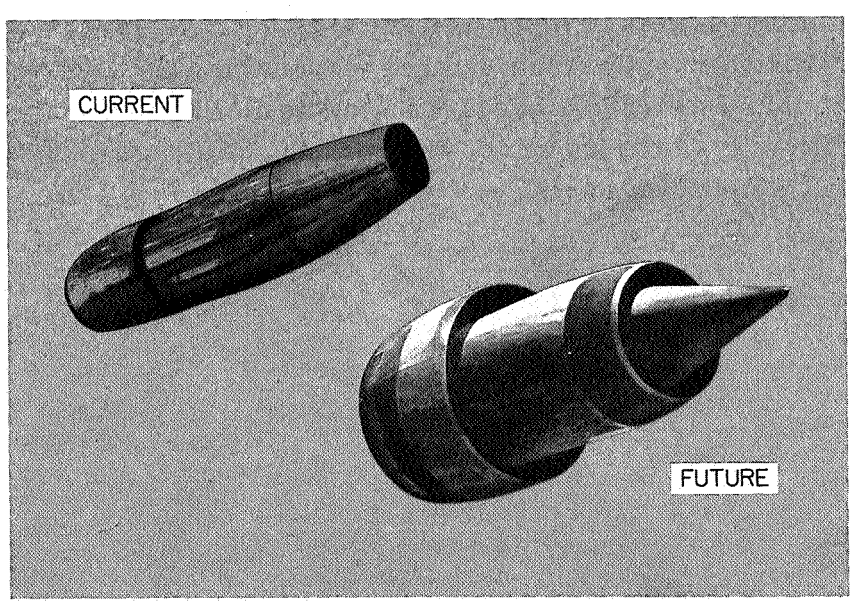

Figure **2**

L-68-8537

SIDELINE NOISE LEVELS FOR CONSTANT THRUST

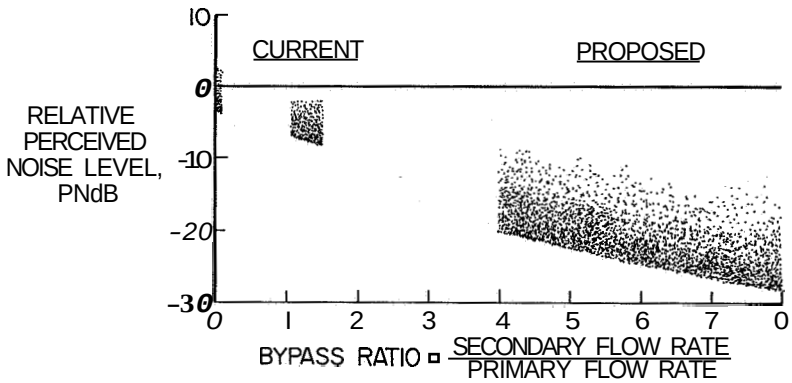

Figure 3

BY-PASS ENGINE NOISE REDUCTION

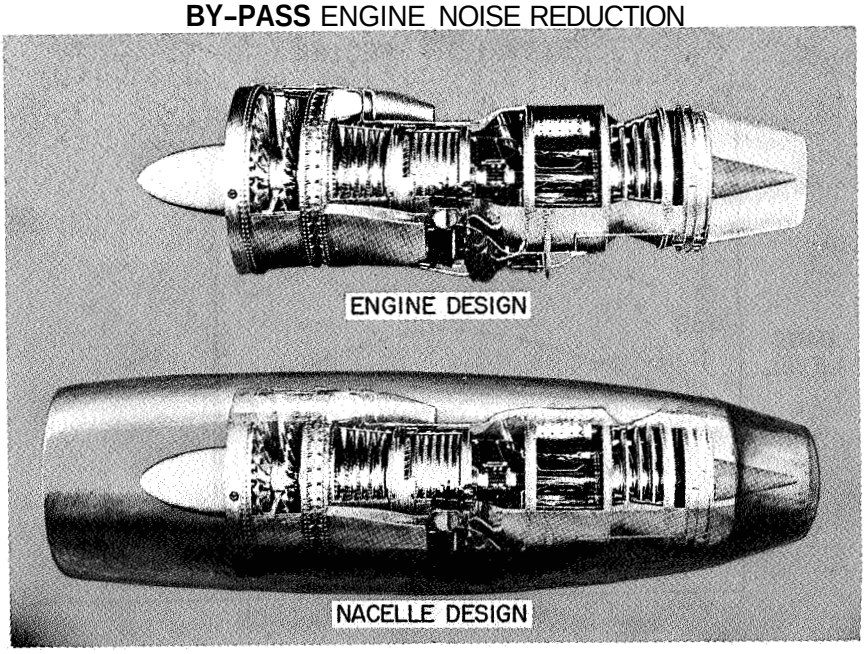

Figure 4 L-68-8538

SCHEMATIC DIAGRAM OF ENGINE NOISE SPECTRA

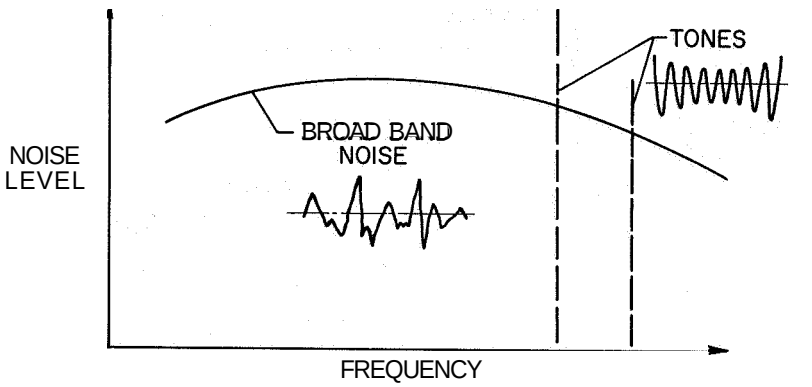

Figure 5

EQUIVALENT SPECTRA

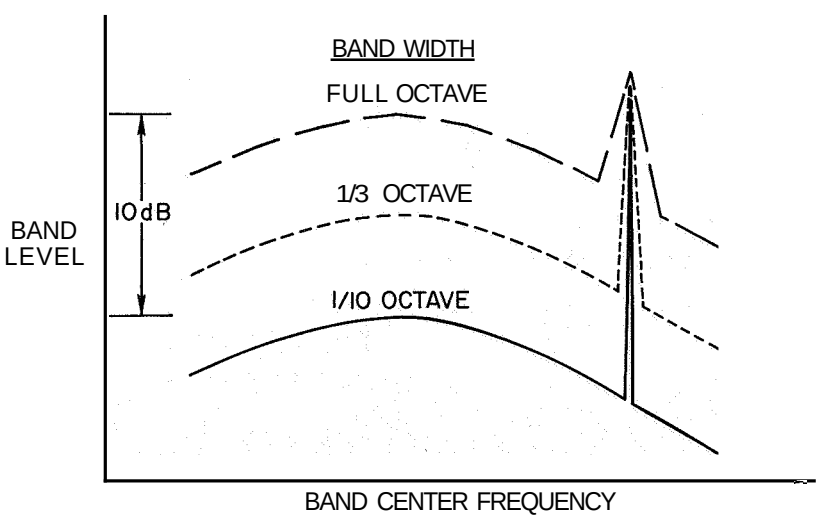

Figure 6

PERCEIVED NOISINESS

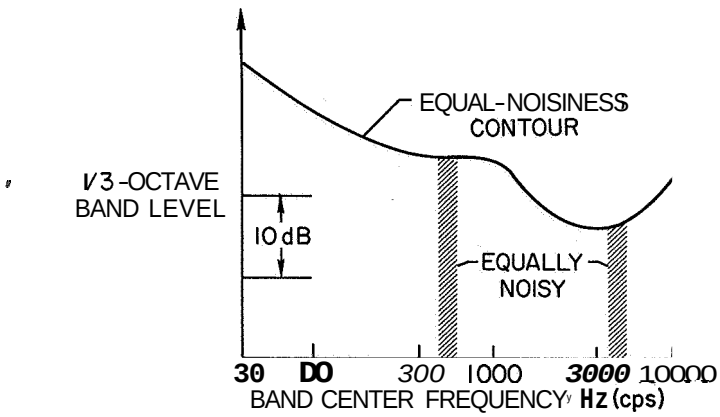

Figure 7

SPECTRUM SHAPES HAVING EQUAL PNL

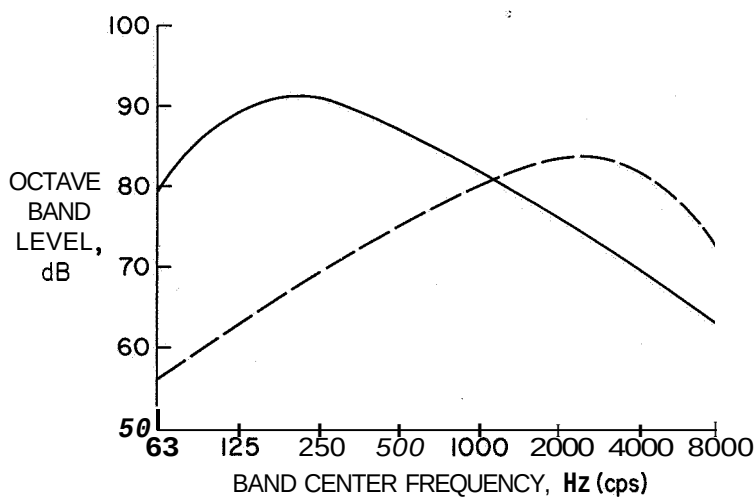

Figure 8

TONE EFFECTS

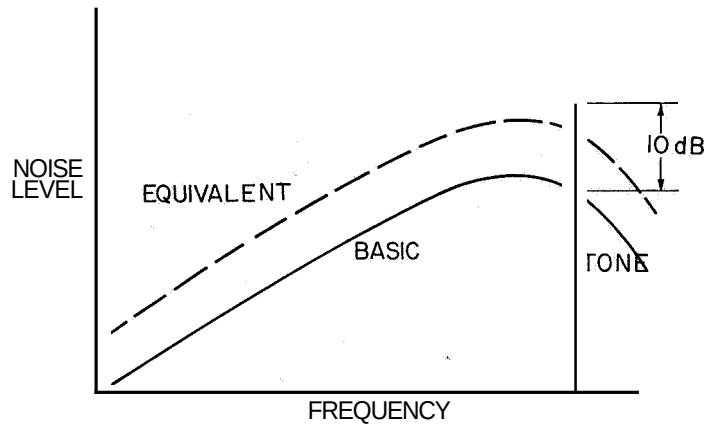

Figure 9

EXAMPLE OF DURATION EFFECTS

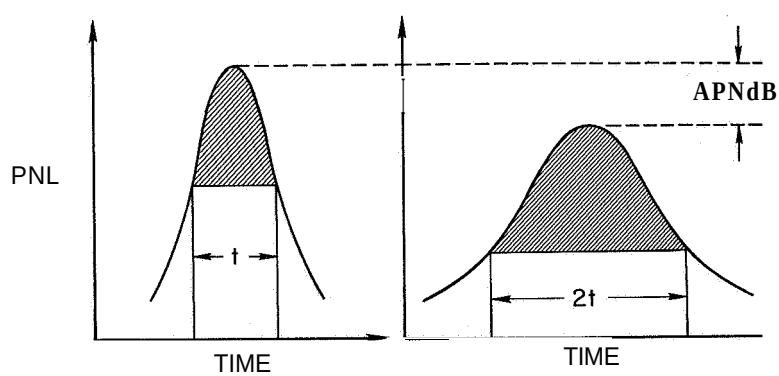

Figure 10

4. NONLINEAR ACOUSTIC THEORY FOR THIN POROUS SHEETS

By William E. Zorumski and Tony L. Parrott

NASA Langley Research Center

SUMMARY

A nonlinear theory is presented which predicts the acoustic properties of thin porous sheets of material in a high-intensity noise environment. The nonlinear theory utilizes two experimental measurements, the low-intensity impedance measurement and the flow-resistance measurement. The basis of the theory is described and results of the theory are compared with experimental data. It is concluded that use of this theory may eliminate the need for impedance tests in the high-intensity range and that nonlinearity can be a useful property of an acoustic absorber.

INTRODUCTION

The purpose of this paper is to discuss some of the basic concepts underlying the acoustical properties of duct-lining materials for airplane engines and nacelles and to construct a mathematical model for these materials which will predict their absorption of high-intensity sound. Sound intensities of the order of 140 to 160 dB are often found in the interior of modern design airplane engines. These acoustic intensities are in the nonlinear range where the classical linear theory of acoustic absorption needs to be modified. This paper presents an acoustic theory for the behavior of thin porous sheets of material in a high-intensity noise environment. The nonlinear theory utilizes two fundamental acoustic measurements, the impedance measurement and the flow-resistance measurement.

For the past 30 years, acoustic materials have been characterized by their impedance, a complex number which uniquely relates the magnitude and phase of a reflected wave to an incident wave. In figure 1 this quantity Z, measured in rayls, is defined as the complex ratio of the pressure to the velocity p/V of the sound waves at the sample. The real or acoustic resistance part of the impedance R is due to viscous action in the sample, and the imaginary or reactive part X is due to the momentum of the air within the sample. The device used to measure the impedance is a simple standing-wave tube or impedance tube. The acoustic intensity or sound pressure level SPL where the impedance begins to depend on SPL determines the nonlinear range for the material. This intensity is often about 120 dB for the thin sheet materials being discussed.

Figure 2 shows another measure of the properties of an acoustic material. The steady flow resistance R, also measured in rayls, is the ratio of the pressure drop

across a sample to the velocity through the sample $\Delta p/V$. In the linear range this ratio is constant, whereas it depends on velocity in the nonlinear range. In the linear region the acoustic and steady-flow velocities are approximately equal; in the nonlinear region they are related by the nonlinear theory.

In the linear range of material behavior, the impedance tube is easy to use, acceptably accurate, and does not need to be supplemented by the flow-resistance test. In the high-intensity or nonlinear range, the impedance tube may still be used; however, many tests are required since the properties of the absorber now depend on SPL and frequency. Also, because of design limitations, the intensity which may be achieved with impedance tubes is often less than that for which data are desired. It is clear that alternate theoretical and experimental methods are needed for extending acoustic properties into the nonlinear range. The following theory shows how the steady-flow test and a low-intensity impedance-tube test may be used to obtain information about material behavior in the high-intensity or nonlinear region.

SYMBOLS

c	speed of sound
d	depth
e	base of natural log system
f	frequency
$i = \sqrt{-1}$	
M	Mach number
N_{Re}	Reynolds number
m,k	integers used in summation limits and corresponding subscripts and superscripts
p	pressure
Δp	change in pressure
R	acoustic resistance; steady-flow resistance

SPL	sound pressure level
t	time
V	acoustic velocity
v	velocity
w	width
X	acoustic reactance
X_L	low-intensity acoustic reactance
x	distance
Z	acoustic impedance
α_N	normal absorption coefficient
ρ	mass density
Φ_a, Φ_b	velocity potential Φ for compartments a and b, respectively

THEORY

The nonlinear acoustic theory is developed from the laws of mechanics and from dimensional analysis as shown in figure 3. Consider a very thin porous sheet which is enclosed by a hypothetical control volume. The thickness of the sheet is assumed to be small compared with the wavelength of sound. On either side of the sheet, there are small acoustic velocities and pressures which must be related. The law of conservation of mass requires that the acoustic velocity, normal to sheet, is the same on both sides. This requirement exists essentially because the sample is too thin to store mass; thus, an inflow on one side must be immediately matched by an outflow on the other side. This simple statement is the first part of the nonlinear theory.

The second statement of the theory is obtained from the momentum law. When this law is applied to the control volume enclosing the screen, it is found that the pressure change, or drop across the screen, depends on two terms which must be determined experimentally. The first term is the steady-flow pressure drop. Dimensional analysis

indicates that this term will depend on the acoustic Reynolds and Mach numbers. Experimental investigation has shown that, for a given sample, the steady-flow pressure drop is a nonlinear function of the acoustic velocity because Reynolds and Mach numbers are proportional to this quantity. The second term is the time rate of change of momentum inside the sample. This term has been found to depend on acoustic velocity and frequency and is related to the reactance measured in the low-intensity impedance-tube test.

The two instantaneous laws which relate acoustic pressures and velocities across the material form the nonlinear acoustic theory. These laws hold continuously in time, in contrast to impedance laws which hold as averages over a cycle. This theory may be compared with the standard impedance theory by using it to solve the impedance-tube problem. In figure 4, a theoretician's view of the impedance tube is shown. The tube is terminated by a speaker at one end and a rigid backing at the other. At these points impedance boundary conditions are used. The tube is separated into two compartments by the material sample. In each part, a velocity potential Φ must satisfy a time-dependent wave equation. The instantaneous laws for velocity and pressure are used across the sample. It is not possible to find a simple harmonic solution to this problem because of the nonlinear effect of the material. It is possible, however, to find a periodic solution by expanding the acoustic velocity at the sample $V(t)$ in terms of a Fourier series. The problem is then to find the coefficients V_k of this series, which are the complex velocities of all the harmonic waves at the screen. The tedious details of solving this problem are omitted here. This solution leads to a nonlinear definition of impedance, which is described by figures 5 and 6.

Experimentally measured pressure differentials $\Delta p/\rho c^2$ for a typical sample are shown in figure 5 as a function of velocity V/c. The extended dashed line indicates how the pressure differential could vary if the material were linear. Actual measurements fall along a curve which bends upward and thus indicates nonlinearity. Shown in figure 6 is the general nonlinear impedance definition which uses these experimental data. The nonlinear impedance Z_k is defined as the ratio of the Fourier pressure coefficient p_k to the velocity coefficient V_k in a periodic wave. The subscript k denotes the kth harmonic of the fundamental period; thus, this equation actually defines a set of impedances Z_1, Z_2, ... The integral term gives the Fourier coefficient p_k. It depends on the experimental function Ap which, in turn, is a function of the complex velocity coefficients V_k. This relationship shows the dependence of the impedance on the amplitude and phase of all harmonics in a wave. In a boundary-value problem, such as the impedance-tube problem, the impedance must be found by an iteration procedure; this procedure also solves the problem. This property is characteristic of a nonlinear problem. The additional term X_L is the low-intensity reactance which is due to internal momentum. If the linear experimental curve is used in the general definition, it is found that the real part is simply the flow resistance R for small velocities, and the imaginary

part is the low-intensity reactance X_L. When the nonlinear experimental curve is used, the integral term has both real and imaginary parts R_k and X_k so that the total reactance, as well as resistance, varies with SPL and frequency.

RESULTS

The theory has been compared with experimental data by making high-intensity impedance-tube tests on the sample of material whose pressure-differential curve is shown in figure 5. This material was selected because flow-resistance tests indicated that it is more nonlinear than several other popular materials and could be expected to show nonlinear features clearly. In figure 7 is shown a typical pressure signal at the face of the sample. This particular signal had a fundamental frequency of 1250 Hz and a fundamental SPL of 153 dB. The distortion of the wave was due to a third harmonic with a SPL of 135 dB. This curve qualitatively demonstrates the nonlinear effect. Figure 8 shows the comparison of experimental and theoretical impedance data for the fundamental wave. The theoretical curves were obtained by assuming a pure incident wave of 1250 Hz and various intensities. The data are presented in nondimensional form in terms of the characteristic impedance ρc of air which is 41.6 rayls (cgs). Theoretical data above 145 dB may be subject to correction because of the uncertainty in the numerical accuracy. This uncertainty is indicated by the short-dashed lines. The measured and computed resistance disagree slightly for low intensities, but agreement improves in the high-intensity range. This low-intensity discrepancy could be easily corrected by the artifice of replacing the low-velocity flow resistance by the low-intensity acoustic resistance. The reactance data automatically correspond with theory for low intensities and fall in the vicinity of the theoretical curves for high intensities, but high-intensity reactance points are scattered between 0 and 0.4 and it was not possible to reach intensities which would clearly show the theoretical dip in the reactance curve.

Many people have assumed that nonlinearity is an undesirable feature in an acoustic absorber. An attempt has been made to determine whether this assumption is true by computing the absorption of a pure wave of varying intensity which is normally incident on a nonlinear absorber. In figure 9, the absorption coefficient, which is the ratio of absorbed wave energy to incident wave energy, is plotted against a frequency parameter. For the sample used here, the absorption is low for low intensities and increases with intensity up until 150 dB. After 150 dB, the maximum absorption decreases slightly, whereas the low- and high-frequency absorption still increases. The resulting flat-topped curve has a widened absorption spectrum which is useful when there are significant variations of frequency. Consequently, nonlinearity can be used to advantage in absorber design.

CONCLUSIONS

The foregoing discussion can be summarized in the following statements: First, the new nonlinear theory uses instantaneous laws instead of impedances. The use of these laws leads to a generalized definition of impedance which has been used to compare this theory with experimental data. Limited data indicate that the theory is fairly accurate. The theory, therefore, may eliminate the need for high-intensity impedance testing. The material would be completely characterized by a low-intensity impedance-tube test and a steady-flow test. Finally, the theory indicates that nonlinearity can be useful.

ACOUSTIC IMPEDANCE

DEFINITION

$$Z = \frac{P}{V} = R + iX$$

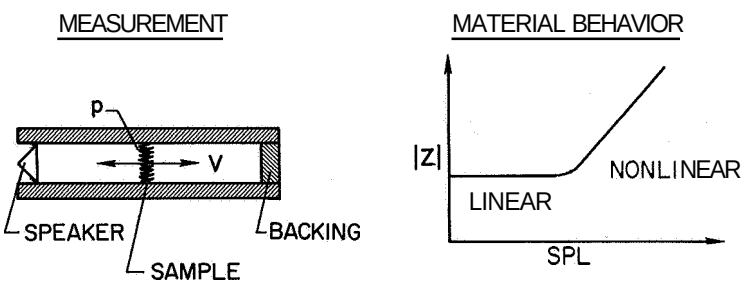

Figure 1

FLOW RESISTANCE

DEFINITION

$$R = \frac{\Delta p}{\dot{V}}$$

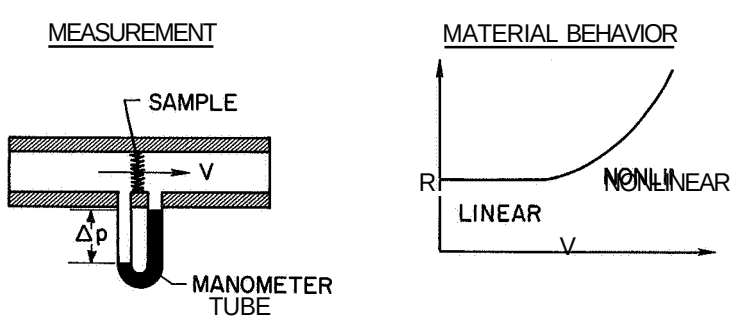

Figure 2

BASIS OF THE THEORY
INSTANTANEOUS ACOUSTIC LAWS

CONSERVATION OF MASS:

$$V_a = V_b$$

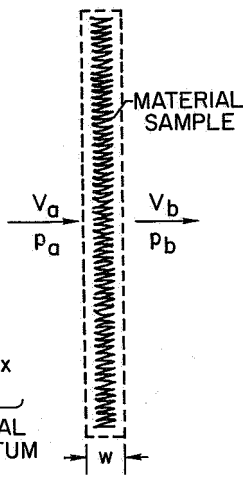

CONSERVATION OF MOMENTUM:

$$p_a - p_b = \underbrace{f(N_{Re}, M)}_{\text{PRESSURE DROP}} + \frac{\partial}{\partial t} \underbrace{\int_0^w \rho v dx}_{\text{INTERNAL MOMENTUM}}$$

Figure 3

IMPEDANCE-TUBE THEORY

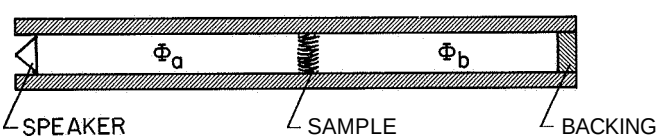

WAVE EQUATIONS:

$$\frac{\partial^2 \Phi_a}{\partial x^2} = \frac{\partial^2 \Phi_a}{\partial t^2} \; ; \; \frac{\partial^2 \Phi_b}{\partial x^2} = \frac{\partial^2 \Phi_b}{\partial t^2}$$

NONLINEAR LAWS:

$$V_a(t) = V_b(t); \; p_a(t) - p_b(t) = \Delta p\left[V(t)\right] + \frac{\partial}{\partial t} \int_0^w \rho v dx$$

PERIODIC SOLUTION:

$$V(t) = \sum_{k=-\infty}^{\infty} V_k e^{ikt}$$

Figure 4

MEASURED FLOW RESISTANCE
5-RAYL MATERIAL SAMPLE

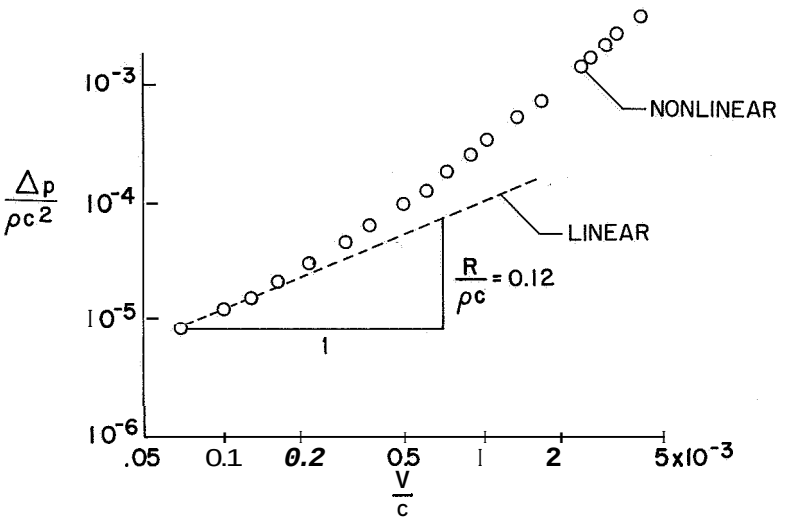

Figure 5

IMPEDANCE DEFINITIONS

GENERAL:

$$Z_k = \frac{p_k}{V_k} = \frac{\frac{1}{2\pi}\int_{-\pi}^{\pi} e^{-ikt}\,\Delta p\left[\sum_{m=-\infty}^{\infty} V_m e^{imt}\right] dt}{V_k} + ikX_L$$

LINEAR:

$$Z_k = R + ikX_L$$

R: FLOW RESISTANCE
ikX_L: INTERNAL MOMENTUM

NONLINEAR:

$$Z_k = R_k + iX_k + ikX_L$$

$R_k + iX_k$: FLOW RESISTANCE
ikX_L: INTERNAL MOMENTUM

Figure 6

EXAMPLE OF PRESSURE SIGNAL IN IMPEDANCE TUBE

153 dB

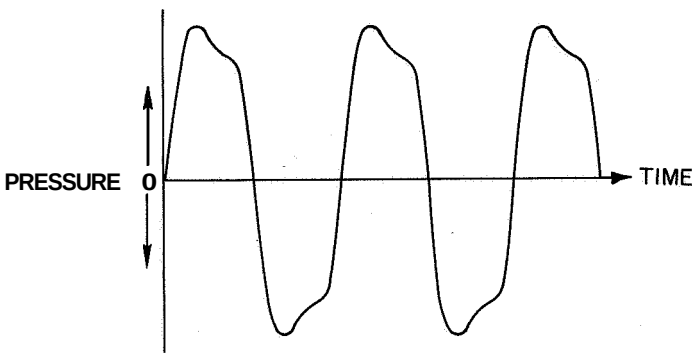

Figure 7

COMPARISON OF THEORY AND EXPERIMENT

5-RAYL MATERIAL; 1250 Hz

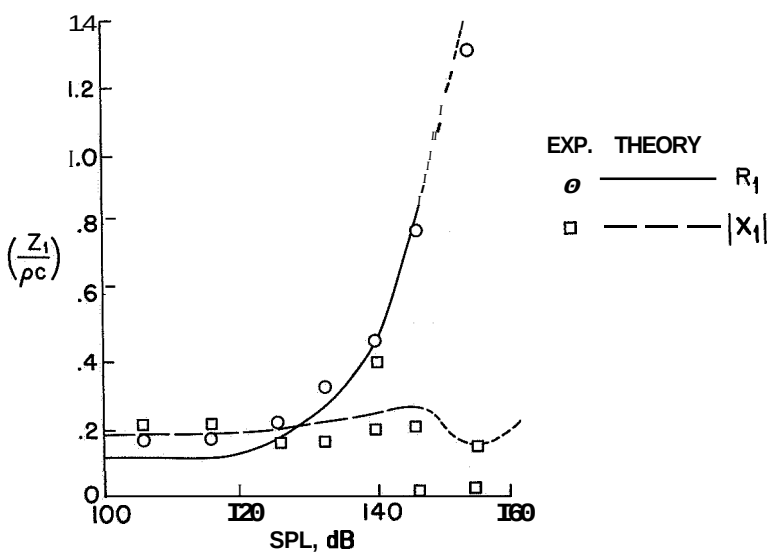

Figure 8

EXAMPLE OF NORMAL-INCIDENCE ABSORPTION

$$\alpha_N = \frac{\text{ABSORBED ENERGY}}{\text{INCIDENT ENERGY}}$$

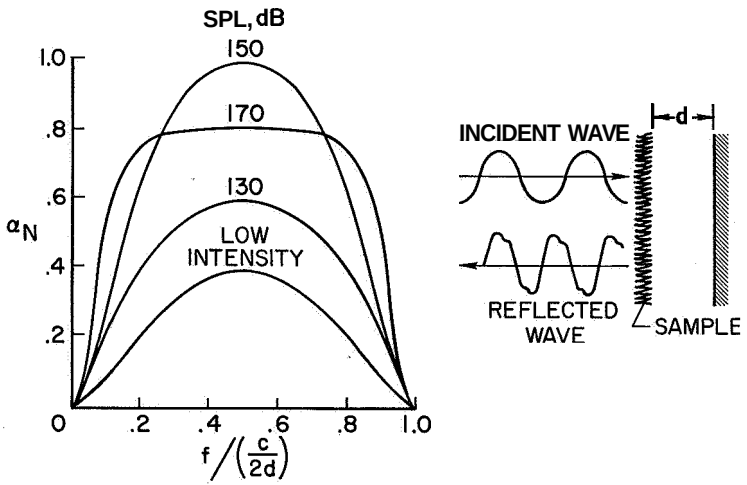

Figure 9

5. DUCT-LINING MATERIALS AND CONCEPTS

By R. A. Mangiarotty,

The Boeing Company

Alan H. Marsh,

McDonnell Douglas Corporation

and Ernest Feder

Pratt & Whitney Aircraft

SUMMARY

This paper summarizes the experimental and theoretical studies conducted by The Boeing Company, McDonnell Douglas Corporation, and Pratt & Whitney Aircraft to evaluate the acoustical characteristics of various metallic and nonmetallic materials and lining concepts. The use of a flow-resistance apparatus and an impedance tube and their role in the initial determination of the suitability of a material are explained. A synopsis of the materials tested and the results obtained is presented. Concepts and guidelines developed for design of acoustically absorptive linings are also presented. A summary of the theoretical studies relating to duct linings is given. In addition, the flow-duct results are compared with full-scale-engine results.

INTRODUCTION

Presented herein is a discussion of some of the aspects of the studies that led to the choice of duct-lining materials and the basic concepts used in the development of acoustically treated inlets and fan ducts for flight tests. (See refs. 1 to 3.)

As an introduction to the subject, figure 1 shows the environment in which acoustic linings must operate. The high airflow velocities in the inlet and fan ducts generate turbulence pressures on the walls that require materials which will not disintegrate under such conditions. (For example, rock wool would not be suitable.) Also, the high sound pressure levels may cause structural damage; a sound pressure level of 170 dB represents a fluctuating pressure of 100 pounds per square foot.

Figure 2 shows a typical spectrum of the far-field sound pressure levels (SPL) generated by the JT3D turbofan engine at a landing-approach power setting. Below 800 Hz the spectrum is controlled by noise from the primary jet exhaust. The spectrum between 800 and 10 000 Hz contains several discrete frequency components that are the principal

cause of annoyance to airport neighbors. The duct-lining materials and concepts are to be selected to attenuate these discrete frequency components.

SYMBOLS

a	duct width (appendix A)
a_i	pressure amplitude constant
b	duct height (appendix A)
c	speed of sound
C_x, C_y	coefficients of mode function
d	cavity depth; lining depth
D	acoustic attenuation, decibels (dB)
f	frequency, hertz (Hz) or cycles per second (cps)
h	duct height; separation between linings
i	integer
$j = \sqrt{-1}$	
k	wave number, $2\pi/\lambda$
k_x, k_y, k_z	components of complex wave number
l	treatment length; duct length
L	acoustic admittance
m,n	duct-mode harmonic integers
M	Mach number
p	acoustic pressure

Δp	pressure drop across material
R	flow resistance, rayls (cgs system of units)
SPL	sound pressure level, decibels (dB)
S_x, S_y	coefficients of mode function
t	time
u	acoustic particle velocity
V	airflow velocity through material
x,y,z	rectangular coordinates (subscripts 1 and 2 indicate stations along duct)
T,X,Y,Z	variable functions
Z	acoustic impedance
α	wave-number propagation constant
α_N	acoustic absorption coefficient
β	wave-number phase constant
λ	acoustic wavelength
ω	angular frequency

Double primes denote second derivatives and the notation ∇^2 denotes the nabla squared.

EXPERIMENTAL STUDIES

The three steps that were taken to evaluate and test various duct-lining materials and concepts are outlined as follows:

(1) Search for materials suitable for use as acoustical linings.

(2) Evaluate the materials and the concepts using a flow-resistance apparatus and an impedance tube.

(3) Test the materials (and the concepts) as duct linings in a flow-duct facility. (In a few cases, some lining concepts have been tested in a full-scale-engine fan duct.)

The desired characteristics of porous sheet materials for potential use as duct-lining treatments are summarized in table I. These characteristics were evolved on the basis of previous experience in the development of lining technology and were modified in view of current work. The candidate materials considered in the program and a list of the evaluation methods are given in table II. Part of the process of material selection and evaluation depends upon the type of lining concept. The three basic kinds of lining concepts that were studied are shown in figure 3, and their acoustic lining mechanisms are outlined in figure 4. The perforated plate and honeycomb combination resembles an array of Helmholtz resonators. As indicated by the solid curve for the lining mechanism, the attenuation spectrum is that of a sharply tuned resonator effective over a narrow band of noise when used as a duct lining in an environment of low airflow velocities and low sound pressure levels, and resembles an array of Helmholtz resonators. This concept can also provide a broader bandwidth of attenuation (see dashed curve in fig. 4) at very high noise levels or by the addition of a fine wire screen which provides acoustic resistance. The addition of the wire screen, however, complicates manufacture and adds weight to such an extent that other concepts are more attractive. The homogeneous absorber blanket is effective over a wide frequency range, but the materials available are not suitable for an engine environment because of their tendency to absorb and retain fluids and because of their fragility when exposed to airflow and high sound pressure levels. The broadband-resistive-resonator concept shown at the bottom of figure 3 was selected because it provides substantial acoustic attenuation over a wide frequency range and was judged, in particular, the most suitable concept for use in an engine environment. This concept incorporates the basic principles of the other two types of linings.

An extensive search was made for metallic and nonmetallic materials suitable for the broadband-resistive-resonator concept. Over 40 materials were evaluated. Most of these materials turned out to be unsuitable for use as lining materials because of their structural brittleness, for example, or their low acoustic performance.

Flow-Resistance Tests

Potentially suitable materials were screened for their flow-resistance properties by means of the flow-resistance apparatus illustrated schematically in figure 5. The

quantity measured is the acoustic flow resistance of the porous material, which is defined as

$$R = \frac{\Delta p}{V} \tag{1}$$

where Δp is the pressure drop across a sample of porous material and V is the airflow velocity through the material. The flow resistance of a porous material is related to the acoustic resistance of the material when it is used as a duct lining. The steady airflow velocity may be related to the root-mean-square (rms) particle velocity, over a range of frequencies, of the sound waves incident on the lining. The variation of flow resistance with airflow velocity for different materials may be roughly defined as turbulent or laminar to indicate the type of flow through the material. In general, the flow resistance should vary as little as possible for materials used to attenuate a narrow band of frequencies, but the variation may be of less importance where a broadband of frequencies is to be attenuated.

Impedance-Tube Tests

If the flow resistance of a sample of material was between about 1 and 100 rayls (cgs), the material was then evaluated with a normal-incidence acoustic-impedance tube to measure acoustic-impedance characteristics, as indicated in figure 6.

The normal-incidence acoustic impedance of a material Z is defined as the complex ratio of the rms acoustic pressure p at the surface of the sample to the rms acoustic particle velocity u at the same surface:

$$Z = \frac{p}{U} \tag{2}$$

This impedance has a resistive component $Re(Z)$ that is analogous to the flow resistance defined in equation (1) and a reactive component $Im(Z)$ that is dependent upon the resonance of the air cavity behind the material as well as the resonance characteristics of the air in the linings. Thus,

$$Z = Re(Z) + j\, Im(Z) \tag{3}$$

For the purpose of evaluating the acoustic properties of materials before they are used as part of a duct lining, the resistive part of the impedance is of prime interest because it provides an indication of the change of flow resistance with frequency. The reactive impedance of a material alone is small compared with the impedance of a lining on the wall of a duct.

The designation "small pores" in figure 6 indicates woven or felted types of materials, whereas "large pores" indicates coarsely woven or perforated plate materials. In the flow-resistance tests, the airflow through the woven or felted types of materials is generally laminar or turbulent with a fine-grain scale of turbulence. The airflow

through the perforated plate materials is generally fully developed turbulent flow. The small-pore materials show much less variation of the real part of the impedance with frequency and therefore are more desirable for applications as acoustical duct linings in turbofan engines.

The acoustic absorptivity of a material can also be determined from the data obtained with the impedance tube. The absorption coefficient, as shown in figure 7, serves to indicate the relative acoustic efficiency of a material as a function of the frequency of the incident sound waves. The depth of the cavity d behind the sample determines the frequency of peak absorption of the lining. The smaller the cavity, the higher the frequency of peak absorption.

To supplement the standard impedance-tube tests in which there is no airflow over the surface of the sample, a study was conducted to measure the acoustic impedance of materials with one surface of the sample exposed to airflow. The study was done by mounting an impedance tube on the side of a flow duct so that one surface of the sample was exposed to the airstream in the duct and the other was exposed to sound waves in an impedance tube. A preliminary analysis of the results indicated, as expected, that increasing the airflow generally increased the acoustic impedance in a manner similar to that indicated in figure 6, or, by using the analogy between the flow resistance and the real part of the impedance, in a manner similar to that shown in figure 5.

Flow-Duct Tests

After evaluating many candidate materials and concepts in the flow-resistance apparatus and the impedance tube, a few of the candidates were tested as part of a duct lining by fabricating panels for installation in a flow-duct facility. A diagram of this type of facility is shown in figure 8. Materials are exposed to high sound pressure levels, as well as to high airflow speeds similar to those in an engine. By measuring the sound levels in the source chamber and the receiving chamber for lined and unlined test ducts, the acoustic attenuation of a lining treatment in the test duct is obtained. The configuration shown in figure 8 simulates an exhaust duct configuration where the directions of the sound propagation and airflow are the same; however, by reversing the direction of either the airflow or the sound through the system, an inlet configuration can be simulated. Typical airflow Mach numbers through the test duct ranged from 0 to 0.6.

Typical results obtained with a lining configuration tested in the flow-duct facility for the exhaust mode only are shown in figure 9. The value of the peak attenuation and the peak frequency at which the peak attenuation occurs are functions of many quantities, the most important of which are presented here. Firstly, however, it should be noted that a conclusion from the study is that materials with the same acoustic characteristics (i.e., flow resistance R and acoustic impedance Z) in a given set of duct environmental

conditions yield the same acoustic performance. This result means that once the proper values for R and Z are determined the resultant acoustic attenuation of a lining treatment is determined by the geometry of the configuration.

The attenuation of individual lining configurations typically varies with the airflow velocity in the duct and the nominal flow resistance as illustrated in figure 10. The nominal flow resistance is the average flow resistance from measurements made at several points on a sheet of material at an airflow velocity of 0.2 meter/second. As the airflow velocity is increased, the nominal flow resistance must be adjusted in order to maintain a high level of attenuation. It is therefore necessary to design a treatment for the flow regime in the duct in which it will be used. The influence of the boundary layer over the lining surface was included in the data in figure 10, but it was not studied separately.

As mentioned previously, the attenuation produced by a duct lining depends on the geometry of the duct in which it is installed. Figure 11 shows the large change in attenuation that can result from variation of only the duct height or separation between treated surfaces; that is, the closer the lined walls are to one another, the greater the attenuation for a given type and area of treatment. The results presented in figure 11 indicate how critical this duct height parameter is. In the example shown, the same treatment with the duct height increased from 6 inches to 12 inches resulted in a decrease of 15 dB in the peak attenuation.

A parametric study of a large quantity of experimental data from flow-duct facilities has shown that the three quantities of (1) treatment cavity depth d, (2) duct height h, and (3) frequency of peak attenuation f are highly correlated, as indicated in figure 12. The information presented in figure 12 is useful in selecting a cavity depth for a treatment for a duct with particular duct height and a particular noise spectrum to be attenuated. The speed of sound c was used to obtain nondimensional parameters.

The attenuation of a fixed length of duct lining increases, as to be expected, with the number of surfaces treated (i.e., as the treated area is increased). The typical relative increase obtained by treating the various sides of a duct is shown in figure 13. It is evident that treating a second and opposite surface of a duct produces a substantial increase in attenuation. The small increase in attenuation obtained by adding linings on walls C and D when linings are already on walls A and B is due to the smaller surface areas of the short walls and to the greater separation between them. The aspect ratio between the length of walls A and B and the length of walls C and D was varied from 1 to 4.

Attenuation of noise also increases, as expected, with an increase of treatment length, and figure 14 shows some of the typical results obtained. The initial portion of the treatment is more effective because, at the beginning of the duct, there are many more

acoustic modes (high orders) that are attenuated more rapidly than the remainder of the propagating modes. Since the remaining modes are predominantly of plane-wave type, they attenuate less rapidly with lining length. Sufficient length of treatment is necessary, of course, to attenuate broadband noise which generates both kinds of duct modes.

Full-scale Test

Two fan-exhaust lining materials and configurations were evaluated in the ducts of a full-scale JT3D engine with good results. Figure 15 shows a sample of the correlation achieved between flow-duct data and full-scale-engine data, after adjustments had been made to account for the differences between the sound pressure levels and the duct heights in the engine and in the flow duct.

Summary of Experimental Results

A summary of the test results on porous surface materials that can be used as part of acoustic lining concepts is as follows:

(1) A large variety of porous materials, metallic and nonmetallic, were tested.

(2) The general result, for a given set of duct environmental conditions, was that the same acoustic performance could be obtained from any of the materials examined provided that the flow resistance and acoustic impedance of the lining were identical under the particular environmental conditions. This result means that each type of thin porous surface material considered (i.e., perforated plate, resin-coated fiber-glass cloth, fiber metal, and woven wire screen) can be made to work. Hence, the selection of the material for use as an acoustical duct lining is more concerned with weight, cost, strength, and manufacturing requirements. Each type of material, however, requires certain adjustments to the acoustical and geometrical variables of the material and its support structure to achieve equal levels of noise reduction and compliance with mechanical and economic constraints.

(3) Perforated-plate material requires the greatest amount of adjusting and full-scale development testing to realize the full potential of the mechanical and economic features.

(4) Both resin-coated cloth and fiber-metal material require about the same amount of adjustment, but advantage can be taken of developments in duct-lining technology to minimize the time and cost of the development program.

(5) Fiber-metal material, with low nominal flow resistance and low nonlinearity factor, is desirable when contamination is not serious or when effective methods can be devised to clean contaminated surfaces.

(6) Resin-coated fiber-glass cloth, with low nominal flow resistance and high nonlinearity factor, is desirable when contamination is a serious problem or when it is undesirable or difficult to devise effective cleaning methods.

A chart showing the types of tests that have been conducted in the various test facilities is shown in figure 16. Of the nonmetallic materials, the fiber-glass—polyimide resin was the most successful, although the other two materials shown had similar acoustical properties, Of the metallic materials, the first two were about the same in acoustical performance. The perforated plate required the largest amount of parametric adjustment to perform acoustically in a similar way to other materials. The NASA-developed lining (NASAMET) was also satisfactory but bulkier than the other three.

THEORETICAL STUDIES

Theoretical studies have been conducted by The Boeing Company (and also by Pratt & Whitney Aircraft) to develop methods for predicting the acoustic performance of duct linings. Thus far, the studies have been successful in developing mathematical equations and an associated computer program for predicting attenuation of a treatment in a duct without airflow. Figure 17 shows a comparison of the attenuation predicted for a two-wall lining treatment without air flowing through the duct and that measured for the same configuration with air flowing through the duct at a Mach number of 0.1. The theoretical prediction is considered to be accurate if allowance is made for the small airflow in the duct.

A summary of the theoretical work is given in appendix A.

CONCLUDING REMARKS

It was concluded from the overall study of material and lining concepts that, for a given duct environment, the same acoustic performance could be obtained from any of the materials examined provided that the flow resistance and acoustic impedance of the lining treatments were the same. In view of this conclusion, a material for lining a duct to produce a given attenuation can be selected by giving primary consideration to other factors, such as the weight, strength, and total cost of the installed lining.

The most important parameters for a duct treatment are the duct height (separation of the treated surfaces), the cavity depth (which controls the principal frequencies to be attenuated), the lining length, and the area treated.

A prediction theory for the condition of no airflow has been successfully developed, but requires extension to cover the case when airflow is present.

APPENDIX A

THEORETICAL ANALYSIS

A theoretical analysis was made to develop a method for predicting the attenuation of sound in ducts, with particular application to turbofan engines. The theory is for straight sections of duct with various cross sections ranging from rectangular to concentric cylindrical segments. The method developed also includes duct-lining optimization on the basis of maximum reduction in perceived-flyover-noise level depending on the shape of the input spectrum.

The transmission of sound through lined ducts has been treated by many investigators. The treatment of the problem as described in this appendix follows most closely that of reference 4, but with an extensive broadening of concepts and applications. A brief outline of the analysis is presented to indicate the principal assumptions in the prediction method.

The sound pressure in the duct is assumed to be low enough for the linear wave equation to be valid; thus,

$$\frac{1}{c^2}\frac{\partial^2 p}{\partial t^2} - \nabla^2 p = 0 \tag{A1}$$

By using the method of separating the variables to obtain a solution in terms of the normal modes of the duct, the following equation is obtained:

$$p(x,y,z) = X(x)Y(y)Z(z)T(t) \tag{A2}$$

If harmonic waves are assumed to be traveling in the positive z-direction along the duct, equation (A2) leads to a solution of the form

$$X(x) = C_x \cos k_x x + S_x \sin k_x x \tag{A3}$$

$$Y(y) = C_y \cos k_y y + S_y \sin k_y y \tag{A4}$$

$$Z(z) = \exp\left(-jk_z z\right) \tag{A5}$$

$$T(t) = \exp(j\omega t) \tag{A6}$$

A general solution as a superposition of these solutions is as follows:

$$p = \sum_{i=1}^{\infty} a_i X_i Y_i Z_i T_i \tag{A7}$$

where the constants a_i are chosen in such a way that any particular sound pressure distribution at the sound-source end of the duct can be accurately described.

Expanding equation (A1) yields

$$\frac{1}{c^2}\frac{\partial^2 p}{\partial t^2} - \frac{\partial^2 p}{\partial x^2} - \frac{\partial^2 p}{\partial y^2} - \frac{\partial^2 p}{\partial z^2} = 0 \tag{A8}$$

but $\frac{\partial^2 p}{\partial x^2} = \frac{\partial^2 X}{\partial x^2} YZT$, and similarly for the other variables. Denoting $\frac{\partial^2 X}{\partial x^2} = X''$ leads to

$$\frac{1}{c^2}\frac{T''}{T} - \frac{X''}{X} - \frac{Y''}{Y} - \frac{Z''}{Z} = 0 \tag{A9}$$

By means of separation constants, equation (A9) is transformed into a number of ordinary differential equations.

A solution that represents a wave propagating in the z-direction, restricted to a single frequency component, is

$$Z(z) = \exp\left(-jk_z z\right) \tag{A10}$$

where $k_z^2 = k^2 - k_x^2 - k_y^2$ is the axial wave number and k is the complex wave number of a wave propagating in free air.

Boundary equations are derived from equations (A2) to (A7) and (A9). Each solution corresponds to a mode of propagation in a duct of width a and height b. In order to solve a particular problem, a combination of modes with different values of the modal order numbers m and n must be taken with different amplitude and phase. They must be made to match the sound pressure distribution at the sound-source end of the duct, where

$$x = a, \quad \sin k_x a = 0, \quad k_x = \frac{m\pi}{a} \qquad (m = 0,1,2,\ldots)$$

$$y = b, \quad \sin k_y b = 0, \quad k_y = \frac{n\pi}{b} \qquad (n = 0,1,2,\ldots)$$

The solution is applied to the calculation of sound attenuation in a duct with broadband-resistive-resonator linings by introducing boundary conditions representing the

acoustic admittances $L(0,a)$ and $L(0,b)$ of linings in a duct of width a and height b. (Note that $b = h$ in the experimental studies described previously.) The attenuation of sound per unit length of duct in the positive z-direction can be determined from equation (A10) for the pressure by introducing $k_z = \alpha + j\beta$. Thus,

$$Z(z) = \exp(-j\alpha z) \exp(\beta z) \tag{A11}$$

The attenuation along the duct between stations at z_1 and z_2, expressed in decibels, is then

$$D_{(z_2-z_1)} = 20 \log_{10}\left|\frac{p(z_1)}{p(z_2)}\right| = -8.68\beta(z_2 - z_1) \tag{A12}$$

Thus, the attenuation per unit length is

$$D = 8.68\beta \tag{A13}$$

The wave number k_z (and thus the phase constant β) is solved from the wave number equation

$$k_z = \pm\left(k^2 - k_x^2 - k_y^2\right)^{1/2} \tag{A14}$$

Because the influence of the convective velocity of the gas in the duct is small compared with the influence of airflow turbulence, the solution was obtained for a zero velocity. The influence of airflow turbulence, boundary layers, and other aerodynamic effects can be taken into account by using experimentally derived lining characteristics obtained under the actual conditions of flow.

A computer program was developed which provides duct-lining design characteristics for optimum attenuation. Inputs to the program are the experimentally determined characteristics of a selection of previous materials, constraints on lining thickness, and the geometry of the duct. Optimization of the attenuation can be performed for any number of modes of sound propagation in the duct. A merit function allowing optimization over any frequency range is used to weight the sound spectrum for subjective response so that linings can be selected to provide optimum attenuation in perceived noise.

REFERENCES

1. Pendley, Robert E.: Design Concepts. Conference on Progress of NASA Research Relating to Noise Alleviation of Large Subsonic Jet Aircraft, NASA SP-189, 1,968. (Paper No. 9 herein.)

2. Drakeley, George T.; and McCormick, Ralph B.: Treated Inlets. Conference on Progress of NASA Research Relating to Noise Alleviation of Large Subsonic Jet Aircraft, NASA SP-189, 1968. (Paper No. 14 herein.)

3. McCormick, Ralph B.: Fan-Duct Development. Conference on Progress of NASA Research Relating to Noise Alleviation of Large Subsonic Jet Aircraft, NASA SP-189, 1968. (Paper No. 15 herein.)

4. Cremer, Lothar: Theorie der Luftschall-Dämpfung im Rechteckkanal mit schluckender Wand und das sich dabei ergebende höchste Dämpfungsmass. Acustica, vol. 3, no. 2, 1953, pp. 249-263.

TABLE I.- DESIRED CHARACTERISTICS OF POROUS SHEET MATERIALS

- ACOUSTIC FLOW RESISTANCE
  - Producible with mean values between 1 and 100 rayls (cgs)
  - Uniform over sheet or controlled gradation
  - Nonlinear increase in flow resistance with increasing airflow velocity should be small
- WEIGHT
  - Not over approximately 0.4 lb/ft^2
- THICKNESS
  - Between approximately 0.02 and 0.05 in.
- STRENGTH
  - Effective ultimate tensile strength not less than 10 000 lb/in^2
  - Effective yield tensile strength not less than 4000 lb/in^2
  - Breaking strength no less than 200 lb/in.
- ENVIRONMENTAL FACTORS
  - High airflow velocity (up to Mach number 0.6)
  - High sound pressure levels (up to 170 dB)
  - Subject to contamination – dust and oils
  - May need use of cleaning solvents
  - Anti-icing considerations
  - Exposed to rain – wetting, freezing, erosion, and corrosion
  - Exposed to sunshine and heat from engine
  - Should be able to withstand environment for rest of design life of airplane
- MANUFACTURE
  - Formable into compound curved shapes
  - Should be available in large sheets, nontoxic and nonflammable
- COST OF RAW MATERIAL
  - Approximately $\$15/ft^2$ or less, in 1000-ft^2 production lots

TABLE II.- CANDIDATE MATERIALS AND ACOUSTICAL EVALUATION METHODS

- POROUS SURFACE MATERIALS
  - Metallic
    - Felted wire fibers – sintered
    - Layers of woven-wire screen – sintered
    - Sintered powders
    - Perforated plate
    - NASAMET
  - Nonmetallic
    - Layers of woven fiber-glass cloth – resin or rubber impregnated
- HONEYCOMB-SUPPORT STRUCTURES
  - Metallic
    - Stainless steel or aluminum – welded or brazed
  - Nonmetallic
    - Heat-resistant phenolic-resin-impregnated fiber-glass cloth (bonded)
    - Phenolic-resin-impregnated nylon-coated paper
    - Polyimide-resin-impregnated fiber-glass cloth (bonded)
- ACOUSTICAL EVALUATIONS
  - Laboratory Tests
    - Flow resistance
    - Standing-wave tube with and without airflow
  - Duct-Model Tests
  - Full-Scale-Engine Tests

TREATMENT ENVIRONMENT

MACH	0.2 TO 0.6	0.3 TO 0.5
SPL, dB	120 TO 160	120 TO 170
AIR TEMP, °F	-85 TO 140	0 TO 700

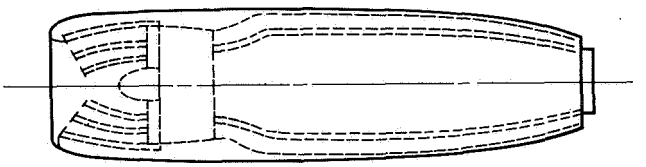

Figure 1

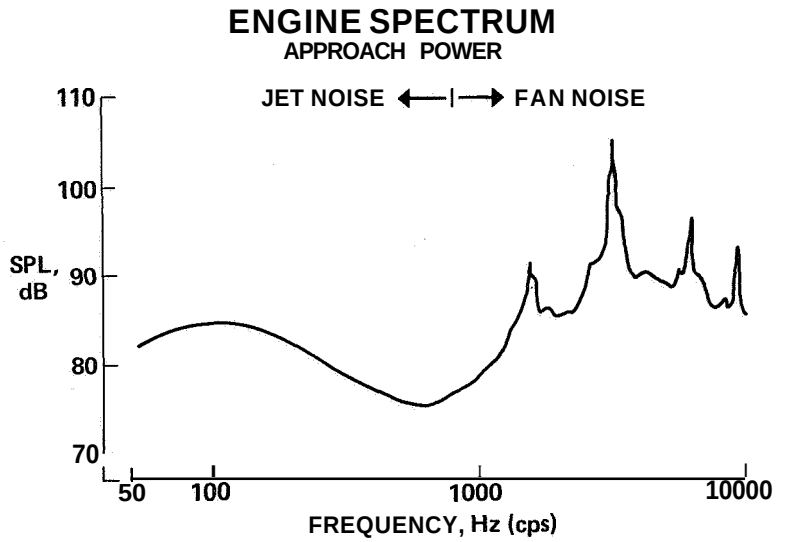

Figure 2

ACOUSTIC LINING CONCEPTS

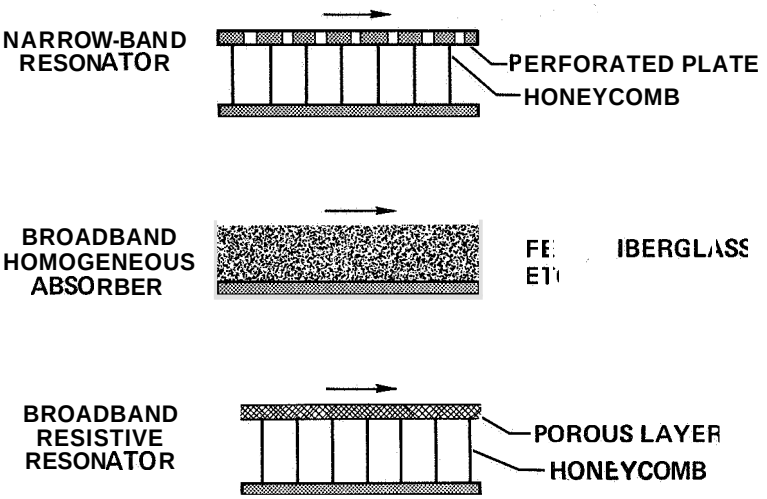

Figure 3

LINING MECHANISMS

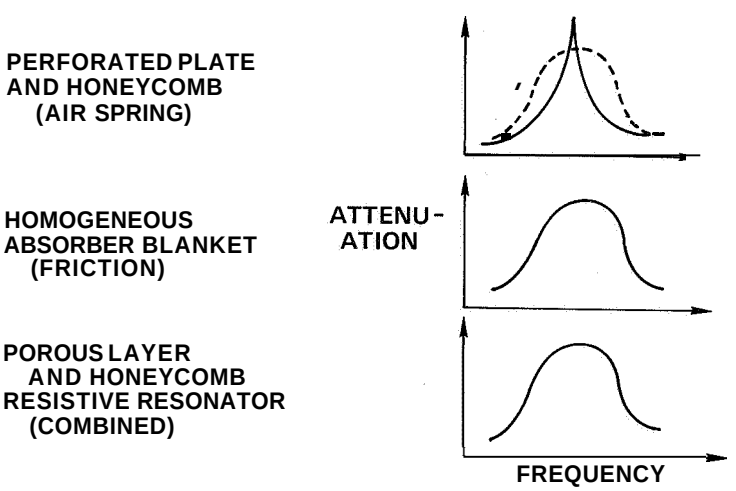

Figure 4

ACOUSTIC FLOW RESISTANCE

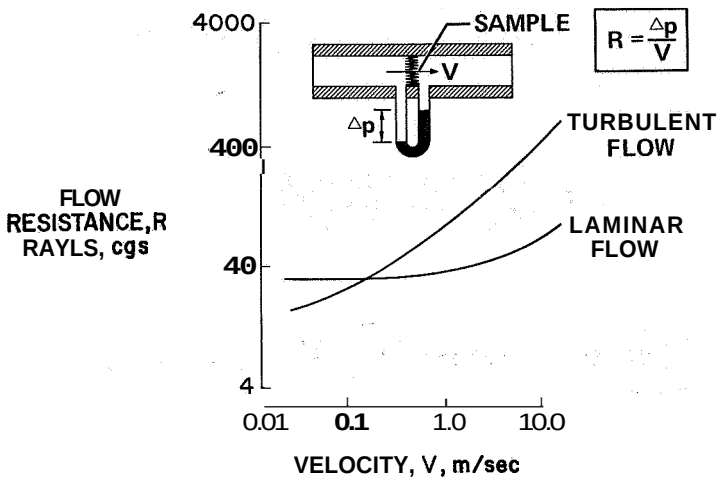

Figure 5

ACOUSTIC IMPEDANCE

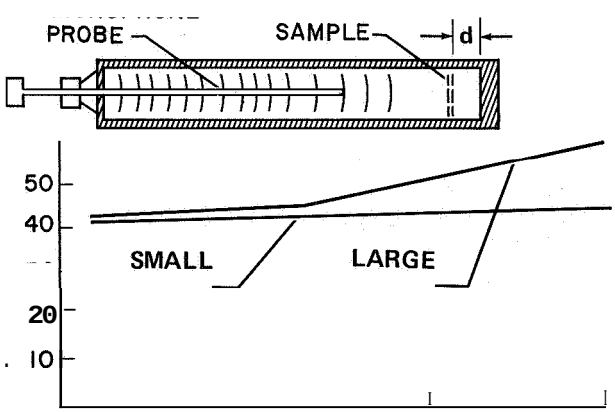

Figure 6

ABSORPTION COEFFICIENT

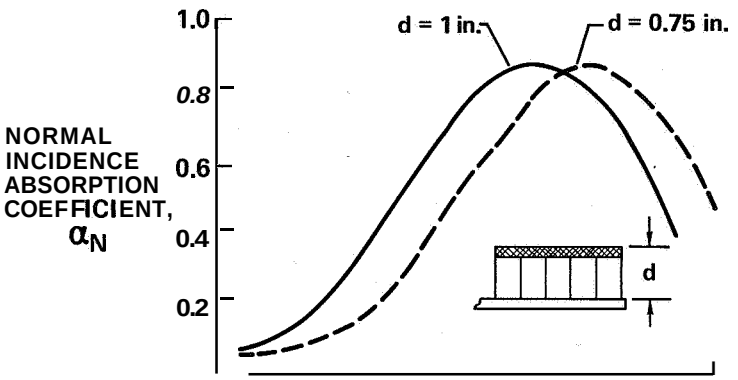

Figure 7

FLOW-DUCT MODEL TESTS

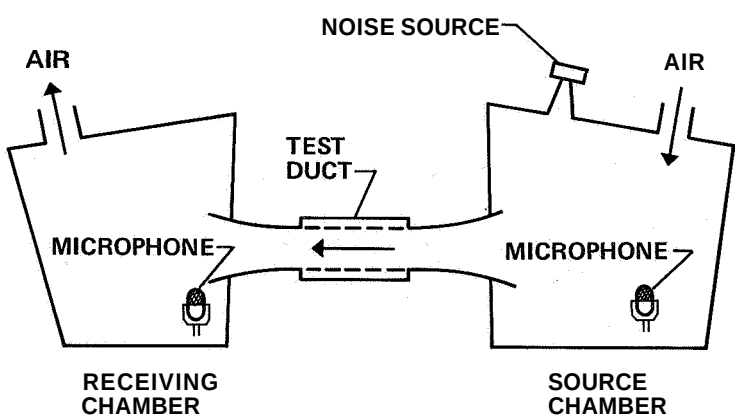

Figure 8

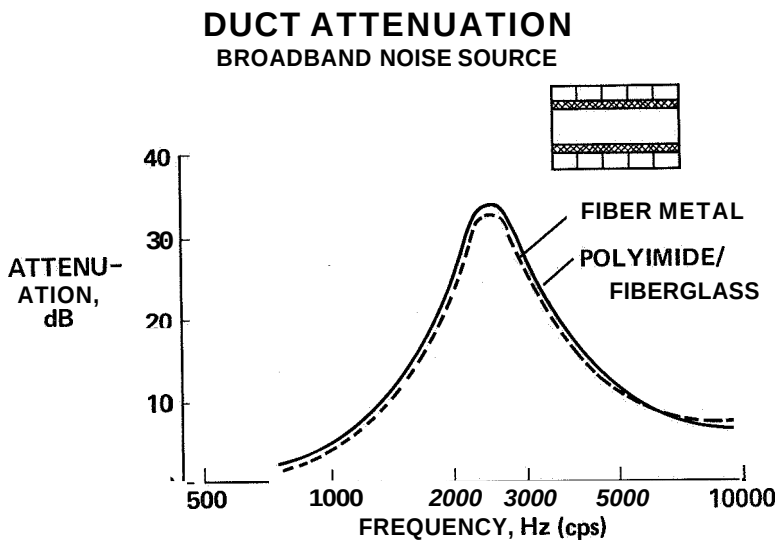

Figure 9

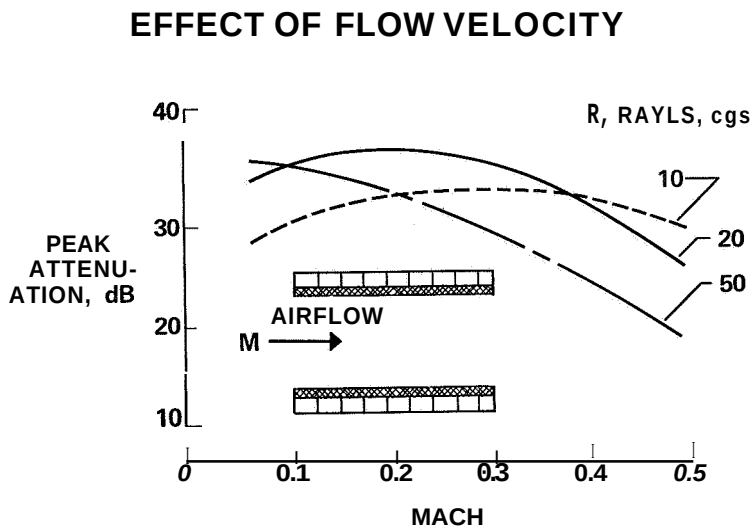

Figure 10

EFFECT OF DUCT HEIGHT

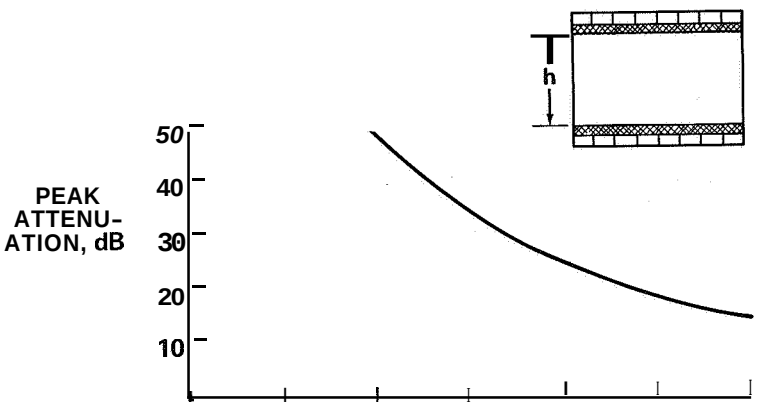

RELATION BETWEEN LINING DEPTH AND DUCT HEIGHT

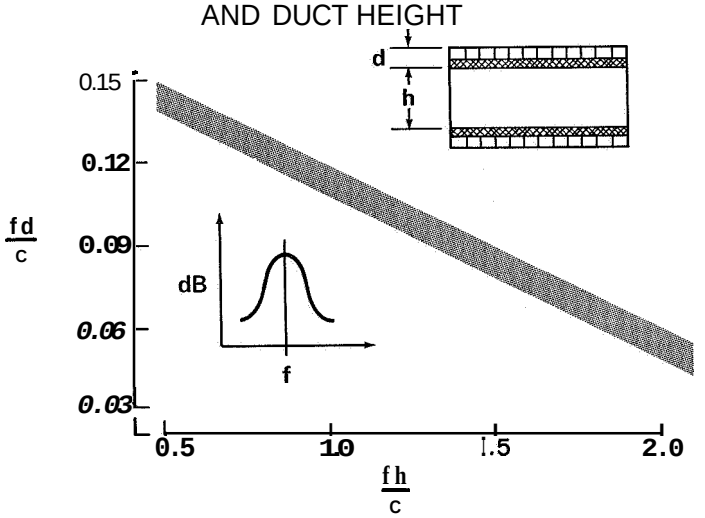

Figure 12

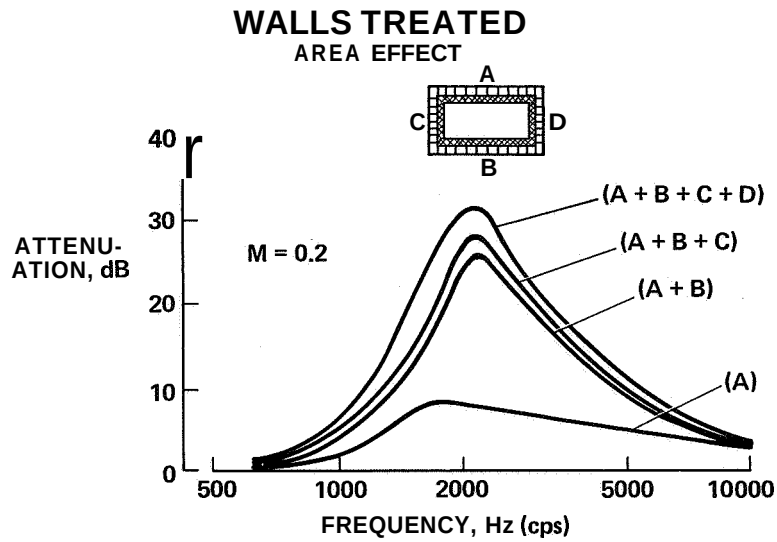

Figure 13

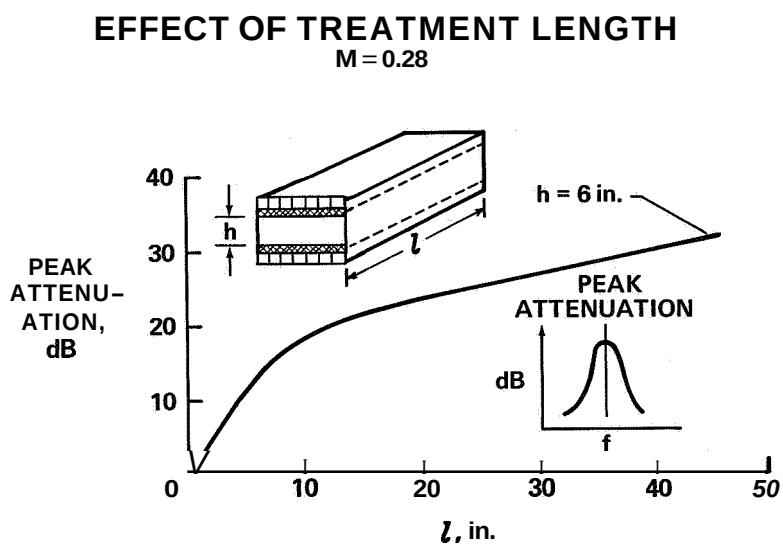

Figure 14

COMPARISON OF ACOUSTICAL DUCT LINING IN JT3D FAN–EXHAUST DUCTS AND IN MODEL FLOW DUCT

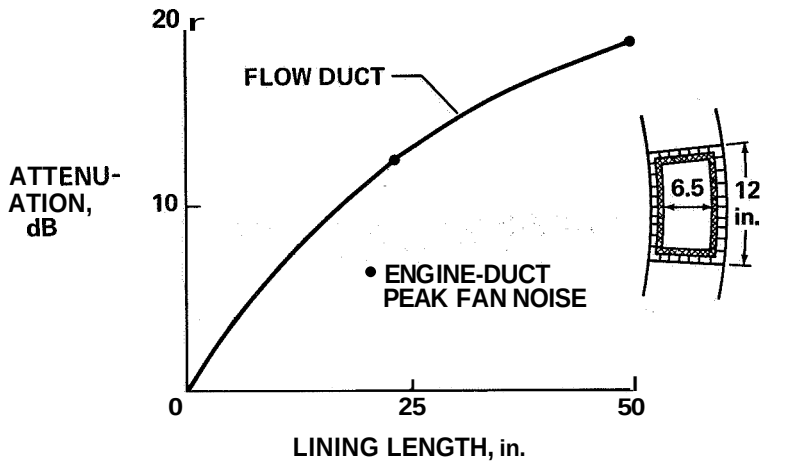

Figure 15

MATERIALS

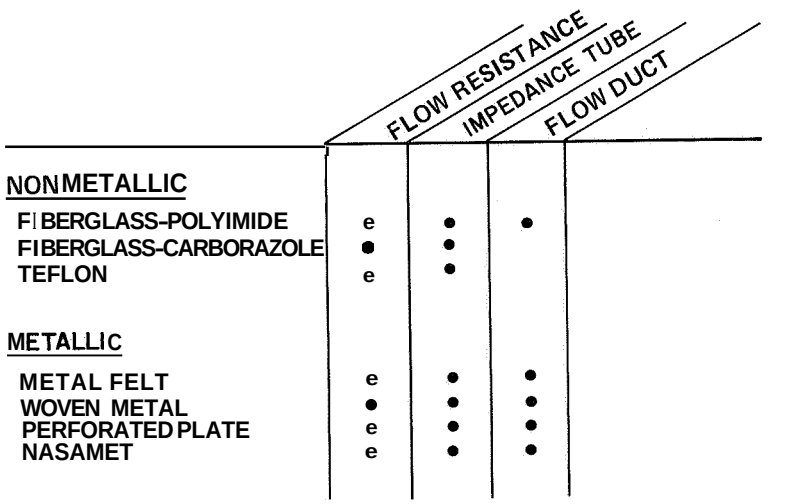

Figure 16

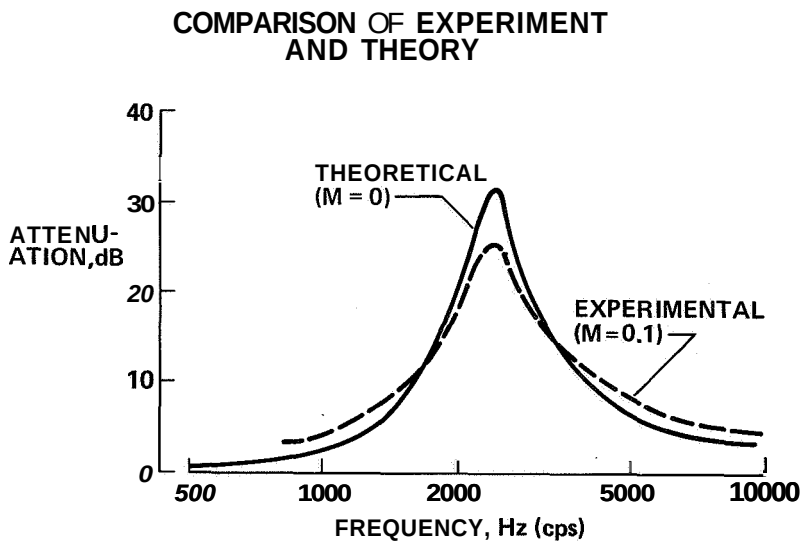
COMPARISON OF EXPERIMENT
AND THEORY
40
30
20
10
0
ATTENU-
ATION,dB
THEORETICAL
(M = 0)
EXPERIMENTAL
(M=0.1)
500
1000
2000
5000
10000
FREQUENCY, Hz (cps)

Figure 17

6. PERFORMANCE OF INLET SOUND SUPPRESSORS

By Charles E. Feiler, Edward J. Rice,
and L. Jack Smith

NASA Lewis Research Center

SUMMARY

The sound power attenuation was experimentally measured for two inlet noise suppressor configurations and compared with the calculated attenuation from a theoretical model. From the agreement observed, it appears that the theoretical model is valid, at least in the range of broadband sound, and can be used in the design of a suppressor. A general description of the theoretical model and the effect of the duct and sound properties on the sound propagation and attenuation are presented.

INTRODUCTION

Theoretical and experimental studies of inlet noise suppressors are being conducted at the Lewis Research Center as a part of the noise research program. The objective of the studies is to extend the understanding of the acoustic behavior of suppressors and of the factors that influence suppressor performance. The studies are general in scope rather than being applied to a specific engine.

In this paper results from the theory are presented which indicate the effects of several parameters on predicted suppressor performance. Some characteristics of the sound propagation found theoretically in a suppressor are also shown. In addition, a comparison is made between the experimental and theoretical sound power attenuation of two suppressor configurations. A detailed discussion of the theoretical calculation is given in reference 1.

SYMBOLS

c	speed of sound
D	duct diameter
L	duct length
R	wall resistance

r	radial distance
X	wall reactance
x	axial distance
A dB	sound power attenuation
$A\,dB_{max}$	maximum sound power attenuation
X	sound wavelength
P	mass density

ANALYTICAL MODEL

Some of the conditions and assumptions for the analytical model are shown in figure 1. Briefly, the theory provides the solution to the linearized wave equation valid for acoustically treated or soft-walled circular ducts. It has been assumed that there was no steady flow, there were no wave reflections from the end of the duct, and the wall impedance was uniform throughout the duct. The solution has been specialized to consider a plane wave entering the duct by calculating the amplitudes of the radial modes such that their sum approximates the plane wave. For this purpose, the first 10 radial modes were sufficient to approximate the initial plane traveling pressure wave.

For these conditions the solution gives the pressure and velocity at any point in the duct. It is therefore possible to calculate the energy passing any cross section and, thus, the sound power attenuation. The parameters that appear in the theory are the ratio of duct diameter to sound wavelength D/λ, the ratio of duct length to diameter L/D, and the wall impedance composed of the wall resistance R, and the wall reactance X.

THEORETICAL RESULTS

In figure 2 is presented the calculated behavior of the initially plane wave as it propagates down the duct. The sound pressure amplitude at any axial distance x relative to that of the plane wave at $x = 0$ is shown as a function of radial position. The calculations were made for a single value of acoustic impedance of the wall and for two values of the frequency parameter D/λ. For $D/X = 10$, the initially plane wave distorts as it propagates until a smooth profile exists at $x/D = 5$; also, the sound energy has been

redistributed or beamed toward the duct center line. The pressure amplitude at the center line has doubled or increased by 6 dB, whereas the pressure amplitude at the wall has decreased by a factor of 10 or 20 dB. For these conditions, calculations show that the acoustic energy of the wave has been attenuated very little. For $D/\lambda = 1$, the wave remains essentially planar as it propagates but is appreciably attenuated. Thus, the results predict a strong influence of the parameter D/X on the sound power attenuation produced by a suppressor.

Figure 3 shows contours of constant sound power attenuation relative to the duct entrance plotted in the wall impedance plane. These calculations were for constant values of D/X of 1 and L/D of 3. The contours are more or less circular and show an upper limit to the attenuation. In general, the upper limit occurs at a negative value of the wall reactance or in the capacitance (stiffness) controlled region. This result is in contrast to the approximate solution for a plane wave which predicts that the maximum attenuation will occur at zero reactance or at the liner tuned point (ref. 2). Generally, the point of maximum attenuation moves at a negative 45° slope to higher wall resistance and more negative wall reactance as D/X is increased. This behavior is discussed in reference 1.

In figure 4, the dependence of the point of maximum attenuation on the frequency parameter D/λ is shown for several values of L/D. The attenuation values have been divided by the L/D value of each curve; this procedure approximately correlated the curves. It is seen from the figure that for D/X values less than about 1, the attenuation does not depend strongly on D/λ. However, for D/X values greater than 1, the attenuation depends strongly on D/λ. A possible reason for this behavior is that sound beaming rather than attenuation was found to occur when the duct diameter exceeded the sound wavelength. This behavior was noted in the discussion of figure 2.

Figure 5 shows calculated attenuation curves for two suppressors that differ only in their diameter. The length and wall impedance were the same for each suppressor. As shown by the curves, the attenuation is much greater for the smaller duct diameter. The increase in attenuation is due to the combined change in L/D and D/X associated with the decrease in diameter. The curves illustrate the gain to be made by the use of configurations that have multiple passages such as those obtained with radial struts or splitter rings. The large attenuation predicted for L/D = 5 may not be observed in practice because of the masking effect of sound transmission through structural members or background noise such as the jet noise.

COMPARISON OF EXPERIMENT AND THEORY

A limited number of experiments for comparison with the theory have been performed on the inlet of a full-scale 5-65 turbojet engine. The base-line configuration of

the J-65 is shown in figure 6. It was equipped with a bellmouth and hard cowl inlet for static testing. Noise measurements were made by an array of far-field microphones in the front quadrant of the engine. In order to produce a more pronounced discrete tone at the blade passage frequency, the space between each third pair of inlet guide vanes was mechanically blocked. The resulting spectrum showed a peak about 10 dB above the background noise at the blade passage frequency and a lower peak at the first harmonic of blade passage frequency. Details of the experimental apparatus and procedures are given in reference 3.

At present, experimental and theoretical data have been obtained for two suppressor configurations. One was a simple cylindrical suppressor with no centerbody. The other was a seven-strut configuration shown without the bellmouth (fig. 7). In these configurations all the suppressor surfaces exposed to the flow were acoustically treated. The facing material in both suppressors was a perforated plate 0.02 in. thick with 0.05-in-diameter holes and an open area ratio of 0.08. The backing cavity depth was 1 in. except that for the struts which was 1/2 in. This backing cavity was partitioned with a honeycomb structure. The two sides of the struts were separated by an impervious septum. The resistance and reactance of this suppressor wall were calculated as a function of frequency according to the method of reference 4. Other conditions used in the wall impedance calculations were flow-by velocity of 150 ft/sec and a sound pressure level of 150 dB (re 2×10^{-4} dyne/cm^2) corresponding, respectively, to the flow velocity and the overall pressure level in the hard cowl inlet.

The geometry of the cylindrical suppressor corresponded to that assumed for the theoretical calculations, A comparison of the calculated and experimental attenuations is shown in figure 8; the agreement is very good. It should be pointed out that there is no empiricism, in the form of an undetermined coefficient, needed for the comparison.

The passages in the seven-strut suppressor were not cylindrical so that the calculated attenuation was obtained essentially by using the wetted perimeter of the passages. The attenuation was calculated for a cylinder with a diameter equal to the actual passage height or width. The calculated result was corrected by the ratio of acoustically treated area to passage cross-sectional area for the actual passage as opposed to the circular passage. The D/X effect was thus accounted for by the exact plane wave theory in a cylinder. The noncylindrical correction was suggested by the approximate theory of Morse (ref. 2). The experimental and calculated attenuations for the seven-strut suppressor are shown in figure 9. At the lower frequencies, where the sound was essentially broadband noise, the agreement was again very good. At the higher frequencies, where discrete tones predominate, the experimental attenuation exceeded the calculated attenuation. A possible reason for this discrepancy may be that the sound at these discrete frequencies propagates as a rotating mode. According to Morse (ref. 2) rotating modes should attenuate faster than a plane wave of the same frequency.

CONCLUDING REMARKS

The limited comparison of sound power attenuation obtained from experiment and theory is very encouraging. The theoretical studies are continuing to ease the restrictions imposed by some of the assumptions. These studies will include the effects of steady flow, wall impedance variation with suppressor length, and annular geometry. Additional experiments are being performed to further explore the validity of the theory and its extensions.

REFERENCES

1. Rice, Edward J.: Attenuation of Sound in Soft Walled Circular Ducts. NASA paper presented at Symposium on Aerodynamic Noise (Toronto, Canada), May 20-21, 1968.
2. Morse, Philip M.: Vibration and Sound. Second ed., McGraw-Hill Book Co., Inc., 1948.
3. Smith, L. Jack; Acker, Loren W.; and Feiler, Charles E.: Sound Measurements on a Full-scale Jet-Engine Inlet-Noise-Suppressor Cowling. NASA TN D-4639, 1968.
4. Phillips, Bert: Effects of High-Wave Amplitude and Mean Flow on a Helmholtz Resonator. NASA TM X-1582, 1968.

ANALYTICAL MODEL

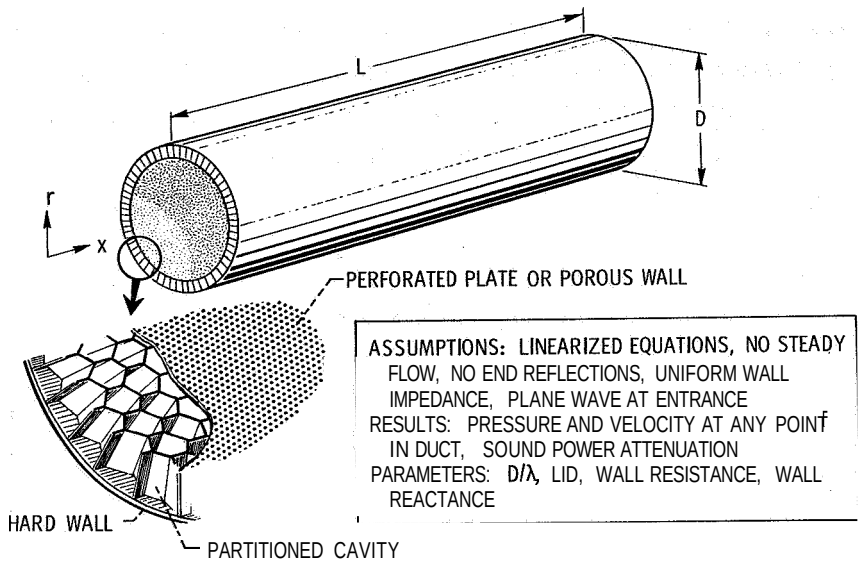

Figure 1

EFFECT OF x/D ON RADIAL PRESSURE PROFILES FOR TWO VALUES OF D/λ

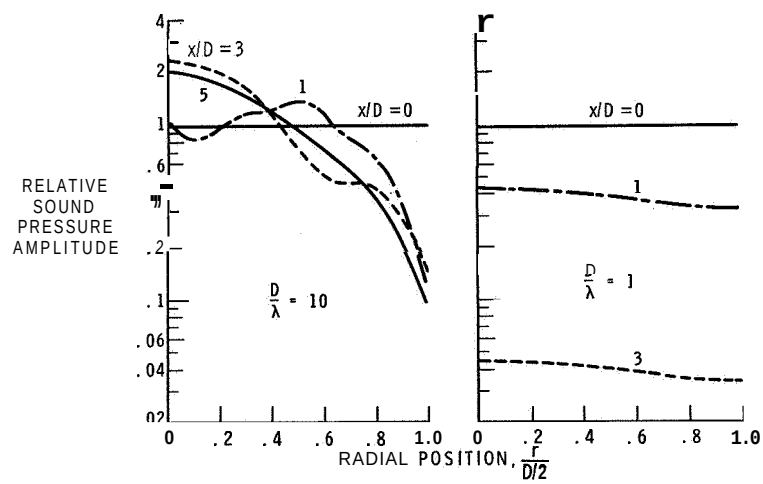

Figure 2

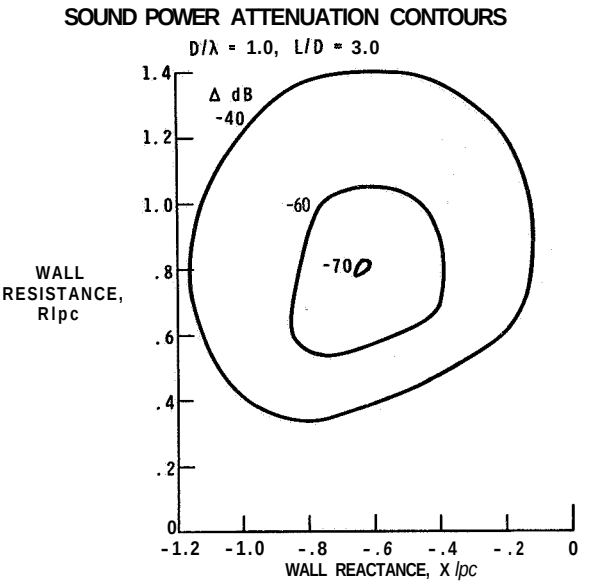

Figure 3

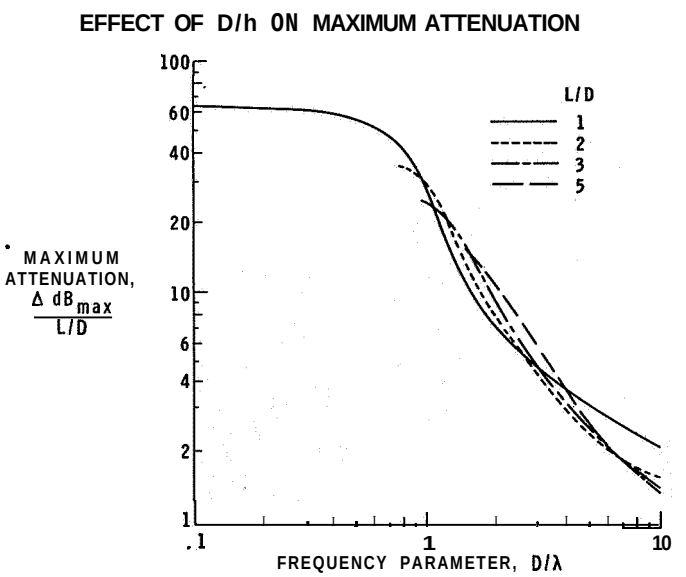

Figure 4

THEORETICAL SOUND POWER ATTENUATIONS FOR L/D=1 AND 5
WITH THE SAME WALL TREATMENT

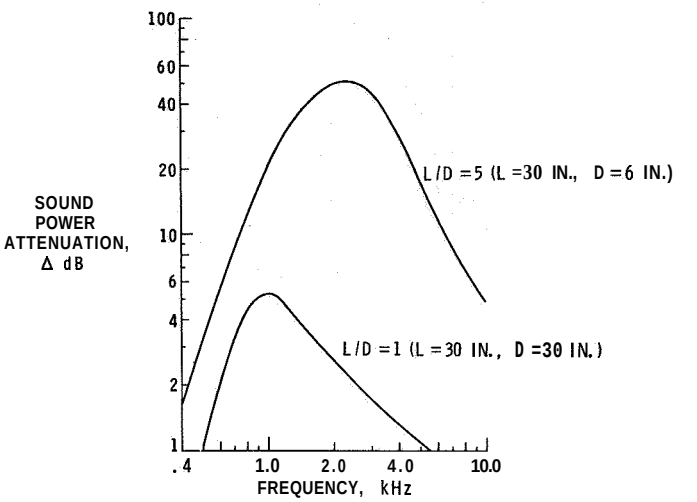

Figure 5

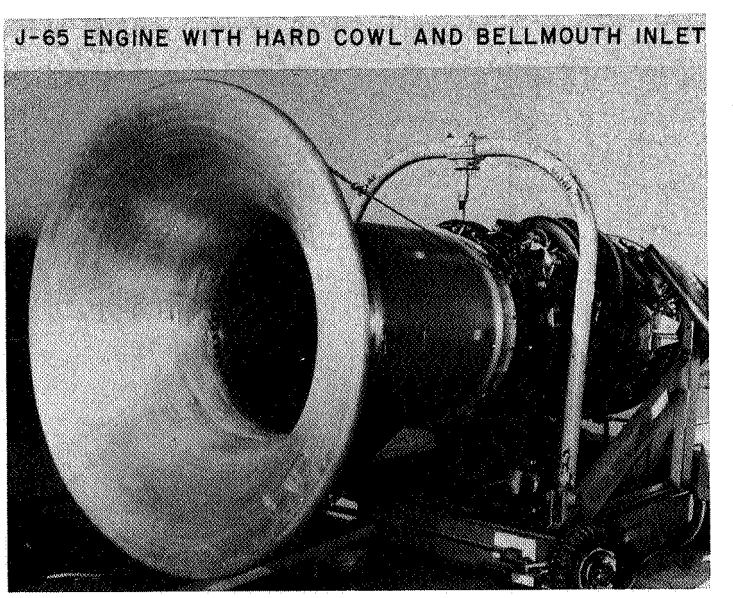

Figure 6 L-68-8539

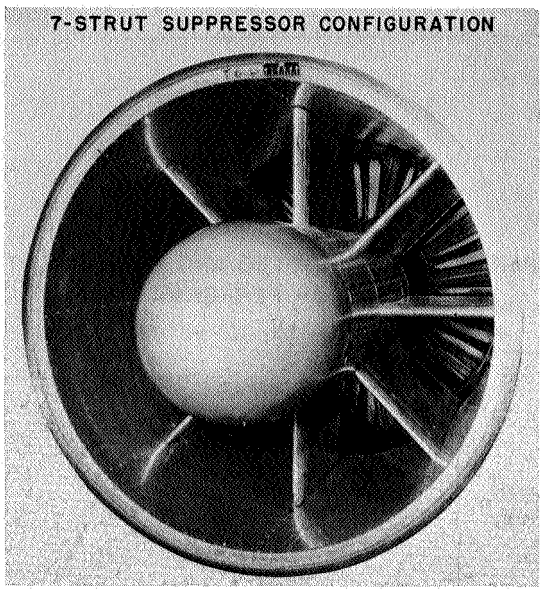

Figure 7 L-68-8540

COMPARISON OF PREDICTED AND EXPERIMENTAL SUPPRESSØR PERFORMANCE

CYLINDRICAL SUPPRESSOR; 1/3-OCTAVE DATA

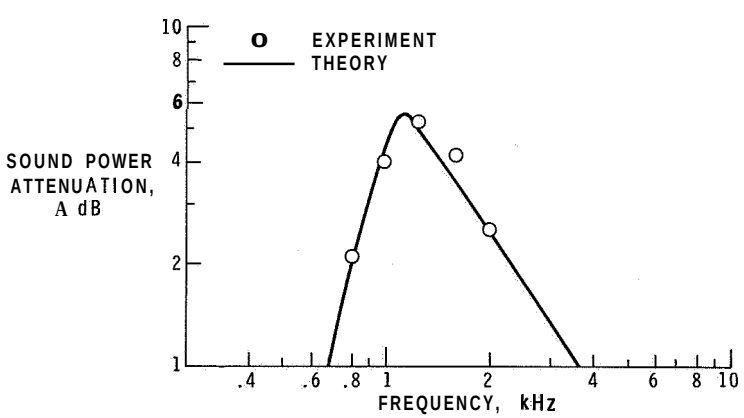

Figure 8

COMPARISON OF PREDICTED AND EXPERIMENTAL SUPPRESSOR PERFORMANCE

7-STRUT SUPPRESSOR; 1/3-OCTAVE DATA

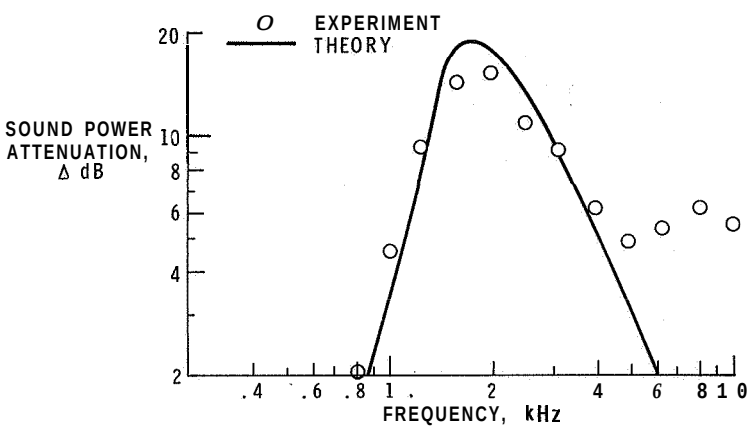

Figure 9

7. STRUCTURAL AND ENVIRONMENTAL STUDIES OF ACOUSTICAL DUCT-LINING MATERIALS

By H. A. Watson, Jr., J. D. Thompson,
McDonnell Douglas Corporation

and

Carl E. Rucker
NASA Langley Research Center

SUMMARY

The structural design criteria for acoustical duct-lining materials depend on the interrelation of aerodynamic, acoustic, and environmental requirements. Environmental conditions are of more-than-normal concern in the design of inlet and fan exhaust ducts which incorporate acoustical materials since the environment is allowed to penetrate the porous facing.

The results of tests reported herein have shown that the acoustical-sandwich structural concepts are feasible. However, without further engineering research, the incorporation of a turbofan noise-suppression system will result in increased weight and complexity with probable loss of aircraft utility. Despite work accomplished to date in the field of structural and environmental testing of acoustical liners, a large amount of additional investigation remains in order to achieve the optimum structural design of a certifiable noise-suppression system for commercial aircraft.

INTRODUCTION

There is an immediate concern for reducing turbojet-aircraft noise which adversely affects the communities adjacent to commercial airports. One promising approach is the development of a noise-suppression system which may be applied to the inlet and exhaust ducts of turbofan engines. An acoustical system of this type requires that the internal wetted surfaces of the ducts be replaced by a porous sheet material backed by acoustical cavities. Honeycomb sandwich is an ideal structural configuration for such a system; but although the duct environment remains unchanged, the exposure of the porous surface, the honeycomb core, and the sandwich interior to the environment introduces a series of problem areas, including corrosion, contamination, and drainage. The subject of this paper will be confined to structural and environmental studies of materials proposed for

use as acoutical duct liners and to the tests, analyses, and design criteria necessary to provide a certifiable noise-suppression system for commercial aircraft.

SYMBOLS

a	acceleration, $in./sec^2$
dS	incremental change in stress
$d\epsilon$	incremental change in strain
EI	sandwich stiffness factor, $lb\text{-}in^2$
$E_T = \frac{dS}{d\epsilon}$	tensile modulus of elasticity, lb/in^2
$F_{t,u}$	tensile strength, lb/in^2
f	frequency, Hz (cps)
f_o	resonant frequency, Hz (cps)
g	acceleration due to gravity, 386 $in./sec^2$
L	length of beam, in. (also thickness or direction of core)
N	number of fatigue cycles to failure
R	stress ratio
S	stress, lb/in^2
T	thickness of core, in.
T_u	tensile ultimate stress, lb/in^2
T_y	tensile yield stress, lb/in^2
t	thickness of sheet or beam, in.

W width or direction of core, in.

A deflection, in.

E strain, μin./in.

P density, lb/in^3

ρ_p density of parent material, lb/in^3

DISCUSSION

General Considerations

Studies related to the structure and environment of duct-lining acoustical materials proposed for use in the noise-suppression system of turbofan aircraft may be more clearly understood when preceded by an explanation of the basic acoustical function of the materials and their location within the nacelle as well as a detailed description of typical duct-liner construction.

The materials discussed in this paper are those that are used primarily in tuned-absorber noise-suppression systems. Basically, these systems function as a series of dead-end labyrinths which, according to their design shape and volume, trap sound waves of a specified wave-length range.

The major noise sources within a turbofan engine are due to the rotating blades of the fan, compressor, and turbine (ref. 1); therefore, the acoustic traps are located within the inlet and exhaust ducts leading to and from these sources. A major restraint upon the noise-suppression system is that disturbances of the aerodynamic flow within the ducts should be minimal. Therefore, the noise traps are logically located flush with or beneath the wetted surfaces of the ducts. When large amounts of suppression are required, additional wetted surface areas, which may be acoustically treated, are usually provided by duct elongation or by the addition of rings, struts, and vanes as shown in figure 1.

A tuned absorber is a composite of sheet and cellular core materials stacked to form a single or multiple sandwich as shown in figure 2. In a single sandwich, the porous facing sheet forms the wetted surface of the treated duct. The cells of the honeycomb core, together with the solid facing sheet, form the dead-end traps. Structurally, the solid sheet acts as the pressure wall of the duct, but the total sandwich reacts imposed loads. In a double sandwich, composed of three facing sheets and two cores, any two of the facing sheets may be porous, according to design. The concentric rings of figure 1 are examples of one type of double sandwich in which the center facing sheets are solid

and the two outer facing sheets are porous, thereby forming two back-to-back simple absorbers. A second type of double sandwich is shown in figure 2. The exposed or wetted surface sheet and the center sheet are of porous material, and the bottom external sheet is solid. In this design, the depths or thicknesses of the two sandwiched cores are often different because they are tuned for different frequency ranges.

Acoustic-Panel Description

In a sandwich structure, the honeycomb core is comparable to the web of an I-beam, which supports the I-beam flanges and allows them to act as a unit. The web of an I-beam and the core of a sandwich carry the beam shear stresses. The core of a sandwich differs from the web of an I-beam in that the core provides continuous support of the facings and thus allows the facings to be worked up to or above their yield strength without wrinkling or buckling. In order that the sandwich will act as an integral unit, the weld or adhesive which bonds the core to its facings must be capable of transm'itting shear loads between the facings and, in the case of pressure loads, of also transferring flatwise tensile loads. The cellular structure of honeycomb core in the acoustic sandwich serves a dual purpose since it also provides the acoustic cavities. In the case of the multiple sandwich, as with the single sandwich, any differential pressure across the plane of the sandwich acts on the solid facing sheet but is reacted by the total sandwich.

In order to determine the structural characteristics of sandwich panels, the mechanical properties of the materials proposed as sandwich elements must first be determined. In the case of an acoustical sandwich, the four types of structural elements are (1) the porous facing sheets, (2) the solid facing sheets, (3) the honeycomb core, and (4) the bond or weld interface between core and facing sheets. (See fig. 3.)

Porous Facing Sheet Materials

Of the four structural elements, the one which presents the most difficulty in selection of material and configuration is the porous facing sheet. This component must be available in thin, formable sheet and have certain acoustic characteristics related to a uniform porosity or flow resistance (ref. 1). In addition, it should be capable of carrying imposed loads and must withstand the environment to which it is exposed as a duct-liner surface. Numerous types of porous facing sheets have been considered. Several of the more promising types are described and discussed briefly in the following paragraphs.

Perforated sheet.- As shown in figure 4, porosity may be accomplished by perforation of solid sheet materials with round holes. If perforated sheets prove to be acoustically acceptable, a multitude of perforated patterns and sheet materials are available for use.

Sintered fiber-metal sheet.- Fiber metal is a randomly interlocked structure of metallic fibers which are sintered to produce a microscopic weld at the fiber intersections, thereby forming an orthotropic three-dimensional truss. Examples of this material are shown in figures 5 and 6. The nose cowl inlet and fan exhaust ducts of the acoustically modified nacelle for the forthcoming McDonnell Douglas flight tests (ref. 2) were fabricated by using this type of porous facing sheet. Numerous types of this configuration are commercially available in sheet gages and fabricated of such materials as copper, silver, AISI types 430 and 347 stainless steel, and 17-4 PH stainless steel. The fiber diameters, dependent upon material, range from 0.0004 to 0.010 inch.

Sintered woven-screen sheet.- As shown in figure 5, sintered woven screen is a sintered composite of two or more finely woven metallic wire screens. These screens are produced in weaves such as plain, twilled, plain dutch, and dutch twilled. The mesh size may vary from 10 by 10 wires per inch to 400 by 2800 wires per inch. A wide variety of materials is available, including AISI types 304, 316, 321, and 347 stainless steel, monel, nickel, inconel, copper, and Hastelloy X. Figure 6 is a micrographic cross section of fiber metal with supporting top and bottom screens.

Sintered continuous-filament sheet.- As shown in figure 5, sintered continuous-filament materials are fine, continuous, unwoven metallic filaments which are sintered in a uniform mat. These sheets are available in the same materials and wire diameters as woven screens.

Woven fiber-glass sheet.- Woven fiber glass (fig. 5) is a woven cloth of fiber-glass filaments available in a wide variety of weaves. With the proper resin matrix and layup methods, this material can be used to produce porous sheets. The porosity may be produced by control of the resin content or by mechanical molding of holes during resin cure. A polyimide resin system may provide a fiber-glass-reinforced structure which will withstand a continuous temperature of 500° F.

Solid Facing Sheet Materials

In the acoustical sandwich panel, the solid facing sheet is the pressure wall of the structure. Therefore, the gage and material of the solid facing are selected to withstand the hoop-tension loads of the duct.

Core Materials

Cellular cores yield the highest strength-to-weight ratio of all geometric structures. Honeycomb core is a lightweight structure of thin ribbons which are bonded or welded at nodes to form, when expanded, any of a large variety of cell sizes and cell shapes, such as squares and hexagons. The cell size is the diameter of an inscribed

cylinder. The ribbon of honeycomb core may be paper, plastic, fiber glass, metal, or any of a vast number of other materials. Figures 2 and 3 illustrate hexagonal and sine-wave cores, respectively. The core used in the fabrication of the McDonnell Douglas flyover nacelles (ref. 2) has a cell size of 0.75 inch, is of sine-wave configuration, and has been grooved for drainage as shown in figure 3. The ribbon is a heat-resistant phenolic resin system reinforced by woven fiber-glass fabric. In the case of welded metallic cores, one unique design with ribbon flanges welded to the facings is shown in figure 7.

Adhesive and Weld Materials

As previously stated, the honeycomb core must be capable of transmitting shear and flatwise tensile loads between the sandwich faces. The dual functions of the acoustic honeycomb sandwich, that is, acoustic attenuation and structural support, require exacting control of the adhesive bonding or weld interface between the honeycomb core and the porous facing sheet. The design objective has been to obtain an adhesive fillet between the honeycomb core and the porous facing which would be structurally adequate (300 psi in flatwise tension) with a minimum blockage of the porous facing material. (See fig. 8.)

In the McDonnell Douglas design of ground- and flight-test hardware described in references 1 and 3, it was found that commercially available structural bonding systems did not have the desired filleting action during cure and that standard adhesive-application methods did not provide uniform distribution of the bonding materials on the ribbon of the core. The solution of the problem involved the adaptation of a carrier-supported, aluminum-filled, modified-epoxy, film adhesive. The unique adaptation involved elimination of the scrim-cloth carrier and revision of the method of applying the adhesive to the core. The materials used in the bonding process are illustrated in the exploded view of the sandwich as shown in figure 9. The bonding method is shown in figure 10 and described in the following steps:

(1) A sheet of adhesive film is detached from its polyethylene separator and spread over the surface of the honeycomb core.

(2) The adhesive is caused to coagulate at the core ribbon by application of localized heat with a heat gun or heat lamp.

(3) The adhesive-core subassembly is then inverted onto the aluminum sheet, bagged, and cured for 1 hour at 350° F in a vacuum of 10 psi. (The term "bagged" refers to enclosing the bonding assembly in a flexible plastic bag and drawing a vacuum to obtain an elastic clamping of the assembly during oven cure.)

(4) When the sheet-adhesive-core subassembly has cooled, adhesive film is spread on the exposed surface of the core, coagulated at the core ribbon by localized heat, as in steps (1) and (2), and allowed to cool.

(5) The porous acoustic facing is then positioned. This operation is not critical since the adhesive hardens after cooling, is not tacky, and does not smear.

(6) The final assembly is bagged and cured for 1 hour at 350° F in a minimum vacuum of 10 psi. The pattern of the bondline is usually visible on the exterior surface of the porous facing material.

In duct areas with elevated temperatures, welded honeycomb becomes a candidate material for the acoustic sandwich. Figures 11 and 12 are micrographic studies of porous sheet welded to metallic ribbon; the material is stainless steel.

Environment

Acoustic requirements dictate that porous surfaces backed by air cavities be used as inlet and fan-exhaust-duct internal surfaces. Thus, the surfaces are structurally more complex than usual and typically require materials, processes, and structural concepts which are not conventionally used for these applications. As a result, particular attention must be paid to the environment in which the acoustic absorbent liners must function.

In the air-intake duct, the treated structure will be exposed to pressures, relative to ambient, ranging from -3 to 4 psi during normal usage. Indications are that on rare occasions of violent engine surges, pressures may peak at values of 15 to 40 psi. Sound pressure levels in the inlet are known to approach 175 dB at high power settings. Treated cowl surfaces will be exposed to atmospheric temperatures ranging from -85° to 125° F or higher. Within the nose-cowl structure, temperatures will commonly be several hundred degrees Fahrenheit, and hot anti-icing plumbing will locally subject surfaces to temperatures of nearly 450° F. In the case of a failed temperature-control valve, temperatures ranging up to 750° F could be encountered locally. In flight operations, the orientation of the engine inlet to oncoming airflow will expose the treated structure to the erosion or damage of rain, hail, and birds and, during ground operations, to the damage of pebbles, slush, and debris.

The fan exhaust ducts must withstand pressures up to 15 psig. Fan-air temperatures will range from about -65° to 250° F. Air velocities within the duct will vary from Mach numbers of about 0.4 to 1.0 between the entrance and exit sections at cruise conditions. Since the ducts form part of the enclosure surrounding the engine compressor case and accessory section, the treated surfaces in this area will be exposed to temperatures within the nacelle which are nominally 300° to 350° F. Locally, compartment

temperatures range up to 750° F near bleed-air piping, where high-pressure leaks may occur. In the event of a fuel fire, temperatures over 2000° F could be encountered. If a fire is started, it is desirable that burnthrough of the fan ducts not occur rapidly. Fire resistance should permit ample time for fire detection and for corrective action to be taken before burnthrough could occur and result in pressurized fan exhaust air being fed to the fire. In concepts featuring long ducts with treated surfaces facing the engine case aft of the compressor section, the treated liner must cope with heat radiation of temperatures up to 1400° F.

The phenomenon of subsurface recirculation losses in the air inlet and fan exhaust ducts is of interest to the power-plant performance engineer. Since the liner surface must be porous and backed by air cavities, and since wall static-pressure gradients exist in the inlet and exhaust flow paths, each cavity has a flow of air entering through regions of high surface pressure and leaving through regions of low surface pressure. There is a resulting small loss of momentum which is additive to the friction loss of the treated surface. Experience has shown that if cavity lengths are kept small, that is, less than 2 inches in the direction of the pressure gradient, the subsurface recirculation losses are small compared with friction losses.

An item which has been of little or no concern in the past, but which is of great concern to the designer of acoustically treated ducts, is porous-surface contamination. Figure 13 illustrates a typical time history of the in-service exposure of a large commercial transport aircraft to various potential contamination conditions.

On the ground, contamination conditions include exposure to oil, solvents, grease, and dirt during maintenance operations. During engine run-up and taxi, treated surfaces will be in the presence of exhaust products, dust, vapors, ground debris, slush, and water. One condition of concern is due to the frequently recurring situation of aircraft lined up awaiting take-off. During this wait, the engines are operating on air mixed with exhaust products from the aircraft ahead. The accumulation of solid particulate matter and vapor in the porous liner surfaces may become significant.

During flight, the treated liners will be exposed to water in the form of solid, liquid, and vapor. Smog and dust will be encountered at low altitudes. Collection of radioactive dust may be of concern at high altitudes. Experience with filters in current aircraft air-conditioning systems has indicated significant collection of radioactive materials. In most types of liners, it may be necessary to include provisions for water drainage from air cavities to protect against loss of sound-absorption qualities, damage due to freezing and expansion within cavities, and weight penalties caused by undrainable water.

Mechanical-Properties Testing

A complete compilation of the mechanical-properties testing performed to date on the noise-alleviation materials proposed for use in noise-attenuation programs is not within the scope of this paper. Therefore, an outline of the tests necessary to determine design allowables for these materials and pertinent data presently available will be presented.

Because the porous sheet materials (particularly the woven and fiber configurations) and the honeycomb core have properties which vary with the direction in the material, they are defined as orthotropic materials (ref. 4). The structural theories of homogeneous, isotropic materials do not apply to orthotropic materials without major revision; but this subject will not be explored in this discussion. However, it may be noted that in order to determine the mechanical properties of isotropic materials, tests along the longitudinal and transverse axes are required, whereas with orthotropic materials, a third test along a diagonal axis is also required in order to define fully the mechanical properties. Figure 14 is a polar orientation plot of fiber-metal tensile strength along three axes.

A component listing of mechanical-properties tests necessary to provide design allowables for noise-alleviation configurations is presented. Tests which are underlined require room temperature, elevated temperature, and special environmental testing.

(1) Porous sheet materials

(a) Tensile tests along three axes to determine tensile yield, tensile ultimate, elongation, and modulus of elasticity (ref. 5)

(b) Flexural fatigue tests along three axes to determine flexural endurance strength (ref. 6)

(c) Interlaminar shear tests along three axes to determine shear strength of resin system or shear strength of sintered fibers (ref. 7)

(d) Bearing tests to determine tear-out shear or bearing strength when sandwich is loaded by mechanical fasteners or rivets (ref. 8)

(e) Photoelastic tests of perforated sheets under biaxial loading to determine stress concentration factors due to hole pattern

(2) Core materials (honeycomb, etc.)

(a) Flatwise tensile tests to determine core tensile strength, usually combined with adhesive or weld test to insure attachment develops full strength of core (ref. 9)

(b) Flatwise compression tests, with specimens bare and supported, to determine strength of core. This test determines the strength loss due to the drainage grooves (ref. 9).

(c) Core shear tests along two or three axes, according to sandwich design. The complete sandwich is usually tested to determine the shear strength of the adhesive or weld (ref. 9).

(3) Adhesive or weld system

As previously outlined, the adhesive or weld system is usually tested in flatwise tension and shear as a component of the total sandwich.

Preliminary lap shear tests are required to determine adhesive-strength allowables. As a special consideration for acoustical sandwich designs, tests are made at elevated temperatures and pressures to determine also the effects of accelerated oxidation and the quality of protective coatings.

(4) Composite sandwich

(a) Flexural beam tests along three axes to determine stiffness factors of the sandwich and compressive buckling allowable of the porous facing sheet (ref. 9)

(b) Flexural fatigue tests of symmetrical beams along three axes to determine flexural endurance strength of the total sandwich. Symmetrical beams are .sandwich panels with equal facing sheets on the exterior surfaces and symmetrical construction about the neutral axis of the panel.

(5) Mechanical fasteners

Fastener tests are made along design axes to determine attachment strength of potted or welded inserts or other mechanical fasteners.

Testing at NASA Langley Research Center. - Flexural fatigue tests of fiber-metal sheet materials were performed at NASA Langley Research Center. The specimens in these tests were fabricated from commercially available AISI 347 stainless-steel fiber-metal sheets. The density of the parent material is 0.29 lb/in^3, the tensile modulus of elasticity is 28.0×10^6 lb/in^3, the tensile ultimate is 9.0×10^6 psi (bar annealed), and the endurance limit is 3.9×10^4 psi (annealed). AISI 347 is an austenitic-type (nonhardenable) stainless steel.

The fibers were tooled to random lengths from 0.0028-inch-diameter wire, bonded together in sheet configurations by heating in a reducing atmosphere (sintered), and formed to the correct volume (thickness) and density. The densities of the materials

tested were 40, 55, and 70 percent of the density ρ_p of an equal volume of the parent material.

Sixteen tensile coupons and 44 fatigue coupons were cut from four 12.5- by 16- by 0.060-inch commercially available fiber-metal sheets. Each sheet was cut into 11 fatigue coupons (seven from the longitudinal direction and four from the transverse direction) and four tensile coupons. Electrodischarge machining was used to cut the specimens (holes included) directly from the sheets. This machining technique resulted in excellent edge conditions, with fibers left relatively undisturbed adjacent to the cut. Fatigue coupons were selected in a random manner to prevent biasing of data due to sheet selection and longitudinal or transverse specimen orientation. Twenty-two fatigue coupons were allocated to these tests, but not all these coupons were tested. Sixteen tensile specimens were tested for each density of fiber metal. Two longitudinal and two transverse coupons were taken from each of four sheets.

Standard tensile tests were run on a conventional hydraulic load machine. An extensometer of 1-inch gage length was used to measure strain. Load-strain curves were recorded on an x-y plotter.

Load-strain curves were obtained from tensile tests, and ET, T_u, and T_y were determined. A sample stress-strain curve for supported fiber metal (based on measured specimen areas and load-strain curves) is shown in figure 15. The tensile modulus of elasticity E_T is defined as the slope of the straight-line portion of a stress-strain curve. The following values of E_T were obtained: 1.91×10^6 for 40-percent ρ_p, 3.01×10^6 for 55-percent ρ_p, and 8.83×10^6 for 70-percent ρ_p.

A 50-lbf electrodynamic shaker system, as shown in the photograph of figure 16, was used to test the 40- and 55-percent-density material specimens. The specimens were mounted as cantilever beams. The 70-percent-density material specimens were tested in the same manner, except that two 50-lbf electrodynamic shakers were operated in tandem and the test specimens were mounted on a yoke between the two shakers. An oscillator was used to set the driving frequency and amplitude.

At the beginning of each test, the driving frequency was increased from a relatively small amplitude in order to determine the first natural bending vibration mode of the specimen. The fatigue tests were then accomplished at the beam natural frequency at various root-stress levels.

The stress levels were determined by means of the output of a piezoresistive or piezoelectric accelerometer on the end of the beam. The specimens were tested over a range of accelerations. In all cases, acceleration measurements were better than ±3-percent accurate.

The specimens were tuned to resonance f_o by monitoring the tip accelerometer at very low loads. The peak deflection **A** and the peak acceleration a are then related by the following formula:

$$a = 0.102\ f^2\ A$$

The beam was assumed to be a constant-strength beam with stress S related to deflection by

$$\Delta = \frac{SL^2}{E_T t}$$

where **L** is the length of the beam, t is the thickness of the beam, and E_T is the tensile modulus of elasticity. For these studies, the thickness t was 0.060 inch, the length **L** was 4.3 inches, as indicated by figure 17, and E_T was determined by averaging data from several tensile tests.

Supplementary instrumentation included a strain gage (single) located at the root of the beam and a reference piezoelectric accelerometer located on the base clamp which held the test specimen.

Test data were monitored by root-mean-square voltage to direct-current converters (voltmeters). The output strain and output tip acceleration analog signals were monitored on a strip-chart recorder. The input frequency was measured from the oscillator on a frequency counter, and the number of cycles accumulated was measured from the tip accelerometer by a counter in the continuous counting mode.

At the start of the test, acceleration was increased quickly to the desired level and was held essentially constant (typical variation was ±0.5g, rms) for the duration of the test. As the test progressed, there was indication that the natural frequency of the model decreased, probably because of reorientation of fibers, fracture of fiber bonds, breaking of fibers, or some combination of these phenomena. These changes of the fibers resulted in a lowering of the resonant frequency, and thus the driving frequency was readjusted to the resonance value. Frequent adjustments of the input frequency and the tip acceleration as the beam stiffness decreased resulted in an essentially constant loading force and constant root strain by comparison with the acceleration and strain records. Although the deflection increased as a function of time, readjustments of input frequency and tip acceleration resulted in an essentially constant root strain.

The endurance limit, which is the limiting value of the stress below which the material can presumably endure an infinite number of stress cycles (where the **S-N** curve becomes horizontal), was determined from figure 18. As an example, an endurance limit of 1500 psi was determined from 16 tests of the 40-percent-ρ_p material, an endurance

limit of 2600 psi was determined from nine tests of the 55-percent-ρ_p material, and an endurance limit of 7600 psi was determined from 17 tests of the 70-percent-ρ_p material. Fatigue curves from figure 18 show that fatigue strength decreases rapidly as density decreases.

Testing at McDonnell Douglas, Long Beach and Santa Monica.- To date, the mechanical-properties testing at McDonnell Douglas has been concerned with determining the strengths of the acoustic materials involved in the design of the NASA Langley flight-test nacelles. (See ref. 2.) The interim results of this program are presented in tables I to VII and figures 14 and 19. These tests were performed according to the test methods indicated in the previous section.

The absence of an acceptable inspection method for bonded honeycomb structure and the necessity of a sonic fatigue environmental test of the inlet and fan exhaust ducts have combined to produce a comparative fatigue test which has proved to be an excellent method of detecting flaws in bonded structure and a flexural fatigue method of comparing the relative endurance of honeycomb-sandwich structure.

Testing was conducted by the Acoustics and Dynamics Environmental Laboratories of the Engineering Laboratory and Service (EL&S) Department of the Missiles and Space Systems Division of the Douglas Aircraft Company. The test facility used consisted primarily of a progressive wave tube (PWT), a bank of 10 Ling electropneumatic transducers coupled to 10 Ling exponential horns 72 inches *long,* a Cooper Bessemer motor-driven air compressor, and an instrumented control room. The PWT, constructed of 0.5-inch-thick sheet steel plates, was 6 inches wide and capable of accommodating test panels as large as 5 by 10 feet. This high-intensity sound system (HISS) was housed in a building constructed of 12-inch-thick concrete walls.

The fatigue resistance of the acoustically treated panel designs tested was evaluated by comparing the test conditions which caused the panels to fail, that is, the overall sound pressure level (OASPL) of the excitation that caused the initial failure, the approximate length of time the panel was exposed to the OASPL, and the extent of damage incurred. The spectrum of the sound pressure level (SPL) used to excite the test panels simulated, for the most part within i 2 dB from 50 to 800 Hz, the SPL existing at the walls of the inlet and fan exhaust ducts attached to a JT3D fan-jet engine operating at take-off power. The average spectrum was determined from measurements at five microphone locations. It was not possible to alter the level of the 80-Hz peak and the 125-Hz dip to produce a more uniform distribution without significantly changing the entire spectrum because of the inherent nature of the HISS. Typical variations in OASPL over the surface of each test panel were about i1 dB.

Each panel was subjected to an QASPL of 150 dB for a period of 2 hours and thereafter, to a series of 1-hour exposures to OASPL's varying from 153 dB to the maximum output capability of the HISS (165 to 166 dB), in 3-dB increments until failure occurred or until a total of 10 hours of sonic-fatigue-free time (including the initial 2 hour's of exposure to 150 dB) had been accumulated. Periodically, the tests were stopped and the panels were visually inspected for signs of fatigue. The inspection intervals varied somewhat with each test panel and with the nominal QASPL.

The test panel was mounted in the wall of the PWT and held in place with 0.25-inch-diameter bolts spaced 4 inches on center along the horizontal edges and with U-shaped clamps along the vertical edges. The U-shaped clamps along the vertical edges of the test panel were also bolted to the wall of the PWT (but not through the test panel) with 0.25-inch-diameter bolts spaced 4 inches on center. In order to ensure a smooth and continuous transition between the inner surface of the PWT and the surface of the installed test panel, the small gaps (0.1 to 0.2 inch in width) between the horizontal edges of the panel and the inner surface of the PWT were filled with putty; the larger gaps (0.5 to 1.25 inches in width) between the vertical edges of the panel and the inner surface of the PWT were stuffed with a solid foam plastic. All skin and rib panels were installed in the PWT so that the Z-frame with the most closely spaced rivets was closest to the sound source.

A portion of the wall of the PWT opposite the wall to which the test panels were mounted was replaced by a 48- by 96-inch sheet of 0.75-inch-thick plexiglass to permit visual inspection of the acoustically treated surface of the test panels. Typical damage due to high-intensity sound is shown in figure 20.

Environmental Testing

Rectangular-duct (exhaust-soot) test. - Since the rate, degree, and physical characteristics of liner clogging due to sooting (while aircraft operate in close proximity awaiting take-off) are unknown, an experiment is being performed with the apparatus shown in figures 21 and 22. Six disk-shaped specimens of treated construction may be fitted into the test flow duct. The specimens are located in various positions with respect to the flow passing through the duct. For instance, some are placed parallel to the duct center line, while others are positioned on surfaces inclined into or away from the flow. In addition, some are located in a constant-area duct section, while others are in areas of effusion or diffusion such that pressure gradients are imposed and subsurface recirculation is induced.

In general, the test procedure is to position the test duct, with specimens installed, about 100 feet behind ground run-up locations such that the duct is alined with a turbofan-engine exhaust. A log is maintained to record time exposure to engine exhaust flow at

high and low powers. Periodically, the specimens are removed for inspection. Flow-resistance measurements are made and the specimens are examined microscopically. Although the actual aircraft in-service environment is not simulated, these tests will provide qualitative information in the following areas:

Identification of contaminates

Relative clogging rates of forward-facing, tangent, and aft-facing surfaces

Relative clogging rates in effuser, constant-area, and diffuser sections

Relative clogging of various surface materials

Clogging rate, oil-film aggravation, and mechanisms of clogging

Effect of subsurface recirculation upon clogging

In-service structural and contamination evaluation of acoustic materials.- Various airline operators have expressed an interest in the development, handling, and maintenance of acoustic liner materials. As a result, a program has been initiated by Douglas and several cooperating airlines to install test specimens of acoustic-material construction within the fan exhaust ducts of operational Boeing 720B airplanes. The installations of these specimens are shown in figures 23 and 24.

An existing removable panel (fig. 25) has been modified to accept two specimens which are approximately 8 inches in diameter. The specimens are removable and are periodically returned to Douglas for examination. They are visually inspected for structural damage and subjected to flow-resistance tests to determine the degree of contamination or clogging. In addition, each specimen is carefully weighed and, should a specimen be damaged, a micrographic study is performed. After inspection, the specimens are returned to the airline and reinstalled in a fan duct for continued environmental exposure.

It is anticipated that this program will provide basic data for a better understanding of the performance of several types of liner construction in terms of contamination rate and structural integrity in an environment of actual operation. Two fiber-metal honeycomb specimens have been returned to Douglas for initial inspection after 198 flight hours of exposure in the Western United States, Mexico, and Canada. No significant damage or clogging was noted, although the exposed surfaces showed some discoloration. In the near future, interwoven polyimide-fiber-glass specimens and welded stainless-steel specimens will be introduced into the program.

Water-drainage tests.- In typical applications of acoustical liners, the probability exists that water or other liquids will collect within the resonant cavities, particularly where the porous liner surface is oriented upward as, for instance, in the lower section of the inlet duct. Analysis of a DC-8 nacelle modified to incorporate sound-absorbing

ducts indicated that approximately 100 pounds of water could be trapped. Because of concern about corrosion, loss of sound-absorption qualities, and added weight to the airplane, it is desired that provisions for overboard drainage be incorporated.

To resolve this problem, a subscale drainage fixture (fig. 26) was built and tested. The fixture featured a typical sandwich composed of a fiber-metal facing sheet, a 0.75-inch cell with a depth of 0.75 inch, and a solid aluminum backing sheet. Drainage passages to interconnect cells were formed by notching the honeycomb with slots 0.125 inch wide and 0.25 inch deep. Care was taken to form interconnections circumferentially rather than longitudinally so that water could drain downward. Longitudinal interconnections were avoided because significant wall pressure gradients exist in that direction within the duct and damming of the cavities is required to prevent subsurface air recirculation. A manifold, by which liquid could be collected from each row of slots and drained overboard, was provided at the bottom of the fixture.

In tests of the fixture under simulated rain conditions, it was determined by weight evaluations that drainage effectiveness was about 65 percent for this particular liner construction and drainage concept. Failure to achieve complete drainage resulted primarily from an inability to position the drainage passage at the lowest physical level in each honeycomb cell. If structural considerations permit, the drainage slots should be properly located.

Panel burnthrough test.- Figure 27 shows results of a burnthrough test of an 8- by 8-inch panel constructed of 0.75-inch fiber-glass honeycomb sandwiched between a fiber-metal porous surface and a 0.25-inch laminated-fiber-glass backing sheet. This panel construction is similar to the fan-duct liner construction to be used in the flight-test program of reference 2. When exposed to a 2000° F flame, the 0.25-inch fiber-glass backing sheet resisted burnthrough for 9 minutes. This was considered to be adequate for the limited flight-test program. For production applications, however, a 15-minute burnthrough resistance is required, as mentioned earlier, to provide ample time for fire recognition and corrective action in the event of an accessory-section fire.

CONCLUDING REMARKS

The structural design criteria for acoustical duct-lining materials depend on the interrelation of aerodynamic, acoustic, and environmental requirements.

The results of tests reported herein have shown that the acoustical-sandwich structural concepts are feasible but that further intensive engineering research is required before such concepts can be safely employed in commercial aircraft.

Two of the important items that need further research are the effect on the fatigue life and the corrosion of the duct-lining structure caused by permitting the honeycomb core and the backing structure to be exposed to the environment because of the porosity of the facing sheets. Additional engineering research must also deal with the problems of inspection, maintenance, and repair that are brought about by complex sandwich structure, as well as with the problem of weight that is in excess of the minimum required for acceptable fatigue life.

REFERENCES

1. Mangiarotty, R. A.; Marsh, Alan H.; and Feder, Ernest: Duct-Lining Materials and Concepts. Conference on Progress of NASA Research Relating to Noise Alleviation of Large Subsonic Jet Aircraft, NASA SP-189, 1968. (Paper No. 5 herein.)

2. Coxon, J. S.; and Henry, C. A.: Flight-Test Nacelles. Conference on Progress of NASA Research Relating to Noise Alleviation of Large Subsonic Jet Aircraft, NASA SP-189, 1968. (Paper No. 11 herein.)

3. Marsh, Alan H.; Zwieback, E. L.; and Thompson, J. D.: Ground-Runup Tests of Acoustically Treated Inlets and Fan Ducts. Conference on Progress of NASA Research Relating to Noise Alleviation of Large Subsonic Jet Aircraft, NASA SP-189, 1968. (Paper No. 10 herein.)

4. Faupel, Joseph H.: Engineering Design. John Wiley & Sons, Inc., c.1964.

5. Anon.: Tentative Method of Test for Tensile Properties of Plastics. ASTM Designation: D 638-67 T. Pt. 27 of 1968 Book of ASTM Standards With Related Material. Amer. Soc. Testing Mater., 1968, pp. 189-202.

6. Anon.: Tentative Methods of Test for Repeated Flexural Stress (Fatigue) of Plastics. ASTM Designation: D 671-63 T. Pt. 27 of 1968 Book of ASTM Standards With Related Material. Amer. Soc. Testing Mater., 1968, pp. 217-234.

7. Anon.: Plastics: Methods of Testing. Fed. Test Method Stand. No. 406 (Method 1042), Gen. Serv. Admin., Oct. 5, 1961. (Supersedes Fed. Specif. L-P-406b.)

8. Anon.: Standard Method of Test for Bearing Strength of Plastics. ASTM Designation: D 953-54. Pt. 27 of 1968 Book of ASTM Standards With Related Material. Amer. Soc. Testing Mater., 1968, pp. 391-397.

9. Anon.: Sandwich Constructions and Core Materials; General Test Methods. MIL-STD-401B, U.S. Dep. Def., Sept. 26, 1967. (Supersedes MIL-STD-401A.)

TABLE I.- FIBER-METAL SHEET TENSILE TEST RESULTS

[Material: AISI 347 stainless steel]

Specime	Mesh orientation deg	Dimensions, in		Area, in^2	Rayl	Fiber	tensity, lb/in^3	Load lb	Tensile stress, psi	Gage, in.	Elongation in.	Elongation percent
		T	W									
F1-1	0	0.047	1	1.047	31	C-28	0.151	778	16 500	2.19	0.250	11.4
F1-2	0	.047	1	.047	31	C-28	.151	822	17 500	2.19	.300	13.7
F1-3	0	.047	1	.047	31	C-28	.151	758	16 100	2.19	.300	13.7
F1-4	90	.047	1	.047	31	C-28	.151	807	17 200	2.16	.244	11.2
F1-5	90	.047	1	.047	31	C-28	.151	776	16 500	2.19	.268	12.2
F1-6	90	.047	1	.047	31	C-28	.151	770	16 400	2.19	.294	13.4
F1-7	45	.047	2	.094	31	C-28	.151	1489	15 900	2.13	.313	14.7
F1-8	45	.047	2	.094	31	C-28	.151	1600	17 000	2.06	.313	15.2
F1-9	45	.047	2	.094	31	C-28	.151	1532	16 300	2.13	.288	13.5
F2-1	0	0.049	1	1.049	78	C-28	0.176	1065	21 800	2.19	0.301	13.7
F2-2	0	.049	1	.049	78	C-28	.176	883	18 000	2.13	.206	9.7
F2-3	0	.049	1	.049	78	C-28	.176	941	19 200	2.03	.281	13.8
F2-4	90	.049	1	.049	78	C-28	.176	912	18 600	2.16	.238	11.0
F2-5	90	.049	1	.049	78	C-28	.176	990	20 200	2.16	.294	13.6
F2-6	90	.049	1	.049	78	C-28	.176	852	17 400	2.08	.253	12.2
F2-7	45	.049	2	.098	78	C-28	.176	1821	18 600	2.06	.288	14.0
F2-8	45	.049	2	.098	78	C-28	.176	1844	18 900	2.06	.278	13.5
F2-9	45	.049	2	.098	78	C-28	.176	1775	18 100	2.06	.294	14.2
F3-1	0	0.049	1	1.049	12	C-28	0.112	500	10 200	2.16	0.294	13.5
F3-2	0	.049	1	.049	12	C-28	.112	469	9 580	2.13	.281	13.2
F3-3	0	.049	1	.049	12	C-28	.112	485	9 900	2.19	.295	13.4
F3-4	90	.049	1	.049	12	C-28	.112	464	9 500	2.22	.271	12.2
F3-5	90	.049	1	.049	12	C-28	.112	483	9 870	2.19	.269	12.3
F3-6	90	.049	1	.049	12	C-28	.112	490	10 000	2.16	.274	12.7
F3-7	45	.049	2	.098	12	C-28	.112	793	8 000	2.19	.255	11.6
F3-8	45	.049	2	.098	12	C-28	.112	812	8 300	2.16	.269	12.4
F3-9	45	.049	2	.098	12	C-28	.112	600	6 120	2.16	.213	9.9
F4-2	0	0.041	1.020	1.0418	8	C-38	0.129	497	11 890	2.00	0.390	19.5
F4-3	0	.041	1.025	.042	8	C-38	.129	424	10 100	2.00	.325	16.3
F4-4	0	.041	1.019	.0417	8	C-38	.129	436	10 420	2.00	.295	14.8
F4-5	0	.041	.996	.0408	8	C-38	.129	462	11 310	2.00	.355	17.8
F4-6	0	.040	1.013	.0405	8	C-38	.129	486	12 000	2.00	.340	17.0
F4-7	0	.041	1.029	.0422	8	C-38	.129	464	11 000	2.00	.300	15.0
F4-8	0	.040	1.003	.040	8	C-38	.129	440	11 000	2.00	.350	17.5
F4-9	0	.041	1.001	.041	8	C-38	.129	454	11 050	2.00	.310	15.5
F5-1	0	0.049	0.985	1.0483	10	C-38	0.135	536	11 100	2.00	0.305	15.3
F5-2	0	.048	1.017	.0488	10	C-38	.135	552	11 300	2.00	.360	18.0
F5-3	0	.053	.984	.0521	10	C-38	.135	456	8 750	2.00	.305	15.3
F5-4	0	.051	.977	.0498	10	C-38	.135	552	11 080	2.00	.280	14.0
F5-5	0	.051	1.047	.0534	10	C-38	.135	612	11 480	2.00	.270	13.5
F5-6	0	.049	1.016	.0498	10	C-38	.135	546	10 960	2.00	.295	15.5

Specimen	Core density, lb/ft^3	Cell size, in.	Ultimate compressive load, lb	Compressive stress, psi
(-314	1.9	3/4	3340	93
(-3)5	1.9	3/4	3300	92
(-3)6	1.9	3/4	3210	89
(-5)4	1.6	1 1/8	2640	73
(-5)5	1.6	1 1/8	2200	61
(-5)6	1.6	1 1/8	2050	57
(-7)4	1.9	3/4	6640	184
(-7)5	1.9	3/4	6180	172
(-7)6	1.9.	3/4	6420	179
(-914	1.6	1 1/8	4660	130
(-9)5	1.6	1 1/8	4470	124
(-9)6	1.6	1 1/8	4900	136

TABLE III.- CORE AND ADHESIVE FLATWISE-TENSILE TEST RESULTS

[Heat-resistant, phenolic, fiber-glass-reinforced, sine-wave configuration]

Specimen	Core density, lb/ft^3	Cell size, in.	Adhesive	Adhesive weight, lb/ft^2 (**)	Film thickness, in. (**)	Area, in^2	Ultimate load, lb	Tensile stress, psi
(-3)1	1.9	3/4	X-10-95-3	----	----	36.0	12400	344
(-3)2	1.9	3/4	X-10-95-3	----	----	36.0	-----	---
(-313	1.9	3/4	X-10-95-3	----	----	36.0	8300	231
(-5)1	1.9	3/4	Narmco 328	0.075	0.008	36.0	11625	323
(-5)2	1.9	3/4	Narmco 328	.075	.008	36.0	14000	389
(-5)3	1.9	3/4	Narmco 328	.075	.008	36.0	14150	393
A3-1	4.5	3/8	Narmco 328	0.055	0.007	4.0	1085	271
A3-2	4.5	3/8	Narmco 328	.055	.007	4.0	1500	375
A3-3	4.5	3/8	Narmco 328	.055	.007	4.0	1470	368
A3-4	4.5	3/8	Narmco 328	.055	.007	4.0	1220	305
A3-5	4.5	3/8	Narmco 328	.055	.007	4.0	1280	320
A4-1	4.5	3/8	Narmco 328	0.110	0.014	4.0	1560	390
A4-2	4.5	3/8	Narmco 328	.110	.014	4.0	1445	361
A4-3	4.5	3/8	Narmco 328	.110	.014	4.0	1420	355
A4-4	4.5	3/8	Narmco 328	.110	.014	4.0	1490	373
A4-5	4.5	3/8	Narmco 328	.110	.014	4.0	1420	355
CT1-1*†	2.0	3/4	Narmco 328	0.110 / 0.055	0.014 / 0.007	36.0	11110	309
CT1-2*†	2.0	3/4	Narmco 328	0.110 / 0.055	0.014 / 0.007	36.0	10750	299
CT1-3*†	2.0	3/4	Narmco 328	0.110 / 0.055	0.014 / 0.007	36.0	11580	322
CT1-4*†	2.0	3/4	Narmco 328	0.110 / 0.055	0.014 / 0.007	36.0	11580	322
CT1-5*†	2.0	3/4	Narmco 328	0.110 / 0.055	0.014 / 0.007	36.0	12100	336
CT1-6*†	2.0	3/4	Narmco 328	0.110 / 0.055	0.014 / 0.007	36.0	11640	323
CT2-1*	2.0	3/4	Narmco 328	0.110 / 0.055	0.014 / 0.007	36.0	11460	318
CT2-2*	2.0	3/4	Narmco 328	0.110 / 0.055	0.014 / 0.007	36.0	13325	370
CT2-3*	2.0	3/4	Narmco 328	0.110 / 0.055	0.014 / 0.007	36.0	10000	278
CT2-4*	2.0	3/4	Narmco 328	0.110 / 0.055	0.014 / 0.007	36.0	11560	321
CT2-5*	2.0	3/4	Narmco 328	0.110 / 0.055	0.014 / 0.007	36.0	11150	310
CT2-6*	2.0	3/4	Narmco 328	0.110 / 0.055	0.014 / 0.007	36.0	14125	393

*Specimens which had adhesive failures.

†Specimens which have drain-hole grooves.

**Two values indicate different bond weights or thicknesses at upper and lower surfaces.

TABLE IV.- CORE- AND ADHESIVE-SHEAR TEST RESULTS

Feat-resistant, phenolic, fiber-glass-reinforced, sine-wave configuration

Specimen	Dimensions, in.			Direction of applied load	Applied load, lb	Shear area, in^2	Core density, lb/ft^3	Shear stress, psi	Shear modulus, psi	Cell size, in.
	L	W	T							
C3-1†	6	2	1/2	L	1450	12	1.9	120.9	2780	3/4
C3-2†	6	2	1/2	L	1464	12	1.9	122.Q	2380	3/4
c3-37	6	2	1/2	L	1713	12	1.9	142.9	2780	3/4
C4-1†	2	6	1/2	W	1097	18	1.9	60.9	1279	3/4
C4-2†	2	6	1/2	W	1114	18	1.9	62.0	1139	3/4
C4-3*†	2	6	1/2	W	813	18	1.9	----	----	3/4
C4-47	2	6	1/2	W	1288	18	1.9	71.5	1220	3/4
C4-57	2	6	1/2	W	1280	18	1.9	71.2	1280	3/4
C4-6†	2	6	1/2	W	1236	18	1.9	68.7	1170	3/4
C4-77	2	6	1/2	W	1180	18	1.9	65.6	1110	3/4
C4-8†	2	6	1/2	W	1186	18	1.9	65.9	1289	3/4
C4-97	2	6	1/2	W	1248	18	1.9	69.4	1229	3/4
C4-10†	2	6	1/2	W	1176	18	1.9	65.4	1160	3/4
C4-11†	2	6	1/2	W	1241	18	1.9	69.0	980	3/4
C4-12†	2	6	1/2	W	1280	18	1.9	71.1	1210	3/4
C4-13†	2	6	1/2	W	1088	18	1.9	60.4	1036	3/4
C4-14†	2	6	1/2	W	1304	18	1.9	72.5	1250	3/4
C4-15†	2	6	1/2	W	1168	18	1.9	64.8	1062	3/4
C2-6	2	6	1/2	W	1188	18	1.9	65.8	1310	3/4
C2-7	2	6	1/2	W	1092	18	1.9	60.7	1332	3/4
C2-8	2	6	1/2	W	1284	18	1.9	71.4	1139	3/4
C2-9	2	6	1/2	W	1289	18	1.9	71.6	1059	3/4
c2-10	2	6	1/2	W	1366	18	1.9	75.9	1069	3/4
c2-11	2	6	1/2	W	1347	18	1.9	74.8	1307	3/4
c2-12	2	6	1/2	W	1283	18	1.9	71.4	1110	3/4
C2-13	2	6	1/2	W	1304	18	1.9	72.5	1435	3/4
C2-14	2	6	1/2	W	1428	18	1.9	79.4	1852	3/4
C2-15	2	6	1/2	W	1266	18	1.9	70.3	1685	3/4
CS5-1†	8	3	1/2	L	3650	24	2.0	152.0	1768	3/4
CS5-2†	8	3	1/2	L	3130	24	2.0	130.2	1714	3/4
CS5-37	8	3	1/2	L	3400	24	2.0	141.8	1609	3/4
CS5-47	8	3	1/2	L	3240	24	2.0	135.0	1609	3/4
CS5-57	8	3	1/2	L	3450	24	2.0	143.8	1595	3/4
CS5-6†	8	3	1/2	L	3120	24	2.0	130.0	1547	3/4
CS5-77	8	3	1/2	L	3460	24	2.0	144.2	1500	3/4
CS5-8†	8	3	1/2	L	3270	24	2.0	136.2	1620	3/4
CS5-97	8	3	1/2	L	3370	24	2.0	140.3	1595	3/4
CS5-10†	8	3	1/2	L	2870	24	2.0	119.5	1660	3/4

†Specimens which have drain-hole grooves.

*All failures were core shear except that for C4-3, which was an adhesive failure.

TABLE V. - SYMMETRICAL HONEYCOMB SANDWICH FLEXURAL TEST RESULTS

[Static quarter-point loading; honeycomb core – HRP 3/4 GF14-1.9; adhesive – Narmco 328]

Specimen	Top face skin	Bottom face skin	Ultimate load, lb	Elongation, in.	Type of failure	EI of sandwich, lb-in^2
SS1-1	FM-119	FM-119	187	0.295	Face wrinkle	29 100
		FM-119	199	.230	Core shear	39 600
		FM-119	203	.238	Adhesive shear	39 100
SS1-4	FM-119	FM-119	227	.36	Face wrinkle	28 900
SS2-1	FM-121	FM-121	222	0.45	Core crushed	22 600
SS2-2	FM-121	FM-121	159	.329	Core shear	22 150
SS2-3	FM-121	FM-121	150	.173	Core shear	39 800
SS2-4	FM-121	FM-121	199	.42	Core crushed	21 700

TABLE VI.- SYMMETRICAL SANDWICH FLEXURAL-FATIGUE TEST RESULTS

All specimens used fiber-glass HRP 3/4 GF14-1.9 honeycomb core (ungrooved). One layer of Narmco 328 adhesive was used to bond both faces of the honeycomb core to the porous facings of all specimens. Gage of all facing sheets is 0.040 inch.

Specimen	Top face skin	Bottom face skin	Maximum facing stress, psi	Minimum facing stress, psi	Stress ratio, R	Alternating stress range, psi	Mean stress, psi	Ultimate stress, psi	Cycles to failure	Type of failure
SS1-12	FM-119	FM-119	7940	1980	0.25	5960	4960	11 000	47 000	Tension
SS1- 5	FM-119	FM-119	7940	1980	.25	5960	4960	11 000	35 000	Tension
SS1-13	FM-119	FM-119	----	----	----	----	----	-----	----	Delaminated
SS1- 9	FM-119	FM-119	5950	1980	.333	3970	3965	11 000	93 000	Tension
SS1-10	FM-119	FM-119	5950	1980	.333	3970	3965	11 000	179 000	Tension
SS1-11	FM-119	FM-119	5950	1980	.333	3970	3965	11 000	98 000	Tension
SS1- 6	FM-119	FM-119	3970	1980	.50	1990	2975	11 000	2 620 000	Tension
SS1- 7	FM-119	FM-119	3970	1980	.50	1990	2975	11 000	10 320 000	No failure
SS1- 8	FM-119	FM-119	3970	1980	.50	1990	2975	11 000	3 166 000	Tension
SS2-12	FM-121	FM-121	7940	1980	0.25	5960	4960	10 500	15 000	Tension
SS2-13	FM-121	FM-121	7940	1980	.25	5960	4960	10 500	13 000	Tension
SS2-14	FM-121	FM-121	7940	1980	.25	5960	4960	10 500	29 000	Tension
SS2- 9	FM-121	FM-121	5950	1980	.333	3970	3965	10 500	41 000	Tension
SS2-10	FM-121	FM-121	5950	1980	.333	3970	3965	10 500	71 000	Tension
SS2-11	FM-121	FM-121	5950	1980	.333	3970	3965	10 500	53 000	Tension
SS2- 6	FM-121	FM-121	3970	1980	.50	1990	2975	10 500	1 317 000	Tension
SS2- 7	FM-121	FM-121	3970	1980	.50	1990	2975	10 500	460 000	Compression
SS2- 8	FM-121	FM-121	3970	1980	.50	1990	2975	10 500	892 000	Tension

TABLE VII.- MECHANICAL JOINT EVALUATION, SANDWICH-BEAM FLEXURAL TEST RESULTS

(a) Fan-duct wall simulation

Single-sandwich construction:
Top face skin - FM-121
Bottom face skin - 1/4-inch fiber glass
Honeycomb core - HRP 3/4 GF14-1.9
Adhesive - Narmco 328

Specimen	Initial failure load, lb	Deflection, in.	Type of failure
J1-1W	550	0.0678	Flatwise tensile of adhesive, core to fiber glass
J1-2W	860	.1148	
J1-3W	880	.095	
J1-4W	600	.110	
J1-5W	920	.155	

(b) Splitter simulation

Double-sandwich construction:
Top and bottom face skin - FM-121
Center face skin - 0.020 corrosion-resistant sheet, type 321 stainless steel
Honeycomb core - HRP 3/4 GF14-1.9
Adhesive - Narmco 328

Specimen	Yield load, lb	Deflection due to yield load, in.	Ultimate load, lb	Deflection due to ultimate load, in.	Type of failure
J1-1S	1840	0.100	3100	0.330	Rivet shear
J1-2S	1350	.675	2750	.235	Rivet shear
51-35	1750	.835	3000	.292	Rivet shear
J1-4S	1915	.910	2900	.295	Rivet shear
J1-5S	1810	.760	2775	.210	Rivet shear

48" TREATED FAN EXHAUST DUCT AND TWO-CONCENTRIC-RING TREATED INLET

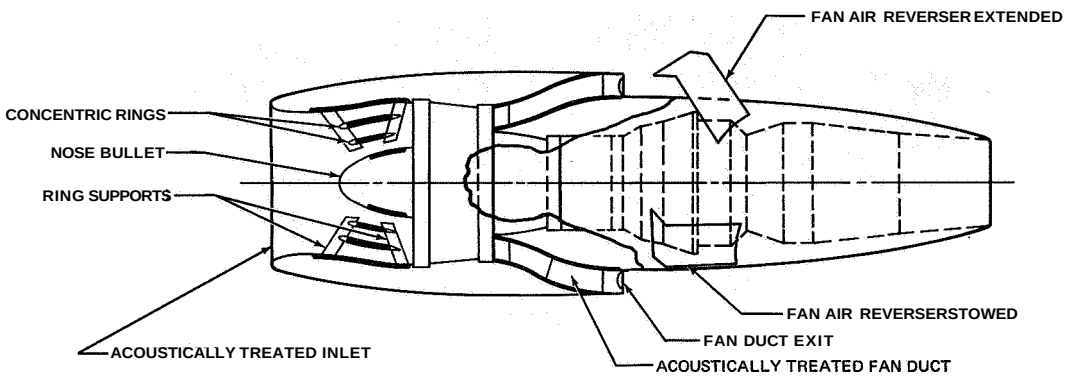

Figure 1

ACOUSTICAL DUCT-LINING COMPONENTS

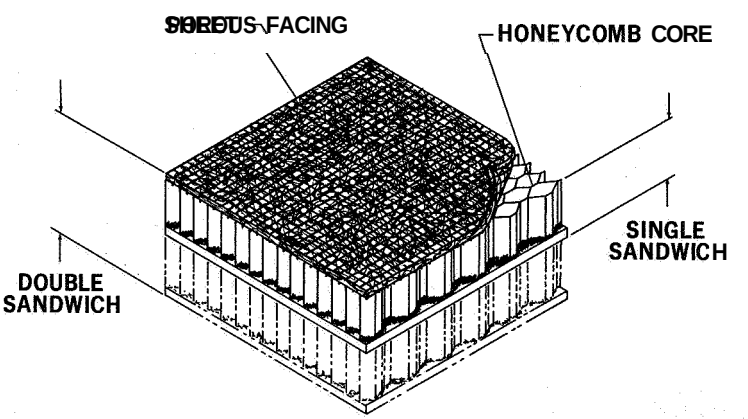

Figure 2

ACOUSTICAL-SANDWICH COMPONENTS

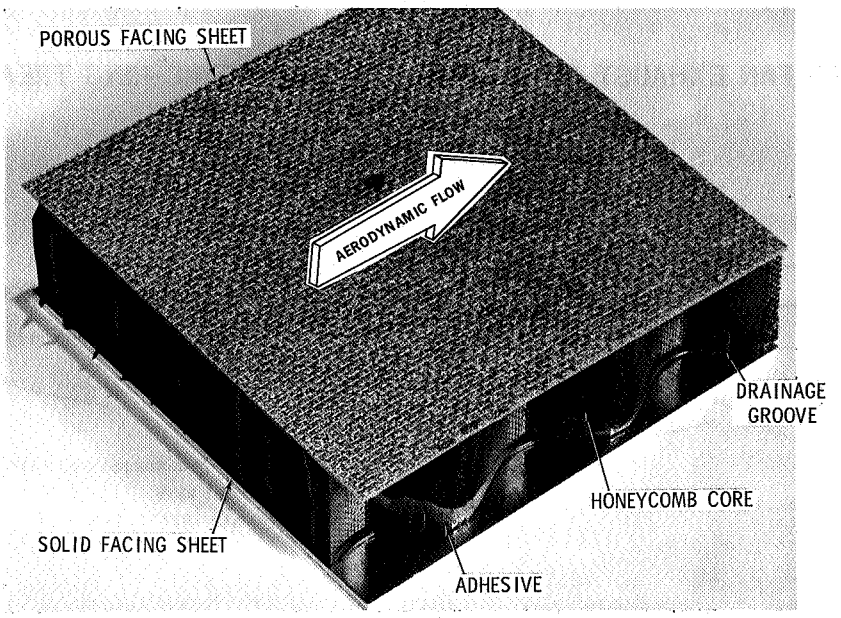

Figure 3 L-68-8546

EXAMPLE OF PERFORATED SHEET

Figure 4 L-68-8547

TYPICAL POROUS SHEET CONFIGURATIONS

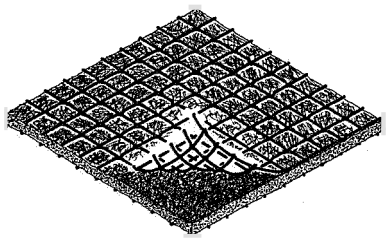

SINTERED FIBER METAL

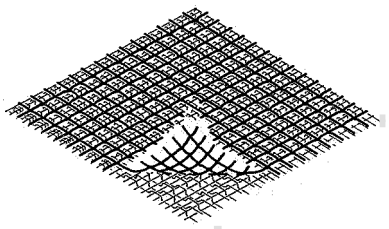

SINTERED WOVEN WIRE

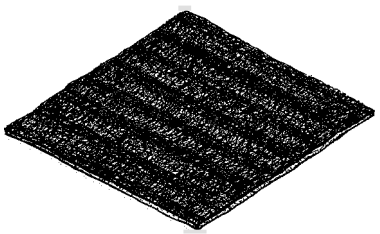

SINTERED CONTINUOUS FILAMENT

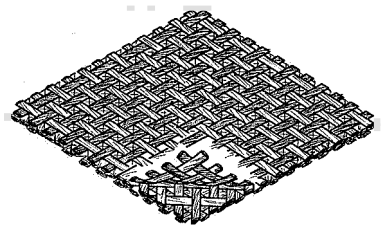

WOVEN FIBER GLASS

Figure 5

FIBER-METAL MICROGRAPH CROSS SECTION - 10 RAYL

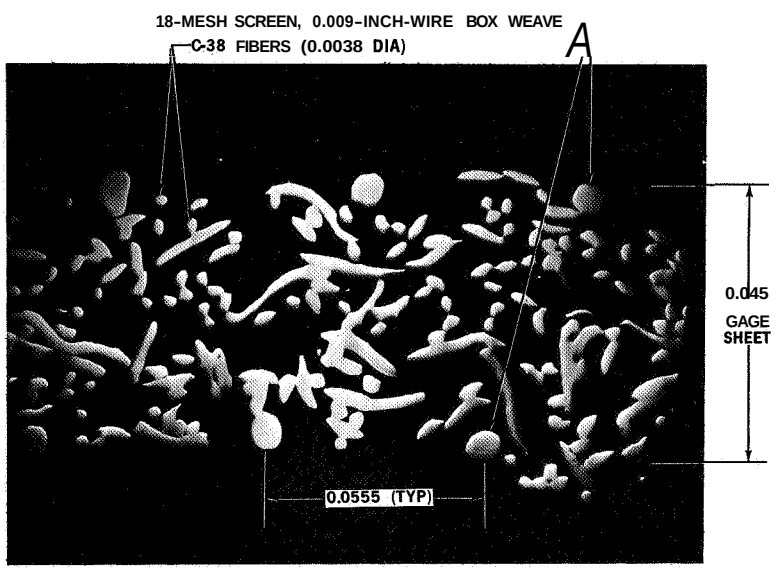

Figure 6

L-68-8548

TYPICAL POROUS-SHEET–CORE INTERFACE

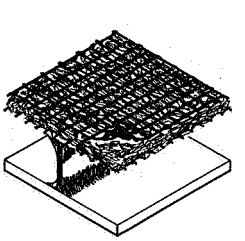

FIBER METAL BONDED TO FIBER-GLASS CORE

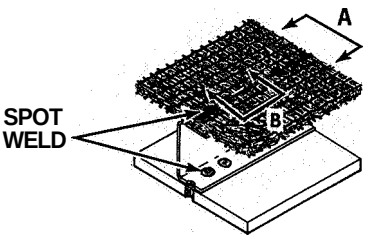

FIBER METAL OR SCREEN WELDED TO METAL CORE

INTERWOVEN STRUCTURE (RESIN SYSTEM OMITTED)

Figure 7

MICROGRAPHIC STUDY OF BONDED INTERFACE

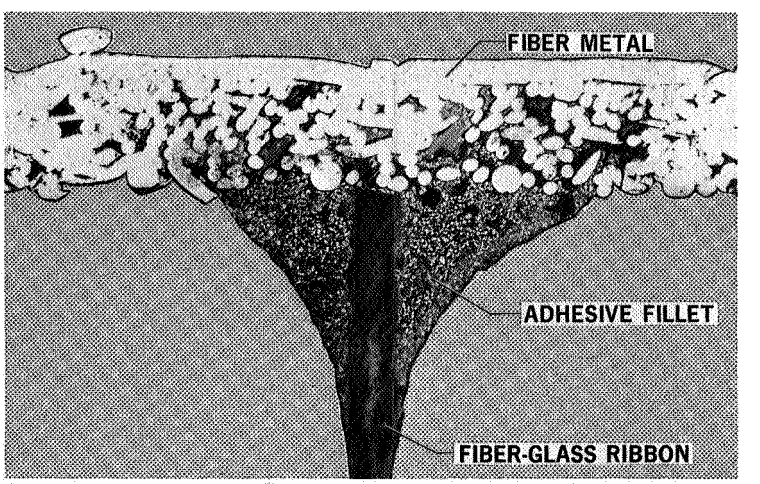

Figure 8

L-68-8541

EXPLODED VIEW OF TYPICAL ACOUSTIC-SANDWICH MATERIALS

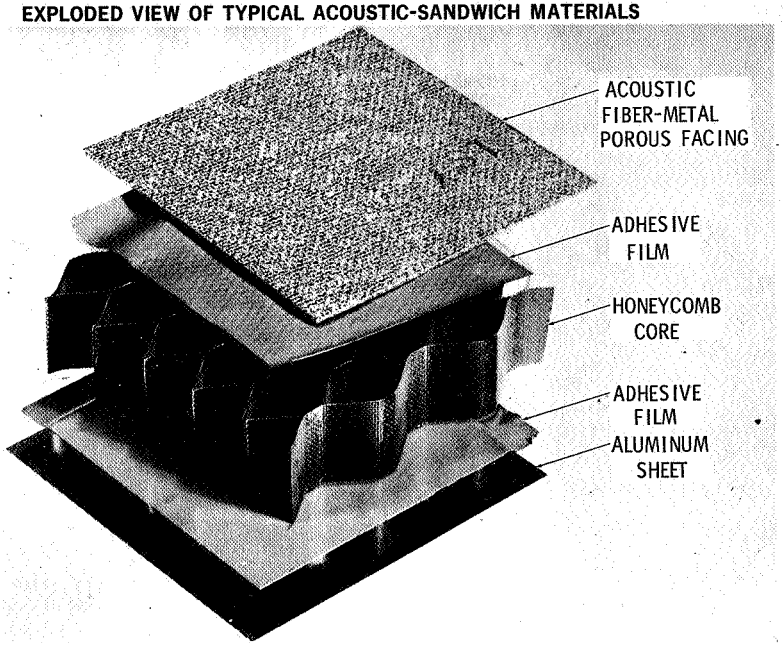

Figure 9

L-68-8549

ACOUSTIC-SANDWICH BONDING PROCESS

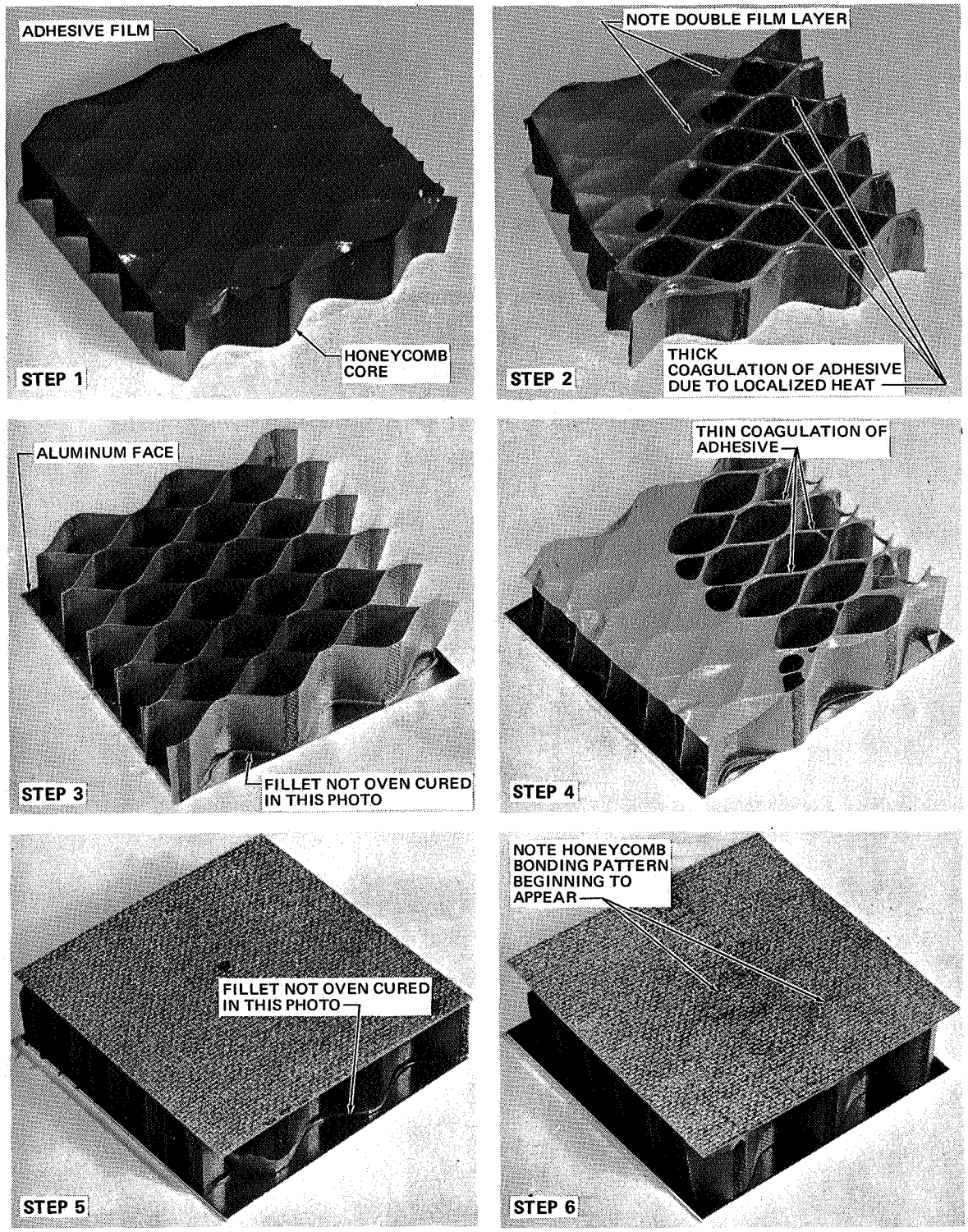

Figure 10 L-68-8550

MICROGRAPHIC STUDY OF WELDED INTERFACE
SECTION A

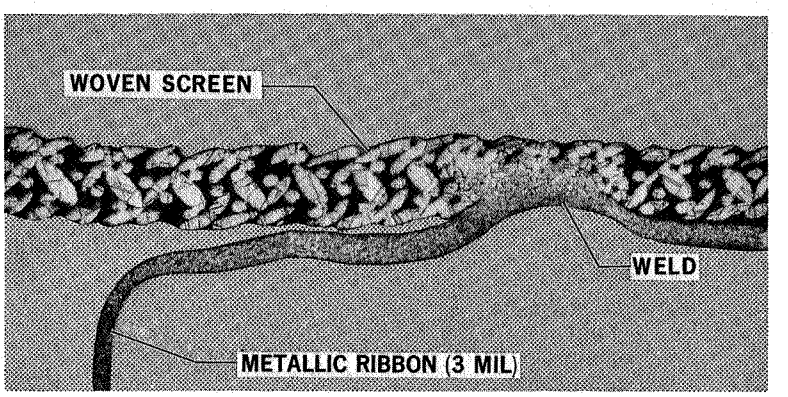

Figure 11 L-68-8542

MICROGRAPHIC STUDY OF WELDED INTERFACE
SECTION B

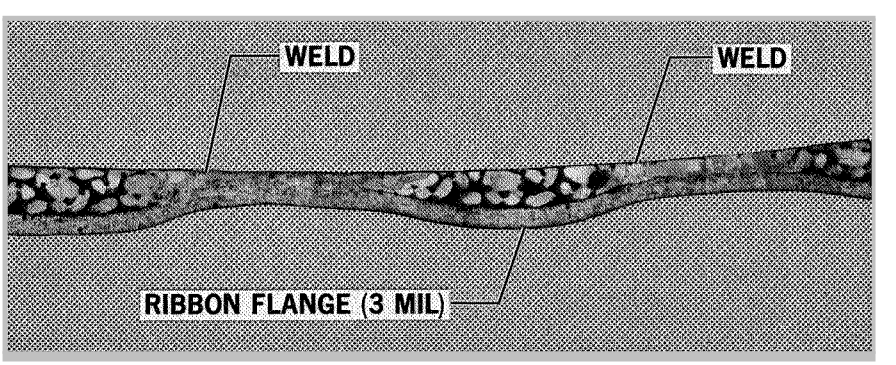

Figure 12 L-68-8551

TYPICAL TIME - OPERATION HISTORY

AIRCRAFT CONTAMINATION EXPOSURE OF ACOUSTIC LINER

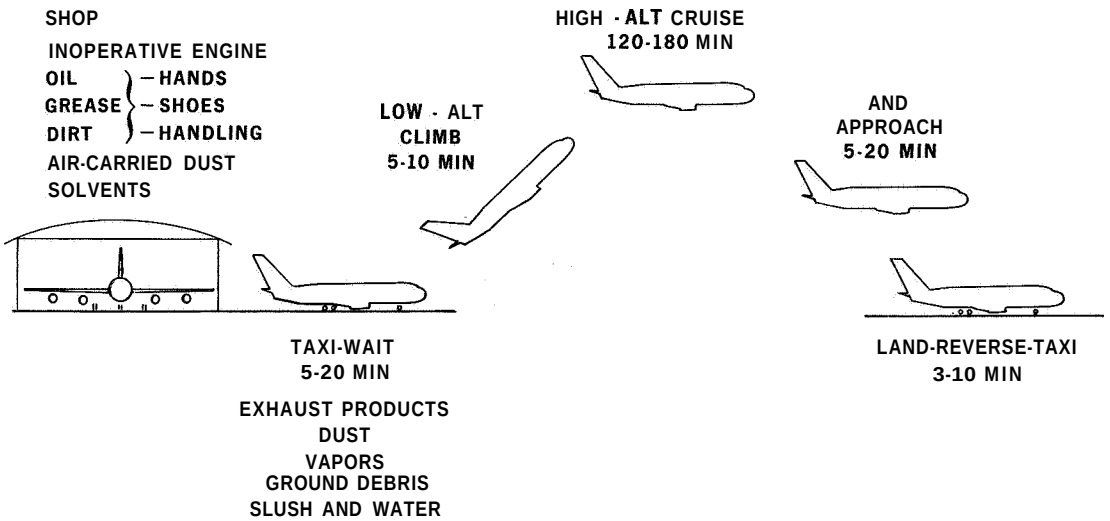

Figure 13

POLAR ORIENTATION PLOT OF FIBER-METAL TENSILE STRENGTH

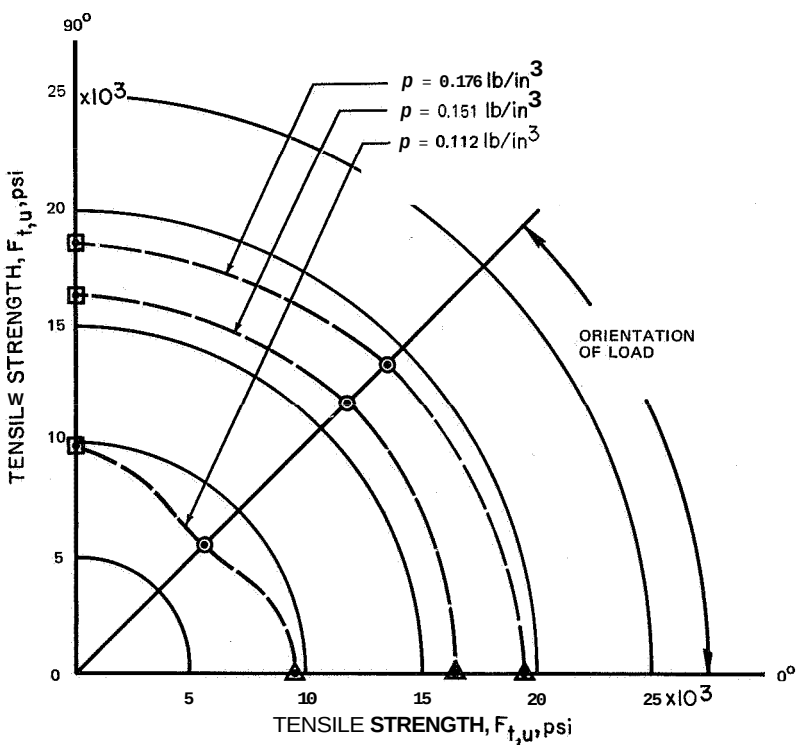

Figure 14

TYPICAL STRESS-STRAIN CURVE
POROUS FACING SHEET MATERIAL:

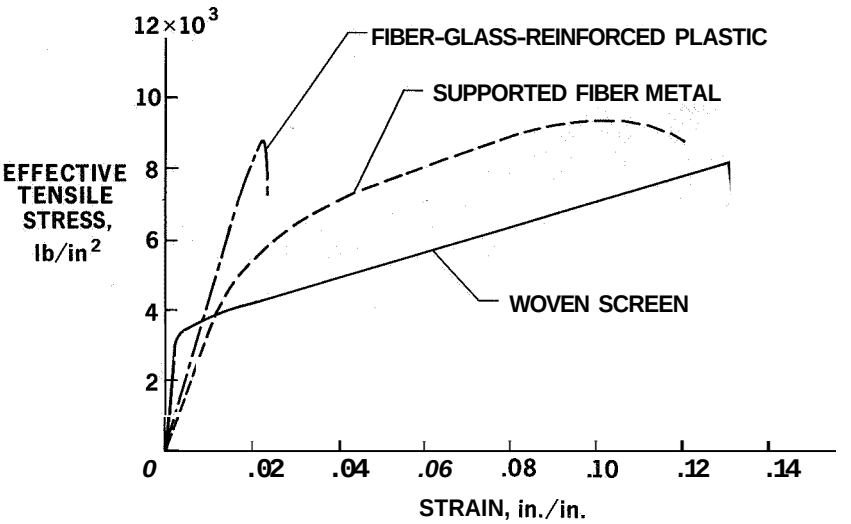

Figure 15

FLEXURAL-FATIGUE ELECTRODYNAMIC SHAKER

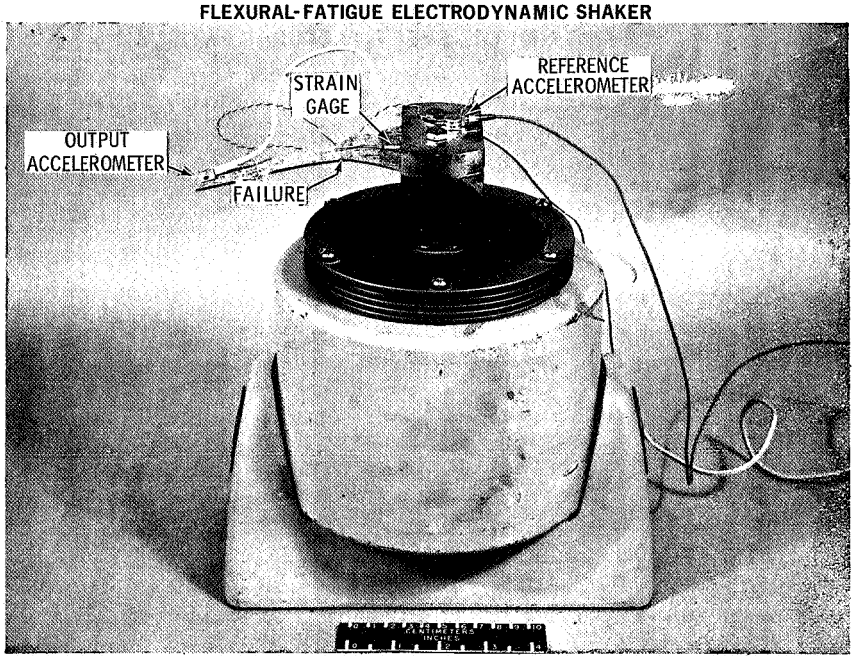

Figure 16 L-68-8552

FLEXURAL-FATIGUE TEST SPECIMEN

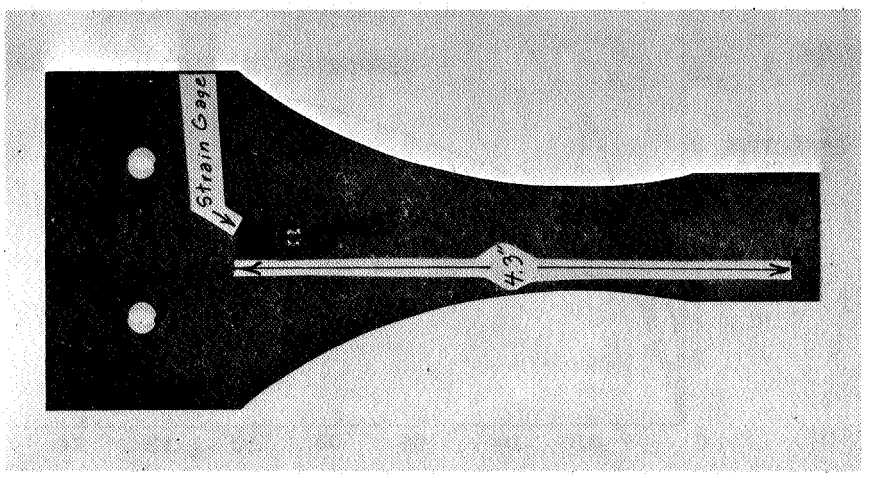

Figure 17 L-68-8553

S-N CURVE
FIBER-METAL SHEET; FLEXURAL FATIGUE

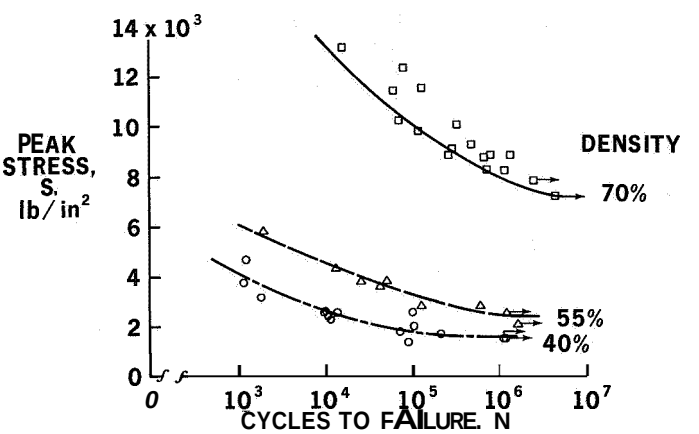

Figure 18

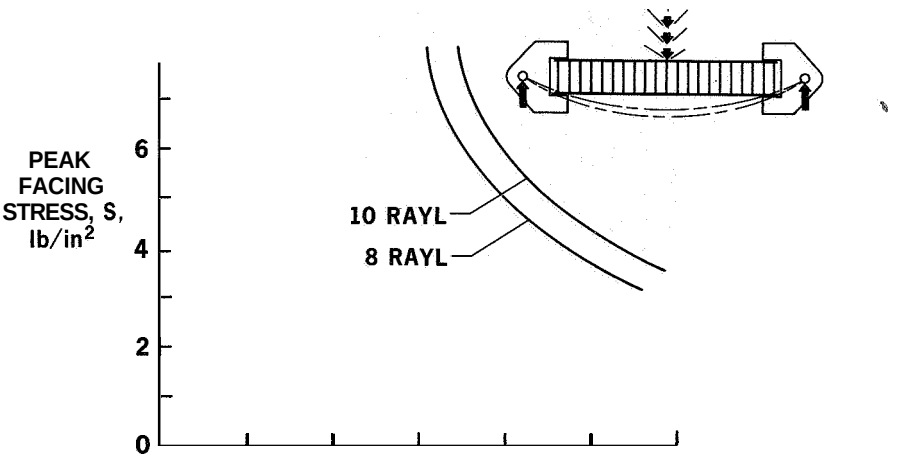

Figure 19

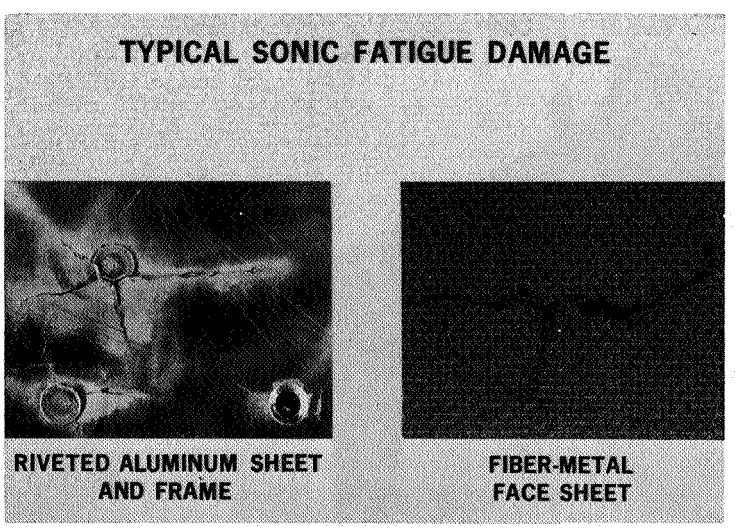

Figure 20 L-68-8543

INTERIOR OF CONTAMINATION TEST FIXTURE

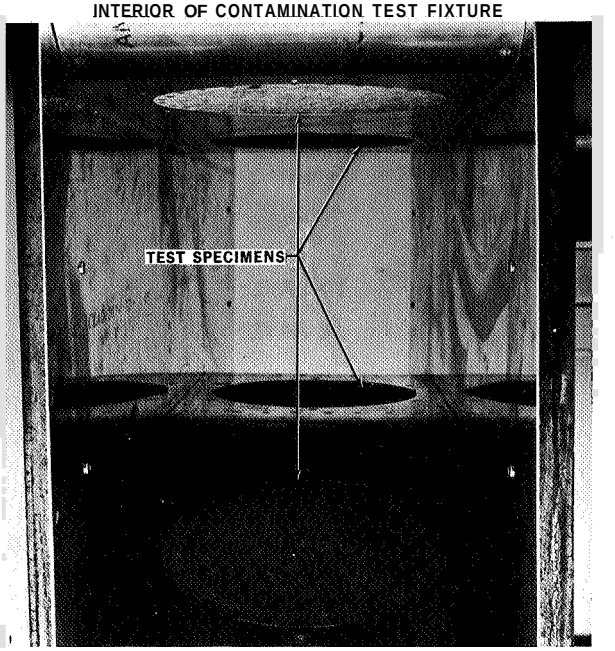

Figure 21 L-68-8554

CONTAMINATION TEST FIXTURE

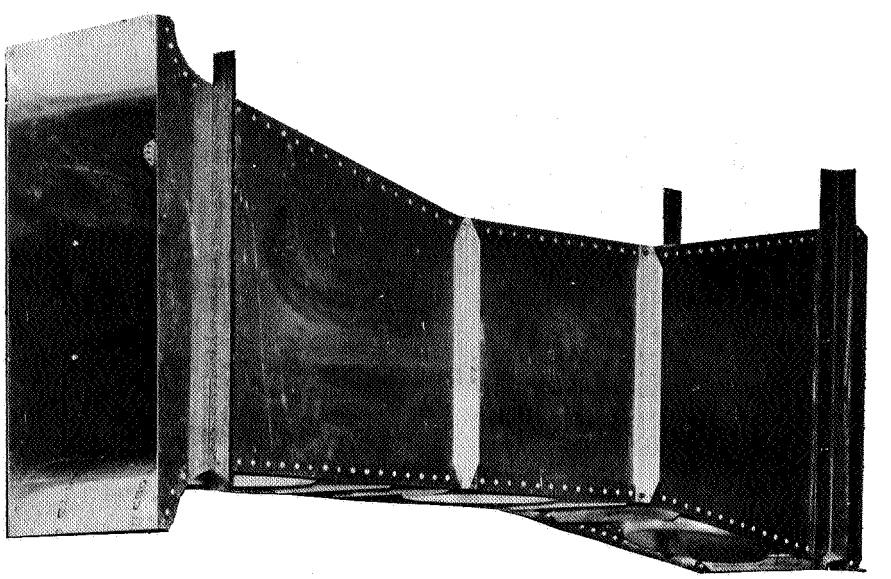

Figure 22 L-68-8600

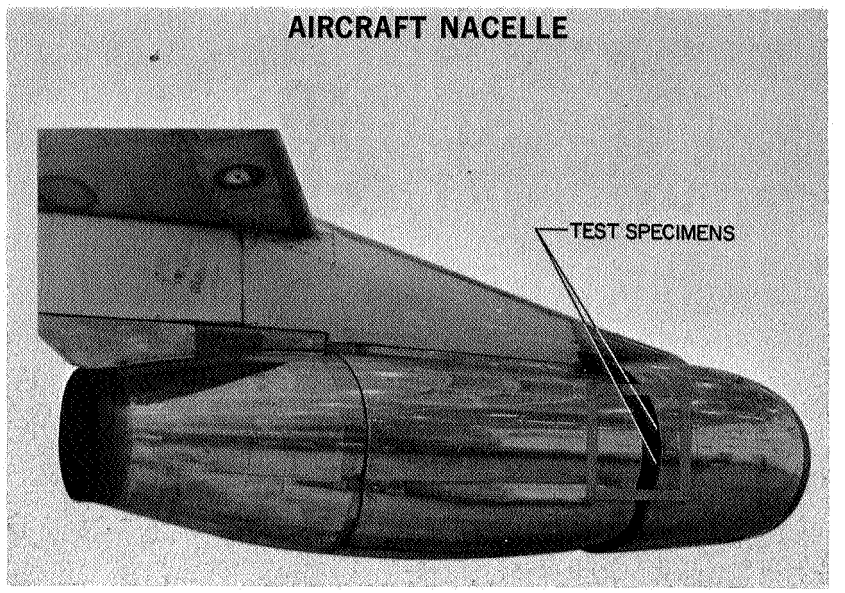

Figure 23 L-68-8544

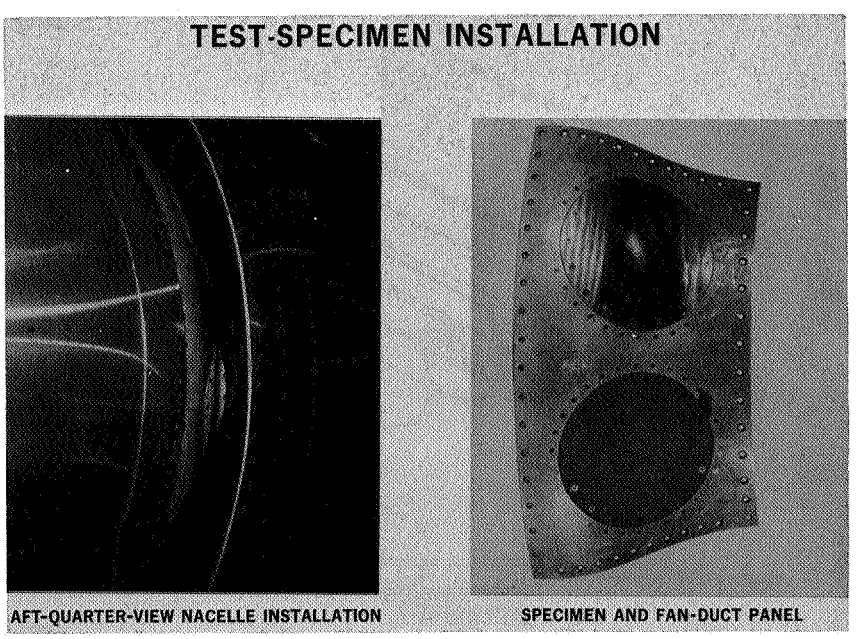

Figure 24 L-68-8545

CLOSEUP OF TEST SPECIMEN

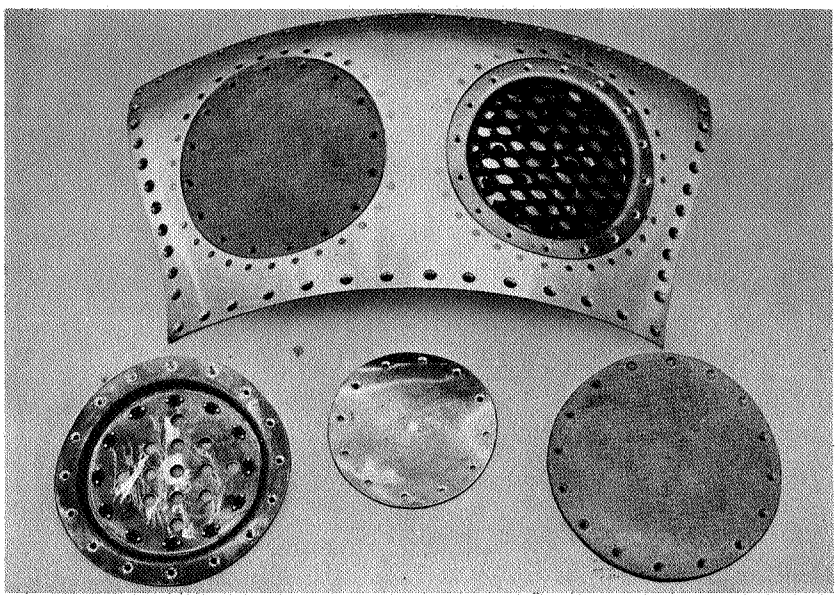

Figure 25 L-68-8555

DRAINAGE TEST FIXTURE

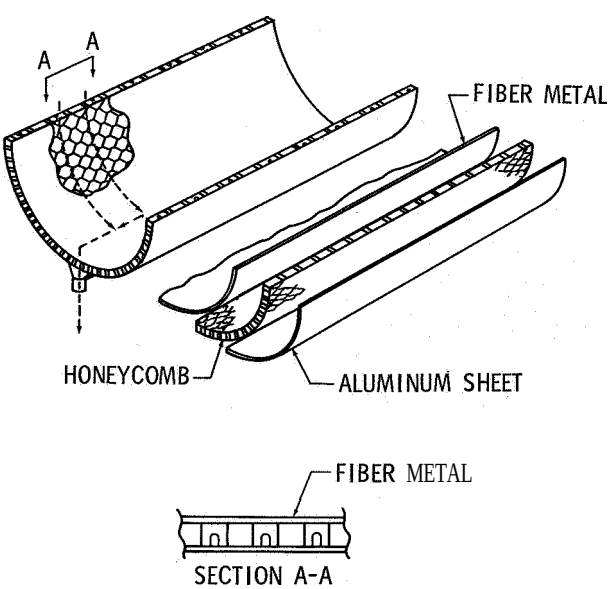

Figure 26

ACOUSTIC-PANEL BURNTHROUGH TEST; 2000° F FLAME

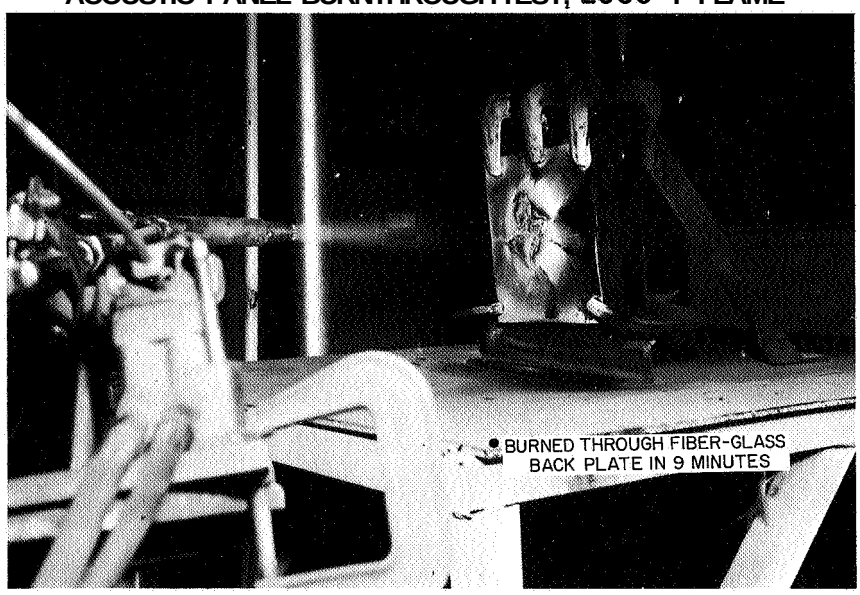

Figure 27 L-68-8556

8. INTRODUCTORY REMARKS ON NACELLE ACOUSTIC TREATMENT APPLICATION

By Harry T. Norton, Jr.

NASA Langley Research Center

These introductory remarks are related to the objective and history of the National Aeronautics and Space Administration Treated-Nacelle Program and the procedure that was used in predicting flyover noise from ground run-up data.

The objective of the program is to identify turbofan-nacelle modifications capable of reducing landing noise with the following constraints: no adverse effect on take-off or climbout noise, no compromise with flight safety, no additional flight-crew workload, and retention of an economically viable airplane.

Figure 1 indicates the sources of the noise radiated from a turbofan engine. Fan noise is emitted from the inlet and the fan discharge ducts, and jet noise is emitted from the fan discharge ducts and the primary nozzle. The effort of this program is limited to reducing the fan noise radiated from the discharge ducts and inlet.

Figure 2 shows the relative strength of the noise from each of the sources as a function of thrust and indicates one reason the program was directed toward reducing the fan noise. The perceived noise level (PNL) under the flight path of a four-engine transport is presented as a function of the thrust of one engine. It can be seen that at the higher thrusts, associated with take-off operations, the fan noise from the fan discharge duct is the controlling factor and would have to be reduced if any reduction in take-off noise is to be obtained. At the thrusts associated with landing approach, the fan noise is considerably above the jet noise. Reduction of the fan noise from the discharge ducts by about 15 PNdB and reduction of the noise from the inlet by about 12 PNdB will be required to reduce the total noise to the jet-noise floor. Because most complaints occur in this landing phase of operation, the greatest benefits can be obtained by attenuating the fan noise in the approach region.

The type of noise spectrum under consideration is illustrated in figure 3, which is a plot of sound pressure level (SPL) in dB as a function of frequency in hertz (cycles per second). This is a typical spectrum of a turbofan engine during landing approach. The spectrum is divided into two regions: (1) the lower frequencies associated with the jet noise and (2) the higher frequencies attributed to the fan noise. The characteristic high-pitched whine associated with the turbofan engine at landing power settings is indicated by the spikes. The fundamental occurs at the fan-blade passage frequency of about 2500 Hz, and the other spikes are harmonics of the blade passage frequency. Suppression of these

high-frequency spikes could reduce the overall noise level as well as alleviate the undesirable fan whine. On the basis of this possibility of noise reduction during landing, the NASA Treated-Nacelle Program was initiated.

In May 1967, contracts to accomplish the objective of the NASA Treated-Nacelle Program were made with McDonnell Douglas Corporation and The Boeing Company. In signing the contracts to accomplish the objective of the program, both companies agreed to make available to the NASA the results of all previous work pertaining to aircraft noise alleviation. Reports of these results have since been transmitted to the NASA.

The approach and goals of the two companies are different. The McDonnell Douglas Corporation approach is to investigate acoustically treated short discharge ducts and acoustically treated inlets, with the goal of a 7- to 10-PNdB reduction. The initial approach of The Boeing Company was to investigate acoustically treated long discharge ducts and sonic or near-sonic inlets, with a 15-PNdB-reduction goal. The reason for the different goals is that at the outset of the program, it was believed that a 7- to 10-PNdB reduction was the maximum that could be obtained by treating the inlet; however, the NASA wanted to evaluate the effects of obtaining a reduction of 15 PNdB. Therefore, McDonnell Douglas was directed to investigate treated inlets, and Boeing was directed to investigate sonic or near-sonic inlets.

Both companies followed certain procedures. They conducted initial studies of materials, duct-lining concepts, and inlet and duct design concepts. The contractor work on materials and duct-lining concepts has been discussed in references 1 and **2.** Both companies used model tests to evaluate inlet and fan-discharge-duct design concepts. On the basis of results from the initial studies, configurations for full-scale ground run-up tests were selected. The full-scale boilerplate nacelles were tested with a Pratt & Whitney JT3D turbofan engine. From the results of these ground run-up tests, configurations for flight testing were to be selected. The economic impact of the nacelle modification was to be considered throughout the program.

Figure **4** presents the scheduled occurrence of events. The dashed line indicates the present date. The companies would be about halfway through the original program, which contemplated flight tests in the latter part of 1969. However, as the results of the McDonnell Douglas ground run-up tests of treated inlets became available in the early part of 1968, it was apparent that McDonnell Douglas could meet its goal of a 7- to 10-PNdB reduction with what is called a single-ring treated inlet in combination with its treated short fan discharge ducts. That is, as a result of the initial studies by both companies, more efficient duct-lining concepts were developed which provided larger attenuation than was thought possible at the start of the program. The results of the McDonnell Douglas tests also indicated that inlet noise suppression on the order of 12 PNdB could be obtained with an acoustically treated inlet.

These results and the results of The Boeing Company ground run-up tests of its treated long fan discharge ducts indicated that Boeing could potentially accomplish the goal of a 15-PNdB reduction with a treated inlet, in combination with its treated long fan discharge ducts, and thereby avoid the complications of the sonic or near-sonic inlet. On the basis of these results and with the concurrence of the contractor in May 1968, Boeing was redirected to flight test a treated inlet and fan discharge duct instead of the sonic inlet. Boeing was also to continue work on the sonic inlet through ground run-up tests. At the same time The Boeing Company effort was redirected, the NASA asked the contractors to accelerate their program so that the flight data could be available on a more timely basis. As a result, the flight tests are scheduled for completion 4 months earlier than originally planned, as indicated by the arrows on the flight-test bars in figure 4.

Figure 5 is a schematic drawing of the flight-test nacelles to be tested by Boeing and McDonnell Douglas. The McDonnell Douglas configuration (top sketch) consists of a single-ring treated inlet and short fan discharge ducts, and the Boeing configuration (bottom sketch) consists of a treated two-ring inlet and treated long fan discharge ducts. The major effort of both companies at this time is manufacturing the nacelles for flight tests. The McDonnell Douglas flight tests are scheduled for completion in March 1969, and the Boeing flight tests, in June 1969.

Figure 6 defines the points at which both contractors will present their predicted flyover noise. An approach reference point 1 nautical mile from the 50-foot obstacle under a 3^{o} glide slope has been selected. For take-off, the reference point under the flight path has been selected as 3.5 nautical miles from brake release.

The overall procedure followed by each contractor to predict flyover noise with the use of ground run-up data is outlined in figure 7. The ground run-up data were taken at predetermined engine power settings with microphones located around the engine at a constant radial distance. A run consists of obtaining data at each of the power settings, and a minimum of three runs were made with each configuration. The data, taken at corresponding power settings, were averaged and corrected to standard-day conditions. These averaged data were then projected along each radius to intersect lines parallel to the engine center line, simulating various altitudes or distances from the engine. This projection takes into account attenuation due to spherical spreading and atmospheric corrections. The next step is to obtain the sound pressure level as a function of time, with corrections applied to the lower frequencies for relative jet velocity and to the higher frequencies for fan-tip Mach number. Finally, the variation of perceived noise level with time is calculated by using the accepted procedures outlined in reference 3.

In conclusion, it should be pointed out that references 4 to 11 are, in essence, status reports of a research and development effort and are presented to show what has been done to date. It should be stressed that the results of the program, presented in terms of

predicted flyover noise and direct operating costs, are based on ground run-up data and that the determination of any final conclusions will have to be reserved until after the flight tests. In addition, the economic viability of the configurations will have to be determined by each airline for its system.

REFERENCES

1. Mangiarotty, R. A.; Marsh, Alan H.; and Feder, Ernest: Duct-Lining Materials and Concepts. Conference on Progress of NASA Research Relating to Noise Alleviation of Large Subsonic Jet Aircraft, NASA SP-189, 1968. (Paper No. 5 herein.)

2. Watson, H. A., Jr.; Thompson, J. D.; and Rucker, Carl E.: Structural and Environmental Studies of Acoustical Duct-Lining Materials. Conference on Progress of NASA Research Relating to Noise Alleviation of Large Subsonic Jet Aircraft, NASA SP-189, 1968. (Paper No. 7 herein.)

3. Anon.: Definitions and Procedures for Computing the Perceived Noise Level of Aircraft Noise. ARP 865, Soc. Automot. Eng., Oct. 15, 1964.

4. Pendley, Robert E.: Design Concepts. Conference on Progress of NASA Research Relating to Noise Alleviation of Large Subsonic Jet Aircraft, NASA SP-189, 1968. (Paper No. 9 herein.)

5. Marsh, Alan H.; Zwieback, E. L.; and Thompson, J. D.: Ground-Runup Tests of Acoustically Treated Inlets and Fan Ducts. Conference on Progress of NASA Research Relating to Noise Alleviation of Large Subsonic Jet Aircraft, NASA SP-189, 1968. (Paper No. 10 herein.)

6. Coxon, J. S.; and Henry, C. A.: Flight-Test Nacelles. Conference on Progress of NASA Research Relating to Noise Alleviation of Large Subsonic Jet Aircraft, NASA SP-189, 1968. (Paper No. 11 herein.)

7. Pendley, Robert E.; and Marsh, Alan H.: Noise Predictions and Economic Effects of Nacelle Modifications to McDonnell Douglas DC-8 Airplanes. Conference on Progress of NASA Research Relating to Noise Alleviation of Large Subsonic Jet Aircraft, NASA SP-189, 1968. (Paper No. 12 herein.)

8. Higgins, C. C.; Smith, J. N.; and Wise, W. H.: Sonic-Throat Inlets. Conference on Progress of NASA Research Relating to Noise Alleviation of Large Subsonic Jet Aircraft, NASA SP-189, 1968. (Paper No. 13 herein.)

9. Drakeley, George T.; and McCormick, Ralph B.: Treated Inlets. Conference on Progress of NASA Research Relating to Noise Alleviation of Large Subsonic Jet Aircraft, NASA SP-189, 1968. (Paper No. 14 herein.)

10. McCormick, Ralph B.: Fan-Duct Development. Conference on Progress of NASA Research Relating to Noise Alleviation of Large Subsonic Jet Aircraft, NASA SP-189, 1968. (Paper No. 15 herein.)

11. Nordstrom, D. C.; and Miller, D. S.: Noise Predictions and Economic Effects of Boeing Nacelle Modifications. Conference on Progress of NASA Research Relating to Noise Alleviation of Large Subsonic Jet Aircraft, NASA SP-189, 1968. (Paper No. 16 herein.)

TURBOFAN-ENGINE NOISE EMISSION

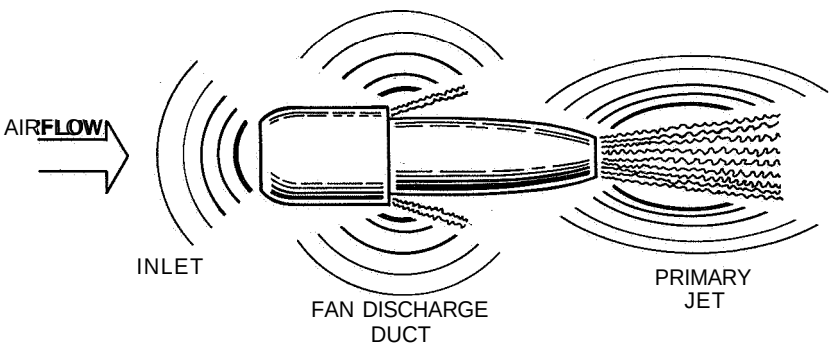

Figure 1

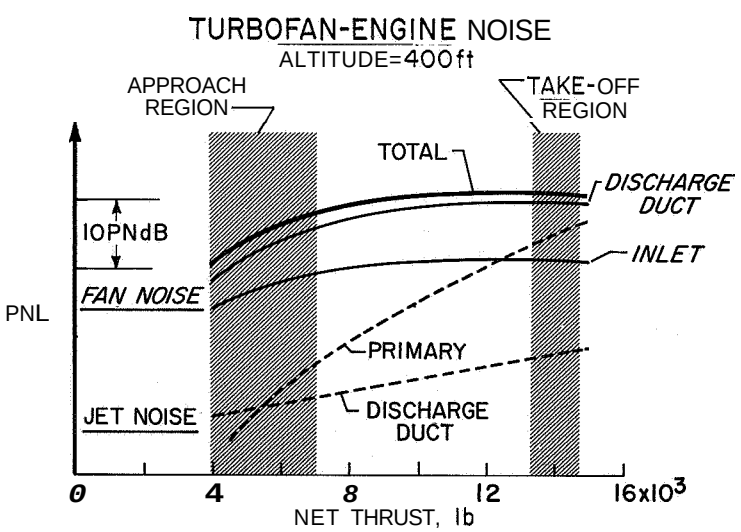

Figure 2

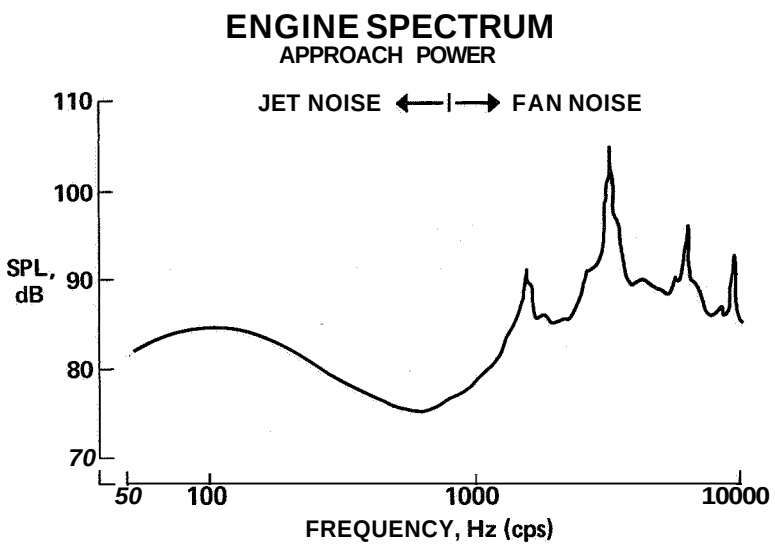

Figure 3

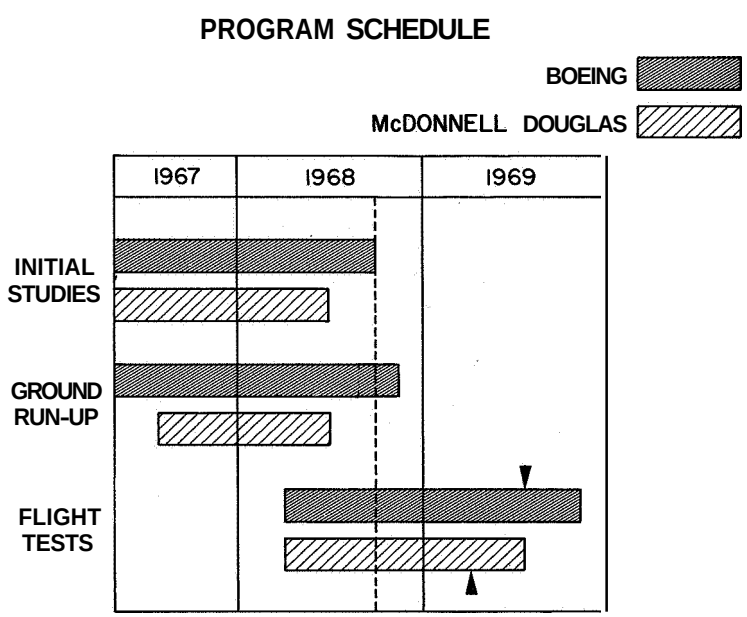

Figure 4

NACELLE TREATMENT CONFIGURATIONS

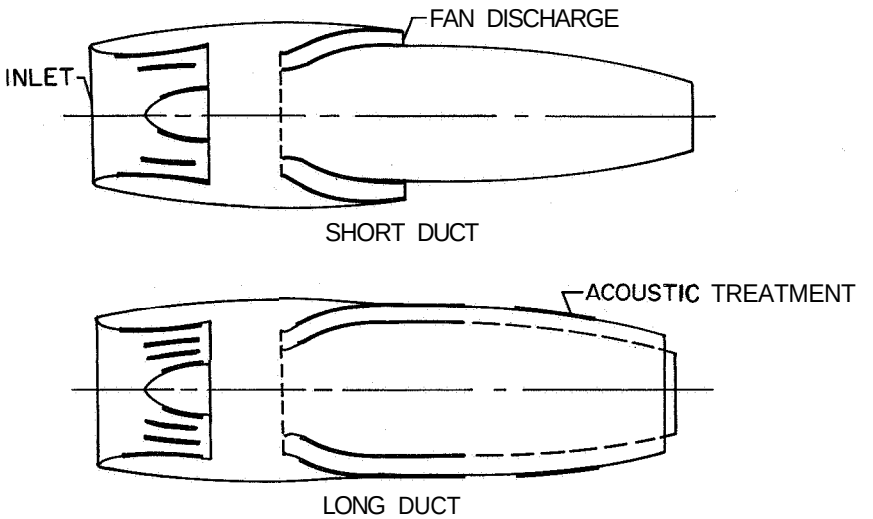

Figure 5

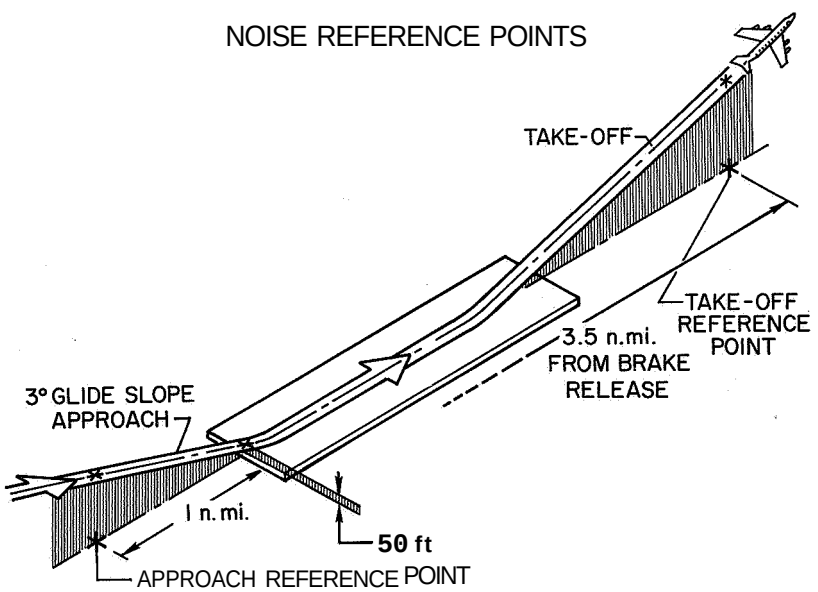

Figure 6

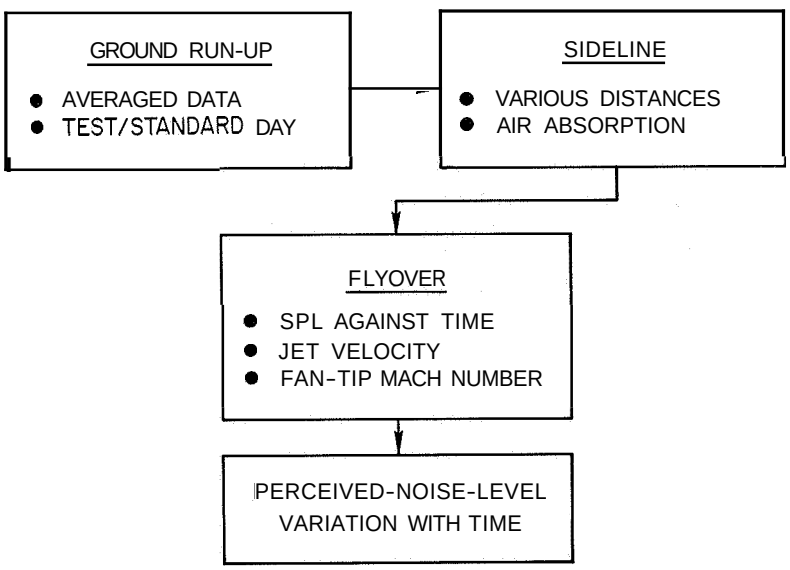
GROUND RUN-UP
AVERAGED DATA
TEST/STANDARD DAY
SIDELINE
VARIOUS DISTANCES
AIR ABSORPTION
FLYOVER
SPL AGAINST TIME
JET VELOCITY
FAN-TIP MACH NUMBER
PERCEIVED-NOISE-LEVEL
VARIATION WITH TIME

Figure 7

9. DESIGN CONCEPTS

By Robert E. Pendley

McDonnell Douglas Corporation

SUMMARY

Engineering design studies were made of alternate approaches to the reduction of noise radiating from the fan section of the Pratt & Whitney Aircraft (P & WA) JT3D engines as installed in McDonnell Douglas DC-8 airplanes with short-duct nacelles. The basic approach studied was to install acoustically absorptive duct linings in the fan inlet and exhaust ducts. A brief investigation was also made of another approach involving the reduction of fan rotational speed at landing thrust by varying the area of the primary exhaust nozzle.

The studies generated several concepts for acoustically treated duct designs for which flyover-noise estimates indicated that the landing approach noise could be reduced approximately 7 to 10 PNdB. Overall evaluation of the results of the design concept studies led to a selection of two treated inlet configurations and one exhaust duct configuration for evaluation in the succeeding ground-test phase of the program. The two inlet configurations incorporated acoustically absorptive linings – (1) on the walls of the cowl and standard center body and on two concentric ring vanes and (2) on the walls of the cowl and an enlarged center body and on one ring vane. The selected fan-exhaust-system design provided acoustical linings in an exhaust duct 24 inches longer than the existing ducts. This design is compatible with the existing primary thrust reversers, but requires a new fan-thrust-reverser design.

Acoustical and engine performance data were measured during JT3D tests with a simulation of the variable-area primary-nozzle concept for fan-speed control. The data obtained indicated that the fan-speed concept could not provide a significant reduction of JT3D flyover noise.

INTRODUCTION

The initial study phase of the McDonnell Douglas Corporation part in the NASA treated-nacelle program required engineering design studies of alternate approaches to the reduction of blade-passage-frequency noise radiated from the fan section of the JT3D engine. The goals and constraints applicable to the approaches are discussed in reference 1. The designs were to produce substantial reductions in landing-approach noise levels, with no increase in take-off noise. It was required that evaluation of the designs be performed, with consideration given to acoustical effectiveness and effects on

airplane and engine performance. At the conclusion of these studies, designs were to be selected for investigation in the succeeding ground-test phase of the program.

The purpose of this paper is to summarize the work performed in carrying out the above tasks. It includes a discussion of the method by which candidate designs were evolved, general descriptions of representative configurations studied, and a discussion of the evaluations performed. The studies were basically concerned with the application of acoustical-lining technology (discussed in ref. 2) to the fan inlet and exhaust ducts. However, another concept was investigated briefly. This concept was intended to reduce the fan speed required for a given landing thrust by controlling the primary-nozzle area. The studies of both concepts are discussed herein.

SYMBOLS

A_{ns}	area of noise source taken as projected annular area of fan inlet or exit, square feet
A_t	treated (acoustically lined) surface area of ducts, square feet
F_g	engine gross thrust, pounds
h	height of duct channel separating acoustically lined surfaces (subscripts **1** and **2** used to denote different regions of inlet duct), feet
N_1	fan rotational speed, rpm
APNL	reduction of perceived-noise level, PNdB
δ_{amb}	ratio of ambient pressure to standard-day sea-level atmospheric pressure
λ	wavelength of sound, feet
θ_{t_2}	ratio of inlet absolute total temperature to standard-day sea-level atmospheric temperature

DISCUSSION

Preliminary Considerations

One of the important constraints of the study was that the nacelle modifications investigated be applicable to the installation of the Pratt & Whitney Aircraft (P & WA)

JT3D engine in the short-duct nacelles of the McDonnell Douglas DC-8 airplane. These nacelles are illustrated in figures 1 and 2.

The fan air-inlet ducts of these nacelles are provided with relatively thick inlet lips to produce high inlet pressure recovery (and therefore thrust) at take-off conditions. (See fig. 1.) As a result, a substantial volume exists between the inlet duct skins and the exterior nose-cowl skins. This volume is utilized for the installation of oil and pneumatic-system heat exchangers, the nose-cowl ice-protection system, and related piping, valves, and ducting. The auxiliary inlet directly beneath the inlet lower lip admits cooling air to the oil and pneumatic-system heat exchangers.

Figure 2 shows the exhaust nozzle of the short fan-exhaust duct, the primary exhaust nozzle, and fan and primary thrust reverser components in the normally retracted (forward thrust) position. The duct splitters indicated extend through the full length of the exhaust duct, and thus divide each exhaust duct into separate channels.

In order to minimize the cost of incorporating noise-suppression features within the nacelle, design solutions were sought that would require the fewest changes to existing nacelle components. Thus, efforts were made to incorporate suppression features without affecting the nacelle components previously mentioned, as well as the equipment between the exhaust duct and the engine case, the pylons, and the mechanical and subsystem interfaces between the nacelles and pylons.

The first step in the study was the definition of the separate reductions required in the noise propagating through the fan inlet and exhaust ducts. A study of available ground- and flight-test data indicated that the landing-approach peak flyover perceived noise from JT3D engines was due to the noise radiated from the fan exhaust and that the peak perceived noise radiated from the fan inlet was approximately 3 PNdB lower. It was therefore considered that achievement of the study goals would require a 10-PNdB reduction of noise from the fan exhaust duct and a 7-PNdB reduction of noise from the inlet.

Next, an estimate was made of the acoustical-lining area A_t needed to accomplish the required noise suppression within the inlet and exhaust ducts. Existing duct-transmission-loss data obtained in the laboratory (ref. 3), together with the meager data previously obtained from flyover-noise tests with treated fan ducts (ref. 4), were used to prepare figure 3. In this figure, the noise-source area A_{ns} is taken as the annular area of the fan inlet or exit, the channel height h is the distance separating acoustically lined duct surfaces, the wavelength λ used is that corresponding to the frequency for which maximum attenuation is desired, and the noise suppression APNL represents the amount of reduction predicted for low altitudes during landing approach.

Figure 3 does not account for a number of factors that may be important, such as the intensity and distribution of noise within the duct, the shape or orientation of lining surfaces with respect to the noise source, and the possible effect of the duct configuration

on the far-field noise distribution. The use of this figure in estimating the potential noise suppression of alternative design concepts was tempered by recognition of, and allowance for, these qualifications.

Figure 3 indicates that the duct channel height is an important variable. Economy in the required lining area can be achieved if the linings can be installed with relatively small channel heights between facing surfaces, although care must then be taken to minimize aerodynamic losses.

Inlet-Duct Concepts

Design. - The first consideration of inlet-noise suppression dealt with the installation of linings on the existing surfaces of the inlet duct and engine center body, as symbolically indicated by the heavy lines in figure 4. On the basis of figure 3, it was predicted that this design concept would fall short of the inlet noise-suppression requirement because of the limited area treated and the unfavorably large channel heights separating the lining surfaces.

During the landing approach, the fundamental blade-passage frequency (the component of the noise that controls the landing perceived-noise level) is about 2500 Hz. The wavelength of the sound waves at this frequency is about 0.47 foot (about 5.5 inches). The annular area of the fan inlet is about 12 square feet. In the region of the center body (where $h = h_1 \approx 18$ inches ≈ 1.5 feet) (see fig. 4), the ratio h/h would be about 3.3, and the treated area required for 7 PNdB (see fig. 3) would be about 25 times 12 or about 300 square feet. In the cowl region ahead of the center body (where $h = h_2 \approx 50$ inches), the ratio h/λ is about 9 and the treated area would be about 700 square feet. Since both of these treated-area requirements are far in excess of the inlet-duct and center-body surface areas, concepts were developed to incorporate the required treated area within narrower channels with more effective values of h/λ.

Two such inlet-duct concepts are illustrated in figure 5. The installation of concentric ring vanes with acoustical linings on each of their sides simultaneously increases the lining area and reduces the channel height. Similarly, the installation of radial vanes with linings on each side of the vanes increases the lining area functioning at smaller channel heights. In this inlet configuration, the channel height corresponds to the circumferential distance between adjacent vanes.

The "light-bulb" inlet illustrated in figure 6 is another concept providing more lining area at reduced channel heights. These objectives are accomplished by enlargement of the acoustically lined center body. The cowl wall must be displaced outward in order to provide sufficient flow area at the center-body maximum-diameter station. The axial distance from this station to the inlet lip and to the fan inlet must be made sufficiently large to prevent excessive curvature to the cowl wall and the downstream center-body

surface. The minimum length of the cowl is thus determined by these aerodynamic shaping requirements. Concentric ring vanes can also be incorporated in the light-bulb inlet concept.

The design illustrated in the right-hand side of figure 6 is one of the retractable lining concepts investigated. Under conditions when noise suppression is not required, the acoustically lined surfaces would be retracted from the aerodynamic flow path, as illustrated by the position of the lined surfaces in the lower part of the sketch. With the linings stowed in this manner, inlet total-pressure (and engine performance) losses, arising from the aerodynamic flow over linings, vanes, or supporting struts, are avoided. When noise suppression is required, the lined surfaces are deployed as illustrated in the upper part of the sketch. The linings are installed on a number of segmented flaps located around the entire periphery of the inlet cowl.

Evaluation.- In evaluating the four concepts shown in figures 5 and 6, it was found that the radial-vane concept offered no advantages in estimated weight or engine performance relative to the two-concentric-ring concept. In addition, the wakes from the radial vanes could be chopped by the fan rotor blades in such a way as to increase the noise that must be absorbed by the treated surfaces in the inlet or exhaust ducts. For these reasons, the radial-vane concept was dropped from further study.

An evaluation of the three remaining configurations is summarized in tables I and II, where the changes tabulated are those estimated relative to the existing nacelles in service.

As indicated in table I, 73.0 square feet of lining area was made available in the two-concentric-ring configuration within the present cowl length. It was estimated that the design could exceed the inlet-noise-suppression requirement of 7 PNdB.

The light-bulb inlet design required an increase in cowl length of 21 inches, owing to the internal aerodynamic shaping requirements mentioned previously. With acoustical linings installed on the internal surfaces and on the concentric ring, 100.5 square feet of lining surface was provided. The incremental nacelle weight was twice that of the two-ring inlet configuration. It was estimated that the design might provide 2 to 4 PNdB more noise reduction than the two-ring design.

The retractable lining design was typical of the other designs of this type that were studied in that only limited lining areas could be provided without substantial increases in cowl length and weight. The large change in weight resulted from the actuating mechanisms and the complicated cowl structure. As table I indicates, the particular retractable concept discussed herein was expected to fall short of the required inlet-noise reduction of 7 PNdB.

The three inlet designs would affect the drag, specific fuel consumption, airplane empty weight, and depreciation and maintenance expense, each to a different degree. The net effect of the changes in these variables is accounted for by an estimated increment in direct operating cost (DOC) as presented in table II. These increments were calculated by using simple change factors that relate changes in operating cost elements to independent changes in drag, specific fuel consumption, and weight.

As table II indicates, the DOC would be increased the least by the two-concentric-ring inlet design. The DOC increment due to the light-bulb inlet design was substantially higher than that of the two-concentric-ring inlet because of its higher predicted weight, drag, and duct total-pressure loss. The retractable lining design would result in the highest DOC increment of the three inlets. Although this design does not have the cruise-fuel-consumption increase associated with linings in the inlet-duct aerodynamic flow path, the additional weight more than eliminated this benefit.

In view of the disproportionate relationship between the estimated DOC increments and noise reductions of the retractable lining concept, this concept was not investigated beyond the initial study phase. Of the remaining two concepts, the two-ring inlet was preferred since it was estimated that the required noise reduction could be achieved with the least DOC increment. However, since the reliability of the methods used to estimate noise reduction had not been validated, it was judged unwise to continue the program into the ground-test phase with only the two-ring inlet design. The light-bulb inlet design was believed to offer added assurance of achieving the inlet-noise-reduction goal; therefore, both the two-ring and light-bulb designs were selected for ground testing. In selecting the two-ring design, the possibility of achieving the required inlet-noise suppression with only one of the two rings installed was recognized. It was therefore required that the ground-test inlet be designed to permit testing with the inner ring removed.

Fan-Exhaust-Duct Concepts

Design.- The first approach studied for the suppression of fan noise was that of installing acoustical linings within the internal surfaces of the existing short-duct configuration. The design provided linings on the inner and outer duct walls and on each side of each of the four splitters in each duct. The treatment on the splitters would be similar to that on the ring vanes in the two-ring inlet or the light-bulb inlet, and would require splitters about 1 inch thick. In order to compensate for the duct area blocked by the thicker splitters, the inner and outer wall contours were expanded. The expansion resulted in an aerodynamically undesirable increase in local wall curvature and an acoustically undesirable increase in channel height. However, the exhaust nozzle outlet was unchanged in shape and, therefore, no change was required to the existing fan thrust reversers or external aerodynamic profiles. (See fig. 2.) It was estimated that a total of 34.7 square feet of linings could be provided within the exhaust ducts of each nacelle.

However, on the basis of figure 3, the design would fall short of the desired noise reduction. Acoustically more effective designs were therefore investigated.

Figure 7 illustrates a concept in which the 34.7 square feet of duct linings within the existing short-duct configuration are supplemented by an additional 17.3 square feet of lining area on two retractable side panels. These panels would normally be stowed flush with the external contours in recesses on the cowl sides forward of the fan exhaust nozzle. When noise suppression is required, they would be translated rearward on a track-and-roller system to the position indicated in the top sketch of figure 7. In this position, additional noise reduction would be accomplished by the absorptive linings on the inside surfaces of the side panels. The panels conformed approximately to the curved shape of the fan discharge jets but they are positioned sufficiently outboard to permit a flow of free-stream air between the panels and the discharge jets.

It would be necessary that the panels be retracted before the fan thrust reversers are actuated. (See fig. 7.) An interlock system would be provided to prevent the inadvertent simultaneous extension of side panels and fan reversers.

Although the side-panel concept was compatible with the continued use of much of the existing nacelle components, it would require the development of a new actuation-and-control subsystem. A comparative study was therefore made of the design illustrated in figure 8. The exhaust ducts were lengthened to provide, internally, the estimated lining area required to meet the noise-reduction goal. The overall exhaust-duct length was increased from 24 inches to 48 inches. The average duct channel height was decreased from 8 inches to 6 inches. Linings would be installed in the inner and outer duct walls and on each side of the splitters.

The existing fan thrust reversers cannot be used with this concept because of the diminished space between the engine case and the nacelle contour immediately downstream from the fan exhaust. A target-type thrust reverser consisting of a single pivoting bucket on each side of the nacelle could be accommodated within this area, however. Although this type of fan reverser is not as effective as the existing cascade reverser, it can provide an overall reverse-thrust effectiveness equal to that of other airplanes known to have satisfactory reverse-thrust levels. The existing primary thrust reversers can be used unchanged with this design.

Evaluation. - Some basic characteristics of the two exhaust systems studied are compared in table III. Although the configuration with the treated short ducts and retractable side panels would increase the nacelle weight by 200 pounds, the 48-inch exhaust-duct design would result in a weight reduction. This result is due to the lower weight estimated for the simpler target-type thrust reverser relative to the weight of the existing cascade reverser. The weight saving in the thrust reversers exceeds the weight increment of the treated 48-inch ducts relative to the existing 24-inch ducts. As table III indicates, more

lining area was provided and a higher probability of achieving the noise-suppression goals was estimated for the 48-inch ducts.

The net effect of the two designs on the estimated direct operating cost is indicated in table IV, which shows a smaller estimated DOC increment for the 48-inch duct design than for the 24-inch duct design. However, the initial retrofit cost would be somewhat higher for the 48-inch duct design than for the 24-inch duct design. Although the 48-inch design does not require development of side panels and their actuating mechanism, it requires a new thrust-reverser development and more change to the nacelle components located between the existing fan-exhaust ducts and the engine case. On the other hand, the 48-inch ducts have less wall curvature and a more favorable flow area distribution than the 24-inch ducts. The effects of these factors, together with the effect of the lighter weight of the design, leads to lower estimated maintenance and fuel costs. These savings were sufficient to offset the increased depreciation due to higher retrofit cost.

The discussion of table III indicates that the target type of fan thrust reverser for the 48-inch exhaust-duct concept results in a substantial weight saving relative to the existing fan thrust reversers. Although the lighter reversers are also compatible with the components in the 24-inch exhaust-duct concept, this reverser design (with its associated weight benefit) was not applied to the 24-inch duct concept. The reason for not using the simple reverser is that the DOC increment would become even less favorable for this concept because there would be an increased depreciation resulting from the target-type reverser that would more than offset the airplane performance improvements resulting from the lighter nacelle weight.

In view of the superior noise reduction and DOC effects estimated for the 48-inch duct design, this concept was selected for testing in the succeeding ground-test phase of the program. (See ref. 5.)

Fan-Speed Control

The concept of controlling the relative speeds of the two rotors of the JTSD engine was investigated to determine its potential for noise reduction. The concept provided for in-flight reduction of the primary-nozzle exhaust area, which reduces the pressure drop across the fan-drive turbine. As a result, at any given level of landing thrust, less power would be available for the low-pressure rotor, and the rotational speed of the fan stages would be decreased while the primary thrust and the exhaust velocity would be increased. The possibility of a net reduction in perceived-noise level would depend on the relative magnitudes of the reduction in discrete-frequency noise from the fan and the increase in broadband noise from the primary jet exhaust.

Three conical primary nozzles of 50, 60, and 80 percent of normal discharge area were tested on the JT3D-3 engine. The test results (fig. 9) show that the concept was successful in the sense that, for a given gross thrust, a substantial reduction in fan speed was realized by the reduction of primary nozzle area. Although the maximum available thrust permitted by engine operating limits would be reduced for operations at reduced nozzle area, sufficient thrust would be available to meet steady-state landing-approach thrust requirements (approximately 4000 to 5500 pounds per engine) at nozzle areas as low as 50 percent of standard. Far-field noise measurements, however, indicated that, for a given thrust, the reductions in fan noise were largely offset by the increased jet noise. It thus appeared that the concept offered little promise, and its investigation was terminated.

CONCLUDING REMARKS

The results of the investigation of design concepts in the initial study phase are summarized as follows:

1. Design concepts based on the installation of acoustically absorptive materials in the fan inlet and exhaust ducts of a JT3D nacelle were studied. It was estimated that several of the concepts could lead to a reduction in flyover noise beneath the landing approach path of 7 to 10 PNdB. These concepts had varying effects on direct operating costs.

2. An inlet configuration with acoustical linings on the duct and center-body walls and on two concentric ring vanes appeared to be the most promising of the inlet concepts studied. Analysis of this configuration indicated that it could achieve the inlet-noise reduction required with the least effect on airplane direct operating costs.

3. It was estimated that the exhaust-duct noise-reduction goal could not be met by the application of acoustical linings to the exhaust-duct surfaces within the existing short-duct nacelle configuration. Of the alternative designs studied that provided the required additional lining area, the most promising design was the one in which acoustical linings were installed on the walls and splitters of an exhaust duct 24 inches longer than the existing ducts. The design was compatible with the existing primary thrust reversers, but it required a new fan-thrust-reverser design.

4. The concept of reducing the fan rotational speed by reducing the primary-nozzle area was found to be incapable of providing significant noise reduction.

5. Two inlet designs and a lengthened exhaust duct design, all incorporating acoustical linings on their internal surfaces, were selected for tests in the succeeding ground-test phase.

REFERENCES

1. Norton, Harry T., Jr.: Introductory Remarks on Nacelle Acoustic Treatment Application. Conference on Progress of NASA Research Relating to Noise Alleviation of Large Subsonic Jet Aircraft, NASA SP-189, 1968. (Paper No. 8 herein.)

2. Mangiarotty, R. A.; Marsh, Alan H.; and Feder, Ernest: Duct-Lining Materials and Concepts. Conference on Progress of NASA Research Relating to Noise Alleviation of Large Subsonic Jet Aircraft, NASA SP-189, 1968. (Paper No. 5 herein.)

3. Marsh, Alan H.; Elias, I.; Hoehne, J. C.; and Frasca, R. L.: A Study of Turbofan-Engine Compressor-Noise-Suppression Techniques. NASA CR-1056, 1968.

4. Pendley, Robert E.; and Marsh, Alan H.: Turbofan-Engine Noise Suppression. J. Aircraft, vol. 5, no. 3, May-June 1968, pp. 215-220.

5. Marsh, Alan H.; Zwieback, E. L.; and Thompson, J. D.: Ground-Runup Tests of Acoustically Treated Inlets and Fan Ducts. Conference on Progress of NASA Research Relating to Noise Alleviation of Large Subsonic Jet Aircraft, NASA SP-189, 1968. (Paper No. 10 herein.)

TABLE I

INLET EVALUATION
BASIC CHARACTERISTICS

CONFIGURATION	CHANGES PER-NACELLE			
	LENGTH, in.	WEIGHT, lb	LINING AREA, ft^2	A PNL PNdB
TWO CONCENTRIC RINGS	*0*	150	73.0	9 TO 11
LIGHT BULB	21	300	100.5	11 TO 13
RETRACTABLE LININGS	6	440	53.0	3 TO 5

TABLE II

ESTIMATED DIRECT OPERATING COST INCREMENTS
INLETS

CONFIGURATION	ΔDOC, PERCENT
TWO-CONCENTRIC RINGS	1.2
LIGHT BULB	1.7
RETRACTABLE LININGS	2.0

TABLE III

EXHAUST SYSTEM EVALUATION
BASIC CHARACTERISTICS

CONFIGURATION	CHANGES PER NACELLE			
	DUCT LENGTH, in.	WEIGHT, lb	LINING AREA, ft^2	APNL, PNdB
24-in. EXHAUST DUCT AND SIDE PANELS	0	200	52.0	6 TO 9
48-in. EXHAUST DUCT	24	-105	70.5	8 TO 11

TABLE IV

ESTIMATED DIRECT OPERATING COST INCREMENTS
FAN EXHAUSTS

CONFIGURATION	Δ DOC, PERCENT
24-in. EXHAUST DUCT AND SIDE PANELS	1.5
48-in. EXHAUST DUCT	1.3

MODEL DC-8 SHORT DUCT NACELLE
THREE-QUARTER FRONT VIEW

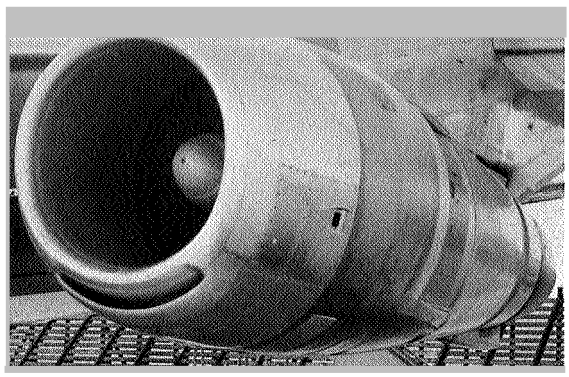

L-68-8557

Figure 1

MODEL DC-8 SHORT DUCT NACELLE
THREE - QUARTER REAR VIEW

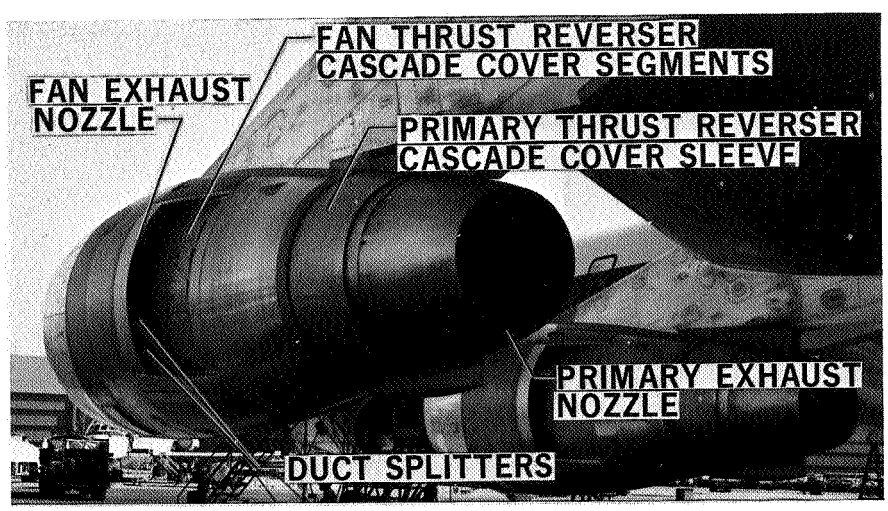

L-68-8558.1

Figure 2

ESTIMATED DUCT-LINING AREA REQUIREMENT

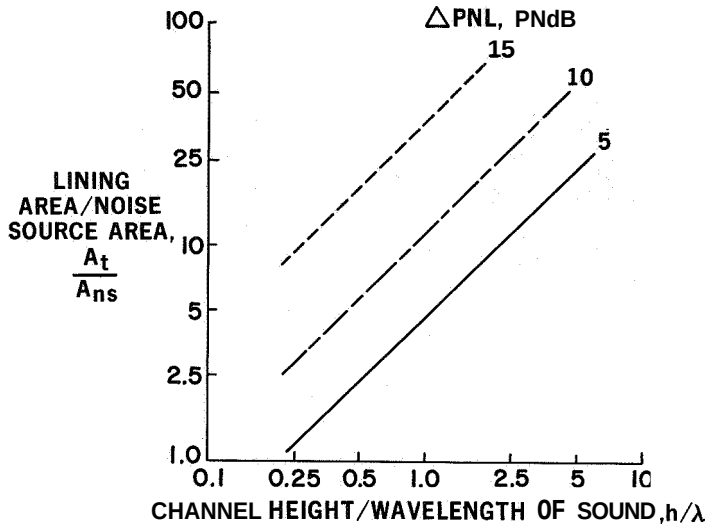

Figure 3

LINING INSTALLATION IN EXISTING INLET DESIGN

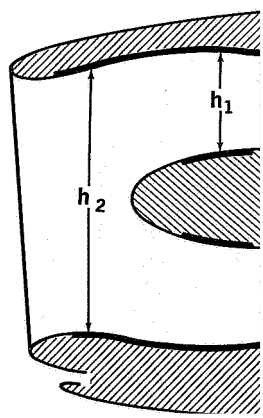

Figure 4

INLET CONFIGURATIONS STUDIED
TYPES OF VANES

CONCENTRIC RING VANES

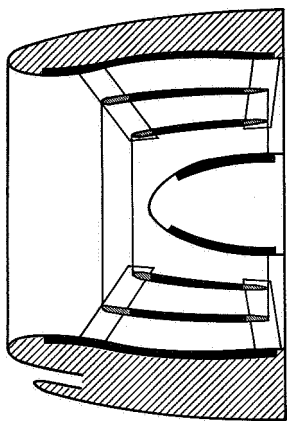

RADIAL VANES

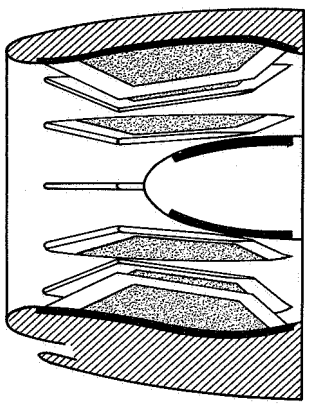

Figure 5

INLET CONFIGURATIONS STUDIED

LIGHT-BULB INLET

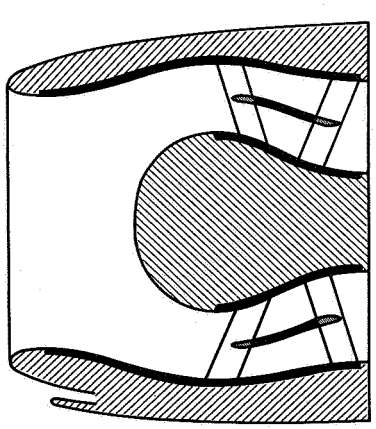

RETRACTABLE LININGS

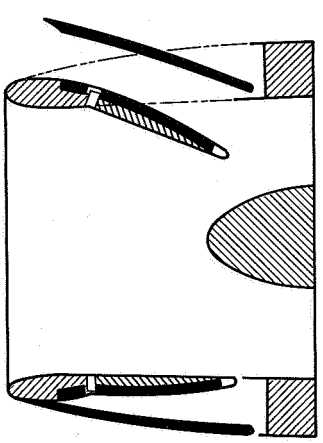

Figure 6

RETRACTABLE-SIDE–PANEL§ CONCEPT

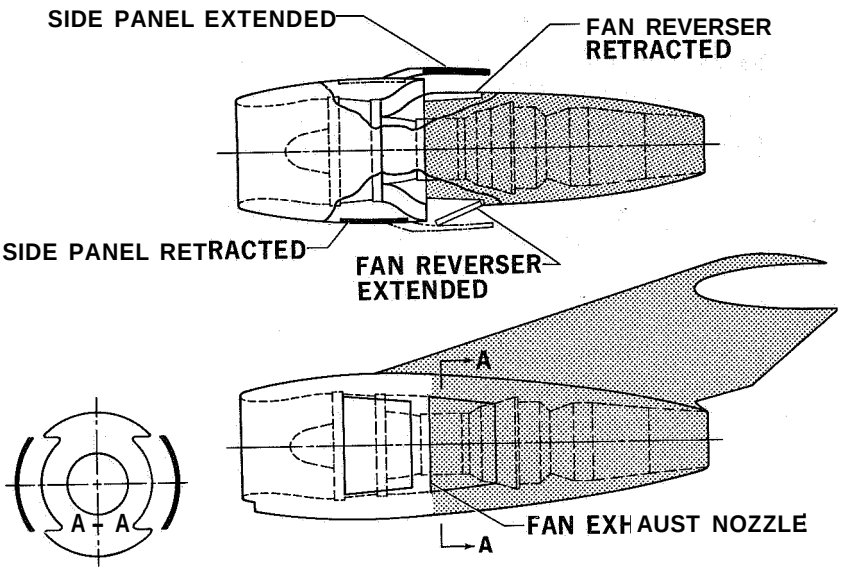

Figure 7

48-INCH FAN EXHAUST DUCT

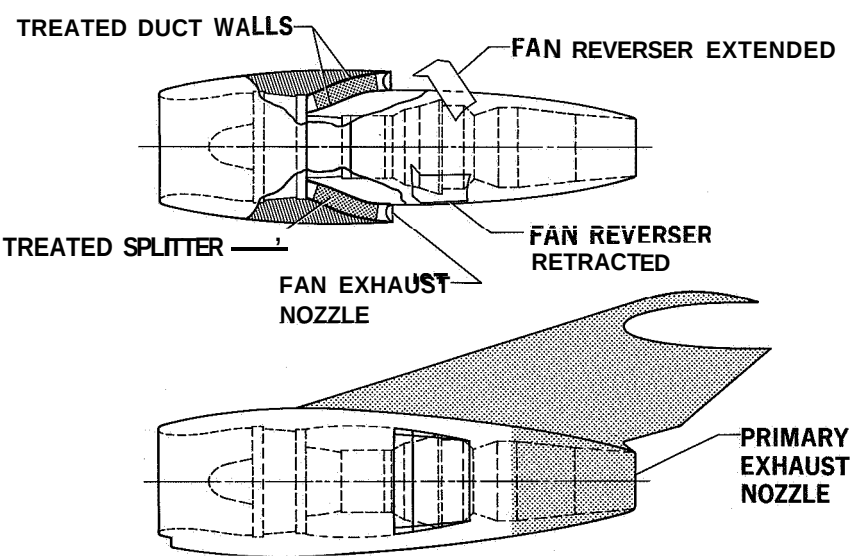

Figure 8

EFFECT OF PRIMARY NOZZLE AREA ON FAN-SPEED–THRUST RELATIONSHIP

JT3D-3 ENGINE

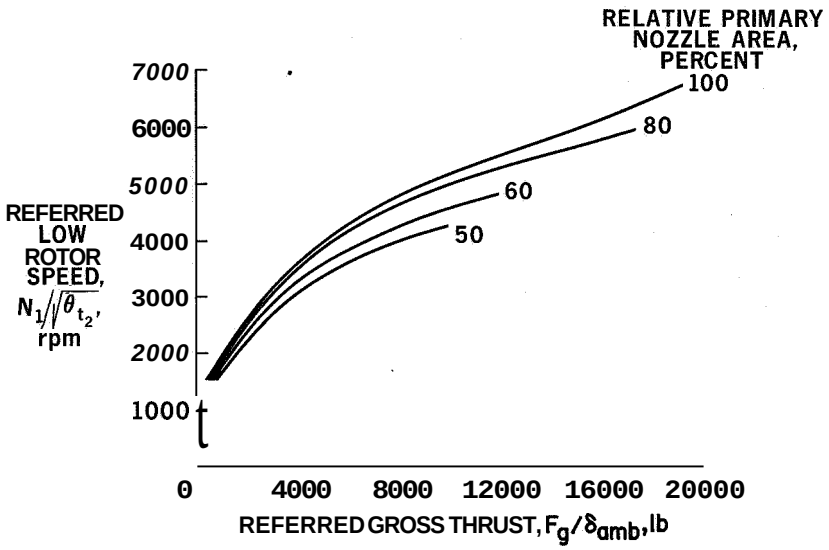

Figure 9

10. GROUND-RUNUP TESTS OF ACOUSTICALLY TREATED INLETS AND FAN DUCTS

By Alan H. Marsh, E. L. Zwieback,
and J. D. Thompson

McDonnell Douglas Corporation

SUMMARY

Two configurations of full-scale acoustically treated inlet ducts and one set of treated fan-exhaust ducts were fabricated and tested. The ducts were installed on a Pratt & Whitney JT3D turbofan engine mounted on an engine test stand. Far-field sound pressure levels and engine-performance data were obtained to evaluate the effects of the duct linings. A description is given of the tests that were conducted and of the configurations of the treated and the reference ducts. The results are presented principally in terms of the quantities that were measured at the test stand, although some estimates of the changes in flyover perceived noise level and basic engine performance are also given. Based on analyses of the test results, a design for a nacelle modification consisting of an inlet duct (with absorptive linings on the surface of the cowl, the center body, and one ring vane) and a fan-exhaust duct (with absorptive linings on the surfaces of the inner and outer duct walls and the flow splitters) was selected for flight testing on a McDonnell Douglas DC-8 airplane.

INTRODUCTION

The development of acoustical duct-lining technology, prerequisite to the selection of a duct-lining configuration, was described in reference 1. Reference 2 presented a description of the mechanical property tests needed to study candidate duct-lining materials which must withstand the environmental conditions encountered in the inlet and fan-exhaust ducts installed on the Pratt & Whitney Aircraft (P&WA) JTSD engines on DC-8 airplanes. The purpose of this paper is to describe the ground-runup tests of the treated inlet and fan-exhaust ducts selected for full-scale testing as a result of the design-concept studies reported in reference 3. Testing and data analysis techniques developed over a period of several years were used in these tests. (See ref. 4.)

This paper will describe: (1) the test procedures used for acquiring and reducing acoustic and engine-performance data and (2) the components that were tested on a JT3D turbofan engine installed on an engine test stand. Four configurations of treated inlets and one set of treated fan-exhaust ducts were tested. The results are presented in

terms of the measured differences from the reference DC-8 ducts (that is, the inlet and exhaust ducts of the existing short-duct nacelle design) and also in relation to the noise-reduction goals described in reference 5.

SYMBOLS

BPF	blade passage frequency, hertz
EPR	engine pressure ratio, P_{t7}/P_{t2}
F_n	net thrust, pounds
N_1	low-pressure-compressor rotor-shaft speed, revolutions/minute
P_{amb}	ambient pressure, pounds/square foot absolute
$P_{amb\ std}$	sea-level ambient pressure, 2116 pounds/square foot absolute
Pt2	total air pressure at engine inlet, pounds/square foot absolute
P_{t7}	total air pressure at inlet to primary-exhaust duct, pounds/square foot absolute
PNL	perceived noise level, perceived-noise decibels (PNdB)
SPL	sound pressure level, decibels (dB) (re 0.0002 microbar)
$T_{amb\ std}$	standard-day ambient air temperature, 518.7 degrees Rankine
Tt2	total air temperature at engine inlet, degrees Rankine
TSFC	thrust specific fuel consumption, (pounds/hour)/pound
δ_{amb}	ambient pressure ratio, $P_{amb}/P_{amb\ std}$
θ_{t2}	temperature ratio, $T_{t2}/T_{amb\ std}$

EXPERIMENTAL ARRANGEMENT

Engine-Noise Test Facilities

Engine test stand.- The McDonnell Douglas full-scale engine-noise test facilities are located at Edwards Air Force Base. Specifically, the engine test stand is situated at the edge of Rogers Dry Lake as shown in the aerial view in figure 1. The test engine is a P&WA JT3D-1 engine with modifications to permit operation at JT3D-3 thrust settings. The P&WA "hush-kit" was incorporated in the engine; as a result, there were 35 first-stage and 32 second-stage fan-compressor blades.

The engine is installed in a simulated DC-8 nacelle with the axis of the engine 5 feet above a concrete pad. The external nacelle surfaces aft of the fan-exhaust nozzle are simulated by an afterbody shroud that is separated from the engine case. The shroud surrounds the engine and primary-exhaust nozzle. The engine is supported by a thrust-instrumented structure designed to simulate the inboard left-hand wing-pylon section of a DC-8 airplane. The simulated wing is suspended from the test stand structure by means of flexures. These flexures permit thrust measurements by means of electronic load cells. However, the forces on the afterbody shroud are carried to the ground and are not included in the thrust balance. This procedure was necessary in order to evaluate internal engine performance separately from scrubbing forces of the fan-exhaust airflow passing over the nacelle afterbody.

The engine control and instrumentation building is located near the engine test stand. The building contains the engine operating controls, provisions for visual monitoring (by windows and closed-circuit television), and the test equipment for data signal conditioning and recording.

Acoustical range.- The acoustical range around the engine test stand has been designed for far-field noise measurements. Fourteen microphones are located on an arc centered at, and 150 feet from, the engine primary-exhaust nozzle. The 0^{o} azimuth for the microphone locations is directly ahead of the engine air inlet. The microphones were located at azimuths between 15^{o} and 157^{o}, the nearest position to the exhaust jet for reliable sound pressure level (SPL) measurements. The surface of the ground plane has been constructed to minimize variations in ground effects in the propagation path between the engine and the microphones. The dirt surface (visible in fig. 1) beyond the concrete surface around the engine stand has been leveled to match the concrete, compacted, and stabilized by an oil covering. A plan view of the engine-noise test facilities is given in the diagram in figure 2.

Background noise and operating limitations.- Because of the meteorological constraints needed to insure valid data and to minimize test time, all acoustical data were acquired during the early morning hours (from 1 a.m. to 7 a.m.). Precautions were

taken to preclude extraneous sounds from the noise field being recorded. An octave-band spectrum of the maximum ambient noise levels at the test facility is shown in figure 3. For an idle power setting (not a normal test condition), the noise radiated from the engine produced a minimum signal-to-background-noise ratio (S/N) of 20 dB over the ambient noise levels in the first and second octave bands (at 63 and 125 Hz); at all frequencies above the second octave band, the S/N ratio was typically 30 to 45 dB at the idle power setting. Thus, for all the normal engine power settings used for test purposes, the S/N ratio was adequate.

Weather conditions.- The high-altitude (2302 feet above sea level) desert location of the engine-noise test facilities, together with the restriction of the testing to the early morning hours, generally results in weather conditions acceptable for far-field noise measurements. Typically, surface winds are from the southwest direction, that is, the direction along which the engine is alined.

Low wind speeds (calm to 6 knots) occur 70 percent of the time (based on hourly measurements) from November to January and decrease to 25 percent of the time during May and June. The ambient air temperature during the early morning acoustical data recording periods ranges from a maximum of about 70° F in July and August to a minimum of about 30° F during December and January. The average moisture content, or absolute humidity, of the air around the noise test facility has been determined to be about 6 grams/meter^3, lower levels of absolute humidity being noted in the autumn and winter months.

The major environmental parameters monitored to determine an acceptable test environment are the speed and stability of the surface wind. The maximum steady wind speed allowed for conducting tests is 8 miles per hour. Winds with speeds less than 8 mph, but with rapidly changing direction, are unsuitable for stable engine operation, and tests are not conducted under this condition.

Fan-exhaust and inlet-noise suppressor enclosures.- One important requirement in the evaluation of acoustical data from the static engine test stand was the need for independent assessments of the acoustical performance of each treated inlet and fan-exhaust duct. Two enclosures were required to satisfy this need: a fan-exhaust-noise suppressor enclosure and an inlet-noise suppressor enclosure. The former enclosure was installed when data were taken to evaluate the acoustical performance of the treated inlet ducts; the latter enclosure, to evaluate the acoustical performance of treated fan ducts.

The acoustical design criteria for the noise reduction to be achieved by each enclosure were established based upon estimates of the relative strengths of the inlet and fan-exhaust noise sources plus an estimate of the amount of noise reduction that the treatment in the inlets and fan-exhaust ducts might achieve plus a factor of 10 dB to ensure an

adequate signal-to-noise ratio. The criteria were specified in terms of the change in SPL to be measured on the 150-foot arc in the 2000-Hz and the 4000-Hz octave bands. The required values were 15 dB in the aft quadrant for the inlet-noise suppressor enclosure and 17 dB in the forward quadrant for the fan-exhaust-noise suppressor enclosure.

The fan-exhaust enclosure, a five-sided structure (no rear wall) having approximate dimensions of 30 feet by 30 feet by 8 feet, was fabricated of 1-inch-thick plywood panels. The acoustical treatment used on the surfaces of the enclosure was unwrapped 4-inch-thick fiber-glass batts. The batts were covered with porous fabric and large-mesh wire screen to prevent erosion. All interior surfaces of the enclosure, including the floor, the ceiling, and the exterior surface of the front, were so treated. The front panel had an opening to allow for a 1-inch clearance around the engine. The opening was packed with fiber glass and soft felt. This flexible seal allowed engine movement yet provided an acoustical seal to eliminate noise leaks. The enclosure was braced to withstand a negative pressure of 0.5 psig within the structure. Figure 4 shows an interior view of the fan-exhaust enclosure.

Figure 5 shows the two major elements of the inlet-noise suppressor, a steel tunnel and a wooden fiber-glass-lined duct that absorbs and redirects the sound from the tunnel. The cylindrical tunnel is approximately 7 feet in diameter and 40 feet long and is fabricated of 3/16-inch-thick sheet steel. The tunnel is mounted on rails and casters to allow longitudinal movement and to facilitate connection to the engine inlet. To reduce the amplitude of sound reflections from the exterior surface of the steel tunnel and to minimize sound leaks, the inlet cowl of the engine and both ends of the tunnel were lagged with batts of 4-inch-thick, unwrapped fiber glass. The lined duct that fits over the screened entrance to the tunnel was fabricated of plywood and fiber glass to the same specifications established for the fan-exhaust suppressor enclosure. The five-sided enclosure functions as a "duct turn," lined on all interior surfaces with 4-inch-thick layers of fiber-glass batts.

An acoustical evaluation of the suppressor enclosures was made by using a high-intensity loudspeaker driven by a power amplifier, excited by octave bands of random noise at 2000 Hz and 4000 Hz. The measured changes in the far-field SPL exceeded the design criteria and the suppressor enclosures were judged to be acceptable.

Sound Pressure Level Measurements

Data acquisition.- The acoustical effectiveness of various nacelle treatments was determined by measuring the far-field acoustic pressures sensed by condenser microphones, 0.5 inch in diameter, located 5 feet above the ground surface along the 150-foot arc. The condenser microphones had a uniform pressure-frequency response and were

oriented on stands to receive the acoustic pressure waves at grazing incidence with their diaphragms in a horizontal plane through the engine.

The microphone signals were routed into the engine control and instrumentation building and monitored, by using oscilloscopes and meters, for waveform and recording level. Amplifiers with 10-dB step-gain adjustments were utilized to set the microphone signals to the optimum levels for tape recording. A 14-channel tape recorder, with frequency-modulation recording capability, was used to record, simultaneously, all far-field microphone signals along with the voice annotation needed for relating the acoustical data with the engine data. Associated equipment, utilized for obtaining supporting data, included the instrumentation indicating the engine operating parameters and the weather conditions. A wind-measuring system, indicating speed and direction and mounted 24 feet above the ground on the roof of the engine control building, was monitored and the readings were tabulated. The air temperatures necessary for determining the moisture content of the air were measured by using hand-held fan-aspirated wet- and dry-bulb thermometers.

Acoustical calibration equipment utilized for the noise-measuring systems included both a precision sound source for system sensitivity calibration at 250 Hz and 124 dB and a variable-frequency constant-amplitude electrical signal source for system frequency response calibration.

Test procedures.- The engine was operated at nine different stabilized power settings to determine basic noise characteristics at referred rotor speeds $\left(N_1/\sqrt{\theta_{t2}}\right)$ ranging from 2200 rpm to 6300 rpm. To obtain acceptable statistical confidence in the measurements, three runs were made at each power setting. Referred rotor speed was used to specify the engine power setting because the ambient air-inlet temperature varies and because the noise level at the source is considered a direct function of the fan-tip Mach number. The procedure of operating the fan section at fixed values of $N_1/\sqrt{\theta_{t2}}$, to keep the tip Mach number constant, minimized the variations in the level of the noise source, but resulted in fundamental fan-blade-passage frequencies varying slightly with ambient temperature.

Even with optimum meteorological conditions, large-amplitude fluctuations were observed in the discrete-frequency far-field fan noise. These fluctuations required noise recordings having durations of 3 minutes at each test power setting to achieve a repeatable average.

Data processing.- Processing of the acoustical data was accomplished at a Douglas facility in Long Beach, California. A diagram of the equipment is shown in figure 6. The essential functions of the equipment include tape signal control and monitoring, 1/1-octave and/or 1/3-octave band filtering, root mean squaring, logarithmic conversion of the filtered signal, digitizing of the analog level, and recording on punch cards. By using an

externally programed digital computer, the digitized records were converted into sound pressure levels corrected for variations in system frequency response. These sound pressure levels were filtered into four 1/1-octave bands with center frequencies of 63, 125, 250, and 500 Hz, and into eleven 1/3-octave bands with center frequencies ranging from 800 to 8000 Hz.

Accuracy and repeatability.- The data processing techniques included procedures for obtaining sound pressure levels having a high degree of statistical validity. These procedures were: (1) use of large values of damping available in the graphic level recorder, typically a pen writing speed of 4 millimeters/second; (2) arithmetic averaging of levels at 10 equally spaced intervals in a 25- to 50-second data sample selected at random from the 180-second data sample available for each microphone location and engine power setting; and (3) arithmetic averaging of comparable sound pressure levels measured for three separate ground-runup tests. Sample-graphic-level recorder traces of 1/3-octave band SPL fluctuations and the 10-sample averaging are shown in figure 7.

The accuracy of the SPL measurements is limited by the accuracy of the piston-phone calibration sound source, that is, about ±0.3 dB. The repeatability of the noise record/reproduce system is about ±0.3 dB. For a given data sample, the data processing techniques result in data repeatability to within ±0.6 dB for 90 percent of the data. The repeatability of the 3-run average 1/3-octave band sound pressure levels is ±1.8 dB for 90 percent of the data.

Engine-Performance Measurements

Data acquisition and reduction.- The test engine was instrumented to provide the data necessary for performance evaluations under static conditions and for "matching" of the effective areas of the fan-exhaust nozzles. Table I indicates the parameters measured and the general types of instrumentation used for performance tests. Instrumentation accuracy was equal to or better than that recommended by the engine manufacturer. In addition to performance instrumentation, instrumentation was available for monitoring engine operations and for observance of the engine operating instructions and limitations.

The large quantity of data obtained was recorded in a format suitable for processing by a digital computer. Instrument calibration corrections and the instructions for reducing the data to nondimensional parameters and to quantities referred to standard-day conditions were programed into the digital computer.

These data acquisition and reduction procedures gave faired results with good repeatability. For example, the repeatability of faired data for thrust specific fuel consumption (TSFC) is considered to be ±0.33 percent; the repeatability of the faired referred net thrust data, at a given EPR, is ±0.25 percent.

Specific test procedures.- Reference engine-performance data for three differing facility configurations had to be established because of the use of the noise suppressor enclosures. The fan-exhaust-noise suppressor enclosure, shown in figure 4, functioned as a zero-flow ejector; thus, the pressure on the aft portion of the engine was reduced by several inches of water relative to the ambient pressure. Because the resulting forces could not be accurately determined by analytical techniques, a reference was established, with the fan-exhaust-noise enclosure installed, to serve as a basis for performance comparisons during the testing of modified inlets.

Similarly, because the inlet-noise suppressor enclosure (fig. 5) affected thrust and fuel flow, reference performance data were established with the suppressor enclosure around the inlet as a basis for comparison of the tests on the modified fan-exhaust ducts.

The two references described were necessary for those tests where simultaneous measurements of noise and engine performance were made. Although care was taken to account for extraneous effects and although measurements were of a quality sufficient for rank-order evaluations of the effects of the various modified inlets and exhaust ducts on engine performance, slight inaccuracies existed because of unaccountable friction and pressure-area forces imposed by the presence of the inlet and exhaust-noise suppressor enclosures. Therefore, once the flight-test modified-nacelle configuration was selected, reference performance data were established again, but without the suppressor enclosures installed, for use in determining the effects of the modified nacelles on basic engine performance.

Components Tested

Inlets.- The engine air inlet used for a reference was the existing DC-8 cowl and center body described in reference 3. Schematic drawings of the two treated engine-air inlets are shown in figures 8 and 9. For convenience in construction, both inlets were made as bodies of revolution, axisymmetric about the inlet center line. The cowl length on the two-ring inlet was 45 inches; on the 47-percent "lightbulb," it was 65 inches. The two-ring inlet was tested with both rings in place, with only one ring (the outer ring) in place, and with both rings removed. The term 47 percent, describing the lightbulb inlet, refers to the percentage of the axial line-of-sight blockage provided by the enlarged center body. The area that is blocked is the annular area at the inlet-guide-vane station on the existing JT3D inlet cowl.

The acoustical treatment was located on the cowls, rings, and center bodies of the two inlet configurations as indicated in figures 8 and 9. The design concept selected by McDonnell Douglas for the duct lining used a single layer of porous stainless-steel fiber metal over air-filled cavities as shown in the two enlarged views in the figures. The acoustical parameters of the duct linings in the inlets are given in table II. The porous

surfaces, fiber-glass honeycomb, and impervious backing structure were bonded together by using the techniques described in reference 2. The impervious backing-support structure consisted of a 0.25-inch-thick fiber-glass laminate.

Fan-exhaust ducts.- The short fan-exhaust ducts used as a reference were described in reference 3. Figure 10 illustrates the configuration of the 48-inch fan-exhaust ducts that were tested. The 48-inch dimension refers to the axial distance between the duct entrance and exit planes. Each duct has acoustical treatment on the outer wall, on the inner wall, on both sides of each of the four flow splitters, and on each "duct end" between the inner and outer walls.

The duct-lining concept used in the fan-exhaust ducts was similar to that used in the treated inlet ducts, as can be seen by comparing the parameters listed in table III with those in table 11. The treatment consisted of a single-layer design of porous stainless-steel fiber metal over air-filled cavities. The nominal flow resistance of the porous surfaces was chosen as 80 mks rayls compared with the 100 mks rayl fiber metal used in the inlet ducts. As indicated in figure 10 and in table 111, the cavity depth on the outer duct wall was greater than that on the inner duct wall. The treatment used on the flow splitters was the same as that used on the ring vanes in the inlets, that is, two 0.5-inch-thick layers on either side of a thin, impervious, steel septum. The duct lining was a bonded construction and, like the inlet ducts, used 0.25-inch-thick fiber-glass laminate for backing-support structure.

RESULTS AND DISCUSSION

Treated Inlet Ducts

Noise level of the reference inlet (existing DC-8 inlet).- Figure 11 illustrates the spectra of the sound pressure levels observed in the forward quadrant at 60^{o} from the inlet center line and 150 feet from the primary nozzle exit. The spectra are shown for the two engine power settings corresponding to those used for DC-8 operations during a landing approach (standard day) and during a take-off (hot day), that is, for referred low-pressure rotor speeds of 4600 and 6300 rpm, respectively. Acoustic performance results, in this and succeeding sections, are presented for one or both of these two engine power settings. The angle of 60^{o} was chosen because estimates of the instantaneous flyover perceived noise level (PNL) during landing showed that the peak PNL of the noise from the existing inlet occurred at an angle of about 60^{o}, when the 150-foot polar SPL measurements were projected to a 400-foot sideline, representative of a landing approach.

The far-field SPL spectra shown in figure 11 illustrate several characteristics of the sounds radiated from the inlet of the P&WA JT3D engine. At the landing power setting, the most prominent features are the intense sound pressure levels in the 1/3-octave bands centered at 2500 Hz and 5000 Hz, that is, in the bands containing the

fundamental and the second harmonic of the blade-passage frequencies (BPF) from the two fan stages. The fundamental BPF tones in the 1/3-octave band at 2500 Hz are from 5 to 6 dB greater than the second harmonic of the BPF tones in the 1/3-octave band centered at 5000 Hz.

At the take-off power setting, the fundamental blade-passage frequencies are between 3400 Hz and 3700 Hz. The SPL at these frequencies contributes approximately equally to the SPL in the 1/3-octave bands centered at 3150 Hz and 4000 Hz. As with the landing power setting, the SPL of the fundamental is also 5 to 6 dB greater than the SPL of the second harmonic. The absolute value of the SPL at the fundamental BPF is less for the take-off than for the landing power setting.

Another interesting feature of the far-field spectra in figure 11 is the appearance of sound pressure levels at frequencies not related to blade passage. These sound pressure levels are technically referred to as combination tones and occur at frequencies which are integral multiples of the rotor speed. Combination tones are produced by a series of randomly spaced weak shock waves propagated forward of those sections of the fan blades that are rotating at supersonic relative tip Mach numbers. Reference 6 contains more detailed information on the formation of these combination tones and notes that the most intense combination tones are at frequencies that are 15 to 20 times the rotational speed of the low-pressure rotor. Thus, at the landing power setting, the combination tones lie within the 1/3-octave bands centered at 1000, 1250, and 1600 Hz and, at the take-off setting, in the 1/3-octave bands centered at 1600, 2000, and 2500 Hz.

Lastly, the broadband noise (in the octave bands centered at frequencies from 63 to 500 Hz) is much less at landing power settings than at take-off power settings. The principal source of broadband noise is normally the primary jet exhaust although with the fan-exhaust-noise suppressor enclosure around the engine, other sources may contribute significantly to the observed sound pressure levels.

Noise reduction of the two-ring inlet.- The noise reduction of the two-ring inlet at the landing power setting is shown in figure 12. In the 1/3-octave band centered at 2500 Hz, the noise reduction was 18 dB with two rings installed, 12 dB with one ring installed, and 3 dB with no rings installed; in the band centered at 5000 Hz, the corresponding noise reductions were 8, 5, and 1.5 dB. These results emphasize the importance of selecting channel heights to give small distances between absorptive surfaces in order to achieve large noise reductions at these high frequencies. The results tend to corroborate the trends that were shown in reference 1 based on transmission-loss tests using duct models with various channel heights and also the trends indicated by the design chart presented in reference 3.

The noise reductions in the 1/3-octave bands centered at 1000, 1250, and 1600 Hz are large because of the apparently efficient absorption of the combination tones by the

treatment on the cowl wall. Addition of the treated rings only makes slight increases in the combination-tone noise reduction, probably because only the outer portions of the fan blades are near sonic speed at the 4600-rpm landing condition and, hence, the combination-tone energy may be concentrated near the cowl wall.

Noise reduction of the 47-percent lightbulb.- Figure 13 shows the acoustical performance at landing power of the lightbulb inlet compared with that of the two-ring inlet (with two rings). The noise reduction observed includes the effects of (1) the acoustical absorptivity of the treated surfaces, and (2) the line-of-sight blockage by the enlarged center body. The results did not indicate any significant additional attenuation from the 27 square feet of additional treatment in the lightbulb inlet, over that in the two-ring inlet, because of the large heights of the channels in which much of the acoustical lining is placed.

Noise reductions at take-off.- Noise reductions achieved at the take-off power setting for the four treated inlet configurations are presented in figure 14. The reductions at take-off are less than those obtained at the landing power setting (at the fundamental and second harmonic blade passage frequencies) because: (1) the sound pressure levels incident on the treated surfaces may be less at take-off than during landing; (2) the airflow velocity over the treated surfaces is greater at take-off; and (3) the absorptivity of the treatment at 3400 to 3700 Hz is less than the absorptivity at 2500 Hz.

The noise reductions at the fundamental and at the second harmonic of the BPF at the take-off power setting (that is, at the frequencies noted by the dashed lines) are approximately equal for each of the four configurations in figure 14. This result contrasts with those shown in figures 12 and 13, where as much as an 11-dB difference between the noise reduction at the fundamental and at the second harmonic was observed. The difference in results is attributed to the relative strength of the BPF tones at the two power settings.

Finally, it is noted that the effect of adding treated ring vanes on the noise reduction at the combination-tone frequencies is different at take-off than at landing. At the landing power setting, the cowl-wall treatment alone (no rings installed) achieved almost as much noise reduction as when the outer ring, or both outer and inner rings, were installed. However, at take-off (with combination tones in the 1/3-octave bands centered from 1600 to 2500 Hz), the reduction was considerably increased by the addition of the treated rings. This result may be related to a spreading out of the combination-tone energy throughout a larger portion of the inlet cowl at the take-off power setting compared with the energy distribution at the landing power setting. A larger portion of each fan blade is rotating supersonically at the take-off power setting than at the landing power setting.

Engine-performance tests.- Figure 15 shows the results of testing three of the four treated inlet configurations with the fan-exhaust-noise enclosure fitted to the test stand.

Engine performance was measured while acoustic tests were being conducted. Referred thrust is shown as a function of engine pressure ratio. To simplify further discussion, the two-ring inlet with just the one outer ring installed is hereinafter referred to as the one-ring inlet.

Thrust decrements observed for the various treated inlets indicate the following rank ordering: (1) one-ring inlet, (2) two-ring inlet, and (3) 47-percent lightbulb inlet It is noted that the configurations producing the larger noise reductions tend to produce more thrust loss.

Pressure survey of one-ring inlet.- An adapter ring, incorporating fixed-position total-pressure rakes, was used to determine pressure recovery characteristics at the inlet station corresponding to the engine inlet. The adapter consisted of two concentric cylindrical sections, 8 inches long, fitted between the engine front flange and the inlet cowl and similarly between the engine hub flange and the center body. Rakes were installed to survey total pressures across the inlet annulus, near the center body and cowl surfaces, and behind the ring and ring-support struts. In addition, six static pressure taps were located with equal circumferential spacing around the adapter ring in the plane of the total-pressure probes.

Figure 16 shows the radial distribution of inlet total pressure. The influences of the cowl-wall boundary layer and the concentric-ring wake are indicated. Although not included in the graph, the wake of one of the ring-support struts was measured (rake 3) at a distance of about 13.5 inches radially from the center body. The peak pressure loss from the ring-support strut was only about one-fourth the loss produced by the acoustically treated ring.

Treated Fan-Exhaust Ducts

Noise level of the reference (existing DC-8) fan-exhaust ducts.- Figure 17 shows the spectra of the sound pressure levels observed at 110° on the 150-foot arc. The 110° angle corresponds approximately to the polar angle at which the peak instantaneous PNL is radiated from the existing short fan ducts during landing.

The spectra are similar to those shown in figure 11 for the reference inlet configuration except that the sound pressure levels are greater by about 10 dB. Combination tones, which should propagate only out the inlet duct because they are related to the shock waves ahead of the supersonic parts of the fan blades, should not be present in the spectra of the noise from the fan ducts. The data presented in figure 17 do not show evidence of strong combination tones.

The noise spectra from the fan ducts also illustrate another important characteristic in that the SPL of the second harmonic of the BPF is now about equal to the SPL

of the fundamental BPF at the landing power setting; whereas a 5- to 6-dB difference was noted in figure 11 between these two frequency components for the inlet noise.

Noise reduction of the 48-inch fan-exhaust ducts.- Figure 18 shows the noise reductions measured at the 110° angle at the landing and at the take-off power settings. At the fundamental BPF, the noise reduction is 23 dB at the landing power setting, and about 12 dB (by interpolation between the values shown for the 3150- and the 4000-Hz bands) at the take-off condition.

On the basis of (a) the relatively greater SPL noted in figure 17 for the second harmonic of the blade passage frequencies compared with the SPL of the fundamental blade passage frequencies and (b) the general results presented in reference 1 for the effects of SPL on the attenuation of sound propagated through treated ducts, it was expected that the noise reduction of the second harmonic tones, compared with that of the fundamental tones, would be relatively larger than was achieved by the treated inlets. As anticipated, at landing power, the noise reduction in figure 18 at the second harmonic of the BPF was relatively larger, compared with that at the fundamental, than the values presented for the treated inlets.

The data presented for the fan-exhaust ducts do not show the significant noise reductions noted for the treated inlet ducts in the 1/3-octave bands containing the intense combination tones. (See figs. 12 and 13.) This observation tends to validate the discussion of the treated inlet ducts that explained the large noise reductions observed in the 1/3-octave bands below the fundamental blade passage frequencies. Since combination tones are not found downstream of the fan blades, no large noise reductions would be expected at these frequencies in the aft quadrant.

Engine-performance tests of the 48-inch fan-exhaust ducts.- The engine-performance tests of the 48-inch treated fan-exhaust ducts, conducted concurrent with the acoustic tests, indicated thrust decrements relative to the existing fan-exhaust ducts of 0.25 percent, or less, at fixed values of engine pressure ratio (EPR). These indicated-fan-duct losses were considered to be less than the uncertainty in the accuracy of the performance measurements with the inlet-noise suppressor enclosure installed.

Relation of Component Test Results to Contract Goals and Inlet Selection

The noise alleviation goals for the modified nacelles, to be designed for the JT3D engine on the DC-8 airplane, were given in reference 5 in terms of a reduction in the peak instantaneous flyover PNL produced by the aircraft passing at an altitude of 370 feet over a listener stationed out of doors 1 nautical mile from the landing threshold. The conditions included an air temperature of 77° F, a runway at sea level, and a 3° landing glide slope. The aircraft specifications were flaps full down, maximum landing weight,

and a net thrust per engine of about 5500 pounds. Perceived noise levels were to be calculated by using the sound-pressure-level—noisiness conversions given by the tables in the latest applicable revision of reference 7.

Although general procedures for accurately predicting the spectrum and directivity of flyover sound pressure levels (and hence the magnitude and time-dependence of instantaneous perceived noise levels) are not yet available, estimates were nevertheless made of the reductions required in peak PNL for the noise radiated from the existing fan-exhaust ducts and the existing inlet duct. These estimates, mentioned in reference 3, were that a reduction in peak instantaneous PNL, under the landing condition described, of about 10 PNdB would be required for the noise radiated from the fan ducts, and about 7 PNdB for the noise radiated from the inlet ducts.

Extrapolating from the 150-foot polar SPL measurements, additional estimates were made, by using the flyover noise prediction techniques described in reference 8, of the reduction in peak landing PNL that would be produced by the four configurations of treated inlet ducts and by the 48-inch treated fan-exhaust ducts. At the landing power setting,

(1) The reduction in peak PNL from the fan ducts would be about 11 PNdB

(2) The reduction in peak PNL from the inlet ducts would be:

(a) For the two-ring inlet with no rings, about 2 PNdB; one ring, about 8 PNdB; two rings, about 11 PNdB

(b) For the 47-percent lightbulb inlet, about 10 PNdB.

No change in peak flyover PNL was predicted at the take-off power condition specified in reference 5.

Based on the estimates presented above and on the preliminary results of the engine-performance tests made with the noise-suppressor enclosures around the engine, the combination of the one-ring treated inlet and the 48-inch treated fan ducts was selected for the modified-nacelle concept for the flight-test phase of the program.

Ground-Test Modified Nacelle

Figure 19 shows the selected components mounted on the JTSD engine simulating the flight-test modified nacelle. There were no noise-suppressor enclosures around the engine for the acoustic and engine-performance tests of the components in this configuration. The T-shaped device visible in figure 19, that is mounted on the ground in front of the engine air inlet, is a vortex barrier that was installed to minimize the effects of ground vortex systems in the inlet airflow on the generation of noise by the fan sections of the engine.

Noise reduction.- The acoustical performance of the existing and the modified JT3D nacelles, measured at the 110° angle, is shown in figures 20 and 21 for the landing and the take-off power settings, respectively. By projecting the sound pressure levels measured throughout the 150-foot arc to the specified landing approach condition, estimates showed that if the DC-8 were to be equipped with a nacelle modification with the same acoustical performance as the combination of the one-ring treated inlet and the 48-inch treated fan-exhaust ducts, the 7 to 10 PNdB perceived-noise-reduction goal during landing would be met. Reference 8 contains additional data on the effects of the nacelle modifications on airport community noise levels.

The spectra in figures 20 and 21 indicate an increase of 1.5 to 2 dB in the sound pressure levels at 63, 125, and 250 Hz. The cause for this increase in the low-frequency sound pressure levels is not known although it is probably related to the difference in the turbulence levels and shear gradients caused by extending the fan-exhaust nozzle 24 inches closer to the primary nozzle. When the fan nozzle on the JT3D engine was made coplanar (or almost coplanar) with the primary nozzle (as on the DC-8 model 62 and 63 airplanes), substantial reductions in low-frequency noise were obtained. Similar low-frequency noise reductions are expected for the long fan-exhaust duct installation being considered for the 707 and 720 turbofan-powered airplanes.

Engine performance.- Figures 22 and 23 present engine-performance data obtained in the tests of the nacelle with modified inlet and fan-exhaust ducts. Figure 22 gives the effects of the nacelle modifications on referred thrust specific fuel consumption (TSFC); figure 23 shows the effects on referred net thrust as a function of EPR. Since the results shown in these figures are for static engine performance only, additional analyses were conducted to provide more meaningful estimates of the effects of these nacelle modifications on airplane performance.

The TSFC penalty, at a constant value of referred net thrust, is considered to be due to the effects on thrust and fuel flow of the losses in total pressure within the inlet and the fan-exhaust ducts. Standard methods of extrapolating these losses to cruise conditions indicated that the cruise TSFC would be increased by about 1 percent for the modified nacelle relative to the existing nacelles.

Whereas the curves presented in figure 23 do indicate a thrust decrement at a given EPR, the decrement in rated power settings will be larger. At take-off rated power, although the data indicated 0.5-percent thrust loss at a constant EPR, reduced EPR settings would be required for the curves used to set take-off thrust for two reasons. First, for airplanes equipped with the existing nacelles, an increase of EPR at ratings over that specified for the basic engine was allowed. This increase was available only with the particular fan-exhaust-duct and fan-thrust-reverser arrangement supplied with the engine for the existing nacelles, and would not be available for the modified nacelles.

Second, an adjustment in EPR would be required to reduce power to prevent engine overboost due to inlet loss. The P_{t2} total-pressure probe in the inlet installation on the DC-8 is located where it does not sense loss in average inlet pressure. The engine, however, does experience inlet-pressure losses and, hence, actually operates at an EPR higher than that indicated by the EPR gage in the cockpit, since the actual average inlet pressure is less than that measured by the P_{t2} probe. Thus, since the parameters that limit the operation of the engine are related to the actual EPR rather than the indicated EPR, a reduction in indicated EPR is required to account for this inlet-pressure loss.

As a result, after making these adjustments to the indicated EPR allowable for the take-off rating and after including the thrust decrement of 0.5 percent once the rated EPR was established, the sea-level standard-day thrust available at the take-off rating will be reduced by an estimated 2.75 percent compared with that for the existing installation. By a similar analysis, on a standard day at an altitude of 35 000 feet, the maximum cruise thrust rating will be reduced by 2.5 percent. The decrease in take-off rated thrust will mean that at fixed distances from start of take-off, airplanes equipped with modified nacelles will be at lower altitudes than airplanes equipped with the existing nacelles and the same gross weight.

CONCLUDING REMARKS

The results of these tests have demonstrated that acoustically treated inlet and fan-exhaust ducts can be designed for the P&WA JT3D turbofan engine that will produce significant reductions in the far-field sound pressure levels, at blade passage frequencies, for landing-approach power settings. The engine-performance penalties associated with these treated ducts result in an increase in cruise thrust specific fuel consumption and a decrease in the thrust available at rated engine power settings. The decrease in thrust at rated take-off power will result in the modified aircraft having a slightly lower take-off flight path.

REFERENCES

1. Mangiarotty, R. A.; Marsh, Alan H.; and Feder, Ernest: Duct-Lining Materials and Concepts. Conference on Progress of NASA Research Relating to Noise Alleviation of Large Subsonic Jet Aircraft, NASA SP-189, 1968. (Paper No. 5 herein.)

2. Watson, H. A., Jr.; Thompson, J. D.; and Rucker, Carl E.: Structural and Environmental Studies of Acoustical Duct-Lining Materials. Conference on Progress of NASA Research Relating to Noise Alleviation of Large Subsonic Jet Aircraft, NASA SP-189, 1968. (Paper No. 7 herein.)

3. Pendley, Robert E.: Design Concepts. Conference on Progress of NASA Research Relating to Noise Alleviation of Large Subsonic Jet Aircraft, NASA SP-189, 1968. (Paper No. 9 herein.)

4. Pendley, Robert E.; and Marsh, Alan H.: Turbofan-Engine Noise Suppression. J. Aircraft, vol. 5, no. 3, May-June 1968, pp. 215-220.

5. Norton, Harry T., Jr.: Introductory Remarks on Nacelle Acoustic Treatment Application. Conference on Progress of NASA Research Relating to Noise Alleviation of Large Subsonic Jet Aircraft, NASA SP-189, 1968. (Paper No. 8 herein.)

6. Kester, J. D.; and Slaiby, T. G.: Designing the JTSD Engine To Meet Low-Noise Requirements for Future Transports. [Preprint no.] 670331, Soc. Automot. Eng., Apr. 1967.

7. Anon.: Definitions and Procedures for Computing the Perceived Noise Level of Aircraft Noise. ARP 865, Soc. Automot. Eng., Oct. 15, 1964.

8. Pendley, Robert E.; and Marsh, Alan H.: Noise Predictions and Economic Effects of Nacelle Modifications to McDonnell Douglas DC-8 Airplanes. Conference on Progress of NASA Research Relating to Noise Alleviation of Large Subsonic Jet Aircraft, NASA SP-189, 1968. (Paper No. 12 herein.)

9. McCormick, Ralph B.: Fan-Duct Development. Conference on Progress of NASA Research Relating to Noise Alleviation of Large Subsonic Jet Aircraft, NASA SP-189, 1968. (Paper No. 15 herein.)

TABLE I.- INSTRUMENTATION FOR ENGINE-PERFORMANCE TESTS

Parameter	Instrumentation
Primary exhaust-duct-inlet total pressure	P&WA averaging rakes and mercury manometer
Engine-inlet total pressure	Probe at nose of center body and water manometer
Fan-duct-inlet total pressure	Six P&WA averaging rakes and mercury manometers
Low-pressure-compressor-exit static pressure	Sensitive manifold pressure gage, 0 to 400-inch mercury absolute
High-pressure-compressor-exit static pressure	Sensitive manifold pressure gage, 0 to 400-inch mercury absolute
Measured net thrust	Load cells and self-balancing indicator
Low-pressure-spool rotor speed	Electronic pulse counter
High-pressure-spool rotor speed	Electronic pulse counter
Fuel flow rate	Turbine flowmeter and electronic pulse counter
Fuel temperature	Iron-constantan thermocouple and precision potentiometer
Engine-inlet total temperature	Four shielded iron-constantan thermocouples and precision potentiometer
Primary-exhaust-duct-inlet total temperature	P&WA averaging probes and precision self-balancing potentiometer

TABLE II.- ACOUSTICAL DUCT-LINING PARAMETERS FOR TWO-RING OR 47-PERCENT LIGHTBULB INLETS

Parameter	Value
Nominal flow resistance of porous surfaces at 0.2 meter/second, mksrayls	100
Cavity depth on cowl and center body. inches	0.75
Cavity depth on either side of impervious steel septum for ring vanes. inches	0.50
Node spacing (cell size) for fiber-glass honeycomb. inches	0.75
Design frequency for maximum noise reduction. hertz	2200 to 2800
Treated area for two-ring inlet. square feet:	
Cowl	35.5
Outer ring	24.0
Innerring	9.0
Center body	4.5
Total	73.0
Treated area for 47-percent lightbulb. square feet:	
Cowl	63.0
Ring	23.0
Centerbody	14.5
Total	100.5

TABLE III.- ACOUSTICAL DUCT-LINING PARAMETERS FOR **48-INCH** FAN-EXHAUST DUCTS

Parameter	Value
Nominal flow resistance of porous surfaces at **0.2** meter/second, mks rayls	**80**
Cavity depth. inches:	
Outer duct wall	**0.75**
Inner duct wall	**0.5**
Flow splitters. either side of impervious septum	**0.5**
Duct ends (between inner and outer duct walls)	**0.5**
Node spacing (cell size) for fiber-glass honeycomb. inches	**0.75**
Design frequency for maximum noise reduction. hertz	**2300** to **2900**
Treated area. square feet:	
Outer duct wall	**24.5**
Inner duct wall	**24.0**
Flow splitters	**19.5**
Duct ends	**2.5**
Total	**70.5**

AERIAL VIEW OF JT3D ENGINE TEST STAND

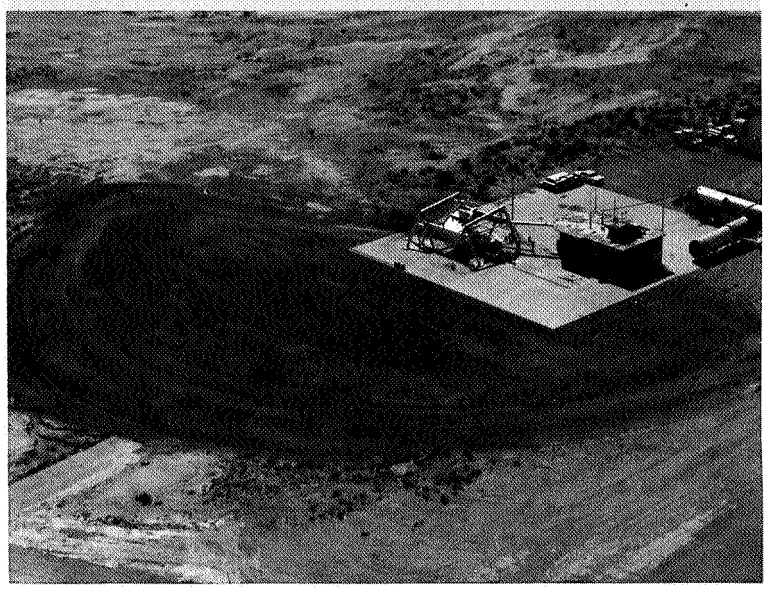

L-68-8559

Figure 1

ENGINE NOISE TEST FACILITIES

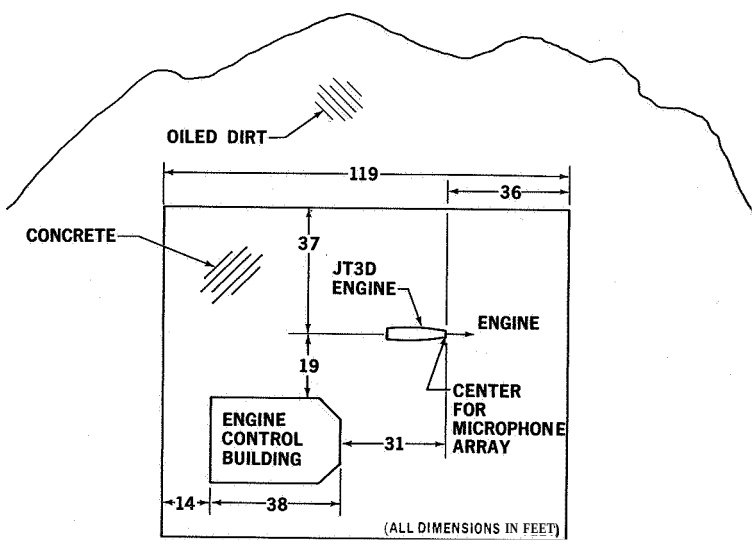

Figure 2

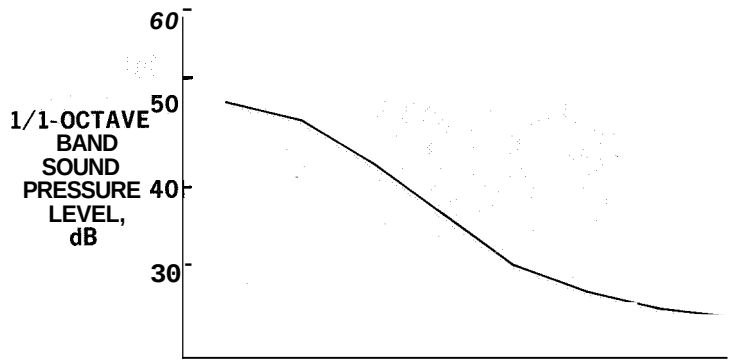

Figure 3

INTERIOR VIEW OF FAN-EXHAUST-NOISE SUPPRESSOR ENCLOSURE

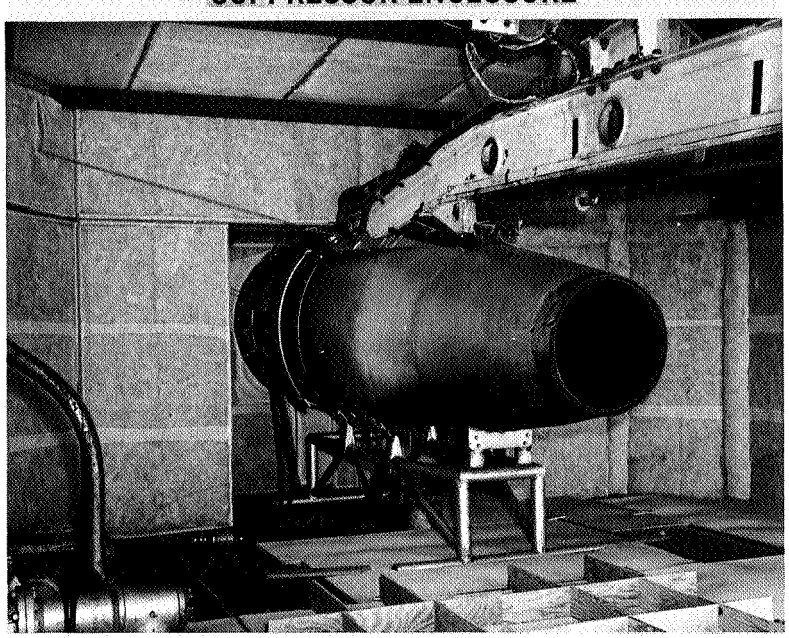

Figure 4 L-68-8561

INLET-NOISE SUPPRESSOR ENCLOSURE

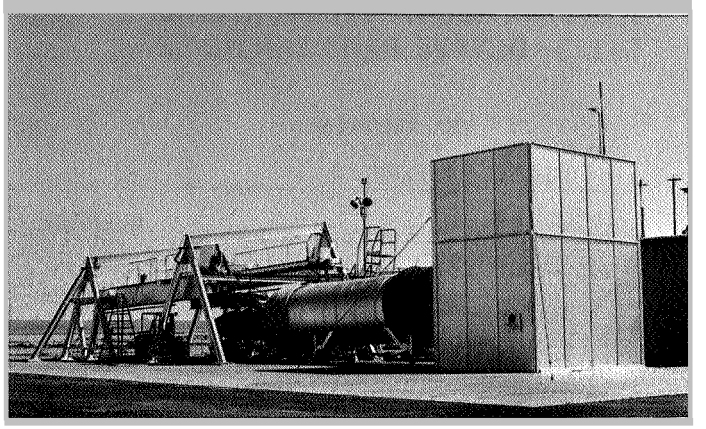

L-68-8562

Figure 5

DIAGRAM OF AUTOMATED PROCESSING SYSTEM FOR ACOUSTICAL DATA

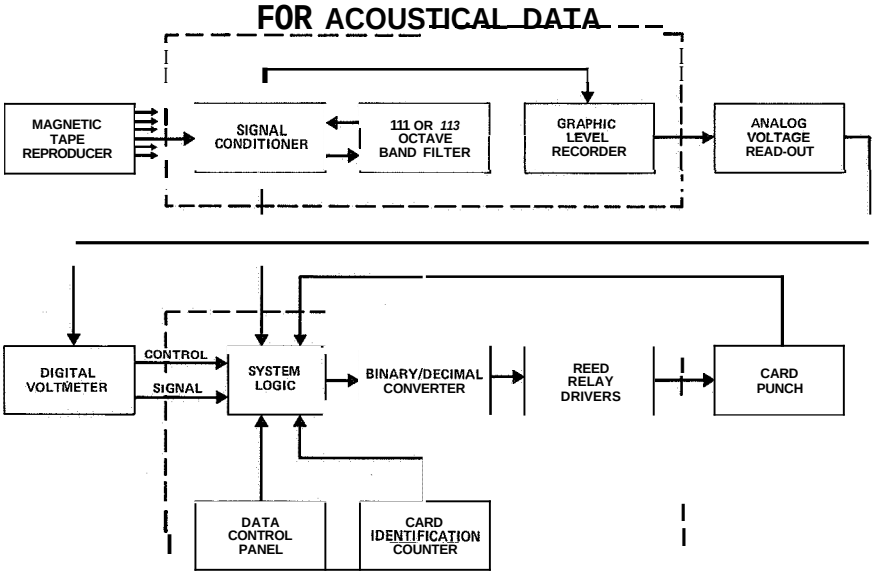

Figure 6

ILLUSTRATION OF FLUCTUATIONS IN 1/3-OCTAVE BAND FAN NOISE

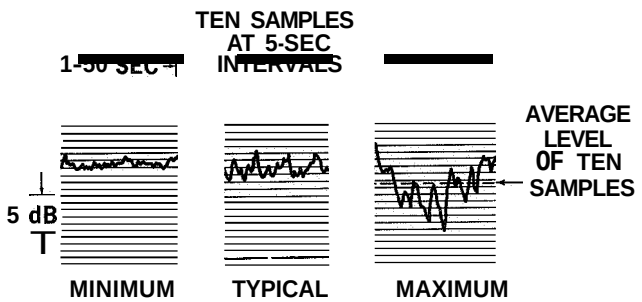

Figure 7

TWO-RING INLET

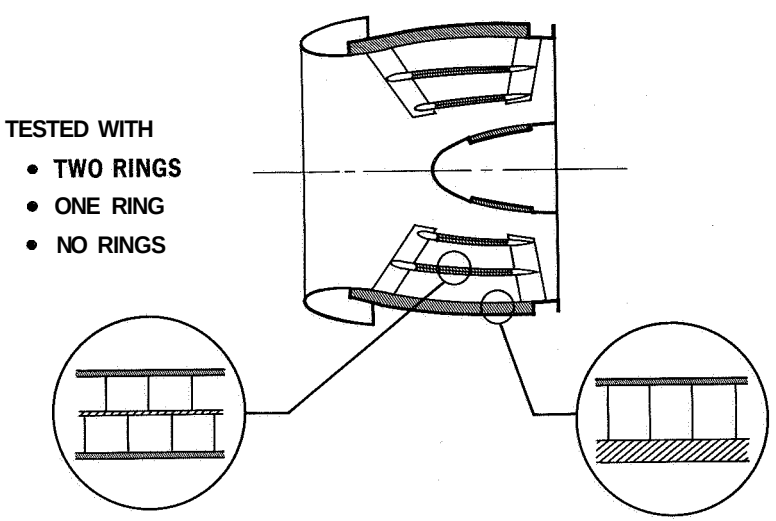

Figure 8

47-PERCENT LIGHTBULB INLET

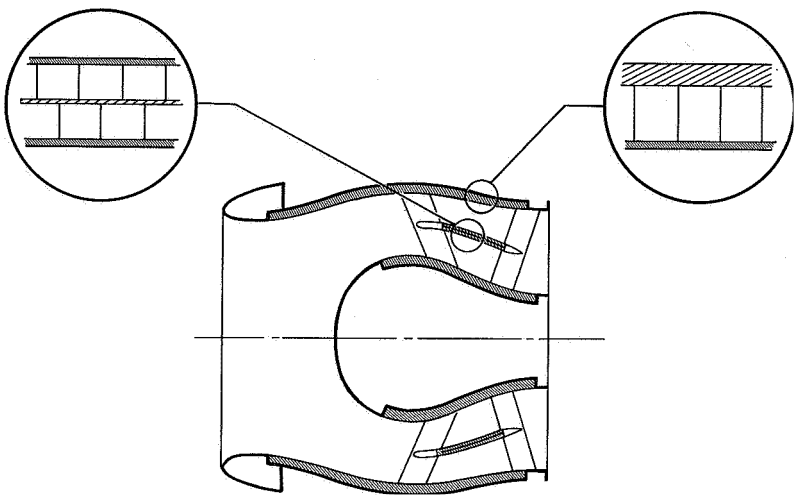

Figure *9*

48-INCH FAN-EXHAUST DUCT§

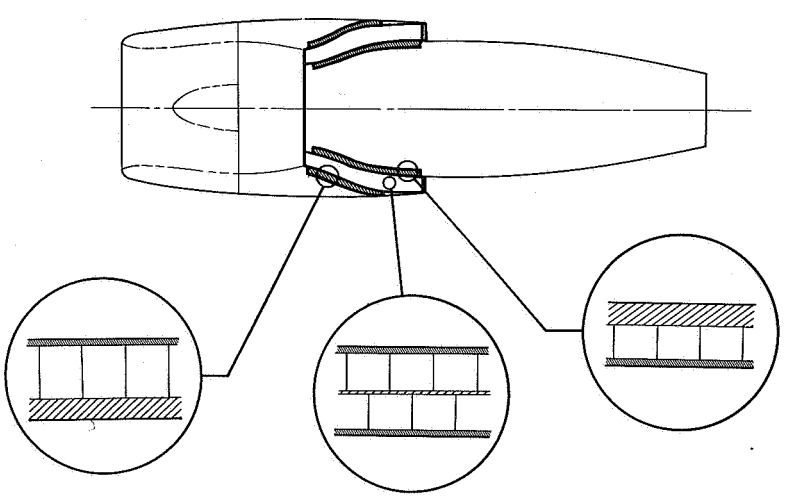

Figure 10

NOISE LEVELS OF EXISTING JT3D ENGINE AIR INLET

DATA AT 60° AND 150-FT RADIUS
FAN-EXHAUST-NOISE SUPPRESSOR ENCLOSURE INSTALLED

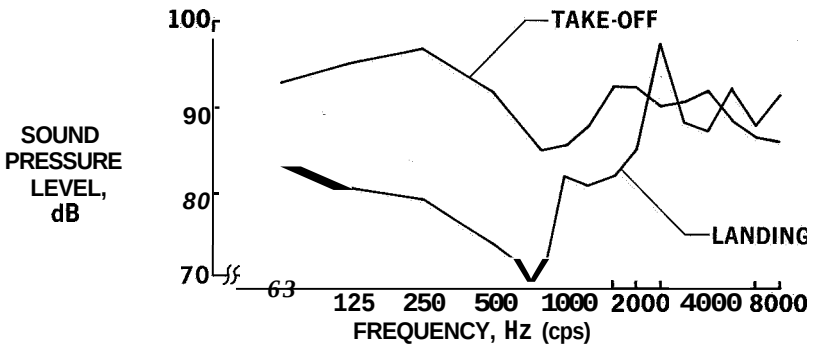

Figure 11

NOISE REDUCTION WITH TWO-RING INLET

DATA AT 60° AND 150-FT RADIUS; LANDING POWER;
FAN-EXHAUST-NOISE SUPPRESSOR ENCLOSURE INSTALLED

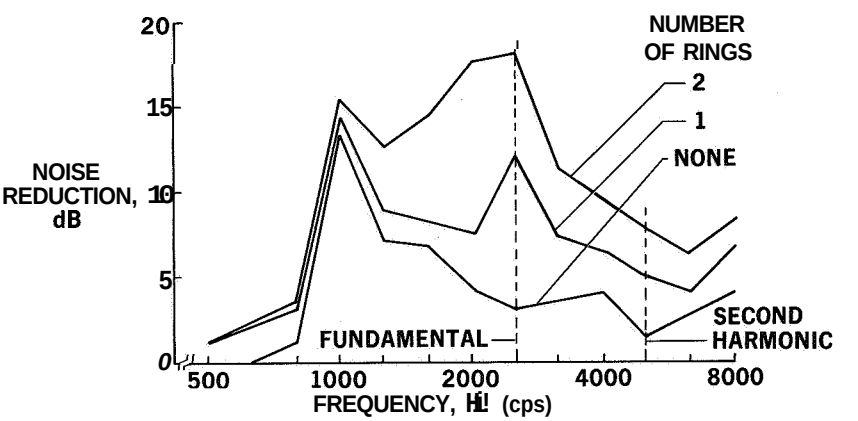

Figure 12

NOISE REDUCTION WITH TREATED INLETS

DATA AT 60° AND 150-FT RADIUS; LANDING POWER;
FAN-EXHAUST-NOISE SUPPRESSOR ENCLOSURE INSTALLED

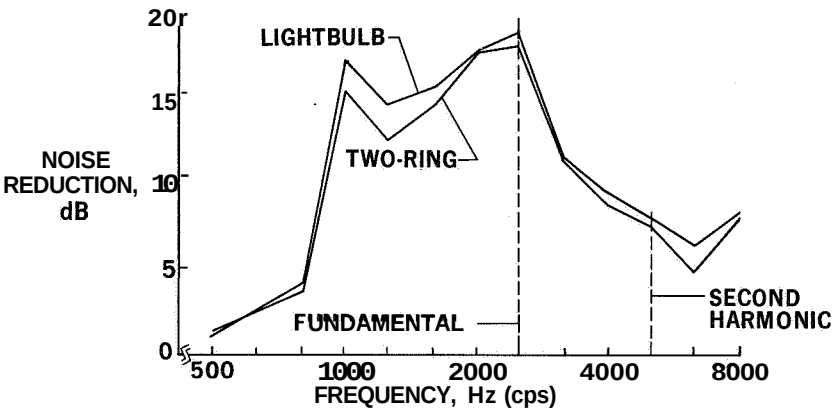

Figure 13

NOISE REDUCTION WITH TREATED INLETS

DATA AT 60° AND 150-FT RADIUS; TAKE-OFF POWER;
FAN-EXHAUST-NOISE SUPPRESSOR ENCLOSURE INSTALLED

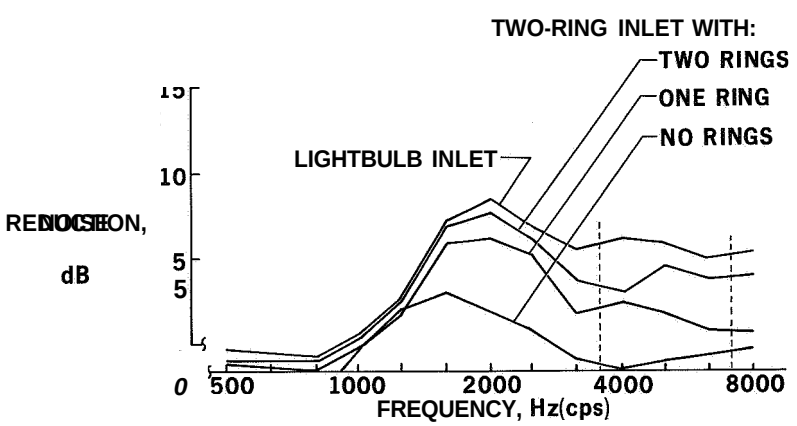

Figure 14

EFFECT OF TREATED INLETS ON THRUST

FAN-EXHAUST-NOISE SUPPRESSOR ENCLOSURE INSTALLED

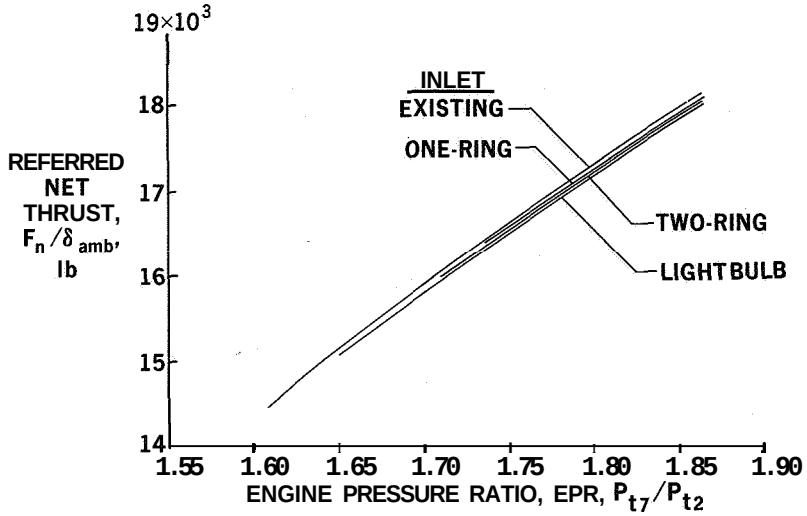

Figure 15

INLET TOTAL PRESSURE PROFILE

JT3D ENGINE WITH ONE-RING TREATED INLET; EPR = 1.795

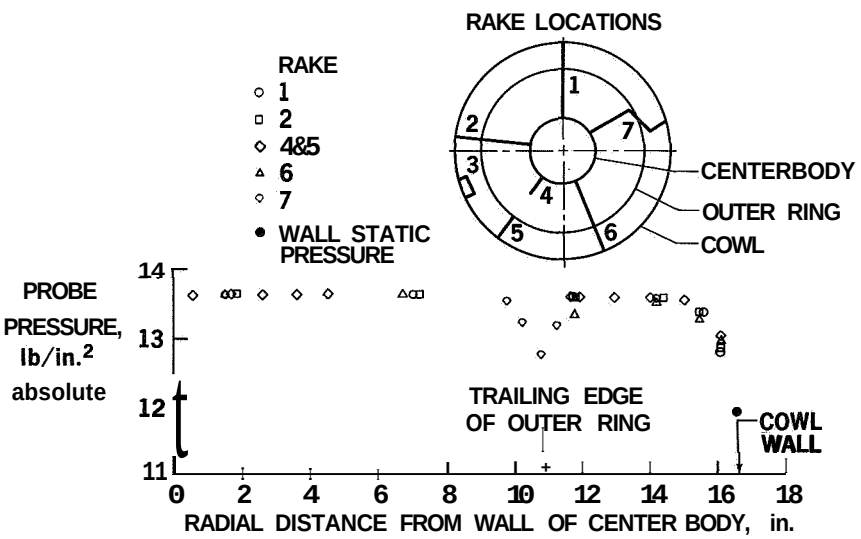

Figure 16

FAN-EXHAUST-DUCT NOISE FROM JT3D ENGINE

DATA AT 110° AND 150-FT RADIUS
INLET-NOISE SUPPRESSOR ENCLOSURE INSTALLED

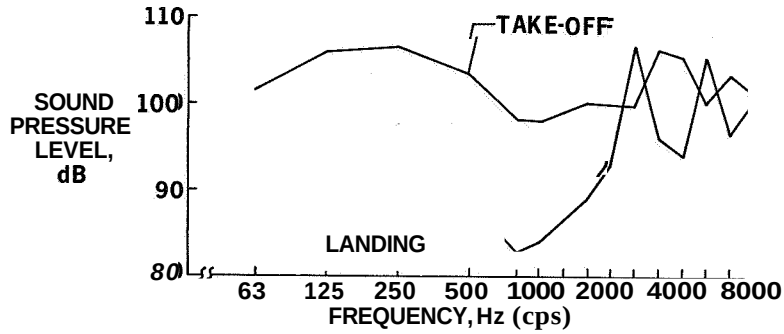

Figure 17

NOISE REDUCTION WITH TREATED FAN-EXHAUST DUCTS

DATA AT 110° AND 150-FT RADIUS;
INLET-NOISE SUPPRESSOR ENCLOSURE INSTALLED

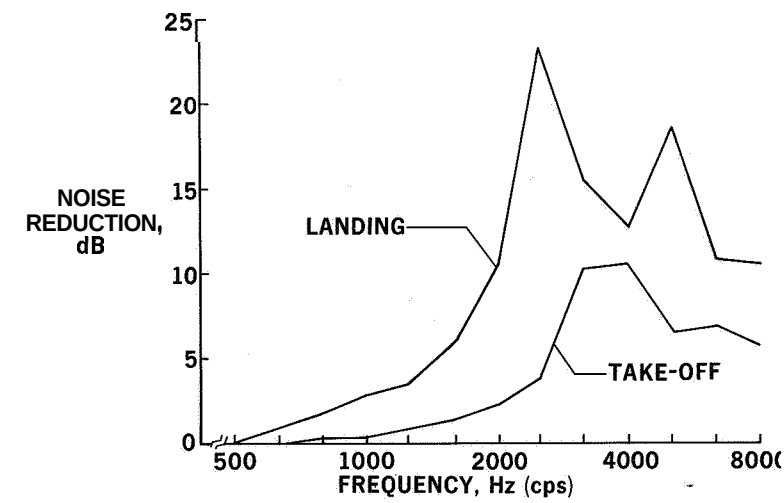

Figure 18

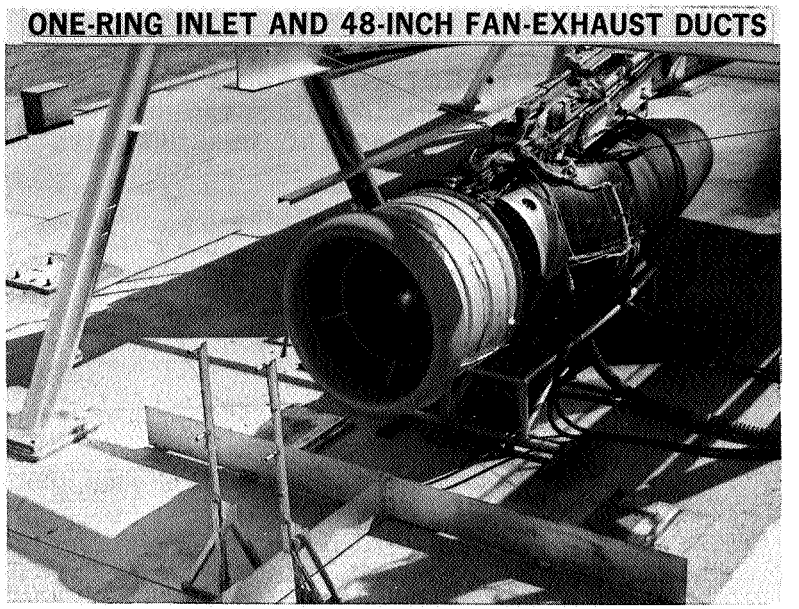

Figure 19 L-68-8560

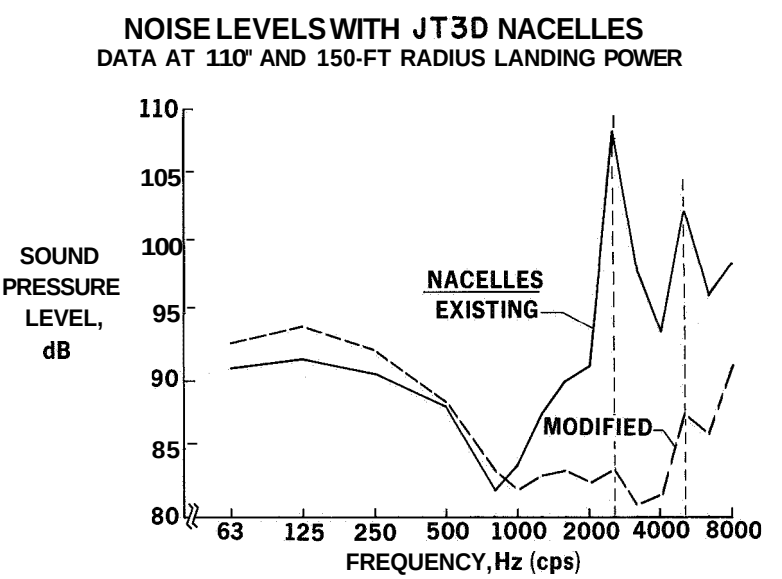

Figure 20

NOISE LEVELS WITH JT3D NACELLES

DATA AT 110° AND 150-FT RADIUS; TAKE-OFF POWER

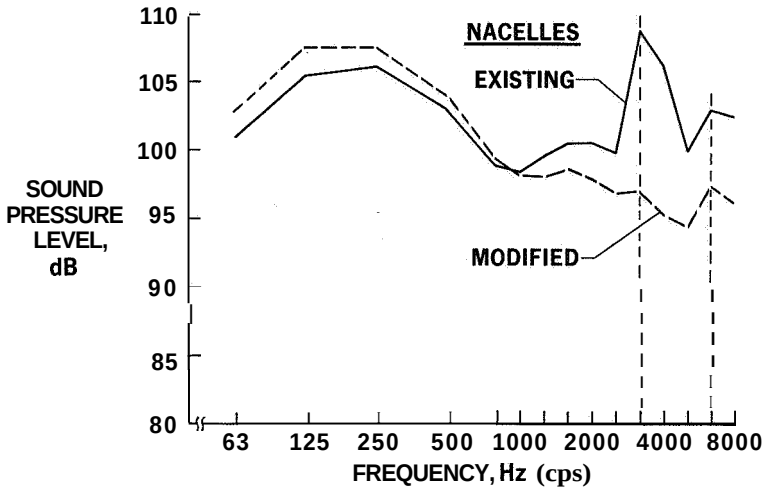

Figure 21

EFFECT OF MODIFIED NACELLE ON THRUST SPECIFIC FUEL CONSUMPTION

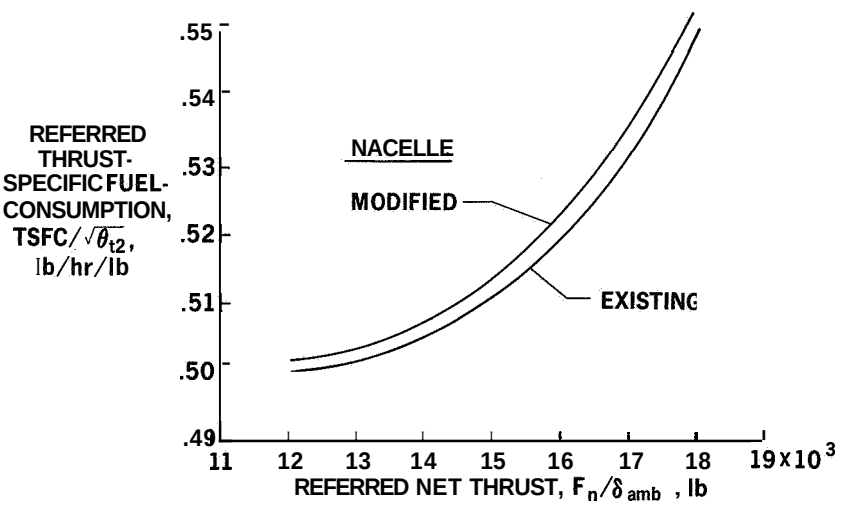

Figure 22

EFFECT OF MODIFIED NACELLE ON THRUST

NO SUPPRESSOR ENCLOSURES AROUND ENGINE

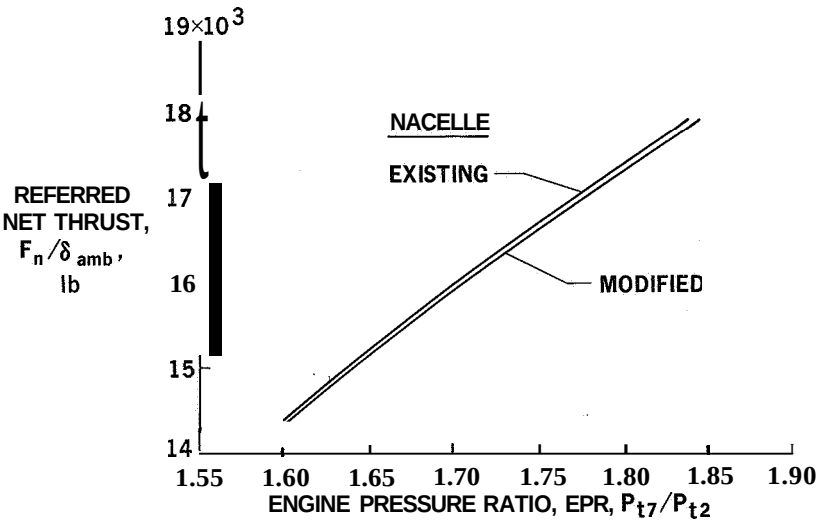

Figure 23

11. FLIGHT-TEST NACELLES

By J. S. Coxon and C. A. Henry
McDonnell Douglas Corporation

SUMMARY

The incorporation of acoustically treated inlet and fan exhaust ducts into present commercial transport aircraft powered by turbofan engines requires redesign of some of the engine nacelle components. During the design of flight-test nacelles intended to validate acoustical design criteria, emphasis has been placed on incorporation of the results of ground tests into the flight nacelle while achieving the most advantageous commonality with the standard short-duct DC-8 nacelle. In addition, the flight-test-nacelle design must provide accurate aerodynamic and acoustic simulations of the nacelle modifications required to retrofit acoustically treated ducting to existing DC-8 airplanes.

INTRODUCTION

On the basis of results of the ground-runup tests reported in reference 1, it was determined that the combination of the one-ring inlet and 48-inch-long fan exhaust ducts would constitute a suitable design for the flight-test phase of the program. This paper discusses the mechanical design of four acoustically treated flight-test nacelles to be installed on a series 55 DC-8 airplane. Particular emphasis is placed on the design requirement that accurate aerodynamic and acoustic simulations of a design suitable for retrofit to present short-duct (24 inches) nacelle DC-8 installations be provided.

DISCUSSION

Flight-Test-Nacelle Design

The inlet duct design incorporates approximately 64 square feet of acoustic treatment on the cowl inner surface, the center body, and both faces of a concentric ring vane located as shown in figures 1 and 2. The overall cowl length of 45 inches is unchanged from the untreated cowl presently in airline service.

The concentric ring vane is supported by four struts attached to the leading edge of the ring and four identical struts attached to the trailing edge, These struts are on the vertical and horizontal center lines of the inlet as shown in figures 2 and 3. The size and shape of the strut reflect the requirement for anti-icing ducting in each strut to provide adequate ice protection for the vane and struts. No operative inlet duct anti-icing system

will be provided for the flight-test nacelles, but space has been made available to assure aerodynamic similarity to the retrofit design.

Because the possibility of increased engine fan-blade vibratory stresses exists with the introduction of the wakes from the ring and struts into the engine inlet, a ground-test evaluation of the fan-blade stresses will be conducted by the engine manufacturer prior to flight testing of the complete nacelle.

The inlet duct also incorporates a 4^{o} downward rake (fig. 2) to correct for wing upwash, nacelle attitude, and angle of attack. This rake duplicates that of the existing inlet duct.

In the interest of simplicity, the flight-test nacelles do not incorporate a full complement of nacelle subsystems. The pneumatic-system heat exchanger is eliminated, and the air-cooled engine-oil heat exchanger is replaced by a fuel-cooled engine-oil heat exchanger. Past experience and recent analysis have shown that satisfactory flight-test performance may be achieved and that limited but satisfactory aircraft pneumatic services may be obtained by using only the low-pressure engine air-bleed system. However, replacement of the engine-oil heat exchanger may require limitation of generator loading or fuel temperature at take-off to preclude exceeding the manufacturer's engine-fuel temperature limits, The auxiliary air inlet, which normally provides ambient air for these heat exchangers, is retained to assure external aerodynamic similarity but is physically blocked to prevent airflow into the cowl. This condition satisfactorily simulates cruising flight during which little or no external airflow is ducted to these subsystems. The engine performance change resulting from the elimination of the high-pressure engine bleed flow will be analytically estimated.

Application of the acoustical design criteria (ref. 1) to the design of fan exhaust ducts results in ducts 48 inches in length to provide the approximately 70 square feet of acoustical lining. This lining is applied to the ducting interior walls and to both faces of the flow splitters as shown in figure 4. The longer ducts require modifications to the engine power controls, to both engine and nacelle pneumatic ducting, to hydraulic system piping, to the engine bleed ducting, and to the engine overboard drains. Two major nacelle items require redesign: the engine access doors and the fan air thrust reverser. The engine access doors are simulated by 0.125-inch-thick aluminum-alloy sheet with no provision made for quick access to the engine. Space considerations do not permit retention of the cascade-type reverser presently in service. Space provisions have been made for a target-type reverser, but the reverser itself is not provided.

The primary exhaust thrust reverser and its fairing, as well as the primary exhaust nozzle and its fairing, are unchanged. However, the primary exhaust thrust reverser will be made inoperative for the flight-test phase.

The acoustic treatment will consist of a sandwich construction composed of an impervious backing, a honeycomb core material, and a porous facing. The specific materials to be used are listed in table I. The sandwich construction is formed by mechanical bonding of the component parts with an epoxy-resin adhesive.

The addition of acoustically treated inlet and fan exhaust ducts will not increase either cockpit instrumentation or crew workload.

Retrofit-Nacelle Design

Although the design of a nacelle suitable for retrofit to existing short-duct nacelle DC-8 airplanes generally follows the design of the flight-test nacelle, a variety of refinements are necessary to assure the reliability and maintainability essential to commercial aircraft.

The retrofit-nacelle design will incorporate a 45-inch-long acoustically treated inlet duct having 64 square feet of acoustic treatment on the inner cowl wall, the center body, and both faces of a concentric ring vane. Inlet cowl subsystems will be similar to those of airplanes presently in service and will require modifications to assure noninterference with the acoustic treatment. However, the cowl ice-protection system will require extensive modification to provide ice protection for the ring vane and its supporting struts. This system will adhere to the design philosophy of the present cowl lip anti-icing system; that is, all anti-icing will be accomplished by engine bleed air, and ice buildup during worst-case icing conditions will not be permitted to exceed a triangular shape 0.152 inch high by 6 inches long. Sufficient heated air will be provided to the leading edge of the ring vane and struts to obviate the need for ice protection for the acoustic treatment itself. This anti-icing concept, illustrated schematically in figure 5, provides engine bleed air to the cowl lip and center body as in existing systems. Additional engine bleed air will be ducted into the leading edge of the ring vane through integral ducting in the two vertical struts, passing through one-half of the leading-edge circumference and exiting through the two horizontal struts to an overboard exhaust exit. This concept avoids mixing the anti-icing air with inlet airflow and, as a consequence, reduces the possibility of additional inlet performance degradation.

Although the maintainability of the nacelle subsystems will remain essentially unchanged, the addition of acoustically treated inlet and fan exhaust ducts will necessitate maintenance requirements in two areas – namely, access to the engine and maintenance of the acoustic treatment. Access to the engine fan blades for routine inspection and minor maintenance will be possible only by removal of 'the entire inlet cowl as a unit. However, access to the engine gearbox and accessories will be provided by an additional joint in the 48-inch-long fan air exhaust ducts. The forward section of the ducts will be

removable in the same manner as the ducts presently in service, while the aft section will be hinged in a manner similar to the engine access doors. The acoustic treatment will require occasional cleaning to remove contaminants as well as repair when damaged by foreign objects ingested into the inlet.

The target-type fan air thrust reverser necessitated by space considerations consists of a hydraulically actuated single-panel deflector mounted on each side of the nacelle. Although the overall nacelle design benefits from the reduced weight of this type of reverser, a reduction in overall thrust-reverser effectiveness will be incurred. However, predicted overall effectiveness is comparable to that of the series 62 DC-8 airplane presently in airline service.

Although a broad variety of acoustic treatment materials are under investigation, the acoustic treatment will be of the general type used for the flight-test nacelles. For purposes of design analysis and cost, the materials of table I have been assumed, with the following exceptions:

Component	Impervious backing in –	
	Flight-test nacelle	Retrofit nacelle
Inlet center body	Fiber-glass laminate	Aluminum
Fan exhaust duct walls	Fiber-glass laminate	Titanium

The magnitude of the effort required to retrofit an acoustically treated nacelle to a JT3D-3B powered short-duct DC-8 airplane is briefly summarized in the following table:

Items changed:
- Air inlet and center body
- Fan exhaust ducts
- Fan air reverser
- Engine power controls
- Engine access doors
- Moderate revisions to engine piping and to hydraulic and pneumatic nacelle systems

Items unchanged:
- Engine mounts (fore and aft)
- Primary reverser and fairing
- Primary nozzle and fairing
- Pylon structure
- Pylon piping and electrical systems
- Pylon-nacelle interfaces
- Cockpit controls and instruments

CONCLUDING REMARKS

Although the nacelle modifications required to retrofit acoustically treated inlet and fan exhaust ducts to present DC-8 airplanes appear relatively extensive, the anticipated modifications do not introduce any insurmountable design or development problems. The simulation of the retrofit nacelles by simplified flight-test nacelles appears practical and promises to provide validation of the acoustic design during the flight-test phase in early 1969. These flight tests will provide final data on the acoustical and performance effects of the nacelle modifications developed in this study.

REFERENCE

1. Marsh, Alan H.; Zwieback, E. L.; and Thompson, J. D.: Ground-Runup Tests of Acoustically Treated Inlets and Fan Ducts. Conference on Progress of NASA Research Relating to Noise Alleviation of Large Subsonic Jet Aircraft, NASA SP-189, 1968. (Paper No. 10 herein.)

TABLE I.- ACOUSTIC-TREATMENT MATERIALS USED IN FLIGHT-TEST NACELLES

Component	Impervious backing	Honeycomb	Porous facing
Cowl	Aluminum	3/4-inch cell, 3/4-inch-deep HRP fiber glass	0.040-inch-thick 10-ray1 fiber metal
Center body	Fiber-glass laminate	3/4-inch cell, 3/4-inch-deep HRP fiber glass	0.040-inch-thick 10-ray1 fiber metal
Ring vane	Steel	3/4-inch cell, 1/2-inch-deep HRP fiber glass	0.040-inch-thick 10-ray1 fiber metal
Inboard wall	Fiber-glass laminate	3/4-inch cell, 1/2-inch-deep HRP fiber glass	0.040-inch-thick 8-ray1 fiber metal
Outboard wall	Fiber-glass laminate	3/4-inch cell, 3/4-inch-deep HRP fiber glass	0.040-inch-thick 8-ray1 fiber metal
Splitters	Steel	3/4-inch cell, 1/2-inch-deep HRP fiber glass	0.040-inch-thick 8-ray1 fiber metal

ACOUSTICALLY TREATED FLIGHT-TEST TURBOFAN NACELLE

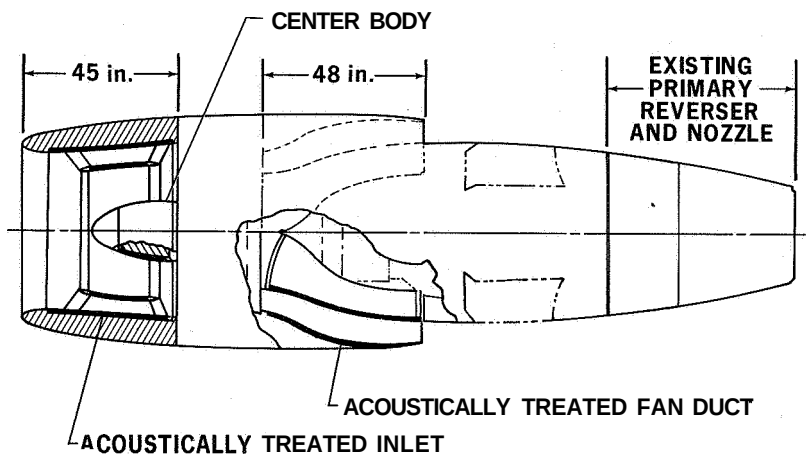

Figure 1

ONE-RING INLET

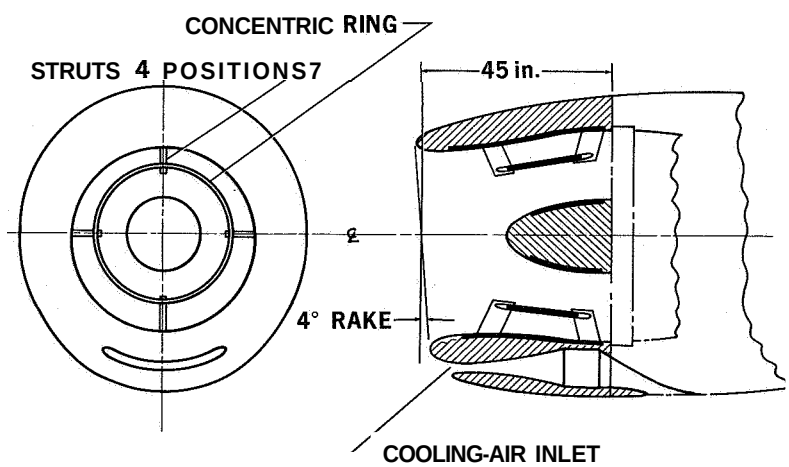

Figure 2

ACOUSTICALLY TREATED TURBOFAN ENGINE INLET

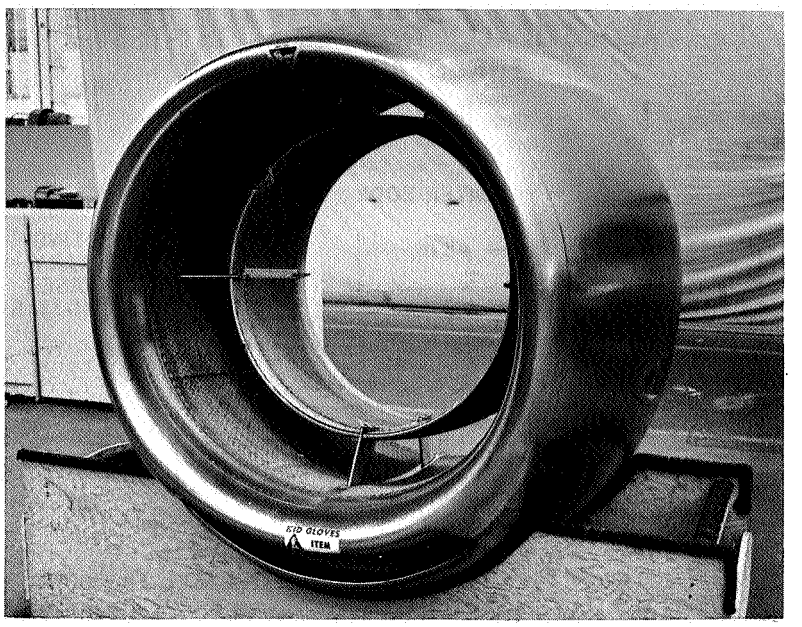

Figure 3 L-68-8563

FAN-DUCT INNER WALL AND FLOW SPLITTERS

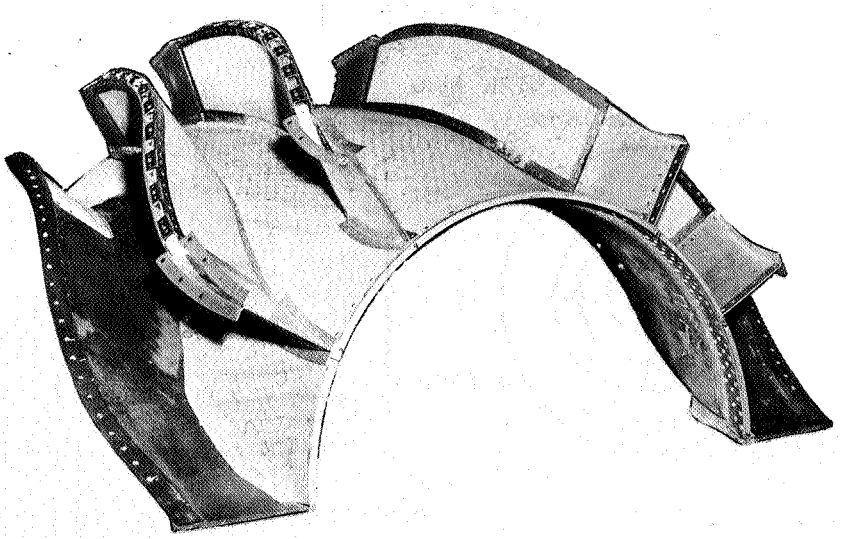

Figure 4 L-68-8564

INLET ICE-PROTECTION CONCEPT

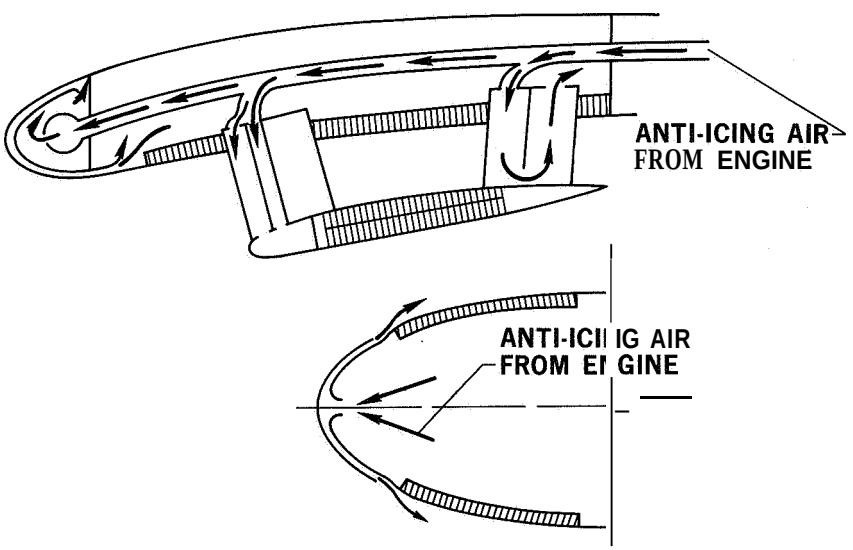

Figure 5

12. NOISE PREDICTIONS AND ECONOMIC EFFECTS OF NACELLE MODIFICATIONS TO MCDONNELL DOUGLAS DC-8 AIRPLANES

By Robert E. Pendley and Alan H. Marsh
McDonnell Douglas Corporation

SUMMARY

Techniques are described that were used for predicting the perceived-noise levels produced by DC-8 airplanes equipped with existing nacelles and with the modified nacelles selected for flight testing. For the landing-approach case with a DC-8 at maximum landing weight at a location 1 nautical mile from the runway threshold, the modified nacelles were predicted to produce a peak instantaneous perceived-noise level that would be about 11 PNdB less than that produced by an airplane equipped with the existing nacelles. The tolerances estimated for the predictions indicate that the reduction expected may be as small as 6 PNdB or as large as 14 PNdB. No change was predicted for the peak perceived-noise level during take-off.

The economic effects of modification to the existing nacelles, in terms of direct operating costs, were estimated by using a method of the Air Transport Association of America with engine-performance data from the test stand extrapolated to flight conditions and with the estimated effects of the modified nacelles on drag. This paper describes the basic assumptions used in the calculations and shows the effects that the nacelle modifications have on the various elements of the direct operating costs. The most significant cost increase is in the acquisition and depreciation of the modified nacelles. The total increase in direct operating costs was about 5.7 percent.

These noise predictions and estimated economic effects apply only to the specific engine and nacelle design considered. Substantial differences may exist in the effects of duct linings on other JT3D installations or on installations of other turbofan engines.

INTRODUCTION

References 1 and 2 described the design, development, and testing of various acoustically treated inlet and fan-exhaust ducts for the JTSD engine. The tests were conducted on an engine test stand where far-field sound-pressure levels (SPL) and engine performance were measured for various configurations of treated inlet and fan-exhaust ducts and for the reference DC-8 inlet and fan-exhaust ducts. On the basis of these measurements, an inlet and fan-exhaust-duct configuration was selected for fabrication and testing in the flight-test program presented in reference 3.

This paper presents predictions of the flyover perceived-noise levels (PNL) produced by DC-8 airplanes equipped with nacelles modified to the configuration selected for the flight-test program. The estimated economic effects of airline operations with the modified nacelles are also presented. The noise predictions and estimated economic effects are based on the acoustical and engine-performance data obtained during the ground tests (ref. 2).

Economic effects were estimated in terms of changes to retrofit costs and to direct operating costs (DOC). In order to estimate DOC's, engine-performance data measured during the ground tests were extrapolated to flight conditions by standard methods. The basic method of calculating DOC's was patterned after that of reference 4. The effects of the modified nacelles on drag were also estimated by standard methods.

SYMBOLS

DOC	direct operating cost, cents/(seat-statute mile)
EPR	engine pressure ratio, P_{t7}/P_{t2}
FAA	Federal Aviation Administration
N_1	low-pressure rotor speed, revolutions/minute (rpm)
$N_1/\sqrt{\theta_{t2}}$	referred low-pressure rotor speed, rpm
PNL	perceived-noise level, perceived-noise decibels (PNdB)
ΔPNL_{peak}	difference between peak value of instantaneous perceived-noise level of an airplane equipped with existing nacelle installation and peak value of instantaneous perceived-noise level of an airplane equipped with acoustically treated nacelles, PNdB
Pt2	total air pressure at engine inlet, pounds/square foot absolute
P_{t7}	total air pressure at inlet to primary-exhaust duct, pounds/square foot absolute
SPL	sound-pressure level, decibels (dB) re 0.0002 microbar
$T_{amb\ std}$	standard-day ambient air temperature, 518.7° Rankine

T_{t2} total air temperature at engine inlet, degrees Rankine

θ_{t2} temperature ratio, $T_{t2}/T_{amb\ std}$

DISCUSSION

Noise-Prediction Techniques

A general description of the noise-prediction techniques used by McDonnell Douglas was given briefly in reference 5. The approach selected took the averaged 1/3-octave-band SPL's, measured on a 150-foot circular arc centered at the exit of the primary exhaust nozzle, and projected them to various sideline distances, that is, to lines drawn parallel to the engine axis at selected distances from 200 to 3000 feet. These sideline projections were made along radial lines, assuming the source of sound to be at the primary exhaust nozzle, by applying corrections to the observed SPL's to account for inverse-square loss and atmospheric absorption. Atmospheric-absorption corrections for the 1/3-octave-band SPL's were determined for an air temperature of 77° Fahrenheit and a relative humidity of approximately 62 percent by using data obtained from reference 6 and by incorporating the modifications of reference 7. No corrections were included for any absorption due to ground effects.

Initial estimates of the flyover SPL's for selected flight conditions were obtained by interpolating the SPL's for each band between the available ground-runup engine-power settings. For example, at the landing power setting of 5000 pounds of referred net thrust per engine, interpolations were made at the referred low-pressure rotor speed $N_1/\sqrt{\theta_{t2}}$ of 4680 rpm and an engine-pressure ratio (EPR) of 1.21. In order to obtain estimates of the SPL's at the take-off power setting (14 500 pounds of referred net thrust per engine at the selected flight condition), the data were extrapolated, beyond the 6300-rpm condition used as the highest engine-power setting in the ground-runup tests, to a referred low-pressure rotor speed of 6500 rpm and an EPR of 1.81.

Estimates of the variation of the SPL with time during a flyover were next made by assuming that the projected sideline SPL's were representative of an airplane flying in straight and level flight over an observer on the ground. These estimates were made for each of the twenty-three 1/3-octave bands and for each of the nine engine-power settings used for the ground-runup tests. By assuming a constant airplane speed (a Mach number of 0.25 or about 280 feet/second), estimates were obtained for 0.25-second intervals of the variation of the 1/3-octave-band SPL's with time during the simulated flyover.

The critical problem in making the interpolations and extrapolations from the ground-runup data was in the selection of the appropriate parameter or parameters. The problem was complicated by the requirement to produce the correct shape, as well as the

amplitude, of the flyover noise spectrum to obtain correct perceived-noise levels. High-frequency noise (for example, frequencies greater than 800 Hz) from the existing, unsuppressed JT3D nacelle is, presumably, related to fan-blade tip Mach number and, hence, was assumed to be a function of $N_1/\sqrt{\theta_{t2}}$. The low-frequency noise (for example, frequencies less than 800 **Hz)** was assumed to be a function of jet-exhaust velocity (or relative jet-exhaust velocity), since previous studies of turbojet engine noise had indicated that the jet-exhaust-velocity parameter produced reasonable correlation between predicted and measured values within this frequency range.

Two problems arose with attempts to utilize the exhaust-velocity parameter. First, the definition of the jet velocity was that derived from the thermodynamic fully expanded velocity determined from the EPR, the turbine-discharge total temperature, and the airplane Mach number. Exhaust velocity, determined in this manner, was representative only of the primary nozzle; the velocity of the air exhausted from the fan-discharge ducts was neglected.

The second problem was that predictions of the flyover SPL spectra from ground-runup SPL measurements of the reference JT3D-powered DC-8 airplanes did not always agree well with measured flyover SPL spectra. At some thrust settings, the predicted SPL's were higher than the measured values; at others, they were lower. Many attempts, using other engine parameters, were made to determine a method that would produce acceptable spectral estimates over a range of engine-power settings.

After considerable experimentation involving comparisons of predictions from ground-runup measurements to actual flyover SPL's (using data from JT3D- and JT8D-powered airplanes; for example, DC-8's and DC-9's), the parameter selected for making spectral estimates for each of the 1/3-octave bands between 50 and 8000 Hz was $N_1/\sqrt{\theta_{t2}}$. Empirical corrections were applied to the initial estimates of the flyover SPL's, for the 1/3-octave bands between 50 and 630 **Hz,** so that the predicted SPL's at the time associated with the maximum value of the instantaneous PNL for the existing JT3D-powered airplane would be close to previously measured values. In order to determine these empirical corrections, comparisons were also made with "composite" spectra consisting of the maximum 1/3-octave-band SPL's noted during a flyover.

The predicted flyover SPL's were adjusted to account for the difference in level owing to four engines by adding 6 dB to all 1/3-octave-band SPL's. Finally, the perceived noisiness of the predicted flyover SPL's, for a given flight condition, was determined by making use of the tables from reference 8 to convert the SPL's to noisiness values. **A** large-capacity digital computer was programed to carry out the computations described.

Selection of Noise-Rating Unit

Probably, most of the airplane noise analyses that have been conducted in the past have been in terms of "composite" PNL's. Composite PNL's are computed from the maximum SPL readings in 1/1- or 1/3-octave bands, irrespective of the times of occurrence of the maximum values. Composite PNL's are the most readily obtainable and require the least sophisticated data-reduction system. "Instantaneous" PNL's are calculated from SPL spectra determined at discrete, closely spaced intervals of time from the beginning to the end of a flyover noise cycle. Both instantaneous and composite PNL's can be determined from the conversion tables in reference 8.

In recent years, it has been suggested that corrections should be applied to the PNL to account for the varying duration of flyover noise exposures and for the presence of intense discrete-frequency components in the spectrum. Proposed techniques for incorporating these effects have been based on instantaneous PNL. (See refs. 9 to 11.)

Noise reductions predicted for the suppression systems are generally larger with peak instantaneous PNL's than with composite PNL's. This fact is due to the relatively greater low-frequency SPL's from the jet-exhaust noise in the composite spectrum than in the spectrum obtained at the instant of the peak PNL. The contribution of these low-frequency sounds to the annoyance of the total spectrum is relatively more important for the sound from the modified nacelles than that from existing nacelles. However, reductions in peak instantaneous PNL's will probably fall between those that would be estimated by using composite PNL's and those estimated by using PNL's with tone and duration corrections.

Instantaneous PNL's were specified to judge the noise-reduction benefits to an airport community because, at the present time, methods for calculating the tone and duration corrections have not been standardized. Specifically, to determine compliance with noise-reduction goals, the difference (referred to as ΔPNL_{peak}) between the peak values of the instantaneous PNL's of the existing and the modified nacelles was calculated for selected altitudes and engine-power settings.

The PNL's used for rating the noise-suppression systems were calculated from the SPL's estimated for an outdoor location. PNL's calculated for interior locations within homes may be more relevant to judgments of the actual effectiveness of noise-suppression systems for airplanes. Typical wall transmission-loss data determined for residential structures (ref. 12) were used to obtain estimates of indoor PNL's.

Limitations and Accuracy of Predictions

The limitations of the flyover noise-prediction technique are rather severe principally because of the nature of the assumptions required and the use of empirical

correction factors. The assumptions and empirical corrections have been tested in a few cases by comparing measured data (a) to predicted flyover peak instantaneous PNL's and corresponding 1/3-octave-band SPL's, and (b) to predicted composite PNL's and corresponding maximum 1/3-octave-band SPL's. Therefore, a reliable estimate of the accuracy of the prediction technique can be made only for airplanes equipped with the existing nacelles.

For existing airplanes, the accuracy of the prediction is such that the peak instantaneous PNL's are estimated to be within ±2 PNdB of the average measured values determined from a series of flyover noise tests, suitably corrected to standard conditions. For airplanes equipped with modified nacelles, the estimated accuracy is at best ±3 PNdB. However, since there is no in-flight experience with the suppression system, the jet exhaust noise may well prevent the actual PNL's from being less than the predicted values. Hence, the estimated accuracy of the PNL predictions for the modified nacelles is +3, -1 PNdB.

Noise Predictions

Landing approach.- The conditions specified in reference 5 for the landing-approach-noise comparison were for 1 nautical mile from threshold, on a day with a temperature of 77° F, with no winds, for a runway at sea level, and with a 3° glide slope to a 50-foot height over the runway threshold. The airplane configuration was for maximum landing weight with flaps full down. The altitude of the airplane at 1 nautical mile from threshold is about 370 feet.

The predicted instantaneous PNL's for the specified landing conditions are shown in figure 1 as a function of time during the flyover. The time scale is relative to an arbitrary zero reference time representative of when the airplane would be approximately directly overhead. The 8-second-time interval shown represents the azimuth limits of 15° to 157° on the 150-foot arc used for the static tests.

The peak-to-peak change in PNL indicated by the predictions in figure 1 is about 11 PNdB between the maximum values of the data represented by the solid- and dashed-line curves. The accuracy of the estimates is shown by the shaded areas around the lines. With the accuracy estimates as shown, the peak-to-peak PNL change that will ultimately result from the flight tests of the modified nacelles could be as much as 14 PNdB or as little as 6 PNdB.

The spectra of the SPL's at the time of peak PNL for an altitude of 370 feet are shown in figure 2. The 1/3-octave bands containing the fundamental and the second harmonic of the blade-passage frequencies are marked by the dashed lines at 2500 and 5000 Hz. The SPL in the 2500-Hz band is about 20 dB less with the modified nacelle than with the existing nacelle; in the 5000-Hz band, the SPL is about 10 dB lower with the

modified nacelle. The SPL in the 1250- and 1600-Hz bands containing the "Combination-tone" frequencies (see discussion in ref. 2) is 4.5 to 5 dB lower with the modified nacelle.

The 1- to 2-dB increase in the low-frequency SPL's (50 to 630 Hz) is of the same order of magnitude as noted in the ground-runup tests. As mentioned in reference 2, this increase in low-frequency noise can probably be attributed to the 24-inch lengthening of the fan-exhaust ducts in the direction of the primary-exhaust nozzle. This lengthening modifies the interaction between the turbulent exhaust flow from the fan ducts and the turbulent flow from the primary nozzle and hence modifies the noise generation process.

Take-off.- The conditions selected for comparison of the noise levels during take-off were: a location 3.5 nautical miles from the start of the take-off roll (brake release), maximum gross take-off weight, 15° flap setting, landing gear retracted, and full take-off thrust. Atmospheric and other parameters were the same as specified for the landing-approach condition. Under these conditions, a 325 000-pound DC-8 airplane will attain an altitude of about 900 feet at the 3.5-nautical-mile point. The altitude attained by the same airplane equipped with the modified nacelles will be about 835 feet if it is assumed that there is a 2.75-percent decrease in rated take-off thrust, as described in reference 2, and a 0.4-percent reduction in scrubbing drag forces.

Estimated instantaneous PNL's for the take-off condition are shown in figure 3. The reference time is again when the airplane is approximately directly overhead. The peak PNL from the modified nacelle occurs about 3 seconds after the peak PNL from the existing nacelle. Essentially no change is indicated for the value of the peak instantaneous PNL, although the duration of the top 10 PNdB of the predicted PNL history is less with the modified nacelles than with the existing nacelles. The shaded areas represent the same accuracy estimates shown in figure 1.

The predicted SPL spectra at the times of the peak instantaneous PNL's are shown in figure 4. The large reductions at the fundamental and the second harmonic of the blade-passage frequencies (indicated by the dashed lines at 4000 and 8000 Hz) and the significant increases in low-frequency SPL's are due to (a) the effects of the selected configuration of the modified nacelle and (b) the difference in the relative times associated with the two spectra. The 3-second difference between the two peak values probably accounts for most of the indicated increase in the law-frequency SPL's and for the indicated decrease in the high-frequency SPL's.

The data shown in figures 3 and 4 are for the specified take-off condition. For airplanes taking off at less than maximum gross weight (probably almost all of the domestic flights and also most of the international flights), there probably will be some reduction in the peak instantaneous PNL since most of the airplanes will reach an altitude where a safe thrust reduction can be made before reaching the 3.5-nautical-mile point.

If the thrust is reduced to that required to maintain a 6-percent climb gradient (about 1000 feet/minute), then some reduction in annoyance may be obtained owing to (a) the reduction in jet-exhaust noise caused by making the thrust reduction and to (b) the reduction of the SPL's at the blade-passage frequencies caused by addition of the acoustical duct linings.

Variation of PNL with distance and thrust.- The variation of the reduction in peak PNL with distance from threshold during the landing approach is shown in figure 5. The reductions are shown to a distance of 7 nautical miles from threshold where the airplane is about 2300 feet above the ground. The reduction is approximately constant to 5 nautical miles and then begins to decrease rather rapidly. No data are presented for the take-off case because essentially no change was predicted for the peak PNL for airplanes at full take-off thrust and at distances of 800 feet or more.

The variation with distance to the airplanes of the estimated peak instantaneous PNL's is given in figure 6 for airplanes equipped with the existing and modified nacelles. This type of presentation shows directly the effect of the suppression system on the noise produced by the existing nacelle installation without consideration of the effect of the acoustical linings on airplane performance. Data are presented for full take-off thrust and for a landing thrust corresponding to maximum landing weight. The same trends noted previously are evident in figure 6; namely, larger reductions are obtained at the landing power setting than at the take-off power setting, and the reductions decrease as the distance to the airplane increases, either directly under the flight path or to the side of the runway.

The data in figure 6 also provide an indication of the changes in PNL that would be expected to the side of the airplane flight path in the vicinity of the airport. For example, at a point about 3000 feet to the side of the runway (assuming that the airplane is just high enough so that ground attenuation effects are not important), the PNL during take-off at full take-off thrust would remain unchanged at about 104 PNdB. During the landing approach, however, the PNL at 3000 feet to the side of the landing path would be reduced from about 92 to about 84.5 PNdB. It is worthwhile to note that, of those airport neighbors who are concerned only with approach noise, the people exposed to the higher values of PNL will experience the larger noise reductions.

The estimated PNL's and PNL reductions which have been presented thus far have all been those which would be experienced outdoors. Because typical house structures attenuate high-frequency noise to a greater degree than low-frequency noise, the low-frequency noise of the JT3D contributes relatively more to the PNL's indoors than to the PNL's outdoors. Thus, suppression of the high-frequency fan noise at the source will generally result in less change to the PNL indoors than outdoors.

Figure 7 presents estimates of the peak instantaneous PNL's that might be experienced inside a dwelling with windows closed. The noise reduction of the structure and insulation of the dwelling was taken from reference 12 and should be representative of modern frame houses located in temperate climates with mild winters. The PNL's inside the dwelling are 22 to 25 PNdB lower than those experienced outdoors (fig. 6) for the same thrust and distance to the airplane. For homes with more insulation (for example, in colder climates), the PNL's at corresponding points will be somewhat lower than those shown in figure 7.

The variations with distance to the airplane of the estimated reduction in peak PNL, at the same landing power setting used in figures 6 and 7, are shown in figure 8 for the noise reductions perceived outdoors and indoors. For the house construction assumed, the reduction indoors is about 2 PNdB less than the reduction outdoors. As pointed out previously, there is a considerable tolerance on the estimated reductions that may be achieved at low altitudes outdoors. The tolerances on the estimates at greater distances and indoors would necessarily be larger. More reliable data to assist in assessing the subjective merits of the suppression system must await flight tests.

Direct Operating Cost Estimates

Direct operating costs have been estimated for JT3D-3B-powered DC-8-55 airplanes equipped with the existing production short-duct nacelles and with the nacelles modified to the retrofit configuration discussed in reference 3. The calculations were based on the method of reference 4 but modified to reflect the specific nature of a retrofit program.

The incremental direct operating cost estimates presented in reference 1 are not consistent with the DOC data presented in this paper. The estimates of reference 1 were made with the aid of change factors that relate changes in DOC to independent changes in weight, drag, and specific-fuel consumption. The change factors included allowances for all elements of DOC. Insurance, maintenance, and depreciation changes were related by simple functions of the weights of new components added to the nacelles. These functions were developed on the basis of 1966 dollar levels and assumed different values of depreciation interval and residual value compared with the more detailed DOC calculations presented in this paper. Similarly, consistency should not be expected in the weight increments quoted herein and those in reference 1, since the weight data presented in this paper are based on later and more detailed design and weight studies.

Basic assumptions used in the calculations are listed in table I. The cost of retrofit includes the cost (for four engines) of new nacelle and engine parts and the cost of installation. The retrofit cost is based on a production run of retrofit kits for 300 airplanes. No salvage allowance was assumed for replaced parts. Depreciation was

computed in two parts for the retrofitted airplane. The depreciation expense for the basic unmodified airplane was assumed (1965 price depreciated over a 12-year interval) plus the additional depreciation expense resulting from amortization of the retrofit and retrofit spares costs over a 5-year interval. Utilization was treated as a variable dependent upon trip block time (fig. 4 of ref. 4). A typical mixed-class seating configuration of 135 seats was used. In an all-tourist configuration at 34-inch seat pitch, the DC-8-55 can accommodate 189 passengers. A 20-percent allowance for initial spares applies to nacelle retrofit kit parts. The initial-spares rate assumed for the new engine parts was 40 percent. It was assumed that the kits will be installed on engines at overhaul or in the spares inventory, and thus will require no airplane out-of-service time for installation.

Incremental maintenance costs were estimated on the basis of an analysis of maintenance tasks and on the assumption that further development of acoustical materials and manufacturing methods will produce linings equal in durability to present inlet- and exhaust-duct structure.

Other assumptions in the maintenance cost analysis were as follows:

(a) A frequency of unscheduled inlet- and exhaust-duct maintenance 50 percent higher than that of present ducts

(b) Eight man-hours of labor and 1 square foot of acoustical lining structure per repair

(c) Five man-hours of labor and $35 material cost for lining cleaning every 500 flight hours

The incremental nacelle-maintenance cost estimated in this manner was $1.06 per flight hour.

Effects of the nacelle modifications on basic changes affecting airplane performance are presented in table 11. The change in airplane empty weight is the net effect of the increased weights of the treated inlet and fan-exhaust ducts, the lower weight of the new fan-thrust reversers, and the change in weight owing to the other nacelle items affected by the retrofit (ref. 3).

The 0.6-percent increase in cruise specific-fuel consumption is the change in fuel flow required to produce a given installed engine thrust less the nacelle drag. The decrease in installed engine thrust is due to changes in the internal performance of the inlet and exhaust ducts and to changes in nacelle drag. For the exhaust ducts, the increased total-pressure losses due to the installation of the acoustical linings are offset to some extent by the more favorable aerodynamic lines of the 48-inch ducts. The decrease in nacelle drag is due to the longer fan-exhaust duct. The longer duct reduces the nacelle surface area wetted by the fan-exhaust stream and thus reduces the scrubbing

drag. However, the longer duct increases the nacelle area wetted by the external flow upstream from the fan nozzle and thus increases the free-stream drag. The contributors to the net change of 0.6 percent in specific-fuel consumption include:

(a) Inlet and exhaust-duct losses, 1.0 percent

(b) Scrubbing drag, -0.7 percent

(c) Free-stream drag, 0.3 percent

The change in maximum cruise thrust indicated in table II applies to the maximum-cruise-thrust rating. Most cruise conditions require a thrust sufficiently below the cruise-thrust rating as not to be affected by this change. The 2.1-percent decrease in the maximum-cruise-thrust rating will affect high take-off weight operations if high initial-cruise altitude is required. None of the cruise performance calculated for the data in this paper was affected by the change in maximum-cruise-thrust rating. The change shown in table II differs from that presented in reference 2 because the installed thrust changes presented herein include the effects of the nacelle modifications on the external drag as well as the internal thrust.

It is predicted that the drag-rise Mach number will be unaffected by the modifications. Cruise-speed changes will therefore be required only through the effects of the change in the maximum-cruise-thrust rating discussed previously.

The contributors to the 2.35-percent take-off thrust loss indicated in table II include:

(a) Inlet- and exhaust-duct loss effects, 2.75 percent

(b) Scrubbing drag, -0.4 percent

Payload-range characteristics for the DC-8-55 airplane with the existing and modified nacelles are presented in figure 9. The maximum range for all payloads is reduced approximately 50 nautical miles by the modified nacelles.

The change in weight-limited payload due to the change in nacelle weight is negligible. The reference payload of 30 175 pounds was calculated on the basis of 205 pounds for each of the 135 passengers and his baggage, plus an additional 2500 pounds for the cargo load typically carried in passenger service. For the passenger airplane considered, the full space-limited payload is 36 175 pounds, assuming 165 pounds for each passenger with the cargo compartment filled with cargo and baggage with a density of 10 pounds/cubic foot. The assumed domestic fuel reserves provided for a 1-hour hold at 99-percent maximum specific range at the final cruise weight, 2 minutes at take-off power for a missed approach, and climb, cruise, and descent to an alternate airport 200 nautical miles from the original destination. The use of international fuel reserves would reduce the maximum range approximately 150 nautical miles, but would not

appreciably affect the relative performance of airplanes equipped with the existing and the modified nacelles.

The effect of the modified nacelles on direct operating cost is shown in figure 10 for cruise at standard-day conditions. For ranges up to the value corresponding to maximum take-off weight (approximately 5350 nautical miles), the operating costs will be increased approximately 5.7 percent. At greater ranges, where passengers must be off-loaded in favor of fuel, the operating costs will be increased approximately 12 percent.

A breakdown of the total increase in direct operating cost for a range of 850 nautical miles is shown in table 111. The selected range corresponds to the present average stage length of DC-8 service. The slight increase in crew expense is the result of the small effect of the modifications on time to climb and therefore block speed. Small changes are predicted in insurance, fuel, and maintenance expenses. The largest element of increased operating cost is the increased depreciation resulting from the added capital investment required by the retrofit.

The data presented in figures 9 and 10 were based on the assumption that sufficient FAA runway length was available to permit take-offs at maximum gross weight with the existing and the modified nacelles. The modified nacelles will have more effect on direct operating cost for operations from short runways than from long runways as shown in figure 11. The data presented in figure 11 were calculated for sea-level take-offs at 77° F, and standard-day cruise with the reference payload of figure 9. The points at which the direct operating cost increments rise sharply correspond to the take-off weight limit for the particular runway length available. At ranges beyond those points, payload off-loading is required.

Since much work is necessary to identify the acoustical lining materials and manufacturing and inspection methods required for satisfactory service in routine airline operations, the retrofit cost estimate presented in this paper is somewhat uncertain. Figure 12 is presented to permit assessment of the impact on direct operating cost of possible variations in retrofit cost.

Similarly, figure 13 is presented to permit assessment of the effects of depreciation intervals other than the 5-year interval used in the preparation of figures 10 to 12.

The direct operating cost data presented in this paper apply only to the two specific nacelle configurations analyzed. The degree to which nacelle structure and equipment items must be changed to accommodate the new treated ducts is peculiar to the two particular nacelle configurations studied. The scope of the changes needed to install nacelle modifications with acoustically treated inlet and fan-exhaust ducts may be substantially different for other engine installations. Similarly, the development of satisfactory internal duct lines in other designs may significantly change the external

aerodynamic lines and the cruise drag. A detailed design study and operating cost analysis is needed to assess the impact of applying duct-lining technology to each specific installation of each specific engine model.

CONCLUDING REMARKS

Flyover noise reductions and direct operating cost changes have been predicted for modifications to the nacelles of DC-8 airplanes. These modifications consist of new inlet and fan-exhaust ducts containing acoustically absorptive duct linings. The predictions were based on data obtained on a static outdoor JT3D-engine test stand equipped with the existing nacelles and with simulations of the modified nacelles.

It was predicted that the peak flyover instantaneous perceived-noise level (PNL) would be reduced approximately 11 PNdB directly beneath the landing-approach path of a DC-8 at maximum landing weight, on a 3^{o} glide slope, and 1 nautical mile from the runway threshold. The peak PNL would not be appreciably changed at a point beneath the take-off flight path, 3.5 nautical miles from brake release for an airplane at maximum take-off gross weight and full take-off thrust.

The magnitude of the noise reduction achieved by DC-8 airplanes equipped with the modified nacelles will vary over a considerable range depending on the thrust level of the airplane, the distance to the airplane (either under or to the side of the flight paths), and the construction of the dwelling if the listener is indoors. Those listeners exposed to the highest noise levels from the existing airplanes during the landing approach will experience the largest noise reductions. Although no change is indicated in the peak PNL for those listeners exposed to noise at full take-off thrust, some noise reduction during take-off may be obtained for those airplanes that can make safe thrust reductions during initial climb. Reliable data to assess the subjective effects of the proposed noise-suppression system must await the results of the flyover-noise tests of the modified nacelles.

The methods used in preparing the flyover-noise predictions were recently formulated and have yet to be validated. The accuracy of the present predictions is therefore uncertain, and caution must be exercised in their use. For example, the accuracy of the flyover-noise predictions requires a tolerance on the 11-PNdB predicted reduction in landing PNL such that the predicted change in peak PNL is in the range from 6 to 14 PNdB.

It was estimated that the direct operating costs of the DC-8-55 airplane would be increased approximately 5.7 percent by the retrofit of the nacelle modifications chiefly because of increased depreciation. This increase applies for operations that are not limited by take-off field length or maximum gross weight.

The predicted effects on flyover noise and operating costs apply only to the specific engine and nacelle designs considered. Substantial differences in the design of the modifications and in their effects on noise and operating costs may be expected in the application of duct-lining technology to other JT3D installations and to other installations of other engines.

REFERENCES

1. Pendley, Robert E.: Design Concepts. Conference on Progress of NASA Research Relating to Noise Alleviation of Large Subsonic Jet Aircraft, NASA SP-189, 1968. (Paper No. 9 herein.)

2. Marsh, Alan H.; Zwieback, E. L.; and Thompson, J. D.: Ground-Runup Tests of Acoustically Treated Inlets and Fan Ducts. Conference on Progress of NASA Research Relating to Noise Alleviation of Large Subsonic Jet Aircraft, NASA SP-189, 1968. (Paper No. 10 herein.)

3. Coxon, J. S.; and Henry, C. A.: Flight-Test Nacelles. Conference on Progress of NASA Research Relating to Noise Alleviation of Large Subsonic Jet Aircraft, NASA SP-189, 1968. (Paper No. 11 herein.)

4. Anon.: Standard Method of Estimating Comparative Direct Operating Costs of Turbine Powered Transport Airplanes. Air Transp. Ass. Amer., Dec. 1967.

5. Norton, Harry T., Jr.: Introductory Remarks on Nacelle Acoustic Treatment Application. Conference on Progress of NASA Research Relating to Noise Alleviation of Large Subsonic Jet Aircraft, NASA SP-189, 1968. (Paper No. 8 herein.)

6. Anon.: Standard Values of Atmospheric Absorption as a Function of Temperature and Humidity for Use in Evaluating Aircraft Flyover Noise. ARP 866, Soc. Automot. Eng., Aug. 31, 1964.

7. Harris, Cyril M.: Absorption of Sound in Air Versus Humidity and Temperature. NASA CR-647, 1967.

8. Anon.: Definitions and Procedures for Computing the Perceived Noise Level of Aircraft Noise. ARP 865, Soc. Automot. Eng., Oct. 15, 1964.

9. Kryter, Karl D.: Prediction of Effects of Noise on Man. Conference on Progress of NASA Research Relating to Noise Alleviation of Large Subsonic Jet Aircraft, NASA SP-189, 1968. (Paper No. 34 herein.)

10. Pearsons, Karl S.: Assessment of the Validity of Pure Tone Corrections to Perceived Noise Level. Conference on Progress of NASA Research Relating to Noise Alleviation of Large Subsonic Jet Aircraft, NASA SP-189, 1968. (Paper No. 36 herein.)

11. Kryter, Karl D.; Johnson, P. J.; and Young, J. R.: Judgment Tests of Aircraft Noise. Conference on Progress of NASA Research Relating to Noise Alleviation of Large Subsonic Jet Aircraft, NASA SP-189, 1968. (Paper No. 37 herein,)

12. Bishop, Dwight E.: Reduction of Aircraft Noise Measured in Several School, Motel, and Residential Rooms. J. Acoust. Soc. Amer., vol. 39, no. 5, May 1966, pp. 907-913.

TABLE I.- BASIC ASSUMPTIONS USED IN DOC CALCULATIONS

Cost of retrofit (1972 dollars), dollars	545 500
Depreciation period, yr –	
For airframe	12
For nacelles	5
Utilization	Variable
Seats	135
Initial spares, percent	20
Down time, hr	0
Maintenance of nacelles	Functional analysis

TABLE II.- BASIC CHANGES AFFECTING AIRPLANE PERFORMANCE

Operating empty weight, lb	332
Cruise specific-fuel consumption, percent	0.6
Maximum cruise thrust, percent	2.1
Cruise speed, knots	0
Take-off thrust, percent	-2.35

TABLE III.- DIRECT OPERATING COST INCREASES

[Model DC-8-55; range, 850 n. mi.]

Element	ΔDOC, percent
Crew	0.02
Insurance	.38
Fuel	.40
Maintenance	.56
Depreciation	4.38
Net change	5.74

ESTIMATED PERCEIVED-NOISE LEVEL DURING FLYOVER

ALTITUDE = 370 FT; LANDING POWER

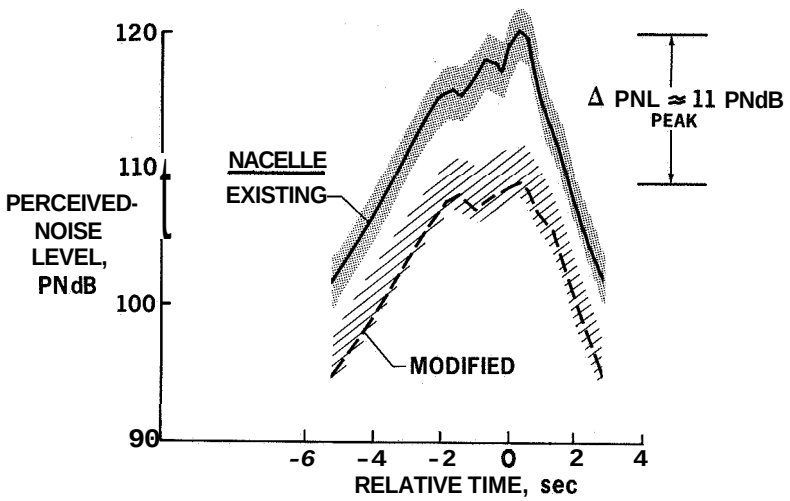

Figure 1

ESTIMATED SPECTRA AT TIME OF PEAK INSTANTANEOUS PNCS

ALTITUDE = 370 FT; LANDING POWER

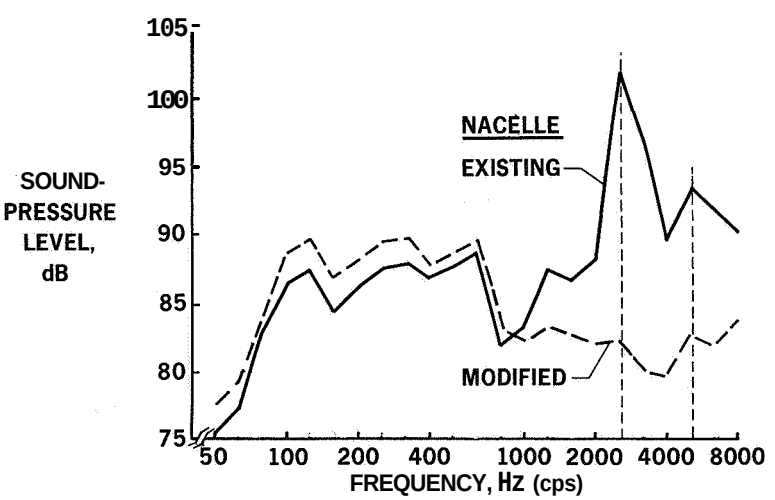

Figure 2

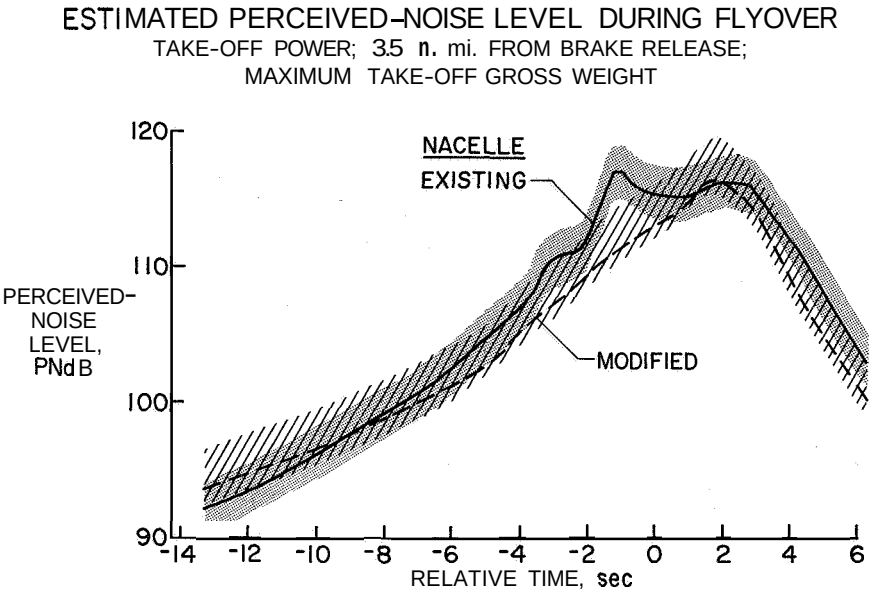

Figure 3

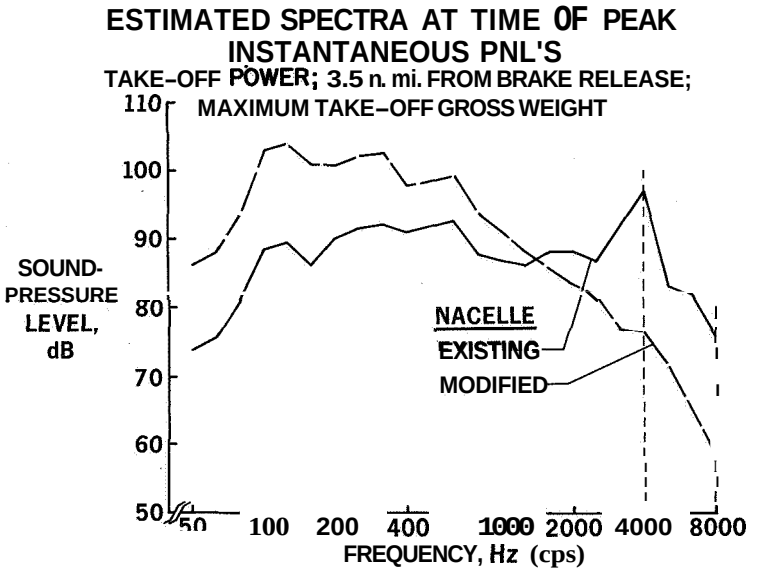

Figure 4

ESTIMATED PERCEIVED-NOISE LEVEL REDUCTIONS UNDER LANDING APPROACH PATH

MAXIMUM LANDING WEIGHT

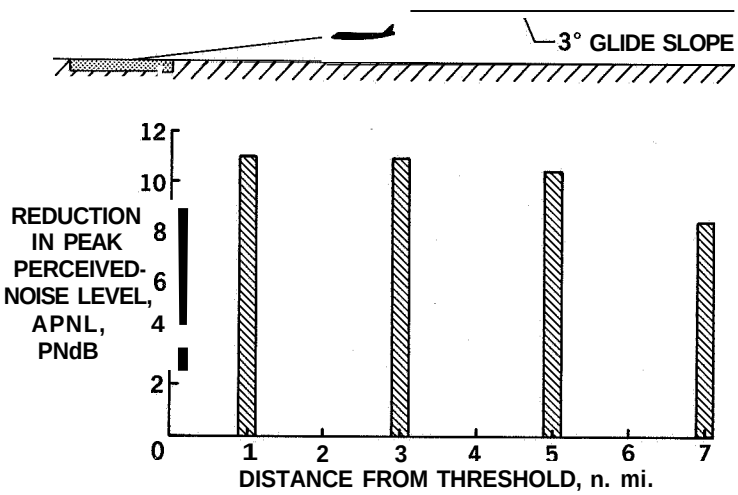

Figure 5

ESTIMATED PERCEIVED-NOISE LEVELS OUTDOORS

DC-8 WITH JT3D ENGINES

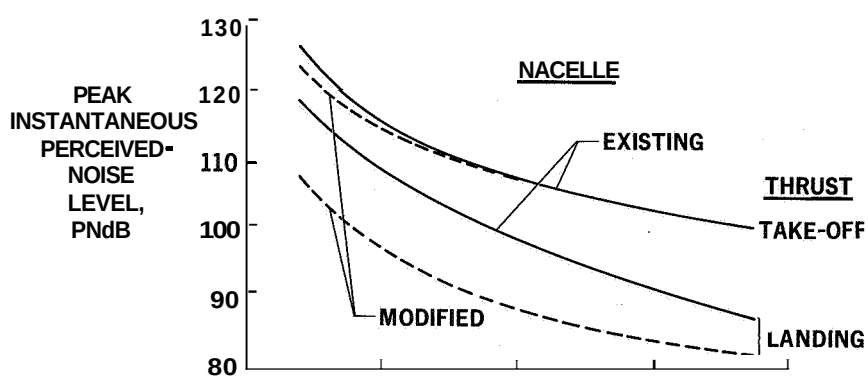

Figure 6

ESTIMATED PERCEIVED–NOISE LEVELS INDOORS
DC-8 WITH JT3D ENGINES

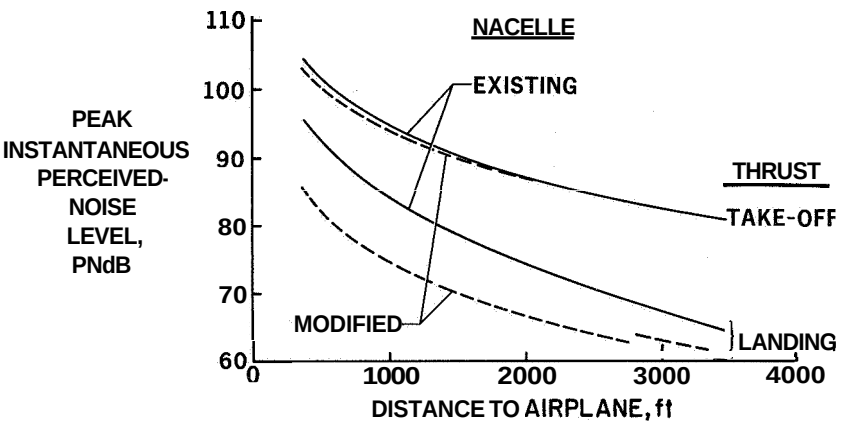

Figure 7

ESTIMATED NOISE REDUCTIONS
JT3D WITH MODIFIED NACELLES;
LANDING POWER

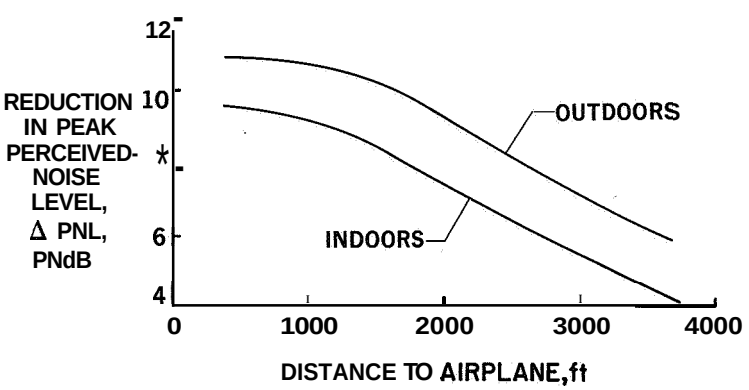

Figure 8

PAYLOAD-RANGE CHARACTERISTICS
DOMESTIC OPERATION; STANDARD DAY;
MODEL DC-8-55

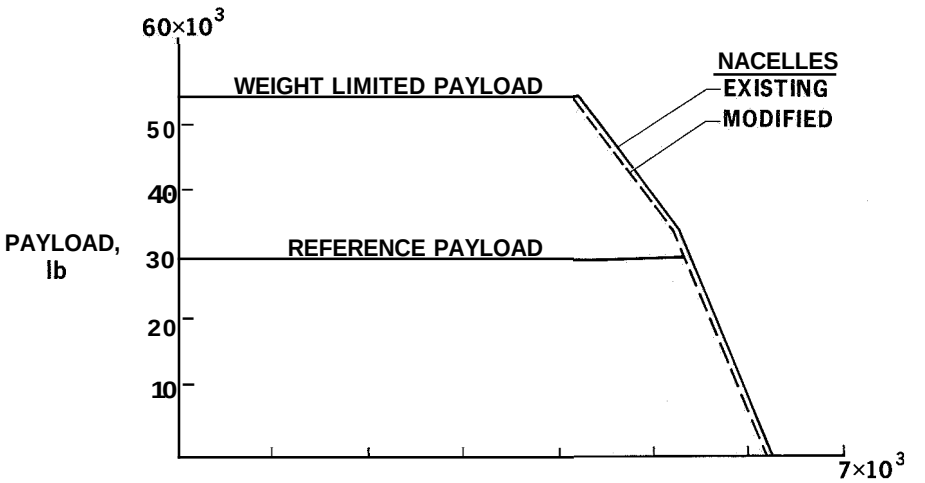

Figure 9

DIRECT OPERATING COST
MODEL DC-8-55

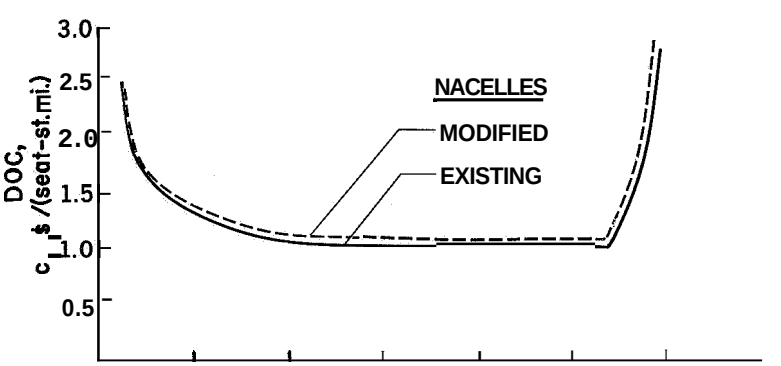

Figure 10

EFFECT OF TAKE-OFF RUNWAY LENGTH ON DIRECT OPERATING COST INCREMENT

MODEL DC-8-55; SEA LEVEL; 77°F

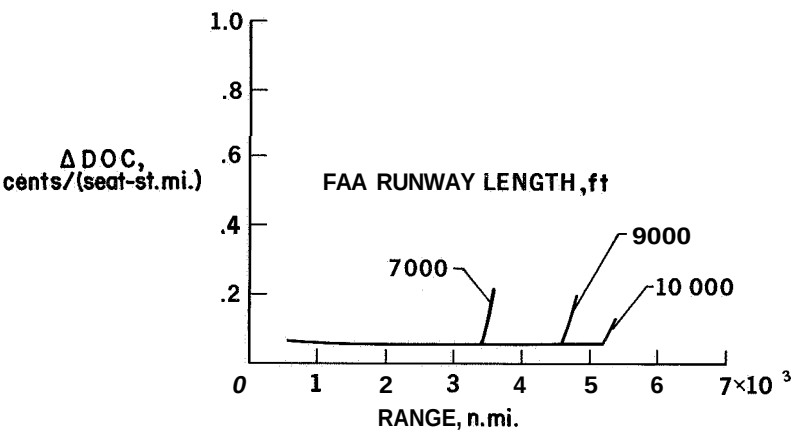

Figure 11

EFFECT OF RETROFIT COST ON DIRECT OPERATING COST

RANGE = 850 n. mi.

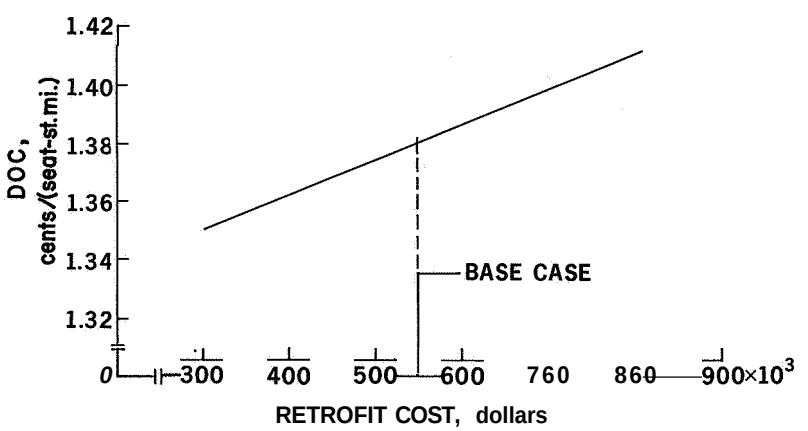

Figure 12

EFFECT OF DEPRECIATION INTERVAL ON DIRECT OPERATING COST

RANGE = *850* n. mi.

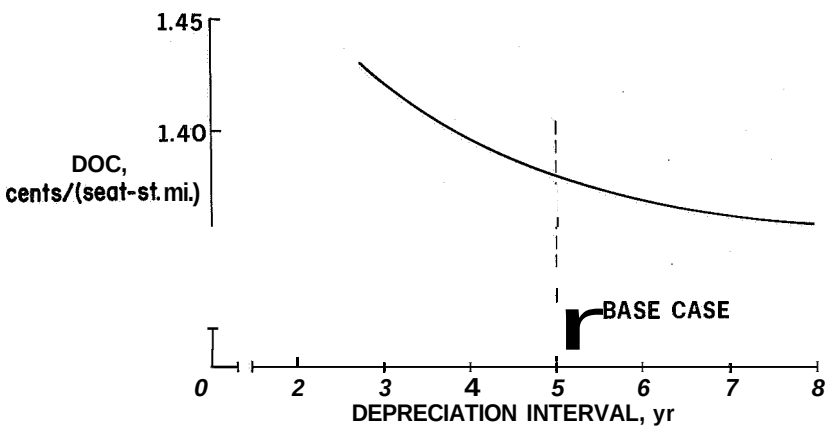

Figure 13

13. SONIC-THROAT INLETS

By C. C. Higgins, J. N. Smith, and W. H. Wise

The Boeing Company

SUMMARY

An investigation of the sonic-throat inlet as a means of reducing the noise of turbofan-powered transport airplanes has been conducted. Of several concepts considered, the variable cowl inlet was selected for further evaluation in both model and full-scale boilerplate inlet configurations. Both model and full-scale test results of an eight-segment variable cowl inlet are presented. Substantial reduction of the forward-radiated discrete frequency fan noise has been achieved at inlet-center-line Mach numbers of 0.7 to 0.8 when operating at two simulated approach power conditions. A mechanized and controllable full-scale inlet configuration for future evaluation is also described.

INTRODUCTION

With the advent of turbofan-powered commercial airplanes, the exposure of communities surrounding major airports to aircraft noise has increased substantially. It has been found that the discrete frequencies associated with the fan are a major contribution to the noise particularly during landing approaches. The discrete frequencies are propagated forward through the inlet, as well as rearward through the fan discharge ducts. Thus, an effective noise reduction program must provide substantial attenuation of the noise propagating along each path.

If only noise propagating forward through the inlet is considered, two distinctly different solutions to the problem are available – namely, (1) insertion of acoustically absorbent panels in the path of propagation or (2) creation of a high velocity flow region to oppose the forward propagation of fan-generated noise within the inlet. If the velocity of the air entering the inlet becomes sonic, sound cannot pass forward through the inlet. Maximum attenuation is obtained when all the flow reaches sonic velocity; however, useful attenuation may still be obtained if the flow attains velocities near the sonic value.

In order to obtain these high velocities, it is necessary to reduce the flow area at some station within the inlet. The sonic or near-sonic velocities occur near the region of minimum area within the inlet; thus, an inlet of this type is designated a "sonic-throat inlet." Figure 1 illustrates the operation of a sonic-throat inlet as contrasted with that of a conventional inlet.

Tests conducted by The Boeing Company (and others) with both model-scale and full-scale inlets indicated that substantial reduction of forward propagating noise was attainable in practice with sonic-throat inlets. Accordingly, The Boeing Company (under NASA Contract NAS1-7129) is now engaged in an extensive program to evaluate and develop the sonic-throat inlet for possible application to large turbofan-powered airplanes. These efforts are described in this paper.

CONCEPTS

Although the sonic-throat inlet is not new, this program represents one of the first attempts to develop an inlet of this type within all the constraints of a practical and viable airplane application. Initial efforts were directed toward definition of the design constraints and selection of promising concepts to satisfy these constraints.

Design constraints established initially in the program included a target of a 15-PNdB reduction in noise during approach, no compromise of safety of flight, and no increase in crew workload. In addition, it was desired to maintain an economically viable airplane.

Other and more detailed design constraints became apparent as the design studies proceeded. Structural limitations associated with the engine were found which prevented use of an inlet longer than 50 inches. The constraint on inlet length was accompanied by a requirement to provide noise suppression at a minimum approach thrust of approximately 3000 pounds per engine. The minimum thrust value then dictated the minimum airflow at which sonic or near-sonic velocities must be attained in the throat region. The throat area which will provide these velocities at minimum approach thrust was found to be approximately 750 square inches, compared with a nominal throat area of 1570 square inches required for cruise operation. Thus, the inlet design problem became basically that of providing an inlet 50 inches long in which the throat area could be varied from 750 to 1570 square inches while providing flow of the quality demanded by the engine for satisfactory operation.

Consideration of the quality of flow required at the engine resulted in two additional constraints upon inlet design. First, the pressure recovery at the engine face must be sufficiently high and uniform to insure engine operation without surge. Second, the disturbances introduced into the flow by the inlet must be compatible with the fan blade vibrational characteristics.

Many sonic-throat-inlet concepts were considered, but all these concepts could be grouped into one of the three general types (or combinations thereof) shown in figure 2. Each concept appeared to offer certain advantages and disadvantages when compared on the basis of performance, weight, cost, controllability, safety, reliability, and

maintainability. It was believed that, with sufficient development, each of the three inlet concepts (i.e., variable cowl, variable center body, and retractable vanes) could provide the desired noise attenuation and aerodynamic performance. However, the variable cowl inlet appeared to offer advantages with respect to the aerodynamic and mechanical design of a sonic-throat inlet, and it was selected for full-scale development.

Advantages found for the variable cowl inlet include an internal flow distribution with high velocities near the cowl wall, least disturbance of the core flow entering the gas generator portion of the engine, adaptability to boundary-layer control, and a geometric arrangement favorable for the mechanical actuation and sealing of the variable geometry components. Experience gained in other full-scale inlet tests prior to the concept selection date also weighed heavily in favor of the variable cowl inlet. Inlet models illustrating the selected concept are shown in figure 3.

SMALL-SCALE MODEL PROGRAM

Tests of a number of sonic-throat-inlet models were conducted by The Boeing Company prior to entering into contract with NASA. These models were

8.50, 14°, 20°, and 29° non-BLC diffusers
29° diffuser with one BLC blowing slot
22° diffuser with two BLC blowing slots
Peripheral choking
Radial vanes (8, 12, 16, 48, and 96)
11° diffuser (long five-door)

Very encouraging results (fig. 4) were obtained with one of the early models tested. This inlet model was characterized by a maximum diffuser angle of 8.50, measured between the diffuser wall and the longitudinal axis of the inlet. Significant and encouraging results were obtained also with boundary-layer control (BLC) applied to inlets with short, high-angle diffusers.

Additional model tests to assist in the definition and evaluation of inlet configurations suitable for full-scale development were conducted during the present program. The small-scale inlet models were evaluated by the use of one or more of the following facilities of The Boeing Company:

(1) Ejector Rig
(2) Powered Model Fan
(3) Low-Speed Wind Tunnels
(4) High-speed Wind Tunnels
(5) Water Table

The ejector rig facility provided a means of inducing airflow through the static model, together with means for measuring static-pressure distributions along the cowl wall and inlet total pressure recoveries at the simulated engine face. The powered model. fan used a single-stage inducer section from a Boeing T-50 gas turbine to simulate turbofan operation behind a sonic-throat inlet. The powered model fan and its air-driven turbine were enclosed within an anechoic chamber, and measurements of the noise emanating from the inlet were made with a boom-mounted microphone for a range of fan speeds and inlet-throat velocities. Tests in these facilities provided information on both noise attenuation and internal aerodynamic performance of inlet models.

Other tests were conducted with small-scale inlet models in both low-speed (up to 200 knots) wind tunnels and in high-speed subsonic wind tunnels (up to Mach number 0.9) both at Cornell Aeronautical Laboratories, Inc., and Boeing. Except for the high-speed wind-tunnel tests (which were 1/8 and 1/15 scale), all models tested were approximately 1/9 scale, based upon an engine face diameter corresponding to the JT3D-3B engine. Tests in the low-speed wind tunnels provided information with respect to internal performance of the inlets and effects of lip geometry upon inlet operation during take-off simulation. The high-speed wind-tunnel tests provided information with respect to the aerodynamic performance of external and internal cowl contours during simulated cruise conditions. All high-speed models utilized "flowthrough" nacelles in which the inlet airflow (and thus stream tube capture area) was varied by means of a movable plug at the discharge nozzle of the nacelle model.

Also, tests of two-dimensional inlet models were conducted on a large water table. These tests permitted observation of the general flow characteristics of several inlet configurations. The water-table tests were also used to supplement analytical studies of suction and blowing boundary-layer control as applied to the diffuser of the inlet.

The various types of small-scale inlet models evaluated in the present program are as follows:

24 retracting vanes
Variable center body
Eight-segment variable cowl:
  Non-BLC (750 sq in. throat area, full scale)
  BLC (750, 900, and 1370 sq in. throat area, full scale)
  Take-off
  Simulated cruise (internal only)
Cruise cowl (flow nacelle)

Following selection of the variable cowl inlet concept for full-scale boilerplate development, 1/9-scale inlet models simulating the take-off, cruise, and approach modes of operation were evaluated. Photographs of these models are shown as figures 5, **6,**

and 7. Boundary-layer-control blowing slots were incorporated in the models intended for use in the acoustic evaluations.

Noise reduction obtained with the eight-segment variable cowl inlet model simulating an approach configuration with a minimum throat area of 750 square inches is shown in figure 8. Results indicate that substantial noise reduction and high inlet recoveries were attained with boundary-layer-control blowing flow approximating 4 percent of inlet airflow. Also, low internal losses were measured with the inlet during cruise simulation. The low-speed wind-tunnel tests indicated that an extended inlet lip would improve inlet performance during static and low-speed take-off operation. Other results obtained in the high-speed wind tunnels indicated that the NACA 1-series external cowl contours would provide low drag during cruise.

Comparison of results from small-scale model and full-scale inlet tests shows excellent agreement. The model inlets have reproduced nearly all important aerodynamic and acoustic characteristics of the full-scale inlets.

BOILERPLATE/PROTOTYPE INLET TESTS

Although some experience with sonic-throat inlets had been acquired by The Boeing Company (and others) prior to the current program, nearly all this experience was related to operation with turbojet engines as opposed to turbofan engines. Because it was suspected that turbofan engines may be more critical with respect to inlet losses and distortion, it was desired to acquire experience with a turbofan engine operating behind a sonic-throat inlet early in the program. Tests were first conducted with a variable cowl inlet configuration installed on a JT3D-1 prototype engine. These initial tests verified that operation was indeed critical with the JT3D-1 engine, with surge encountered near throat Mach numbers of 1.0.

The inlet tested initially was approximately 70 inches long, with a distance between the throat and engine face of 57 inches. Minimum geometric throat area was 928 square inches. This inlet, which was designated the "five-door inlet," consisted of five movable doors separated and supported by five V-shaped longitudinal struts or "prongs." (See fig. 9.) The diffuser was designed with a maximum angle of 11^{o} between the cowl wall and the longitudinal axis of the inlet; the equivalent conical diffuser angle (based upon inlet and exit area and diffuser length) was 6.7^{o}.

As originally designed, the five-door inlet had no provision for boundary-layer control of the diffuser. Following engine surge difficulties encountered in the initial tests, a series of modifications were made in order to improve the flow entering the engine. The modifications included installation of vortex generators at various locations in the inlet, installation of an improved entrance lip, careful sealing of various joints, and

installation of a T-shaped angle on the ground in front of the inlet to destroy or reduce the ground vortex which was formed at the higher airflows. Of these items tested, use of vortex generators at strategic locations within the inlet proved most effective; however, none of these modifications would permit operation at a fully sonic condition.

The inlet was subsequently modified for suction boundary-layer control, then later modified again for blowing boundary-layer control. Suction boundary-layer control proved to be ineffective, but blowing boundary-layer control proved to be particularly effective and fully sonic operation was achieved. The reduction of fan noise obtained during these tests is presented in figure 10.

In the interval following design of the five-door inlet, analyses of the structural limitations of the engine had proceeded sufficiently to establish a maximum length of 50 inches as an acceptable value for the inlet. Also, further consideration of the blade vibratory stresses indicated that eight excitations per revolution were preferable to the five excitations of the five-door inlet. These new design criteria were then integrated with the design experience obtained with the five-door inlet, and a completely new inlet design resulted which was designated the "eight-segment inlet." The eight-segment inlet was characterized by a diffuser 28 inches long, revised contours of the fixed supports, and two boundary-layer-control blowing slots installed downstream of the throat. The diffuser had a maximum angle of 21° between the cowl wall and the longitudinal axis of the inlet and an equivalent conical diffusion angle of 17°, based upon diffuser inlet and exit areas and diffuser length. Minimum throat area attainable with this inlet was 750 square inches.

Two configurations of the eight-segment inlet have been evaluated. In the first configuration (fig. 11), the inlet was constructed of fiber glass with steel inserts for the boundary-layer-control slots and other fittings, The throat area was fixed at 750 square inches, the segments were straight-line elements which formed an octagon-shaped passage through the inlet, and the boundary-layer-control slots were continuous in a circumferential direction. The slots were designed with removable plates that permitted variation of the slot openings from 0.114 to 0.25 inch in height for the front slot and 0.09 to 0.20 inch in height for the aft slot. This configuration served to verify the feasibility of the design concept and to investigate the boundary-layer-control blowing requirements for maintaining attached flow.

Tests of the fiber-glass fixed-throat inlet were quite encouraging, with best results obtained by the use of the larger boundary-layer-control slot sizes. It was also determined that a single boundary-layer slot was sufficient for controlling flow in the diffuser. Limited acoustic measurements obtained with this inlet were also encouraging, and it was decided to proceed with a complete evaluation of an adjustable boilerplate inlet on a specifically prepared acoustic test facility.

Cross sections of the boilerplate inlet with eight manually adjustable segments are shown in the minimum area approach (fig. **12)** and take-off (fig. **13)** configurations, while corresponding views of the inlet installed on a JT3D-3B engine are shown in figures **14** and **15.** Results were again encouraging, with the fan noise reduced by approximately **17** to **20** decibels for Mach numbers of 0.7 or greater, as measured on the center line of the inlet.

As shown in figure 16, the results indicate that the noise levels decreased rapidly with inlet-center-line Mach numbers up to **0.8.** Operations at higher Mach numbers did not result in significantly greater attenuation because of the presence of a noise floor due to other sources. Similar results were obtained with inlet throat areas of **750** and 900 square inches, and it is believed that a family of similar curves will exist for the range of throat areas likely to be used during approach flight. Based upon these results, it is believed that noise reductions in excess of the program goal can be achieved with the eight-segment inlet controlled to maintain center-line Mach numbers between **0.7** and **0.8.**

Internal flow characteristics near the inlet throat were surveyed by means of a static-pressure probe (visible in fig. **14)** which could be translated radially across the inlet. Figure **17** shows the local Mach number distribution within the inlet when operating with a minimum throat area at a nominal center-line Mach number of **0.8.** Highest Mach numbers were present near the cowl wall, with the Mach numbers decreasing progressively as the inlet center line was approached. For this condition, a region of supersonic flow existed near the cowl wall. It is believed that the large values of attenuation achieved with this inlet configuration (for subsonic center-line Mach numbers) is attributable in large measure to the high velocities near the periphery of the inlet throat. With this configuration, the highest velocities occur where the flow area comprises a large percentage of the total flow area and sound pressure levels are likely to be highest.

Measurements of the total pressure recovery at the engine face were obtained for various values of inlet-center-fine Mach number; these results are shown in figure **18.** The influence of boundary-layer-control blowing is evident from the total pressure recovery values greater than **1.0** near the fan tips. At the higher center-line Mach numbers, losses associated with the high velocities near the cowl wall are reflected in reduced values of pressure recovery at the engine face.

Boundary-layer-control blowing quantities of approximately **4** percent of inlet-throat mass flow provided satisfactory engine operation during these tests. Boundary-layer-control blowing air for these tests was supplied from four bleed ports on the high pressure compressor of the engine. As in the previous tests with the fiber-glass fixed-throat inlet, one boundary-layer-control blowing slot was found to be nearly as effective as two blowing slots. However, it is believed that further improvement in the flow from the blowing slots

may be obtained with an improved plenum chamber and the boundary-layer-control distribution system.

Performance of the eight-segment inlet in the take-off configuration was found to be satisfactory, although cross-wind effects were not evaluated. Internal losses were found to be quite low and in excellent agreement with those previously measured in 1/9-scale-model tests.

Following completion of these tests, conversion of the manually adjustable eight-segment inlet to a mechanized and controllable configuration was undertaken. This work is presently in progress, with tests of the modified configuration scheduled before the end of 1968. The mechanized inlet will include eight hydraulically actuated segments, a boundary-layer-control blowing system, and an analog computer programed to control the inlet throat area as a function of engine speed and power lever position. A functional schematic of the control and actuation system is shown in figure 19.

The command signals generated within the computer were fed to eight independent servo amplifiers and hydraulic servo-control valves. These servo valves regulate the flow of hydraulic fluid to each actuator as required to increase or decrease inlet throat area in response to the command signal from the computer. The position of each segment (and thus throat area) is sensed by a potentiometer which provides feedback to the corresponding servo amplifier and control valve. Movement of the segment continues until a null is reached between the command signal and the position feedback signal. Response rates of the control and actuation system have been selected to be compatible with the acceleration and deceleration characteristics of the engine. It should be noted that synchronization of the position of the eight movable segments is thus maintained electrically rather than mechanically.

It is anticipated that the forthcoming tests of the mechanized and controllable inlet will provide verification of the inlet and control system compatibility with the engine during dynamic operation. Operation at inlet-center-line Mach numbers of 0.7 to 0.8 is anticipated, but the control system is sufficiently flexible to permit operation at other center-line Mach numbers if desired.

CONCLUDING REMARKS

Tests of the variable cowl sonic-throat inlet show reductions of 17 decibels or more in discrete fan noise during operation at inlet-center-line Mach numbers of 0.7 or greater. The tests also indicate that substantially greater attenuation of inlet noise can be achieved with the sonic-throat inlet but other noise sources associated with current JT3D-3B-powered airplanes (primary jet, turbine, fan discharge) establish noise levels below which further reduction of inlet noise is not advantageous.

Because of structural limitations on inlet length, boundary-layer control of the flow in the inlet has been found necessary to achieve satisfactory diffusion and surge-free engine operation. High pressure compressor bleed air has been successfully used for this purpose.

Tests to date have been conducted only for selected steady-state operating conditions, hence additional testing is necessary to verify that operation of the inlet and control system will be compatible with that of the engine in a dynamic flight environment. These additional tests with a mechanized and controllable inlet configuration are planned to begin in the immediate future.

The sonic-throat inlet is of necessity more complex than a conventional or non-articulated inlet. Variable geometry, boundary-layer control, and a computer are additional elements which will increase the complexity, weight, cost, and development time of the sonic-throat inlet. It is to be emphasized, however, that the sonic-throat inlet provides a demonstrated capability for further substantial reduction of inlet noise, if required. The added complexity thus may be justified for those applications where the full attenuation potential of the sonic-throat inlet can be utilized effectively.

NOISE PROPAGATION THROUGH CONVENTIONAL AND SONIC-THROAT INLETS

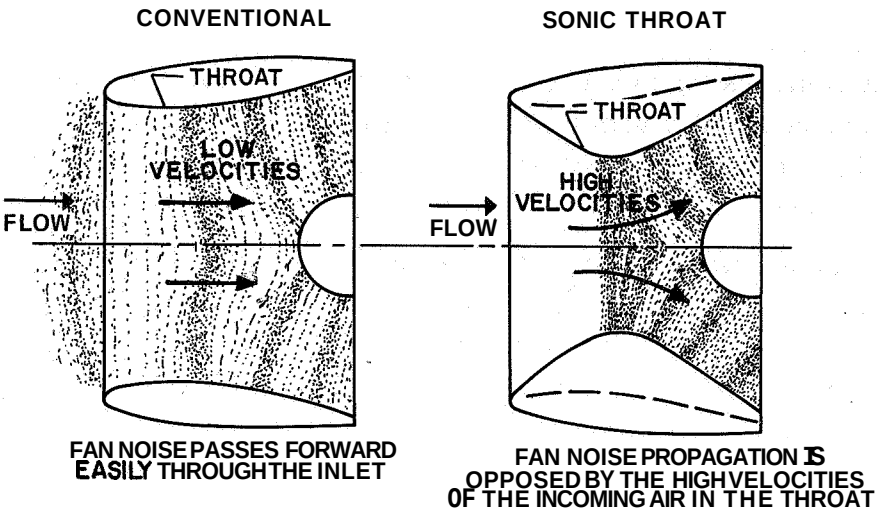

Figure 1

SONIC-THROAT INLET CONCEPTS

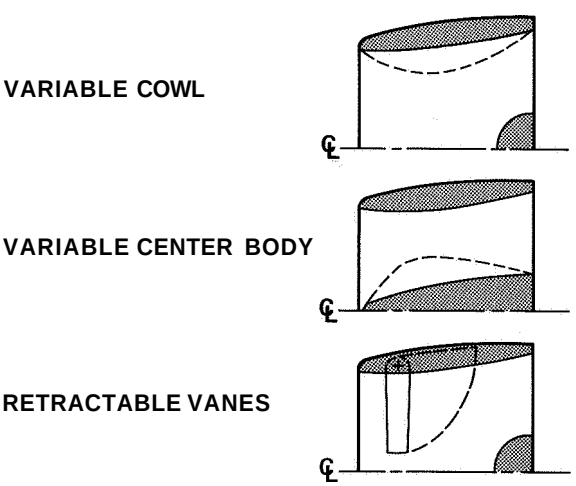

Figure 2

MODELS OF VARIABLE COWL INLET

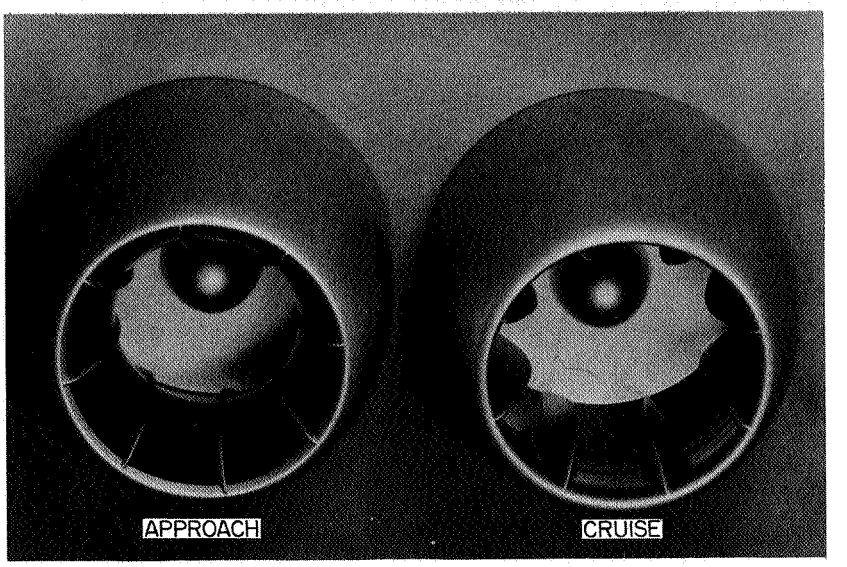

Figure 3 L-68-8565

FAN NOISE ATTENUATION FOR VARIOUS DIFFUSER ANGLES

SONIC-THROAT INLET MODEL TESTS PRIOR TO NASA CONTRACT

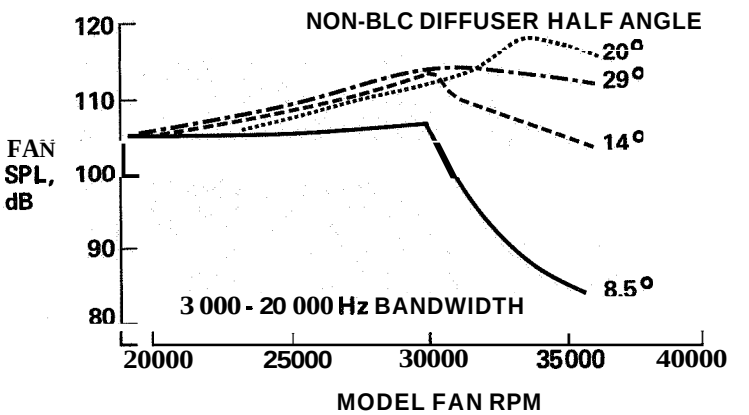

Figure 4

3

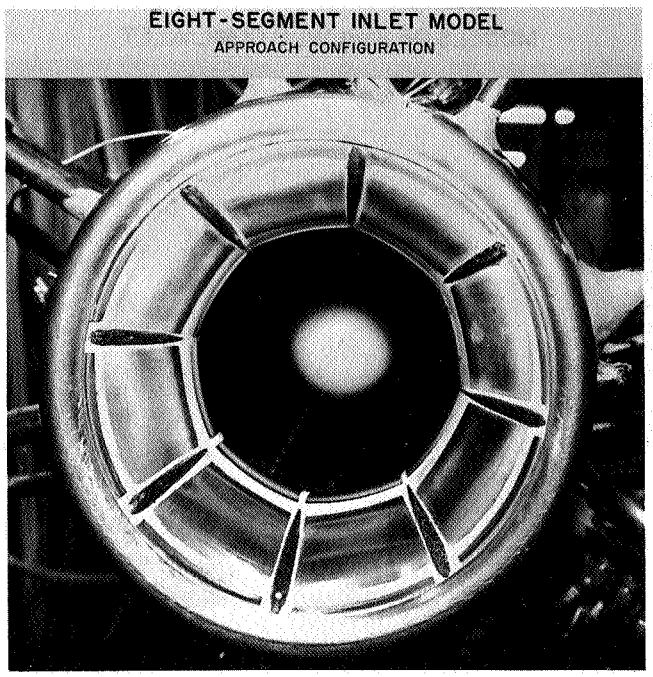

Figure 5 L-68-8568

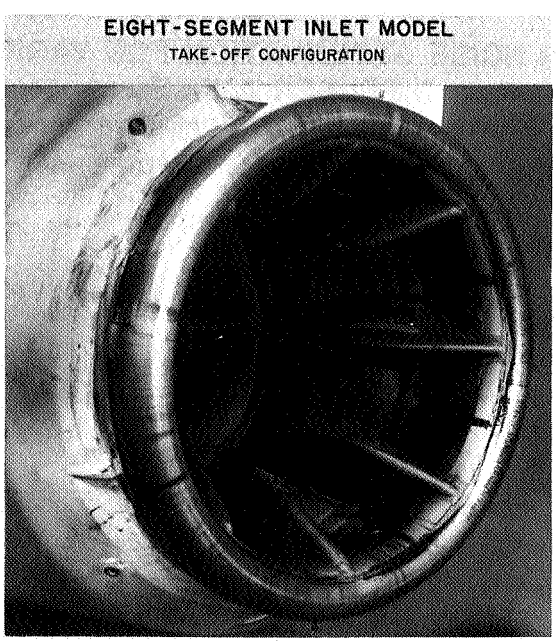

Figure *6* L-68-8569

L-68-8570

Figure 7

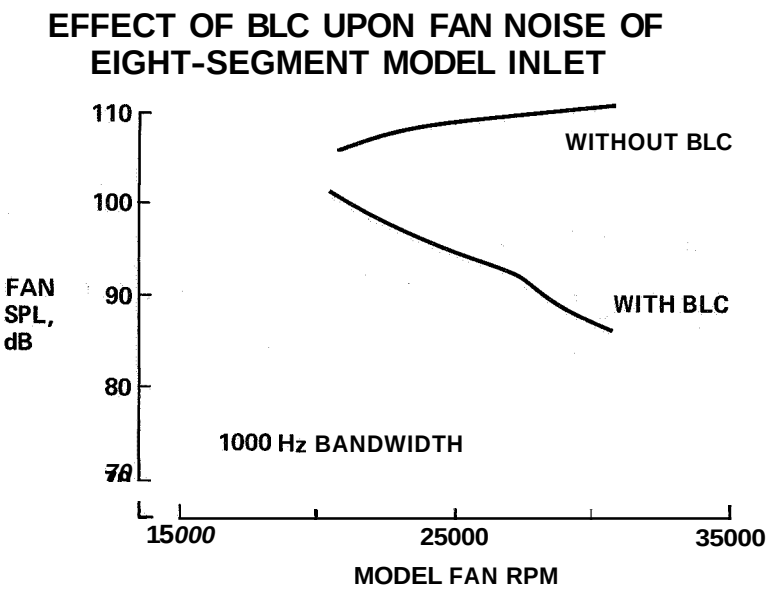

Figure 8

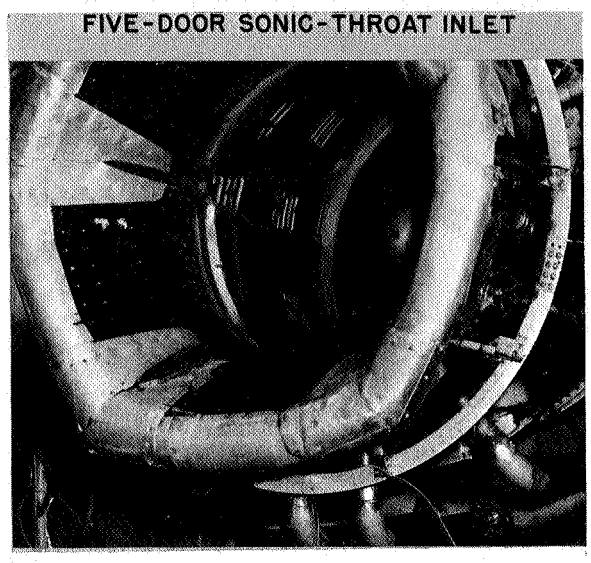

Figure 9 L-68-8571

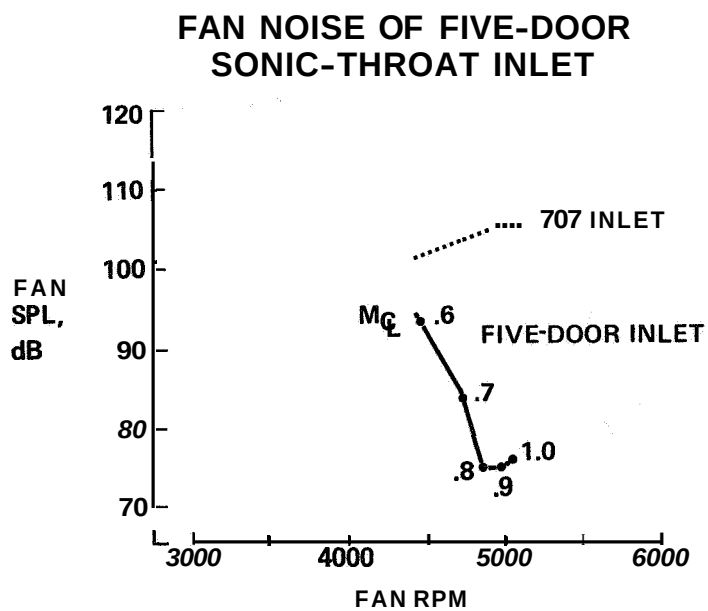

Figure 10

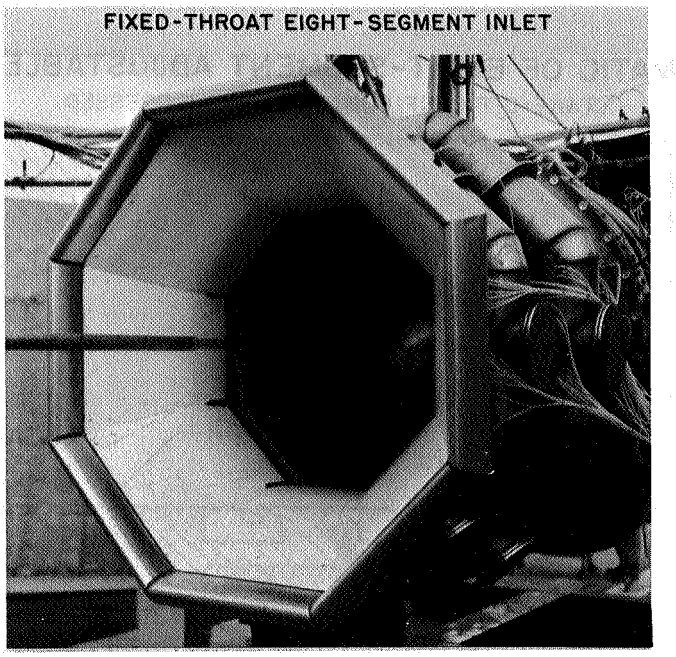

Figure 11 L-68-8572

SCHEMATIC OF EIGHT-SEGMENT ADJUSTABLE INLET

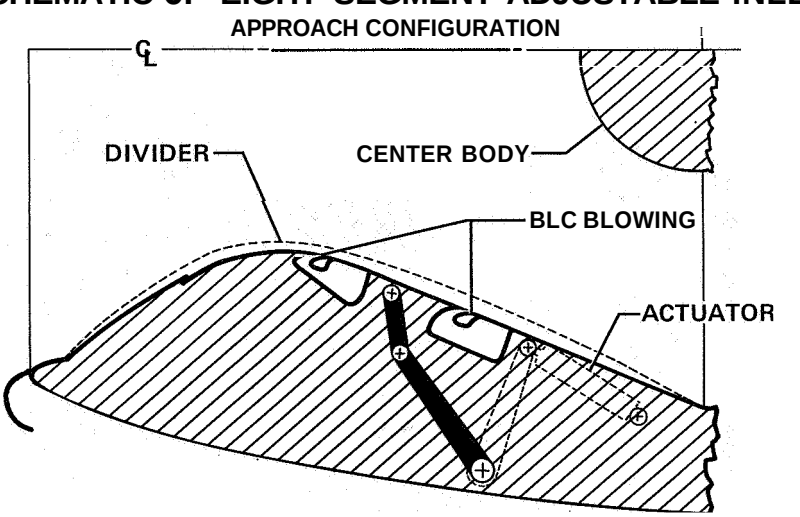

Figure 12

SCHEMATIC OF EIGHT-SEGMENT ADJUSTABLE INLET

TAKE-OFF CONFIGURATION; UNSUPPRESSED

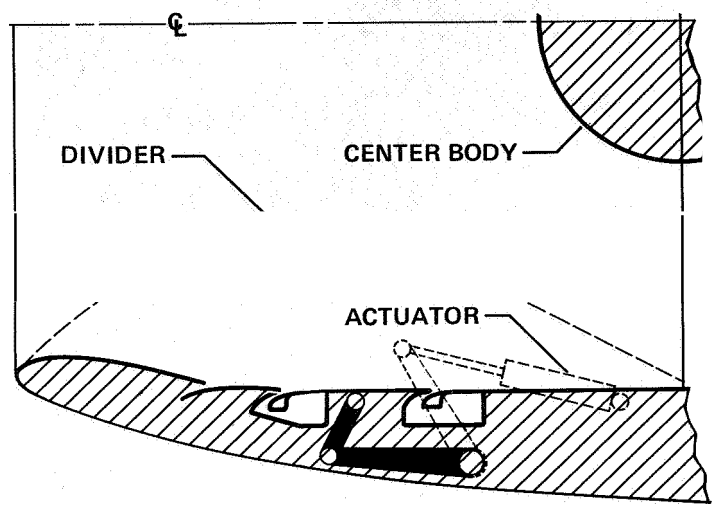

Figure 13

EIGHT-SEGMENT ADJUSTABLE INLET

APPROACH CONFIGURATION

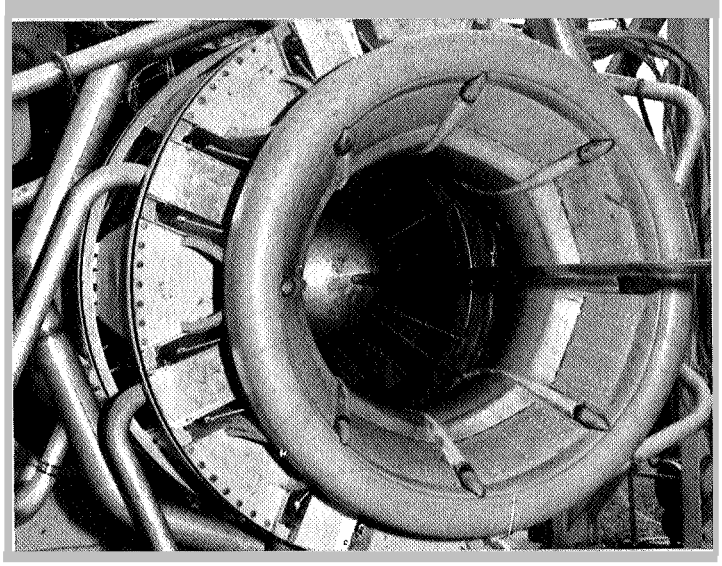

68-8566

Figure 1

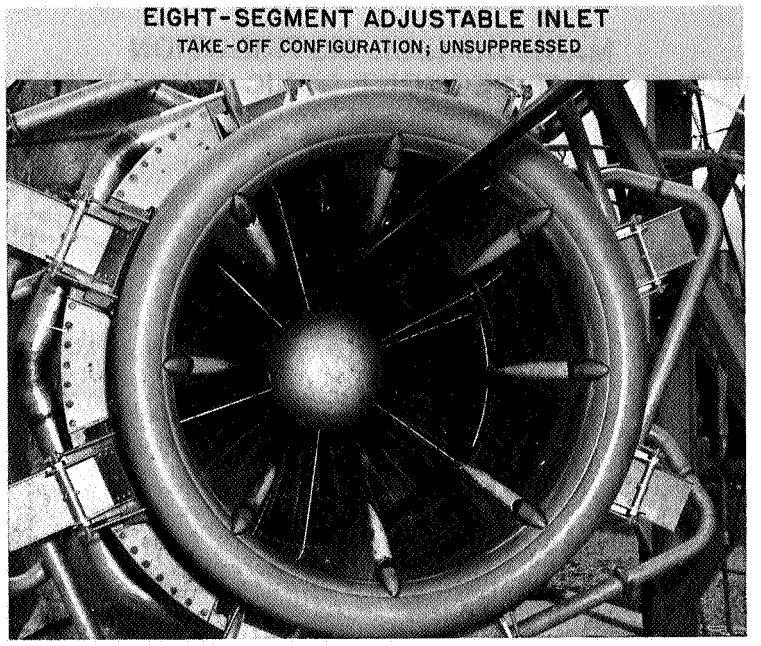

Figure 15

L-68-8567

FAN NOISE ATTENUATION OF EIGHT-SEGMENT SONIC-THROAT INLET

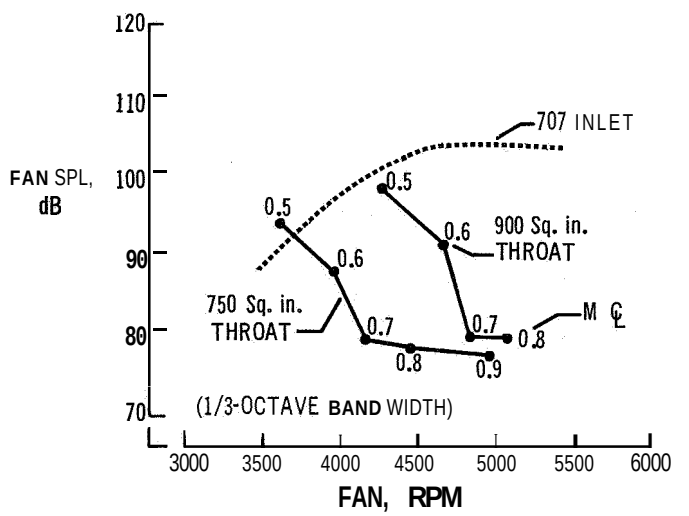

Figure 16

MACH NUMBER DISTRIBUTION IN THE EIGHT-SEGMENT SONIC-THROAT INLET

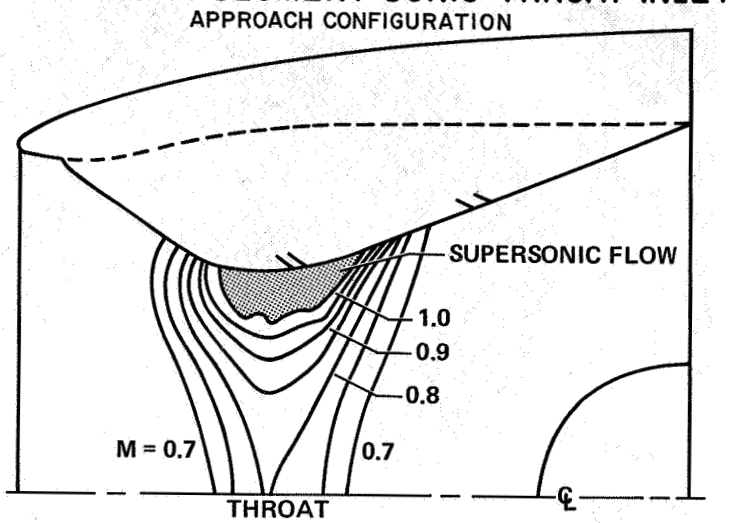

Figure 17

TOTAL PRESSURE RECOVERY AT FAN FOR VARIOUS INLET-CENTER-LINE MACH NUMBERS

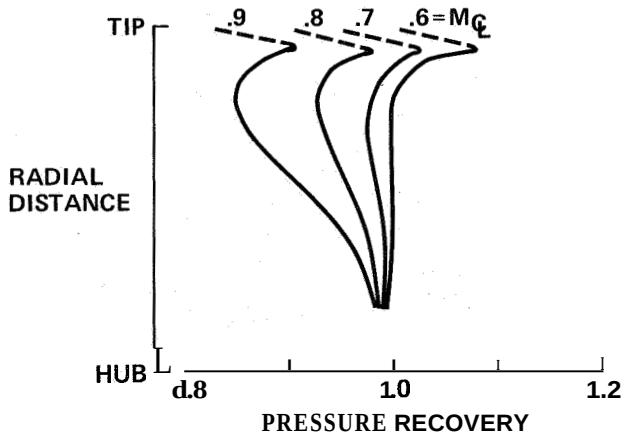

Figure 18

SIMPLIFIED SCHEMATIC OF INLET CONTROL SYSTEM FOR EIGHT-SEGMENT SONIC-THROAT INLET

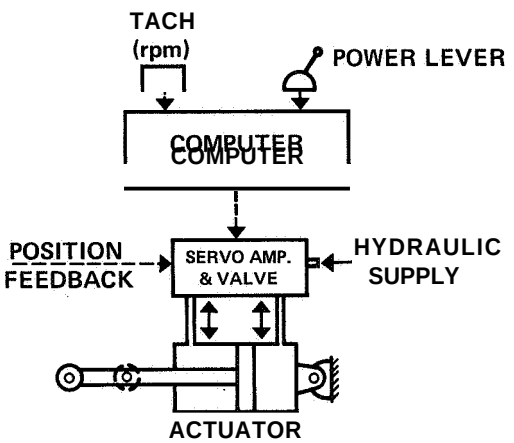

Figure 19

14. TREATED INLETS

By George T. Drakeley and Ralph B. McCormick

The Boeing Company

SUMMARY

The fan noise radiated from the inlet during approach of a Boeing 707-320B airplane is 5 PNdB lower than the noise radiated from the fan exhaust duct. Available information indicates that the inlet noise suppression of 10 PNdB required for an overall airplane fan noise suppression goal of 15 PNdB can be achieved with an acoustically treated inlet. The Boeing Company has designed and is manufacturing acoustically treated inlets for ground and flight tests in mid-1969.

INTRODUCTION

The development of technology to reduce the fan-generated noise of the Boeing 707-320B airplane by 15 PNdB has been the task of the Boeing Company under contract no. NAS1-7129 since May 1967.

Studies of the peak perceived noise levels (PNdB) associated with the JT3D-3B turbofan engine with which the airplane is equipped indicate that with the airplane at an altitude of 400 feet, the contribution of the inlet noise to the total perceived noise level is 5 PNdB lower than the fan exhaust noise. Component noise levels and their relationship to the total are shown in figure 1. To meet a target of 15 PNdB reduction in peak perceived noise, it is therefore required to reduce the forward radiated noise contribution by 10 PNdB.

The reduction of fan inlet noise sound pressure levels (SPL) required to achieve a 10 PNdB reduction in perceived noise level is shown in figure 2. The effect of this attenuation on a typical sound pressure level spectrum of the noise radiated from the inlet is shown in figure 3. The peak noise level after treatment occurs at about 5 or 6 thousand cycles per second. This level is acceptable since these frequencies have less influence on perceived noise level as measured in PNdB than the lower frequencies have. At the start of the program it was expected that a sonic or near-sonic inlet would be required to accomplish the required 10 PNdB suppression of inlet noise. Tests by McDonnell Douglas have demonstrated that this much noise reduction can be achieved with a treated inlet. It was therefore decided to postpone flight testing of a sonic or near-sonic inlet and to design and flight test treated inlets in combination with the acoustically treated fan ducts already under development at Boeing.

CONCEPTS

In the evaluation of any concept designed to meet the target attenuation, consideration must be given to the effect on the propulsion performance of the inlet. Small decreases in pressure recovery can cause significant changes in the performance of the airplane. In general, the performance of the inlet can be influenced by the amount of acoustic material used, the length of the inlet required, and the flow diffusion efficiency. It is desirable to use the least amount of acoustic material required and to arrange it in a configuration that provides the minimum pressure loss.

The quantity of treatment required in an inlet to meet the target noise reduction depends upon the radial distribution of the acoustic pressure level in the inlet, the cross-sectional areas of the flow channels formed by the insertion of the acoustic material, and the separation distance of the acoustic material. Experimental data have shown that the sound pressure level near the outer wall of the inlet is higher than that near the center. To obtain uniform acoustic performance across the inlet, the amount of attenuation provided must also vary across the inlet.

Since the effect of an acoustic lining in an engine inlet is very dependent upon the distribution of treatment across the inlet, a number of different configurations were studied before the 2-ring inlet, similar to the inlet tested by McDonnell Douglas and identified as concept **1** in figure **4,** was selected for design development. Some of the other concepts studied are also shown. In all cases acoustic treatment was used on the inlet wall and on the center body and an increase in the length of the typically short Boeing inlet was required.

The first concept studied was a 2-ring inlet similar to concept **1** but with only three untreated radial struts. Three struts would give adequate support to the treated rings. However, it was found, through coordination with Pratt & Whitney, that the wakes from three struts, if strong enough, would set up harmonic frequencies in certain compressor blades and could develop unacceptably high blade stress. Coordination with Pratt & Whitney established that the minimum number of struts that could be used without extensive testing or analysis to assure no adverse effect on blade stresses was eight. This information led to studies of the other configurations.

By using the prediction techniques developed in the flow duct and full-scale tests of the fan-exhaust duct program, the amount of acoustic treatment required to meet the target attenuation was estimated for each configuration. It was found that treated radial struts would require more acoustic treatment than rings would require to produce the same attenuation. This effect is due to the fact that the radial splitters have the largest treatment separation distance at the cowl wall where the maximum attenuation is required.

The inlet pressure loss for each configuration was estimated by computing the friction drag of the inlet from the flow velocity, the wetted area, and the local skin-friction coefficient. The velocity distribution through the inlet was based upon one-dimensional net area distribution. The skin-friction coefficient for the acoustic material was based upon experimental data that indicated a value 1.5 times greater than that for a smooth flat plate. The results are presented in table I along with the estimated weight of the various configurations. The pressure loss study did not account for diffusion losses or losses that might be generated by any local flow separation or turbulence.

CONCEPT SELECTION

The trade study results show that the ring concept requires significantly less acoustic treatment than radial struts. Consequently, the inlet flow losses are smaller and the weight increase is less. The ring concept was selected for further development.

A ring-placement trade study was made to optimize the radial spacing of the rings and to determine the length of treatment required. A computer program was run to determine the noise reduction obtained from various radial spacings of the rings. The results were based upon various selected flow channel lengths and the center body and cowl wall configuration selected from flow studies. The study indicated that maximum attenuation is achieved with approximately equal spacing of the rings.

By using lining technology developed in the fan-exhaust-duct program, the depth of treatment was selected as 0.3 inch and 0.6 inch on opposite walls of each flow channel to obtain the attenuation over the required freque'ncy bandwidth. The treatment depths were arranged to give the thinnest rings. The flow resistance of the acoustic material was varied with channel length to conform to changes in local sound pressure level due to progressive attenuation. The configuration is shown in figure 5. Boeing developed polyimide-fiber-glass sandwich was selected as the acoustic material. The acoustic sandwich is made of porous sheets, with the selected flow resistance, bonded to honeycomb of the size and thickness selected to provide the required resonance chamber and then bonded to an impervious sheet or, in the case of the rings, to an impervious septum. These sandwiches, in addition to providing noise attenuation, are the basic structures of the cowl wall and both rings. Treatment on the center body is nonstructural.

For the flight-test program a conservative lip design was selected to assure adequate take-off performance since the design would have little effect on the noise reduction and the cruise performance of a more optimum configuration can be reasonably well estimated. The wall contour at the throat is a 2.5 to 1 ellipse and the contraction ratio is 1.25. The throat area is the same as the current production inlets.

The internal cowl contour was developed from consideration of the flow area through the inlet. It was found that a 31-inch-long production 707 center body modified to accept acoustic treatment would provide adequate treatment length and reasonable flow channel heights. Acoustic requirements determined the approximate radial location, thickness, and length of the rings. The station locations of the rings and the cowl wall contour were adjusted to provide a nearly linear flow area distribution through the inlet as shown in figure 6. The length and thickness of the acoustic treatment in the rings was carefully controlled so that the cowl wall angle would be small. An inlet length of 45 inches was selected so that the wall angle would not exceed 9°. The exact shape and placement of the rings were determined from potential flow studies. A computerized relaxation procedure solving the incompressible and compressible potential flow problem was used to map out the streamline patterns and surface velocity distributions for the basic cowl and nose dome configuration. The rings were then fitted to specific streamlines. The complete inlet configuration was then examined by use of the potential-flow program and a boundary-layer program to analyze the flow characteristics at both cruise and take-off conditions. The results showed that in the region of the rings, there was no significant change in the streamline patterns for take-off and cruise conditions. The effects of a crosswind were estimated for take-off conditions from a two-dimensional Streamline pattern with the flow center line. It was concluded from comparing the respective flow patterns that a maximum 3° change in angle would exist at the leading edge of the inner ring and that there would be no appreciable angle difference at the outer ring. The leading- and trailing-edge contour of the ring are based on NACA 64 series airfoil sections and the strut contours are based on NACA 0012 airfoil sections. The basic contour for the external lines was selected as a NACA 1 series with a length of 60 inches and a maximum height of 6.40 inches. However, because of the noncircular shape of the nacelle and the 3.50 droop of the inlet, only the horizontal profile can exactly comply with this requirement. The remainder of the contour was faired as necessary to account for the diameter variations.

The scheduling of this part of the program has precluded any preliminary tests, model or full scale, of this design. The inlet will be ground tested prior to flight to insure adequate flight performance. The estimated performance of the treated inlet, based upon one-dimensional-flow analysis, indicates 1.2 percent less pressure recovery than the current production inlet. The take-off performance should be equal to that of the production inlet.

CONCLUDING REMARKS

The acoustic design of the inlet was based upon meeting the target attenuation. Consideration has been given to possible loss of acoustic effectiveness due to experimental

variations and manufacturing problems and a conservative approach to acoustic design has been used. It is expected that the inlet will meet the noise reduction goal. The estimated inlet performance shows some pressure recovery loss. This loss, the weight increase due to increased inlet length, and the addition of ring struts will result in reduced airplane performance.

TABLE I

TRADE STUDY RESULTS
20-dB PEAK ATTENUATION

CONCEPT	TREATMENT REQUIRED, ft^2	PRESSURE RECOVERY LOSS, %	WEIGHT INCREASE, lb	LENGTH INCREASE, in.
1	84	1.2	93	10.5
2	113	1.3	134	10.5
3	119	1.5	143	10.5
4	157	1.7	201	17.5

TURBOFAN NOISE

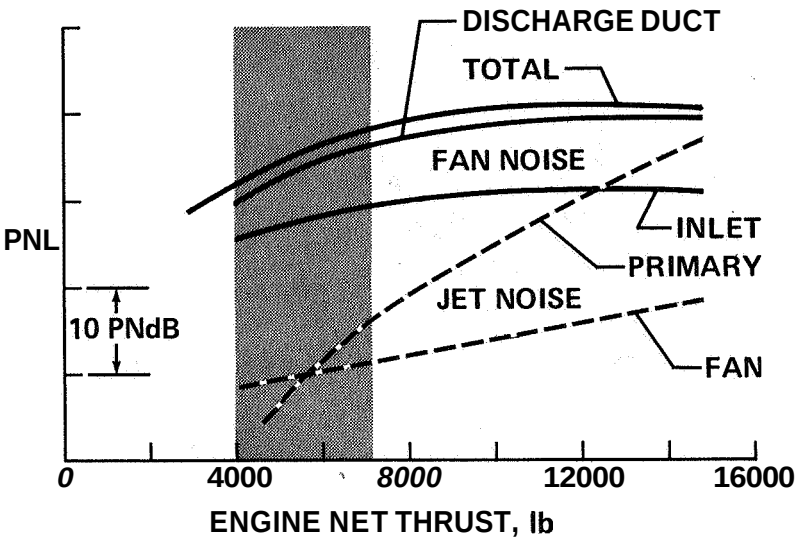

Figure 1

INLET NOISE REDUCTION GOAL

5000 rpm

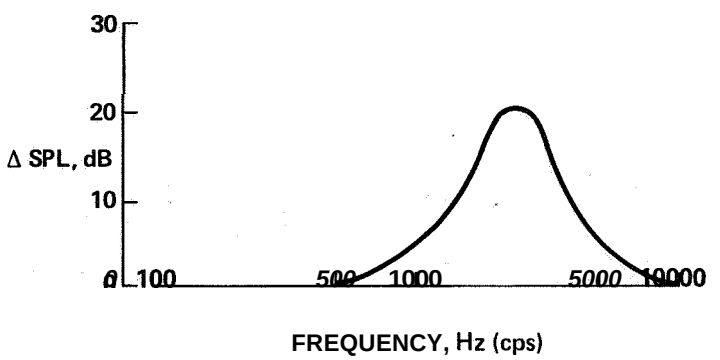

Figure 2

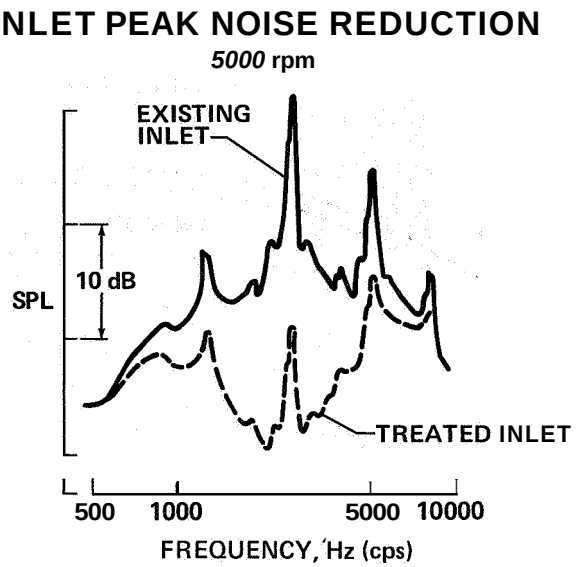

Figure 3

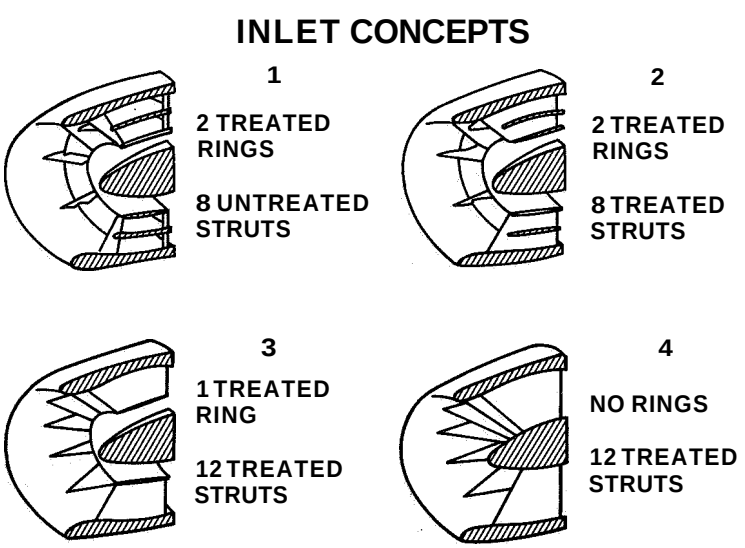

Figure 4

CONFIGURATION

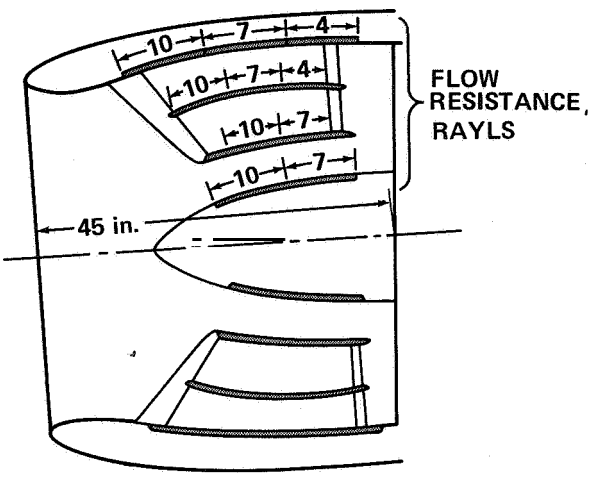

Figure 5

INLET AREA DISTRIBUTION

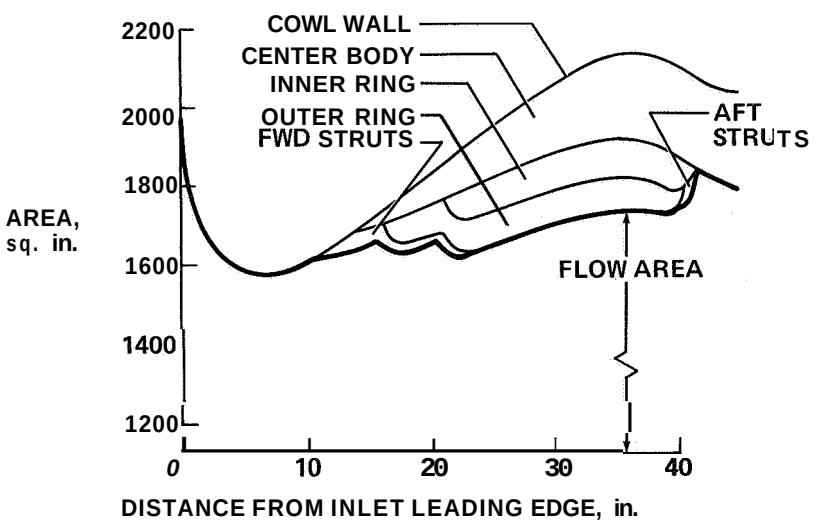

Figure 6

15. FAN-DUCT DEVELOPMENT

By Ralph B. McCormick

The Boeing Company

SUMMARY

The fan noise radiated from the fan discharge duct during the landing approach of current fan jet airplanes is the largest single contribution to the composite engine noise. The Boeing Company has designed and ground tested an acoustically treated long fan duct to reduce this component of engine noise. Data obtained during the tests show a reduction in the peak noise level of the treated duct over the existing duct of 9 to 16 PNdB for approach power settings at a distance of 370 feet. Engine thrust measurements indicate an increase in thrust of approximately 2 percent over the existing short duct. Flight-test fan ducts are being constructed for evaluation in mid-1969. It is estimated that the long treated fan ducts will increase the weight of each nacelle by approximately 750 pounds.

INTRODUCTION

The Boeing Company has been involved in the development and evaluation of a turbo fan nacelle modification to reduce fan noise since the fan whine emitted from the fan duct is the largest single contribution to the composite engine noise. The basic program goal is a 15-PNdB noise reduction of a Boeing 707-320B airplane during landing approach and is to be accomplished by attenuating the fan-duct component of noise by this amount.

The program for development of an acoustically treated fan duct was divided into three phases: **(1)** a trade study of various concepts was made to aid in the selection of a configuration; (2) a ground-test duct was designed and tested for performance evaluation; and **(3)** four flight-test ducts are being constructed for flight evaluation in mid-1969.

OBJECTIVES

An attenuation goal for the fan duct is shown in figure **1.** The goal was selected to give the peak attenuation at the fan frequency during the approach condition. **A** peak attenuation of 30 dB is required and a suitable bandwidth was selected to obtain the required attenuation over the range of power settings associated with a normal approach. Figure 2 shows a typical sound level spectrum of the peak noise attributed to the fan duct at an engine speed of 5000 rpm. The data were obtained from ground tests of a production untreated duct and were adjusted to a 370-ft distance. The effects of the selected

attenuation goal are also shown and indicate the sound level required to achieve a peak noise reduction of 15 PNdB.

The noise reduction must be accomplished without imposing a severe penalty on the performance of the airplane. The current production fan duct on the 707 airplane shown in figure 3 is very short in length. It was designed to minimize the weight and external drag of the nacelle. The limited length and cross-sectional area are not sufficient to install a significant amount of acoustic material. It is necessary to design a substantially longer duct to contain the required amount of acoustic material. This will mean an increase in the nacelle size and weight and will result in an increase in the internal and external drag of the nacelle. The short duct, however, discharges high-velocity air over the nacelle afterbody causing a significant amount of scrubbing drag. This drag can be reduced with a longer duct. A long duct design will require that the duct be bifurcated to clear the support strut at the top of the nacelle and the engine accessories at the bottom to maintain sufficient ground clearance.

TRADE STUDY

To obtain an insight into the most reasonable compromise of fan-duct length, cross-sectional area, and shape, a trade study was made. A number of duct design concepts were studied to determine the amount of acoustic treatment required and the effect on airplane performance. Three of the concepts studied are illustrated in figure 4. This study led to the selection of concept 3 for further development. Concept 1 extended to about seven-eighths of the length of the nacelle and had a kidney-shaped cross section and nozzle. Concept 2 was a full-length duct with a kidney-shaped cross section and nozzle. Concept 3 was also a full-length duct. The cross section was changed to an elongated kidney shape to reduce the internal turning losses and to decrease the separation distance of the acoustic material from approximately 9 to 7 inches. A coplanar annular nozzle was used. All the concepts had the duct divided into five channels on each side to control the turning losses and provide for the structural design. The trade between duct internal flow area and nacelle maximum diameter was studied by considering three duct flow areas at the nacelle maximum diameter. The areas provided for (1) a contraction from 828 sq in. at the fan exit to a flow area of 660 sq in., (2) a constant flow area for much of the duct length, and (3) an expansion from 828 sq in. at the fan exit to a maximum flow area of 900 sq in.

An analysis of the airplane performance was made using a constant payload and field length to determine the effect on range. Consideration was given to the internal flow losses, weight, and external drag of the various concepts. The changes in range as compared with the range of the production airplane are shown in figure 5 for the various flow

areas considered. Concept 3 with a maximum flow area of 900 sq in. has the least effect on airplane range.

The acoustic analysis of these concepts (fig. 6) determined the peak noise reduction as a function of the treatment length. The elongated kidney shape with the smaller treatment separation distance required approximately 67 inches of treatment length to meet the 30-dB peak attenuation goal; whereas, the kidney shape required an additional 15 inches. The analysis was based on experimental data obtained in duct flow tests. Other experimental and theoretical data indicate that an additional noise reduction of about 4 dB can be achieved with coplanar concentric nozzles. These results along with the performance analysis indicated the selection of concept 3 for further development.

The configuration selected (fig. 7) has an internal contour developed from the geometry indicated by the trade study. It was designed in four sections: A bifurcated section turns the flow from the annular fan exit to the bifurcated elongated kidney shape and also expands the flow from 828 sq in. at the fan exit to 900 sq in. A linear flow-area distribution was chosen to preclude a large local diffusion. The constant-area section will contain most of the acoustic material. The flow area is a maximum through this section to give a low velocity over the rough acoustic material and reduce the internal losses. The transition section provides the change from the elongated kidney shape to the annular nozzle, The flow area through this section was determined by the space available between the engine and the required external nacelle contour, The nozzle is annular and approximately coplanar with the primary nozzle.

A 1/5-scale model of the internal configuration of the duct was tested. Measurements of thrust, airflow, and pressure loss confirmed the estimated internal losses used in the trade study.

GROUND-TEST DUCT

A full-scale ground-test duct was constructed to verify the estimated acoustic and propulsion performance. The selected internal configuration was used and the duct was designed so that only minimum changes to the engine systems would be required. Each half of the duct was constructed in four sections as shown in figure 8. The bifurcated section was constructed of epoxy-fiber glass. The side cowl is constructed of polyimide-fiber glass sandwich honeycomb that is designed to provide for both the acoustic and structural requirements. A cost and weight study indicated the use of polyimide-fiber glass construction in this area. A thrust reverser was not developed for this configuration,. but a space provision was provided. The transition and nozzle section is constructed of aluminum sheet and frames. It has a 30-inch-long polyimide-fiber glass acoustic insert panel at the forward end. The panel is removable and will be used to determine the effect of extending the treatment length.

The acoustic treatment used in the side cowl consisted of double-layer treatment in the outside wall and single-layer treatment on the splitters and inside wall. The treatment depth selected to provide noise reduction over the selected bandwidth was 1.0 inch for the double layer and 0.5 inch for the single layer. The flow resistance of the material varies from 5 to 35 rayls for the double layer and from 6 to 30 rayls for the single layer. The value at any location is a function of the local sound pressure level and flow Mach number.

The acoustic treatment for the aft insert panel is the same as for the side cowl, except that the inside wall is not treated. Including the panel there is a total of 267 sq ft of acoustic treatment. This is in excess of the estimated amount required to account for manufacturing problems, accuracy of predictions, and possible deterioration in acoustic effectiveness due to contamination.

Ground tests were run on a test stand at a remote location. Baseline tests of the existing production short duct and the full-length treated ground-test duct have been completed. The tests were run both with and without suppressed inlet noise. The results obtained indicate that the inlet radiated noise interferes with the measurements of duct radiated noise when the inlet noise is not suppressed. All data shown were recorded with the inlet noise suppressed. Acoustic data were obtained from 24 far-field microphones (fig. 9) located around the engine in both horizontal and vertical planes.

Analysis of the data was made in preferred 1/3-octave bandwidths with a signal integration time of about 6 seconds. Perceived noise levels were computed for both horizontal and vertical measurements using sound-pressure-level corrections for distance, atmospheric absorption, and ground absorption when applicable. Noise levels measured from one engine at a distance of 200 ft were considered approximately equal to values for four engines at 370 ft (inverse square relationship and correction for atmospheric absorption).

Preliminary results for the existing duct and the treated duct configuration for three test conditions are shown in figures 10, 11, and 12. The data from both the horizontal and vertical measurements were adjusted to a distance of 370 ft. The engine conditions shown correspond to static thrust settings that approximate in-flight thrust at approach, cutback, and take-off. Values of peak noise reduction between the existing duct and the treated duct configuration for both the horizontal and vertical planes are shown as a function of static thrust in figure 13. Estimated reductions in peak perceived noise level take into account the data scatter between runs and give both maximum and minimum values as shown in figure 14. Although the perceived noise levels computed from the horizontal measurements do not compare directly with the values computed from the vertical measurements, the reductions agree well.

Typical spectral data of the peak noise attributed to the fan duct are shown in figure 15. The data were recorded at 5000 rpm at 110° in the horizontal plane. The data are adjusted to a 370-ft distance. Data accumulated during the test indicate a reduction in peak noise level of 9 to 16 PNdB. The data also show a reduction of 2 to 6 dB in sound pressure level at the frequencies associated with the jet noise. This reduction is attributed to the coplanar annular nozzle configuration. The magnitudes of the peak frequencies have been reduced substantially more than the broadband level. This reduction indicates the presence of a broadband background noise in the 2 to 6 kHz range that limited the noise attenuation measured. Further testing of the treated long duct is planned to provide better definition of the broadband background noise. A more accuracte evaluation of the treated duct will be made when a fully treated nacelle is tested.

Measurements of thrust, fuel flow, and duct pressure losses were made to evaluate the internal performance. The propulsion performance of the engine with the treated duct is shown in figure 16. Gross thrust measurements indicate approximately a 2-percent increase in thrust over the standard production duct. The increase is attributed to the relatively small internal loss and the absence of a scrubbing drag.

FLIGHT-TEST DUCT

A flight-test configuration of the duct (fig. 17) has been designed and is currently under construction. The design is similar to that for the ground test and uses much of the same tooling for manufacture. The internal contour has only minor changes and the external contour was modified to conform to flight requirements. Flight tests are planned for mid-1969.

The amount and location of the acoustic treatment are the same as for the ground test but treatment has been changed. Recent experimental data indicate that a suitable combination of single-layer treatment will meet the target attenuation. The single-layer treatment is much simpler to manufacture and less costly. The treatment depths are 0.75 inch on the outer walls, 0.50 inch in the splitters, and 0.30 inch on the inner wall. The aft acoustic panel has been modified to be part of the nacelle structure. The flow resistance of the acoustic treatment will vary from 18 to 30 rayls. It is estimated that the flight-test treated long duct will increase the weight of each nacelle by approximately 750 pounds. The design will also reduce ground clearance by approximately 3 inches.

CONCLUDING REMARKS

The noise reduction goal of 15 PNdB for a Boeing 707-320B airplane during landing approach appears feasible. Ground tests indicate that the acoustically treated long fan duct will result in a gain in thrust of approximately 2 percent at take-off conditions. The fan-duct modification will result in a weight increase of approximately 750 pounds for each nacelle.

FAN-DUCT ATTENUATION GOAL

5000 rpm, 370 ft

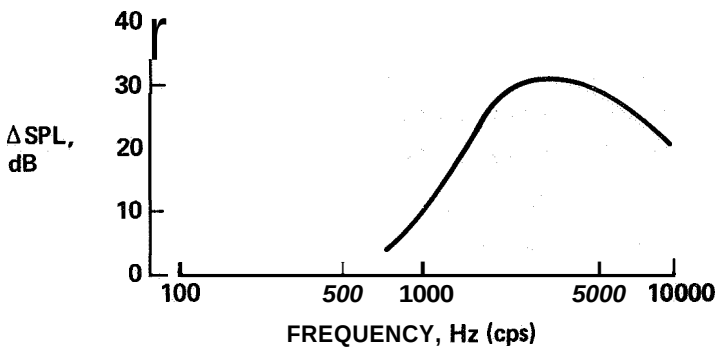

Figure 1

FAN-DUCT PEAK NOISE REDUCTION

5000 rpm, 370 ft

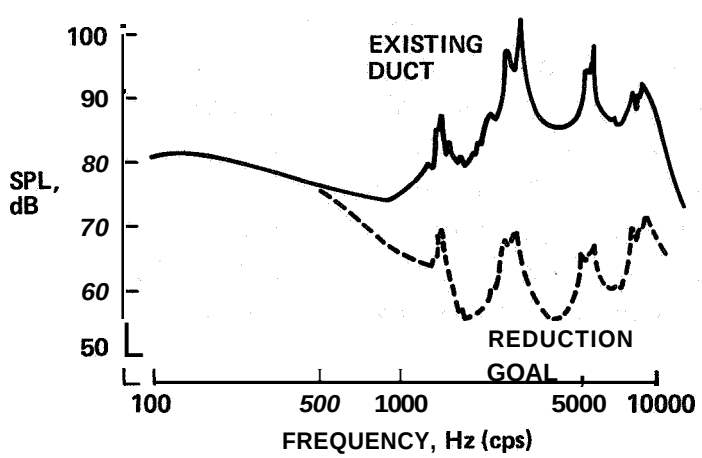

Figure 2

EXISTING NACELLE

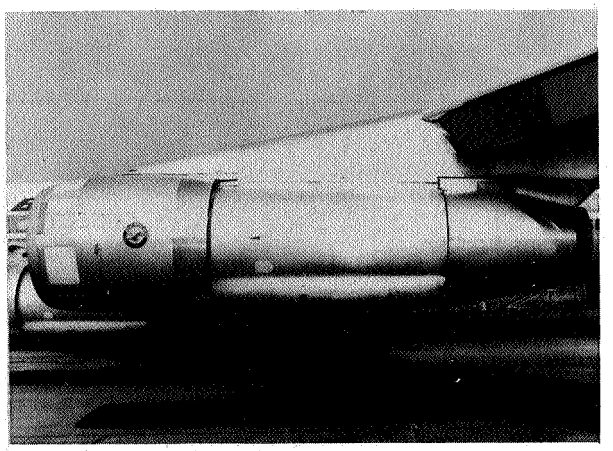

Figure 3 L-68-8573

TRADE STUDY CONCEPTS

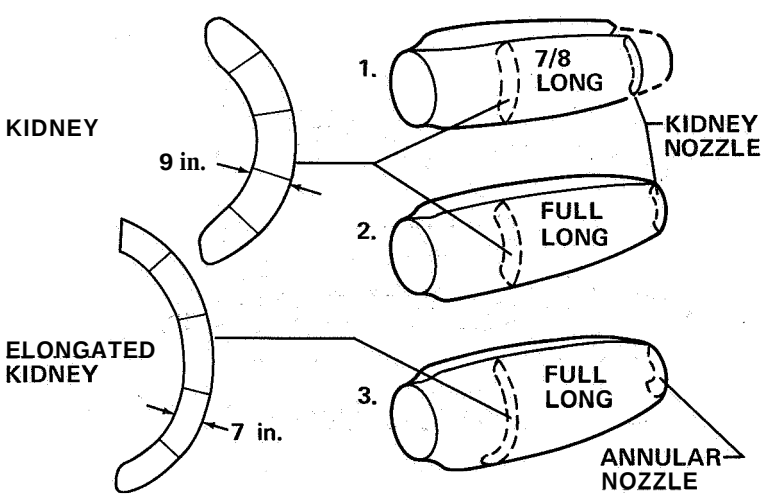

Figure 4

DUCT PERFORMANCE ANALYSIS

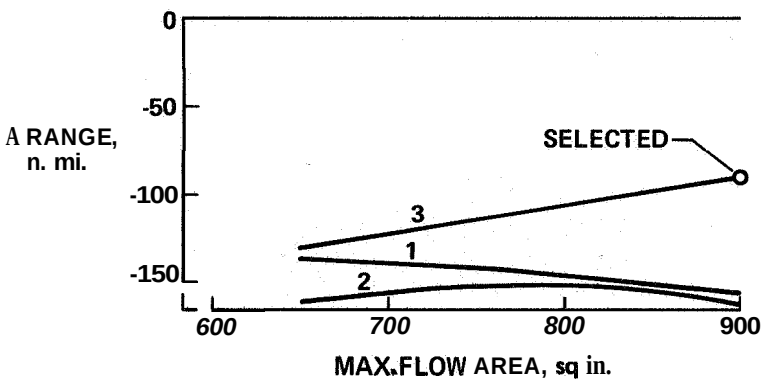

Figure 5

ACOUSTIC ANALYSIS

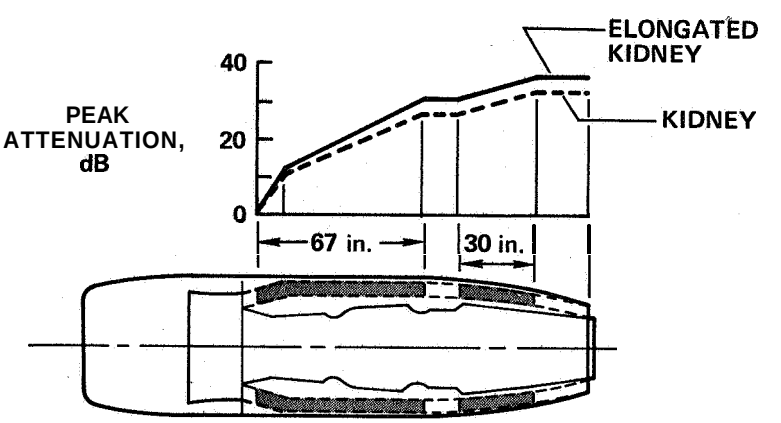

Figure 6

SELECTED DUCT CONFIGURATION

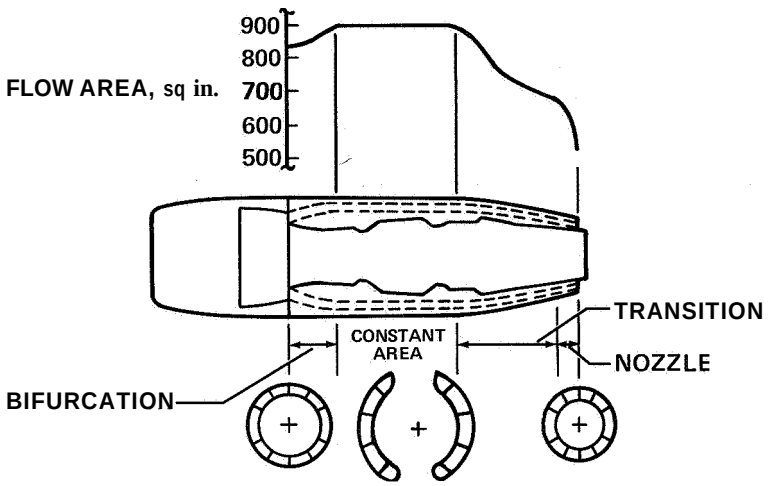

Figure 7

GROUND-TEST CONFIGURATION

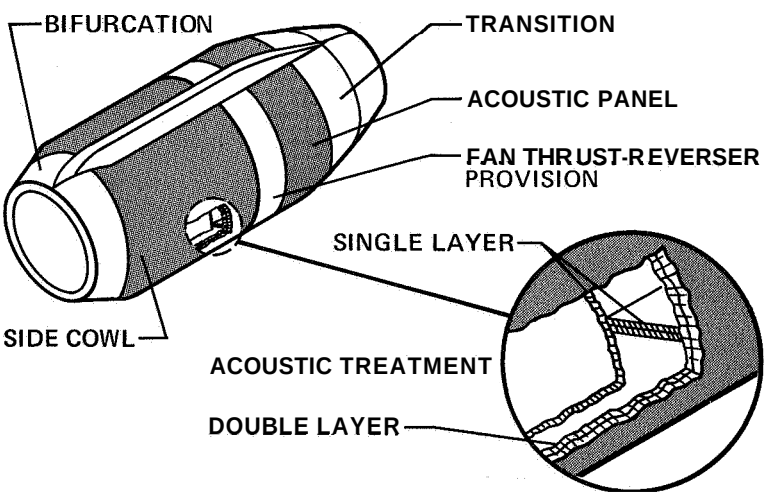

Figure 8

FAR-FIELD MICROPHONES

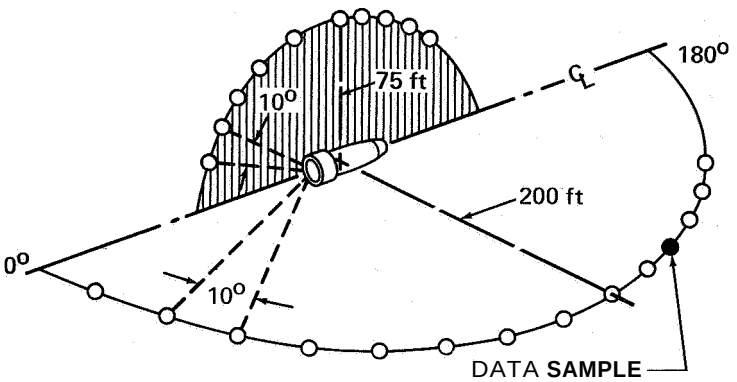

Figure 9

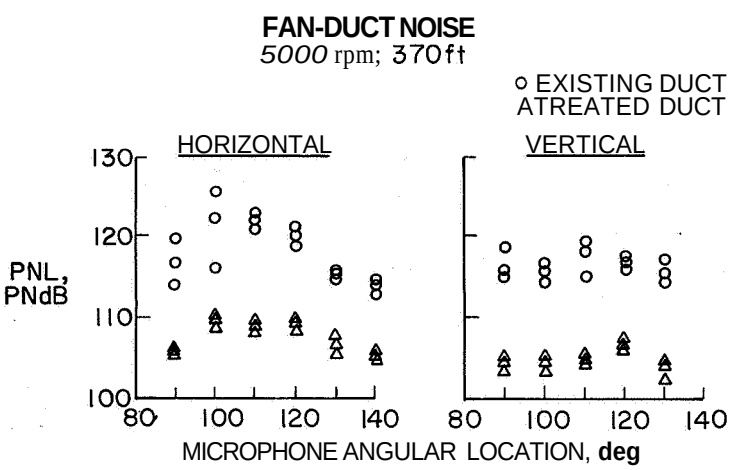

Figure 10

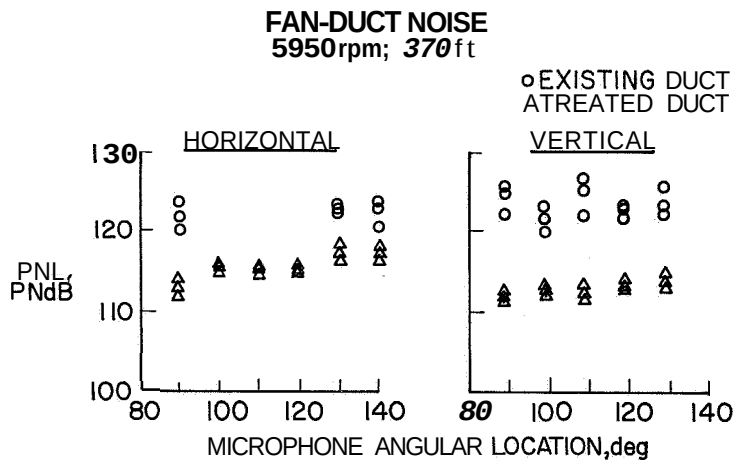

Figure 11

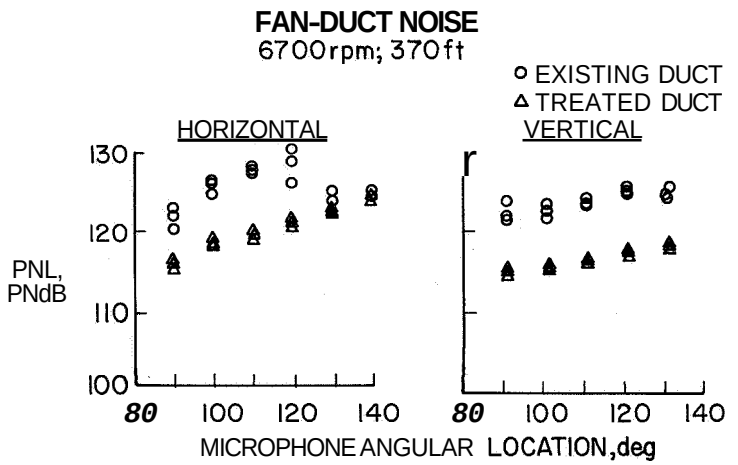

Figure 12

EFFECT OF THRUST ON NOISE REDUCTION
370 ft

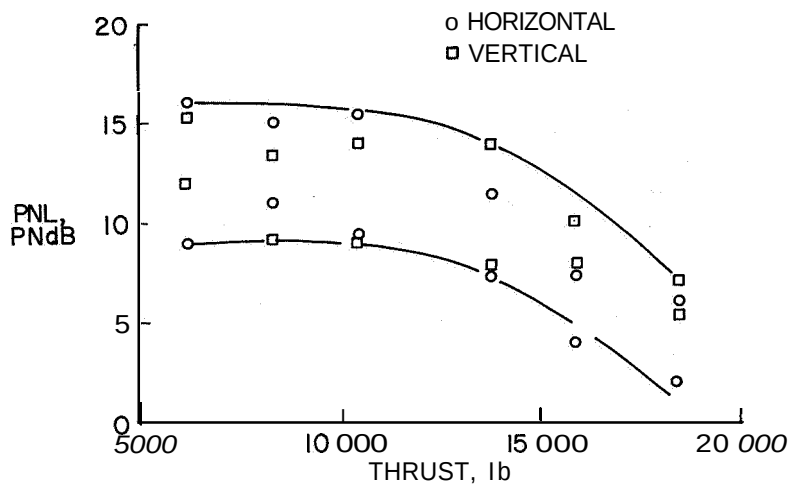

Figure 13

NOISE REDUCTION MEASUREMENT

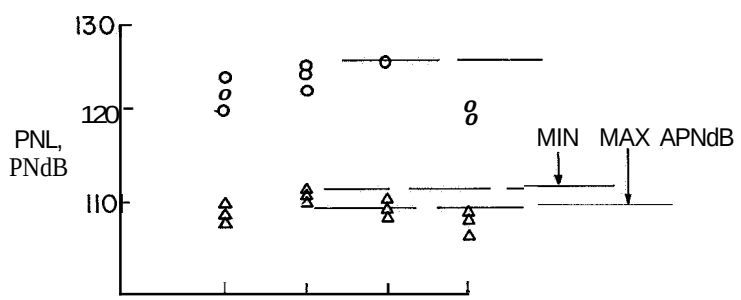

Figure 14

ACOUSTIC RESULTS GROUND-TEST DUCT

5000 rpm, 370 ft

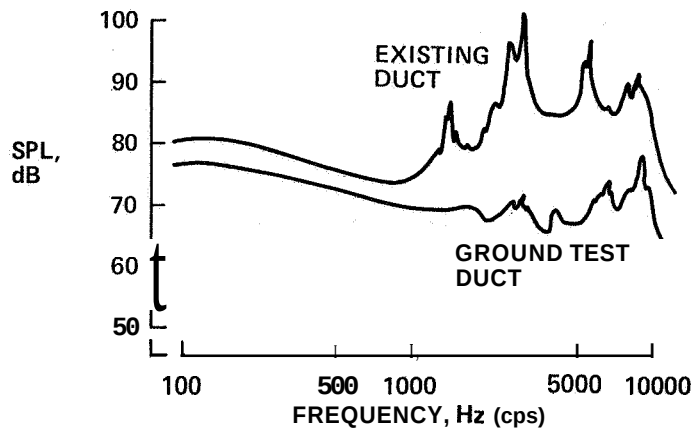

Figure 15

GROUND-TEST ENGINE PERFORMANCE

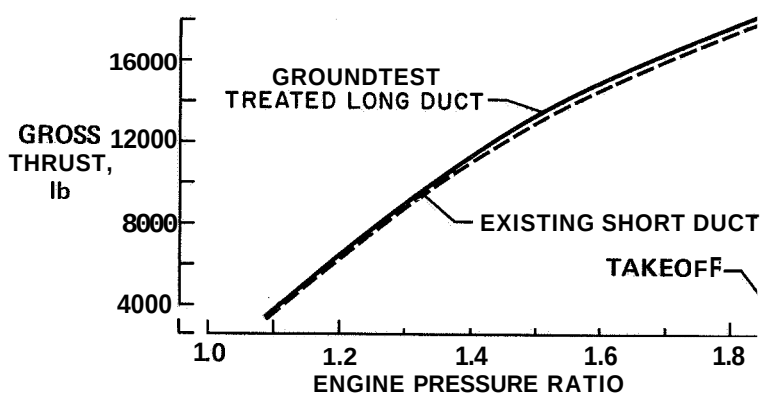

Figure 16

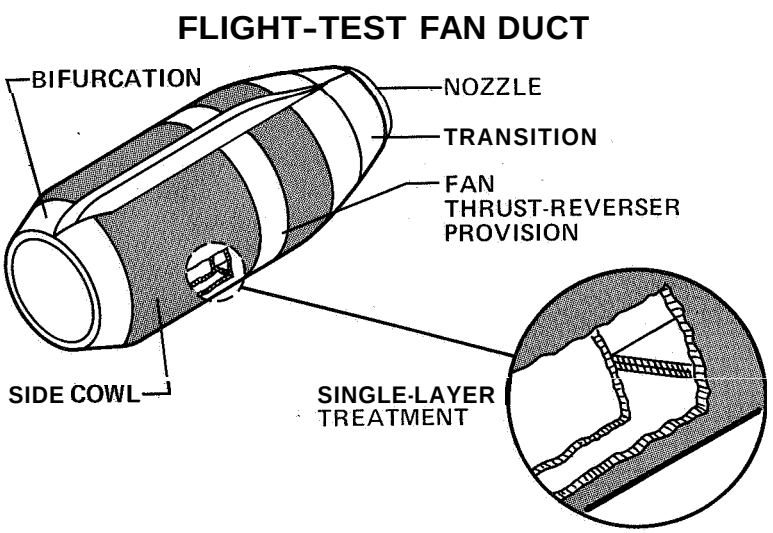
FLIGHT-TEST FAN DUCT
BIFURCATION
NOZZLE
TRANSITION
FAN
THRUST-REVERSER
PROVISION
SIDE COWL
SINGLE-LAYER
TREATMENT

Figure 17

16. NOISE PREDICTIONS AND ECONOMIC EFFECTS OF BOEING NACELLE MODIFICATIONS

By D. C. Nordstrom and D. S. Miller

The Boeing Company

SUMMARY

The features and requirements of an acoustically treated nacelle designed for JT3D turbofan-powered 707 airplanes are described. The acoustic features of this nacelle which make it different from the existing production configuration include (1) a two-ring treated inlet containing 87 square feet of acoustical material within the diffuser to reduce the fan-generated noise radiated forward and (2) a full-long fan duct lined with 267 square feet of sound absorbing material to reduce the aft radiated fan noise. It is predicted that this combination of inlet and fan duct treatment will reduce the fan noise to the level of the jet noise during landing approach. When this treatment is applied to the 707-320B airplane on a 3° glide slope, a reduction in peak flyover noise of approximately 13 to 16 PNdB is realized at a point 1 nautical mile from the runway threshold. In addition, the time of exposure to noise in excess of 100 PNdB is markedly reduced. The increase in jet noise level at take-off thrust settings limits the reductions in peak take-off flyover noise to approximately 5 to 7 PNdB at a point 3.5 nautical miles from brake release. If the airplane could cut back thrust to that required to maintain a 6-percent climb gradient, then a further reduction in flyover noise of 4 PNdB should be realized. Flight validation is required to substantiate that the predicted reductions can be achieved. Flight tests of the modified nacelle are scheduled for May and June 1969.

The nacelle modifications have been developed with the goal of maximizing the landing-approach noise reduction while minimizing the impact on airplane performance and economics. The loss of 180 nautical miles in maximum range capability is a result primarily of the 3360-pound total increase in nacelle weight. Although a slight reduction in take-off thrust is expected, its effects on field length and climbout are negligible.

The major factors affecting direct operating costs (DOC) for an airplane retrofitted with treated nacelles have been determined by using the 1967 Air Transport Association method. The resulting DOC increase of approximately 7 to 10 percent results from depreciating the estimated kit costs of $900,000 to $1,150,000 over a period of 5 years. The kit costs are based on 1972-1973 dollars and reflect the 46-month period, after production go-ahead, required to certify and produce retrofit kits for the six hundred 707 and 720 turbofan-powered airplanes that will be operating in the early 1970's.

INTRODUCTION

Details of the acoustically treated inlets and fan exhaust ducts being developed under NASA Contract NAS1-7129 are presented in references 1 and 2. The purpose of the present paper is to integrate these data in terms of the impact of acoustically treated nacelles on the JT3D-3B powered 707-320B airplane. Some of the characteristics of the basic-specification airplane selected for analysis are a maximum take-off gross weight of 327 000 pounds, 149 passenger seats with 15 percent first class and 85 percent tourist class, and a maximum landing weight of 207 000 pounds.

The effects of retrofitting the airplane with acoustically treated nacelles are considered in the following major areas:

(1) Noise reductions for landing-approach and take-off conditions

These noise-reduction predictions are based directly on Boeing and McDonnell Douglas ground-test results.

(2) Payload range and take-off performance

(3) Direct operating cost (DOC), and nacelle certification and retrofit kit production schedules

These cost and production data are based on a total fleet of six hundred 707 and 720 (including one hundred seventy 707-320B's) turbofan-powered airplanes expected to be operational during 1972-1973.

CONFIGURATION DESCRIPTION

The short-duct nacelle configuration (fig. 1), the design of which took place in 1959-1960, was carefully tailored to provide low weight and minimum cruise drag, The resulting inlet highlight diameter and the 18-percent throat contraction ratio selected required blow-in-doors to provide surge-free engine characteristics during low-speed operation. The large blow-in-doors shown in figure 1 illustrate a second iteration of the basic inlet with the intent of providing improved pressure recovery at the engine compressor face, and thus increased thrust during take-off and climbout. The short fan exhaust duct and the very tightly fitted cowl provide minimum nacelle cross-sectional area. Since the engine nacelle is also cantilevered as far forward of the wing as the structural design concept will permit, the combination effect provides minimum wing-nacelle interference drag. The fan nozzle location selected, however, results in some thrust and specific fuel consumption penalties as a consequence of scrubbing drag caused by the relatively high-velocity fan exhaust air blowing over the aft engine cowl. The manner in which these factors are related makes it difficult to change the nacelle configuration

to obtain substantial noise attenuation and not incur a loss in airplane performance, a deterioration in airplane flutter characteristics, or some other adverse effect.

A number of significant changes from the baseline nacelle are required to accqm-modate the acoustic treatment needed to provide the desired noise attenuation. In the treated nacelle (fig. 2), the inlet design philosophy has been revised completely. The blow-in-doors have been eliminated and the inlet is longer and heavier. The highlight diameter has been increased, the throat contraction ratio has been changed to 25 percent to assure satisfactory low-speed operation, and 87 square feet of acoustic treatment have been provided within the diffuser. Further changes are evident in the installation of the larger diameter, full-long duct containing 267 square feet of acoustic treatment. It can be noted that the annular fan and primary nozzles are essentially "coplanar." These changes will add approximately 3360 pounds to the airplane operating empty weight and will also contribute to some deterioration in cruise performance. However, care has been taken in the detail design in an effort to minimize these adverse performance effects and yet meet the noise attenuation goals.

NOISE ATTENUATION

The noise attenuation attainable from the treated nacelle is very strongly influenced by power setting, as shown in figure 3. At the 707-320B maximum landing weight of 207 000 pounds, a net thrust of 5000 pounds per engine is required when the aircraft is on a 3^{o} glide slope with gear down and landing flaps extended. The noise reduction shown of 9 to 16 PNdB at this power setting represents the extremes of the measurements obtained during ground test at the Boeing Company's Tulalip test facility corrected for flight and extrapolated to a 3'70-foot altitude and includes tolerances in measurement of both the baseline and the treated configurations. Spectral analysis clearly shows that the limiting noise source at this power setting is turbine-blade-generated noise.

At the **707-320B** maximum take-off weight of **327** 000 pounds, approximately **11 700** pounds of thrust per engine are required to maintain a 6-percent all engine climb gradient with take-off flaps extended and gear up. At this cutback power setting, the jet noise levels are relatively higher than those at approach thrusts. Therefore, the effec-tiveness of the treated rings, linings, and splitters of the inlet and duct in reducing fan noise cannot be fully exploited and the noise reduction is correspojndingly reduced. At take-off thrust, the jet noise produced downstream of the primary nozzle becomes even more dominant and effectively limits the noise attenuation available to the values shown.

Figure **4** identifies the noise reference points currently proposed by the Federal Aviation Administration (FAA) and considered in this paper. The approach reference point is **1** nautical mile from the landing threshold and directly beneath the 3^{o} glide-slope

approach path, and the take-off reference point is 3.5 nautical miles from the start of the take-off roll and directly beneath the take-off flight path.

Estimated time histories of flyover noise at the approach reference point are presented in figure 5 for the baseline-nacelle airplane and a treated-nacelle airplane with a thrust per engine of 5000 pounds. The estimates use the limited ground-test data of figure 3 and represent the noise exposure that a ground observer at the approach reference point would receive. In addition, these noise time histories show a 13- to 16-PNdB reduction from the baseline-nacelle-airplane peak perceived noise level of 123 PNdB to the treated-nacelle-airplane peak perceived noise level of 107 to 110 PNdB. Therefore, on the basis of these data it may be observed that the time exposure to noise levels in excess of 100 PNdB will be substantially reduced.

Figure 6 identifies the effect of altitude and distance from the threshold on noise reduction during landing approach for a thrust per engine of 5000 pounds. Noise reduction and altitude are shown at various distances from the landing threshold during a 3° glide-slope approach. Note that the attenuation decreases approximately 1 PNdB per nautical mile from the threshold.

The flyover-noise signature at the take-off reference point is shown in figure 7(a) for the treated-nacelle airplane and the baseline-nacelle airplane. The variation in sound pressure level as a function of thrust measured during ground tests, when extrapolated to flight, results in an estimated 5- to 7-PNdB reduction in take-off noise from the baseline-nacelle-airplane peak perceived noise level of 118 PNdB to the treated-nacelle-airplane peak perceived noise level of 111 to 113 PNdB. The perceived noise levels of figure 7(a) are calculated for an altitude of approximately 900 feet, which is representative of the altitude attained by a maximum take-off gross weight 707-320B airplane at a point 3.5 nautical miles from the start of take-off roll.

Because the airplane with either nacelle configuration is at an altitude of less than 1000 feet, cutback thrust cannot be utilized as a noise abatement procedure under proposed FAA noise certification criteria. If take-off gross weights are less than approximately 320 000 pounds, altitudes at the take-off noise reference point will exceed 1000 feet. When cutback can be employed, the proposed FAA noise rule requires a minimum climb gradient of 6 percent. Figure 7(b) presents the baseline-nacelle and treated-nacelle flyover perceived noise levels estimated for the thrust setting required to maintain a 6-percent climb gradient. The results indicate that acoustic treatment will effect a further reduction of approximately 4 PNdB.

The noise variation with take-off gross weight is presented in figure 8 for the baseline-nacelle and treated-nacelle airplanes. Both configurations are assumed to employ an instantaneous cutback to a 6-percent climb gradient over the 3.5-nautical-mile point for take-off weights below 320 000 pounds. The take-off noise estimates shown in

figure 8 therefore combine the effects of both the altitude increase at the noise reference point and the reduction in the thrust required to maintain climb as weight is reduced.

An interesting feature of the full-long-duct nacelle, which may contain a payoff of significant proportions, is that the annular "coplanar" fan and primary nozzles provide approximately 2- to 6-dB noise reduction from the baseline short-duct nacelle in the jet noise spectra. These reductions exist across the entire range of engine power settings and are believed to result from reduced shear velocity gradients in the primary nozzle mixing zone.

PERFORMANCE EFFECTS

Substantial engineering effort has been devoted to minimizing the adverse effects of the nacelle modifications on airplane performance. The principal nacelle change producing adverse performance effects is the full-long aft fan duct. The long-duct nacelle, compared with the existing short-duct production nacelle, results in a threefold increase in wetted area to be accounted for in drag calculations as well as an increase in the interference drag as a result of increased cross-sectional area adjacent to the wing. More important, the long duct, and the acoustic treatment that it contains, is responsible for an appreciable increase in nacelle weight.

The increase in airplane drag is estimated to be approximately 3.1 percent at Mach 0.80 and a 35 000-foot altitude, the conditions typical of long range cruise. The increase in skin-friction drag due to increased nacelle wetted area accounts for more than 80 percent of the total increase at Mach 0.80 and the increases in interference drag account for most of the rest of the penalty. These estimates contain a 10-percent allowance in skin friction to account for typical production surface roughness and excrescencies. The initial set of flight-test nacelles is not being fabricated with production tooling and the surfaces might not achieve the smoothness that would be demanded for airline equipment. Except for surface smoothness, it is believed that the estimated increases in drag are reasonably accurate. Some confirmation of these estimates is obtained from results of a wind-tunnel test of a generally similar sonic-throat-inlet nacelle model conducted under Contract NAS1-7129. The results of this test, when adjusted to account for configuration differences, bracket the estimated 3.1-percent increase. A long-duct—sonic-throat-inlet nacelle configuration and the existing short-duct production configuration were tested on an 0.068-scale half-model. The data obtained in this test are used to establish the drag rise characteristics. At the Mach 0.83 minimum DOC cruise condition, the added interference drag of the treated nacelles is estimated to result in an increase in drag of approximately 5.1 percent.

The installed engine performance at take-off and cruise has been estimated for the acoustically treated nacelle configuration. Engine performance changes resulting from

estimated inlet pressure recovery losses, fan duct pressures (based on measurements obtained during ground tests), and fan exhaust nozzle velocity coefficients were applied to Pratt & Whitney specification engine performance. This analysis indicates that thrust increases of 3.1 percent and thrust specific fuel consumption (TSFC) improvements of 3.5 percent might be obtained for the Mach 0.80 long range cruise condition. This potential improvement results primarily from the elimination of the scrubbing of relatively high-velocity fan exhaust on the afterbody of the existing short-duct nacelle. This scrubbing drag is absorbed as an installed engine performance penalty of more than 4 percent of cruise thrust and TSFC so that its elimination can more than balance the inlet losses. The inlet pressure recovery losses are calculated on the basis of the estimated flat-plate skin-friction drag (with an allowance for the roughness) of the acoustic material and the ring-strut intersection drags. Duct and nozzle velocity coefficients are expected to change only a small amount in a favorable direction at cruise conditions.

At take-off, however, duct velocity coefficients change in an adverse manner by about 1/2 percent and contribute to the 70-pound reduction in take-off thrust that is estimated for a treated nacelle. At take-off, elimination of scrubbing drag, at best, represents an improvement of approximately 1.5 percent in thrust, about the same magnitude as the magnitude of the inlet losses which is also estimated to be about 1.5 percent and, thus, the inlet losses will balance the scrubbing-drag improvements.

Weight estimates indicate an increase in operating empty weight of 3360 pounds, 840 pounds for each nacelle, to account for acoustic material, increased length and diameters of the inlet cowls, long fan ducts, and new fan thrust reversers. These estimates are based on analysis of the weights of an assumed production configuration which would necessarily be different in many respects from the test configuration to be flown in this program.

Field lengths and take-off profiles were calculated for the existing production and acoustically treated nacelle airplanes by methods which account (empirically) for important parameters such as flare and rolling friction. The estimated effects on engine and airplane performance of the treated nacelle previously described are included in the calculation. The effect of the nacelle installation on take-off length and climbout profile is small. For a temperature of 77° F and for a 327 000-pound maximum take-off gross weight, the take-off field length of the airplane with treated nacelles is lengthened by 50 feet from a baseline of 10 710 feet and the altitude at 3.5 nautical miles from brake release is decreased by 15 feet from a baseline of 900 feet.

The effect of the treated nacelles on payload range is defined in figure 9 for domestic and international operations. Both long range cruise and minimum DOC cruise conditions are shown for the baseline 707-320B airplane and the treated-nacelle airplane. A step climb cruise procedure was used for long range cruise, whereas a constant altitude

was utilized for minimum **DOC** cruise. Inasmuch as detailed differences exist between the basic-specification airplane selected for analysis and individual airlines' configurations, the performance shown in the figure can only be considered representative of airplane capability. The performance penalties ranging from 165 to 180 nautical miles for international and domestic long range cruise (fig. 9) are almost entirely due to the 3360-pound increase in operating empty weight because of the expectation that the ***drag*** increase of the treated-nacelle configuration will be balanced by an increase in installed engine performance at Mach 0.80 cruise. The domestic range penalty of 240 nautical miles at Mach 0.83 minimum **DOC** cruise is larger than the range penalty at long range cruise; this reflects the effect of the increase in interference drag with Mach number. The 1967 Air Transport Association (ATA) fuel reserve rules were applied. The difference in the fuel reserve requirements of these ground rules is responsible for the small differences in range penalties between the domestic and international performance shown in figure 9.

RETROFIT **ECONOMICS**

The economic consequences of the range penalties shown in figure 9, coupled with retrofit cost considerations, must be evaluated for each airline's route structure to determine how critical long range routes or take-off limited fields are affected and how these changes will affect the airline profit structure. A study of this magnitude is beyond the scope of this paper but considerable insight into the economic consequences of retrofitting treated nacelles into airline operations can be determined by analyzing changes caused in direct operating costs. For this purpose, direct operating costs have been calculated for airplanes equipped with baseline and treated nacelles by using the 1967 ATA method for domestic and international operations (except that actual maintenance estimates are used for the treated nacelles). Major **DOC** considerations are as follows:

Retrofit cost (including installation)	$900,000 to $1,150,000
Initial spares	20%
Depreciation period:	
Airframe	12 years
Nacelle	5 years
Airplane utilization	ATA curve
Passenger seats	149
Firstclass	15%
Tourist class	85%
Airplane downtime	Assumed zero
Nacelle maintenance	Functional analysis

Two retrofit cost estimates are given, which correspond to the maximum and minimum estimates of the kit cost. This cost range represents the uncertainties in estimating

production costs for the polyimide—glass-fiber acoustic construction currently being considered for this nacelle. The airplane kit costs of $900,000 to $1,150,000 are estimated for 1972-1973 dollars. A factor of considerable importance to the DOC estimate is the inclusion of a 20-percent initial spares allowance for the retrofit nacelle. This allowance is based on current experience with the existing short-duct production nacelles which are requiring from 13 to 24 percent spares for various major nacelle components. This allowance is in line with the ATA 1967 formula because the nacelle is built up of "airframe" components, for example, inlet and fan discharge duct cowlings (13 to 17 percent initial spares) and "engine" components, for example, thrust reversers and quick engine change items (15 to 24 percent initial spares). The ATA method's new airplane depreciation period of 12 years is assumed. The 5-year depreciation period for the treated nacelle is being used in other noise-alleviation studies sponsored by the Air Transport Association and Aerospace Industries Association. This depreciation period accounts to some degree for the fact that the average airplane being considered for retrofit has already been in service for some time and, therefore, has a limited useful life. Each airline has its own individual depreciation philosophy however, and these philosophies must be extended to this particular problem in each individual case. Downtime was not included as an economic factor on the basis of the assumption that retrofit would be accomplished concurrent with airplane overhaul. If this assumption should prove to be incorrect, additional airplane out of service costs would have to be included.

The calculated direct operating costs, based on the aforementioned ground rules, are presented as a function of ATA range in figure 10 and the data indicate an increase of approximately 7 to 10 percent in DOC as a result of retrofit for both domestic and international operations. The most significant factor causing this increase is the kit cost of $900,000 to $1,150,000 and the assumed 5-year depreciation period.

The significance of the change in value to be depreciated can be better understood by a comparison of depreciation, crew pay, insurance, maintenance, and fuel costs for the baseline-nacelle airplane and the treated-nacelle airplane. As can be seen in figure 11, retrofit causes an increase in depreciation from 26 percent to 31 percent of the DOC. Crew pay does not change, but insurance costs will increase slightly as a function of the retrofit kit cost. Fuel costs will increase by an amount about equal to the increase in insurance costs.

The baseline maintenance costs were also calculated by the 1967 ATA maintenance cost analysis procedure. If this ATA procedure had been used for the retrofit maintenance cost calculations, instead of actual estimates based on functional analysis of the proposed configuration, the value would be 0.344 cent per seat statute mile rather than

0.341 cent as shown in figure 11. Should the retrofit kit costs be written off over a different time period from the 5-year period assumed, then the depreciation costs can change substantially as shown in figure 12. In this figure the percentage increase in DOC is established for assumed depreciation periods ranging from 2 to 12 years. As can be seen, depending on the period assumed for depreciation, the impact of retrofit on DOC can be almost halved or doubled. Again, depending on the depreciation period, the spread in estimated kit costs could result in a change of from 2 to 4 percent in DOC.

Some insight into the implications of the timing of the treated-nacelle retrofit program can be gained from the possible production schedule shown in figure 13. Significant program events are identified with respect to an assumed production program go-ahead. The program schedule could vary somewhat from the estimated timing shown, depending on factors such as timing of production go-ahead, urgency of program, certification rule application, total production requirements and production rates. However, the program is believed to be quite representative considering current and proposed production capability and capacity. The first significant milestone occurs 14 months after production go-ahead when the first complete production kit is available for flight test. Precertification and certification flight testing leads to a certified retrofit for the 707-320B airplane 22 months after go-ahead. Delivery of kits to the airlines could begin at this time and, based on an assumed production rate of 25 kit shipments per month, production of kits for 600 airplanes, not including spares, would be completed approximately 4 years after production go-ahead.

It must be understood that use of DOC as a measure of airplane operating profitability for a massive retrofit program, such as that envisioned for the acoustically treated nacelle, extends the 1967 ATA method beyond its designed intent. Also, the DOC is only one measure of the impact of retrofit. Questions arise such as, Will an old airplane be retired and new equipment purchased? Or, Will the outlay of substantial monies for quiet nacelles preclude the purchase of much of the planned new equipment? Nearly $1 billion in financing must be arranged over a relatively short period. Will the public pay? How elastic is the market? These questions are not part of the contract with NASA, but these and other questions must be both asked and answered in the near future.

CONCLUDING REMARKS

An acoustically treated nacelle designed for the JTSD turbofan-powered 707 series airplanes is currently being constructed and is scheduled to be flight tested in May-June 1969. Although technology evolved during the development of this nacelle is applicable to other turbofan engines installed on other airplanes, the magnitudes of the noise reductions estimated for the acoustically treated JTSD nacelle are not applicable to any other type of

turbofan engine, primarily because of the variation in the relative intensity of the individual noise sources within the engine. Similarly, performance and DOC penalties are not applicable to aircraft other than the 707-320B airplane used as an example. The most important results of this program to date are as follows:

1. Significant reductions in JT3D engine noise appear to be technically feasible. In the landing-approach configuration, maximum noise reductions of 13 to 16 PNdB are predicted. Maximum noise reductions of 5 to 7 PNdB are possible at take-off thrust and 9 to 11 PNdB at cutback thrust.

2. The range penalty at long range cruise conditions, 180 nautical miles for domestic ATA fuel reserves, is due almost entirely to the 3360-pound increase in operating empty weight.

3. Changes in take-off and climb performance are considered negligible.

4. The direct operating cost increase of 7 to 10 percent is a direct result of the $900,000 to $1,150,000 kit cost and 5-year depreciation period adopted and can change considerably if other assumptions are made.

5. Delivery of certified quiet nacelle kits to the airlines could start as early as 22 months from a production go-ahead. Manufacture of 600 airplane kits could be completed 2 years later.

A word of caution is necessary with regard to application of these predicted noise reductions and associated performance effects. First, these predictions are based upon extrapolation of limited model and full-scale ground-test data applied to a proposed retrofit treated-nacelle airplane and, second, the noise reductions and performance have yet to be validated by flight demonstrations. This paper is an interim status report only.

REFERENCES

1. Drakeley, George T.; and McCormick, Ralph B.: Treated Inlets. Conference on Progress of NASA Research Relating to Noise Alleviation of Large Subsonic Jet Aircraft, NASA SP-189, 1968. (Paper No. 14 herein.)

2. McCormick, Ralph B.: Fan-Duct Development. Conference on Progress of NASA Research Relating to Noise Alleviation of Large Subsonic Jet Aircraft, NASA SP-189, 1968. (Paper No. 15 herein.)

BASELINE NACELLE

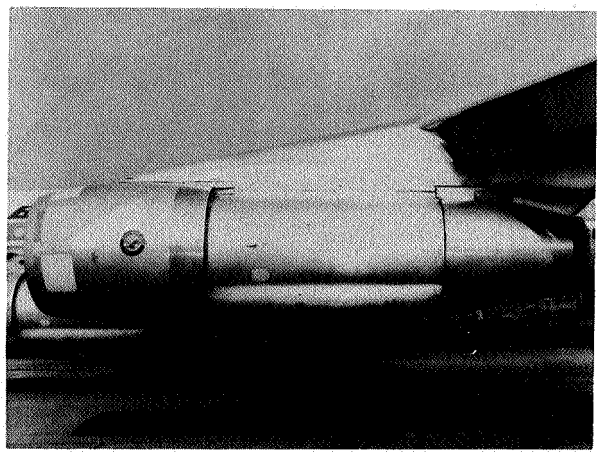

Figure 1

L-68-8573

TREATED NACELLE

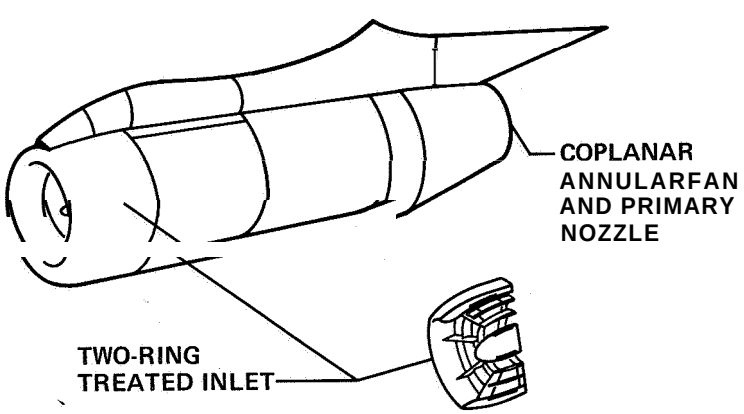

Figure 2

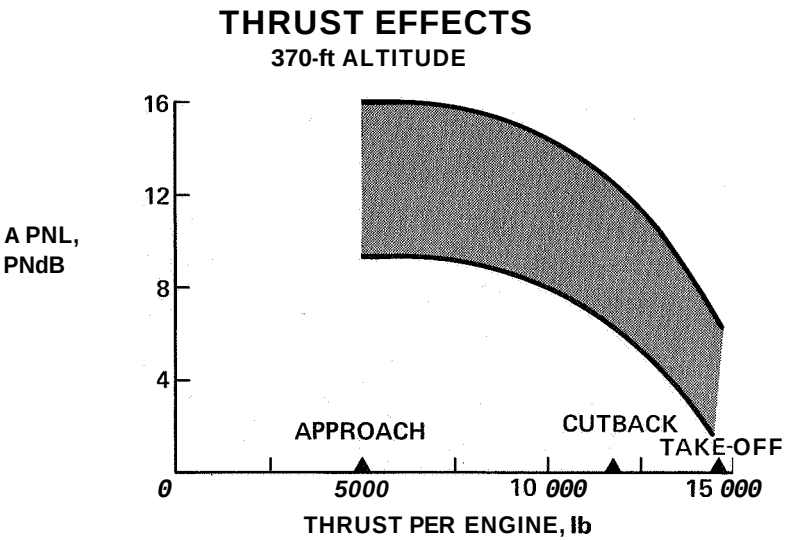

Figure 3

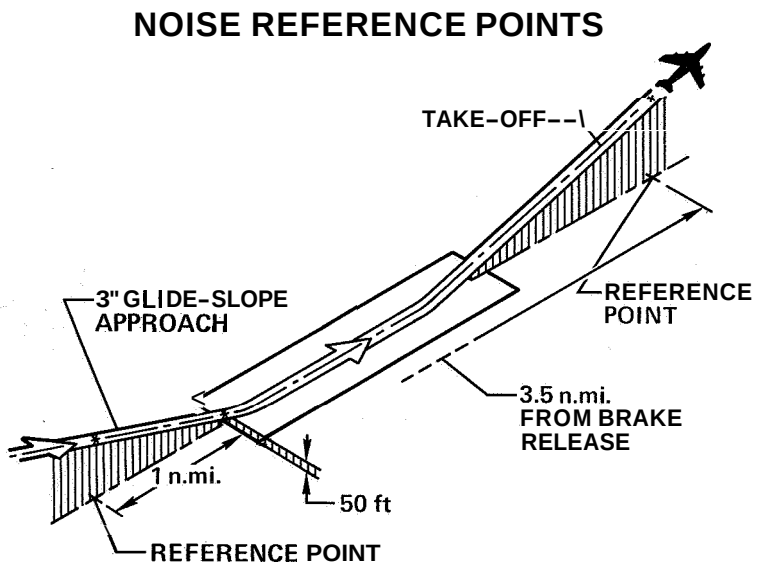

Figure 4

FLYOVER NOISE AT APPROACH REFERENCE POINT

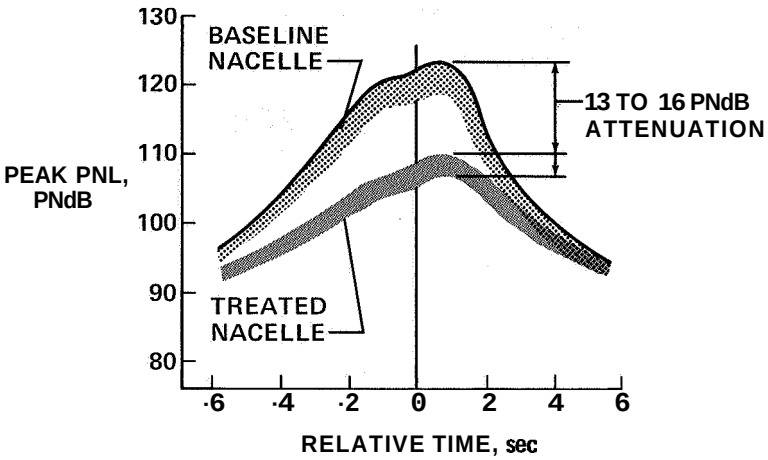

Figure 5

NOISE REDUCTION DURING LANDING APPROACH

THRUST PER ENGINE, 5000 lb

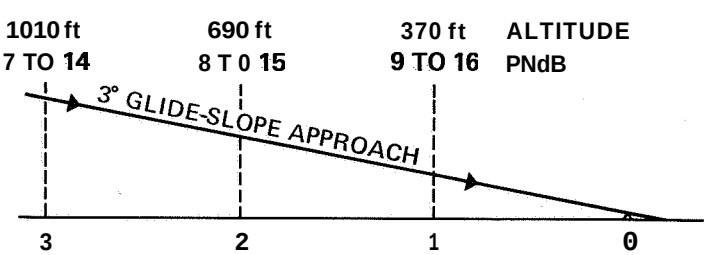

Figure 6

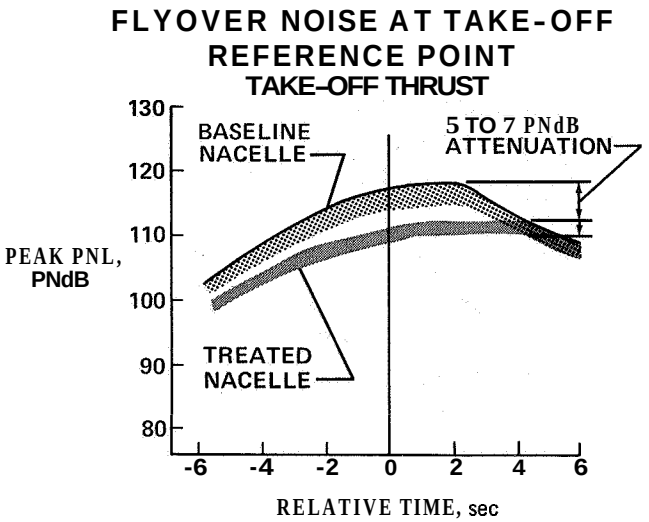

(a)

CUTBACK THRUST

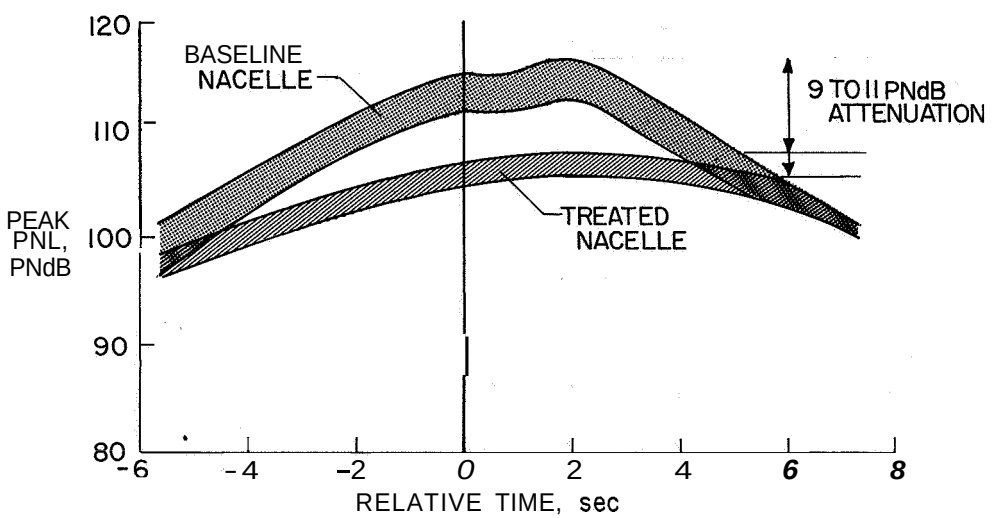

(b)

Figure 7

FLYOVER NOISE AT TAKE-OFF

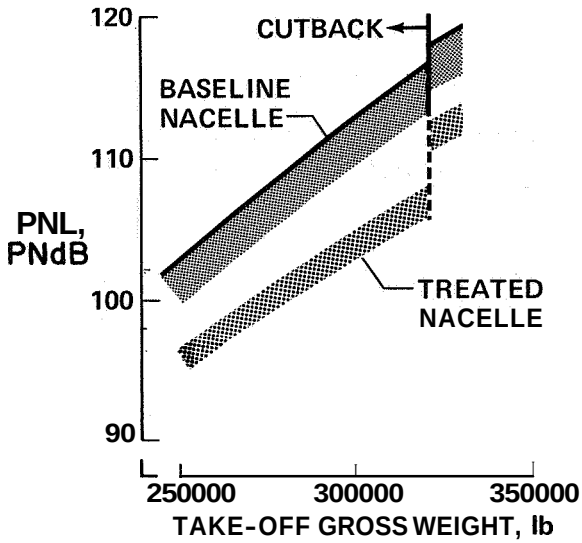

Figure 8

PAYLOAD RANGE

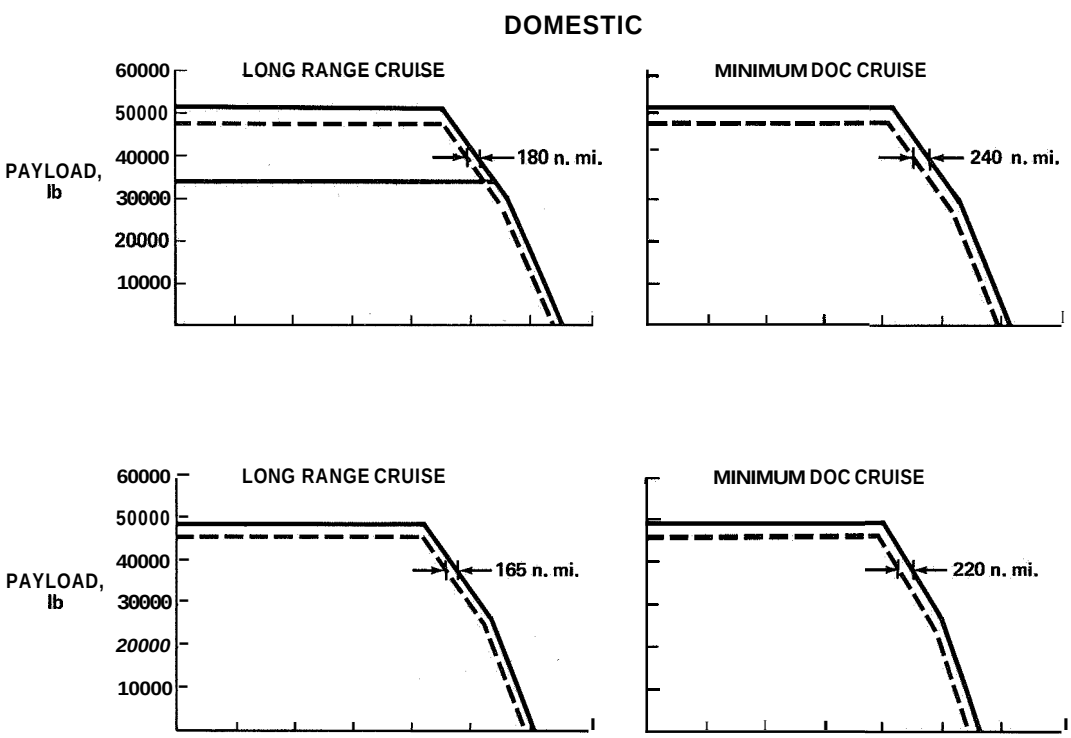

Figure 9

DIRECT OPERATING COST

DOMESTIC OPERATIONS

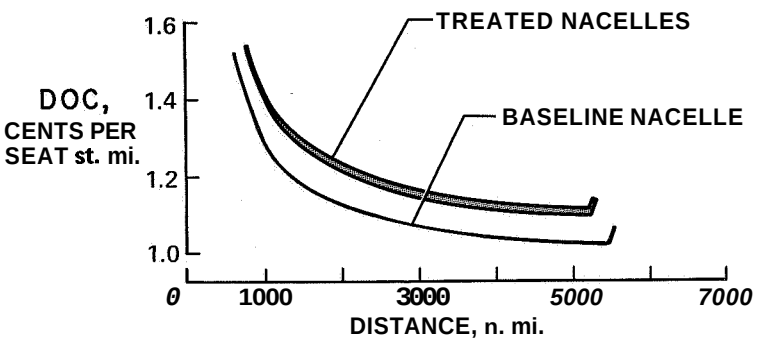

(a)

INTERNATIONAL OPERATIONS

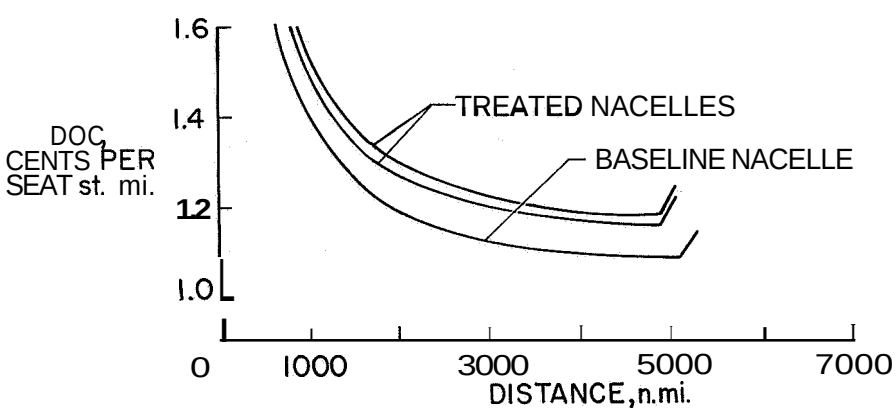

(b)

Figure 10

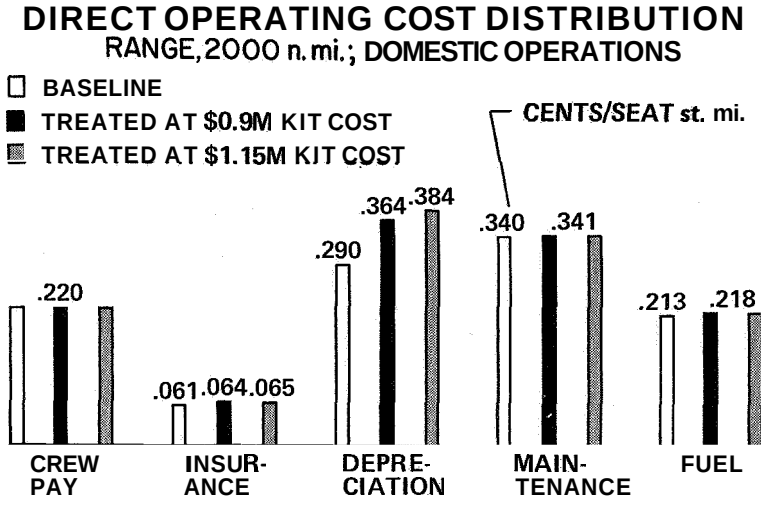

Figure 11

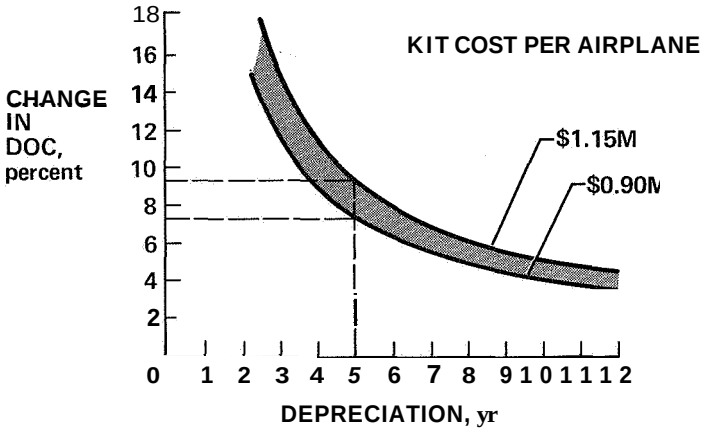

Figure 12

RETROFIT KIT PRODUCTION SCHEDULE

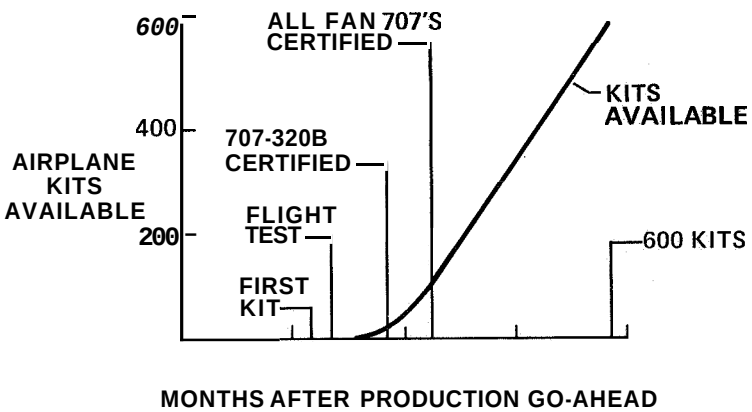

Figure 13

17. CONCLUDING REMARKS ON NACELLE ACOUSTIC TREATMENT APPLICATION

By John G. Lowry
NASA Langley Research Center

The flyover noise data presented in the preceding papers were, in general, referred to a point directly under the approach flight path 1 mile from the end of the runway. In order that no one will be misled by this type of presentation, figure 1 has been prepared to show the variation of noise around the end of the runway for a four-engine turbofan-powered transport approaching for a landing. Figure 1 presents lines of equal perceived noise level for the basic untreated airplane and the associated attenuations for the airplane with the modified nacelles as a function of the distance from the end of the runway. These data are for outside conditions and for a nacelle modification that gives about an 11 PNdB reduction at the reference point. It should be noted that the distance along the runway is in nautical miles and the side line distance is in feet. This arrangement was used to make the figure more intelligible by separating the curves. As a person proceeds away from the end of the runway, the perceived noise levels reduce; the APNdB resulting from the nacelle modifications show the same trends. The results do, however, show that the people who experience the greatest noise exposure also experience the greatest noise reduction. Since there has been some concern that people inside houses would not experience any significant benefit from nacelle modifications, figure 2 has been prepared to show the noise exposures of people inside a house for the same flyover conditions and nacelle modifications as used in figure 1. The house selected is one with attenuation characteristics about midway between the extremes of houses from several parts of the United States (ref. 1). There is a significant attenuation due to the house itself; for example, the noise level decreases from 120 PNdB to 93 PNdB at the measuring point. Despite this large attenuation due to the house, the benefit of the nacelle acoustical treatment is still significant, being only about 2 PNdB less than that experienced outdoors. More complete data of this type will be available for the modified airplane after the flight tests. These data will include take-off noise footprints, the results being presented in effective perceived noise level.

The presentations of the economic impact of a retrofit program have been given in terms of direct operating costs only. It is realized that direct operating costs present only part of the picture; however, since all the data are estimated from ground-test results, it was felt that direct operating costs are probably the best indicator at this time. Certainly many of the more pertinent economic considerations including those that are unique to any given airline will have to be considered in evaluating the economic impact on the airlines. The final reports of these studies will, based on the flight-test results,

present a more comprehensive analysis of the economic impact on the airlines. Each airline will, of course, have to evaluate its own operations on the basis of the flight-test results.

Since airplanes powered by the Pratt & Whitney JTSD engine are only part of the noise problem, the application of these data to other engines including the high-bypass-ratio engines is important. It is believed that the treatment technology and concepts can be applied by correctly taking into account the differences in physical size and shape of the engine and nacelle and the noise spectrum of the untreated engine. The values of attenuation obtained from the JT3D engine would not, of course, be expected to apply directly to other engines since the relative strengths of the several noise sources differ from engine to engine. It is believed, however, that the reductions can be estimated by considering the characteristics of individual engines.

Finally, it should be again emphasized that the preceding papers are only a progress report and that the noise attenuation, airplane performance, and direct operating costs are estimates based on ground runup data only. These estimates will be verified after the flight-test results are obtained and analyzed sometime next summer.

REFERENCE

1. Mayes, William H.; Findley, Donald S.; and Carden, Huey D.: House Vibrations Significant for Indoor Subjective Response. Conference on Progress of NASA Research Relating to Noise Alleviation of Large Subsonic Jet Aircraft, NASA SP-189, 1968. (Paper No. 39 herein.)

NOISE FOOTPRINT
LANDING APPROACH, OUTSIDE

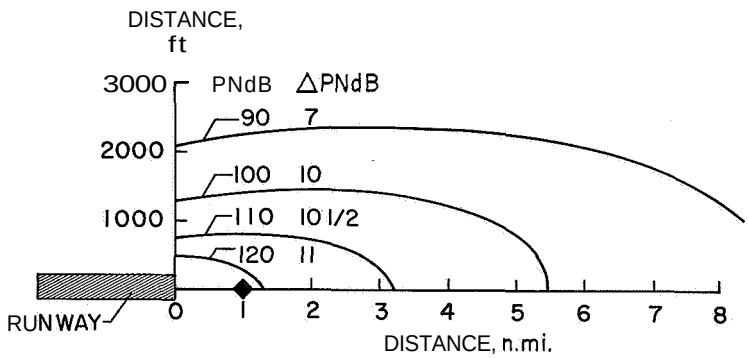

Figure I

NOISE FOOTPRINT
LANDING APPROACH, INSIDE

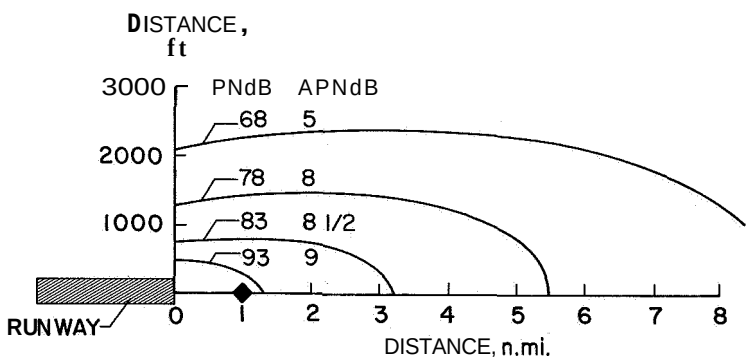

Figure 2

18. QUIET ENGINE PROGRAM

PRELIMINARY ENGINE DESIGN AND AIRCRAFT INTEGRATION

By Joseph F. McBride

NASA Lewis Research Center

SUMMARY

Design studies sponsored by National Aeronautics and Space Administration have resulted in identification of engine cycle characteristics, engine mechanical configurations, and component aerodynamic design parameters which allow turbofan airplane power plants to operate with lower noise output. Preliminary designs of such engines have been made to define the weight and size compromises resulting from design considerations for engine quieting. Engine noise output is predicted to be significantly lower than that produced by currently operating engines. Integration of the quiet engine with a typical subsonic jet transport has been investigated. Study results indicate that useful turbofan engines designed for low noise production are compatible with subsonic jet transport systems.

INTRODUCTION

The acoustic suppression technology reviewed earlier holds great promise of allowing reduction of the turbomachinery noise produced by airplane engines. In addition, the NASA is very interested in quieting engines by minimizing production of noises at their sources.

Design considerations for the quieting of airplane jet engines have been the subject of a NASA study program over the past 2 years. This Quiet Engine Definition Program has been directed toward selection of thermodynamic cycle characteristics and mechanical design features which will produce quiet engines to power subsonic commercial jet transports. An engine would be considered quiet if it produced take-off and landing-approach noise levels on the ground significantly lower, by ≈15 PNdB, than those of the JT3D and JT8D engines. If such noise reductions can be gained through engine design features alone, further reductions through the application of suppressors would produce a truly quiet airplane power plant.

The quiet engine program at the NASA Lewis Research Center began in late 1966 with a study of the effects of high bypass turbofan cycle characteristics on engine jet noise levels, fuel economy, engine size, and airplane payload and range. The quieter engine

was known to be most needed for the long-range four-engine airplanes; therefore, compatibility with the Boeing 707 and McDonnell Douglas DC-8 was made an engine design guideline.

Many years of NACA and industry experience in jet-exhaust noise-suppression work have indicated that little reduction in jet noise through the application of mechanical devices such as lobe and tube suppressor nozzles can be expected. Therefore, emphasis was placed on achieving the lowest practicable level of jet noise through proper selection of turbofan-engine cycle parameters. The turbofan engine has the well-known feature of allowing the slowing of average exhaust velocity and, as a result, lowered jet noise production and improved propulsive efficiency.

DISCUSSION

The results of the calculations in determination of turbofan jet noise and physical size as functions of the various cycle characteristics can be plotted on a single map such as that in figure 1. This figure shows the noise produced by the fan and core exhaust streams at take-off power over a range of bypass ratio and fan pressure ratio for a selected combination of turbine temperature ratings and for a fixed overall cycle pressure ratio. The trends in jet noise output and physical size of the engine shown in this figure are indicative of those found at all other chosen temperature and cycle pressure ratio values.

When jet-exhaust noise is reduced through proper application of a high bypass ratio cycle, the fan of the turbofan engine becomes the dominant noise source. Core engine compressor noise and turbine noise must be contended with, but until fan noise is greatly reduced, they do not become dominant. The jet noise levels possible at bypass ratios greater than 4.0 in figure 1 are very low compared with the total noise developed by current engines. If the fan noise can be reduced through design and acoustic suppression to those jet noise levels, a truly quiet power plant will be achieved.

The cycle studies performed at NASA Lewis Research Center provided a field of interesting cycle points around bypass ratio 5.0. More detailed engine configuration studies in cooperation with the turbine engine industry were then initiated. Pratt & Whitney Division of United Aircraft Corporation was contracted (Contract no. NAS3-10497) under the Quiet Engine Definition Program in July of 1967 and began a parametric study of engine performance, size, weight, and jet and fan noise output for turbofan engines covering the following range of cycle characteristics:

Cruise thrust, lb	4900
Take-off thrust, lb	20 000 to 25 000
Bypass ratio	3 to 8
Fan pressure ratio	1.3 to 1.7
Compressor pressure ratio	15 to 30
Turbine inlet temperature, cruise, °F	1600 to 2100
Turbine inlet temperature, take-off, °F	1600 to 2300

The results of this study provided no clearly best choice for a quiet engine cycle, but indicated that potentially attractive engines were possible at any bypass ratio between 3.0 and 8.0.

Selected sets of engine parameters were given to Pratt & Whitney and to a second definition program contractor (Contract no. NAS3-10496), the Allison Division of General Motors, for the preliminary design phase of this program. These seven sets of engine characteristics are shown in table I. Designs of these engines were done in such detail that those considerations in mechanical arrangement, flow-path configuration, and component design which would lead to selection of a single quiet engine candidate could be identified for a more detailed design analysis.

The seven preliminary designs provided good basis for comparison of several engine mechanical design features and their influence on size, weight, and predicted noise output of the engines. Air flow-path considerations, mechanical arrangement, and component operating problems were identified for two- and three-spool engines, for one- and two-fan stages, and even for the unconventional concept of counterrotating fan stages.

Throughout these preliminary designs, the presently known design features for fan quieting were applied. Fan inlet guide vanes were avoided. Fan mechanical speeds giving subsonic blade relative velocities were maintained. Fan rotor-to-stator spacing was made as great as practically feasible. No detailed fan aerodynamic designs were made in these preliminary studies; thus, only the major effects of fan slowing and spacing were investigated.

Schematic arrangements of the resulting designs for the four engines at bypass ratio 5.0 are shown in figures 2 to 5. The predicted noise levels quoted in these figures are peak values for a four-engine airplane at take-off power during a flyover at an altitude of 1000 feet and for approach power at an altitude of 300 feet. The corresponding total noise and 118 and 100 PNdB on approach. None of these noise levels assume the use of acoustic suppression materials in the engine nacelles.

Comparison of the characteristics of these bypass ratio 5.0 engines reveals these facts about the fan configurations studied:

(1) A two-stage fan, properly spaced out for noise purposes, causes an engine to be very long and heavy.

(2) Based upon the fan noise prediction techniques available today, a two-stage fan would be somewhat noisier than its single-stage equivalent.

The second point mentioned is very important to the development of a quiet turbofan engine. Both contractors agreed in their noise predictions (and NASA has found no data to dispute them) that the two-stage fan must be at least 3 decibels noisier than a single-stage fan without inlet guide vanes. The point in question is the influence that the level of aerodynamic loading has on the noise output of a blade now, since each stage of the two-stage fan can be more lightly loaded than a single-stage fan which does the same work. At this time it is predicted that the quietest fan will be a single-stage fan.

The counterrotating two-stage fan has been dropped from further immediate consideration because considerable development time and effort would be required to supply the aerodynamic design data needed for incorporation of such a fan into an operating engine system.

The two-stage fan noise and weight penalty considerations tend to rule out an engine lower in bypass ratio than about 5.0 as a candidate for a quiet engine. The turbofan cycle energy balance causes low bypass ratio to optimize with higher fan pressure ratio, both for low jet noise and for best fuel economy. A single-stage fan cannot be designed to produce a high fan pressure ratio greater than about 1.60, particularly when mechanical speed of the fan rotor is being kept low for noise reasons. The quiet engine should have a bypass ratio somewhat greater than 5.0, therefore, to give near-optimum cycle performance with the single-stage fan and to gain the jet-exhaust velocity and jet-noise reductions attainable with the higher bypass ratio.

Engines of higher than 6.0 bypass ratio were dropped from consideration in this engine definition program because of installation and noise output considerations. The fans of very high bypass engines must be very large, as can be seen in figure 1, so that installation under the wings of the current four-engine jet transports would be difficult and integration into new airplane designs would be a severe problem. *Also,* the aerodynamic drag penalty associated with the large nacelle body housing of such an engine tends to counterbalance the fuel economy advantages of higher bypass ratio. Secondly, the study results for Pratt & Whitney engine C indicated very little jet and fan noise improvement for an 8.0-bypass-ratio engine compared with that for the 5.0-bypass-ratio engine with a single-stage fan.

Another consideration in choice of mechanical configuration developed from our design studies for the several engines. It became apparent that the most desirable spool arrangement for a quiet engine would be one which isolated the fan, apart from any compressor stages, on the low pressure rotor. The fan drive turbine is compromised in work output per stage and in stage efficiency because of the low rotational speed imposed by fan speed limitations for noise reasons. If the low turbine is made to produce only the work required by the fan and no core engine compressor work, the engine benefits in size, weight, and performance. Isolation of the fan spool also allows modification of the aerodynamic design of the fan, to slow it down or speed it up, or even to change its size and bypass ratio, independently of the core engine. Major changes in core compressor and turbine design need not be made with each modification in fan design as an engine is developed aerodynamically, mechanically, and acoustically.

On the basis of these considerations, it was determined that the engines to be designed in more detail under our definition program would have a bypass ratio between 5.0 and 6.0, would use a single-stage fan operating at low speed on an isolated rotor spool, and would incorporate the rotor-to-stator spacings found feasible in the preliminary designs. Specific descriptions of the two engines resulting from the subsequent design work are included in reference 1.

NASA has required that the selection of quiet engine cycle characteristics, mechanical arrangement, and component designs be made with minimum noise output as a major constraint. It has been apparent from the start that design for attainment of low noise output will unfavorably affect the engine in size, weight, and perhaps, performance. Sacrifices in these areas are inevitable when the fan is limited in speed, the blade rows are spaced out, and turbine inlet temperatures are limited on take-off because of noise considerations. On the other hand, the engine resulting from these studies is intended to be an operational and completely usable power plant for subsonic jet transports. In order that the goal of airframe compatibility might be upheld and that the question of the possibility of quiet engine "retrofit" on today's airliners might be answered, NASA initiated an engine/airframe integration study program with Douglas Aircraft Company (Contract no. NAS3-11151). This program parallels the engine definition program; thus, installation considerations can be used in engine selection decisions.

The Douglas program began in January of this year. The first task in that study provided preliminary nacelle and pylon design for installation of a single-stage-fan version of a 5.0-bypass-ratio quiet engine on the DC-8 model 61. Fan-inlet and fan-discharge duct suppressors were included in the nacelle design so that realistic installed-engine weights and dimensions for a very quiet power plant would be maintained. Figure 6 shows the resulting installation on the inboard position of the DC-8 wing. The study ascertained that engine integration was possible, that ground clearance was adequate, and that no

modifications to the airframe would be required for installation of an engine of this size and weight.

The second task in the Douglas program involved analytical determination of performance of the DC-8 with this preliminary engine and comparison with the present airplane configuration. Some results of this performance study follow:

Weight increase of 6720 lb per airplane

1800-foot shorter take-off field length

No cruise Mach number decrement

400-mile better range at volume-limited payload

2000-foot higher initial cruise altitude

Minimum retrofit cost ≈ 4 million dollars

It is a heartening fact that no serious compromises in airplane performance result from replacing the current DC-8 power plant with the larger and heavier quiet engine. Indeed, general improvement is expected in range, take-off distance, and initial cruise altitude. The economics of engine retrofit however are formidable. The replacement of four engines, nacelles, and pylons will cost at least $4 000 000.

Subsequent tasks in the integration program involve determination of detailed performance and retrofit information for the final selected engine configuration from the engine definition program. Aerodynamic model tests are being conducted with the DC-8 quiet engine configuration in the Ames 12-foot-high Reynolds number tunnel and the Ames 11-foot transonic tunnel. Flutter tests are being performed to determine whether wing structural modifications would be required because of aeroelastic limitations. Detailed costs of nacelle and pylon retrofit kits and the costs of retrofit labor and out-of-service time are being determined. Operating costs for the airplane with quiet engines are being predicted.

CONCLUDING REMARKS

Nothing to date in the engine definition and engine integration studies has indicated that the goal of producing an engine system which can be both significantly quieter in operation than current turbofan engines and completely compatible with subsonic transport airplane systems is being compromised.

REFERENCE

1. Kramer, James J.: Quiet Engine Program – Detailed Engine Designs. Conference on Progress of NASA Research Relating to Noise Alleviation of Large Subsonic Jet Aircraft, NASA SP-189, 1968. (Paper No. 19 herein.)

TABLE I

PRELIMINARY ENGINE DESIGNS

	ALLISO			PRATT AND WHITNEY			
	A	B	C	A	B	C	D
BYPASS RATIO	3	5	5	3	5	8	5
FAN PRESSURE RATIO	1.7	1.5	1.5	1.7	1.6	1.35	1.6
ENGINE SPOOLS	3	3	3	2	3	2	3
FAN STAGES	2	2	1	2	2 (COUNTER-ROTATING)	1	2

SIDELINE TAKE-OFF JET NOISE

NOISE FOR 4 ENGINES SIZED FOR 4900 lb CRUISE THRUST

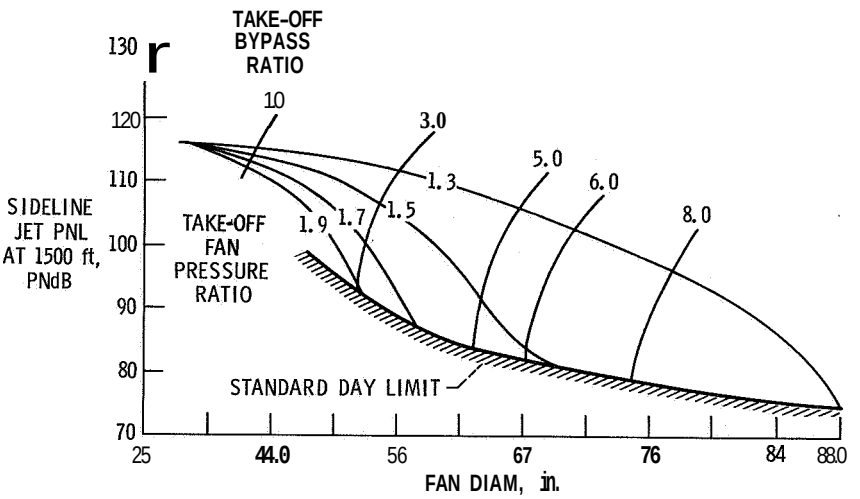

Figure 1

ALLISON "B" BYPASS RATIO 5.0

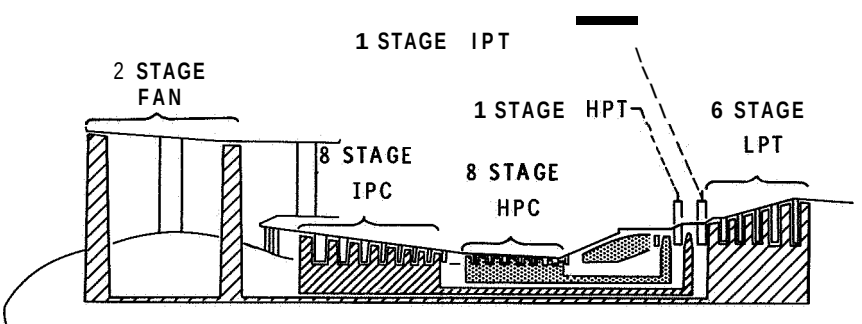

LENGTH	190 IN.
DIAMETER	73 IN.
WEIGHT	6000 LB
NOISE, PNdB	
TAKE-OFF	109/93
APPROACH	108/92

Figure 2

ALLISON "C" BYPASS RATIO 5.0

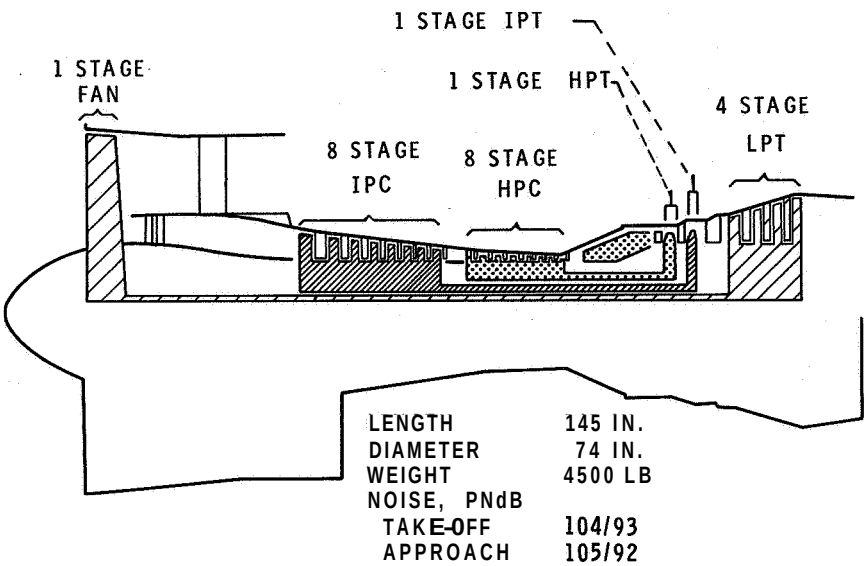

Figure 3

PRATT AND WHITNEY "B" BYPASS RATIO 5.0

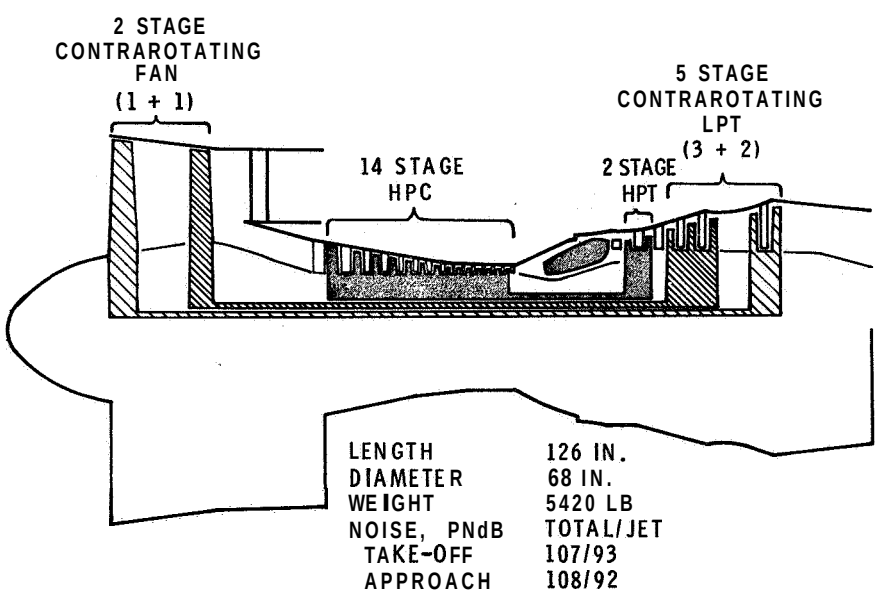

Figure 4

PRATT AND WHITNEY "D" BYPASS RATIO 5.0

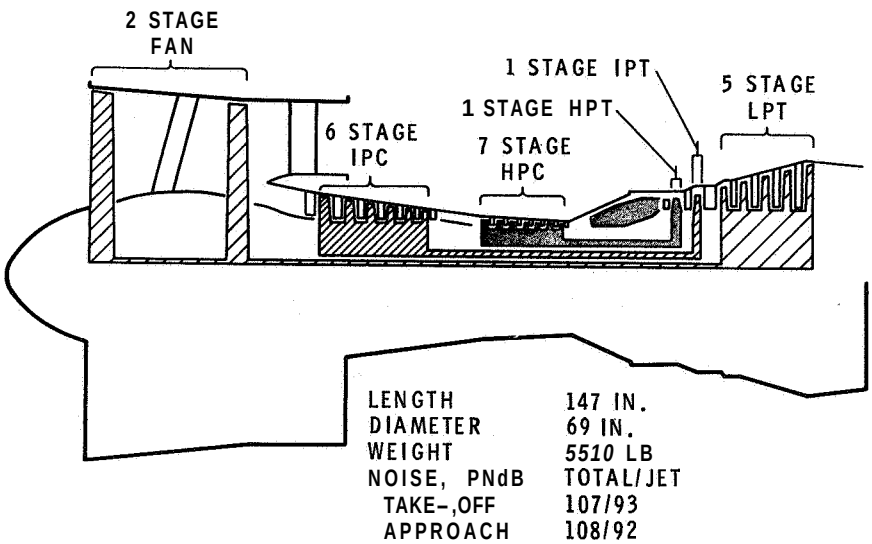

Figure 5

DC-8-61 QUIET ENGINE NACELLE

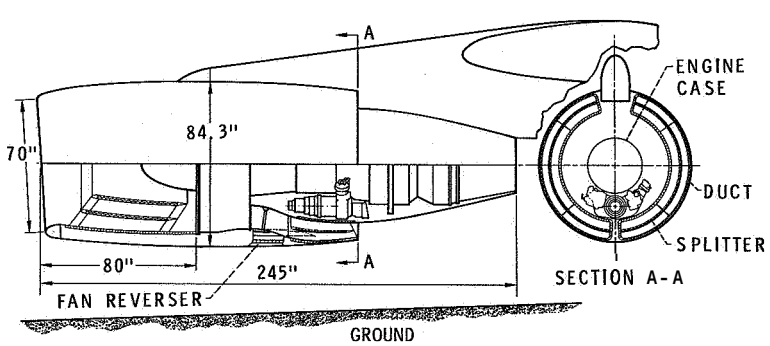

Figure 6

19. QUIET ENGINE PROGRAM

DETAILED ENGINE DESIGNS

By James J. Kramer
NASA Lewis Research Center

SUMMARY

The engine design constraints developed to insure maximum turbofan engine quieting are reviewed. Two engines designed within these constraints are discussed and their noise levels estimated, The supporting fan noise research program is briefly discussed and some preliminary fan noise data presented.

INTRODUCTION

In the early part of the Quiet Engine Definition Program a rather wide range of engine configurations was examined as discussed in reference 1. Later, a set of design constraints was selected within which engines were designed in more detail under contract by Allison Division of General Motors Corporation (Contract NAS3-10496) and Pratt & Whitney Division of United Aircraft Corporation (Contract NAS3-10497). These engines are reviewed and the supporting fan noise research program is discussed in this paper.

QUIET ENGINE DESIGN CONSTRAINTS

The design constraints that were chosen for the final phase of the design study activity for the Quiet Engine Definition Program are given in table I. The general considerations which led to these constraints are discussed in this section.

Engine

The screening of various engine layout designs resulted in the conclusion that a quiet engine should have a bypass ratio in the range of 5 to 6. The cruise thrust was set at 4900 lb; the corresponding take-off thrust for such an engine, about 22 000 lb.

Fan

Because the fan dominates the noise output of such an engine, the specification of the fan design was a prime consideration. The anticipation that considerable information will be learned about fan noise in the next few years made it desirable to be able to

incorporate that technology in the quiet engine as it was developed. Therefore, the fan was specified to be mounted on a shaft by itself with no compressor stages so that changes in fan configuration and speed could be achieved with the least impact on the rest of the engine.

The effect of blade loading on the fan noise production is not well known at this time. In order to have lightly loaded blades, it is necessary to use two or more fan stages. For a bypass-ratio-5 engine, the fan pressure ratio can be achieved with one heavily loaded stage. The noise predictions did not indicate a noise advantage for the two-stage fan, but these predictions have considerable uncertainty associated with them. A weight penalty is associated with a two-stage fan compared with a single-stage fan. A single-stage fan was selected for the engine design, but investigations of the noise performance of both two-stage fans and single-stage fans will be part of the supporting experimental program.

In order to minimize the noise associated with the single-stage fan, inlet guide vanes were ruled out and the spacing between rotor and stator blade rows was specified to be at least 2 rotor chords. It was desired to have the flow subsonic over the blades in order to eliminate the noise associated with supersonic relative velocities, the so-called "shock noise" or "buzz-saw noise." In order to achieve subsonic relative flow, the tip speed at take-off could be a maximum of about 1000 ft/sec. These engines operate so that the tip speed at take-off is about 10 percent lower than the value at the cruise condition. Thus, the take-off tip-speed limit of 1000 ft/sec corresponds to a cruise tip speed of 1100 ft/sec. The engine is designed for the cruise condition. In figure 1, fan pressure ratio is plotted against a blade loading parameter D factor for a tip speed of 1100 ft/sec. The present state of the art is such that allowable D factors are 0.5 or lower. Figure 1 shows that a fan pressure ratio of the order of 1.6 can be achieved with state-of-the-art blade loading limits with this tip-speed limitation.

In figure 2, engine specific fuel consumption is shown as a function of fan pressure ratio. There is a marked increase in fuel consumption at fan pressure ratios below 1.5 for an engine with a bypass ratio on the order of 5. Thus, for good economy a fan pressure ratio of 1.5 is required and reasonable blade loading limits the ratio to a maximum of 1.6.

Compressor

Parametric engine performance studies have indicated that the specific fuel consumption of these engines began to increase rapidly as the cycle pressure ratio (overall compression ratio) decreased below 18. The specific fuel consumption continued to decrease as cycle pressure ratio increased but not very rapidly as shown in figure 3. Therefore, the minimum cycle pressure ratio for good fuel economy, specific fuel

consumption, was determined to be 18. In order to achieve an overall compression ratio of 18 with a fan pressure ratio of 1.5 the pressure ratio required of the compressor is 12. Both two-spool and three-spool engines were considered. They differ in that the main compressor is made up of one or two rotors. A limit of 12.5 was set as the maximum pressure ratio per compressor rotor in order to avoid any problems associated with high-pressure-ratio compressors. A two-spool engine with a 1.5-pressure-ratio fan and a single-rotor compressor with a 12:1-pressure-ratio compressor has an overall cycle pressure (compression) ratio of 18. Thus, this limit permits the use of a single-rotor compressor – that is, a two-spool engine. Dual-rotor compressors as used in a three-spool engine develop a pressure ratio across each rotor on the order of 4 or 5; therefore, the limiting value of 12.5 does not influence the three-spool engine.

Turbine

The turbine temperatures at cruise and take-off are important because they set the jet noise level. The fan noise suppressor technology has progressed to the point where there is some hope that a 10-PNdB suppressor can be developed even for large-diameter engines. In order to achieve the quietest power plant possible, this quiet engine would be used with a fan inlet and exhaust suppressor. The hot jet mixing noise represents the floor for engine noise output. Reductions in fan noise below this floor are of no benefit to the observer. Therefore, the jet noise should be at least 10 PNdB below the fan noise if advantage is to be taken of the fan noise suppressor technology being developed. The rough estimate of the fan noise at 1000-ft altitude at take-off power was 105 PNdB; the jet noise maximum should then be 95 PNdB. In figure 4 the jet noise level in PNdB for an observer of a 1000-ft flyover is plotted against design turbine inlet temperature. The design turbine temperature must be 1775° F or lower in order to assure adequately low jet noise levels. This design-turbine-temperature limit of 1775° F corresponds to a take-off turbine temperature of 2000° F.

ENGINE DESIGNS

Allison Division of General Motors Corporation and Pratt & Whitney Division of United Aircraft Corporation conducted detailed design studies of these engines under contract for Lewis Research Center and did a complete aerodynamic and mechanical design of the fan.

The engine designed by Allison is a three-spool engine and is shown in figure 5. The single-stage fan develops a pressure ratio of 1.5 at cruise and has a diameter of 74 in. The tip speed at take-off is 1020 ft/sec. The fan blade has a chord at the tip of 6.2 in. and an aspect ratio of 3. The fan is driven by a five-stage turbine, offset somewhat from the gas generator turbine in order to obtain higher tip speed at a given

rotational speed. The overall compression ratio of 24 is achieved with a 16:1 compressor consisting of two rotors having eight stages and pressure ratios of 4. Each rotor is driven by a single-stage turbine. The overall length is 153 in. and the weight is estimated at 4790 lb. The noise performance is summarized in table II. An observer on the ground 3 miles from the start of take-off roll would be subjected to 105 PNdB by a fully loaded four-engine airplane of the DC-8 type equipped with engines of this design without suppressors as it passed overhead at an altitude of 1000 ft. The jet noise is estimated at 93 PNdB so that further fan noise reduction with suppressors would be beneficial. The Allison noise estimation procedure is an empirical correlation based on several fan parameters, the most important of which is the flow Mach number relative to the blades. It takes into account the blade spacing, loading, and the presence of upstream blade rows, if any.

The Pratt & Whitney engine designed within the constraints given in table I is shown in figure 6. The single-stage fan has a take-off tip speed of 1000 ft/sec and develops a pressure ratio at cruise of 1.6. The rotor blade has a rather long chord at the tip, 7 in., and an aspect ratio of 2.2. The fan diameter is 68.9 in. The engine has two spools. The single-rotor compressor develops a pressure ratio of 12.5 and has five stages of variable stators. The compressor is driven by a two-stage high-pressure turbine. The first stator, first rotor, and second stator are air-cooled. This is also true of the Allison engine. The fan turbine is a five-stage in-line turbine. The overall length is 118 in. and the weight is 4950 lb.

The noise performance of this engine is summarized in table 11. A ground observer would hear 106 PNdB as a fully loaded four-engine airplane of the 707 type equipped with engines of this design passed overhead at an altitude of 1000 ft at take-off power. A mile from touchdown on approach an observer hears 104 PNdB. The corresponding jet noise levels at these observation points are 94 PNdB and 84 PNdB, respectively. The jet noise estimates for both the Pratt & Whitney and Allison engines are not as precise as the usual jet noise estimates because the jet velocities have been reduced to the point where the jet noise is not following the familiar eighth-power-of-velocity correlation law. Even at take-off power at 1000-ft altitude the jet velocity is less than 1000 ft/sec relative to the surrounding atmosphere.

The fan noise is still the dominant source and suppressors would benefit the ground observer. The fan noise prediction method at Pratt & Whitney is based on test data obtained with the JT3D and JT9D engines. The prime correlating parameter is the rotational tip speed of the fan. It is interesting that the estimated fan noise outputs from Pratt & Whitney and Allison are quite comparable although the prediction methods differ considerably in format.

These design studies have indicated several things. The combination of the high-bypass-ratio engine and moderate turbine temperatures result in sharp reductions in jet

noise. Estimates of the fan noise reduction possible with a low-tip-speed fan are significant but the fan remains the dominant noise source. There is a weight penalty associated with the low-tip-speed fan but it is not such as to rule out the use of this quieting feature in practical aircraft propulsion systems.

The NASA plans to build and test several engines of the general character discussed herein. This experimental engine program will demonstrate the amount of quieting that can be achieved in complete engine systems.

FAN NOISE RESEARCH

The main noise problem is the fan. The experimental research program on fan noise supporting the Quiet Engine Program has begun. One of the fan experiments was conducted under contract by the General Electric Company (Contract NAS3-11166) with a modified version of the TF39 engine. The fan section of the unmodified TF39 engine is shown in figure 7. The inner portion of the fan is a two-stage device with no inlet guide vanes. The outer portion is a single stage with a row of inlet guide vanes. General Electric modified the fan section of a TF39 engine by removing the outer portion of the fan and spacing the blade rows of the inner portion to provide a distance of approximately 1 chord between rows. The modified fan is shown in figure 8. The inner portion of the fan developed a pressure ratio of 1.5 at a tip speed of 1000 ft/sec.

As mentioned previously, a single-stage fan was specified for the quiet engine design but tests of two-stage fans were to be part of the supporting research program. The modified TF39 engine was tested and some preliminary engine noise data are shown in figures 9 and 10. Figure 9 is a plot of perceived noise level as a function of angular position around the engine as measured at a 225-ft radius for take-off power setting. The maximum occurred at the 110° position at take-off power setting. The corresponding perceived noise levels for a four-engine airplane flying 1000 ft overhead at take-off power and at 325-ft altitude at approach power are 110 PNdB and 115 PNdB. These values are not as low as those estimated for the single-stage low-tip-speed fan.

In order to obtain data on single-stage fans such as this, a fan test rig is being constructed at Lewis in order to obtain far-field noise data. A sketch of the facility is shown in figure 11. It will drive 72-in-diameter fans up to tip speeds of 1200 ft/sec.

The first fan model to be tested in the facility has been designed and built at the Lewis Research Center. It is a single-stage device designed to produce a 1.5 pressure ratio and to operate at a take-off tip speed of 1000 ft/sec, has a chord of 5.5 inches and an aspect ratio of 3.5, and is designed to produce a uniform pressure ratio along the span. The blade loading is rather high and the blade turns approximately 15° past axial at the hub.

Following this initial test, the facility will be used to test a series of full-scale model fans and fan noise suppressors to be used with the quiet engine,

CONCLUDING REMARKS

The design study of turbofan engines for subsonic transport propulsion systems has indicated that substantial reductions in jet noise can be achieved by the proper selection of engine cycle parameters. Substantial fan noise reductions below current fan noise levels are predicted for engines with low-speed single-stage fans without inlet guide vanes and with large spacing between rotors and stators. Further reductions in fan noise resulting from the use of fan noise suppressors will result in overall installed power-plant noise levels about 20 PNdB lower than current levels.

REFERENCE

1. McBride, Joseph F.: Quiet Engine Program – Preliminary Engine Design and Aircraft Integration. Conference on Progress of NASA Research Relating to Noise Alleviation of Large Subsonic Jet Aircraft, NASA SP-189, 1968. (Paper No. 18 herein.)

TABLE I.- QUIET ENGINE DESIGN CONSTRAINTS

Engine:	
Bypass ratio	5 to 6
Cruise thrust, lb	4900
Take-off thrust, lb	22 000
Fan:	
Number of stages	1
Inlet guide vanes	None
Spacing between rotor and stators	2 rotor chords
Tip speed -	
Take-off, ft/sec	1000
Cruise, ft/sec	1100
Pressure ratio, cruise	1.5 to 1.6
Compressor:	
Rotors	1 or 2
Maximum pressure ratio per rotor	12.5
Turbine:	
Inlet temperature -	
Take-off, °F	2000
Cruise, °F	1775

TABLE II.- FLYOVER PERCENED NOISE LEVELS

	Allison		Pratt & Whitney	
	Total PNdB	Jet PNdB	Total PNdB	Jet PNdB
Take-off power, 1000-ft altitude	104	93	106	94
Approach power, 325-ft altitude	105	80	104	84

VARIATION OF FAN PRESSURE RATIO WITH BLADE-LOADING PARAMETER

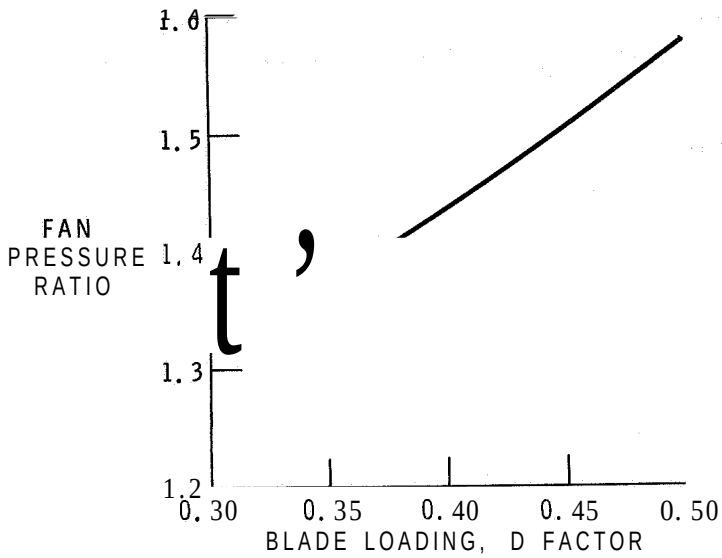

Figure 1

EFFECT OF FAN PRESSURE RATIO ON ENGINE CRUISE SPECIFIC FUEL CONSUMPTION

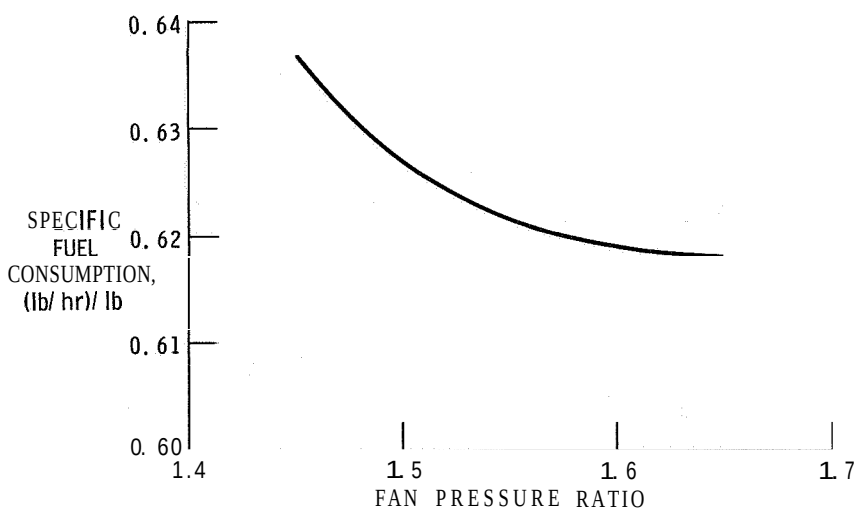

Figure 2

EFFECT OF CYCLE PRESSURE RATIO ON ENGINE CRUISE SPECIFIC FUEL CONSUMPTION

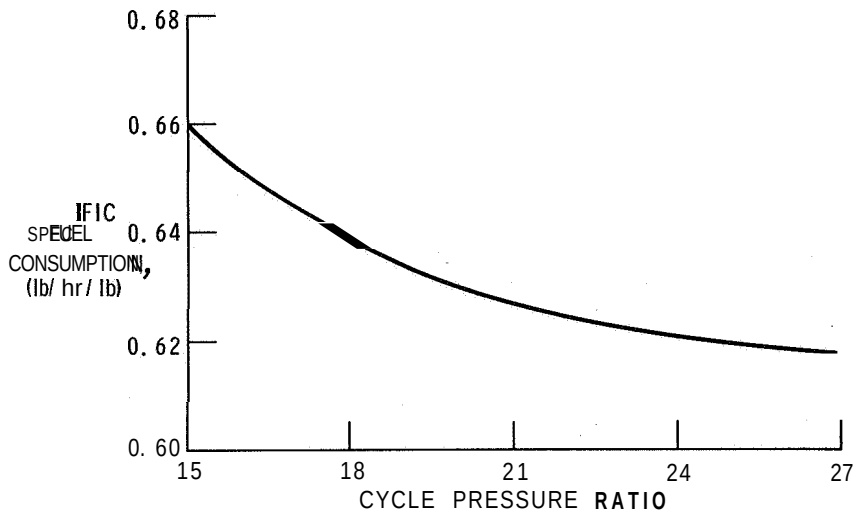

Figure 3

VARIATION OF JET NOISE WITH TURBINE INLET TEMPERATURE

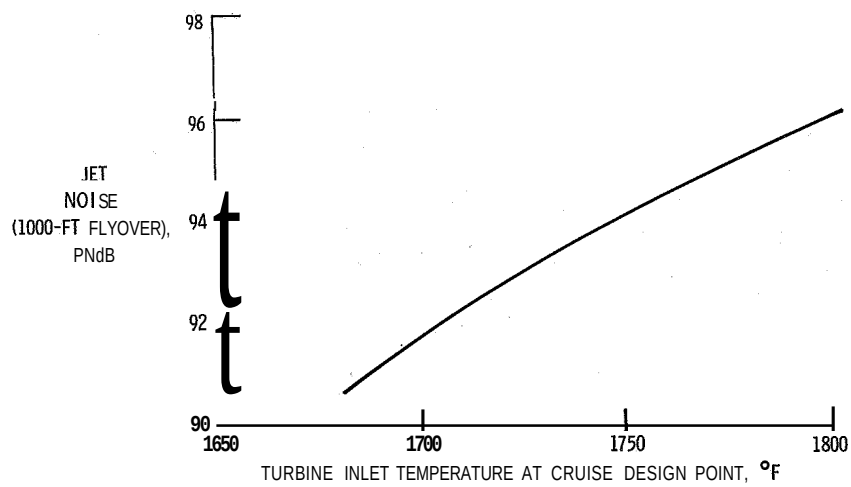

Figure 4

ALLISON 5.5- BYPASS-RATIO ENGINE

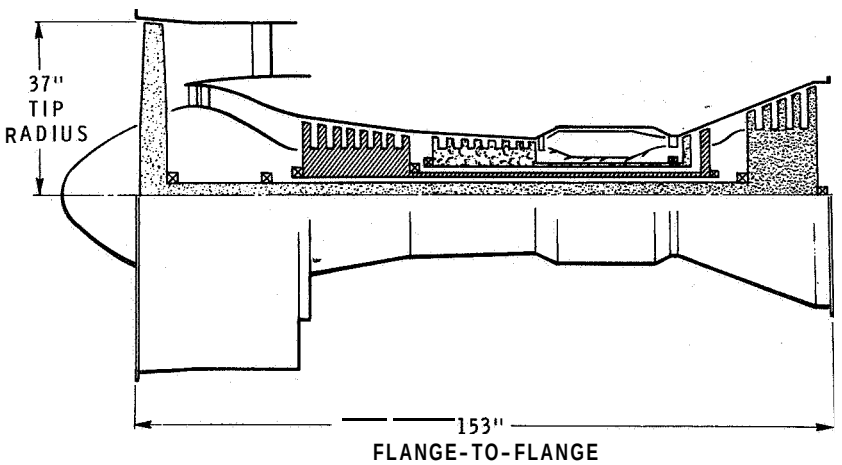

Figure 5

PRATT & WHITNEY 5.4- BYPASS-RATIO ENGINE

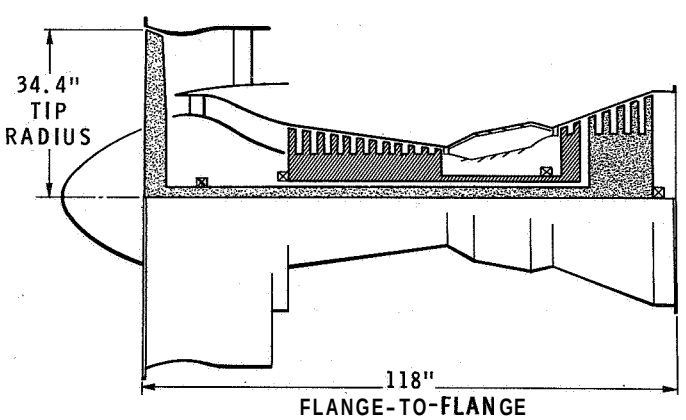

Figure 6

UNMODIFIED TF39 FAN

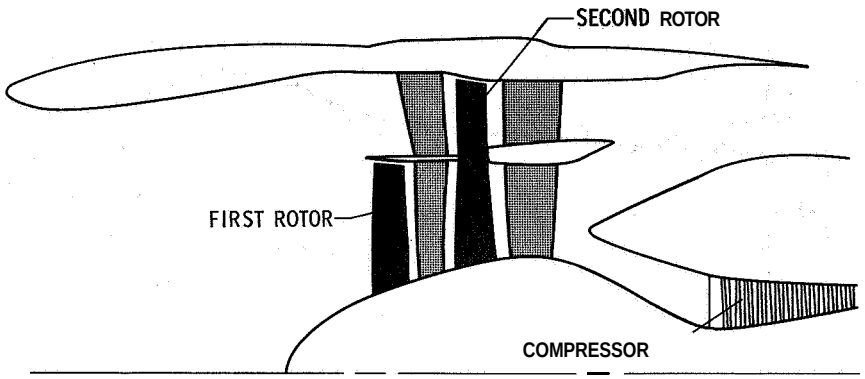

Figure 7

TWO–STAGE LOW TIP SPEED FAN

MODIFIED TF39 INNER PANEL ONLY

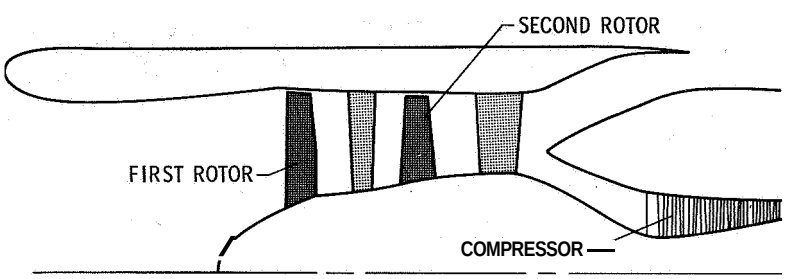

Figure 8

PERCEIVED NOISE LEVEL AS A FUNCTION
OF ANGULAR POSITION

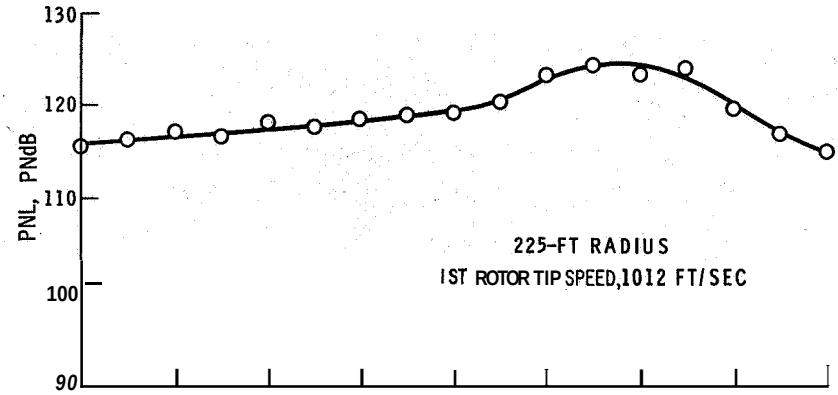

Figure 9

FREQUENCY SPECTRUM OF MODIFIED TF39 FAN
1/ 3-OCTAVE DATA; 225-FT RADIUS

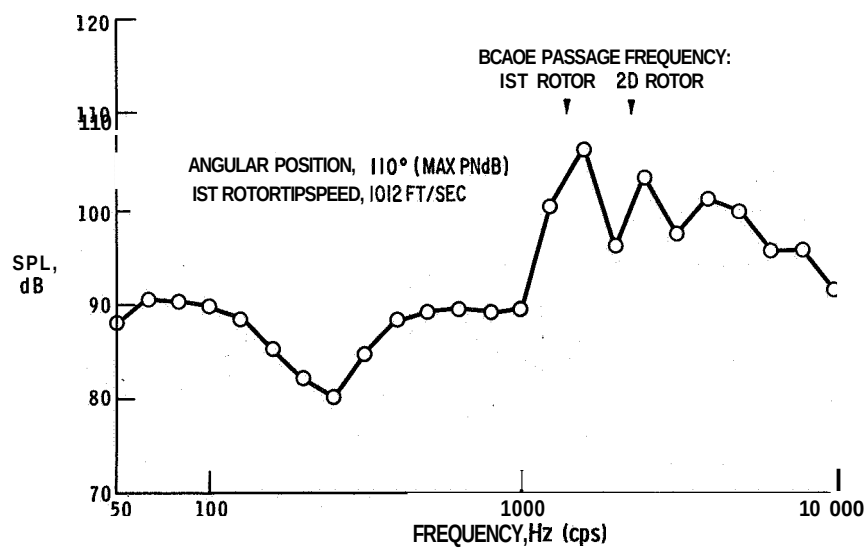

Figure 10

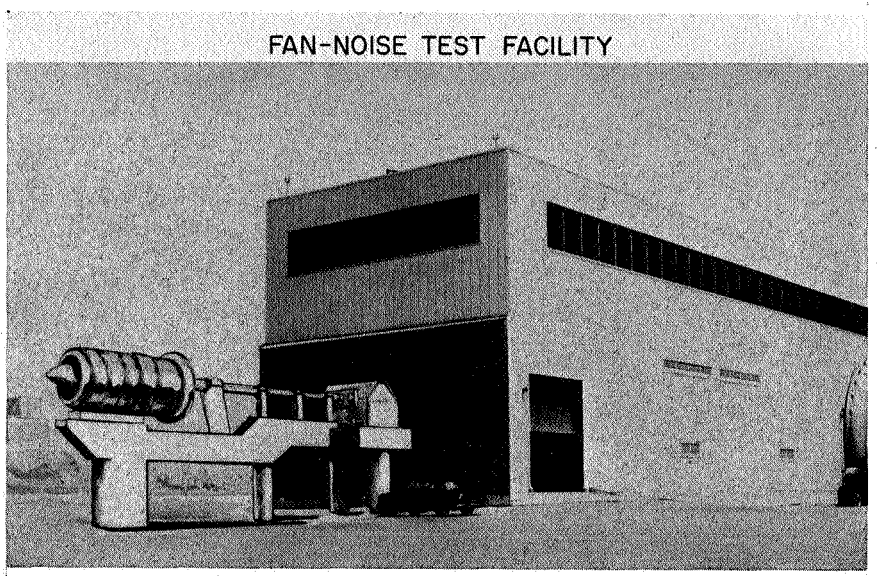

Figure 11 L-68-8575

20. COMPRESSOR NOISE ANALYSIS

By Martin V. Lowson

Wyle Laboratories

SUMMARY

The results of a general theory for the prediction of noise radiation by fans and compressors are described. Emphasis is placed on the basic mechanisms underlying the noise radiation and the leading results from the application of the theory. Preliminary agreement with experiment is shown. The theory is capable of including virtually all the major design variables of a compressor and is thought to be of direct use in trade-off studies to minimize noise at an early stage of engine design.

INTRODUCTION

This paper is concerned with the application of theory to the prediction and the understanding of the noise radiation by compressors and fans. The noise produced by these devices has been increasing in importance as a source of community noise, and the projected introduction of fans with very high bypass ratios, possibly operating at supersonic tip speeds, will lead to the domination of the observed sound field of an airplane by the sound radiation from this source. The objective of the theory is to give an understanding of the basic mechanisms underlying the compressor noise with the hope that it will lead to improved methods for the control and the prediction of noise radiation. One of the key problems facing the engine designer at the present time is that no method is available for predicting the detailed acoustic effects of design changes; therefore, it becomes extremely difficult to make the appropriate design trade-offs to minimize the noise radiation at the initial design stages of any given engine.

Much important work has now been accomplished on compressor noise, both theoretically and experimentally (refs. 1 to 13). A review of the available information on compressor noise is given in reference 11. The work reported herein is a condensation of work reported in more detail in reference 14. In the present paper, only the basic physical mechanisms underlying the compressor noise will be discussed together with the leading results from the application of the theory. For more details of the mathematical methods and physical models used in the theory, the reader is advised to consult reference 14.

The model used in the analysis regards the fan as an isolated rotor or stator in free space on which fluctuating forces are acting. The effect of the upstream or

downstream blade rows are included only in terms of the fluctuating forces which result from their presence. Methods for calculating these fluctuating forces have also been derived.

Several other sources of noise are feasible. Fluctuating thickness and'fluctuating mass source terms can be significant (ref. 14). The acoustic stresses acting around the blade can also give rise to both discrete and broadband radiation (ref. 13). There is also a possibility of interactions between various sources inside the compressor giving rise to additional noise terms. However, it is thought that most of these other sources will be negligible, and certainly the mass source terms calculated in reference 14 were found to be very small. Furthermore, the basic phase effects discussed in this paper will apply to any type of acoustic source function so that many of the key results and design trends should be applicable regardless of the specific type of acoustic source which is acting.

It is important to realize the complexity of the compressor noise radiation problem. Figure 1 shows the cause and effect chain which leads to compressor noise radiation. The aerodynamics of the compressor necessarily involve unsteady flow components. These unsteady flows cause unsteady forces to act upon the compressor blades so that dipole-type sound is radiated from each blade. The radiation from each blade combines to give the sound output of the rotor or stator disk, and the efficiency of propagation of this sound down the inlet and/or outlet duct is governed by the acoustic modes of the duct. The final sound which reaches the observer is the result of radiation from the end of this duct. This complexity is both an advantage and a disadvantage. It is an advantage because the many different parameters which can affect the noise radiation by the compressor can all be altered substantially independently to achieve a minimum noise radiation by the compressor. It is a disadvantage because each of these many parameters requires consideration. This introduces considerable complexity into any theoretical development or into any analysis of data from various types of engines. However, the present theory is capable of taking into account most of the effects which occur in the compressor, and it can be shown that many of the other effects are, to a large extent, negligible (ref. 14). Therefore, the theory developed is thought to have some general utility in compressor design.

SYMBOLS

B	number of rotor blades
c	speed of sound in undisturbed atmosphere
c_m	magnitude of mth harmonic of sound radiated
D	compressor diameter

D_k	magnitude of kth torque harmonic
F_i	components of external force (i = 1, 2, 3)
J_μ	Bessel function of first kind and of order μ, where $\mu = mB - kV$
k	summation parameter (order of stator wake harmonic)
M	rotational Mach number
m	order of sound harmonic
P	sound pressure
Q	mass source strength
R	typical radius
r	distance from observer to source
r_1	distance from observer to hub
T_{ij}	acoustic stress tensor (i,j = 1, 2, 3)
T_k	magnitude of kth thrust harmonic
t	time
U	phase velocity of sound radiated
V	number of stator vanes
V_T	compressor tip velocity (mechanical tip speed)
W	wake velocity
x,y	Cartesian coordinates of observer position
x_i,x_j	Cartesian coordinates of source (i,j = 1, 2, 3)
θ	angle of radiation

X loading harmonic ($\lambda = kV$)

μ modal order $\mu = |n - \lambda| = |mB - kV|$

ρ perturbation density

τ retarded time, $\tau = t - \frac{r}{C}$

Ω angular velocity of rotor

MECHANISMS OF NOISE GENERATION

First of all the basic mechanisms by which the noise is generated will be reviewed. It is important to realize that sound is wave phenomenon. Sound travels through the air at a well-defined wave speed, and because of this, sound heard at any one instant must have been generated at some earlier instant. As is illustrated in figure 2, the exact earlier time at which the sound was generated is dependent on the distance from the observer to the sound source. Thus for an extended source, sound heard at the same time t will in general have been generated at different retarded times τ where $\tau = t - \frac{r}{c}$. Here, r represents the distance from the observer to the point under consideration and c is the speed of sound in the undisturbed atmosphere. It is therefore vitally important to account for the retarded time effects over the source if any accurate solution for the acoustic source characteristics is to be obtained.

In general, the lines of equal phase in this source region are in motion. Thus, the phase velocity in this source region becomes of considerable importance. An example is shown in figure 3. Consider that the sound radiated by some disturbance is moving with a phase velocity u. From figure 3 it can be seen that $u = \frac{c}{\cos \theta}$. Note that the phase velocity which couples into the wave is always greater than the speed of sound. As is shown in figures 3(b) and 3(c), increases in phase velocity can be accommodated by increases in the angle of radiation θ, but when the phase velocity is reduced below the speed of sound, no coupled acoustic wave is possible. For the infinitely long system illustrated here, the sound radiation from the source with a subsonic phase velocity would be identically zero. All contributions will cancel. But because the compressor has finite dimensions, cancellation is incomplete and subsonic phase velocities in the compressor can still give rise to some radiated sound. Conversely, when the phase velocity is supersonic the acoustic radiation is large. It should be noted that the phase velocity of the source is only rarely equal to its physical velocity. Figure 4 gives an example. Suppose that the two rows represent the rotor and stator of the compressor. Suppose also that a

pressure pulse is generated when any two members of the rows are in line, as shown by the arrows; this is closely analogous to the real situation. If the rotor row moves, pulses will occur as shown when the second pair comes into line. It can be seen that the effective phase velocity corresponding to the successive pulses is much higher, triple in this case, than the actual velocity of the rotor; thus both the rotor and the stator can act as "phased arrays" with a high effective velocity. Therefore, even though the rotor itself is moving at subsonic speeds, the phase velocities of the pressure fluctuations can be supersonic, and this causes efficient and undesirable radiation from the compressor. It might also be noted that when the rotor itself is moving at supersonic speeds, it can couple directly into the sound field without any requirement for these interaction effects; consequently, supersonically moving rotors are particularly efficient generators of sound. Subsonic rotors on the other hand generate significant sound levels only by the interaction process described above and are therefore more amenable to treatment at early stages of design.

Figure 5 shows, diagrammatically, the aerodynamic field existing in a compressor. Wakes stream from an initial stator and are intercepted by the rotor. As shown by the velocity diagram, the basic effect of the velocity defect in the stator wake is to cause a fluctuating downwash at the rotor disk, which will be reflected in fluctuating forces on the rotor blades. Exactly equivalent effects occur at the second stator, which experiences a fluctuating force on its vanes due to the rotor wake. Because the number of rotor and stator blades varies, the forces on the rotor or stator blades will vary in phase from blade to blade. As discussed above, these cascade phase effects are of extreme importance in determining the efficiency of the final radiation.

Several important effects related to the frequency characteristics of the compressor radiation may also be deduced from a study of figure 5. Consider first of all the rearmost stator row. Each blade is stationary and undergoes a force fluctuation due to the velocity profile of the rotor wakes. The time variation of these fluctuations is governed by the rotor speed. Thus the frequency of the noise radiated by the stator is directly related to the rotor frequency. If the rotor has B blades and rotates at angular velocity Ω, then the fundamental frequency of the stator radiation will be $B\Omega$.

The wake velocity field behind the rotor can be analyzed into spatial Fourier components. Because of the rotation, each spatial harmonic of the rotor wake is transformed into a single temporal harmonic of the stator radiation. Now immediately behind the rotor the wake velocity profile is very sharp and thus contains all spatial frequencies, but as the wake expands downstream, it becomes smoother and less intense so that at large rotor-stator separations only the first spatial harmonic of the wake may be significant. Thus it may be predicted that the stator radiation for small rotor-stator separations will contain substantial noise at all multiples of the blade passage frequency $B\Omega$ and that the effect of increasing rotor-stator separation will be to reduce preferentially the higher harmonics of the sound radiated by the stator.

The effects at the rotor, however, are rather different. The rotor field passes through what is essentially a stationary velocity field due to the wakes from the first stator. (See fig. 5.) The frequency of the fluctuating forces on, and thus of the acoustic radiation by, the rotor is governed by the rotor speed. Thus the angular velocity of the rotor governs temporal frequencies at both the rotor and the stator. Clearly, the stator wake can still be analyzed into spatial Fourier components, and their relative magnitude will depend on stator-rotor separation in the same way as discussed previously; that is, at large separations only the first spatial harmonic of the stator wake will be significant. Furthermore, successive spatial harmonics of the stator wake will give rise to successive loading harmonics on the rotor. However, in contrast to the stator case, each loading harmonic on the rotor gives rise to more than one sound harmonic in the radiation field.

This is due to the motion of the rotor blades. As is well known, relative motion between source and observer gives rise to Doppler frequency shifts, the observed frequency rising as the source approaches the observer and reducing as the source recedes. Thus the rotation of a particular frequency source moving with the rotor causes a periodic variation of the frequency observed at a fixed point. The effects are very similar to those of frequency-modulated radio signals. It is found that the frequency modulation causes any single frequency input to be observed as a series of frequencies, each displaced from the input frequency by some multiple of the modulation frequency. Thus fluctuating forces at one harmonic will cause radiation in all harmonics. For this reason increase of stator-rotor separation may be expected to reduce the noise basically in all the sound harmonics radiated by the rotor. This may be contrasted with the predominant reduction in the higher harmonics predicted above for the equivalent stator radiation effect.

It can be shown (ref. 14) that each loading harmonic λ gives rise to a different mode of radiation from the rotor, in a manner very similar to that described in the work of Tyler and Sofrin (ref. 1). Each mode will have different acoustic radiation characteristics, so that the observed radiation level from the rotor is dependent on both the acoustic radiation efficiency of each mode and the relative magnitude of its contribution from the various loading harmonics λ. The overall radiation pattern is thus given by the sum of all the modes.

THEORETICAL DEVELOPMENT

It is not appropriate herein to give in detail the theoretical development of the equations which describe the sound radiated by the compressor. However, a brief description is justified. Any source of a sound can be described by the basic equation which was first derived by Lighthill (ref. 15) and is given as

$$\frac{\partial^2 \rho}{\partial t^2} - c^2 \frac{\partial^2 \rho}{\partial x_i^2} = \frac{\partial Q}{\partial t} - \frac{\partial F_i}{\partial x_i} + \frac{\partial^2 T_{ij}}{\partial x_i \, \partial x_j} \tag{1}$$

The left-hand side of equation **(1)** is the wave equation and the right-hand side can be regarded as being a collection of the various possible acoustic sources which can occur. The first term $\partial Q/\partial t$ gives the effect of mass introduction. This corresponds to the siren action of the compressor which, as mentioned previously, is small. The second term $\partial F_i/\partial x_i$ gives the effect of fluctuating forces. As was noted above, substantial fluctuating forces can act in the compressor because of the action of the wakes and this is the key term in the development of the present theory. The last term in equation **(1)** $\partial^2 T_{ij}/\partial x_i \, \partial x_j$ incorporates several effects, the most important of which, in general, is the direct sound radiation by turbulence. The symbol T_{ij} may be regarded as an acoustic stress tensor. Thus equation **(1)** can be used to describe the sound radiation by the compressor provided that the forces acting upon the compressor can be specified. The requirement then is merely to manipulate this equation into a form which gives explicit analytical results for the sound radiation at any point. This was done in detail in reference **14.** Only the final result for a typical case which is the sound radiation due to the steady and fluctuating forces acting on the rotor will be quoted herein. The expression is given as

$$c_m = \frac{imB^2\Omega}{2\pi c r_1} \sum_{k=-\infty}^{+\infty} (-i)^{mB-kV} \left(\frac{xT_k}{r_1} - \frac{mB - kV}{mBM} D_k \right) J_\mu \left(\frac{mBMy}{r_1} \right) \tag{2}$$

Somewhat surprisingly an almost identical expression was found to apply to the sound radiation from the stator. Rather than describe these equations in detail, some typical results of computations using the equation will be given herein. Note particularly that all the results will apply to radiation from either rotor or stator and that both inlet and exhaust discrete-frequency radiations by a fan are included.

RESULTS AND DISCUSSION

There are two features of the sound output which are important: the directionality and the acoustic power output, both of which are predicted by the present theories. Acoustic power is the principal gross feature of the sound and is affected by the gross features of engine design, such as mass flow and revolution rate. However, directionality can also play a significant role, especially since it is more readily modified by detail design and because the sound radiated radially outward has the most significant effect on community noise. This effect can be appreciated by reference to figure **6.** It can be seen that the sound radiated forward (or aft) must travel very much farther than

that radiated downward before reaching an observer on the ground. In the case shown, there is a difference in the path length of a factor of 10. Sound is attenuated proportionally to the inverse square power of distance traveled. Thus, sound radiated along the forward path would be, in this case, 20 dB lower in intensity on reaching the ground than sound radiated downward. It is clear that community noise problems would be minimized if the sound could be chosen to radiate in an axial direction rather than radially outward. This fact is often overlooked in discussions of compressor noise. The two features, overall power and directionality, will be discussed separately subsequently.

The two key parameters are the modal order $\mu = |n - \lambda| = |mB - kV|$, and the frequency parameter $nM = mBM$. Essentially, the frequency parameter includes the effects of rotational speed and blade number, whereas the modal order is governed by the difference in blade numbers between rotor and stator. Note that $nM = kR$, where k is the wave number and R a typical radius, and in this form may be more familiar to acousticians. Because of its more direct relevance to compressor parameters, nM is used herein.

For the purposes of this discussion, consider a 16-blade rotor ($B = 16$) operating at $M = 0.5$. The solid curve in figure 7 shows the result for the effect on the first-harmonic noise ($m = 1$) of the first-mode radiation ($k = 1$) due to the fluctuating force terms. As has been pointed out previously the effect of large stator-rotor separation will be to emphasize the contribution of the $k = 1$ term, so that this is of principal interest. The curves are symmetrical about $V = 16$, the $\mu = 0$ case. Figure 7 also shows how for small numbers of stator vanes, efficiency is very low. Beyond $V = 8$, the acoustic radiation becomes more efficient, reaching a maximum at $V = 10$. Then there is a lowering of efficiency as stator vane numbers are increased up to 16. Past this point efficiency again increases up to a maximum of about 2.6 dB additional at $V = 22$. It may also be noted that $V = 10$ and $V = 22$ correspond to the most unfavorable side-line directivity pattern as well as the highest power, as will be shown below. For $V = 10$ the peak would be in front of the compressor and for $V = 22$, behind. For further increases in blade number, efficiency then drops off rapidly. Equivalent results will occur on all compressors. The efficient and inefficient radiation regions apparent in figure 7 correspond to supersonic and subsonic phase velocities for the interaction tones, as was discussed above.

Clearly the optimum way to utilize the results shown in figure 7 is to choose the stator vane number so that radiation is in the inefficient region of the curves. Unfortunately, this is difficult on practical compressors, Apart from the effects of multimode input and higher harmonics, the high idling Mach number of modern compressors is very restrictive. Figure 7 also shows the effect of rotational Mach number. It can be seen that the region of efficient radiation spreads out considerably and reaches down even to

zero vane numbers for $M = 1$. Thus excessive numbers of stator vanes are necessary to achieve low acoustic radiation unless the engine has been specifically designed to run at a low Mach number. Similar conclusions were reached by Tyler and Sofrin (ref. 1).

The directivity pattern of compressor noise radiation is important because of the effects discussed previously with reference to figure 6. It is desirable to radiate noise in an axial direction to minimize community noise. Figure 8 shows some directivity curves typical of the three important cases in the acoustic power plots of figure 7. Figure 8 gives the directivity factor in dB as a function of an angle from the compressor hub. The dashed lines give lines of equal side-line noise level and were calculated assuming the inverse square law and the compressor axis parallel to the ground. The sound level relative to these dashed contours will generally be the most significant parameter from the community noise point of view.

The curves in figure 8 for sound radiation are not symmetrical about the compressor disk. This is because for small values of X ($X = kV$) the thrust and drag terms cancel in the forward quadrants but are additive in the rear quadrant, so that more sound is heard behind the compressor disk than in front. This effect is well known in propeller noise theory (ref. 16). However, as can be seen from equation (2), the situation is reversed when $X > n$; that is, when $kV > mB$. For this case more sound is radiated forward out of the compressor inlet than rearward. The effect of the $X > n$ case is given quite accurately by simply inverting the directionality patterns shown in figure 8. The effect could have practical application, since it gives a method by which the designer can choose the more intense sound to radiate forward or rearward into any available sound-absorbing device in the duct.

The two patterns on the right-hand side of figure 8 correspond to efficient radiation, whereas the radiation pattern on the left corresponds to inefficient radiation conditions. Thus, the least efficient radiation cases from the acoustic-power point of view have the worst directivity pattern from the point of view of community noise. Fortunately, the effects of the decreased efficiency will generally overcome any directivity effects. However, there are other significant features. As can be seen in figure 7, there are two maximums in the radiation efficiency. The center curve in figure 8 corresponds to this case and shows strong radial radiation. Thus it is desirable from the standpoint of both directivity and power to design compressors away from these points. Conversely, figure 7 shows how it is desirable to go to low-order modes in the center of the curves to reduce sound power., Figure 8 shows that this also has favorable directivity effects with minimal radial radiation.

COMPARISON WITH EXPERIMENT

Because of the large number of unknowns in the problem, particularly in specifications of the aerodynamic source characteristics, detailed correlation with experiment must be deferred. However, it is of interest to make some comparison herein. Figures 7 and 8 suggest the rather surprising conclusion that if the compressor had to operate in the efficient radiation region, then it would be desirable to go to equal numbers of rotor and stator blades ($\mu = 0$) for minimum noise radiation. Figure 9, taken from a report by Crigler and Copeland (ref. 7) provides a verification of this prediction. Figure 9 shows that the acoustic power radiated for 53 guide vanes ($\mu = 0$) is about 8 dB less than for 31 guide vanes and 7 dB less than for 62 guide vanes. Note in figure 9 how the peak levels for the $\mu = 0$ case are higher but carry very little acoustic power, so that power levels are low. The major reduction in sound radiation occurring for the $\mu = 0$ case here, particularly in the radial direction, is obviously of practical significance.

A further comparison with experiment may be accomplished by the introduction of a very simple model, discussed in more detail in reference 14. If it is assumed that the wake is of pure sinusoidal form with a momentum defect equal to the blade profile drag, then numerical values may be assigned to the fluctuating force coefficients. The fluctuating forces may be calculated by the methods of Kemp and Sears (refs. 17 and 18) as discussed in more detail in reference 14. If the asymptotic expressions for the various results are also taken, then a simple result for overall acoustic power is obtained. Using typical values for the parameters and assuming spherical spreading give the result for the side-line noise level at 200 feet as

$$p = 50 \log_{10} V_T + 20 \log_{10} D - 75 \qquad (3)$$

where V_T is the compressor tip velocity in ft/sec and D is the compressor diameter in inches. This curve is shown in figure 10, along with data points from several sources. In view of the large number of assumptions made it is very encouraging that the theoretical curve even falls on the data points.

The V_T^5 law implied by equation (3) has also been found in several experiments, but it is of interest that in the basic formulation (ref. 14) a V_R^5 law was derived where V_R is the relative speed of the blade as opposed to V_T, the mechanical tip speed. This dependence of noise of V_R has also been suggested by several investigators. The dependence of the sound on diameter squared is also eminently reasonable. However, it should be noted that the result of equation (3) is the end result of many approximations and cannot be applied indiscriminately. The uncertainties associated with any simple approach are indicated by the wide scatter of the experimental data in figure 10. It can be seen that variations of ±10 dB are probable.

CONCLUDING REMARKS

A theoretical description of the noise radiated by the fluctuating forces on the rotor and stator of a fan or compressor has been derived. The theory enables the designer to account for most of the design features of the compressor. Parameters which can be included in the theory include

Rotational speed
Blade and/or vane numbers
Separation between rotor and stator
Broad features of blade and vane geometry
Stage aerodynamic and performance parameters
Multistage radiation
Compressor hub velocity

Effects which are not included in the theory include

Duct treatment
Passage of sound through blade rows
Effects of flow velocity on sound propagation
Noise radiation due to thickness or acoustic stress

The theory also suggests that the following features will not have substantial effects on the sound:

Hard-wall duct phenomena
Detailed compressor geometry

The key problem is in predicting the aerodynamic characteristics of the shed wakes. Once these are established, the theory allows, at least in principle, very comprehensive predictions of the acoustic radiation to be made. Even off-design conditions including such effects as rotating stall can be described by general theory. Preliminary agreement with experiment has been shown. Thus, it appears that the theory can be used with reasonable confidence in design trade-off studies, and it is hoped that this will lead to the design of quieter engines in the future.

REFERENCES

1. Tyler, J. M.; and Sofrin, T. G.: Axial Flow Compressor Noise Studies. SAE Trans., vol. 70, 1962, pp. 309-332.

2. Bragg, S. L.; and Bridge, R.: Noise From Turbojet Compressors. J. Roy. Aeron. Soc., vol. 68, no. 637, Jan. 1964, pp. 1-10.

3. Morfey, C. L.: How to Reduce the Noise of Jet Engines. Engineering, vol. 198, no. 5148, Dec. 18, 1964, pp. 782-783.

4. Morfey, C. L.: Rotating Pressure Patterns in Ducts: Their Generation and Transmission. J. Sound Vib., vol. 1, no. 1, Jan. 1964, pp. 60-87.

5. Sharland, I. J.: Sources of Noise in Axial Flow Fans. J. Sound Vib., vol. 1, no. 3, July 1964, pp. 302-322.

6. Hetherington, R.: Compressor Noise Generated by Fluctuating Lift Resulting From Rotor-Stator Interaction. AIAA J., vol. 1, no. 2, Feb. 1963, pp. 473-474.

7. Crigler, J. L.; and Copeland, W. L.: Noise Studies of Inlet-Guide-Vane-Rotor Interaction of a Single-Stage Axial-Flow Compressor. NASA TN D-2962, 1965.

8. Smith, M. J. T.; and House, M. E.: Internally Generated Noise From Gas Turbine Engines. Measurement and Prediction. Trans. ASME, Ser. A: J. Engr. Power, vol. 89, no. 2, Apr. 1967, pp. 177-190.

9. Hulse, B. T.; and Large, J. B.: The Mechanisms of Noise Generation in a Compressor Model. Trans. ASME, Ser. A J. Engr. Power, vol. 89, no. 2, Apr. 1967, pp. 191-197.

10. Morfey, C. L.; and Dawson, H.: Axial Compressor Noise – Some Results From Aero-Engine Research. Paper Presented at 11th Annu. Gas Turbine Conf., Amer. Soc. Mech. Engrs. (Zurich), Mar. 1966.

11. Lowson, M. V.: Reduction of Compressor Noise Radiation. J. Acoust. Soc. Amer., vol. 43, no. 1, Jan. 1968, pp. 37-50.

12. Slutsky, Simon: Discrete Noise Generation and Propagation by a Fan Engine. Paper Presented at AFOSR – UTIAS Symp. on Aerody. Noise (Toronto), May 20-21, 1968.

13. Ffowcs Williams, J. E.; and Hawkings, D. L.: Theory Relating to the Noise of Rotating Machinery. Brit. A.R.C. 29,821, Jan. 1968.

14. Lowson, M. V.: Theoretical Studies of Compressor Noise. Rep. WR 68-15P (Contract No. NAS 1-6885), Wyle Lab., July 1968.

15. Lighthill, M. J.: On Sound Generated Aerodynamically. I. General Theory. Proc. Roy. Soc. (London), ser. A, vol. 211, no. 1107, Mar. 20, 1952, pp. 564-587.

16. Gutin, L.: On the Sound Field of a Rotating Propeller. NACA TM 1195, 1948. (From Physik. Zeitschr. der Sowjetunion, Bd. 9, Heft 1, 1936, pp. 57-71.)

17. Kemp, Nelson H.; and Sears, W. R.: Aerodynamic Interference Between Moving Blade Rows. J. Aeronaut. Sci., vol. 20, no. 9, Sept. 1953, pp. 585-612.

18. Kemp, Nelson H.; and Sears, W. R.: The Unsteady Forces Due to Viscous Wakes in Turbomachines. J. Aeronaut. Sci., vol. 22, no. 7, July 1955, pp. 478-483.

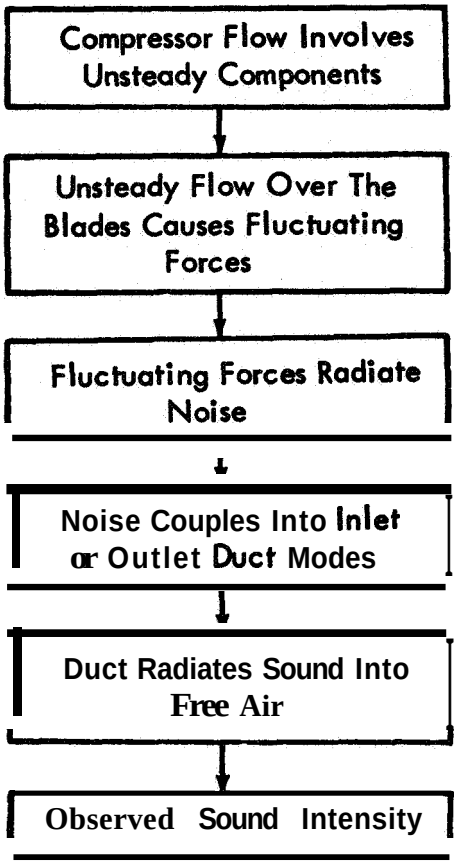

Figure 1.- The cause and effect chain of compressor noise radiation.

Signals received at the same instant will have been generated a time $(r_1 - r_2)/c$ apart.

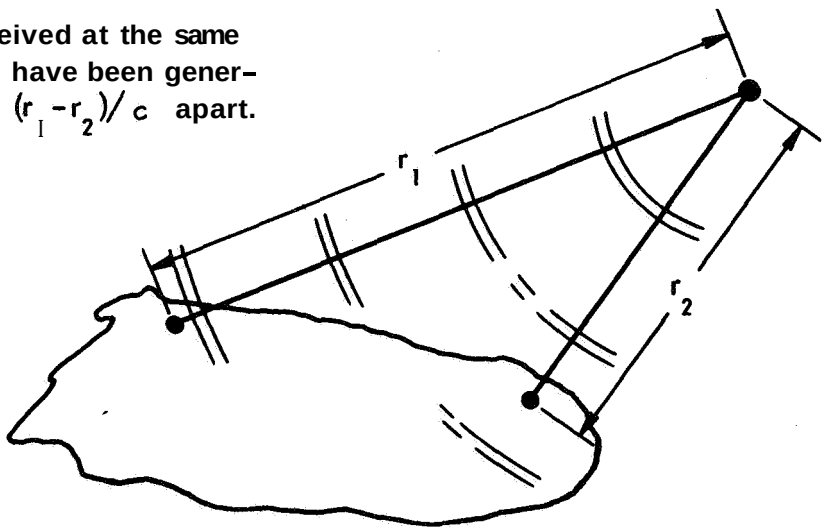

Figure 2.- Effects of retarded time.

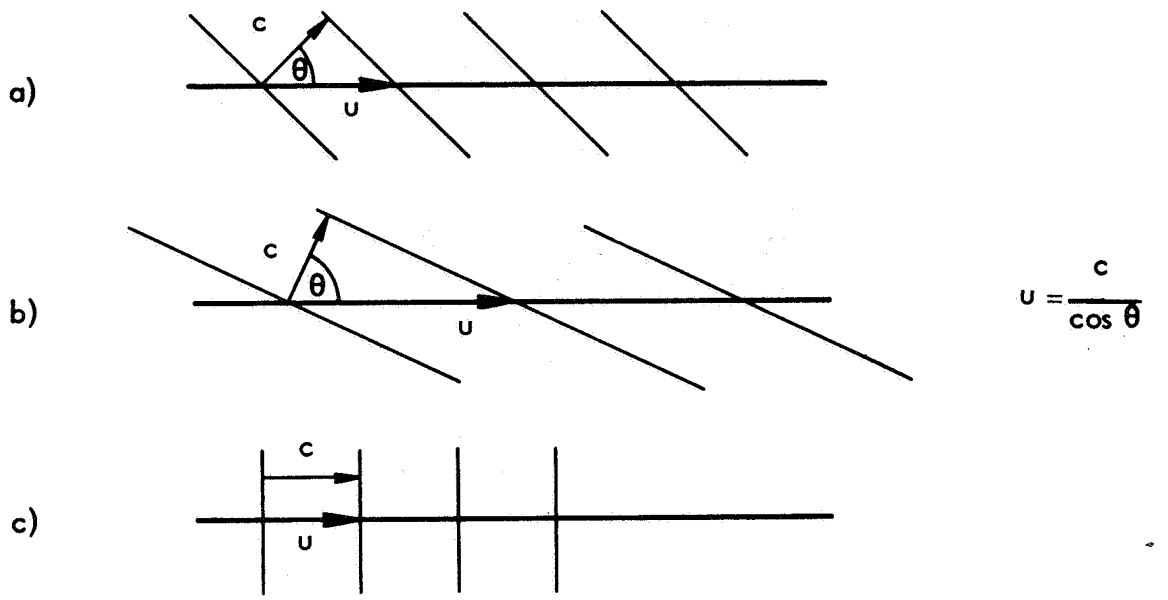

Figure 3.- Effects of source velocity.

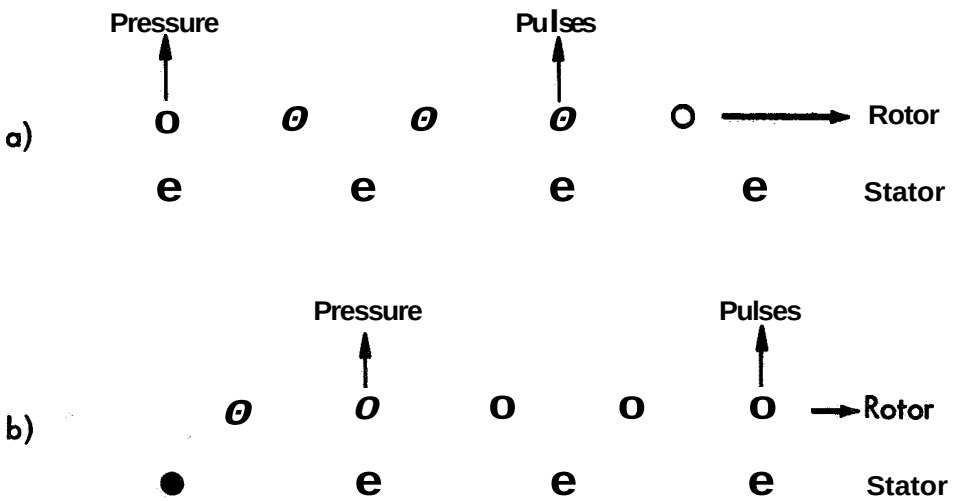

Figure 4.- Rotor-stator phase effects.

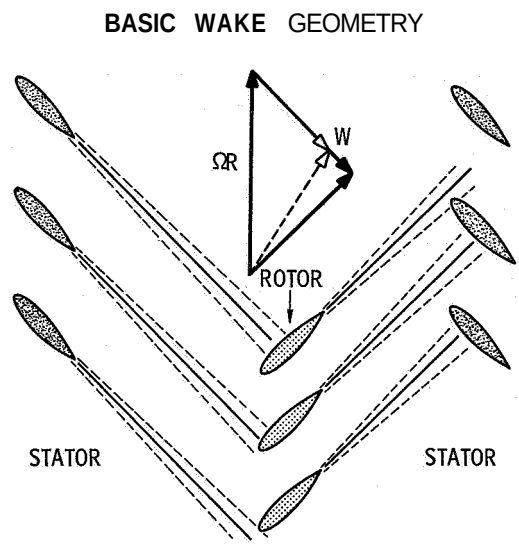

Figure 5.- Basic wake geometry.

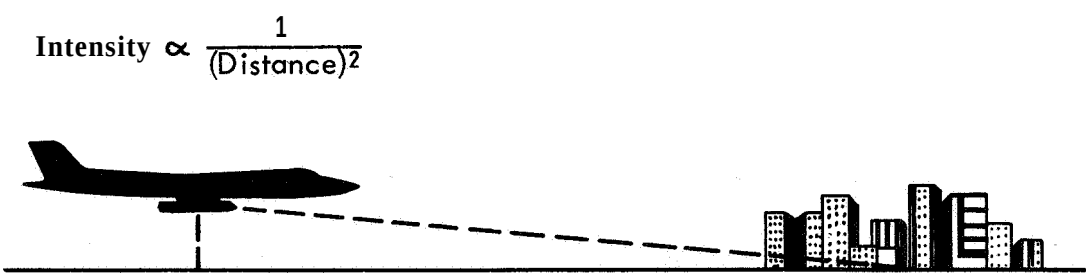

Figure 6.- Effect of directionality on observed noise levels.

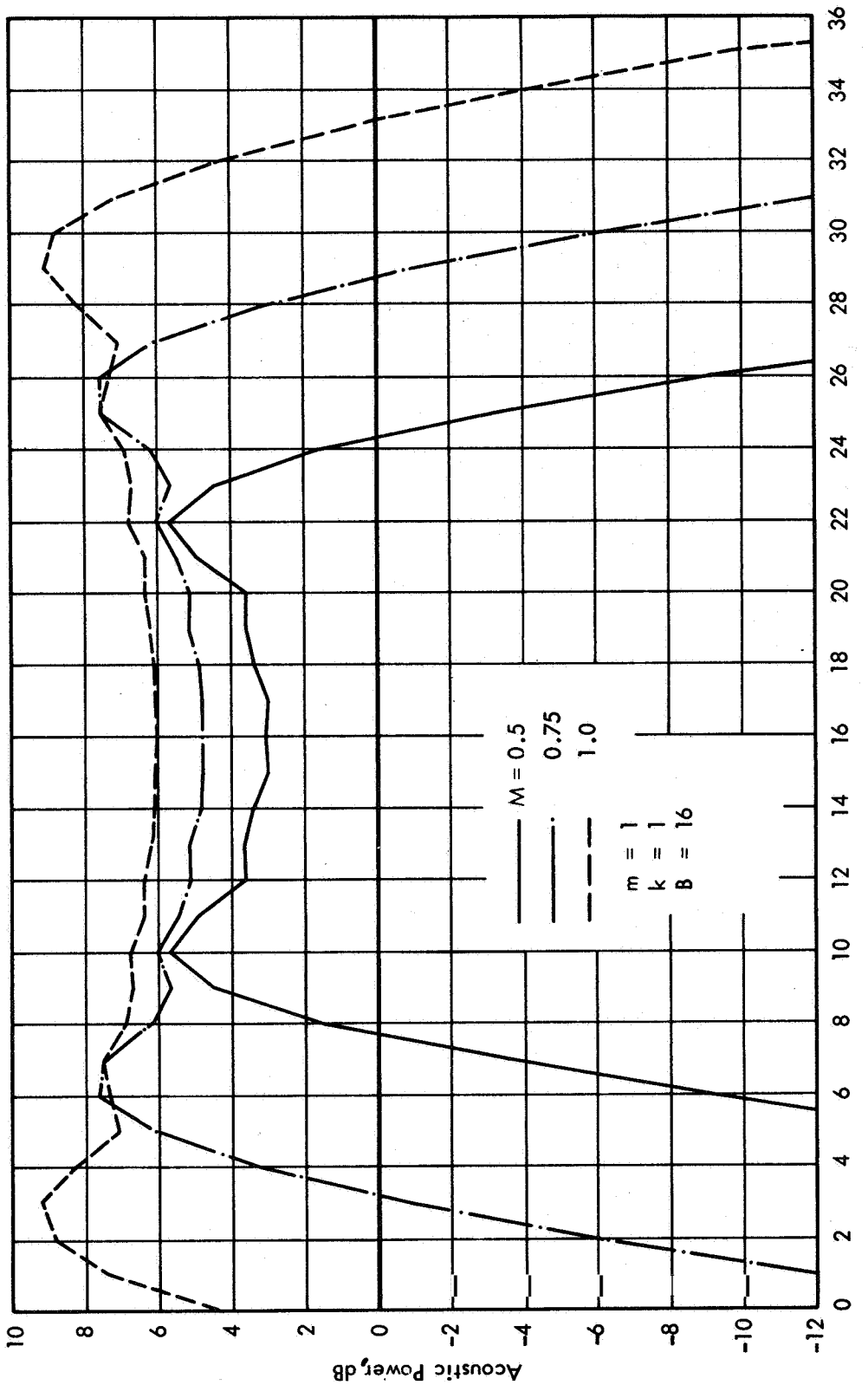

Figure 7.- Effect of rotational Mach number on acoustic power.

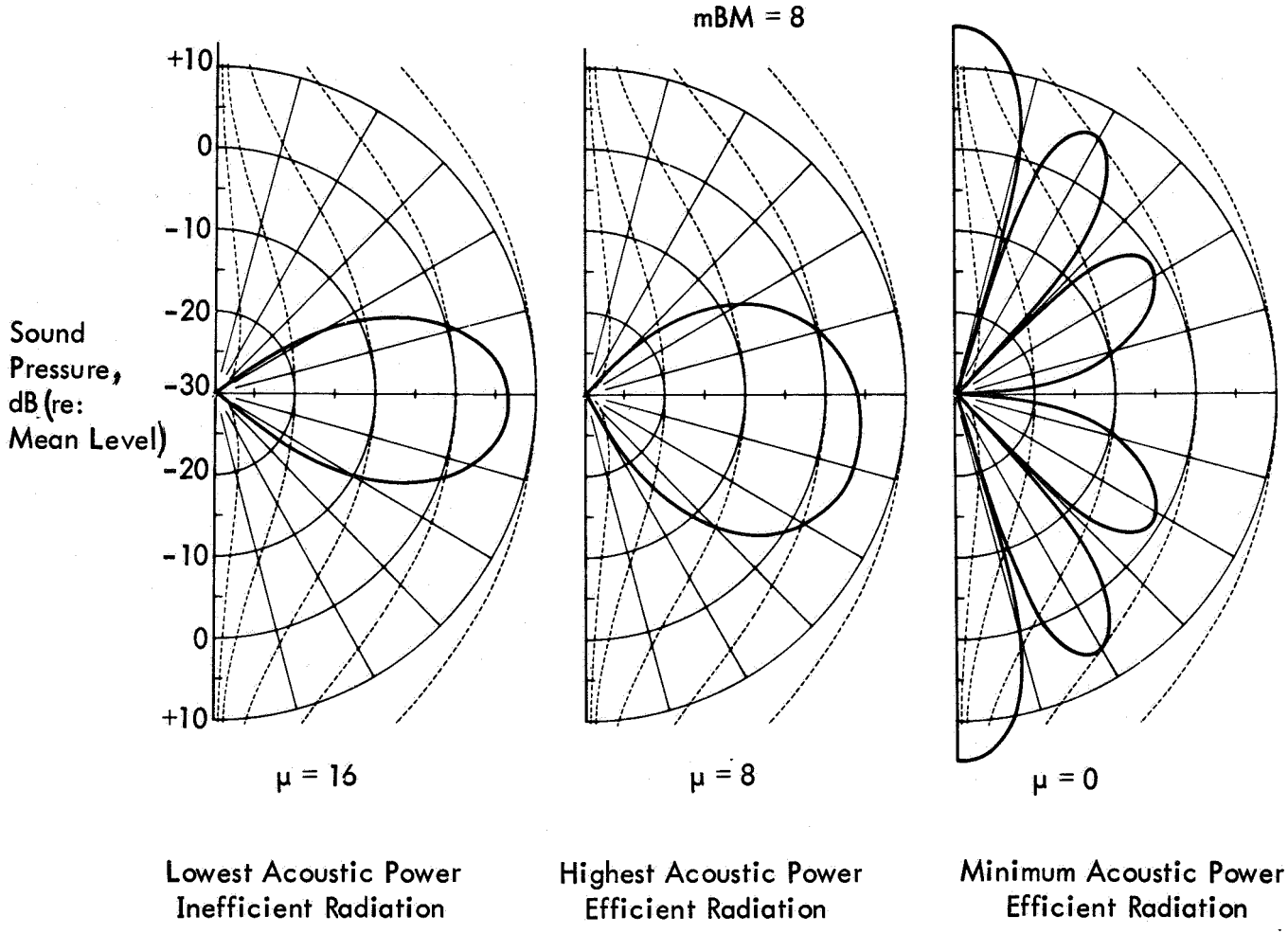

Figure 8.- Compressor noise directivity patterns.

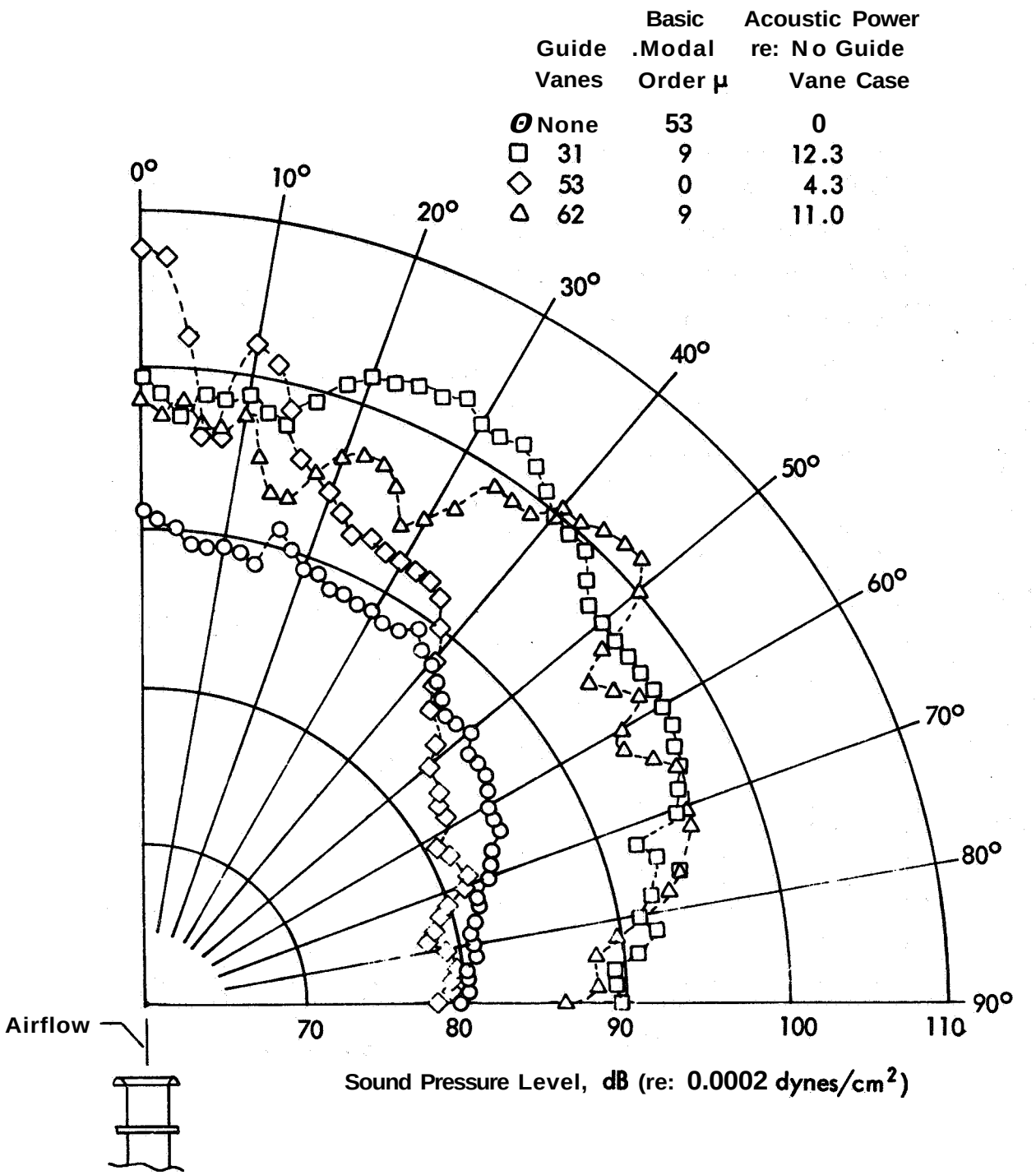

Figure 9.- Measured one-third octave (at blade passage frequency) radiation patterns for various rotor – quide-vane configurations. Rotor tip Mach number M_t, *0.346.* From Crigler and Copeland (ref. 7).

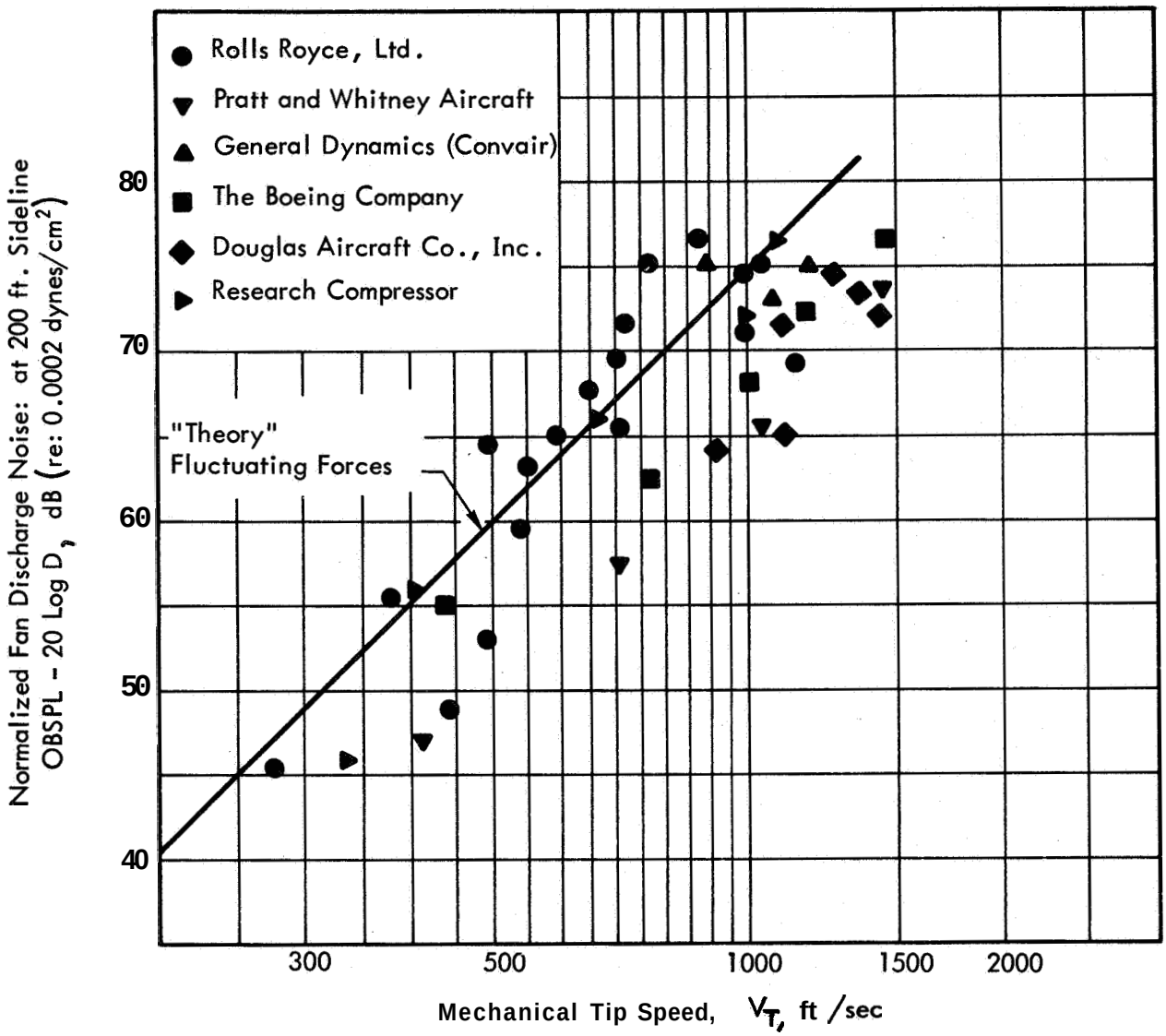

Figure 10.- Comparison of "theory" and experiment. Maximum fan discharge noise in octave band containing fundamental blade passage frequency.

21. POTENTIAL OF INLET-GUIDE-VANE CONFIGURATION FOR INLET NOISE REDUCTION

By David Chestnutt and John L. Crigler

NASA Langley Research Center

SUMMARY

The effects of inlet guide vanes on the noise radiated from the inlet of an axial flow compressor are discussed. It is found that an inlet-guide-vane—rotor spacing of 2 to 3 chords appears to be an optimum configuration. It is shown that inlet guide vanes can be used to aerodynamically choke the flow to produce a sonic barrier to inlet noise radiation. This sonic barrier has reduced the inlet noise up to 30 dB and has been obtained over virtually the entire operating range of the test compressor. In addition, inlet noise reduction is shown to be a function of average Mach number between guide vanes above Mach 0.65. Performance losses during choked-flow operation are shown to be modest.

INTRODUCTION

Recent research has indicated that inlet guide vanes can favorably reduce the radiation of noise from the inlet of a compressor. The role of inlet guide vanes (IGV) in the alleviation of inlet noise is presented schematically in figure 1. Shown in this figure is a turbofan engine which emits noise from three major sources: namely, the primary jet, the fan discharge, and the inlet. The inlet noise and fan discharge noise are made up mainly of broadband and discrete tones radiating from the rotating machinery. Inlet guide vanes may be axially spaced to control the strengths of the wakes encountered by the rotor (illustrated in the sketch at the lower left in fig. 1). The effects of such wake interactions on the compressor noise are included in reference 1. Inlet guide vanes may also be used for locally choking the inlet flow (illustrated in the sketch at the lower right in fig. 1). Both the wake-interaction and the choked-flow phenomena are discussed from the standpoint of their effect on noise reduction.

INLET-GUIDE-VANE—ROTOR SPACING

The effects of aerodynamic interactions on the noise of a turbojet engine are shown in figure 2. Observe the differences in 1/3-octave band sound-pressure-level (SPL) spectra for 30° azimuth in front of the engine with inlet guide vanes (IGV) at two different axial spacings. The solid-line record represents a noise spectrum for a spacing of 1/8 chord; the dash-line record represents a spectrum for a spacing of 6 chords. It can be seen that

there are significant noise reductions at all band center frequencies. These noise reductions result apparently from reduced aerodynamic interaction effects due to increased inlet-guide-vane—rotor spacing.

A summary of all available data (refs. 2 to 8) related to the effects on noise of inlet-guide-vane—rotor spacing is presented in figure 3. Included are data for the fundamental-blade-passage frequencies from engines as well as those from single-stage subsonic compressors and from multistage transonic compressors. All noise levels are referred to those at an axial spacing of 0.125 chord. As axial spacing is increased, the relative noise levels generally decrease. These effects of spacing are greater for small axial spacings, where potential flow effects as well as strong wake interactions may be present, and become less at the larger axial spacings. The noise reductions obtainable for large IGV-rotor spacings approach those resulting from total removal of the inlet guide vanes. An inlet-guide-vane—rotor spacing of **2** to **3** chords appears to be an optimum configuration.

INLET-GUIDE-VANE CHOKING

Test Arrangement

All inlet-guide-vane choking studies at the Langley Research Center were made with a three-stage transonic axial-flow air compressor (fig. **4).** This photograph was taken during the installation phase and shows the bellmouth inlet and downstream diffuser. The inlet noise from this compressor radiated into an anechoic chamber in which far-field measurements were taken. The compressor embodying current compressor design technology can operate as a one-, two-, or three-stage machine. Provision is made for changing the number of rotor blades and stator vanes. The three-stage transonic configuration was used in this investigation. The compressor is driven by a 3000-hp variable-speed electric motor and has a maximum design speed of 25 000 rpm.

Figure 5 presents the performance curves for this three-stage transonic compressor. Both the efficiency and pressure-ratio curves are fairly typical of those for transonic compressors. Note especially the flat pressure-ratio curves in the subsonic region and the nearly vertical curve denoting transonic operation. Whenever noise data were collected for this compressor, corresponding compressor performance data were also taken. During this investigation the compressor was operated over the range of pressure ratio and at the rotational speeds indicated. Further details regarding this equipment are given in reference 3.

Effects of Mach Number Between Inlet Guide Vanes

Figure 6 shows the relative overall sound pressure level as a function of average axial Mach number M_{av} between adjacent inlet guide vanes. This relationship was

originally presented in reference 3 for choking obtained either by turning the inlet guide vanes in a direction opposed to rotor rotation or by thickening the inlet guide vanes. The data of figure 6 are representative of either method for obtaining choking. In reference 9, choking in the compressor inlet was effected by a variable cowl. Aerodynamic choking is defined as a condition at which the air velocity has reached the acoustic velocity and no sound can be propagated upstream through the choked region. At an average Mach number of about 0.65, there begins a gradual reduction in noise level as the Mach number is increased. At an average Mach number of approximately 1.00 where the full effect of choking is realized, there is a dramatic reduction in the noise level. The measured noise reduction of 30 dB shown was obtained from a compressor configuration with IGV-rotor spacing of 1/2 chord. Had the spacing been less, the noise reduction would have been correspondingly greater because of the higher initial noise level.

Far-Field Radiation Patterns and Spectra

In figure 7 are seen the far-field radiation patterns for both choked and unchoked flow conditions. These patterns were obtained by using a traversing microphone spaced 10 inlet diameters from the compressor inlet. The outer pattern represents a typical unchoked condition with an inlet-guide-vane—rotor spacing of 1/2 chord and shows a marked variation in the noise level. The inner pattern represents a typical choked condition for which inlet-guide-vane—rotor spacing is not believed significant, the noise levels are lower, and there is less noise variation with azimuth. The corresponding spectra for these patterns are shown for comparison in figure 8. The upper 1/10-octave spectrum was taken at 30° azimuth and is representative of the unchoked condition. The lower 1/10-octave spectrum was taken at the same azimuthal value and is representative of the choked condition. The two important observations to be made are that as a result of choking, the sound pressure level has been reduced considerably across the entire spectrum and the peaks at the fundamental-blade-passage frequency and its harmonics have been eliminated. Because of the higher rotational speed mentioned previously, the fundamental-blade-passage frequency is higher than that encountered in larger slower rotating compressors.

Effects of Compressor Speed

The relative merits of retaining inlet guide vanes to effect choking, yet spacing them properly for minimum interaction noise when the compressor is operating in an unchoked mode, are established by the data in figure 9. The inlet guide vanes used in this figure were designed for choking at a compressor speed of 100 percent design corrected speed (rpm). An inlet configuration with an IGV-rotor spacing of 1/2 chord is represented by the dash-line curve with square symbols. As the compressor speed is increased from 70 percent to 100 percent rpm, there is a sharp reduction in the noise level and the inlet

is aerodynamically choked. The dash-line curve with circular symbols represents an inlet configuration with no inlet guide vanes and for which the noise levels are decidedly lower at 70 percent rpm but, as the compressor speed is increased, there is only a relatively small additional noise reduction. The obvious compromise is to space properly the inlet guide vanes to minimize the aerodynamic interactions when the compressor is operating in an unchoked mode. This configuration is represented by the solid-line curve. As the compressor speed is increased for this configuration, the same minimum noise level is obtained at 100 percent rpm as with the configuration with 1/2-chord IGV-rotor spacing. Therefore, variable-geometry inlet guide vanes with appropriate axial spacing would produce relatively lower interaction noise levels and could provide substantial noise reductions by means of flow choking.

The experimental work accomplished to date with the three-stage transonic research compressor is shown in figure 10. The hatched area at the top of the figure indicates the noise reductions available at the fundamental-blade-passage frequency by increased axial spacing. A reduction in noise of approximately 10 dB was obtained with increased IGV-rotor spacing to the point of removal of the inlet guide vanes. A combination of increased IGV-rotor spacing and choking by means of increased IGV turning provided an additional 20-dB noise reduction which has been obtained at compressor speeds from approximately 72 percent rpm to 100 percent rpm.

Compressor Performance

Some consideration should be given to the effect of choking on compressor performance. The experimental data presented in table I provide a partial answer to this effect and show that performance is a function of how choking is obtained. Choking has been obtained by thickening the inlet guide vanes, by turning the inlet guide vanes, or by a combination of thickening and turning. Compressor efficiency losses of 4 to 5 percent and pressure-ratio losses of 4 to 10 percent were measured during choked-flow operation, and an increase in surge sensitivity was observed.

Although the adverse performance results indicated in table I are known to be critical for full-power operation, they may not be critical for off-design operation, such as might occur during an airplane second-segment climb or landing approach for which noise reduction is an important consideration. If a choked-flow inlet is incorporated in the initial compressor design, it is believed that the performance penalties noted in the table could be minimized.

CONCLUDING REMARKS

The results of this study suggest that variable-geometry inlet guide vanes with appropriate inlet-guide-vane—rotor spacing can provide large inlet noise reductions.

Such a design concept seems to be worthy of consideration for reducing noise of future axial-flow compressors even though some additional mechanical complexity may be involved.

REFERENCES

1. Lowson, Martin V.: Compressor Noise Analysis. Conference on Progress of NASA Research Relating to Noise Alleviation of Large Subsonic Jet Aircraft, NASA SP-189, 1968. (Paper No. 20 herein.)

2. Crigler, John L.; and Copeland, W. Latham: Noise Studies of Inlet-Guide-Vane—Rotor Interaction of a Single-Stage Axial-Flow Compressor. NASA TN D-2962, 1965.

3. Chestnutt, David: Noise Reduction by Means of Inlet-Guide-Vane Choking in an Axial-Flow Compressor. NASA TN D-4682, 1968.

4. Lowson, M. V.: Reduction of Compressor Noise Radiation. J. Acoust. Soc. Amer., vol. 43, no. 1, Jan. 1968, pp. 37-50.

5. Crigler, John L.; Copeland, W. Latham; and Morris, Garland J.: Turbojet-Engine Noise Studies To Evaluate Effects of Inlet-Guide-Vane—Rotor Spacing. NASA TN D-4690, 1968.

6. Dawson, H.; and Voce, J. D.: The Effect of Axial Spacing on Compressor Tone Noise. 5e Congrès International d'Acoustique, Vol. 1b, Daniel E. Commins, ed., Congr. Int. Acoustique, 1965, pp. [L14]1-4.

7. Bateman, David A.; Chang, Stephen C.; Hulse, Bruce T.; and Large, John B.: Compressor Noise Research. Tech. Rep. ADS-31, FAA, Jan. 1965.

8. Kilpatrick, D. A.; and Reid, D. T.: Transonic Compressor Noise – The Effect of Inlet Guide Vane/Rotor Spacing. R. & M. No. 3412, Brit. A.R.C., 1965.

9. Higgins, C. C.; Smith, J. N.; and Wise, W. H.: Sonic-Throat Inlets. Conference on Progress of NASA Research Relating to Noise Alleviation of Large Subsonic Jet Aircraft, NASA SP-189, 1968. (Paper No. 13 herein.)

TABLE I.- EFFECTS OF CHOKING ON COMPRESSOR PERFORMANCE

Means of choking	Comparison with unchoked operation		
	Surge sensitivity	Efficiency loss, percent	Pressure-ratio loss, percent
IGV thickening	Increased slightly	---	8 to 9
IGV turning	Increased	4 to 5	8 to 10
IGV turning and thickening	Increased slightly	---	4 to 5

ROLE OF INLET GUIDE VANES

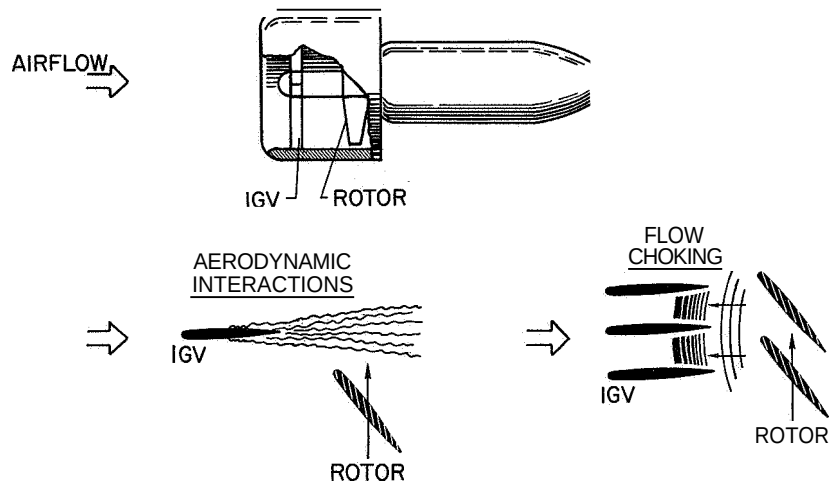

Figure 1

EFFECTS OF INLET-GUIDE-VANE—ROTOR SPACING

TURBOJET ENGINE

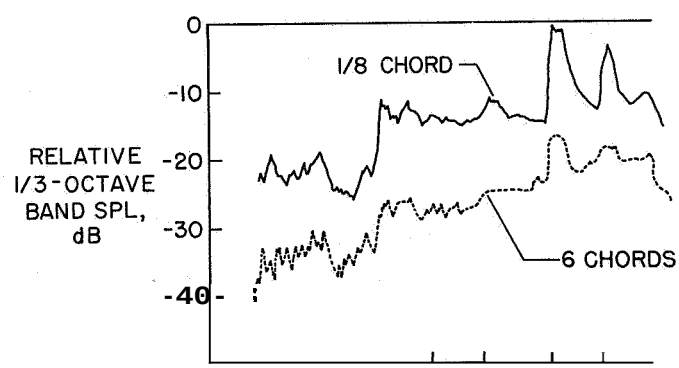

Figure 2

SUMMARY OF IGV–ROTOR SPACING EFFECTS ON NOISE

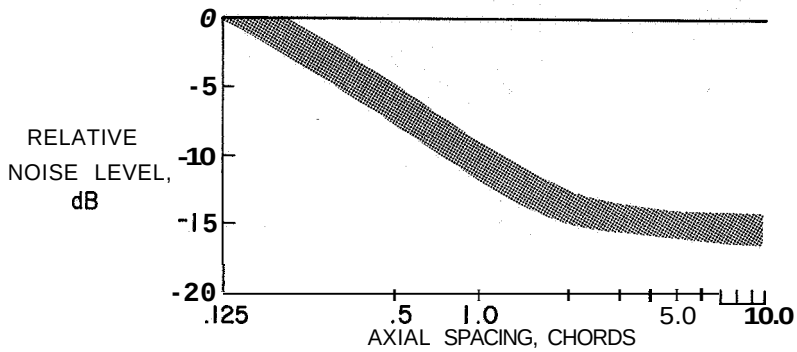

Figure 3

TEST ARRANGEMENT

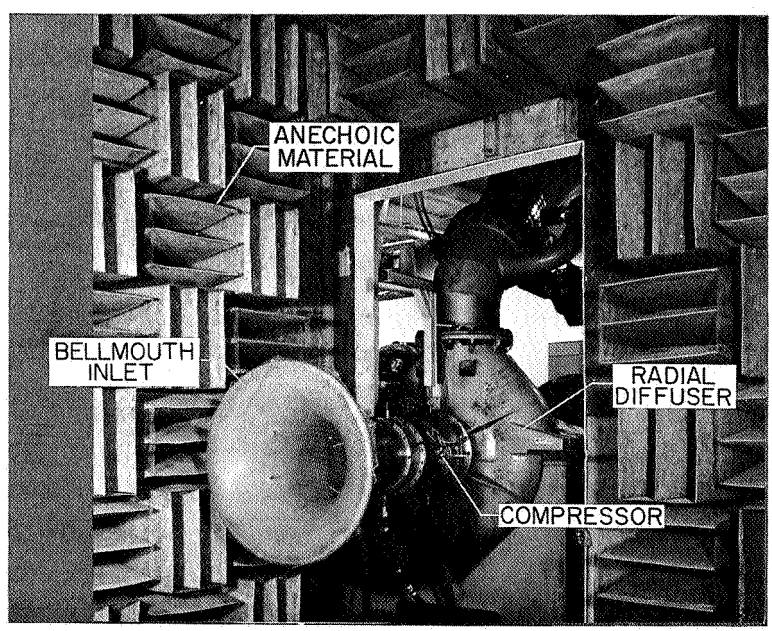

Figure 4 L-68-8577

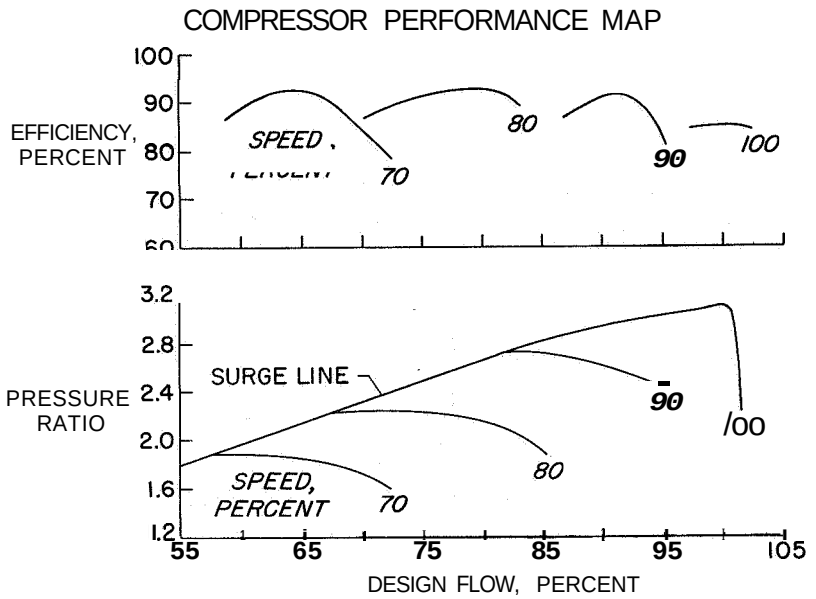

Figure 5

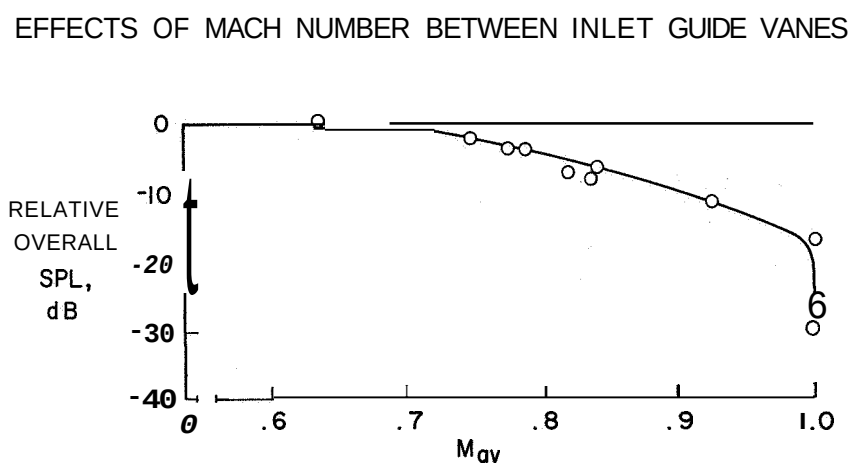

Figure 6

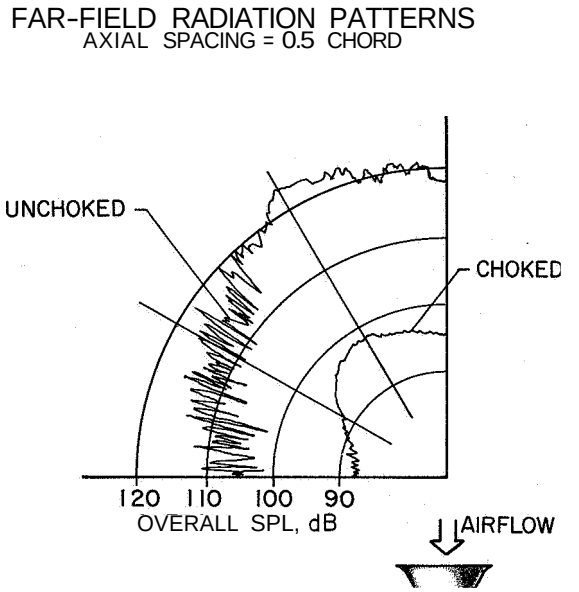

Figure 7

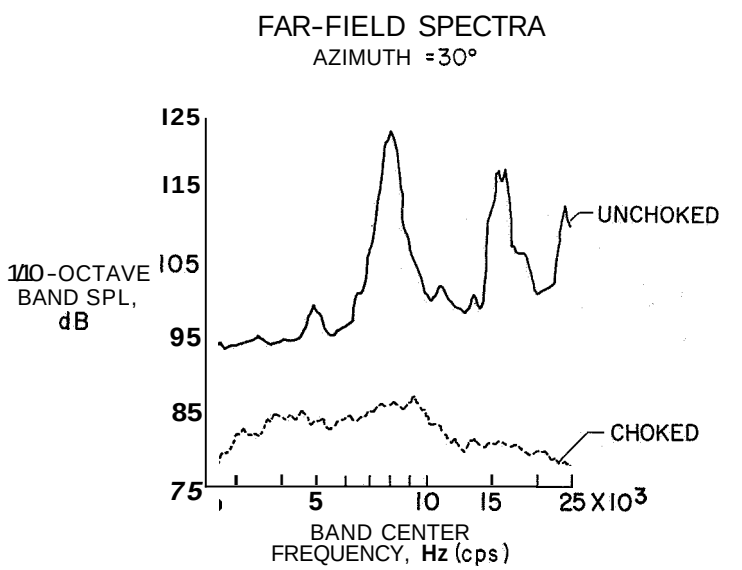

Figure 8

EFFECTS OF COMPRESSOR SPEED

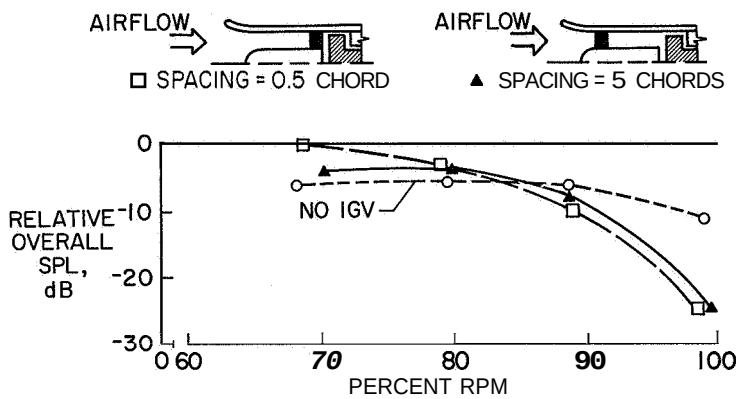

Figure *9*

NOISE REDUCTION INVOLVING INLET GUIDE VANES

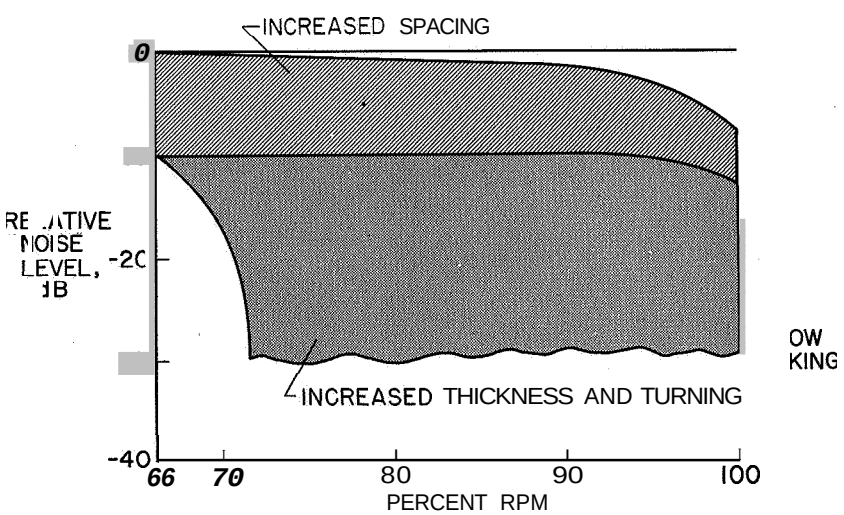

Figure 10

22. A STUDY OF EXHAUST NOISE AS IT RELATES TO THE TURBOFAN ENGINE

By Colin G. Gordon

Bolt Beranek and Newman, Inc.

SUMMARY

At the relatively low exhaust velocities of current and projected high-bypass-ratio engines, it may be expected that noise from the free expanding jet will be dominated by sources produced within the engine ducting by the exhaust stream. These sources will result from the highly turbulent flow within the duct and the interaction of this turbulence with surface discontinuities, struts, and the like.

An experimental program has been performed on a laboratory jet to study these new sources of exhaust noise. The influence of the insertion of discontinuities and obstructions into the jet pipe has been examined and related to the flow parameters. Results to date suggest that the acoustic power generated by a flow discontinuity can be correlated with the pressure drop which it produces in the flow.

These studies are felt to have significant bearing on the prediction and control of exhaust noise of current and future turbofan engines.

INTRODUCTION

Perhaps the most fundamental result that can be elicited from aerodynamic noise theory describes the process whereby the intense turbulence in the exhaust stream of a jet engine generates sound. The theory predicts that the sound from this turbulence will increase with the eighth power of flow velocity. This result has been verified experimentally in the laboratory and by measurement on turbojet engines over much of their operating range.

An eighth-power-of-velocity law suggests immediately that exhaust velocities need only be reduced by a small amount to obtain quite significant reductions in sound output. For example, a 25-percent reduction in exhaust velocity should effect a noise reduction of about 10 decibels; a 50-percent reduction would be accompanied by a 24-decibel reduction in noise.

In the modern generation of turbofan engines, the thrust is developed by accelerating a larger volume of gas through a smaller velocity range than was typical of the older turbojet vehicles. A silhouette of an engine of the high-bypass-ratio type is shown in figure 1. The turbulent mixing sources are identified as external sources in this figure and, in this regard, the contribution made by the bypass exhaust must not be omitted. It might be

supposed that reduction of the velocities in this mixing region would remove, or significantly reduce, the problem of exhaust noise. By judging the increasing concentration of effort on fan- and compressor-noise problems, it might be assumed that the problem has indeed been solved.

A closer look at the problem indicates however that the solution is not quite so simple. Real engines and laboratory jets at low, but still high subsonic, speeds often show a marked deviation from the eighth-power-of-velocity law (refs. 1 to 4). The exponent of the velocity is reduced. At these reduced speeds, it is believed that broadband exhaust noise is no longer dominated by the sources in the freely expanding turbulence, but that sources arise which are associated with the highly turbulent flow in the exhaust ducting itself. These sources are distinct from sources generated by the air-moving equipment within the engine and are identified as internal sources in figure 1.

The significance of the proposed change in source type and location is twofold. Firstly, a reduced velocity exponent means that less benefit will be derived from low tailpipe velocities than might be supposed. Secondly, methods of noise suppression appropriate to the classical jet source may not be effective and, in fact, may be harmful when the dominant sound source is located within the exhaust duct.

The purpose of the study described in this paper is to model in a very simple sense the condition of a highly turbulent flow exhausting into the free atmosphere and to examine the sound generating properties of this flow. The basic form of the experiment is shown in figure 2.

SYMBOLS

c	speed of sound
D	diameter of pipe
$\tilde{F}$	fluctuating-force amplitude
f	frequency
f_o	constant having dimensions of frequency and found to be approximately equal to cutoff frequency for plane-wave propagation
I	acoustic intensity
k	constant

$k(s),k'(s)$	spectrum-shape constants
S	Strouhal number
U	flow velocity
U_c	constricted-flow velocity
W	radiated power
Δp	pressure drop across obstruction
δ	geometric thickness of wake
P	gas density

SOURCES OF AERODYNAMIC NOISE

As a prelude to subsequent discussions, a brief description of the three fundamental mechanisms of aerodynamic noise generation is presented herein. The relation of these mechanisms to the experiment is illustrated in figure 2.

The process whereby the free turbulence in an expanding jet generates noise has been mentioned previously. The noise sources associated with the turbulence exist in the absence of solid surfaces. These sources are inefficient radiators of sound, having the equivalence of acoustic quadrupoles and, as such, they are generally referred to as aerodynamic quadrupoles. The acoustic intensity I from these sources can be shown to have the parametric dependence

$$I \propto \frac{\rho U^8}{c^5} \tag{1}$$

where ρ is the gas density, U is the flow velocity, and c the speed of sound.

When turbulence is generated by a surface or when turbulent flow impinges on a surface, fluctuating drag or lift forces are exerted. These forces when applied to the fluid constitute sources of acoustic power. These sources have the equivalence of the acoustic dipole and are sometimes termed aerodynamic dipoles. They are more efficient radiators than the quadrupole sources. It can be shown that the parametric dependence of the acoustic intensity is

$$I \propto \frac{\rho U^6}{c^3} \tag{2}$$

The aerodynamic dipole thus displays a dependence upon the sixth power of flow velocity.

The final source which can be elicited from current aerodynamic noise theory arises if the turbulence within the jet pipe produces a gross fluctuation of the volume flow across the exit plane of the pipe. Such a source is piston-like in its form and is, therefore, appropriately called the aerodynamic monopole. The monopole is the most efficient of aerodynamic sources that can be postulated, with the dependence

$$I \propto \frac{\rho U^4}{c^3} \tag{3}$$

It should be noted that the intensity relations given in equations (1) to (3) assume that each source is located in a free-field acoustic environment. In a subsequent section of this paper, the influence of the restricting environment of the pipe is discussed.

EXPERIMENT

A most important requirement of the experiment was that a high degree of measurement accuracy be obtained so that the different source mechanisms could be identified on the basis of the measured velocity exponents.

A schematic of the measurement system is shown in figure 3. Air from the airflow apparatus was passed via a sound attenuating muffler to a 6-inch-diameter pipe which penetrated the wall of the anechoic measurement chamber. This pipe then decreased in diameter to the diameter of the experimental jet, generally 2 inches. The airflow in the pipe was measured by a Pitot-static tube some distance upstream from the test section which carried the flow disturbance. The pipe was constructed in such a way that the spoiler could be readily inserted and removed. The distance of the spoiler from the exit plane could also be changed. Throughout most of the experiments the spoiler was located three pipe diameters (6 inches) from the exit plane. The total length of jet pipe (following the transition) was some 36 inches. Thus fully developed pipe turbulence was established before the spoiler location.

The sound field in the anechoic chamber was scanned in a single (horizontal) plane centered on the pipe exit. A simple traverse for each flow condition was used, the total noise signal being recorded on magnetic tape. The reduction of these data into octave bands of frequency was made subsequently. A graphic computer technique was used to compute the radiated sound power.

OVERALL RADIATED SOUND POWER

In the preliminary studies, attention was focused on the overall sound power (that is, measured over the entire frequency range) radiated by the system. The principal findings can be summarized as follows: The level of the overall radiated sound power from a plain unobstructed jet is shown in figure 4 as a function of the exit-plane velocity. Results are

shown for three separate experiments made over a 4-month period. These results demonstrate the high order of repeatability made possible by the experimental equipment. The plain pipe radiation shows an eighth-power-of-velocity dependence at the higher velocities but tends, however, to a sixth-power dependence as the velocity decreases. The eighth-power dependence is identified with free jet turbulence and agrees closely with theoretical predictions (solid-line curve in fig. 4) based on constants determined experimentally by Fitzpatrick and Lee (ref. 3). The sixth-power dependence may be identified with aerodynamic dipole mechanisms within the pipe – perhaps associated with the exit lip.

When a flow obstruction is inserted into the pipe, the radiated power increases as is shown in figure 5 and a sixth power of velocity becomes established over the total operating flow range. This result is typical in that a sixth-power-of-velocity law was consistently and accurately observed throughout the studies for most cases in which the pipe flow was obstructed. If this velocity exponent is assumed to be indicative of an aerodynamic dipole mechanism within the pipe, at least two possible locations of the noise sources can be postulated. These locations are:

(1) On, or close to, the flow obstruction associated with turbulence generation

(2) At the exit plane associated with the interaction of the highly turbulent wake with the exit lip

Figure 6 shows the result of an experiment, the object of which was to define the location of these sources. An acoustic muffler was placed immediately downstream from the spoiler. The purpose of the muffler was to attenuate the acoustic energy propagating downstream from the spoiler without influencing, sensibly, the form of the downstream turbulence. The data in figure 6 indicate that the spoiler-generated sound must be located in the vicinity of the spoiler rather than at the exit lip. In a second experiment, the muffler was replaced by flow straighteners which attenuated the downstream propagating turbulence without significantly interrupting the acoustic propagation path. The same conclusion was reached; that is, the sources of obstruction-generated sound are located on, or close to, the surface of the obstruction.

Sound-power data for three different obstruction geometries are presented in figure 7. The data are presented as a function of exit-plane velocity. While each geometry displays an approximate dependence upon the sixth power of velocity, a very considerable scatter occurs between the data of one geometry and another. Exit-plane velocity is apparently not a good correlating parameter for obstruction-generated sound.

When, however, these same data are plotted against the total pressure drop that occurs across the flow obstruction, the degree of correlation is excellent as shown in figure 8. The sound power from a pipe-immersed obstruction can, apparently, be expressed in terms of the third power of the pressure drop across it. . The dimensions of the obstruction seem to be of little importance.

The result demonstrated in figure 8 was found to hold for a wide variety of obstruction geometries and sizes. It seemed that herein lay the basis for a prediction scheme for obstruction-generated sound. A physical model on which to base the analysis was needed to help derive the appropriate prediction formula.

The observed dependence of obstruction sound upon the sixth power of flow velocity is a strong indication that the source mechanism is the aerodynamic dipole. It can therefore be postulated that the acoustic source is the fluctuating force field exerted by the flow on the obstruction.

The schematic of the jet pipe appropriate to this model is shown in figure 9. Airflow passing along a pipe is constricted as it passes the flow obstruction. The flow then expands to form a highly turbulent wake behind the obstruction. The process of vortex shedding by the obstruction causes fluctuations in the drag and lift forces exerted on it. These fluctuating forces form the dipole source of sound.

The power radiated from a force field in a free-field acoustic environment is given by

$$W \propto \tilde{F}^2 f^2 \tag{4}$$

where $\tilde{F}$ is the amplitude and f is the characteristic frequency of the force. For this model, equation (4) is assumed to be valid even in the confines of the pipe. Furthermore, the drag forces, rather than the lift forces, are assumed to be primarily responsible for the radiation.

The characteristic frequency of vortex shedding from the obstruction is given by the quotient of the constricted velocity U_c and the geometric thickness of the wake 6. If constant proportionality between the steady and fluctuating drag components is assumed, then the fluctuating force field can be expressed by the product of the constricted velocity pressure $\frac{1}{2}\rho U_c^2$ and the area of the wake. Thus, the expression for radiated power can be derived as

$$W = \frac{k\,\Delta p^3 D^2}{\rho^2 c^3} \tag{5}$$

where Δp is the pressure drop across the obstruction, D is the diameter of the pipe, and ρ and c are, respectively, the density and speed of sound of the air, and k is a constant. Equation (5) is identical in form with that developed by Yudin (ref. 5) some years ago from studies of air-duct elements (related to low-velocity ventilating systems). This equation is observed to provide a good degree of overall-power data correlation in the present study. Indeed, for this study the value of k (for overall power) has been observed to lie close to 2.5×10^{-4}.

FREQUENCY SPECTRUM

The result of the dipole model is found to describe quite accurately the overall noise radiation from many different obstruction configurations. Its correctness as a physical model is less certain, however, when the frequency spectrum of the obstruction-generated sound is examined.

The octave-band spectrum, for a typical obstruction geometry, normalized in accordance with the dipole-model formula of equation (5) is presented in figure 10. As is usual, the normalizing frequency is the Strouhal number. In the present study the Strouhal number is based on the constricted velocity U_c and the geometric thickness δ of the wake. The data collapse is quite good at low Strouhal numbers but is less complete at high Strouhal numbers. At this stage of the study it was concluded that the dipole model of obstruction-generated sound as formulated in equation (5) was less powerful than had been hoped. The next step in the analysis was to search for a means of improving the data correlation.

A QUADRUPOLE MODEL OF OBSTRUCTION-GENERATED SOUND

The data collapse shown in figure 10 is incomplete. These same data take the form shown in figure 11 when the normalizing formula is modified to

$$W = k'(s)\,\frac{\Delta p^3 D^2}{\rho^2 c^3}\left[1 + \left(\frac{f}{f_o}\right)^2\right] \tag{6}$$

where f is the center frequency of the band, $k'(s)$ is the spectrum-shape constant, and f_o is a constant having the dimensions of frequency. The constant f_o takes a value approximately equal to the acoustic cutoff frequency (for plane-wave propagation) of the jet pipe. The degree of data collapse is quite excellent, and equation (6) has been equally successfully applied to spectrum data for several different flow obstructions. In each case the range of data scatter lay within ±2 decibels.

The first term of equation (6) is similar to equation (5) and as such is derivable from the dipole model described previously. The second term, however, has an additional frequency-squared term. For aerodynamic noise mechanisms, frequency is proportional to velocity, and thus the second term has the velocity dependence of a quadrupole source. At first sight, therefore, both dipole and quadrupole source mechanisms are involved, the dipole dominating at frequencies below the cutoff frequency f_o and the quadrupole at frequencies above cutoff. Both mechanisms appear under the same spectrum-shape constant $k'(s)$, thus implying a strong interrelation between the two.

An acceptable physical model of the sound generating process can be developed as follows. Throughout the preceding discussion the assumption is made that the aerodynamic

source phenomena within the confines of the pipe can be described in terms of their free-field radiation formulas. This assumption is justifiable primarily on the basis that much of the measurement data show a sixth-power-of-velocity dependence for a physical setup that, one might intuitively feel, should be dominated by aerodynamic dipole sources.

Theoretical arguments presented in reference 6 indicate that enclosure of aerodynamic sources within a pipe will quite drastically change their radiation characteristics. This argument is discussed briefly with reference to figure 9. The dipole force field existing on the obstruction is accompanied, for a hard-walled pipe, by an array of wall images. From the viewpoint of an observer situated farther down the pipe, these images serve to reinforce the sound field to which he is exposed – particularly those images that are phase-correlated with the primary source. It can be shown that the effect of this reinforcement is to introduce a frequency-squared term into the denominator of the free-field source equation. It can also be argued that this frequency-squared term disappears for frequencies above the plane-wave cutoff frequency of the pipe.

The argument may be summarized as follows: Below the cutoff frequency for the pipe the dipole field can be expected to display the velocity dependence appropriate to a monopole source. Similar reasoning applies to a pipe-enclosed quadrupole field; below cutoff the quadrupole field will radiate with the velocity dependence of a dipole source. Above the acoustic cutoff frequency, when the presence of the pipe ceases to influence the radiation impedance seen by the aerodynamic source, the quadrupole and the dipole sources will revert to their normal free-field behavior.

Such a conclusion is presented for an aerodynamic-source field located in an infinitely long pipe. A complication arises when the pipe is truncated and the energy that passes through the exit plane of the pipe into the free field beyond is considered. Acoustic theory indicates that below the plane-wave cutoff frequency for the pipe the transmissibility of the exit plane varies directly with the second power of frequency, thus canceling completely the modification to the sound source imposed by the pipe enclosure. In most practical situations in the experiment and in the real engine, however, the exhaust-flow velocities across the exit plane are quite high. It can be argued that under these conditions the acoustic transmissibility (and reflection) influences of the exit plane will disappear.

The arrangement shown in figure 12 is now considered. The dominant sources are assumed to be associated with the intense turbulence in the wake of the obstruction. These sources are therefore quadrupole in character, and at frequencies above the cutoff of the pipe will radiate according to the expression

$$W \propto \frac{\rho U^8 D^2}{c^5} \tag{7}$$

Equation (7) may be written in terms of the pressure drop across the obstruction

$$W \propto \frac{\Delta p^4 D^2}{\rho^3 c^5} \tag{8}$$

Below the cutoff frequency equation (8) is modified to the form

$$W \propto \frac{\Delta p^4 D^2}{\rho^3 c^5}\left(\frac{f_o}{f}\right)^2 \tag{9}$$

The generalized expression for radiated power may thus be derived as

$$W \propto \frac{\Delta p^3 D^2}{\rho^2 c^3}\left[1 + \left(\frac{f}{f_o}\right)^2\right] \tag{10}$$

Equation (10) is precisely the expression used for data correlation.

CONCLUDING REMARKS

The principal result of the present study is perhaps the development of a prediction formula for obstruction-generated sound. This prediction formula seems to have relevance to a wide range of current problems such as the exhaust noise of turbofan engines and the noise of components in low-velocity ventilation systems. The results of this study also seem to be pertinent to the problem of noise generation in fluid piping systems.

Some confusion still exists as to the exact physical model by which the sound-generating mechanism can be described. The dipole model

(1) Is based on a conceptually acceptable physical model of the aerodynamic dipole

(2) Provides a good, but not outstanding, fit to the experimental data

(3) Suggests that the shed turbulence, rather than the impacting turbulence, is responsible for the radiating force field

The quadrupole model

(1) Is based on a mechanism somewhat at odds with what might be intuitively expected

(2) Provides an excellent fit to the experimental data

(3) Hinges on unproven theories relating to the influence of pipe enclosure upon aerodynamic sources

This work specifically relates to the exhaust noise of the turbofan vehicle in the following manner. It may be anticipated that the combined parameters of high exhaust turbulence and relatively low exhaust velocity will conspire with surface discontinuities in the

exhaust duct (including the exit lip) to generate noise at a level significantly higher than that associated with the free expanding jet. Unless these sources are accounted for in engine-noise prediction techniques, estimates of the exhaust noise levels of future vehicles may be significantly underestimated. Also, the application of current methods of jet noise suppression (multijet nozzles, and so forth) to these vehicles may increase the level of exhaust noise by intensifying the exhaust-duct sources.

REFERENCES

1. Mawardi, Osman K.; and Dyer, Ira: On Noise of Aerodynamic Origin. J. Acoust. Soc. Amer., vol. 25, no. 3, May 1953, pp. 389-395.

2. Lassiter, Leslie W.; and Hubbard, Harvey H.: Experimental Studies of Noise From Subsonic Jets in Still Air. NACA TN 2757, 1952.

3. Fitzpatrick, H. M.; and Lee, Robert: Measurements of Noise Radiated by Subsonic Air Jets. Rep. 835, David W. Taylor Model Basin, Navy Dept., Nov. 1952.

4. Ffowcs Williams, J. E.; and Gordon, C. G.: Noise of Highly Turbulent Jets at Low Exhaust Speeds. AIAA J., vol. 3, no. 4, Apr. 1965, pp. 791-793.

5. Yudin, E. Ya.: The Acoustic Power of the Noise Created by Airduct Elements. Soviet Phys. - Acoust., vol. 1, no. 4, July-Dec. 1955, pp. 383-398.

6. Davies, H. G.; and Ffowcs Williams, J. E.: Aerodynamic Sound Generation in a Pipe. J. Fluid Mech., vol. 32, pt. 4, June 1968, pp. 765-778.

LOCATION OF AERODYNAMIC NOISE SOURCES
ASSOCIATED WITH TURBOFAN EXHAUST

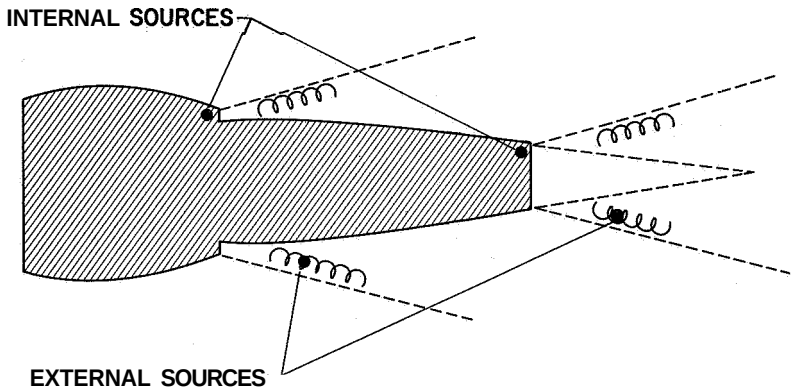

Figure 1

AERODYNAMIC NOISE SOURCES IN
TURBULENT JET FLOW

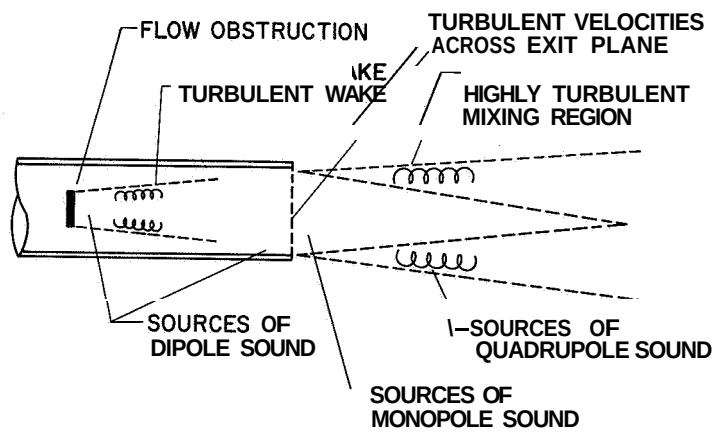

Figure 2

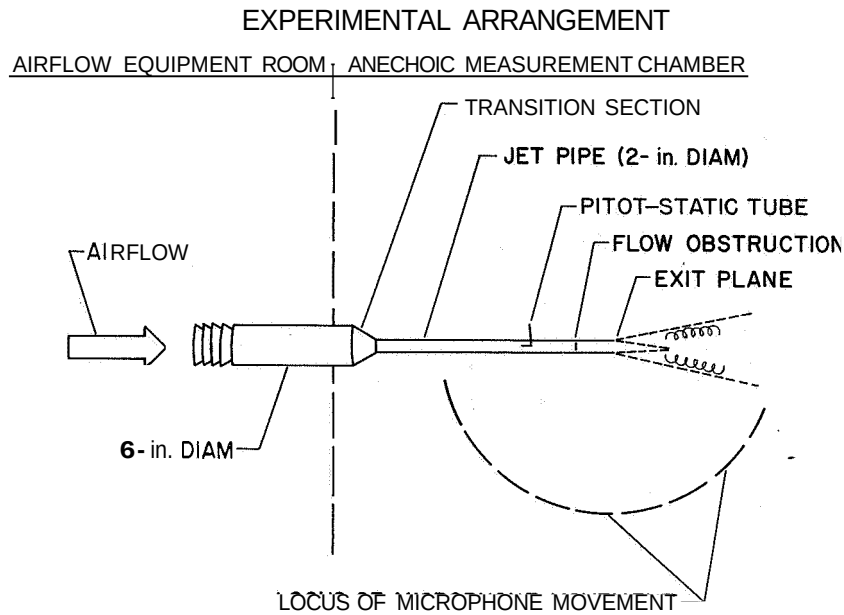

Figure 3

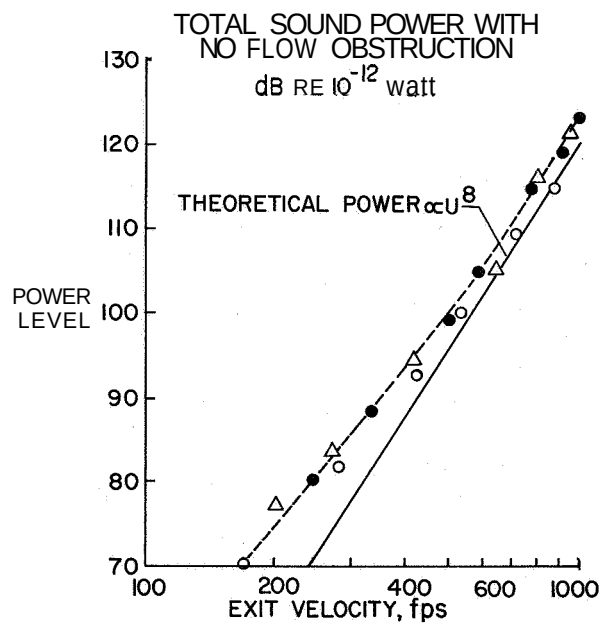

Figure 4

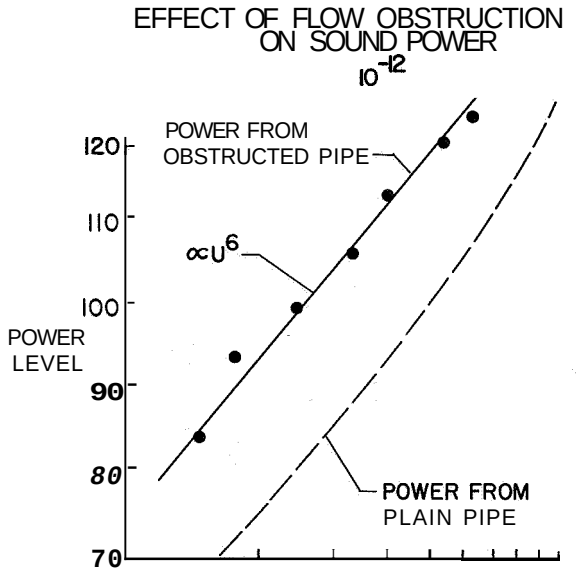

Figure 5

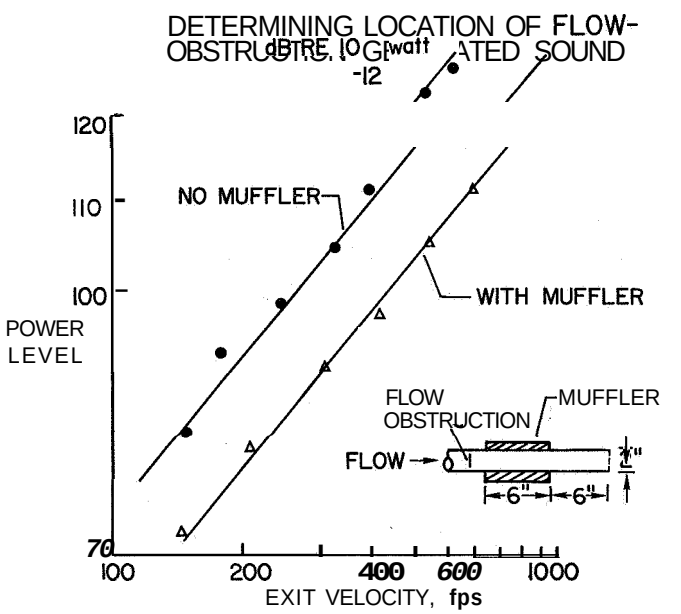

Figure 6

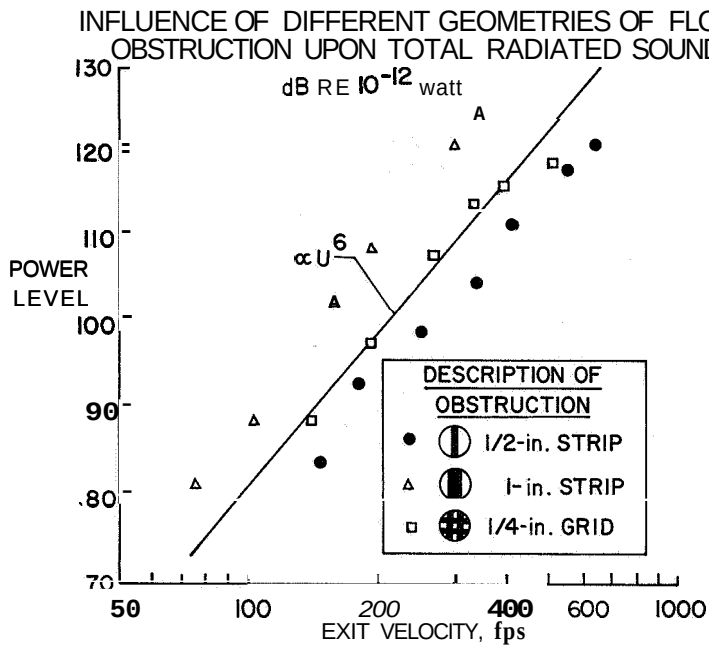

Figure 7

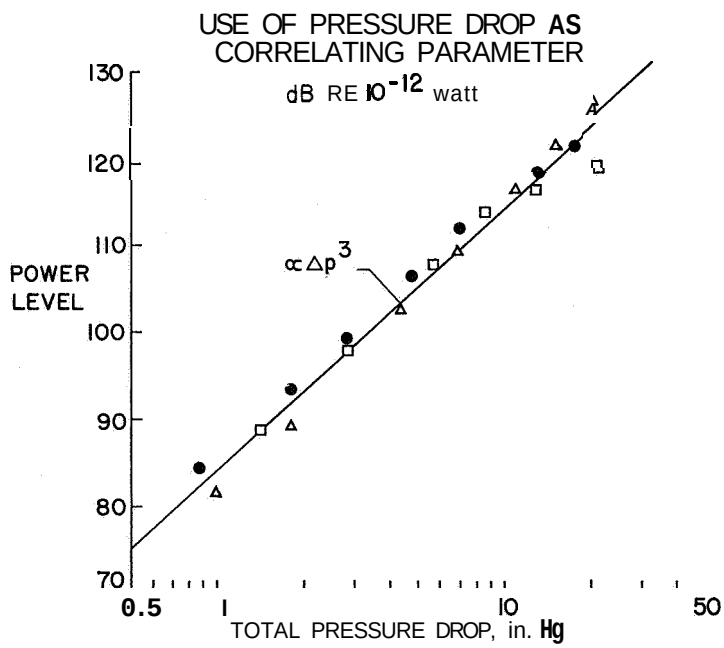

Figure 8

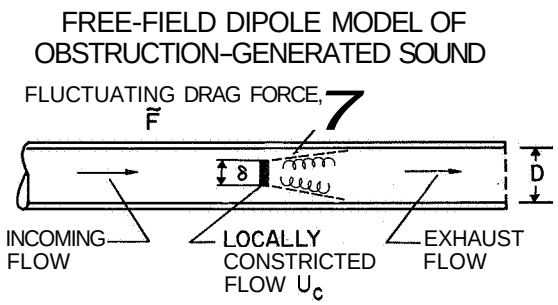

Figure 9

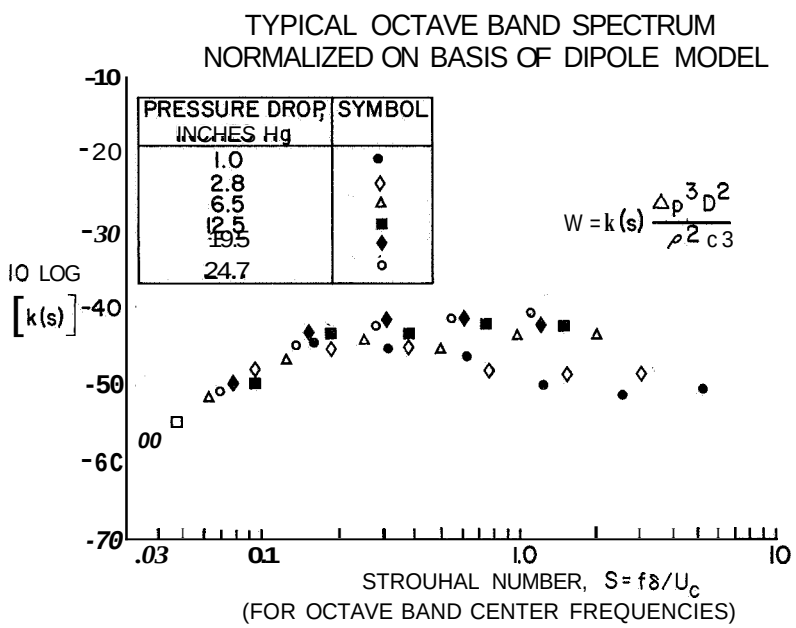

Figure 10

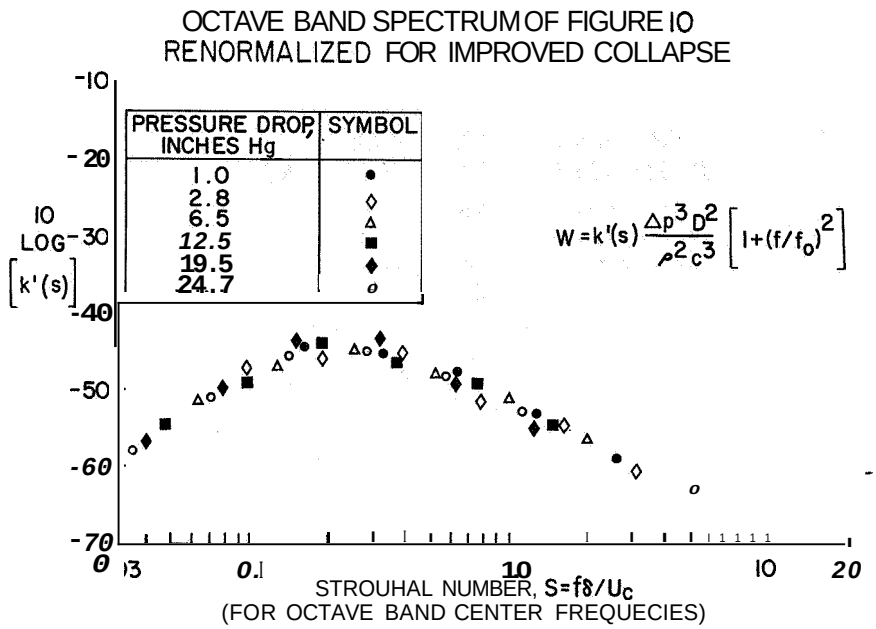

Figure 11

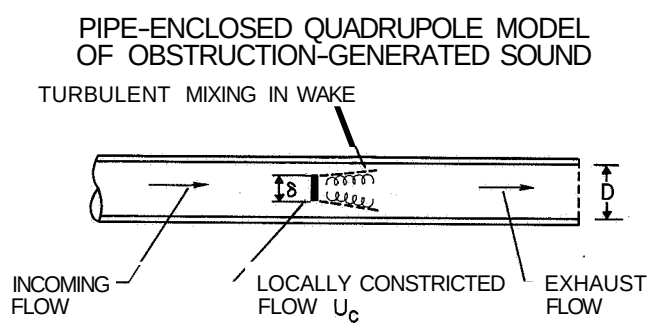

Figure 12

23. OPTICAL CROSSED-BEAM INVESTIGATION OF LOCAL SOUND GENERATION IN JETS

By Fritz R. Krause

NASA George C. Marshall Space Flight Center

and

Lennox N. Wilson

IIT Research Institute

23

SUMMARY

Optical cross-correlation techniques are being developed to provide many of the experimental inputs which semiempirical models need for prediction of noise generation at the source.

The location of sound source intensities in jet shear layers requires area integrals of correlated density fluctuations. Two narrow light beams are set to detect sound sources in the flow by triangulation. A digital cross correlation of the optical signals from the two beams is then used to approximate the desired area integration of correlated disturbances. This optical integration over correlation areas is confirmed experimentally by verifying the radial resolution and spectra that are expected for point-area-product mean values. The determination of noise sources in jet shear layers will be started as soon as a new infrared crossed-beam system, which should give density-related local beam modulations, is finished.

The measurement of streamwise velocity variations in supersonic jets is required to apply present models of noise generation in turbulence—shock-wave interaction zones. Mean velocity profiles have already been measured in supersonic flows by using a statistical cross-correlation between streamwise separated and delayed beams. The measurement of root-mean-square velocity fluctuations will be started as soon as the appropriate sample reduction and digital filtering techniques are completed.

INTRODUCTION

The prediction of jet noise intensities and spectra requires, in many instances, that the source of the noise be found. Present theoretical studies indicate that the shear layer and the turbulence in the jet are significant generators of noise. The problem is thus to formulate present mathematical noise prediction models in terms of experimentally

accessible shear layer and turbulence parameters and to develop probes which could measure these parameters in the jet. This problem was recognized early while trying to predict and to suppress the extreme jet noise levels that are produced during the firing of large rocket motors. One possible set of experimentally accessible shear layer and turbulence parameters is provided by the point area correlation of density fluctuations and by the statistical distribution of streamwise velocity variations. Both of these parameters can conceivably be measured in remote or inaccessible flow regions through the digital correlation of the photometer outputs from two narrow light beams. The progress in developing this crossed-beam concept and the experimental technique is now reported.

This paper includes many unpublished analytical and experimental results. The details of the mathematical derivations will be covered in a future **NASA** publication. The experiments with ultraviolet beams in supersonic jets were performed by M. J. Fisher and R. J. Damkevala. (See ref. 1.)

SYMBOLS **AND NOTATIONS**

a	speed of sound
b	shear-layer width
D	nozzle exit diameter
f	frequency
G	normalized two-beam-product mean value, defined by equation (12)
G_ρ	point-area-product mean value, defined by equation (5)
I	detected radiative power (watts)
i	beam modulation, $I - \langle I \rangle$
K'	fluctuation of extinction coefficient, $K - \langle K \rangle$
M	Mach number
P	probability distribution
P	pressure

S	turbulence spectrum
T	integration (averaging) time
t	time
$\vec{U}$	velocity components in earth-fixed frame, (U,V,W)
U_c	group velocity (convection speed of turbulence)
x	longitudinal coordinate along jet axis
Y	lateral coordinate in microphone plane
z	lateral coordinate normal to microphone plane
ξ	minimum beam separation distance (space lag)
η	length coordinate along beam B
ζ	length coordinate along beam A
$\vec{\xi}$	point vector in beam-oriented frame, (ξ,η,ζ)
P	density
X	optical wavelength
AX	optical band pass
τ	time lag
< >	time average

Superscripts:

→	vector
'	fluctuation

*	drifting or vortex-fixed system
–	mean value of point property

Subscripts:

A	beam A
B	beam B
crit	critical
f	far field
max	maximum
o	nozzle exit

EXPERIMENTAL INPUTS FOR MATHEMATICAL NOISE PREDICTION MODELS

The noise generation of rocket engines is often so intense that individual sound waves become visible on shadowgraphs. Figure 1 illustrates such sound emanation from a cold model air jet. Three distinct sets of sound waves are clearly recognizable outside the jet and have been enhanced by white lines for illustration purposes. The origin of these sound waves may be found by tracing the wave normals back to the jet. The sound sources are apparently located at the nozzle lip, in the jet shear layer, and in the turbulence-shock interaction zone. It is therefore hoped that the mathematical jet noise prediction models which have been developed for shear layers and turbulence in aircraft engine jets may also be applied to supersonic rocket exhausts. Experimental input parameters which could be used in both subsonic and supersonic jets are sought. Such parameters would allow the noise investigations in rocket engines to be based on the large body of experience that has been accumulated for present aircraft engines. Using such parameters to design experiments on sound generation at the source would result in instrumentation and data reduction systems that could be applied to both aircraft and rocket engines, as well as to the supersonic transports.

The main results of the literature search for suitable experimental inputs are illustrated in figure 2. Sound generation in subsonic and supersonic shear layers is predicted as a consequence of vortices that are not alined in the flow direction. The main experimental input that could be used to study the sound generation by such vortices

is a point-area correlation of density fluctuations. In supersonic jets additional noise is predicted for streamwise velocity variations upstream of shocks. Such velocity variations produce a shock-wave oscillation which will, in turn, generate sound even if no vortices are present. The main experimental input that could be used to study sound generation by turbulence-shock interaction is thus the probability $P(U)$ of streamwise velocity fluctuations.

Sound Generation Studies in Jet Shear Layers

The theory of sound generation in subsonic jet shear layers was formulated by M. J. Lighthill in 1952 and 1954. (See refs. 2 and **3.)** His quadrupole sources are physically identical with the deformation of vortex rings (ref. 4). Any vortex which is not alined to the local flow direction will exert a force on the surrounding fluid particles and thereby slightly change the local pressure. This pressure change will, in turn, slightly change the local gas density in an almost isentropic fashion. Consider many different realizations of a vortex that is traversing the nozzle-fixed point $\vec{x}$ during the moment t of the realization. The deformation of this vortex could be recognized by the temporal variations of the density $\partial\rho/\partial t$ in a vortex cross section. The size of the deformed cross section will then depend on the area within which the density changes are correlated. The expected jet noise contribution per cross section of a moving vortex may thus be expressed by the following average E over all realizations:

$$F_{\text{supersonic}}(\vec{x}, \ldots) = \int_{\substack{\text{Vortex-fixed} \\ \text{frame}}} E\left[\frac{\partial}{\partial t}\rho\left(\vec{\xi}^{*} = 0, t\right) \frac{\partial}{\partial t}\left(\vec{\xi}^{*}, t\right)\right] d\eta^{*}\, d\zeta^{*} \tag{1}$$

The integrand represents a correlation between the traveling vortex center $\vec{\xi}^{*} = 0$ and the vortex cross section $\xi^{*} = \text{Constant}$. It can be related to a similar correlation in a nozzle-fixed frame through the following translation of the separation coordinates:

$$\left.\begin{aligned} \xi &= \xi^{*} + U_c \tau_1 \\ \eta &= \eta^{*} \\ \zeta &= \zeta^{*} \end{aligned}\right\} \tag{2}$$

Lighthill (ref. 2) further assumes that the density time derivative in the nozzle-fixed spot $\vec{x} + \vec{\xi}$ may be represented by a statistically stationary time series. In this event, the ensemble average over realizations E may be replaced with a time average $\langle\rangle$ and the correlation of the time derivative may be replaced .with the time-lag derivative of the temporal fluctuations:

$$p' = p - \langle p \rangle \tag{3}$$

As a result of the translation and time-averaging procedures, the noise contributions from a deforming-vortex cross section might be expressed by an experimentally accessible point-area correlation of density variations:

$$F(\vec{x},\xi) = \lim_{\tau_1 \to 0} \frac{\partial^2}{\partial \tau_1^2} \int_{\substack{\text{Moving-vortex} \\ \text{cross section}}} \langle \rho'(0;t)\, \rho'(\vec{\xi}^*; t+\tau_1) \rangle \, d\eta^* \, d\zeta^*$$

$$= \lim_{\tau_1 \to 0} \frac{\partial^2}{\partial \tau_1} \int_{\substack{\text{Nozzle-fixed} \\ \text{frame}}} \langle \rho'(x;y;z;t)\, \rho'(x+\xi+U_c\tau_1;\ y+\eta;\ z+\zeta;\ t+\tau_1) \rangle \, d\eta \, d\zeta \tag{4}$$

The integrand represents one special case of the following point-area-product mean value:

$$G_\rho(\vec{x},\xi,\tau) = \int_{\substack{\text{Nozzle-fixed flow} \\ \text{cross section}}} \langle \rho'(\vec{x};t)\, \rho'(\vec{x}+\vec{\xi};\ t+\tau) \rangle \, d\eta \, d\zeta \tag{5}$$

The desired relation between such correlation measurements in the flow and the associated mean-square pressure fluctuations in the far field follows by substituting equations (1), (4), and (5) into the mathematical model of quadrupole sound. The result is a fourth-order integral that accounts for all jet locations $\vec{x}$ and all cross sections ξ.

$$\langle p'^2(x_f) \rangle_{\text{Subsonic shear layer}}$$

$$= \frac{1}{16\pi^2} \int_{\text{Jet}} \frac{(x_f - x)^2 (y_f - y)^2}{\left[|\vec{x}_f - \vec{x}| - \frac{U_c(\vec{x}_f - \vec{x})}{a_o} \right]^6} \left[\frac{\partial}{\partial y} \left(\frac{a^2}{a_o^2} U \right) \right]^2 \times$$

$$\left(\int_{\substack{\text{Eddy} \\ \text{length}}} \frac{\partial^2}{\partial \tau_1^2} G_\rho(\vec{x};\ \xi(\tau_1 \to 0);\ \tau = \tau_1 \to 0)\, d\xi \right) dx\, dy\, dz \tag{6}$$

Vortices generate very intense and directional sound waves outside the jet as soon as their speed exceeds the speed of sound at the microphone $(U_c/a_o > 1)$. Such vortex speeds will occur both in hot subsonic jets and in cold or hot supersonic jets, and the

associated "Mach wave sound emission" may be of primary importance for rocket engines and the supersonic transport. Ffowcs Williams and Maidanik (ref. 5) predicted this type of sound radiation from a theoretical study of the singularity that arises in equation (6) along the particular direction

$$\theta = \cos^{-1}\frac{a_o}{\overline{U}_c} \tag{7}$$

His mathematical model can also be represented in terms of point-area correlation of density fluctuations (ref. 6), except that the area deformation must be applied to a nozzle-fixed flow cross section instead of a drifting cross section. To a nozzle-fixed observer, the cross section of a passing vortex will change because of the variation of the vortex shape. Sound is thus generated even if the vortex is not deformed at all. The sound waves which emanate from the traveling vortex are very similar to the Mach waves which a bullet traveling along the same streamline would generate.

The desired relation between density correlation measurements in heated subsonic or any supersonic shear layer and the associated mean-square pressure fluctuations at the microphone follows by substituting equations **(4)** and **(5)** into the mathematical model of Mach wave sound emission. This substitution gives

$$\langle p'^2(\vec{x}_f)\rangle_{\text{Supersonic or heated shear layer}} = \frac{1}{16\pi^2}\int_{\text{Jet}} \frac{(x_f - x)^2 (y_f - y)^2}{|\vec{x}_f - \vec{x}|^6}\left(\frac{\partial \overline{U}}{\partial y}\right)^2 \left(\int_{\substack{\text{Nozzle-fixed}\\ \text{frame}}} \frac{\partial^2}{\partial \tau^2} G_\rho(x,\xi;0)\, d\xi\right) dx\, dy\, dz \tag{8}$$

The integrand of equation (8) closely resembles the integrand of equation (6). The main difference between the associated density correlation measurements in subsonic and supersonic shear layers is in the interpretation of the temporal correlation function. Equation (8) requires the curvature $\partial^2 G/\partial \tau^2$ of the temporal correlation between a point and an area at a fixed separation ξ. Equation (6) requires the curvature $\partial^2 G/\partial \tau_1^2$ of the envelope to all time correlation curves $G(\tau)_\xi$ that have been obtained for different point-area separations.

Sound Generation Studies in Turbulence-Shock Interaction Zones

Streamwise velocity fluctuations upstream of a shock create a nonuniform pressure jump across the shock. The shock starts oscillations which, in turn, propagate pressure waves into the downstream flow. In 1967, H. S. Ribner (ref. 7) established a mathematical

relation between axial acoustical flux I_{ac} downstream of the shock ($x \to \infty$) and the mean-square velocity variation $\langle U'^2 \rangle$ upstream of the shock ($x \to -0$).

$$I_{ac}(x \to \infty) = \frac{3}{2} \frac{\overline{p}^2}{\rho a} \left(\vec{x} \to \infty, \ldots\right) \frac{\langle U'^2(x \to -0) \rangle}{a^{*2}} \chi$$

$$\int_{\theta=\theta_{crit}(M;\gamma)}^{\theta=\pi/2} |P(\theta)|^2 \cos^3 \theta \left[1 + M \sin \theta_2 (\theta;M;\gamma)\right] \left(1 + \sin \theta_2\right) d\theta \qquad (9)$$

In this relation, M is the Mach number upstream of the shock, γ denotes the ratio of specific heats, and a* is the critical speed of sound. The functions a* and θ_{crit} can be obtained from isentropic flow and oblique-shock tables. The functions θ_2 and $P(\theta)$ were tabulated by Ribner in 1955. (See ref. 8.)

The flux of acoustic energy is steady across the jet boundaries. Just outside the jet, the acoustic flux should be the same as that calculated inside the jet. This invariance allows the estimation of the mean-square pressure fluctuation, just outside the jet, which turbulence-shock interaction will generate far downstream of the shock:

$$\langle p'^2(\vec{x}_f) \rangle_{\substack{\text{Shock-turbulence} \\ \text{interaction}}} = \rho_o a_o I_{ac} \qquad (10)$$

In equation (10), the acoustic flux may be calculated numerically for any given Mach number from equation (9). In fact, a similar integral applicable to oblique shocks can be obtained. Thus, there is a direct relationship between the mean-square pressure fluctuation at the downstream microphone and the longitudinal root-mean-square velocity. This model is still idealized since the finite extent of the potential core and the interaction between the shear layer and the shock root are not yet included. However, Ribner's formulation could be extended to these more realistic flow fields. Within this model, or any of its future extensions, the measurement of the streamwise velocity variations upstream of shocks seems to be the most important input that would be required in future investigations of jet noise at the source.

CROSSED-BEAM MEASUREMENT OF POINT-AREA CORRELATIONS

Two narrow light beams are set to select by triangulation a point in the jet, as shown in figure 3. Each of these beams is then collected by photodetectors A and B. Consider now the passage of vortices, which are slightly more opaque or transparent than the surrounding gas. The passage of such a vortex will slightly change the received

radiative power. The fluctuations of the photodetector output signals therefore contain information on the vortices that traverse the beams. These fluctuations i_A and i_B are recorded by using ac-coupled amplifiers. Each recorded signal will account for any vortex that is traversing the line of sight, whereas information is sought on only those vortices that pass the beam intersection. These "common" signal components can now be retrieved by a digital cross-correlation computation. During such a calculation, all radiative power modulations which occur only in one beam without affecting the other beam are canceled.

The cancellation of "noise" components depends on the number of oscillations in the record and will be very complete, if the digital cross-correlation computations are applied to a very long record. Noise components may thus be suppressed to the level of the temporal variations of the boundary conditions by integrating over a long record. All the crossed-beam data have been reduced with a special digital computer program which provides for a time integration of any desired length, by accumulating the time integral in a recursion formula. In this recursion, only one short data piece at a time is used on the computer memory. The associated "piecewise" correlation computations have successfully retrieved common signal components, which have been an order of magnitude smaller than the root-mean-square values of the recorded signals i_A and i_B.

Practical limitations, such as dynamic interchannel time displacement errors of the data acquisition system and temporal trends in the experimental boundary conditions, provide a lower limit for the smallest signal that can be retrieved, The continued development of piecewise correlation techniques fortunately shows promise for the partial elimination of the variations of boundary conditions in uncontrolled environments. (See ref. 9.) Environmental variations have been partially eliminated through piecewise modification of the signal time histories. (See ref. 10.)

Optical Approximation of Point-Area Correlations

The common signals which remain after the digital cross-correlation computations are produced only by those vortices which passed the beam intersection. All beam modulations by other vortices and by light source and detector noise should cancel each other. (See ref. 11.) The physical interpretation of the common signals thus needs to consider only those vortices which passed through the beam intersection point. Analytical studies of the optical integration along those beam elements which intersect the "common" vortices now indicate that this optical integration may be arranged to provide the desired point-area correlation. (See ref. 6.) The main results of these and more recent analytical studies are summarized in figure 4 and in the following equation:

$$\frac{\langle i_A(t)\, i_B(t)\rangle}{\langle I_A\rangle \langle I_B\rangle} - \int_{\substack{\text{Eddy cross}\\ \text{section}}} \langle K'(x;y;z;t)\, K'(x;\, y+\eta;\, z+\zeta;\, t)\rangle \, d\eta \, d\zeta \qquad (11)$$

The left-hand side of equation **(11)** is an experimentally accessible quantity and is denoted by the term "two-beam-product mean value." The numerator is calculated by adding the instantaneous product of the ac-coupled photometer outputs i_A and i_B. The denominator is given by the mean value of the dc-coupled photometer records I_A and I_B. The time average $\langle\ \rangle$ has been obtained by integrating over a record length T which was sufficient to reduce all remaining variations of the two-beam-product mean value below a desired error margin $\left(\text{rms noise}/I \leqq 10^{-4}\right)$.

The right-hand side is identical with the desired point-area integration. The point is selected by the beam intersection. The area is generated by moving one beam parallel to the other. The integral may thus be described as a "point-area-product mean value." The correlation refers, however, to the local changes of radiative power, which are caused by the changes of opacity or transparency between passing vortices and the surrounding gas. The scalar K' is thus given by the local variation of light extinction or light emission coefficients. Two-beam-product mean values (eq. **(11))** would therefore give the desired point-area integration of density variations (eq. (5)) only if the local variations in radiative power K' can be related to density variations ρ'.

The optical approximation of point-area approximation can be extended to points and areas which are separated along a streamline. Let the beams A and B intersect the common streamline at the positions x and $x + \xi$. The optical point-area correlation would then be given by

$$G(T;x;y;z;\xi;\ldots) = \frac{\langle i_A(t)\, i_B(t)\rangle}{\langle I_A\rangle \langle I_B\rangle}$$

$$= \int_{\substack{\text{Vortex cross}\\ \text{section}}} \langle K'(x;y;z;t)\, K'(x+\xi;\, y+\eta;\, z+\zeta;\, t)\rangle \, d\eta \, d\zeta \qquad (12)$$

The claim of point-area correlation (eq. (12)) cannot be verified with point probes, since such a test would require a large number of phase-matched probes which possess a linear and time-invariant frequency response and which do not interfere with the flow. However, the point-area correlation does lead to two important conclusions on spatial resolution and spectral characteristics, which can be verified rather easily. The first conclusion is obtained by considering the isolation of individual streamlines through the location of the outside point. Thus individual streamlines which are separated by no more

than a beam diameter could be distinguished. In flows with a dominant direction, the spatial resolution of streamlines should thus be possible inside a typical vortex. The spatial resolution of flow traverses should therefore approach the resolution of point probes.

The second conclusion is reached by considering cross-flow components. Any directional fluctuation will displace a vortex only inside the beam front. The area integral across the vortex is not changed by such a displacement, and the associated two-beam product mean value will therefore not depend on cross-flow components. This discrimination against cross-flow components is the essential difference between one- and three-directional wave number spectra. Crossed-beam spectra should approximate three-dimensional spectrum function and not the one-dimensional spectrum that is given by point probes.

Experimental Verifications

The first crossed-beam tests were designed to check the optical approximation of point-area correlations by verifying these conclusions. All tests were conducted in the initial portion of two supersonic jet shear layers, which were generated by expanding highly dried and unheated air through two nozzles. These nozzles produce shock-free jets of the same thrust at Mach numbers of 2.42 (D = 4.57 cm) and 3.34 (D = 5.47 cm).

The shadowgraph of figure 1 illustrated the jet from the M = 3.34 nozzle at off-design conditions. Typical sound pressure levels exceed 150 dB in the area where most of the crossed-beam instrumentation was located. All measurements were thus performed under extremely adverse noise and vibration environments.

Most crossed-beam measurements used focused ultraviolet beams generated by projecting the image of a hydrogen discharge (ref. 12) on the desired points of minimum beam separation. The beams were mounted on a lathe bed in such a manner that the points of minimum beam separation would always be parallel to the jet axis, that is, to the dominant direction of the streamlines. This point pair could traverse the jet axially and radially, and the separation could be varied in an axial direction. The light was extinguished in the flow by using the ultraviolet absorption of oxygen at an optical wavelength of 1850 Å inside a spectroscopic bandpass of 50 Å. Additional light extinction occurred by scattering from natural tracers, generated by condensation of entrained wet ambient air, and from air liquefaction at high chamber pressures. Crossed-beam tests with collimated helium-neon laser beams of approximately 2 mm in diameter were performed more recently to obtain additional information on scattering without simultaneous absorption.

The modulations of the ultraviolet beam were recorded with two photomultiplier tubes, EMR Model N 541A-05-14. The output signals from the two phototubes were

amplified by specially built amplifiers and stored on an FM tape recorder, CEC, Model VR-3600, at a speed of 120 ips. Special multiplex equipment was integrated into the FM tape recorder so that any dynamic interchannel time displacement errors could be avoided by using two center frequencies (450000 cps and 825000 cps) on the same tape track. This multiplexing technique led to a flat frequency response from 500 cps to 500000 cps and relative phase distortions of less than 3^{o}. The analog tapes were then converted to digital tapes by running them through the analog-digital conversion systems of the Marshall computation laboratory at the reduced speed of 15 ips. Because of this stretching of the time scale, the effective sampling rate'was 160000 samples per second. The digital tapes were then processed on an IBM 7094 computer by using the piecewise correlation program.

The cancellation of cross-flow components by optical area integration may be judged from the spectral measurements summarized in figure 5. The ordinate displays crossed-beam spectra which have been calculated by including a time delay in the cross-correlation calculations:

$$S(f) = \frac{1}{2\pi} \int_{\tau=-0.003\ \text{sec}}^{\tau=0.003\ \text{sec}} \frac{\langle i_A(t)\, i_B(t+\tau) \rangle}{\langle i_A^2 \rangle^{1/2} \langle i_B^2 \rangle^{1/2}} \cos(2\pi f \tau)\, d\tau \qquad (13)$$

These spectral estimates were then normalized with the maximum value; thus, the peak of the spectrum is always equal to one. The abscissa gives a normalized frequency which was based on the shear-layer width b and the turbulent convection speed U_c (given subsequently in fig. 8). This normalization has been successful in collapsing hot-wire spectra in subsonic jet shear layers on a universal curve.

The points in figure 5 represent crossed-beam spectra for six different locations in both the subsonic and the supersonic portions of the two jet shear layers. These points do approach a "universal" spectrum shape for the high frequencies. Thus, the local beam modulations in the supersonic flow seem to have the same length and velocity scales as the modulations in the subsonic flow.

The two solid lines in figure 5 represent the one-dimensional and three-dimensional spectra which the Heisenberg-Kolmogoroff theory would predict for locally isotropic turbulence. The position of these lines is immaterial; only the slope of the lines is important. One-dimensional spectra, which include cross-flow components, should follow a -5/3 power law and are thus indicated by a -5/3 slope. Three-dimensional spectra, which do not include cross-flow components, should follow a -11/3 power law. The measured spectra obviously approximate this -11/3 slope. This approximation of a

three-dimensional spectrum function gives confidence in the optical approximation of point-area-product mean values.

The location of local sound sources may be judged from the crossed-beam intensity measurements summarized in figure 6. Intersecting light beams measured point-area correlations, and a pitot probe measured velocities at several traverses in the two jets. The results in figure 6 refer to one traverse of the M = 3.34 jet. The inner and outer edges of the shear layer are indicated by the velocity profile and are located at y/D = 0.4 and 0.8. The shear-layer thickness b is thus (0.8 - 0.4)5.47 × 2.2 cm. A typical vortex cross section would extend over approximately 1/3 of this width.

Inspection of the two-beam-product mean values indicates that both the ultraviolet and the laser systems clearly resolve common beam modulations of less than 0.1 percent of the mean radiative power in the beam. These common modulations show a clear structure. The ultraviolet system produces, in the outer edge of the shear layer, a peak correlation which is probably associated with the condensation of the wet ambient air that was entrained by the jet. The laser system produces a peak correlation at the inner edge of the shear layer, which could probably be associated with the condensation of the natural CO_2 content of air.

The radial resolution of the two-beam-product mean values may be judged by comparing the width of the intensity peaks with the anticipated vortex diameter, ≈b/3. Both peaks have clearly been resolved inside a vortex. The beam diameter was approximately 2 mm; some of the experimental points show a clear and consistent variation of two-beam-product mean value along a 2-mm interval. The claim that the spatial resolution should approach the beam diameter seems therefore to be verified for this initial part of a supersonic shear layer.

There is thus every reason to believe that crossed beams do integrate over correlation areas as predicted by the analytical formulation in the section "Optical Approximation of Point-Area Correlations."

The successful approximation of point-area correlations would allow us to locate sound sources in jet shear layers if the local beam modulations are proportional to density variations. The laser beams show a peak intensity at the supersonic edge of the shear layer, and the ultraviolet beams show a peak intensity at the subsonic edge of the shear layer. However, the theory of Mach wave emission would predict the maximum sound source intensities in the center of the shear layer. It is therefore unlikely that the two systems have located sound sources; that is, the local beam modulations are not density related. Density-related beam modulations might be achieved by suppressing light scattering.

The local emission and absorption processes, which remain after scattering has been reduced, are uniquely determined by concentration, temperature, and density fluctuations. (See ref. **13.)** Furthermore, most jet noise theories assume that all thermodynamic variations in supersonic shear layers occur isentropically and do not change the composition of the gas. Small disturbances of densities and temperatures are then proportional to each other, and a relation to density is justified. However, chemical reactions in actual rocket exhausts will change the gas composition in an irreversible manner. Fortunately, the radiative power contributions due to temperature variations may then be suppressed by special settings of the wavelength **A** and the spectroscopic bandpass **AA.** (See ref. **14.)** It is therefore believed that local infrared beam modulations which are directly porportional to density fluctuations might be found in many jet noise investigations of practical interest.

Scattering will be reduced in future noise investigations by using infrared beams in heated flows. Heating should reduce the production of natural tracers by wet air entrainment or air liquefaction in the jet. The few remaining natural tracer particles should scatter the infrared light much less than the visible and ultraviolet beams now in use. Contamination by solid tracer particles might, however, present problems in some applications,

To study such problems, a special optical calibration cell which can be resonated like an organ pipe is being built. Wall pressure measurements in the cell should then provide a direct estimate of the local density fluctuations. The relation between beam modulation and density variation could thus be studied for various settings of the spectroscopic band pass and various gas samples.

VELOCITY MEASUREMENTS WITH STREAMWISE SEPARATED BEAMS

Streamwise separated beams may still contain a considerable amount of common signals, even if the separation exceeds several vortex diameters. Such commonality is a consequence of the flow, which transports the same emitting, absorbing, or scattering centers from the upstream to the downstream beam. A finite correlation might be expected if the signal of the downstream beam is delayed by the approximate transit time between the beams before the product mean value is calculated. Conversely, variable time delays might be introduced into the data reduction to analyze the motion along the streamline which has been selected by the beam triangulation. Without such time delays, widely separated beams could not contain common signals.

Conceptual Velocity Measurements

Consider the conceptual crossed-beam experiment illustrated in figure 7. Two mutually perpendicular beams have been separated along a streamline by the distance ξ. The ac-coupled signal from the downstream beam is delayed by the time interval τ, and the delayed and the undelayed signals $i_B(t - \tau)$ and $i_A(t)$ are then fed into a digital cross-correlation program. The output of this program will reach a maximum when the time delay is equal to the transit time which the average vortex needs to travel from the upstream to the downstream beam. The peak of the correlation curve may thus be used to identify the most probable velocity, as indicated in figure 7.

The digital correlation computations may be so arranged that the shape of the correlation curve indicates streamwise velocity components other than the most probable value. The analytical studies indicate that the following correlation of the signal time derivatives should approximate the probability P that the streamwise velocities U had the value ξ/τ:

$$P\left(U = \frac{\xi}{\tau}\right) = \frac{\tau}{\xi} \frac{< \frac{a}{at} i_A(t) \frac{a}{\partial t} i_B(t - \tau) >}{\int_{-\infty}^{\infty} \frac{< \frac{a}{at} i_A(t) \frac{a}{at} i_B(t - \tau) >}{\tau} d\tau} \tag{14}$$

Equation (14) is thus the key to the desired measurement of streamwise velocity variations. The root-mean-square value $<U'^2>^{1/2}$, which is required for sound generation studies in shock-turbulence interaction zones, could be read directly from the width of the correlation curves.

The approximation of the streamwise velocity distribution function P with crossed-beam measurements may be understood physically by identifying the time derivative of the common signal components with the slope of a passing vortex surface. A large oscillation is expected only if the head or the tail of a vortex traverses the beam. The correlation calculation of equation (14) then represents the correlation of traveling interfaces instead of the entire vortex. An interface will need only a very short time interval to travel its own length, and the correlation curve $P(\xi/\tau)$ should therefore resemble a very sharp peak if all interfaces would travel at the same transit time. Conversely, the spread of the correlation curve will give the distribution of interface transit time or speeds. The correlation of time derivatives is thus different from the usual correlation of the signal fluctuations, where the width of the curve is identified with the time a vortex needs to travel its own length and not with the spread of transit times.

Measurements of Convection Speed Profiles

Crossed-beam measurements of convection velocities have been made in several radial and axial positions in both of the supersonic jets using the ultraviolet and the laser systems. The main results are plotted in figure 8 in a nondimensional form with the width of the shear layer as a length scale and the nozzle exit speed as a velocity scale. Pitot tube traverses of subsonic and supersonic jets suggest that this particular normalization should give a "universal" velocity profile that is valid for both subsonic and supersonic jets. (See ref. 15.) A similar result is predicted by identifying the turbulent velocity field with the random walk of a single fluid particle. The velocity measurements with pitot probes did collapse on the universal curve shown. The dashed curve represents subsonic convection speed measurements with a pair of hot wires that were also separated along streamlines. (See ref. 16.)

Inspection of the crossed-beam results leads to the following observations:

(a) In the subsonic portion of supersonic shear layers, crossed-beam measurements agree with scaled group velocity profiles from subsonic hot-wire measurements. The same agreement with hot-wire group velocities was found in our previous investigations of subsonic shear layers. (See refs. 17 and 18.)

(b) In the supersonic portion of the jet shear layers, laser crossed-beam measurements tend to follow the mass average speed indicated by pitot tubes. Convection velocities from ultraviolet measurements also tend to be higher than those predicted from hot-wire measurements in subsonic flows. Unfortunately, the scatter of the velocity points is still too large for any detailed analysis. This lack of resolution is probably due to the electronic and computational problems associated with retrieving very small signals out of noise. It is believed that the experience from these first crossed-beam tests in supersonic shear layers will allow us to improve data acquisition and reduction so that the spatial resolution of velocity profiles will be considerably better in future tests.

(c) Both laser and ultraviolet beams give approximately the same velocity profile although each beam responds to different light extinction processes.

Apparently, velocity measurements are independent of the type of local extinction phenomena to which the beams respond. This independence of the local extinction process suggests that velocity and length scale measurements can be conducted whether or not the beams respond to density variations. Scaling studies between subsonic and supersonic jets, between cold and hot jets, and between model jets and the prototype engine exhaust are thus within the capability of existing crossed-beam technology.

The measurement of streamwise velocity fluctuations and length scales requires the correlation of time derivatives. In the digital program, a time derivative is replaced

with the moving central difference between three adjacent data samples. These differences are so small that the quantization errors are relatively large. Quantization errors can be reduced by sample reduction techniques whenever the sampling frequency exceeds the data frequency by one to two orders of magnitude. Adding many samples to obtain one data point reduces quantization errors since the average is more accurate than any of the original samples. Appropriate time-scale stretching, sample reduction, and digital filtering techniques for correlation of time derivatives are being developed. Preliminary checks of these techniques are encouraging, and it is believed that the measurement of streamwise root-mean-square velocity will be experimentally feasible.

CONCLUSIONS

Theoretical and experimental studies of crossed-beam test arrangements indicate that the statistical correlation of optical signals has the potential to provide many of the measurements which are required for jet noise investigations at the source. Remote, or inaccessible, source areas are studied optically without the probe interference problems that plague present hot-wire investigations.

The intensity and spectra of jet noise may be related mathematically to the point-area correlation of density fluctuations in jet shear layers and to streamwise velocity fluctuations in shock-turbulence interaction zones.

The optical integration along the beams has been used to obtain point-area correlations that are not accessible to any point probe.

Sound sources may be located by varying the position of the beam intersection point in the jet. The two-beam-product mean value should provide direct estimates of sound source intensities and spectra, if an optical wavelength region can be found that provides density-related light extinction or emission processes.

The distribution of streamwise velocity variations could conceivably be measured in subsonic and supersonic jets with streamwise separated and delayed beams.

The velocity and length scale measurements in subsonic and supersonic jets show that present crossed-beam technology could be used for scaling studies between cold and hot jets and between model engines and the prototype.

REFERENCES

1. Fisher, M. J.; and Damkevala, R. J.: Shock Wave Shear Layer Interaction in Clustered Rocket Exhausts. Contract No. NAS8-20408, IIT Res. Inst., Oct. 9, 1967.

2. Lighthill, M. J.: On Sound Generated Aerodynamically. I. General Theory. Proc. Roy. Soc. (London), ser. A, vol, 211, no. 1107, Mar. 20, 1952, pp. 564-587.

3. Lighthill, M. J.: On Sound Generated Aerodynamically. II. Turbulence as a Source of Sound. Proc. Roy. Soc. (London), ser. A, vol. 222, no. 1148, Feb. 23, 1954, pp. 1-32.

4. Powell, Alan: Vortex Sound. Rep. No. 61-70 (Contract No. Nonr-233(62)), Dep. Eng., Univ. California, Oct. 1961.

5. Ffowcs Williams, J. E.; and Maidanik, G.: The Mach Wave Field Radiated by Supersonic Turbulent Shear Flows. J. Fluid Mech., vol. 21, pt. 4, Apr. 1965, pp. 641-657.

6. Krause, F. R.; and Fisher, M. J.: Optical Integration Over Correlation Areas in Turbulent Flows. 5e Congrès International d'Acoustique, Vol. 1, Daniel E. Cummins, ed., Cong. Intern. Acoustique, 1965, pp. [K65] 1-4.

7. Ribner, H. S.: Shock-Turbulence Interaction and the Generation of Noise. NACA Rep. 1233, 1955. (Supersedes NACA TN 3255.)

8. Ribner, H. S.: Acoustic Energy Flux From Shock-Turbulence Interaction. UTIAS Tech. Note No. 108 (AFOSR 67-0221), Univ. of Toronto, July 1967.

9. Krause, Fritz R.; and Hablutzel, Benjamin C.: Noise Elimination by Piecewise Cross Correlation of Photometer Outputs. NASA paper presented to National Academy of Sciences Committee on Atmospheric Sciences, Panel on Remote Atmospheric Probing (Chicago), May 17, 1968.

10. Jayroe, R. R., Jr.; and Su, M. Y.: Optimum Averaging Times of Meteorological Data With Time-Dependent Means. Proc. Third National Conference on Aerospace Meteorology, Amer. Meteorol. Soc., 1968, pp. 208-217.

11. Krause, F. R.; and Fisher, M. J.: Remote Sensing of Local Flow Instabilities and Turbulence. Flow Measurement Symposium, K. C. Cotton, ed., Amer. Soc. Mech. Eng., c.1966, pp. 171-194.

12. Cann, M. W. P.: Light Sources for Remote Sensing Systems. NASA CR-854, 1967.

13. Krause, F. R.; Davies, W. O.; and Cann, M. W. P.: The Determination of Thermodynamic Properties With Optical Cross-Correlation Methods. Aero-Astrodynamics Research Review No. 6, William D. Murphree, ed., NASA TM X-53647, 1967, pp. 116-132.

14. Krause, F. R.; and Stephens, J. B.: Remote Detection of Local Temperatures and Local Partial Pressures With Crossed-Beam Spectroscopy. Specialist Conference on Molecular Radiation and Its Application to Diagnostic Techniques, R. Gaulard, ed., **NASA** TM **X-53711, 1967,** pp. **297-327.**

15. Nash, J. F.: *An* Analysis of Two-Dimensional Turbulent Base Flow, Including the Effect of the Approaching Boundary Layer. R. & M. **No. 3344,** Brit. A.R.C., **1963.**

16. Davies, P. **O. A.** L.; Fisher, M. J.; and Barratt, M. J.: The Characteristics of the Turbulence in the Mixing Region of a Round Jet. J. Fluid Mech., vol. **15,** pt. **3,** Mar. **1963,** pp. **337-367.**

17. Fisher, M. J.; and Krause, F. R.: The Crossed-Beam Correlation Technique. J. Fluid Mech., vol. **28,** pt. **4,** June **22, 1967,** pp. **705-717.**

18. Fisher, M. J.; and Damkevala, R. J.: Optical Measurements With High Temporal and Spatial Resolution. Contract No. **NAS8-11258,** IIT Res. Inst., Sept. **5, 1967.**

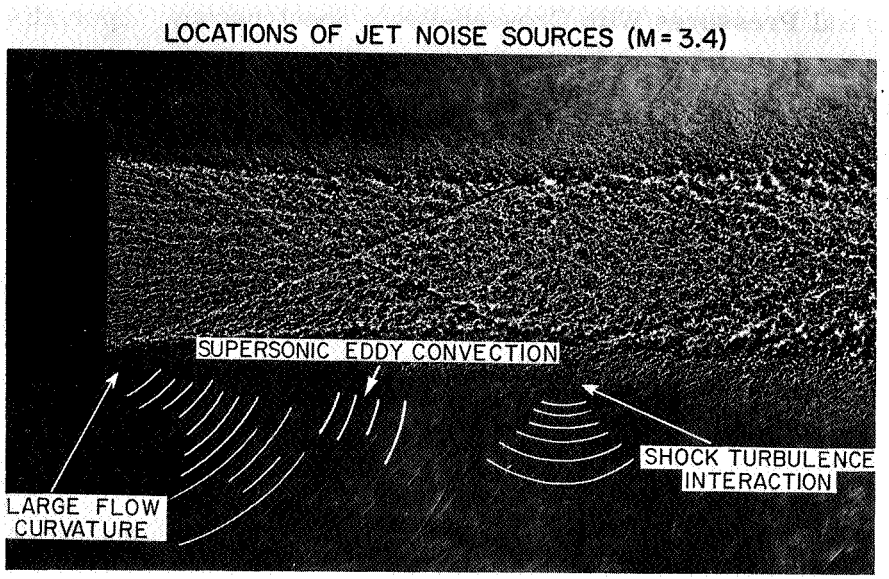

Figure 1 L-68-8578

EXPERIMENTAL INPUTS TO JET NOISE PREDICTION MODELS

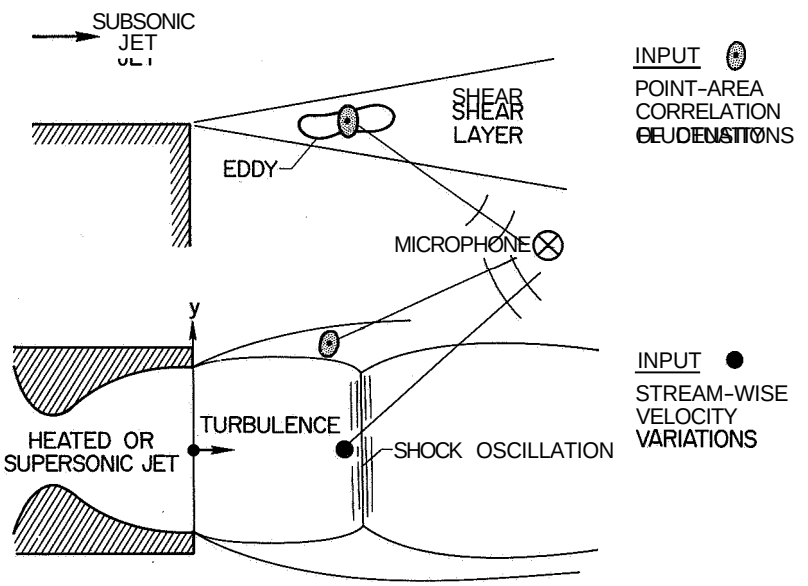

Figure 2

SOUND SOURCE IDENTIFICATION IN SUPERSONIC JETS

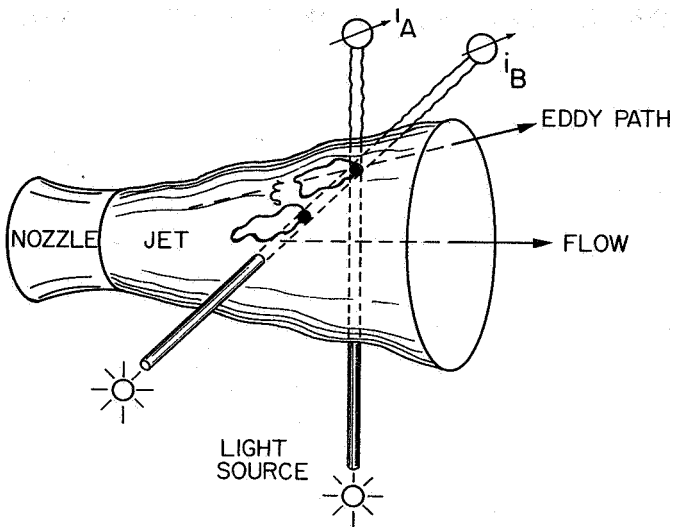

Figure 3

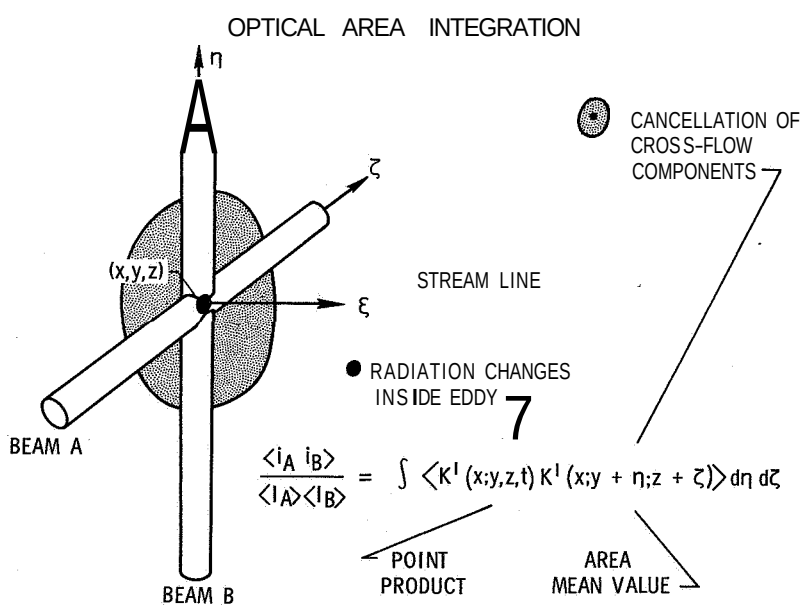

Figure 4

CROSS–BEAM SPECTRA IN JET–SHEAR LAYER

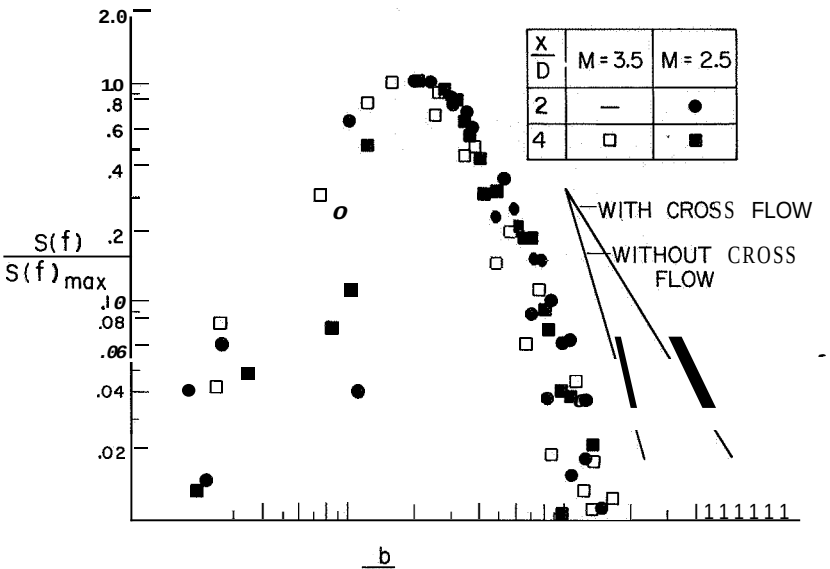

Figure 5

CROSS-BEAM RESOLUTIONS OF POINT-AREA CORRELATIONS

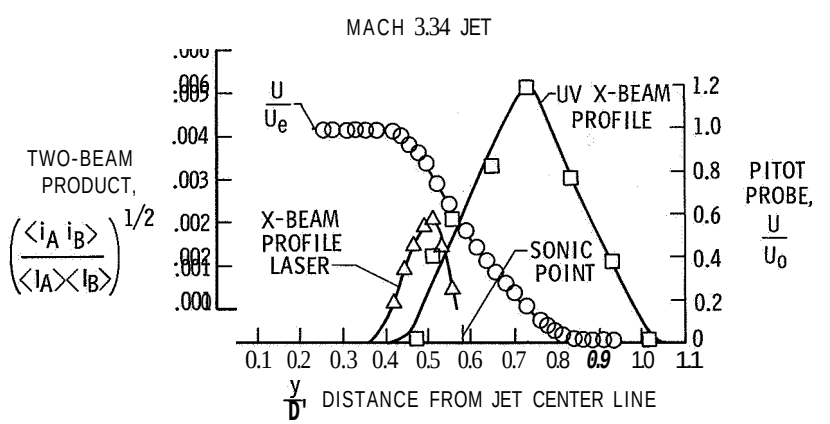

Figure 6

MEASUREMENT OF STREAMWISE VELOCITY VARIATIONS

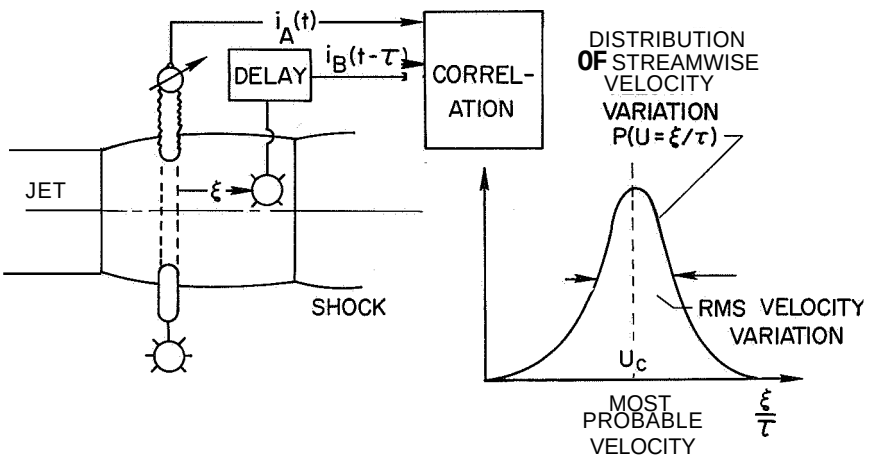

Figure 7

CONVECTION SPEED MEASUREMENTS
IN JET SHEAR LAYER

$\frac{x}{D}$	U_0 = 624 m/s	U_0 = 556 m/s	
2	o	●	U-V SYSTEM
4	□	□	U-V SYSTEM
4	+		LASER SYSTEM

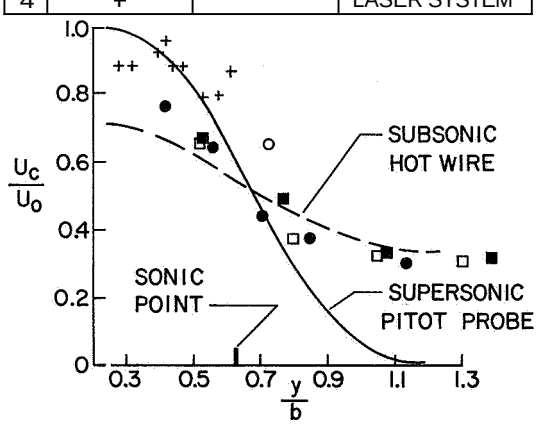

Figure 8

24. VARIABILITY IN AIRPLANE NOISE MEASUREMENTS

By David A. Hilton and Herbert R. Henderson

NASA Langley Research Center

SUMMARY

This paper presents some of the acoustic data obtained during two measurement projects involving a 727 turbofan airplane and an 880 turbojet airplane *along* with information relating to airplane position and meteorological conditions during the tests. Data apply to ground-to-ground and air-to-ground measurement situations for distances of about 1500 feet.

The studies indicate that, even under controlled conditions, variations can occur in acoustic measurements. Such variations are due to several factors, some of which can be compensated for. Weather and terrain are significant factors in measurement variability, particularly at long distances and for the higher frequencies.

INTRODUCTION

In making measurements to evaluate the noise characteristics of an airplane, there are several factors that can cause variations in such measurements. These factors are the airplane operating conditions, weather, terrain, and instrumentation and procedures. In order to demonstrate the manner in which such factors can affect measured acoustic data, the results from practice noise evaluation exercises are presented. These data were obtained in cooperative projects of the National Aeronautics and Space Administration with the Federal Aviation Administration. At the National Aviation Facilities Experimental Center (NAFEC) a 727 airplane was used in landing and take-off noise studies; at the NASA Wallops Station an 880 airplane was used in flyover studies. The purpose of this paper is to present the pertinent results of these studies and to indicate the nature of the variations observed in the measured quantities.

NAFEC PROJECT

Test Arrangement

Figure 1 contains the general layout for the NAFEC noise measurement project. The purpose of the project was to define the noise footprint of a representative commercial turbofan airplane during take-off and landing. Noise measurements along the sideline during the take-off roll of the airplane, under the airplane during the climbout phase,

and under the airplane during the approach phase were required. In order to make these measurements, microphones were located along a line 1500 feet from the runway center line as shown in figure 1 and also under the flight track in the climbout and landing-approach areas.

Noise Data

Figure 2 contains a plot of the overall sound pressure levels (SPL) as measured at the microphone stations along the 1500-foot sideline array. Data are included for 10 controlled flights of the 727 airplane during a 3-hour period. The maximum sound pressure levels are measured to the rear of the airplane while it is still in a near static condition. Then, as the airplane begins to roll and the forward speed increases, the sound pressure levels decrease. After the airplane rotates and clears the ground, a slight increase in overall sound pressure level is observed. As the airplane climbs out and gains altitude, the sound pressure levels begin to decrease slightly as the slant distance increases. The square symbols represent measurements made on the opposite side of the runway from the circle symbols and have been included in the plot to show that comparable measurements were approximately equal on both sides of the runway. The spread in the acoustical data at each station is of the order of 5 dB. The data in figures 3 and 4 show the spectral content as measured at two of the microphone stations.

In figures 3 and 4, $\frac{1}{3}$-octave band measurements are plotted for two different microphone positions. One microphone was located at the 1500-foot sideline distance but to the rear of the airplane, the measurement being made while the airplane was in a near static configuration (fig. 3). The other microphone was under the flight path of the airplane, and the measurements were taken when the airplane passed overhead at an altitude of about 1600 feet (fig. 4). In both figures the hatched area represents the spread of the sound pressure levels in each frequency band for the 10 flights. In the ground-to-ground case (fig. 3) the lower frequency band levels (below 100 Hz) varied about 5 dB, whereas the higher frequency band levels (above 500 Hz) varied as much as 20 dB. In the air-to-ground case (fig. 4) the variations across the full range of the spectra were markedly less and exceeded 5 dB only at frequencies above 2000 Hz. In both cases the overall noise levels varied about 5 dB because they were controlled by the lower frequency portions of the spectra. The data of figures 3 and 4 are believed to be representative of measurements for conditions when the airplane was under close control. The variations observed are judged to result from several sources.

Sources of Measurement Variability

The four main sources of measurement variability are believed to be instrumentation, terrain, operating parameters of the airplane, and changes in meteorological conditions.

Instrumentation and terrain. - Instrumentation and terrain were not varied in the tests. The terrain was uniformly flat, open, and had sparse grassy ground cover in all measurement areas. The instrumentation was of the same type and was operated in the same manner at each station. Changes in the characteristics of the instrumentation and the terrain during the 3-hour test period are believed to be minimal.

Airplane operations. - Figure 5 contains a plot of the airplane lateral displacement and altitude time histories for 10 flights. Take-off power was applied to the engines at the start of the roll and was held constant until the airplane passed the last measuring station. The airplane position over the measuring station varied approximately 400 feet in lateral displacement and approximately 600 feet in altitude during the 10 flights. These variations in flight path are sufficient to affect the noise-level values. Corrections can be made for variations in distance, but no attempt was made to include such corrections in the data of this paper.

Meteorological conditions. - The other significant variable that affects the acoustic data is the local meteorology. Figure 6 shows variations in some meteorological quantities for the time period during which these 10 flights were made. Temperature, absolute humidity, wind velocity, and wind direction are plotted as functions of altitude. The hatched regions represent the variations in the measurements at the various altitudes. These data were obtained by means of modified rawinsondes that gave continuous readings of temperature and relative humidity. The balloons were tracked by dual theodolites to obtain the wind information. Throughout the test period the wind velocity did not exceed 7 knots at the surface, did not exceed 18 knots at any altitude of interest, and the direction remained constant at an azimuth angle of about 200°. During the test period there were no sharp temperature inversions. Temperature and relative humidity values changed somewhat; however, the absolute humidity remained essentially constant during this time. Some atmospheric variables can be accounted for; however, in a situation such as the one described, insufficient data are available to accomplish meaningful corrections.

WALLOPS STATION PROJECT

Longer term variations in acoustic measurements are shown in figure 7 which contains data measured during 57 flights of an 880 turbojet airplane. These flights were made at a constant altitude of 1400 feet and a constant power condition (engine pressure ratio (EPR) equals 2.0) over a 10-day period. These acoustic data were measured during subjective noise studies at the Wallops Station, and the meteorological conditions that existed during these flights were of the same order as those shown in figure 6.

Statistical Analysis

In figure 7 a histogram has been plotted of the acoustic data that were measured directly under the flight track of the airplane. The maximum value of the overall sound pressure level was determined as the airplane passed overhead. The number of events associated with each maximum sound pressure level value are plotted in figure 7. The spread in the measurements amounts to approximately 6 dB. The standard deviation σ for these data is 1.1 dB; that is, 68 percent of the data are within -11.1 dB of the mean value.

SUMMARY OF VARIABILITIES

Data have been presented from two flyover measurement projects, and it has been shown that variations occur in the measured acoustic data. In table I an attempt is made to evaluate the effects of several factors contributing to variations in acoustic measurements. The various factors which are sources of measurement variability are listed, and values are assigned to each of these. Instrumentation stability is within ±0.2 dB over the entire spectrum. Instrument calibration and data reading operations have associated with them a ±0.5-dB error across the spectrum. It is estimated that changes in the outside air temperature may cause noise-level changes of ±1.0 dB even though the engine pressure ratio was held constant. When the airplane was flown under radar control, ±1.5-dB variations were caused by variations in airplane distance from the measurement locations. Standard procedures are available to compensate for distance. If reasonable care is not taken in conducting the operation, instrumentation and airplane effects on the

TABLE I.- SUMMARY OF VARIABILITIES

Variable	ΔdB low frequency	ΔdB high frequency
Instrument stability	rt0.2	±0.2
Instrumentation operations	±.5	±.5
Airplane power	±1.0	±1.0
Airplane position	±1.5	-11.5
Atmosphere (air to ground)	±2.0	±3.0
	±2.0	±10.0
distance, 1500 ft		

data can be greater than those indicated. The data in the last two items of table I contain the effects of the factors just discussed plus those associated with the atmosphere and terrain. For air-to-ground propagation, where mainly the atmosphere is involved, variations of ±3.0 dB were observed; however, for ground-to-ground propagation where the atmosphere and terrain may affect the data, variations of up to ±10.0 dB were observed. For measurement distances of the order of 1500 feet, the atmosphere and terrain are significant factors.

CONCLUDING REMARKS

Under controlled conditions variations can occur in acoustic measurements. These variations are due to several factors, some of which can be compensated for. Atmosphere and terrain are significant factors in measurement variability, particularly at long distances and for the higher frequencies.

TEST ARRANGEMENT

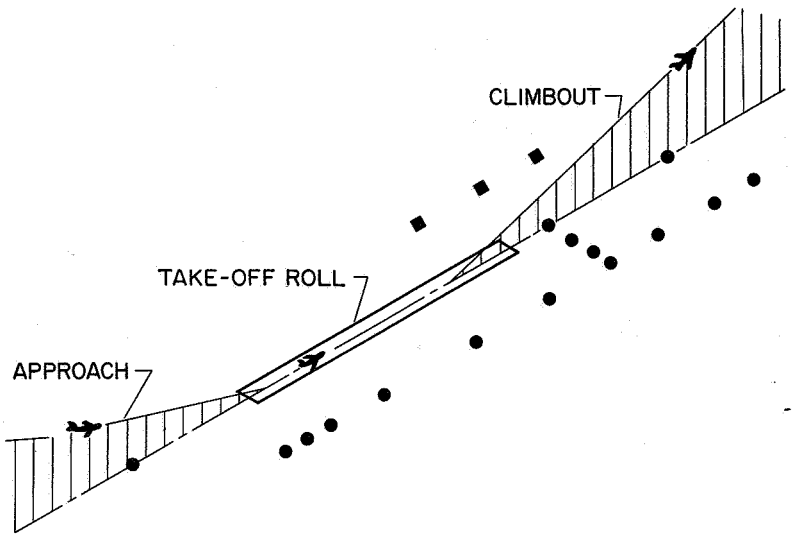

Figure 1

SIDELINE NOISE MEASUREMENTS
DISTANCE = 1500 ft

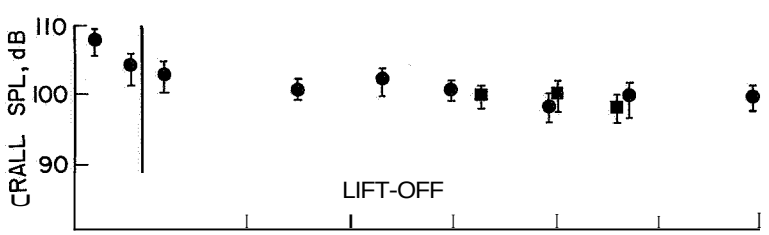

Figure 2

VARIABILITY OF MEASURED SPECTRA
GROUND TO GROUND; DISTANCE = 1500 ft

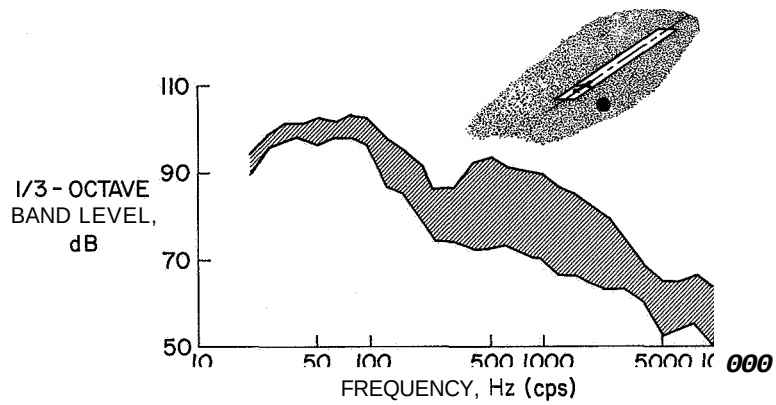

Figure 3

VARIABILITY OF MEASURED SPECTRA
AIR TO GROUND; ALTITUDE = 1600 ft

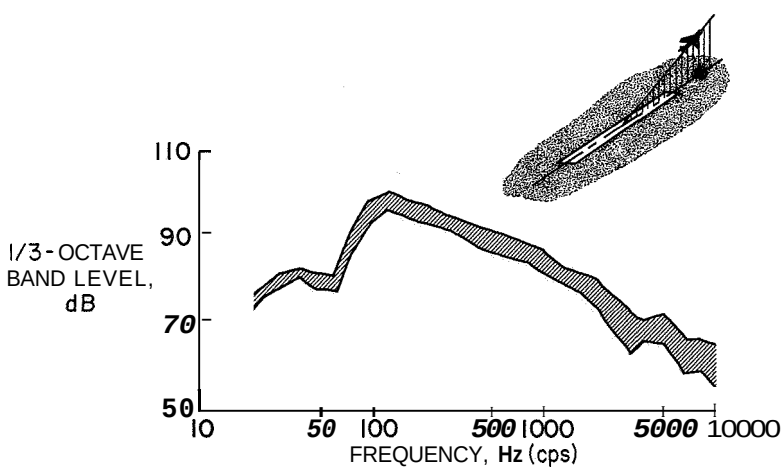

Figure 4

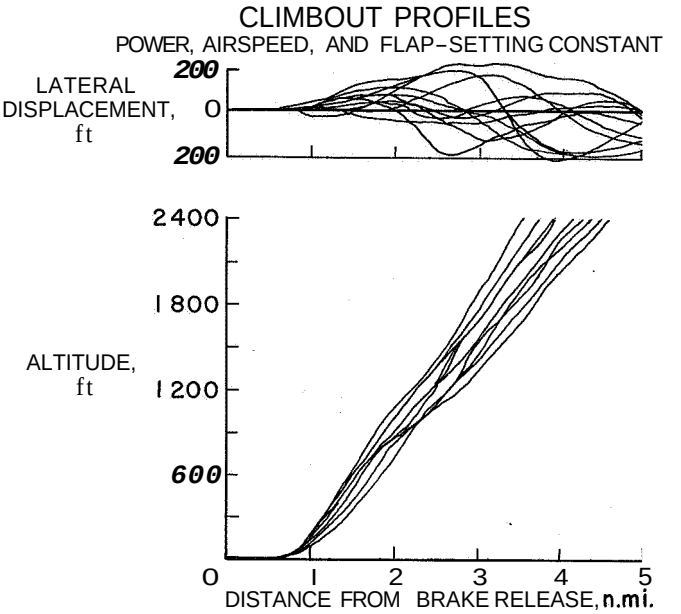

Figure 5

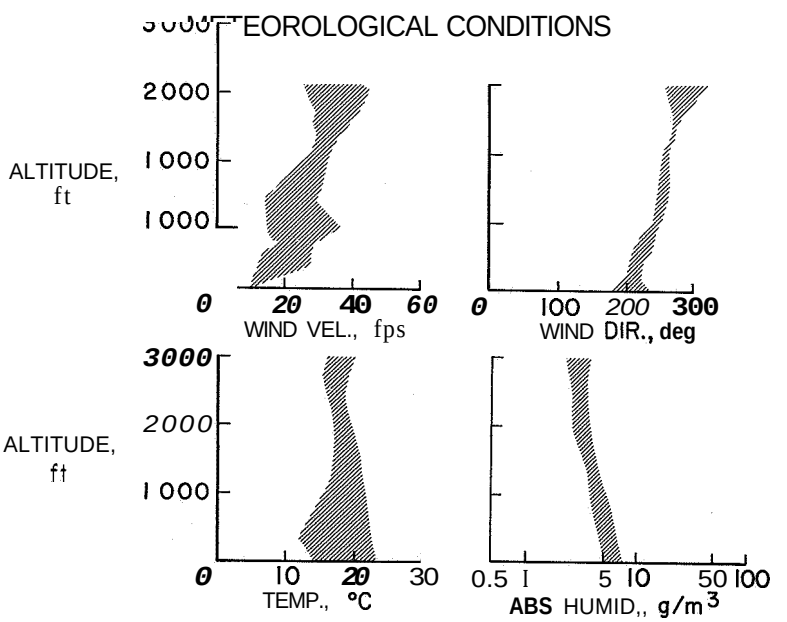

Figure 6

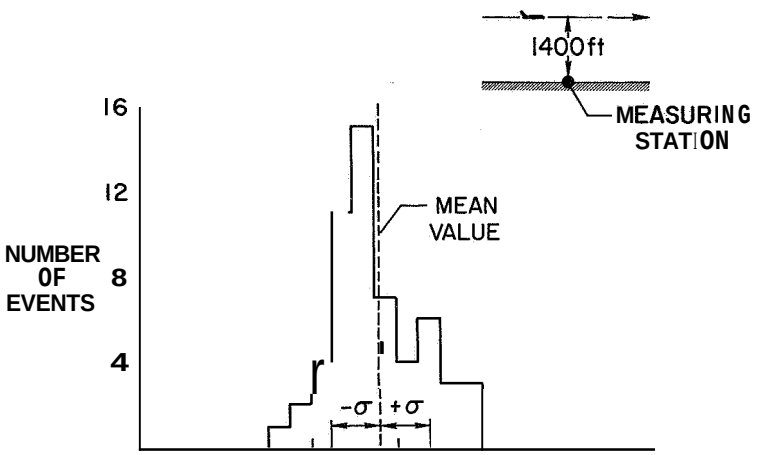
NOISE MEASUREMENT VARIATIONS FOR 57 FLYOVERS
1400ft
MEASURING STATION
16
12
8
4
NUMBER OF EVENTS
MEAN VALUE
-σ
+σ

Figure 7

25. TWO METHODS OF EVALUATING CLIMBOUT NOISE

By W. Latham Copeland

NASA Langley Research Center

SUMMARY

Data have been collected under controlled conditions on several jet-powered transport airplanes to determine operating procedures for minimizing noise exposures and to evaluate a proposed means for performing rapid acoustic evaluations of new airplanes.

Power cutbacks during climbout are shown to be beneficial in reducing noise levels under the climbout path, the amount of reduction being a function of the detail design of the airplane and its engines. A special flight procedure is described which produced sufficient level-flight parametric data for predicting the ground noise levels during climbout without the need for repeated take-offs and landings.

INTRODUCTION

Noise during take-off—climbout operations of jet-powered transport airplanes is an important consideration because of possible adverse reactions in communities near airports (ref. 1). Data have been collected under controlled conditions on a jet-powered transport airplane (ref. 2) to determine operating procedures for minimizing noise exposures and to evaluate a proposed means for performing rapid acoustic evaluations of new airplanes. The objective of this paper is to present some of the results of flight research studies in which the measured noise levels are closely correlated with airplane operations.

The material discussed in this paper is divided into two parts. The first part deals with climbout noise measurements and illustrates the effects of climbout profile and power and airplane configuration. The second part deals with the results of parametric studies which are used in a procedure for estimating the climbout noise for a particular profile when the altitude, power, flap angle, airplane speed, climb rate, and airplane weight are known.

CLIMBOUT OPERATIONS

Test Setup and Test Airplanes

A schematic diagram of the test arrangement for the climbout operations is shown in figure 1. These flight tests were conducted in the vicinity of the NASA Wallops Station, Wallops Island, Virginia. Various climbout procedures were flown, and airplanes were

accurately tracked by ground radar during each flight. The flight tracks in all cases were made over an array of noise measurement stations deployed along the ground track at distances varying from 1.5 to 7.5 nautical miles from brake release.

The airplanes used in the test program are shown in figure 2. These test airplanes were: a four-engine turbojet owned and operated by the Federal Aviation Administration; a four-engine turbofan owned and operated by the Boeing Company; a three-engine turbofan owned and operated by Eastern Airlines; and a two-engine turbofan owned and operated by American Airlines.

Test Results

Figure 3 shows noise-measurement results obtained from the four-engine turbojet airplane, This figure illustrates different climbout procedures employed for noise evaluations and the measured perceived noise levels (PNL) associated with these respective climbout procedures. Progressively lower noise levels are obtained for the slower climb rates which involve lower levels of thrust.

Figure 4 illustrates a climbout procedure employed to reduce the noise over a small area. The four-engine turbojet airplane was used for this test. Take-off power was employed to a 1500-foot altitude. Power was then reduced to that required for a 500-foot/minute climb rate; this reduced power was maintained for 10 seconds and then was followed by a return to take-off power. This figure also shows the measured perceived noise levels resulting from this procedure. Relatively higher noise levels were experienced following the return to take-off power than when take-off power was maintained throughout.

The amount of noise-level reductions obtainable by power cutbacks will vary for airplanes having different types of jet power plants as illustrated in figures 5 and 6. Figure 5 demonstrates the amount of perceived-noise-level reductions as measured for a four-engine turbojet airplane and a four-engine turbofan airplane. Figure 5 shows that the reduction in perceived noise level for the four-engine turbojet airplane at the time of power cutback is of the order of 10 PNdB. Similar data for the four-engine turbofan airplane indicate a smaller perceived-noise-level reduction. The lesser reduction obtainable for the turbofan airplane is due to the presence of fan noise which reduces at a slower rate with reduced velocity than does jet noise.

Figure 6 illustrates the amount of perceived-noise-level reductions obtainable for two different airplanes powered by turbofan engines. This figure shows measured data for the three-engine and the two-engine turbofan airplanes. The same order of reductions is obtainable for both airplanes. The amount of noise-level reductions obtainable for the three-engine and two-engine turbofan airplanes is greater than those for the four-engine turbofan airplane. This difference results from special airplane and engine design

features to reduce fan noise and from more favorable thrust-to-weight ratios which allow a greater power cutback than for the four-engine airplane.

PARAMETRIC FLIGHT STUDIES

Test Procedure

Several factors, such as airplane altitude, engine thrust level, flap setting, airplane speed, airplane climb rate, and airplane weight, may be important when predicting noise from climbout operations. A test procedure has been devised which involves controlled flights and noise measurements to account properly for all these factors. Figure 7 is a schematic diagram showing the nature of this test procedure. A four-engine turbofan airplane under radar control was flown in a level-flight attitude to the vicinity of the noise measurement range. Just prior to reaching the noise measurement range, the engine throttle settings were adjusted to provide various rates of climb from 750 to 2400 feet/minute. Each test flight was made over an array of noise measurement stations deployed along the ground-track center line. Data were recorded at each station as the airplane passed overhead. Tests were repeated for each of the climb rates with initial level-flight altitudes of 500, 800, and 1100 feet. These flights were conducted with flap settings of 0^{o} and 14^{o} which are representative settings for take-off and climbout operations for this particular airplane.

By this means acoustic data were obtained for various airplane altitudes, various engine thrust levels, and at the flap setting of interest. Results from this flight-test procedure have been plotted such that the noise levels during the climbout operations of the test airplane can be accurately predicted. The usefulness of such parametric data for predicting the noise for a given climbout profile is illustrated in figure 8.

Comparison of Measured and Predicted Noise Levels

Figure 8 shows a comparison of the measured and predicted noise levels of the four-engine turbofan airplane for a climbout profile employing take-off power with a 14^{o} flap setting to a 1500-foot altitude, then a power reduction to that required for a climb rate of 500 feet/minute. This figure illustrates the range of altitudes associated with three nearly identical test flights for which noise data are also presented. The pilot was instructed to fly the same profile each time, and the hatching represents the variation in this operation. Perceived-noise-level data as measured from the three flights are shown in the sketch at the bottom of figure 8. For comparison, noise predictions (hatched bands) have been made for the flown profiles based on the parametric flight data. Good correlation exists between the measured and predicted levels.

Encouraging results such as those of figure 8 suggest that this simulation method of prediction may be very useful in evaluating the noise characteristic of various types of airplanes under various operating conditions. Parametric flight procedures can establish basic noise characteristics of a particular airplane and the range of noise leveis associated with various operations, and these can be accomplished without the need for repeated take-offs and landings or for an instrumented airport range.

CONCLUDING REMARKS

Power cutbacks during climbout are shown to be beneficial in reducing noise levels under the climbout path, the amount of reduction being a function of the detail design of the airplane and its engines. A special flight procedure is described which produced sufficient level-flight parametric data for predicting the ground noise levels during climbout without the need for repeated take-offs and landings.

REFERENCES

1. Jet Aircraft Noise Panel: Alleviation of Jet Aircraft Noise Near Airports. Office Sci. and Technol., Mar. 1966.
2. Copeland, W. Latham; Hilton, David A.; Huckel, Vera; Dibble, Andrew C., Jr.; and Maglieri, Domenic J.: Noise Measurement Evaluations of Various Take-Off—Climbout Profiles of a Four-Engine Turbojet Transport Airplane. NASA TN D-3715, 1966.

TEST ARRANGEMENT FOR CLIMBOUT STUDIES

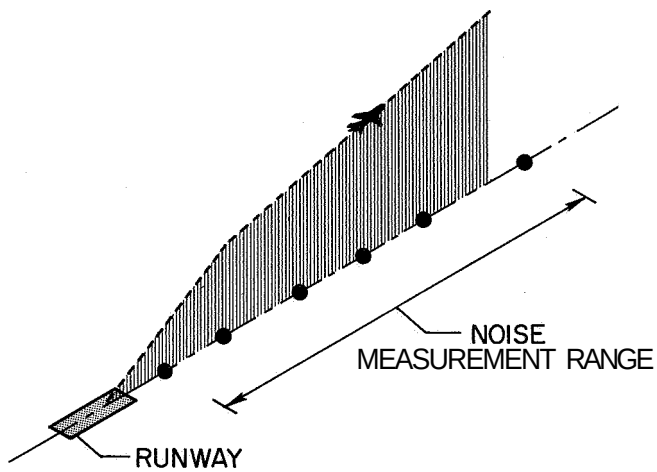

Figure 1

TEST AIRPLANES

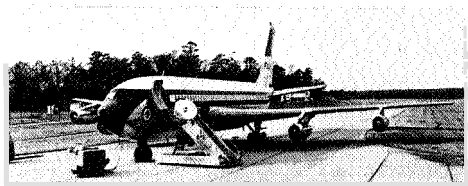

4-ENGINE TURBOJET

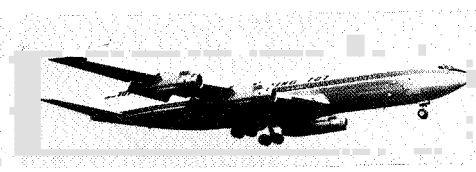

4-ENGINE TURBOFAN

3-ENGINE TURBOFAN

2-ENGINE TURBOFAN

Figure 2

EFFECTS OF ENGINE POWER SCHEDULING
4-ENGINE TURBOJET

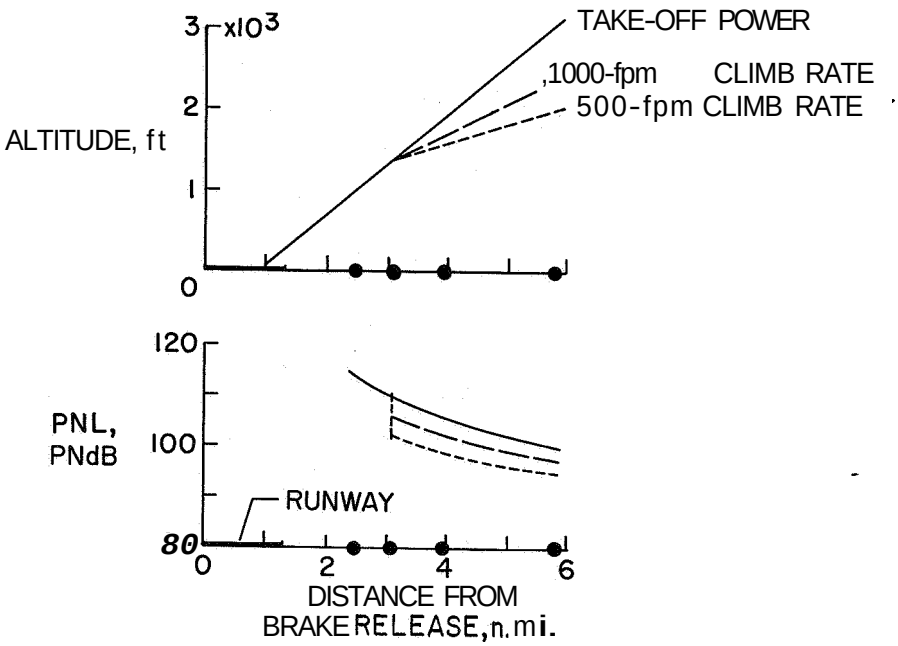

Figure 3

EFFECTS OF ENGINE POWER SCHEDULING
4-ENGINE TURBOJET; 10 sec AT 500-fpm CLIMB RATE

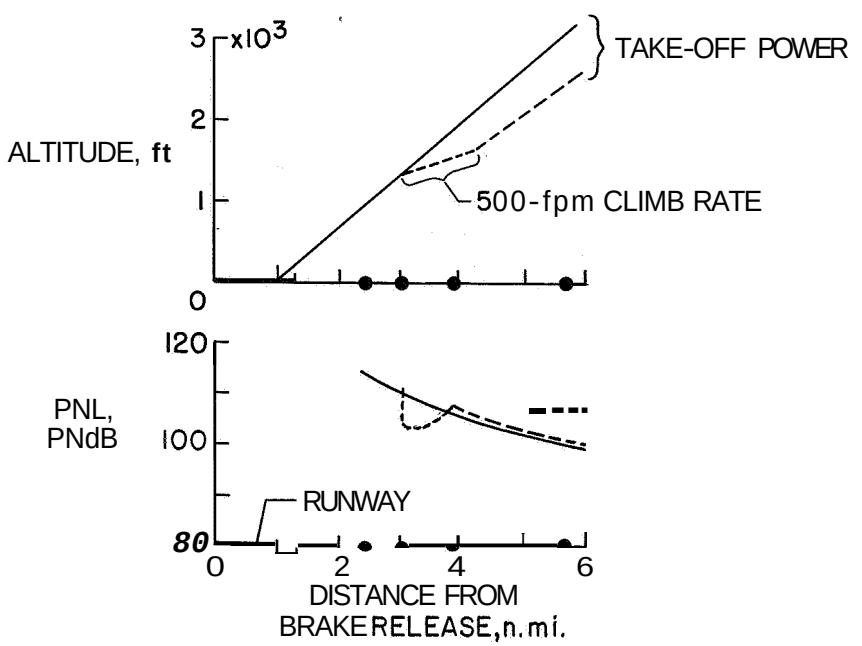

Figure 4

NOISE REDUCTIONS DUE TO POWER CUTBACK
4-ENGINE AIRPLANES

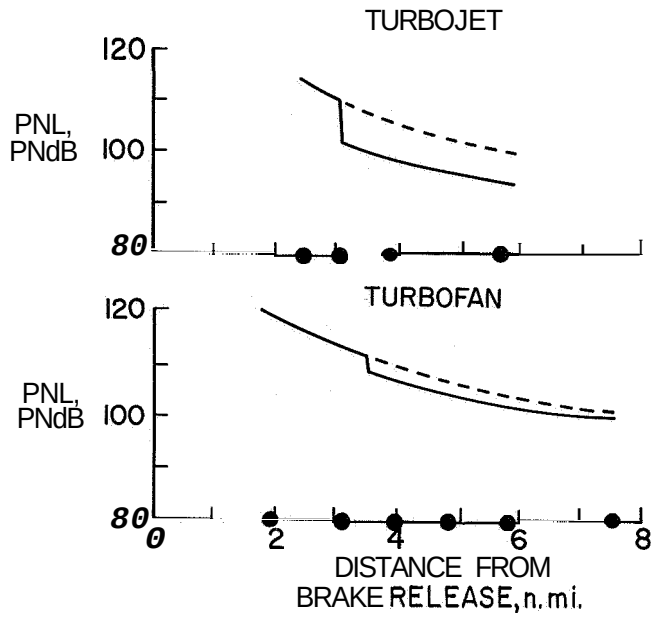

Figure 5

NOISE REDUCTIONS DUE **TO** POWER CUTBACK

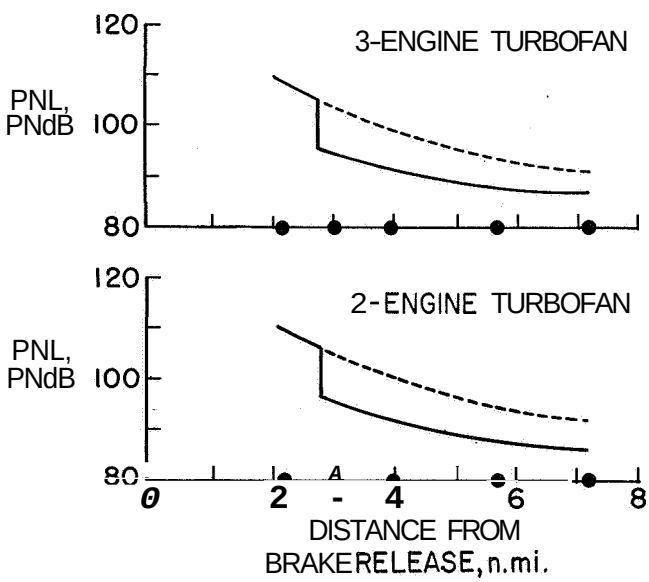

Figure 6

TEST PROCEDURE

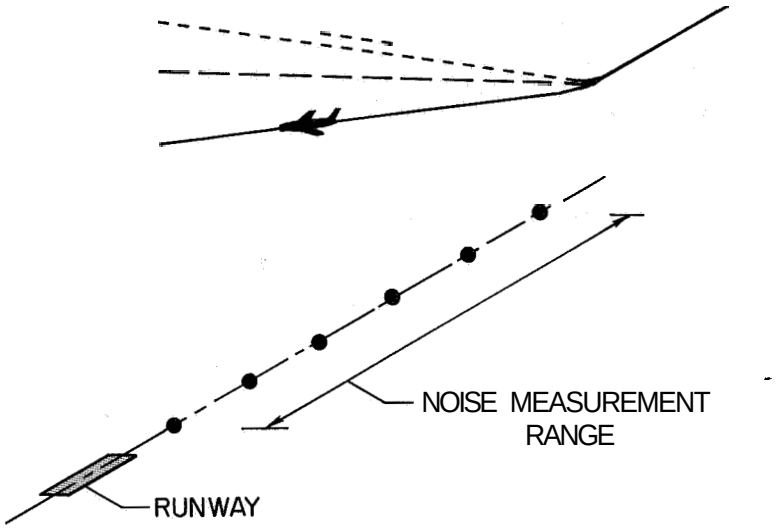

Figure 7

COMPARISON OF MEASURED AND PREDICTED DATA
4-ENGINE TURBOFAN

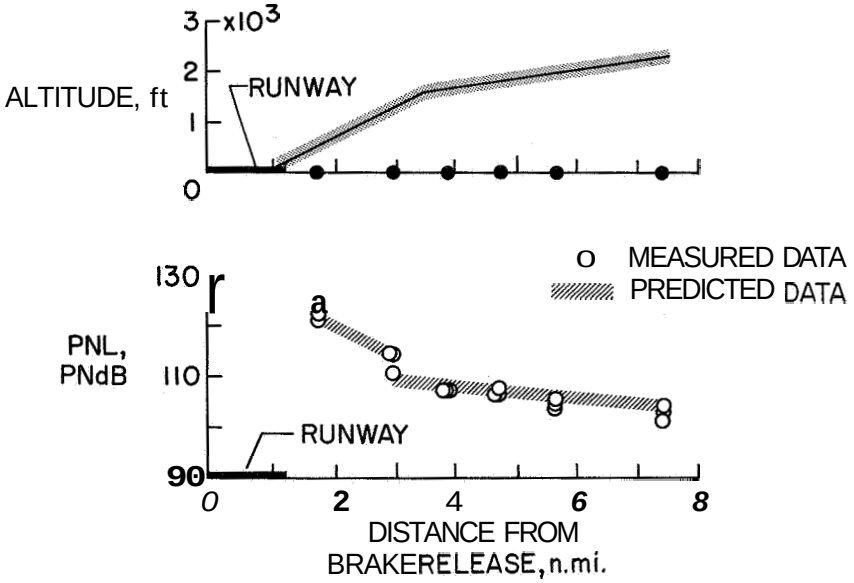

Figure 8

26. FLIGHT INVESTIGATION OF METHODS FOR IMPLEMENTING NOISE-ABATEMENT LANDING APPROACHES

By Hervey C. Quigley, Robert C. Innis, and Emmett B. Fry

NASA Ames Research Center

SUMMARY

A flight and simulation investigation has been conducted to determine the requirements that will enable pilots to fly steep two-segment noise-abatement landing-approach profiles with the precision common to conventional instrument landing approaches without an increase in pilot workload. The amount of noise reduction depends on the altitude of intercept of the two segments. Profiles with an intercept altitude of 400 feet resulted in a noise reduction of 10 PNdB or more $1\frac{1}{2}$ nautical miles from the runway threshold and beyond.

The profiles were evaluated by 11 pilots by using a research jet transport. The airplane had improvements over current jet transports including a flight director modified for two-segment profiles, an autothrottle, and both longitudinal and lateral directional stability augmentation. The two-segment approaches could be flown in the modified airplane with the same precision as conventional instrument landing approaches without a significant increase in pilot workload in the nearly ideal conditions of the tests. Further tests are needed to examine the requirements and operational limitations of two-segment approaches in an environment more representative of airline operations.

INTRODUCTION

Operating problems associated with landing-approach profiles that will reduce the noise level of jet transports have been the subject of NASA research for several years. Much of the research (refs. 1 to 3) has concentrated on the problems of steep landing approaches. Reference 1 showed that the use of increased approach angles is a feasible method for decreasing the noise of jet transports. As reported in references 1 and 4 and as shown by figure 1, the approach noise is reduced in two ways when the approach angle is increased. First, an increase in the approach angle requires a reduction in thrust of the engines; and second, a steeper approach places the airplane higher above the ground. The combination of reduced thrust and higher altitude results in a significant reduction in noise.

Another operational method that can reduce the noise in landing approach is the use of a decelerating approach. In the deceleration technique the approach is started at a

high airspeed, the engine thrust is reduced to a low value, and the airplane decelerates to the landing-approach speed at a point near the runway. The amount of noise reduction will depend on how much reduction in engine thrust can be tolerated during the deceleration period.

A flight and simulation investigation has recently been conducted to determine the requirements that will enable pilots to fly steep and decelerating noise-abatement landing approaches with the precision common to normal instrument landing approaches without an increase in the pilot workload. The evaluation flights were flown under simulated instrument conditions in daylight and in near-ideal weather. Preliminary results of only the studies on the use of increased landing-approach angle are reported in this paper.

SYMBOLS AND ABBREVIATIONS

h	altitude, feet
T	thrust, lb
V_{APP}	approach velocity, knots
ε	instrument landing error, degrees

Abbreviations:

BLC	boundary-layer control
DLC	direct lift control
EADI	electronic attitude director indicator
ILS	instrument landing system
PNL	perceived noise level

AIRPLANE AND SIMULATOR

Test Airplane

A four-engine jet transport, the Boeing 367-80 (707 prototype), was used and is shown in figure 2. This airplane is described in reference 5 except for certain modifications made for this investigation. Details of the modified flap system are shown in figure 3. The modified boundary-layer-control (BLC) flap enabled the airplane to be operated at moderately high lift coefficients in landing approaches with low engine thrust and to provide a means for direct lift control. The main flap and BLC system are described in reference 5. The new slotted auxiliary flap provided additional lift by increasing angle-deflection capabilities and by the impingement of the jet exhaust from

the inboard engines on the slotted auxiliary flap. A high-rate actuation system (30°/sec) was installed on the auxiliary flap to provide direct lift control. Maximum travel step inputs (±20°) of the auxiliary flap gave approximately ±0.15g at the landing-approach speed. The normal trim deflection for the auxiliary flap was 10° greater than that for the main flap.

The evaluation pilots flew the airplane from the right seat by a "fly-by-wire" control system which was programed onto a general-purpose analog computer located in the forward section of the fuselage. The computer also provided the computations and drive signals required for the direct lift control, autothrottle, flight director, and flight-path angle on the electronic attitude director indicator (EADI).

The fly-by-wire control system could be used as the basic airplane control system by gearing control inputs directly to the elevator or as a rate command control system to improve airplane pitch response and stability.

The auxiliary flaps for direct lift control were driven in combination with the elevators through a computer interconnection from the control column. Also available was a control-wheel-mounted thumb controller for direct lift control.

The EADI, which was developed by the Boeing Company, was a black and white cathode-ray-tube display with exposed dimensions of 5.4 by 7.2 inches. (See figs. 4 and 5.) In addition to the information usually found on current electromechanical attitude director indicators, the EADI included symbols for digital radio altitude, flight-path angle, potential flight path (proportional to longitudinal acceleration), and a television picture. The television picture was provided by a closed-circuit system with the television camera mounted under the nose of the airplane.

Simulator

The Ames moving base transport simulator, described in reference 5, was used for the simulation studies. The control-force characteristics and pilot instrumentation represented those of the test airplane and included a left-hand throttle arrangement and an electronic attitude director indicator. The simulator was programed with 367-80 aerodynamic parameters by using the equations of motion described in reference 6. These equations were modified to provide for the effects of the modified flap system, proper engine response, autothrottle, rate command control system, and direct lift control. Continuous computations of the noise on the ground directly below the airplane were made on all simulator runs. Approximations of the measured variation of PNdB with engine thrust and with airplane altitude of a Boeing 707-320 were used for the computations.

DISCUSSION

Problem Areas of Steep Landing Approaches

The results of previous tests of steep landing approaches (ref. 1) and the initial-flight and simulator results of the present program have shown that the following problem areas make noise-abatement landing approaches more demanding of the pilot than normal approaches:

(1) Rate of descent near the ground

(2) Flight-path control

(3) Pilot workload

(4) Guidance and display information

(5) Engine response

The first of these problems is of major concern for steep landing approaches because of the higher rate of descent associated with steep approaches. The variation of the rate of descent with approach angle for three approach airspeeds is shown in figure 6 along with the computed noise reduction of an airplane with an approach speed of 115 knots. These data show that the rates of descent for present-day jet transports on normal 2.5° to 3° instrument approaches are between 500 and 800 feet per minute. The curve in the lower part of the figure shows that substantial reductions in noise (approximately 18 PNdB) are possible as the approach angle is increased to 6°. Approach angles of 6° are near the maximum that can be considered for most current jet transports at minimum landing-approach speeds when allowances for overshoots of $7\frac{1}{2}^{\circ}$ to 8° and engine response are considered. An approach angle of 6°, however, will result in a rate of descent of 1600 feet per minute at an approach speed of 150 knots. Evaluation by two NASA pilots in the initial phase of the program indicated that rates of descent greater than 900 to 1000 feet per minute were unsatisfactory at altitudes less than 200 feet above the ground in simulated instrument landing approaches. The data in figure 6 indicate that a reduction in noise of 5 PNdB or more is possible by an increase in approach angle to about 4° without a large increase in rate of descent if approach airspeeds are kept on the low side of the range used by current jet transports. The landing-approach speeds must be reduced to 90 knots or less for the rates of descent to be satisfactory for approach angles of about 6°.

Two-segment landing-approach profiles were used in the earlier tests (ref. 1) to reduce the high rate of descent near the ground. Figure 7 illustrates a typical two-segment approach and shows the computed noise reduction. The two-segment approaches that were considered in this program had an upper segment with an approach angle of 6° which intercepted a lower segment with an approach angle of 2.650. (The angle of the

instrument landing system (ILS) at the Oakland International Airport, where the tests were conducted, is 2.65°.)

The noise reduction for a two-segment approach is less than that for a straight 6° approach. At a point 2 nautical miles from the runway threshold in the two-segment approach (fig. 7), the airplane is not as high above the ground; and therefore, the noise reduction is only 12 PNdB compared with 18 PNdB for the straight 6° approach. The noise reduction goes to zero when the airplane intercepts the lower segment of the approach profile because the thrust must be increased to normal approach thrust and the airplane altitude remains the same. The noise reduction on a two-segment approach is related, therefore, to the altitude of the intercept of the two segments. When the intercept altitude is low, the noise reduction is high, but the high rate of descent must be continued closer to the ground. The altitude for the intercept was, therefore, one of-the variables in the program.

The other four problem areas listed at the beginning of this section are related to the pilot's ability to comfortably fly the nonlinear portion of the two-segment approaches. Figure 8 shows a typical flight path of an airplane (solid line) when the pilot is flying a two-segment approach (dotted line) by using instrumentation common to current jet transports. Primarily because of inadequate guidance, the pilot will continue to fly a 6° glide slope at the intercept. The correction of the resulting deviation from the intended flight path is a demanding task and greatly increases the pilot workload. Since the engines are at a low thrust value on the 6° glide slope, the pilot is also concerned about the effect of low response time of the engines. Most jet engines have response times from low thrust to maximum thrust of several seconds; therefore, pilots cannot accomplish a wave-off as quickly as in a normal approach.

The inadequate guidance on the two-segment approach also affects the noise as shown in figure 8. Since a fairly large undershoot error can develop, it is necessary to use thrust values greater than those required for a normal approach. This excess thrust results in more noise. Obviously, the two-segment approaches must be flown precisely and smoothly to alleviate these problems.

Method to Alleviate Problem Areas in Steep Approach

Since the test airplane was a fly-by-wire airplane, it was possible to program the onboard computer to obtain the desired characteristics that would alleviate some of the problems of flying two-segment approaches with the precision and pilot workload of a normal landing approach. To improve flight-path control, a rate command control system on the longitudinal axis and direct lift control were incorporated; to reduce pilot workload,

an autothrottle was included; and to improve guidance and display information, modifications to the flight-director computations were made and an advance cathode-ray-tube display was used.

The lateral-directional characteristics of the test airplane were also augmented to give the airplane good lateral-directional handling qualities. The augmentation consisted of roll damping, turn coordination, and directional damping.

Rate command control system.- One of the most important characteristics that the pilots desire for good flight-path control is precise control of the pitch attitude of the airplane. A rate command control system was provided on the longitudinal axis of the test airplane to provide the desired pitch response. Rate command control systems have been demonstrated that give good pitch response. Reference 7 gives examples of early tests of a rate control system. The rate command control system that was used had performance similar to the stick-steering autopilots being installed on some late-model jet transports and was of the general type of control system being proposed for the supersonic transports. With a rate command control system, the pilot's fore and aft control column commands pitch rate as a function of control force. When the control force is returned to zero, the airplane will stay at the new command altitude. This altitude-hold feature of the rate command control system and the ability to command a change in pitch attitude without control reversals helped to reduce the pilot's workload on the approach. The pilots' evaluation of the rate command control system showed that the system was an improvement over the conventional method for changing and controlling the flight path of the airplane in the approaches. There were, however, some unusual characteristics of the rate command control system which required some change in control technique for flare and touchdown. Further discussion of these characteristics is beyond the scope of this paper,

Direct lift control (DLC).- The direct lift control (DLC) was also incorporated into the airplane to improve flight-path control. Flight tests with other airplanes such as the F-8C (ref. 8) and Convair 990 have shown that DLC provides a more rapid vertical response of the airplane for flight-path control. When the DLC is interconnected to the pitch control as in this program, the DLC affords a quickened vertical response of the airplane to commanded pitch-angle changes. The pilots' evaluation of the DLC in the two-segment approaches indicated that the DLC provided little improvement in the tracking of the ILS on the landing approach for an airplane with good pitch response and adequate guidance. The pilot appreciated the quickened vertical response of the DLC, however, especially in the flare-and-touchdown task. The pilots recognized the potential advantage of DLC to help arrest rates of descent rapidly in case of emergency on a steep landing approach.

Autothrottle.- An autothrottle system was included as a means for reducing the pilot workload on the approach. An autothrottle relieves the pilot of the job of making adjustments in engine thrust to keep the airspeed on the approach within acceptable limits. Autothrottles have been used by airlines and others and have been shown to be effective in reducing the pilot workload. In two-segment approaches where both attitude and thrust changes are required late in the approach, the evaluating pilots considered the autothrottle to be necessary to keep the workload at a level comparable to a normal landing approach.

Flight directors.- Guidance for the pilot on the approaches was provided by a flight-director system. A flight director provides the pilot with computed commands to assist him in flying precise instrument landing approaches. Because computations used in current flight directors are designed for low-angle linear approaches, modifications to the computations were required to provide precise guidance on the two-segment approaches. As in most modern flight-director systems, the airplane attitude and ILS error information were used to compute the commanded flight-director needle displacement. The modifications to the computation and logic provided for the intercept of the 6° upper segment of the approach profile, for an increase in sensitivity, and for guidance on the nonlinear portion of the two-segment approaches by commanded attitude changes. Compensation for the powered-lift effects of the flap and for off-speed effects improved the accuracy of the guidance following transition to the lower segment. A detailed discussion of the modified flight-director computations is beyond the scope of this paper. The pilot evaluation of the flight director will be included in a later section of the report.

Advanced instrument display.- Besides the basic guidance information furnished by the flight director, the pilot requires sufficient additional information to assess the progress of the approach. This information traditionally is provided by several instruments on the instrument panel. The advantages that might be gained by including most of this information along with the flight-director guidance on a single cathode-ray-tube display (EADI) was evaluated in the program.

Although the display contains many elements (fig. 5), after a brief familiarization time on the simulator, the display could be effectively used. The pilots appreciated the expanded scale for much of the information and felt that the information presented was useful on the approach; however, the symbology that was used on the display was not considered optimum by all the pilots. They felt further development of this type of display was warranted. The pilots did not agree on the relevance of the television, but most considered a real-world display useful.

Profiles and Guidance

The two-segment approach profiles that were evaluated by the pilots are shown in figure 9. This figure also shows the computed noise reduction for the profiles. The two profiles have a 6° approach angle for the upper segment and a 2.65° for the lower segment. The intercept altitudes are 250 and 400 feet. The 250-foot intercept altitude was chosen to give a computed noise reduction of about 10 PNdB 1 nautical mile from the runway threshold and beyond. The second profile with the intercept at 400 feet was chosen to give about 10-PNdB noise reduction $1\frac{1}{2}$ nautical miles from the threshold and beyond. These two intercept altitudes also provided the pilots with an opportunity to evaluate a low and a moderately high intercept altitude on two-segment approaches.

Two guidance systems were used on both the 250-foot- and the 400-foot-intercept profiles. The instrument landing systems for the guidance were generated by using an approach radar especially programed for these tests. The two systems are illustrated in figure 10. In the top part of the figure, a system with two separate ILS beams is represented. The upper segment of the profile was a 6° beam generated by the radar system, and the lower segment was the standard 2.65° ILS at the Oakland International Airport. This system required two ILS receivers in the airplane and special flight-director logic for switching near the intercept altitude. The flight-director computations for the two-beam ILS consisted of a capture of the 6° beam at an altitude of about 2500 feet,and a second capture from above of the 2.65° beam near the intercept. The other type of guidance shown in figure 10 represents a single ILS beam that was curved at the intercept point. The radius of curvature was about 40 000 feet which corresponds to a flight-path rate of change of 3.5 seconds per degree at an approach speed of 115 knots. The curved ILS system was generated by the approach radar. The flight-director computation for the curved beam required special logic information from the radar to identify the point where the curvature started. The flight-director computation for approximating the curved portion of the beam was accomplished on board the airplane.

Landing-Approach Speed

Two ranges of landing-approach speed were used to evaluate the benefits of a reduced approach speed on two-segment approaches. An approach airspeed of between 145 and 135 knots was used as representative of current jet transport operation. A lower airspeed of between 122 and 112 was used as representative of a jet transport with special high-lift devices.

Pilots' Evaluation

The two-segment approach profiles were evaluated by one commercial airline, four NASA, and six FAA pilots. The primary objective of the evaluation was to compare the

ILS flying precision and the pilot workload on the two-segment approaches with those on normal 2.650 approaches. Pilot opinion was obtained from the results of both simulation and flight evaluations. The pilots made extensive evaluation of variations in each of the devices incorporated on the simulator to alleviate the problems on two-segment approaches. The results of the simulation were used to determine the airplane configurations for flight evaluation.

Results of evaluation of profiles.- The evaluation by the 11 participating pilots of the two-segment approach profiles has shown that the two-segment approach can be flown with the same precision as a normal approach when the methods to alleviate the problem areas discussed earlier were incorporated into the test airplane. Figure 11 shows a comparison of the tracking of a typical curved two-segment approach having a 400-foot intercept with a normal approach. Comparable magnitude and frequency of glide-slope errors are also shown. The results for an approach with a 250-foot intercept altitude or with the two-beam ILS were similar to those for an approach with a 400-foot interoept altitude (fig. 11). The tracking was within the accuracy required for Category II landing weather minima. The overall pilot workload on any of two-segment approaches was no higher than a normal approach without autothrottle.

The pilots' comparison of the approaches with the 250-foot and the 400-foot intercepts shows that the pilots preferred the higher intercept altitude. The pilots felt that the 400-foot intercept allowed a little more time to become stabilized on the lower segment before initiating the flare. The pilots were slightly rushed on some of the approaches with 250-foot intercepts. Because of the importance of the time element, most of the pilots preferred the lower approach speed. When the approaches were flown smoothly and precisely, the pilots did not consider the low response time of the engines a problem on the two-segment approaches.

The opinion of the pilots was mixed on their preference to the type of guidance for the two-segment approaches. Although either system gave the required guidance, some of the pilots preferred the two-beam system because they felt that having the steep upper segment intercept the lower segment enabled them to determine more accurately their position on the nonlinear portion of the profiles. The transition could be made a little faster, and thus more time on the lower segment was available. Other pilots preferred the single-beam curved profile because they felt that this profile required the least increase in pilot workload. The curved ILS eliminated the discontinuity of the two-beam system and was easier to follow. The transition on the curved ILS was considered to be smoother to fly by most of the pilots,

Requirements for two-segment approaches.- The pilots were asked to evaluate the significance of the various devices incorporated to alleviate the problems of the

two-segment approaches. The following list shows what the pilots felt were the primary and secondary requirements for the two-segment approaches evaluated in this program:

Primary requirements

(1) Guidance system for two-segment profiles

(2) Modified flight director

(3) Autothrottle

Secondary requirements

(1) Rate command control system

(2) Advanced displays

(3) Direct lift control

The primary requirements are considered essential for the two-segment approach. A guidance system for two-segment profiles must include the necessary ground-based equipment required for a two-segment instrument landing system and the equipment in the airplane to receive and display the information. The second requirement follows very closely in that a modified flight-director system must be provided that is compatible with the guidance system. The pilots felt that for the two-segment approaches an autothrottle was a primary requirement for keeping the workload at the level of a normal approach.

The secondary requirements are those that the pilots felt were not essential but which gave some improvemeqt. The rate command control system improved flight-path control by providing precise control of pitch attitude. Since the pitch response of the test airplane without the rate command control system was considered satisfactory and the basic airplane control system included automatic trim, the two-segment approach could be flown with or without the new control system without significant change in workload. It should be pointed out, however, that good pitch response is an important requirement and improvement in the pitch-response characteristic would probably be required for some current jet transports for two-segment approaches.

Displays that will improve the method of presenting the information the pilot needs in the approach are definitely required for any landing approach. The advanced cathode-ray-tube display used in the present program was recognized as having the potential to achieve some improvement required for pilots' displays. It was not found, however, to be essential in making the two-segment approach. In one series of approaches made by one pilot, an electromechanical altitude director indicator was used in place of the cathode-ray-tube display. The pilot was able to perform the task equally well with either display.

Since the airplane had satisfactory vertical response to control inputs, the direct lift control was not considered a requirement by the pilots for making the two-segment approach. The benefits of the quickened vertical response were appreciated, however, by the pilots in the flare-and-touchdown task.

CONCLUDING **REMARKS**

The results of a flight and simulation study have shown that a significant reduction in landing-approach noise can be achieved by flying a steep two-segment approach profile. For the jet transport used in this study, a reduction in noise of approximately 10 PNdB or more at a point 1 nautical mile from the runway threshold and beyond was achieved when a two-segment profile with an intercept altitude of 250 feet was flown. The pilots preferred, however, the two-segment profile with an intercept altitude of 400 feet, which gave a noise reduction of 10 PNdB $1\frac{1}{2}$ nautical miles from the runway threshold and beyond.

The two-segment landing approaches that were evaluated in this program could be flown by a modified jet transport with the same precision as conventional instrument landing approaches without a significant increase in pilot workload. It must be recognized, however, that the research airplane had improvements over current jet transports including a flight director modified for two-segment profiles, an autothrottle, and both longitudinal and lateral directional stability augmentation. The evaluation flights were flown under simulated instrument conditions in daylight and in near-ideal weather. Further tests are needed to examine the requirements and operational limitations of two-segment approaches in an environment more representative of airline operations.

REFERENCES

1. Zalovcik, John A.; and Schaefer, William T., Jr.: NASA Research on Noise-Abatement Approach Profiles for Multiengine Jet Transport Aircraft. NASA TN D-4044, 1967.

2. Hall, Albert W.; and McGinley, Donald J., Jr.: Flight Investigation of Steep Instrument Approach Capability of a C-47 Airplane Under Manual Control. NASA TN D-2559, 1965.

3. Hall, Albert W.; and McGinley, Donald J., Jr.: Flight Investigation of Steep Instrument Approach Capabilities of a T-33 Airplane Under Manual Control. NASA TN D-2775, 1965.

4. Zalovcik, John A.: Effect of Thrust and Altitude in Steep Approaches on Ground Track Noise. NASA TN D-4241, 1967.

5. Condit, Philip M.; Kimbrel, Laddie G.; and Root, Robert G.: Inflight and Ground-Based Simulation of Handling Qualities of Very Large Airplanes in Landing Approach. NASA CR-635, 1966.

6. Jackson, Charles T., Jr.; and Snyder, C. Thomas: Validation of a Research Simulator for Investigating Jet Transport Handling Qualities and Airworthiness Criteria During Takeoff. NASA TN D-3565, 1966.

7. Russell, Walter R.; Sjoberg, S. A.; and Alford, William L.: A Flight Investigation of the Handling Characteristics of a Fighter Airplane Controlled Through a Rate Type Automatic Control System. NACA RM L56F06, 1956.

8. Gralow, R. T.; Peace, J. D., III; and Shipley, J. L.: Evaluation of the Direct Lift Control System Installed in the F-8C Airplane. Final Report, Rep. No. FT-51R-65 (RA1300001), U. S. Naval Air Test Center (Patuxent River, Md.), Aug. 13, 1965. (Available from DDC as AD 468464.)

NOISE REDUCTION DUE TO THRUST AND ALTITUDE

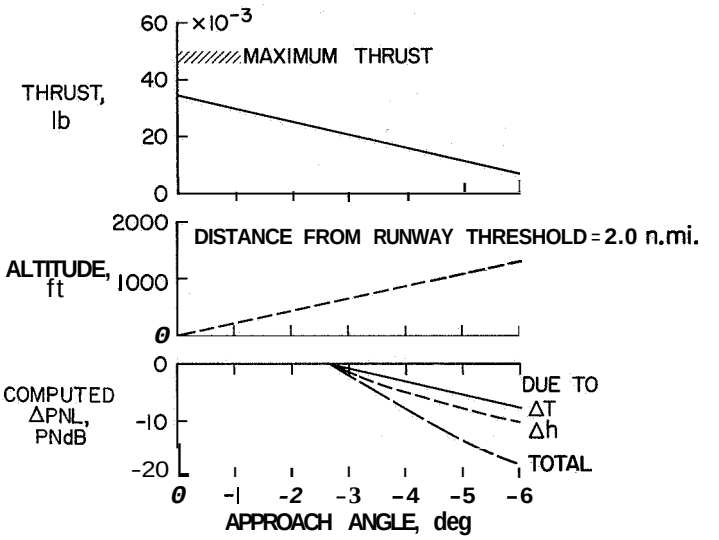

Figure 1

TEST AIRPLANE BOEING 367-80

Figure 2 L-68-8580

BOEING 367-80 AIRPLANE MODIFIED FLAP

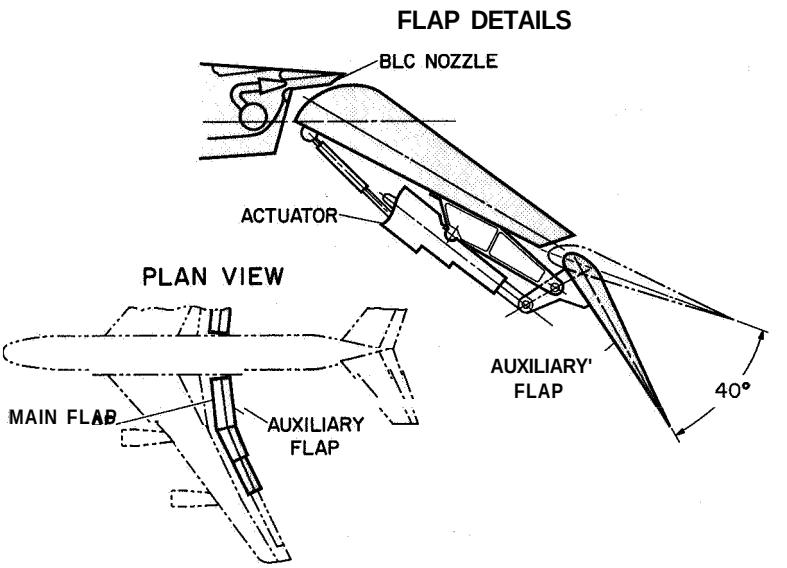

Figure 3

BOEING 367-80 AIRPLANE COCKPIT

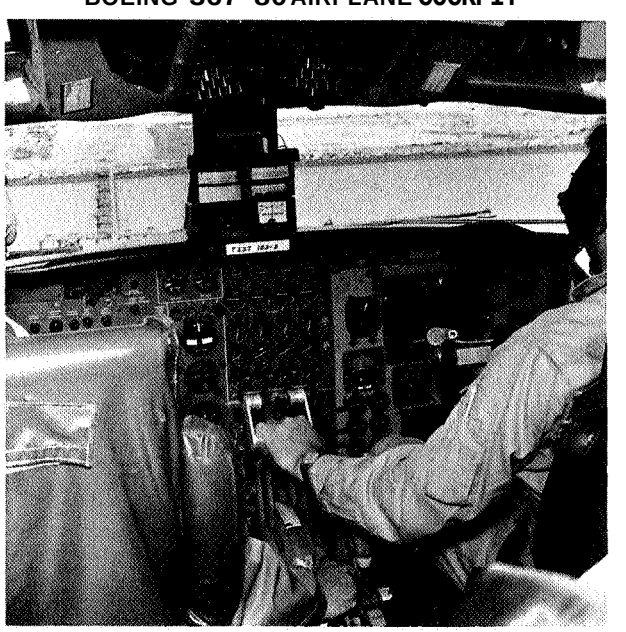

Figure 4 L-68-8581

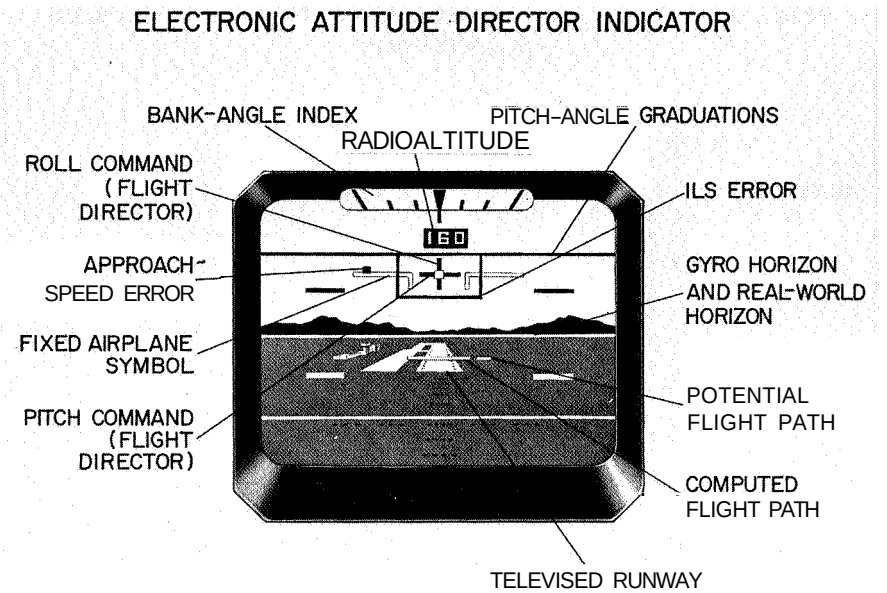

Figure 5

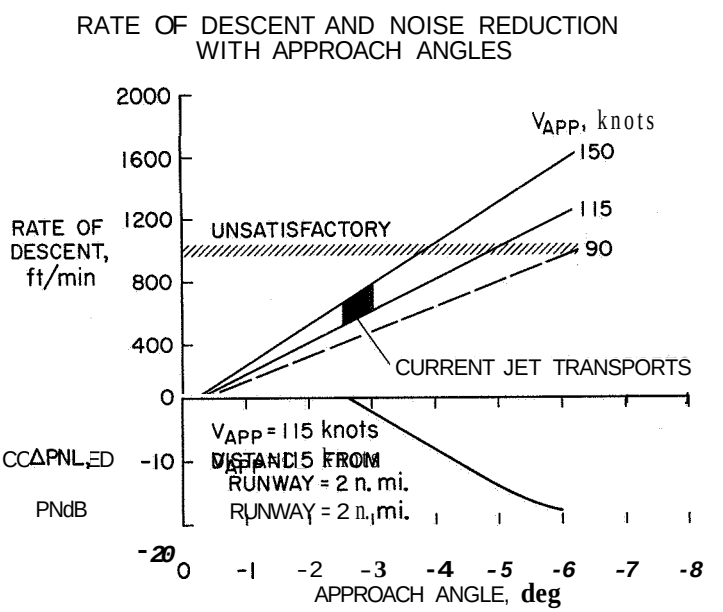

Figure 6

NOISE REDUCTION FOR TWO-SEGMENT APPROACH PROFILES
V_{APP} = 115 knots

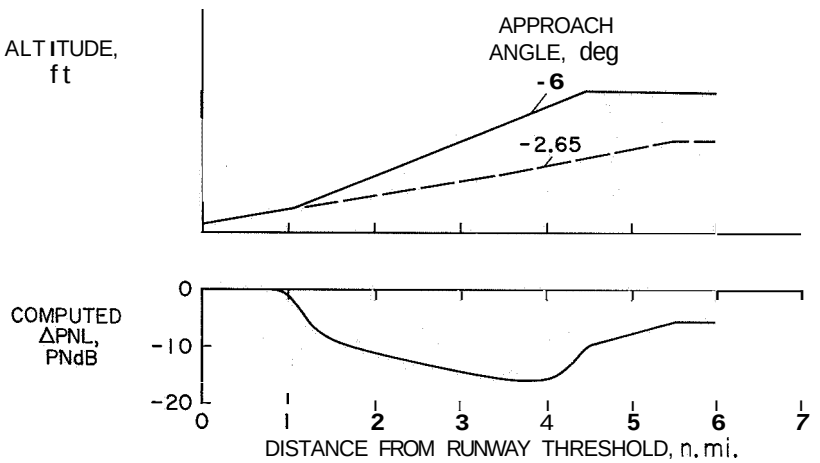

Figure 7

EFFECTS OF INADEQUATE GUIDANCE

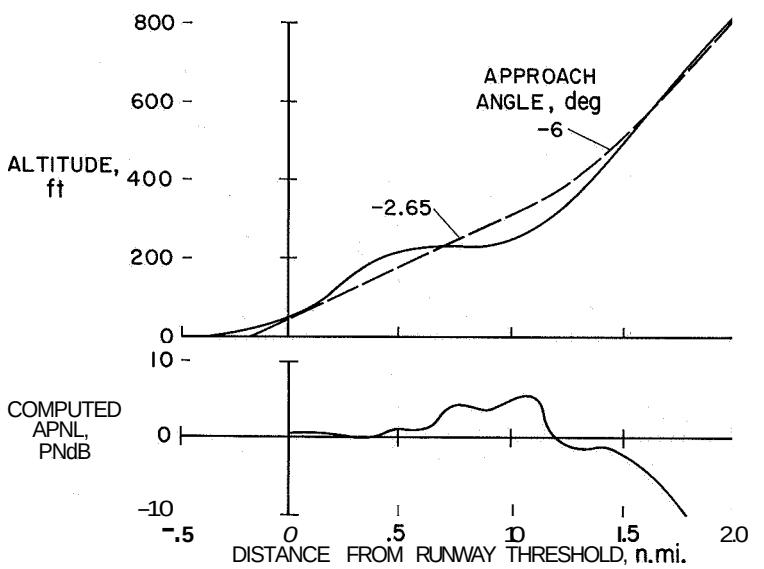

Figure 8

COMPUTED NOISE REDUCTION FOR TEST PROFILES

V_{APP} = 115 knots

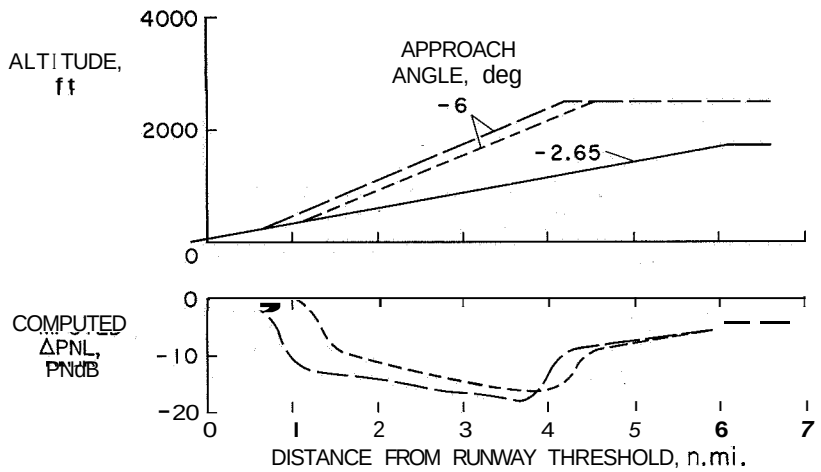

Figure 9

GUIDANCE FOR TWO-SEGMENT **PROFILES**

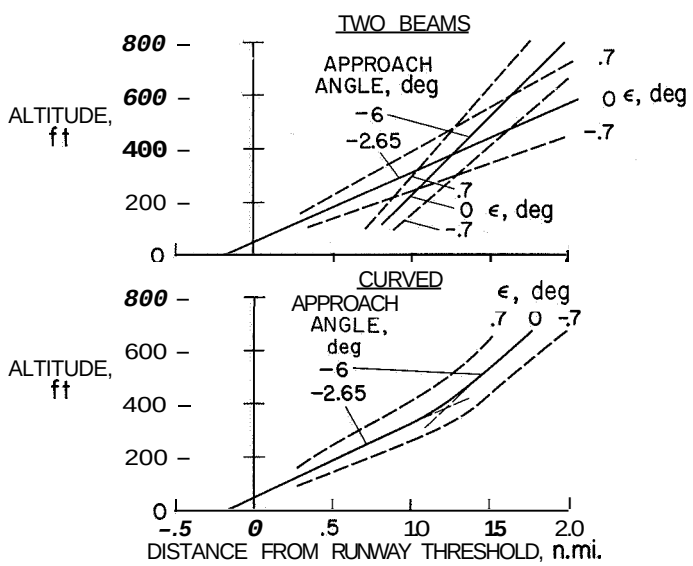

Figure 10

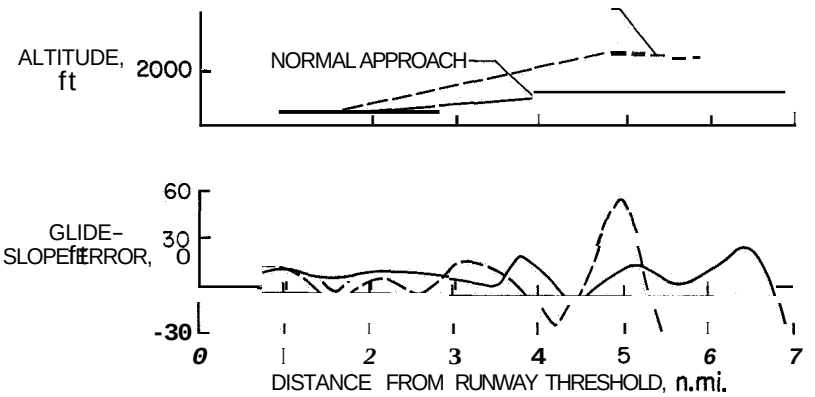
ALTITUDE, ft
2000
NORMAL APPROACH
GLIDE-SLOPE ERROR, ft
60
30
0
-30
0
2
3
4
5
6
7
DISTANCE FROM RUNWAY THRESHOLD, n.mi.

Figure 11

27. TECHNIQUE FOR CALCULATING OPTIMUM NOISE-ABATEMENT TAKE-OFF PROFILES

By Heinz Erzberger, Homer Q. Lee, H. Rodney Peery, and Fred J. Drinkwater III

NASA Ames Research Center

SUMMARY

An analytical technique has been developed for determining take-off and climbout profiles of jet aircraft that minimize the noise in a noise-sensitive area near an airport. Because the technique is analytical, it is especially suited to the study of the effect of such factors as engine noise characteristics, location of noise-sensitive area, and operational constraints on the optimum profile for noise abatement.

Two important elements of the technique are the division of the ground track of the profile into a section near the airport having low sensitivity to noise, followed by one that is noise sensitive, and the formulation of a criterion for comparing the noisiness of different profiles. The criterion used in this study was the average perceived noise along the noise-sensitive section of the ground track. Any other criterion could be used instead.

The technique was applied to the calculation of optimum profiles for a typical currently inservice jet transport. Although the complete specification of the profiles generally depends on the noise characteristics of the engines and on other factors, the optimum profiles calculated herein can be characterized by a period of acceleration as soon as possible after take-off, followed by a steep climb, which in turn is followed by thrust reduction when the noise-sensitive area or a specified altitude is reached. Before the transition from accelerating to climbing, the optimum profiles achieved an airspeed that permitted full retraction of flaps. This acceleration caused some altitude loss at the beginning of the noise-sensitive area, but the disadvantage of a slightly lower altitude can be outweighed by the advantage of greater thrust reduction that is possible in the clean airplane configuration. Thus, in the trade off between airspeed and altitude, gaining airspeed until it is permissible to retract flaps can be more important than gaining altitude, if the objective is to minimize the average perceived noise along the noise-sensitive ground track.

A piloted fixed-base simulation of take-off profiles demonstrated the reduction in average perceived noise that is possible with the optimum climbout profile. No unusual difficulties in flying this profile on the simulator were encountered by the pilot.

INTRODUCTION

In this paper a technique is developed for determining take-off and climbout profiles of jet aircraft that minimize the flyover noise in a noise-sensitive area located near an airport. The technique offers an analytical approach to the take-off noise minimization problem and differs therein from earlier work on this problem which consisted mainly of analyzing noise signatures obtained from flight testing preselected take-off profiles (refs. 1 and 2). The paper emphasizes the mathematical formulation of the problem and the interpretation of results in terms of basic aerodynamic theory and the properties of jet noise. This analysis yields an improved understanding of the interplay between the many factors that affect flyover noise and offers to reduce considerably the amount of flight testing needed to establish noise-abatement procedures.

The analytical technique developed in this paper for calculating take-off profiles that minimize flyover noise was closely guided by methods found in optimum-control theory. Thus, the development of the technique begins with a description of the take-off profile problem; then a numerical criterion for the noisiness of a take-off profile is formulated. The proposed criterion requires calculation of perceived noise level. For turbojet noise, the noise prediction method of the Society of Automotive Engineers (SAE) can be utilized, but for turbofan noise, measured noise data must be used until more accurate analytical methods for predicting fan noise become available.

By means of the dynamic programing algorithm programed on a digital computer, take-off profiles that minimize the chosen noise criterion are generated. These optimum profiles are then simplified in order to make them easier to fly along. Simplified optimum profiles are calculated for both turbofan- and turbojet-powered aircraft.

In order to keep the computational difficulties associated with the optimum-profile calculations within manageable bounds, it was necessary to use simplified equations of motion for the aircraft. The effect of these simplifications as well as the pilot's ability to fly along the profiles were evaluated in a piloted simulator study,

SYMBOLS

C_D	drag coefficient
C_L	lift coefficient
F	total thrust, pounds force

F_i total thrust used to compute noise in ith segment of noise-sensitive section of ground track, pounds force

g acceleration of gravity, 32.2 feet/second^2

h altitude, feet

h_i altitude used to compute noise in ith segment of noise-sensitive section of ground track, feet

i integers representing segments of noise-sensitive section of ground track

J performance function

L total number of small segments of the noise-sensitive section of ground track

$N = 2^{(Z-40)/10}$

S wing reference area, feet2

$\Delta t_i = \frac{\Delta x}{V_i}$

Δt_{ref} reference time for duration of noise perceived in each short segment of noise-sensitive section of ground track, seconds

V airspeed, knots

V_2 take-off safety speed, knots

V_i airspeed used to compute noise in ith segment of noise-sensitive section of ground track, knots

W gross take-off weight (GTOW), pounds

x distance along ground track, feet

Δx length of each short segment of noise-sensitive section of ground track, 750 feet

Z	perceived noise level, PNdB
α	angle of attack, radians
γ	flight-path angle, degrees
δ	flap-deflection angle, degrees
ρ	air density, slugs/foot^3

ANALYSIS

Description of Take-Off Profile Problem

For the purposes of this study, the ground track corresponding to the take-off and climbout path of an aircraft consists of two major sections. The first section, which is assumed to have low sensitivity to noise but which could have a limitation on maximum sideline noise, begins at brake release and ends at the beginning of the noise-sensitive area. Typical values for its length are 3 to 5 miles.

The section of the ground track that traverses the noise-sensitive area is designated as the second section, and it is typically 4 to 8 miles long. The length of both sections generally depends on conditions existing at a particular airport. A complete take-off and climbout path showing the location of the two sections along the ground track is illustrated in figure 1.

The entire ground track is taken to be a straight line parallel to the runway. This assumption is justified whenever the noise-sensitive area cannot be avoided by early turning maneuvers either because of unfavorable terrain or because the airport is closely surrounded by populated areas, all sensitive to noise.

In simplest terms, the objective of the study is to determine the flight path, subject to the operating limits of the aircraft, that is least annoying to people living in the noise-sensitive area. In determining this optimum flight path one must take into consideration the assumption that the ground track is composed of two adjacent sections, one having low sensitivity to noise and the other being noise sensitive. The implication is that the flight path cannot be optimized independently for each section since the flight path over the first section strongly affects the noise over the second section through the altitude, airspeed, and power setting at the beginning of the second section.

Mathematical Criterion for Noisiness of Profile

Application of optimum-control theory to the noise problem requires the defining of a performance function or noise criterion to be minimized by the take-off profiles. An obvious requirement of the performance function is that it be closely related to the perceived noise level in the noise-sensitive area, but this restriction still permits considerable latitude in its selection. For instance, one could simply establish as the noise criterion the perceived noise level in units of PNdB measured at the boundary of the noise-sensitive area (point B in fig. 1 as well as in subsequent figs.) after thrust has been reduced to meet some specified flight condition. This performance function has the advantage of simplicity and would be adequate if the noise-sensitive area were concentrated at a single point on the ground track. However, if the noise-sensitive section of the ground track is several miles long, as it is at most airports, minimizing the-noise at only a single point may be unrealistic since this procedure discriminates against other points along the noise-sensitive section.

The performance function defined below attempts to overcome the difficulty with measuring the noise at only a single point by averaging the noise levels perceived along all points of the noise-sensitive second section. An approximate but sufficiently accurate method for computing the average noise along the second section is to divide this noise-sensitive section into L short segments, to compute the maximum flyover noise for each segment, and then to average these values. Except for the factor $\sqrt{\frac{\Delta t_i}{\Delta t_{ref}}}$, which models the duration effects and which is discussed in greater detail subsequently, the essential content of the performance function is

$$J = 10 \log_2 \frac{1}{L} \sum_{i=1}^{L} N\left(F_i, h_i, V_i\right) \sqrt{\frac{\Delta t_i}{t_{ref}}} \tag{1}$$

The quantity N rather than Z is used in equation (1) because it puts heavier penalty on high noise levels than the logarithmically dependent Z does, and also because it is convenient computationally.

It is well known that the subjectively judged noisiness of a sound depends not only on acoustic power and spectral content but also on duration (ref. 3). The complete relationship between duration and perceived noise is too complex to be considered herein, but an approximation sufficient for the purpose of this study is to assume that doubling the exposure time of a noise increases the perceived noise level by 5 PNdB. Since the values of N entering into equation (1) are antilogarithmically related to the perceived noise level in PNdB units, the equivalent operation on them for a 5-PNdB increase per

doubling of duration is multiplication by $\sqrt{\frac{\Delta t_i}{\Delta t_{ref}}}$. The reference duration Δt_{ref} is arbitrary in this study, since it affects J only by a constant and thus has no influence on the determination of the profiles.

Method for Computing Perceived Noise

The performance function discussed in the previous section requires calculations of the perceived noise level as a function of thrust, altitude, and airspeed. For turbojet noise, the SAE noise prediction method described in references 4, 5, and 6 is employed to perform these calculations with the use of parameters of a typical turbojet engine. This method is reasonably accurate for predicting the maximum flyover noise for turbojet engines with standard exhaust nozzles. Fortunately, high accuracy in predicting noise levels is not needed in this study, since in minimizing such functions as the performance measure for noisiness, the absolute value of the function to be minimized is irrelevant. The important items in the minimization are the trade offs among the factors of thrust, altitude, and airspeed that enter into the evaluation of the function, Hence, a model for jet noise that preserves these trade offs, as the SAE model does, is sufficient.

For profile calculations involving turbofan noise, however, the currently available SAE noise prediction method, even with refinements introduced specifically to model the fan-generated noise, is inadequate. Comparison with measured turbofan noise data has often shown considerable error both in the absolute value of the calculated noise and in the accuracy of the trade offs between altitude and thrust. As just pointed out, it is the latter type of error that prohibits the use of this method for optimum-profile calculations. Instead, measured noise data as functions of thrust and altitude for a currently inservice turbofan were used directly. These data are reproduced in figure 2. The effect of changes in airspeed on noise, which is not given in figure 2, was assumed to be the same as for turbojet noise calculated by the SAE prediction method.

Since the optimum profiles are influenced mainly by the trade offs in the noise measure among altitude, thrust reduction, airspeed, and duration, it is instructive to tabulate the change in perceived noise caused by a doubling of each of these quantities. The following table shows the results for turbojet- and turbofan-generated noise:

Factors affecting flyover noise	Change in perceived noise caused by doubling of quantity, PNdB, for –	
	Turbojet	Turbofan
Thrust	9 to 15	4 to 9
Altitude	-9	-9
Airspeed	-2 to -8	Unknown
Duration	2 to 6	2 to 6

Particularly noteworthy is the fact that sensitivity of the noise to thrust changes is considerably higher for turbojets than for turbofans. This difference in noise characteristics of the two engine types has some effect on the optimum-climbout procedures.

Equations of Motion and Method for Computing Optimum Profiles

In order to evaluate the noise criterion described previously, one must be able to generate histories of altitude and airspeed along the ground track corresponding to a specific take-off procedure. In this study, it is convenient to describe a take-off procedure by giving the thrust, the flight-path angle, and the flap-deflection angle as functions of the distance along the ground track. These three quantities are the only control variables that need to be considered, since the ground track of the climbout is assumed to be a straight line, with lateral control maneuvers therefore excluded. The equations of motion are then given as

$$\frac{dV}{dx} = \frac{g}{WV\cos\gamma}\left[F\cos\alpha - \frac{1}{2}\rho SV^2 C_D(\alpha,\delta) - W\sin\gamma\right] \tag{2}$$

and

$$\frac{dh}{dx} = \tan\gamma \tag{3}$$

These equations are in standard form except that x plays the role of the independent variable rather than time, as is usually the case. The angle of attack α, which is needed to solve equation (2), is calculated by solving the following equation for α:

$$\frac{1}{2}\rho SV^2 C_L(\alpha,\delta) - W\cos\gamma + F\sin\alpha = 0 \tag{4}$$

Equation (4) is based on the assumption that the centripetal acceleration during changes in flight-path angle is negligibly small. This equation can be solved for α by approximating $\sin\alpha$ with α and by approximating C_L with a linear function in α and δ. Equations (2) to (4) allow one to generate take-off profiles if the initial altitude and airspeed are specified and if the control variables F, γ, and δ are assigned specific functions of x. However, these equations were used only for generating the part of the profile that begins at a point where the aircraft has reached a 400-foot altitude and the take-off safety speed V_2 (point A in fig. 1). The location of this point can be calculated for a particular aircraft by using the procedure described in its flight manual.

Calculating take-off profiles that minimize the chosen criterion for noisiness can now be interpreted as a problem in optimum control in which the state variables are

airspeed and altitude and the control variables are thrust, flight-path angle, and flap-deflection angle. Solutions of this optimum-control problem were obtained by implementing the dynamic programing algorithm on a digital computer (ref. 7).

RESULTS OF THEORETICAL CALCULATIONS

General Properties of Optimum Profiles

Optimum profiles computed for the previously introduced noise criterion have been found to depend strongly on the engine type (whether turbojet or turbofan), on the length of the first and second sections of ground track, and on operational constraints. Although influenced by many variables, an optimum profile, represented herein as a history in altitude-airspeed coordinates, typically has the form shown in figure 3. For the purposes of this study, the optimum profile is assumed to begin at a point, marked A in figure 3, where the aircraft has achieved the take-off safety speed V_2 and a 400-foot altitude, since before reaching this airspeed and altitude no unusual maneuvers are permitted. Thus, starting at point A, the aircraft accelerates in level flight until a certain climb speed, which is often close to the minimum drag speed, has been attained. During this acceleration period, flaps are retracted as soon as the minimum speed for flap retraction is achieved. After the acceleration period, the aircraft enters a steep climb that is essentially constant until a point just ahead of the noise-sensitive area, At that point, the climb steepens to become a decelerating climb. Then a large power reduction occurs as the noise-sensitive area is penetrated at point B. The remainder of the profile, although depending somewhat on the length of the second section of the ground track, consists of a slightly decelerating climb at the minimum permissible power setting.

Profiles that minimize the perceived noise only at the beginning of the noise-sensitive area (point B), although not shown herein, have similar characteristics. In such profiles, the climb speed has been found to depend more strongly on the length of the first section than in the previously discussed profiles; here the climb speed decreases and eventually approaches V_2 as point B moves toward point A.

Simplification of Optimum Profiles

In assessing the practical value of noise-optimum profiles, one must consider the difficulty that a pilot would experience in flying along them and the number of parameters required to describe them. Examined in this light, the optimum profile shown in figure 3 is too complicated and therefore must be simplified before it can be put to practical use. Such simplification of optimum profiles is found to be necessary in most practical applications of optimal control.

The optimum profile between points A and B consists essentially of a period of maximum acceleration followed by a period of maximum climb. Therefore, a logical choice for a simplified optimum profile would be one that accelerates as fast as possible to a certain airspeed, then climbs at constant airspeed, and finally enters a reduced-power flight near the beginning of the noise-sensitive area. Such a simplified optimum profile is indicated in figure 3 by the dashed line. In effect, this simplified profile needs to be optimized only over two parameters, namely the climb speed and the amount of thrust reduction. The computation is thus simplified, and a profile that is easier for the pilot to fly along is produced.

However, the decisive test of acceptability of the simplified optimum profile is given by the penalty measured in terms of the noise generated by it in comparison with the minimum noise. In all profiles examined, the noise generated by the simplified profile exceeds that of the optimum profile by less than 0.5 dB. Hence, only simplified optimum profiles are presented in the next section, although they are also referred to as optimum profiles.

Minimizing Average Noise Over Noise-Sensitive Area With Altitude Constraints

Profiles that minimize the performance function defined by equation (1) are presented. The profile calculations were performed for a typical large jet transport powered by either turbofans or turbojets at a gross weight of 280 000 pounds. The length of the first section of ground track was chosen as 21 000 feet and that of the second section as 26 000 feet. In the second section, thrust was constrained to be not less than that needed to maintain level, unaccelerated flight at the chosen climb speed. Constraints on the thrust based on maintaining some nonzero rate of climb over the noise-sensitive area have also been investigated and were found to yield similar results. Since operational or safety reasons may dictate that the aircraft first achieve some minimum altitude above ground level before power is reduced in a noise-abatement climbout, the optimum profiles were calculated subject to the constraint that maximum power reduction not take place until an altitude of 1500 feet is attained. However, some power reduction is assumed to take place at point B, even if the aircraft is at a lower altitude, in order not to exceed an upper limit on the perceived noise that is assumed to exist at the beginning of the noise-sensitive area. Thrust after this initial power reduction was taken as 40 000 pounds, which is assumed to satisfy the maximum noise limitation.

In calculating the optimum profiles a search was conducted not only over all climb speeds but also over the amount of thrust reduction after a 1500-foot altitude is achieved in order to find the combination that minimizes equation (1). But it was found that the optimum thrust after final thrust reduction for either turbofans or turbojets was always very close to the smallest thrust allowed by the constraint. It should be pointed out,

however, that for second-section lengths much longer than 5 miles, the optimum thrust after power reduction does increase above the smallest value allowed by the constraint.

Figure 4 shows optimum profiles for turbofan- and turbojet-powered aircraft and also a nonoptimum profile consisting of a steep climbout with maximum take-off flaps. The optimum profiles, which at initial penetration of the noise-sensitive area obviously produce more noise than the steep-climbout profile, nevertheless produce a lower average noise value. The chief reason is the fact that with fully retracted flaps, considerably less thrust is required to maintain level, unaccelerated flight than with 25° take-off flaps. As mentioned previously, noise produced by an overflight of a jet aircraft depends very strongly on the amount of thrust developed by its engines, along with the altitude and airspeed of the aircraft. Thus, acceleration to airspeeds at which flaps can be retracted, even at the expense of some altitude loss, permits flight at lower thrust levels than is possible with take-off flaps and thereby helps to reduce the noise. In addition to the effect of airspeed and flap setting on noise through the influence of these factors on thrust reduction, an increase in airspeed also helps to reduce the perceived noise by decreasing its duration, The computed profiles in figure 4 optimize the trade off between using the available thrust to gain altitude, on the one hand, and to gain airspeed, on the other, so that the average noise level produced along the noise-sensitive section of the ground track is minimized. The steep climbout profile attains the minimum altitude of 1500 feet just as the noise-sensitive area is penetrated at point B and, therefore, immediately permits maximum power reduction to take place. The optimum profiles, however, first accelerate to the indicated climb speeds, then climb at full power as far as the noise-sensitive area and continue to climb at reduced power to 1500 feet, where the final power reduction occurs. The values of thrust used on the three profiles after power reduction has occurred are given in figure 4.

Figure 4 also gives the differences between the values of the performance function (eq. (1)) obtained for the steep-climbout profile and those obtained for the optimum profiles. The noise reduction is higher for the turbojet than for the turbofan because of the greater effect of thrust reduction on turbojet noise.

The profiles as well as the reductions in average noise level given in figure 4 are based on the performance of a large, currently inservice jet transport and on representative noise characteristics of jet engines. These data are presented herein to illustrate the theory and could easily be recalculated for specific aircraft and airport conditions.

SIMULATION RESULTS

This section describes the results of flying noise-abatement profiles on a fixed-base simulator for a large jet transport. Flying the profiles on a simulator was thought

to provide an independent means of checking the basic theory developed herein and to uncover difficulties that a pilot may encounter in flying along the optimum profiles. A gross weight of 300 000 pounds was simulated in this study.

The performance function was again assumed to be the average perceived noise along the second ground-track section. In agreement with current operational thinking, an altitude constraint of 1500 feet was again placed on the initial point for power reduction. However, in the theoretical study, thrust after final power reduction could be as low as necessary to maintain level flight at constant airspeed, whereas in the simulation, the pilot's goal after achieving a 1500-foot altitude was a throttle setting that would yield a 500-ft/min rate of climb and would thereby ensure a positive climb gradient over the noise-sensitive area. This positive climb gradient is desirable for operational and safety reasons.

The noise-level calculations performed in the simulation were based on the turbofan noise data given in figure 2. The perceived noise level calculated from this figure was reduced by 1.5 PNdB for the optimum profile in order to account for airspeed and duration differences between the steep-climbout and optimum profiles.

The profiles are shown in figure 5; one is a steep-climbout noise-abatement profile described previously, and the other is a typical pilot's approximation of an optimum profile. The beginning of the noise-sensitive area was assumed to be located at point B, 29 000 feet from brake release, where the steep-climbout noise-abatement profile achieves a 1500-foot altitude. Figure 5(a) shows that the optimum profile requires an additional distance of 2500 feet *along* the ground track to achieve the same altitude. This distance is the penalty for accelerating from V_2+18 knots, with 25° flaps used on the steep-climbout profile, to V_2+50 knots, with retracted flaps used on the optimum profile. As expected, along this section of the ground track the perceived noise is higher for the optimum than for the steep-climbout profile (see fig. 5(c)). However, once the aircraft reaches 1500 feet on the optimum profile, the pilot reduces the thrust 28 percent more than on the steep-climbout profile, as shown in figure 5(b). This greater thrust reduction causes the noise level to drop and remain below that of the steep-climbout profile for the remaining 24 000 feet of the noise-sensitive area.

Generally, the pilot encountered no exceptional difficulty in flying along the simplified optimum profiles. However, practice did improve his timing in initiating flap retraction and his accuracy in setting the throttles for a 500-ft/min rate of climb.

CONCLUDING REMARKS

A rational technique for determining take-off and climbout profiles that minimize the annoyance from jet take-off operations in communities located along the climbout

path has been established. What distinguishes this technique from others used in the past is the mathematical formulation of the problem and its solution by purely analytical methods. The technique permits computation of optimum take-off trajectories for a particular aircraft operating from a particular airport subject to prescribed operational constraints.

A mathematically defined criterion for noisiness of a take-off procedure was formulated and then used as a basis for arriving at noise-optimum profiles. The criterion was taken as the average noise level, including a penalty on the duration of the noise, produced by an overflight of a noise-sensitive area. Any other criterion can be easily used instead.

The technique was applied to the calculation of optimum take-off profiles for a typical large jet transport. Although the optimum profiles were found to depend upon many factors, such as the noise characteristics of the jet engines and the length of sections of ground track, some generally valid properties of the profiles can be discerned. The optimum profiles calculated have a period of acceleration as soon as possible after take-off, followed by a steep climb, which in turn is followed by thrust reduction when the noise-sensitive area or a specified altitude is reached. Before the transition from accelerating to climbing, the optimum profiles achieve an airspeed that permits full retraction of flaps. This acceleration causes some altitude loss at the beginning of the noise-sensitive area, but the disadvantage of a slightly lower altitude can be outweighed by the advantage of greater thrust reduction that is possible in the clean airplane configuration. Thus, in the trade off between airspeed and altitude, gaining airspeed until it is permissible to retract flaps can be more important than gaining altitude, if the objective is to minimize the average noise along the noise-sensitive ground track.

A piloted fixed-base simulation of take-off profiles demonstrated the reduction in average perceived noise that is possible with the optimum climbout profile. No unusual difficulties in flying along this profile were encountered by the pilot.

REFERENCES

1. Copeland, W. Latham; Hilton, David A.; Huckel, Vera; Dibble, Andrew C., Jr.; and Maglieri, Domenic J.: Noise Measurement Evaluations of Various Take-Off - Climbout Profiles of a Four-Engine Turbojet Transport Airplane. NASA TN D-3715, 1966.

2. Galloway, W. J.; Pietrasanta, A. C.; and Pearsons, K. S.: Study of the Effect of Departure Procedures on the Noise Produced by Jet Transport Aircraft. ADS-41, FAA, Oct. 1965.

3. Pearsons, Karl S.: The Effects of Duration and Background Noise Level on Perceived Noisiness. ADS-78, FAA, Apr. 1966.

4. Anon.: Definitions and Procedures for Computing the Perceived Noise Level of Aircraft Noise. ARP 865, Soc. Automot. Eng., Oct. 15, 1964.

5. Anon.: Jet Noise Prediction. AIR 876, Soc. Automot. Eng., July 10, 1965.

6. Lee, Robert; Farrell, James; Henry, George; and Lowe, Albert: Procedures for Estimating the Effects of Design and Operational Characteristics of Jet Aircraft on Ground Noise. NASA CR-1053, 1968.

7. Bellman, Richard: Dynamic Programming. Princeton Univ. Press, 1957.

TWO-SECTION CLIMBOUT

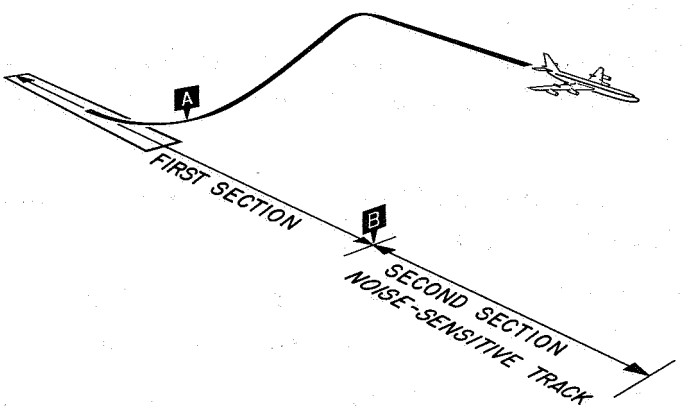

Figure 1

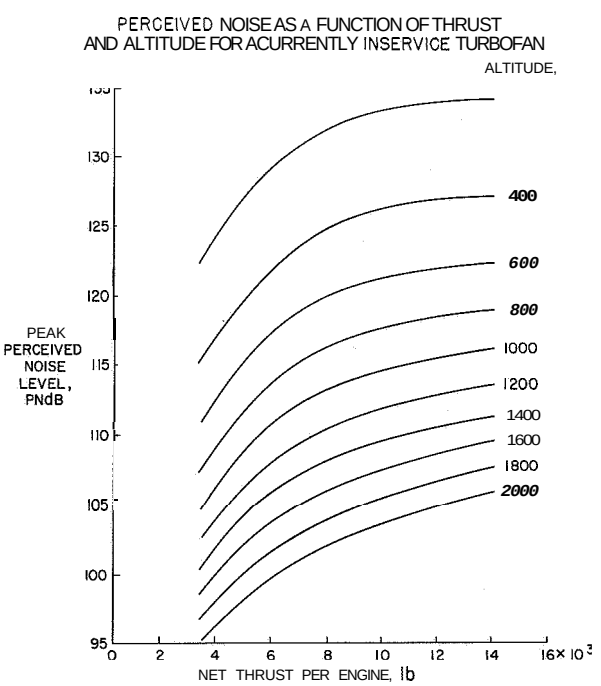

Figure 2

OPTIMUM AND SIMPLIFIED OPTIMUM PROFILES

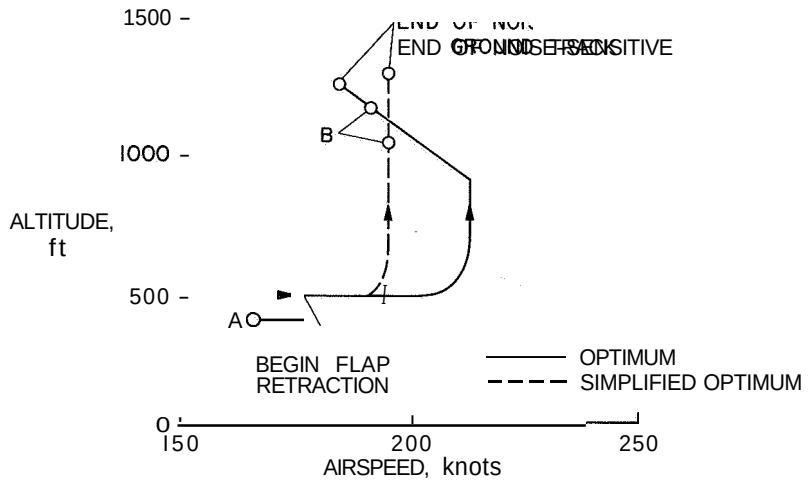

Figure 3

OPTIMUM PROFILES WITH 1500-ft ALTITUDE CONSTRAINT

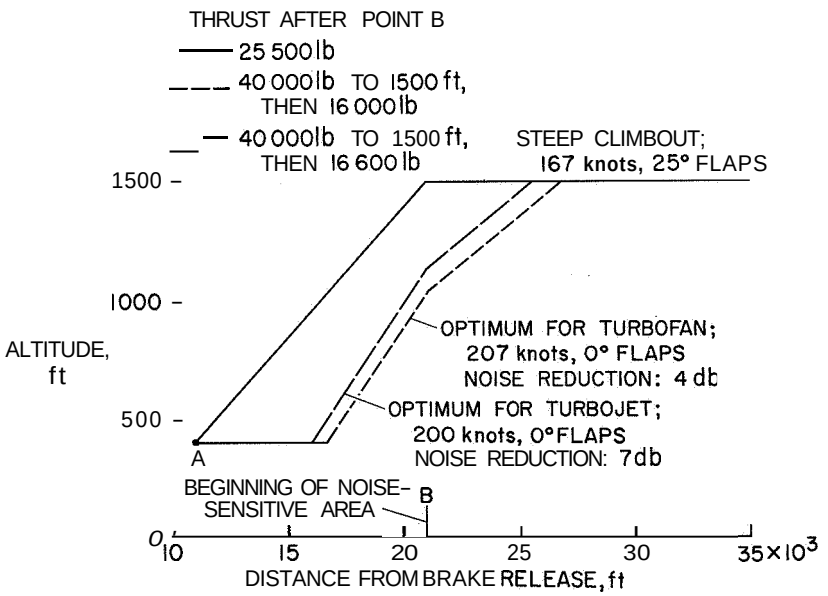

Figure 4

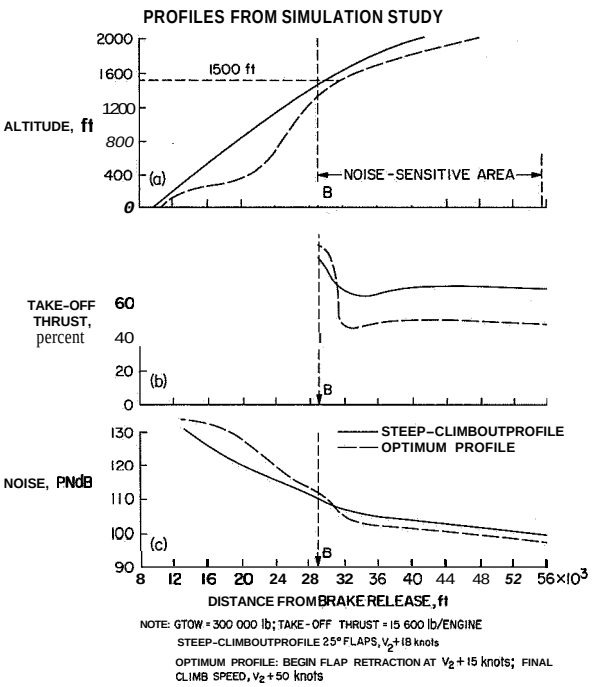
PROFILES FROM SIMULATION STUDY
ALTITUDE, ft
2000
1600
1200
800
400
0
1500 ft
(a)
NOISE-SENSITIVE AREA
B
TAKE-OFF THRUST, percent
60
40
20
0
(b)
B
NOISE, PNdB
130
120
110
100
90
(c)
B
STEEP-CLIMBOUTPROFILE
OPTIMUM PROFILE
8 12 16 20 24 28 32 36 40 44 48 52 56×10³
DISTANCE FROM BRAKE RELEASE, ft
NOTE: GTOW = 300 000 lb; TAKE-OFF THRUST = 15 600 lb/ENGINE
STEEP-CLIMBOUTPROFILE 25° FLAPS, V2+18 knots
OPTIMUM PROFILE: BEGIN FLAP RETRACTION AT V2+15 knots; FINAL CLIMB SPEED, V2+50 knots

Figure 5

28. PROCEDURES FOR ESTIMATING THE EFFECTS OF DESIGN AND OPERATIONAL CHARACTERISTICS OF JET AIRCRAFT ON GROUND NOISE

By James H. Farrell

Conesco Division of Flow Corporation

SUMMARY

Procedures have been developed for estimating the effects of design and operational characteristics of jet aircraft on ground noise including various engine-cycle parameters, aircraft-design characteristics, and aircraft-flight characteristics. Parametric plots have been prepared to show how these different interrelated factors influence noise; and, when possible, assessments have been made of the accuracies and limitations of the graphs, nomographs, and equations that have been developed. This paper presents a review of these studies.

INTRODUCTION

One very important aspect of the noise-control problem is that it is a system problem, and any noise reduction, if it is to be attempted at an early design stage, requires knowledge of how various design and operation factors of the engine-airplane system are combined to influence the noise level on the ground. Along with this fact is the consideration that because of the complexity of the problem, noise control will involve the efforts of people who are not experienced acousticians, and it is important that acoustical data and design procedures be put in a form easily understood and used by engineers who do not have acoustical experience.

The present program was organized with these two important considerations in mind. Specifically, it was concerned with the study of how various factors inherent in the design and operation of any engine-airplane system are combined to influence the noise level on the ground. The aim of the program was to identify the various factors of importance and to develop quantitative descriptions of how they are related to noise. A further aim of the program was to develop and present simplified and easy-to-use parametric charts, nomographs, and formulas that might enable designers and others to relate quickly and directly the important engine and airplane design parameters to noise.

A detailed report of the program is presented in reference 1; this paper is a synopsis of that report.

SYMBOLS

A	exhaust nozzle area, compressor flow area, humidity-absorption coefficient
C_D	drag coefficient
C_L	lift coefficient
$C_{\hat{L}}$	maximum lift coefficient
CPR	overall cycle pressure ratio
F_n	net thrust of aircraft
FPR	fan pressure ratio
H	distance of closest approach
PNdB	unit of perceived noise level (PNL)
PNL	perceived noise level
P_r	nozzle pressure ratio
Q	log of ratio of perceived noise to thrust, $PNdB_O - 10 \log F_n$
S	wing reference area, initial distance between observer and aircraft
S'	ground-roll distance
S_o	distance to observer from starting roll position
SFC	specific fuel consumption
T	net thrust of aircraft
T_t	nozzle total temperature
T_4	turbine inlet temperature

V or V_0 aircraft velocity

W weight of aircraft

β bypass ratio

γ flight-path inclination

INFLUENCING FACTORS

The factors that influence the noise at specific ground locations are as follows: First, the engine-noise source can vary in sound-power level, spectrum shape, and directionality pattern, depending upon the engine-design characteristics. Second, the distance between the noise source and the ground observer depends upon aircraft-design characteristics and the chosen flight paths, and third, the noise-attenuation characteristics of the air depend upon such things as temperature and moisture content. This program has been concerned with the interrelation of these factors, and an effort has been made to show how the existing knowledge of jet-engine noise can be used to develop explicit relations among these factors. The work has been primarily analytical, and much experimental verification is needed to establish accuracies. The program has included the following efforts:

(1) Noise-prediction procedures for jets and compressors have been established. This program has involved

(a) A review of "SAE" method of predicting jet-exhaust noise and the development of a direct method for estimating jet perceived noise levels (PNL)

(b) The development of a procedure for calculating the initial perceived noise levels (PNL_0) of combined jets in fan engines

(c) The modification of several suggested compressor noise-prediction methods into one unified method

(2) An analytical investigation of noise as a function of engine-cycle parameters for jet and fan engines has been performed, The parameters considered include:

Nozzle parameters:

Exhaust velocity
Density
Total temperature
Pressure ratio
Weight flow
Nozzle area

Fan parameters:

Tip velocity
Weight flow

Cycle parameters:

Cycle pressure ratio
Fan pressure
Turbine inlet temperature
Bypass ratio

Parametric plots have been prepared that show how jet and fan noise vary as these different parameters are changed.

(3) Several simplified calculational methods have been developed for determining PNL for various situations including:

(a) Jet and compressor noise PNL from overall sound-pressure level

(b) PNL of the combined jet and compressor noise from individual PNL values

(c) Prediction of the variation of PNL with distance for jet, compressor, and jet combined with compressor noise

(4) An analytical investigation has been made of aircraft separation distances and, hence, noise as a function of design and flight characteristics. The parameters considered include wing loading $\frac{\text{Weight}}{\text{Wing reference area}}$; drag-weight ratio $\frac{\text{Drag}}{\text{Weight}}$; power loading $\frac{\text{Thrust}}{\text{Weight}}$; and maximum lift coefficient of wing $C_{\hat{L}}$.

Parametric plots have been made relating these parameters to ground noise.

(5) Both graphical and analytical procedures have been developed for establishing ground noise at specific points or over specific areas when an aircraft is in flight. The graphical procedure allows direct comparisons of ground PNL contours for different flight paths.

(6) To show what can be done with some of the methods that have been developed, PNL contours, magnitudes of ground areas as functions of PNL, and annoyance levels have been calculated for several flight paths, and the results have been compared.

To illustrate the work, consider the following examples from the program.

Engine-Cycle Parameters and Noise

Engine-cycle parameters can be related to jet-exhaust noise by use of the SAE method of predicting jet noise. In this method, the engine-reference noise level is a function of the exhaust density, the exhaust nozzle area, and the relative velocity between the

jet exit velocity and the aircraft speed. The three variables – density, nozzle area, and jet velocity – can be related to such parameters as nozzle-pressure ratio, nozzle total temperature, overall cycle pressure ratio, turbine inlet temperature, and engine size (represented by either area, thrust, or weight flow); thus, the engine-reference noise level can be given directly as a function of these variables. Once the reference noise level is known, perceived noise levels can be determined. Figure 1 shows a plot of sideline perceived noise levels as functions of pressure ratio, total temperature, area, and aircraft velocity. This particular graph is plotted for an area of 5 square feet. If there is a total temperature of 1200° F, a pressure ratio of 2.5, and the aircraft is traveling at 300 ft/sec, then the reference PNdB is 130. As can be seen, such graphs can be conveniently used by engine designers, and the values obtained are within 1/2 dB of what would be obtained by a calculation using the SAE method.

In the case of compressor noise, there is no standard calculational procedure available for determining sideline noise; however, several empirical methods have been combined to give results that are accurate to about ±6 dB, and which can give qualitative information on noise trends. Figure 2 shows how such variables as bypass ratio, fan pressure ratio, turbine inlet temperature, and specific aircraft velocities are related to a noise parameter Q which has been defined as the log of the ratio of perceived noise to thrust and which is an expression of the amount of perceived noise per pound of thrust. Figure 2 is for an aircraft velocity of 200 ft/sec; other graphs for three other velocities have been developed.

Even though figure 2 is representative of trends, some interesting results are obtained by relating the cycle variables to noise and an important factor such as specific fuel consumption. Specific fuel consumption is directly related to the parameters: bypass ratio, flow-pressure ratio, cycle pressure ratio, and turbine inlet temperature. Figure 3 shows a sample graph of the noise parameter Q as a function of specific fuel consumption for various combinations of engine parameters. It can be seen that a low Q is generally associated with a low specific fuel consumption. From a consideration of several such graphs, it appears that in optimum high-bypass-ratio designs, the compressor noise per unit flow, the jet noise Q, and the specific fuel consumption all tend to be minimized and, thus, on an equal thrust basis, high-bypass-ratio designs are favorable for both noise and economy.

Airframe Design and Noise

Aerodynamic design of an airframe can indirectly influence the amount of noise received on the ground in several ways: (1) by affecting the flight path relative to the observer, and hence the distance between the observer and the noise source, (2) by affecting the engine-power requirement at various modes of take-off and landing operations, and hence the noise-source intensity, and (3) by affecting the aircraft speed

characteristics which, in turn, affect both the noise source characteristics and the exposure time of the observer to the noise.

Airframe design parameters that are of special importance in noise studies include the gross weight W, wing reference area S, coefficients of lift and drag C_L and C_D at various airplane flap configurations, and the thrust T. Once these parameters or their limiting values are adequately defined, it is generally possible to establish the limits in flight path, power setting, and speed within which the airplane can operate.

For a powerplant operating at a specific power setting during take-off, the most important variable which determines the noise level experienced by an observer on the ground is the minimum separation distance between the observer and the flight path. This minimum separation distance is denoted by the symbol H. If the observer is directly under the flight path and the climb angle of the aircraft is not very steep, the minimum separation distance is almost exactly equal to the altitude of the aircraft when directly overhead.

Figure 4 is a schematic diagram of a take-off where the climb angle is given by γ, the closest approach distance between the observer and the plane is given by H, and the equivalent ground-roll distance is given by S'. Equivalent ground-roll distance can be empirically related to such aircraft-design parameters as weight, thrust, wing area, and maximum lift coefficient, whereas the climb angle y is related to thrust, drag, and weight. It is thus possible to express the distance of closest approach in terms of the distance between the observer and the starting roll position S_0 and various airframe-design parameters. If an observer is considered to be at the 3-mile point (so that S_0 is known), then the distance of closest approach can be expressed solely in terms of design parameters, and it is now possible to calculate the maximum noise level at the 3-mile point, only the airframe parameters and the engine characteristics being known. This procedure has been followed, the following assumptions being made: (1) the climb-out path of the airplane follows a constant angle of attack, (2) there is a constant speed procedure, and (3) the powerplant design is fixed. Under these conditions, the effect of airframe-design parameters on noise is due simply to their effect on separation distance. For example, figure 5 shows the effect of power loading T/W on the relative PNL (APNdB) for several values of wing loading. This effect is very strong, and increasing the thrust-weight ratio from 0.25 to 0.35 can mean a noise reduction of approximately 5 to 7 PNdB for both jet and compressor noise.

Although the engine noise may be known and the effect of airframe-design parameters on noise may be known, the picture is incomplete if the effect on ground noise of various aircraft maneuvers is not determined. Two methods have been developed for determining the PNdB of an aircraft at selected positions on the ground. The first method is graphical and gives a quick and simple procedure for determining the time

history and magnitudes of PNL at selected ground points. The second method is an analytical method and gives the same answers, but in a form suitable for computer applications. Of central importance in the graphical method is the concept that the aircraft noise field may be considered as fixed and that the ground observer can be considered as moving relative to the stationary aircraft and its noise field. Thus, different observer points and flight paths may be represented by properly oriented flight paths drawn on noise contour maps of the airplane. The analytic method utilizes the concept of the angle of maximum radiation and distance of closest approach to determine the maximum PNL that a ground point experiences. By means of these concepts, a computer program has been written and used to determine the contours of constant PNL produced by various take-off procedures.

The graphical procedure is most useful for showing how variations in the airplane flight path can influence the noise at a specific ground location, whereas the computer analysis is most useful for calculating contour plots of noise levels for various assumed take-off and landing procedures. The graphical procedure is illustrated in figure 6, which shows a typical take-off flight path. To visualize the development of the two-dimensional tracking plot, it is necessary to imagine how a fixed point on the ground appears to an observer in the airplane. In figure 6, at the start, the ground-observation point will be in line with the runway and several miles from the start of the ground roll. Thus, the ground point appears, to the observer, to be approaching along the airplane axis. At rotation, the airplane pitches upward, which causes the ground point to rotate down, as seen by the observer. Thus, the pitch maneuver, if negotiated quickly, can be projected on the plot as an instantaneous rotation of the ground point at constant range. The airplane then continues to climb at a constant rate, and this flight path is a straight line parallel to the axis of the airplane on the noise plot.

As can be visualized, because of the axial symmetry of the noise field around the aircraft, any straight-line flight path will resolve itself into a straight line parallel to the aircraft axis on the noise plot, and each such segment of straight-line flight will have a corresponding distance of closest approach. The effects of a power cutback are also shown in figure 6. As can be seen, before the track reached the point of closest approach and the point of maximum PNL, a rotation at constant slant range has been shown. This rotation corresponds to the downward pitch of the aircraft at power cutback. In this illustration, it has been assumed the power cutback would lower the PNL values of the contour by 10 PNdB. This effect is indicated by the dashed-line sections showing the after-cutback values of the PNL contours. From such a diagram, if the flight velocity is known, the complete time history of the observation point can be constructed.

CONCLUDING REMARKS

The illustrations presented give some idea of what can be accomplished with existing theory. Obviously, what has been done is only a beginning, and it is to be hoped that those engineers who are actively concerned with engine or airframe design or with operational problems will extend the approaches presented in the report so that the prediction of ground noise becomes part of the routine of aircraft design or of flight analysis.

REFERENCE

1. Lee, Robert; Farrell, James; Henry, George; and Lowe, Albert: Procedures for Estimating the Effects of Design and Operational Characteristics of Jet Aircraft on Ground Noise. NASA CR-1053, 1968.

PERCEIVED NOISE LEVEL AS FUNCTION OF PRESSURE RATIO,
TEMPERATURE, AREA, AND VELOCITY

AREA = 5 SQ FT

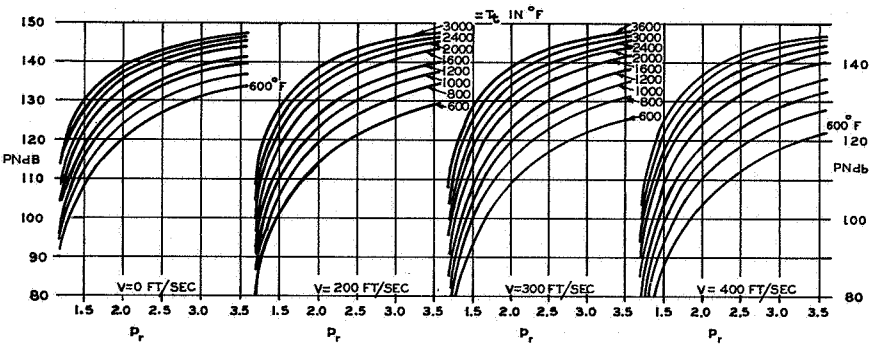

Figure 1

Q AS A FUNCTION OF BYPASS RATIO, FAN PRESSURE RATIO,
TEMPERATURE, AND OVERALL CYCLE PRESSURE RATIO

AIRCRAFT VELOCITY, *200* FT/SEC

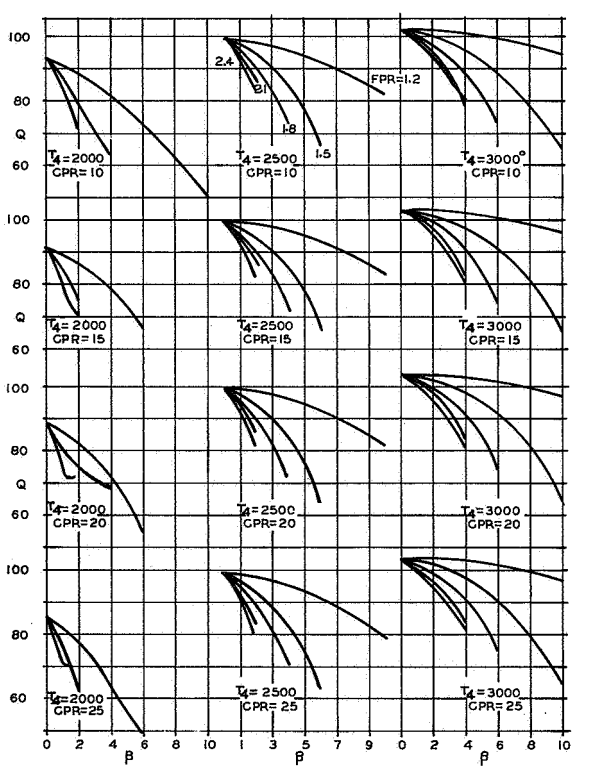

Figure 2

Q AS A FUNCTION OF SPECIFIC FUEL CONSUMPTION FOR VARIOUS OVERALL CYCLE PRESSURE RATIOS, FAN PRESSURE RATIOS, BYPASS RATIOS, AND TEMPERATURE

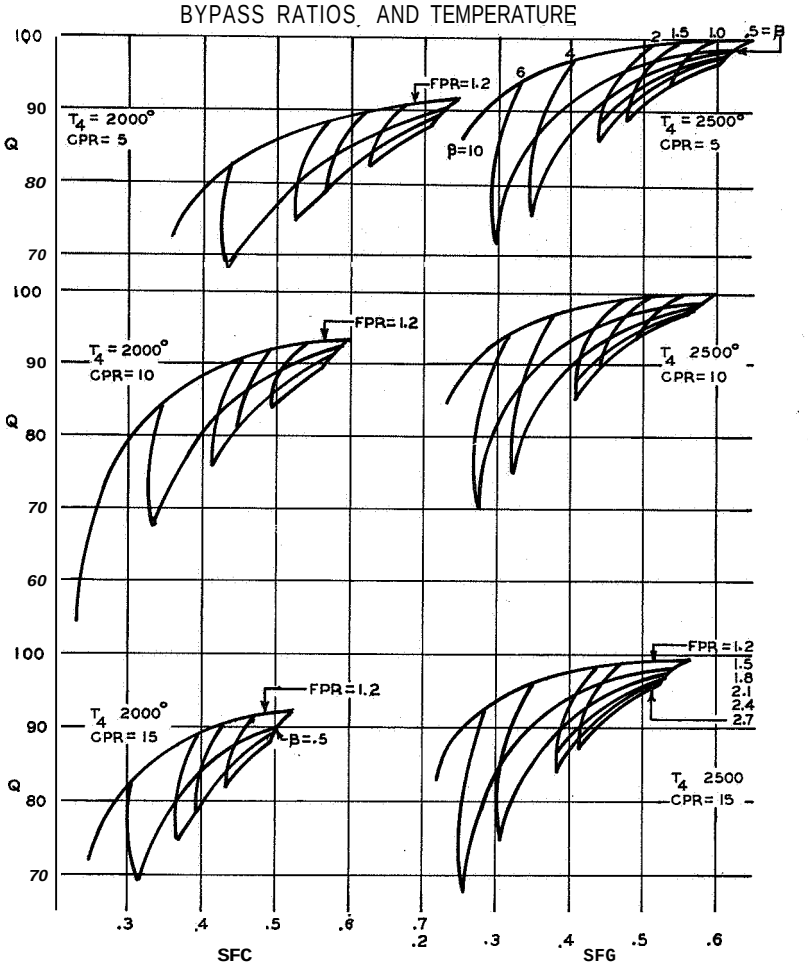

Figure 3

TAKE-OFF SCHEMATIC

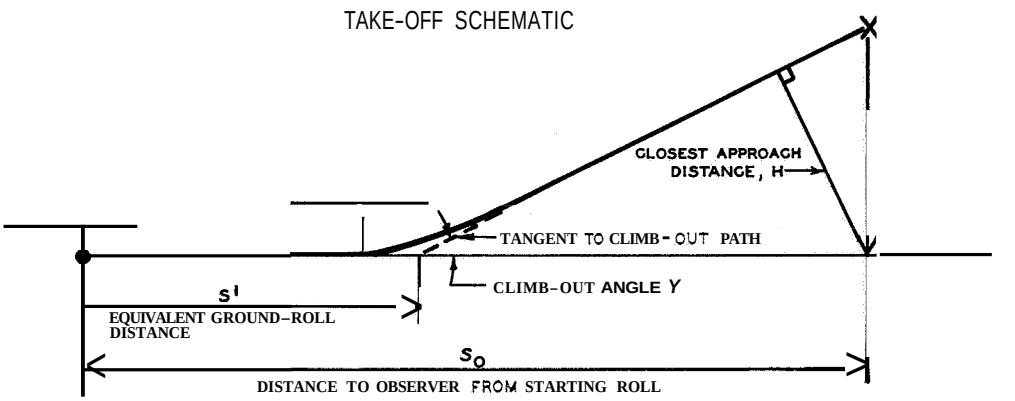

Figure 4

APNdB AS A FUNCTION OF POWER LOADING

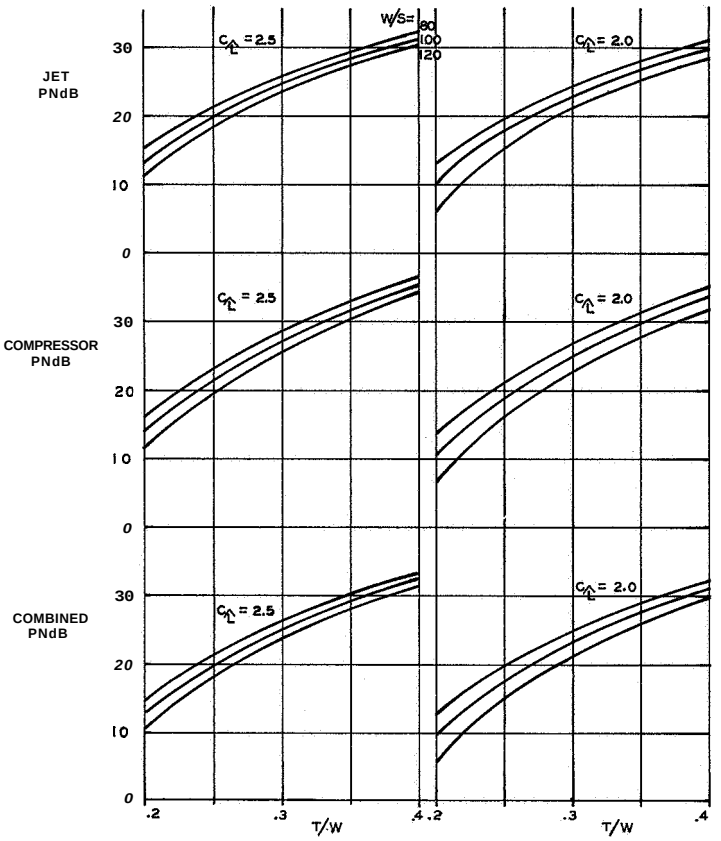

Figure 5

GROUND-TRACK PLOT OF AIRPLANE TAKE-OFF

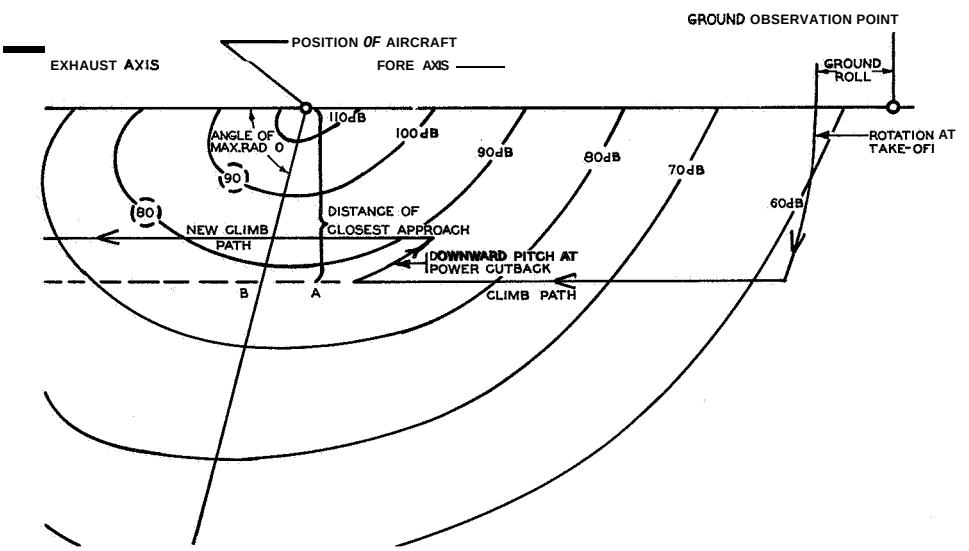

Figure 6

29. PREDICTED AND MEASURED XB-70 GROUND-TO-GROUND ENGINE NOISE

By Norman J. McLeod, Paul L. Lasagna,
and Terrill W. Putnam

NASA Flight Research Center

SUMMARY

Measurements have been made of XB-70 engine noise during ground runs. The effect of engine power settings and engine spacing on the noise spectra during the ground runs is presented. Some of the data obtained during the ground runs were analyzed to determine the amplitude variation, and the effect of averaging time was determined. The SAE method was used to predict the noise levels for various test conditions, and comparisons of predicted and measured spectra are presented.

Tests indicate some limitations for the SAE prediction method. During ground operation of the XB-70 airplane, the amplitude variations in the acoustic data during quasi-stable engine thrust indicate that similar variations might occur when flyover noise spectra are being measured. Atmospheric attenuation predictions were greater than the measured attenuation for the high-frequency octave bands at the specific conditions of these tests.

INTRODUCTION

Because present commercial jet airplanes have caused community reaction to the noise produced, research is being conducted to reduce the noise. Future large jet transports will be equipped with even larger engines, and the engine designer must be able to predict the noise that will be created by the new engines. The Society of Automotive Engineers (SAE) prediction method (refs. 1 and 2), which is widely used, was empirically derived from measurements of smaller jet engines. This method requires knowing the exhaust-nozzle diameter, mass flow, and the exhaust-nozzle exit velocity relative to the free-stream velocity. An investigation was, therefore, carried out at Edwards Air Force Base, California, to determine whether the SAE method would adequately predict the noise created by large jet engines and to determine whether any other problems would develop when measuring or predicting the noise with the XB-70 as a noise source. The tests were a joint program conducted by the U.S. Air Force, North American Rockwell Corporation, General Electric Company, The Boeing Company, and NASA.

This paper presents the results of the comparison of measured noise levels and levels computed with the SAE method and the problems caused by the varying noise levels encountered during supposedly constant engine operating conditions.

TEST AIRPLANE

A photograph of the XB-70 airplane mounted on the Air Force thrust stand, taken approximately 1 month prior to the date on which the data presented in this paper were obtained, is presented as figure 1. Edwards Dry Lake was comparatively dry on the day of the tests. The XB-70 is a large, six-engine, prototype bomber equipped with six YJ93-GE-3 engines installed in the aft part of the fuselage. The engines are approximately 11 feet above the ground. Each of the inlets supplies air to three of the engines.

A photograph showing the engines installed in the XB-70 is presented as figure 2. The engines are numbered 1 to 6, from left to right, and are mounted on approximately 5-foot centers. Each engine is equipped with a fully convergent-divergent nozzle, and the exhaust flow becomes choked at approximately 93 percent rpm (compressor speed) for zero forward velocity. Each engine is in the 30 000-pound-thrust category for full afterburner operation. At military power, each installed engine produces approximately 20 000 pounds of thrust. Military power is the maximum power without afterburner and is analogous to take-off power of commercial jet airplanes. This paper is limited to non-afterburning engine operation.

DATA-ACQUISITION INSTRUMENTATION

The microphone locations in relation to the XB-70 are presented in figure 3. The microphones were located at 10^{o} intervals at radii of 500 and 1000 feet from 90^{o} to 160^{o}, where 0^{o} is along the airplane center line toward the nose of the airplane. The radius for each microphone was taken as the distance from the intersection of the airplane center line and the plane of the exhaust nozzle. Microphones were also positioned at 120^{o}, 130^{o}, and 140^{o} at a distance of 1500 feet.

The signals from the condenser-type microphones were conditioned and then conducted by land lines to wide-band-type instrumentation magnetic-tape recorders. The acoustic data-acquisition system was laboratory calibrated for frequency response prior to and after the tests. The data-acquisition system was acoustically calibrated for level and linearity on the day of the test.

There was special instrumentation, independent of the pilot's instruments, onboard the XB-70 for determining thrust by means of the gas generator method (ref. 3), which provided adequate instrumentation for determining the parameters necessary in using the SAE method of computing the sound levels in decibels.

DATA REDUCTION

The data recorded on magnetic tapes were played back through octave-band filters and recorded on strip-chart recorders. The averaging time used during data reduction was 2.7 seconds. The last 10 seconds of each time history was faired to determine the sound pressure level (SPL) and effectively provided an averaging time of 10 seconds. The SPL was then corrected for data-acquisition- and data-reduction-system response, angle of sound impingement on the microphone diaphragm, and background noise. The data-reduction system was an averaging system, and the average SPL is considered to be accurate to ±1 dB (referenced to 0.0002 dyne/cm^2).

TEST CONDITIONS

The pilot set the engine conditions required for a given data point. The engine conditions presented in this paper include data from 70 percent and 90 percent rpm and military power. Data are included for engine 1, engines 1 and 2, engines 1 and 6, and engines 1, 2, 3, 4, 5, and 6 operating. All runs were 2 minutes long with the acoustic, onboard, and thrust-stand data recorded during the last minute of the run. The temperature at the time of the tests was 27° F and the relative humidity was 70 percent. The winds were less than 10 knots from the nose of the airplane.

DISCUSSION

Varying Sound Levels

One specific problem encountered during the tests was that the SPL varied during quasi-stable engine thrust conditions. Quasi in this instance means that the pilot's engine-monitoring instruments showed no variation in engine thrust, and the thrust-stand data also indicated stable engine thrust.

A time history of the 2000-Hz octave band SPL for two different averaging times is presented in figure 4. The variation of SPL was the maximum found in examining 300 samples of quasi-stationary XB-70 engine noise data. The longer averaging time smooths the data and reduces the variations. This reduction is reflected in the amplitude-distribution graphs obtained by sampling the time histories every 0.1 second with a class interval of 1 decibel. The graph for an averaging time of 1.8 seconds shows a variation of 7 decibels, while an averaging time of 0.03 second shows a variation of 14 decibels.

By using statistical methods, the standard deviation of the data can be computed from the graphs. Typical octave-band standard deviations obtained during these tests by using

various averaging times are presented in figure 5. Increasing the averaging time from 1.8 seconds to 3.4 seconds resulted in only a small improvement in the standard deviation. All octave bands show an increase in standard deviation as the averaging time is decreased. These data also show a decrease in the standard deviation for any specific averaging time with an increase of frequency through the 500-Hz octave band. Frequencies above the 500-Hz octave band show an increase in standard deviation with an increase in frequency for any specific averaging time. At this time, it is not known whether this increase in standard deviation with increase in frequency and the large increase in the standard deviation between the 500-Hz and 1000-Hz octave bands is typical of large engines or due to unknown factors in the XB-70 engines.

Overall Sound Pressure Levels

The overall SPL in decibels at a distance of 500 feet with engine 1 operating is presented in figure 6 for three power settings. The direction of maximum sound propagation appeared to be 130°. The results for various engines operating are presented in figure 7 at two power conditions, and the angle for propagation of maximum SPL was 130°. Results at a distance of 1000 feet were the same; in this paper, the data and the computed levels presented are for an angle of 130°. This angle is only 5° from the SAE specified angle of propagation of maximum SPL, which for the direction angles used in this paper would be 135°.

A comparison of measured and computed sound pressure for engine 1 at a distance of 500 feet is presented in figure 8. The computed levels used parameters obtained from the gas generator method. The thrust computed by using the gas generator method varied slightly from the measured thrust. The computed noise level using the measured thrust would be 0.05 decibel higher at the maximum jet exit velocity and 0.65 decibel lower at the lowest jet velocity. Since this is within the accuracy of the sound measurements, the gas generator method was used to obtain the parameters for all computations in this paper. At the highest jet velocities, the predicted and measured overall SPL agreed but at the lowest jet velocity the measured level was 3.5 decibels higher than the computed SPL.

The difference between measured and computed overall sound pressure levels at a distance of 500 feet for the various engine combinations is presented in figure 9. As in the previous figure, the measured overall sound pressure levels at the lower jet velocities were greater than the computed overall levels for all engine combinations. At maximum jet velocities, the measured and computed values agreed when engine 1 or engines 1 and 6 were operating; however, when the engines were close together, that is, engines 1 and 2 or all 6 engines, the computed level was higher than the measured level for the plane in which these measurements were made.

Octave-Band Sound Pressure Levels

A comparison of measured and computed octave-band sound pressure levels for engine 1 at an angle of 130° and a distance of 500 feet is presented in figure 10. The computed levels were for a temperature of 27° F and a relative humidity of 70 percent, actual atmospheric conditions. At military power, the computed and measured levels agreed except for the two highest frequency octave bands. At 80 percent rpm, the measured levels were higher than the computed levels, as was noted previously for the overall levels.

One of the important reasons for predicting octave-band sound pressure levels is to enable perceived noise levels, in PNdB, to be calculated in order to estimate community response. The perceived noise levels for the computed and measured octave-band levels were the same at military power. At 80 percent rpm, the perceived noise level for the measured data was 9 PNdB higher than the perceived noise level for the computed SPL, which could cause the community response to be underestimated.

The difference between measured and computed octave-band sound pressure levels for engine 1 and engines 1 and 2 at military power and 80 percent rpm are presented in figure 11. As for figure 10, the measured and computed octave bands for engine 1 at military power agreed except for the two highest octave bands. Though not shown, the results for engines 1 and 6, which provide maximum engine spacing, were essentially the same as for engine 1. The measured octave-band levels were less than the computed values for engines 1 and 2 at military power for octave bands less than 4000 Hz and higher than the computed SPL for the 8000-Hz octave band. The results for all six engines operating at military power were essentially the same as for engines 1 and 2. At 80 percent rpm, the measured octave-band levels were higher than the computed values for all frequencies except one for both engine combinations. The result for other engine combinations were the same.

Atmospheric Attenuation

The actual value of atmospheric attenuation is important when predicting sound pressure levels for distances other than specified in the SAE method. A comparison of the actual attenuation and the theoretical attenuation for the day of the tests is presented in figure 12. The solid line is the attenuation due to spherical spreading, assuming the ground is a perfect reflector. The dashed line is the attenuation due to spherical spreading plus the theoretical atmospheric attenuation for the day of the tests. The measured data are shown by the symbols, which have some scatter. The distance of 500 feet at an angle of 130° was an arbitrary zero point for both the measured and the theoretical data. The attenuation of the 63-Hz band was the same as the predicted

attenuation. In general, the attenuation was greater than predicted for the actual day for the 125-Hz through the 1000-Hz octave bands. The attenuation for the 2000-Hz and higher octave bands was definitely less than the predicted attenuation. The reason the attenuation was less than predicted for the higher frequency octave bands is unknown.

CONCLUDING REMARKS

The data in this paper have indicated that the predicted levels using the SAE method compare very well for one large engine at military power and multiple engines when they are widely separated, and they provide a conservative prediction when the engines are close together. At the lower power settings, the SAE method underpredicted the levels by an amount that could be significant during landing or noise-abatement climbouts. The theoretical atmospheric attenuations based on the actual-day conditions were larger than the actual atmospheric attenuation for the higher frequency octave bands.

Although the XB-70 shows significant noise variation during quasi-stable engine operations, it is unknown whether this noise variation will be present in future large engines. Should such variations occur, it will be necessary to use long averaging times during data analysis. When flyover noise is measured and shorter averaging times are required, sufficient data must be obtained in order to determine the amplitude distribution.

REFERENCES

1. Anon.: Jet Noise Prediction. AIR 876, Soc. Automot. Eng., July 10, 1965.

2. Anon.: Standard Values of Atmospheric Absorption as a Function of Temperature and Humidity for Use in Evaluating Aircraft Flyover Noise. ARP 866, Soc. Automot. Eng., Aug. 31, 1964.

3. Beaulieu, Warren; Campbell, Ralph; and Burcham, William: Measurement of the XB-70A Propulsion Performance Incorporating the Gas Generator Method. AIAA Paper No. 68-594, June 1968.

XB-70 AIRPLANE

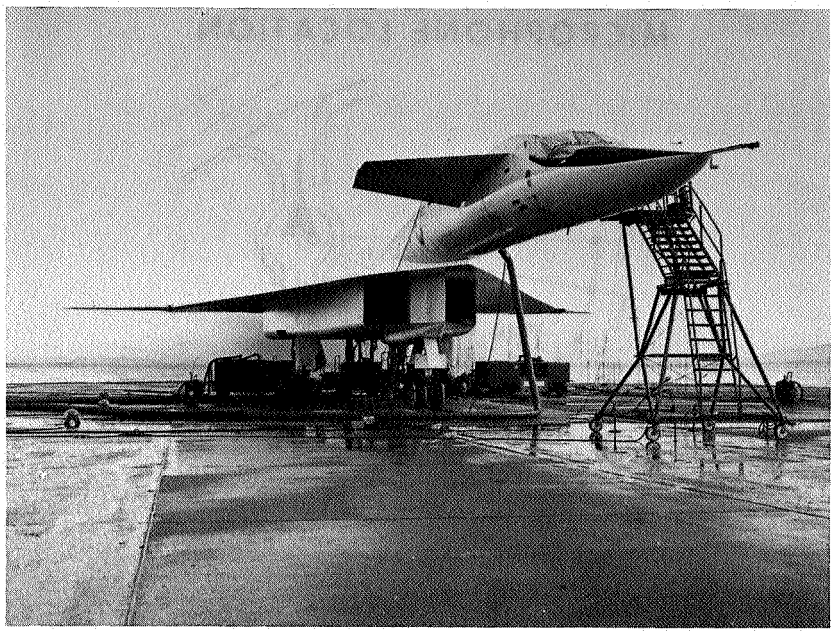

Figure 1 L-68-8582

ENGINES INSTALLED IN THE XB-70

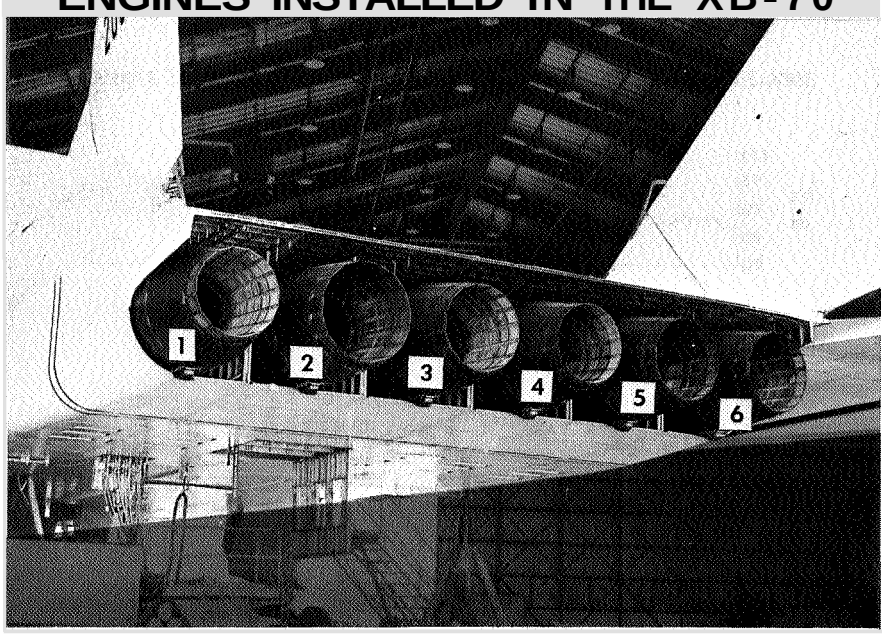

Figure 2 L-68-8583

MICROPHONE LOCATION

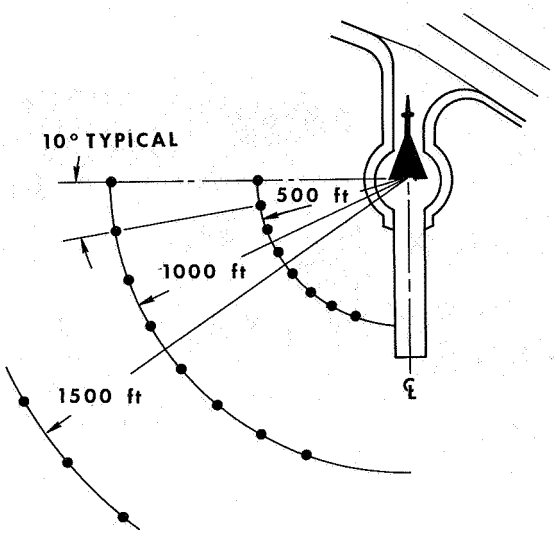

Figure 3

EFFECT OF AVERAGING TIME ON AMPLITUDE DISTRIBUTION OF SPL

2000-Hz OCTAVE BAND, ENGINES 1 AND 2, *90%* rpm AT 130° ANGLE

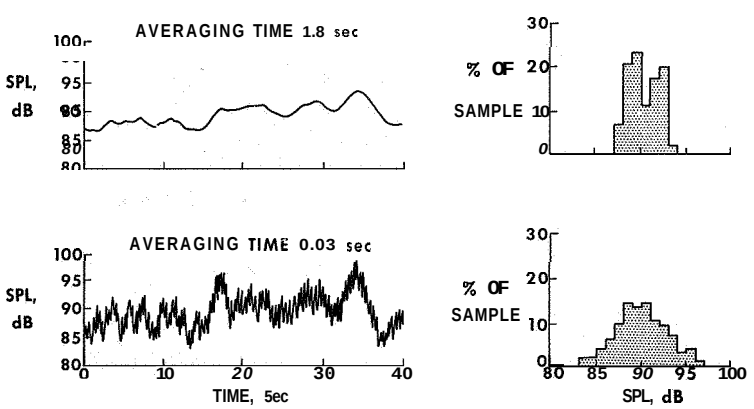

Figure 4

OCTAVE-BAND STANDARD DEVIATIONS FOR VARIOUS AVERAGING TIMES

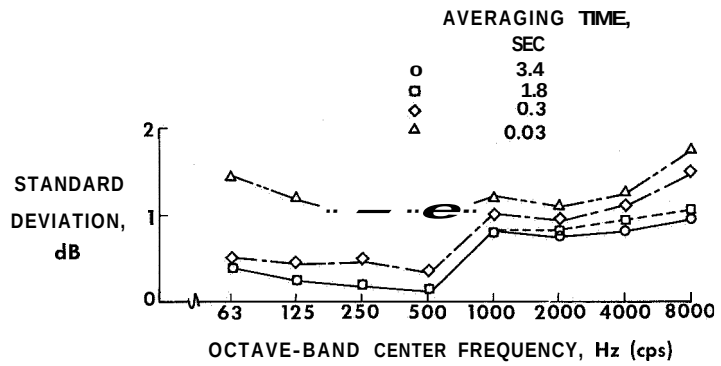

Figure 5

OVERALL SOUND PRESSURE LEVELS (SPL)

ENGINE 1 AT 500-FOOT DISTANCE

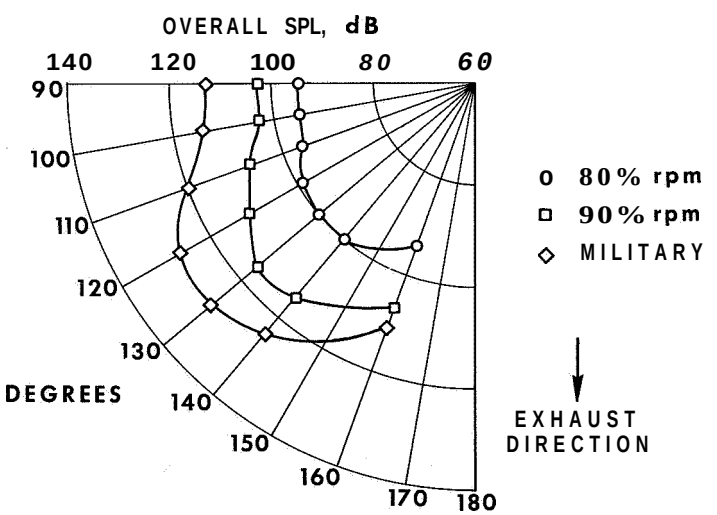

Figure 6

OVERALL SOUND PRESSURE LEVELS
VARIOUS ENGINES AT 500–FOOT DISTANCE

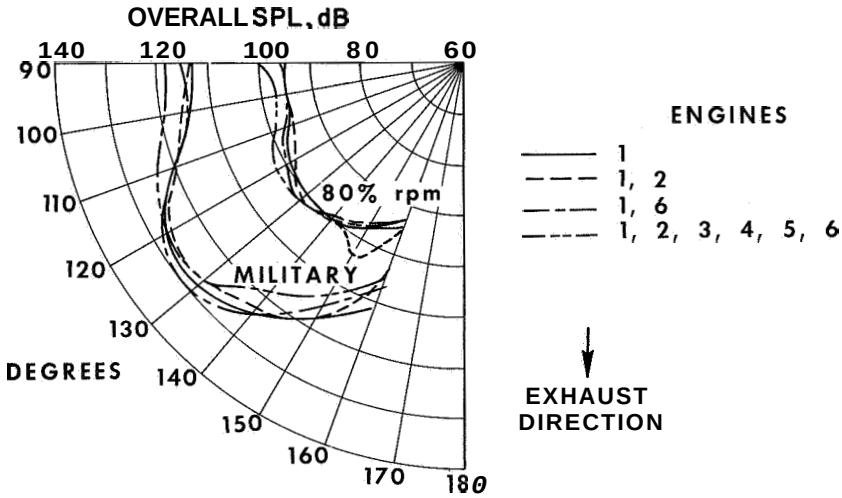

Figure 7

MEASURED AND COMPUTED MAXIMUM OVERALL SPL

ENGINE 1 AT 500-FOOT DISTANCE AND 130° ANGLE

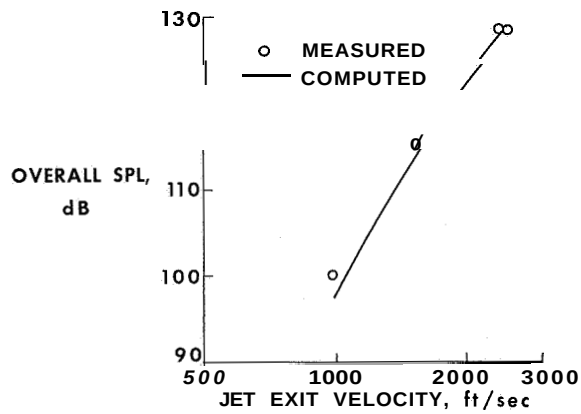

Figure 8

DIFFERENCE BETWEEN MEASURED AND COMPUTED MAXIMUM OVERALL SPL

500-FOOT DISTANCE AT 130' ANGLE

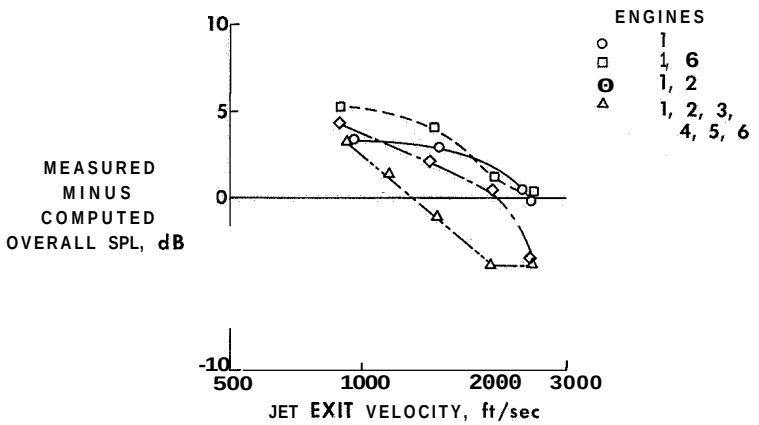

Figure 9

MEASURED AND COMPUTED OCTAVE-BAND SPL

ENGINE 1 AT 500-FOOT DISTANCE AND 130' ANGLE

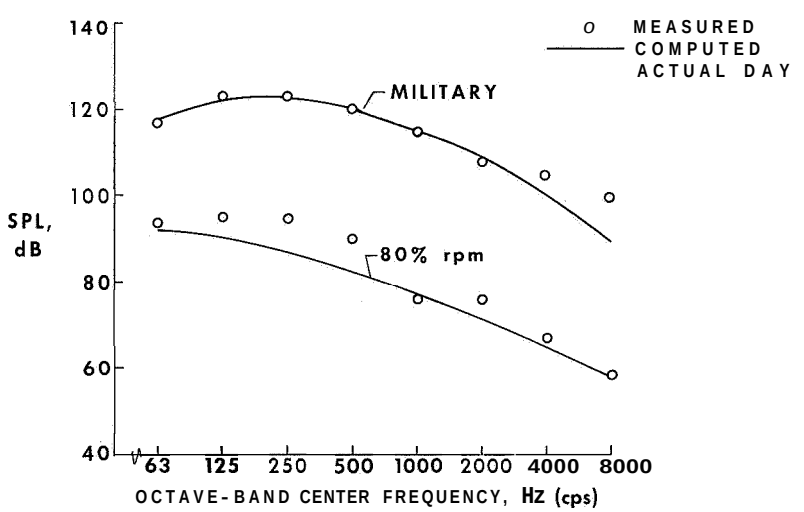

Figure 10

DIFFERENCE BETWEEN MEASURED AND COMPUTED OCTAVE-BAND SPL

500-FOOT DISTANCE AT 130° ANGLE

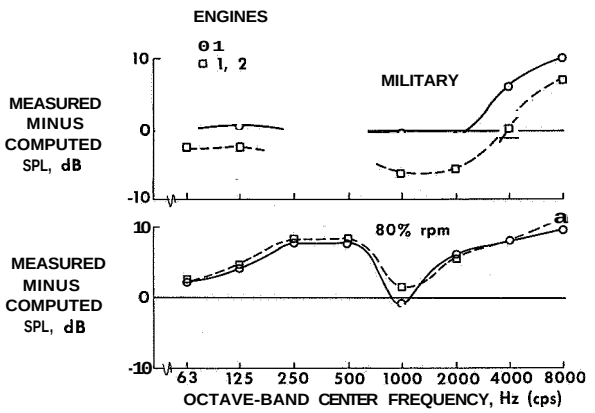

Figure 11

COMPARISON OF MEASURED AND PREDICTED ATTENUATION OF SOUND

MILITARY POWER AT 130° ANGLE

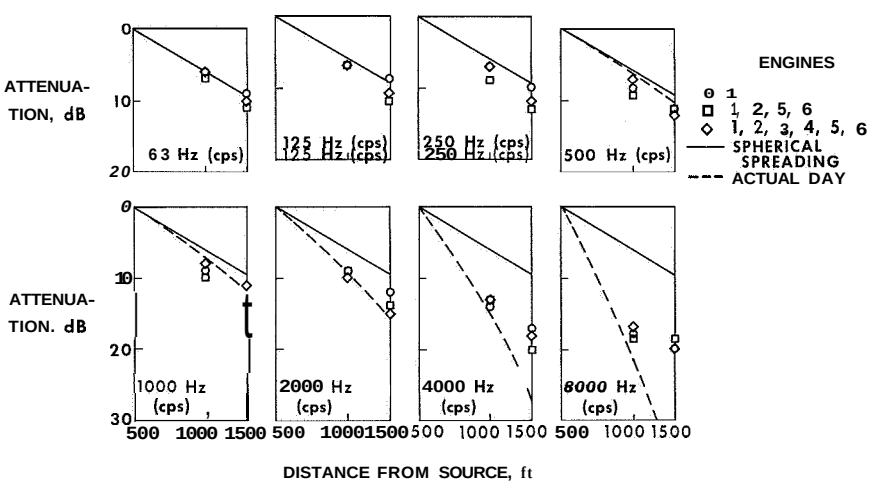

Figure 12

30. PROPAGATION OF SOUND FROM AIRCRAFT GROUND OPERATIONS

By Dwight E. Bishop and Peter A. Franken

Bolt Beranek and Newman, Inc.

SUMMARY

An experimental study has been performed to investigate the sound propagation losses associated with aircraft ground operations. The study emphasized downwind propagation because the highest levels observed on the ground generally occur when the receiver is downwind from the source. Noise from the initial part of jet aircraft take-offs was measured at distances up to 9000 feet from the aircraft in field measurements at Los Angeles International and Denver Stapleton airports.

The results show a pronounced increase in low-frequency attentuation reaching a maximum in the frequency range of 125 to 250 Hz. The results also indicate that current industry procedures for estimating atmospheric absorption lead to overestimation of attenuation at frequencies above 1000 Hz. A simple engineering procedure for estimating downwind propagation losses is given.

INTRODUCTION

The operation of aircraft in and around airports has become a major contributor to the American urban and suburban noise environment. Effective planning of such matters as airport layout or adjacent land usage therefore requires realistic estimates of the aircraft noise in nearby areas. (See refs. 1 to 3.) These noise estimates depend upon a knowledge of the source characteristics of the various aircraft and the losses associated with propagation from the source to the receiver. Although there is considerable engineering information available describing many of the aircraft noise sources currently encountered, there is considerable uncertainty as to the proper engineering procedures to use in estimating noise levels at positions distant from the aircraft source.

Figure 1 shows the elements of the aircraft noise problems described in terms of sources, paths, and receivers, This paper is concerned with the propagation of sound arising from aircraft ground operations – either from ground runups or noise generated by aircraft during the take-off roll. This paper is based upon an experimental study (ref. 4) to investigate sound propagation losses associated with aircraft ground operations. Of concern in this study was the relationship between the noise levels measured near an aircraft on the ground with the noise levels measured at distant points in areas or

communities around an airport. The primary purpose of the study was to determine how well one could relate the changes in noise levels between near and distant positions with the basic weather information that is typically available at an airport – surface measurements of temperature, winds, and humidity. A second purpose was to develop engineering procedures for estimating aircraft noise levels at relatively large distances from aircraft.

Many of the previous studies of ground-to-ground propagation were concerned with long-range communication systems. Hence, they focused attention of the question as to the least favorable conditions for sound propagation. In this study, concerned with predicting aircraft noise in communities, interest was in the opposite question – what are the noise levels expected under the most favorable conditions for sound propagation?

In general, propagation from a source on the ground to a receiver on the ground is most favorable when the wind is blowing in the direction from the source to the receiver (downwind propagation). *Also,* the lobes of maximum noise from a jet engine lie in the rear quadrants of the aircraft, which are also generally in the downwind direction. For these reasons, the highest noise levels observed in nearby areas are generally associated with downwind propagation. Hence, downwind propagation was emphasized in this study.

MEASUREMENT PROGRAM

Although modern airports are indeed noisy places, it is difficult to find an airport noise source that permits consistent measurements out to 5000 feet, a typical distance of interest in the present program. Of the many types of noise sources found at an airport, field experience soon showed that the noise generated during the initial part of a jet aircraft take-off was the most consistently useful source for the program.

Field measurements using jet aircraft take-offs as sources were made at the Los Angeles International airport over a 6-month period and at the Denver Stapleton airport during a 1-week measurement period. Subsequent analysis is based upon results from measurements at both airports.

The noise was measured during the initial part of a jet transport take-off at three positions as shown in figure 2. One position was located within about 300 feet of the airplane. The other two positions were located at greater distances on a line with the innermost position (station 1) and the airplane. The most distant position was located typically 1 mile or more from the airplane.

Use of the noise from jet airplanes during the initial part of the airplane take-off roll imposed some significant limitations in analysis of the data. Because most jet transport airplanes started their take-off roll before or immediately upon reaching full thrust, the noise source was constantly changing in magnitude and geometrical location.

Thus, each airplane take-off produced a time-varying signal with a usable duration of about 5 to 10 seconds. The fact that the signal amplitude and geometrical location were changing rapidly with time introduced the need for careful time correlation of the recordings made in the field.

Simultaneous magnetic tape recordings were made at all stations. Annotation by the observer at station 1, recorded directly on the tapes at each of the stations, signaled the start of each event and provided synchronization for all three stations. A tone burst was placed on the station 1 tape as the airplane moved past position A, shown in figure 2. A second tone burst was placed on the tape as the airplane moved past position B on its take-off roll. The recorded signal between the two tone bursts denoted the usable position of the signal at station 1 for that event. During laboratory analysis of the recorded data, octave frequency band levels were examined at the three positions obtained for the same usable time interval (adjusted for the sound propagation time), and the differences in noise levels observed between the three measurement positions were compared.

Meteorological conditions, in terms of wet- and dry-bulb temperatures, wind speed and direction, barometric pressure, and cloud cover were noted at each measurement station at approximately hourly intervals. Hourly sequence surface weather observation data were obtained from the U.S. Weather Bureau offices located at the Los Angeles and Denver airports, for each measurement period. Weather Bureau radiosonde information was utilized to estimate temperature profiles. In the data analysis, the Weather Bureau information was relied upon as the primary description of the weather, field measurement data being used to supplement the Weather Bureau information.

To illustrate some of the actual field measurement locations, figure 3 shows two different measurement radials at Los Angeles International airport. Typically, noise would be measured during several aircraft take-offs with measurement stations located along one radial. Then, during the same period, measurement locations would be shifted to another radial and the noise measurements repeated during several other aircraft take-offs. The two outer positions were usually located in the communities surrounding the airport and only the innermost station had direct line of sight to the aircraft. As the figure indicates, between the innermost station and the outer two stations, there were intervening buildings, elevated freeways, and other obstructions which interfered with direct line-of-sight sound propagation.

SOUND ATTENUATION FACTORS

Figure 4 provides an example of the difference in noise levels that might be measured downwind during favorable sound propagation conditions. The zero reference refers to the noise levels measured at 200 feet from an aircraft source. The first band

indicates typical differences in levels between those measured at 1000 feet and those measured at 200 feet from the aircraft source. The lower band indicates the typical differences for downwind sound propagation between those measured 200 feet and 4000 feet from the aircraft. The difference in noise levels at the 1000-foot and 4000-foot positions are shown as shaded bands to provide an indication of the variability that might be expected, even under the same reported surface weather conditions. If noise levels taken at these distances at different times under different reported surface weather conditions were compared, one would likely find much greater spread than is indicated by the bands shown in figure 4.

In the following table are listed the primary factors determining the differences in noise levels at various distances from an aircraft source for downwind propagation:

Noise attenuation component	Dependent upon
Inverse-square spreading	Geometry, distance
Classical attenuation } Standard atmospheric Molecular attentuation } attenuation	Absolute humidity
Miscellaneous meteorological and ground effects – "residual" attenuation	Wind and temperature profiles, terrain

The first component listed, the attenuation due to inverse-square radiation of the sound, may be evaluated from the measurement geometry and distance relationships.

The classical and molecular attenuations are grouped together under the term "standard atmospheric attenuation." The standard atmospheric attenuation is primarily determined by the absolute humidity of the air. This attenuation can usually be predicted from knowledge of the air temperature and relative humidity. There are accepted industry procedures and tables (given in ref. 5) for estimating the standard atmospheric attenuation. The attenuation values given in these procedures are based upon rather precise laboratory measurements of air under uniform temperature and humidity conditions. Although there is little question about the accuracy of these values for air under uniform conditions, there is a question as to the accuracy of using simple surface measurements of temperature and humidity to predict the atmospheric attenuation for propagation over the ground under typical field conditions.

What is left after the first three components (inverse-square spreading and classical and molecular attenuation) have been removed from the sound pressure level differences is associated with the meteorological and ground effects and is denoted as "residual attenuation." The residual attenuation is likely to vary drastically for upwind and

downwind conditions. It results from such factors as scattering due to inhomogeneities in the atmosphere and from temperature and wind gradients which cause bending of the sound waves. It also is affected by the terrain which causes absorption and reflections.

Figures 5 and 6 provide some indication as to the relative size of these four components at low frequencies and at high frequencies. Figure 5 shows the expected downwind sound attenuation at 250 Hz. The major factors contributing to the attenuation are the inverse square spreading and the residual attenuation. The standard atmospheric attenuation due to the air absorption is relatively small. At these low frequencies, even considerable error in estimating the standard atmospheric attenuation values would not lead to serious errors in estimating the total attenuation.

Figure 6 shows the expected downwind attenuation at high frequencies, in this case, 4000 Hz. Typically, the total attenuation is much greater. The two primary contributors are now the inverse-square spreading and the standard atmospheric attenuation. The residual attenuation may be very small. In this case, it is easy to see that errors in estimating the standard atmospheric attenuation may lead to large errors in estimating the total sound attenuation.

In the field measurements, only the total attenuation was measured directly. The inverse-square losses were determined from knowledge of the distances between the measurement positions, and the standard attenuation was estimated from the surface measurements of temperature and relative humidity. These calculated values were then subtracted from total observed field attenuations and the remaining residual attenuation values were examined. Thus, the residual attenuation values from the field measurements contained the true residual attenuation plus any measurement errors or errors in the determination of the standard atmospheric attenuation. Particularly at high frequencies, errors in the estimation of the standard atmospheric attenuation could cause large errors in the determination of the residual attenuation from the field measurements.

In the field measurements, many data were taken at many different distances and under many different weather conditions. In the analysis, the residual attenuation information was grouped in terms of three distance ranges. Different groupings of the data were then examined in terms of absolute wind speed, wind vector magnitudes, and temperature profile behavior. For all these groupings, there was considerable scatter of the data, and it was not possible to give any more consistent presentation than that based on a division of data in terms of absolute wind speed – greater than 10 knots per hour and less than 10 knots per hour.

Typical results of the measurements are shown in figures 7 and 8. These figures show the mean residual attenuation, observed in octave bands, for three distance ranges. The solid line is for a mean distance of 2600 feet; the short-dashed line, for a mean

distance of 5200 feet; and the long-dashed line, for a mean distance of 7000 feet. Figure 7 presents data for wind speeds less than 10 knots; figure 8, for wind speeds greater than 10 knots. In these figures, the attenuation is positive in an upward direction; thus, the higher the line is on the graph, the greater the amount of residual attenuation. One will note that there is considerable residual attenuation at the low frequencies; as a result, there is a peak in the attenuation in the 125- and 250-Hz octave bands.

In the frequency bands above 1000 Hz, there are three features of unusual behavior:

(1) The attenuation values become negative and represent "amplifications" that are as large as 40 dB and 50 dB at the highest frequencies

(2) The order of the mean attenuation curves becomes inverted so that the largest distances show the smallest (rather than the largest) attenuations

(3) The standard deviations become large, typical values rising from 6 dB to 12 dB below 1000 Hz to 30 dB to 40 dB at 4000 Hz.

Although it is true that greater level fluctuations are expected at high frequencies than at low frequencies, the fact that the increases in standard deviation are coupled with these other effects suggests strongly that the procedure for standard atmospheric attenuation at high frequencies has generated values that are very high. In other words, by using the standard atmospheric attenuation values of reference 5, "amplifications" have been artificially introduced at the higher frequencies and have also increased the scatter in the data. Based on this reasoning, the high-frequency attenuation values were recalculated, the SAE procedure being modified in two steps. In one set of data (figs. 9 and 10), the values obtained from the SAE procedure in the frequency bands centered at 2000 and 4000 Hz were arbitrarily halved. In the second step, the standard SAE attenuation was omitted completely.

From figures 9 and 10, it may be seen that the removal of half of the standard attenuation in the highest frequency bands reduces the artificial amplifications of figures 7 and 8. Furthermore, data scatter and standard deviations were also significantly reduced at 2000 and 4000 Hz. Complete removal of the standard attenuation forces the resulting attenuation values negative and suggests that the values are now overcorrected by removing all the high-frequency air attenuation.

The most pronounced feature of the curves shown in figures 9 and 10 is the low-frequency peak occurring around 125 and 250 Hz mentioned earlier. This low-frequency peak in residual attenuation was observed occasionally by earlier workers (refs. 6 to 9) and has been ascribed to destructive interference between the direct sound and sound partly reflected from the ground surface. However, the field-measurement geometry does not fit in with any such interference models. Some earlier workers had also suggested that the presence of a wind greater than about 5 miles per hour would destroy

this interference effect. However, the data shown here for winds much greater than 5 miles per hour show the effect very markedly. Parkin and Scholes making measurements with a jet engine in Great Britain have also seen this low-frequency behavior and present some data to show that the effect is dependent upon the source and measurement height. (See ref. 10.) However, no detailed understanding of the effect is available.

By cross plotting the residual attenuation data shown in figure 10, one has some of the information needed for an empirical engineering procedure for estimating attenuation for downwind sound propagation. Such a procedure is presented in the appendix, together with an example of its application. The residual attenuation values to be used in this procedure are shown in figure 11. In figure 11, the attenuations for different octave frequency bands from 31.5 to 500 Hz are plotted as a function of distance from the source. The residual attenuation at large distances is greatest at 125 and 250 Hz and decreases in magnitude at higher as well as at lower frequencies.

Within the last several years, other procedures have been suggested by industry (ref. 11) for predicting downwind sound propagation.* These procedures use values for the residual attenuation that do not provide for the large attenuation values that were observed at 125 and 250 Hz. These procedures also predict sizable residual attenuations at the higher frequencies, contrary to what has been found in this investigation. Thus, if one were to compare the two procedures by applying them to predict noise levels at large distances from an aircraft located on the ground, one would arrive at significantly different answers. The results presented herein would produce lower estimates of noise levels at the lower frequencies and higher estimates of the noise levels at the higher frequencies.

CONCLUSIONS

The study of the residual attenuation associated with the downwind propagation of noise from an aircraft on the ground provides the following conclusions:

1. The attenuation data show a pronounced increase in low frequencies. This increase reaches a maximum in the frequency range of 125 to 250 Hz, a frequency range of considerable interest for turbojet engine noise.

2. Current industry procedures for estimating the standard attenuation associated with classical and molecular absorption lead to overestimation of attenuation at frequencies above 1000 Hz. This effect may be of particular interest for large bypass-ratio turbofan engines.

---

*In reference 11, the term "extra ground attenuation" corresponds to the term "residual attenuation" used in this paper.

3. Under the most favorable conditions, the values of standard deviations associated with propagation over distances of 3000 to 6000 feet are in the range of 6 dB to 12 dB. Thus, under typical downwind conditions, rather large variations in distant noise levels may be expected even for the same gross weather conditions as measured in terms of surface temperature, humidity, and surface winds.

4. A simple engineering procedure for estimating downwind propagation losses has been developed. This procedure incorporates the findings of conclusions **1** and **2.**

5. Like many experimental programs, this study has raised a number of questions. The low-frequency residual absorption peak is not fully understood even though it is certain that it exists. Also, the reason that the standard absorption values appear to be so excessive at high frequencies is not known. Thus, considerably more work remains to be done to develop reliable methods for predicting ground-to-ground noise propagation. There is also reason to suspect that the application of current methods for estimating standard atmospheric absorption for air-to-ground propagation during aircraft flyovers may also be in error. For these reasons, **NASA** has recently begun a study to examine the propagation losses observed in a number of carefully controlled aircraft flyovers undertaken during recent tests at Wallops Island, Virginia.

APPENDIX

SUGGESTED PROCEDURE FOR ESTIMATING DOWNWIND ATTENUATION

The purpose of this procedure is to suggest a method for predicting the propagation of noise over open terrain from an aircraft on the ground to other locations in nearby residential areas. The procedure is restricted to the case of downwind propagation, that is, a nonnegative component of the wind in the direction from the aircraft source to the residential receiver. This case of downwind propagation is expected to be the most favorable for sound propagation to nearby areas. Upwind propagation, that is, a negative component of wind velocity in the direction of source to receiver, tends to provide larger values of residual attenuation and under some circumstances produces marked attenuation regions called shadow zones.

For the purpose of this procedure, the wind velocity is assumed to be 10 miles per hour. The wind velocity averaged for about 60 airports in the United States has been found to be approximately this value. The source and receiver heights are also assumed to be approximately 6 feet above the ground.

The following information is required to calculate the attenuation between point A (a convenient reference point located within a few hundred feet of the aircraft) and point B (the residential measurement point of interest):

x_A, x_B distances from aircraft to points A and B, respectively

T ambient temperature

RH ambient relative humidity

The total downwind attenuation (TDA) is given as the sum of three components

$$TDA = IA + SA + EA$$

where

IA inverse-square attenuation, $20 \log_{10}\left(x_B/x_A\right)$

SA standard atmospheric attenuation, calculated from reference 5, as modified

EA residual attenuation

APPENDIX

Figure 11 presents plots of residual attenuation **EA** as functions of propagation distance, for frequency bands below 1000 Hz. For frequency bands at or above 1000 Hz, **EA** is taken to be zero.

For frequency bands centered at 1000 Hz and below, the standard atmospheric attenuation **SA** is calculated directly from reference 5 as a function of temperature T and relative humidity RH. For frequency bands centered at 2000 **Hz** and above, **SA** as a function of temperature and humidity is taken as one-half the values obtained from reference 5.

If one-third octave frequency bands are used, the values of **TDA** for the frequency bands between the octave band center frequencies should be obtained by interpolation from a smoothed curve based on the octave band values. The standard deviations associated with the predicted values of **TDA** are of the order of 6 dB to 12 dB.

For the example shown in table I, the total downwind attenuation in preferred octave frequency bands between two points that are 200 ft and 4000 ft from an airplane was determined. The temperature was 59° F and the relative humidity, 70 percent.

TABLE I.- EXAMPLE OF TOTAL DOWNWIND ATTENUATION CALCULATIONS

Octave band center frequency, Hz	Inverse-square attenuation, dB	Standard atmosphere attenuation per 1000 ft[1], dB	Standard atmosphere attenuation[2], dB	Residual attenuation[3], dB	Total downwind attenuation, dB
31.5	26	0	0	6	32
63	26	0	0	10	36
125	26	0	0	15	41
250	26	0	0	15	41
500	26	.7	3	2	31
1000	26	1.4	5	0	31
2000	26	3.0	6	0	32
4000	26	7.7	15	0	41
8000	26	14.4	28	0	54

[1]Reference 5, paragraph 5.0.

[2]Based upon one-half the values of the third column for frequencies of 2000 Hz and higher.

[3]From figure 11.

REFERENCES

1. Anon.: A Study of the Optimum Use of Land Exposed to Aircraft Landing and Takeoff Noise. NASA CR-410, 1966.

2. Anon.: Land Use Planning With Respect to Aircraft Noise. AFM 86-5, TM 5-365, NAVDOCKS P-98, U.S. Dep. Defense, Oct. 1, 1964. (Available from DDC as AD 615015.)

3. Anon.: Land Use Planning Relating to Aircraft Noise. Tech. Rep., Bolt, Beranek & Newman, Inc., Oct. 1964. (Available from DDC as AD 615015.)

4. Franken, Peter A.; and Bishop, Dwight E.: The Propagation of Sound from Aircraft Ground Operations. NASA CR-767, 1967.

5. Anon.: Standard Values of Atmospheric Absorption as a Function of Temperature and Humidity for Use in Evaluating Aircraft Flyover Noise. ARP 866, Soc. Automot. Eng., Aug. 31, 1964.

6. Ingard, Uno: The Physics of Outdoor Sound. Proceedings of the Fourth Annual Noise Abatement Symposium, Vol. 4, Oct. 23-24, 1953, pp. 11-25.

7. Wiener, Francis M.; and Keast, David N.: Experimental Study of the Propagation of Sound Over Ground. J. Acoust. Soc. Amer., vol. 31, no. 6, June 1959, pp. 724-733.

8. Parkin, P. H.; and Scholes, W. E.: The Horizontal Propagation of Sound From a Jet Engine Close to the Ground, at Radlett. J. Sound Vib., vol. 1, no. 1, Jan. 1964, pp. 1-13.

9. Parkin, P. H.; and Scholes, W. E.: The Horizontal Propagation of Sound From a Jet Engine Close to the Ground, at Hatfield. J. Sound Vib., vol. 2, no. 4, Oct. 1965, pp. 353-374.

10. Scholes, W. E.; and Parkin, P. H.: The Effect of Small Changes in Source Height on the Propagation of Sound over Grassland. J. Sound Vib., vol. 6, no. 3, Nov. 1967, pp. 424-442.

11. Anon.: Method for Calculating the Attenuation of Aircraft Ground to Ground Noise Propagation During Takeoff and Landing. AIR 923, Soc. Automot. Eng., Mar. 1, 1968.

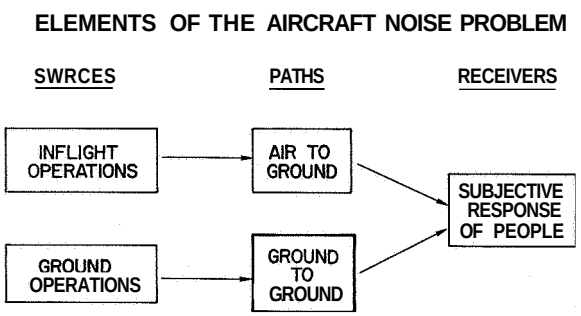

Figure 1

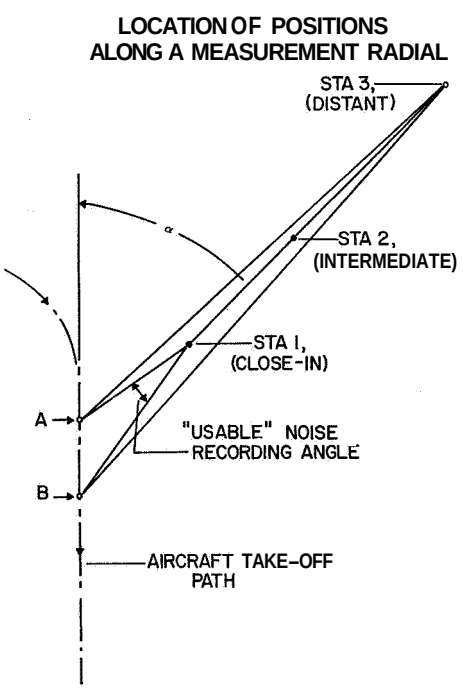

Figure 2

TYPICAL MEASUREMENT POSITIONS
(TAKE-OFFS FROM RUNWAY 25R)

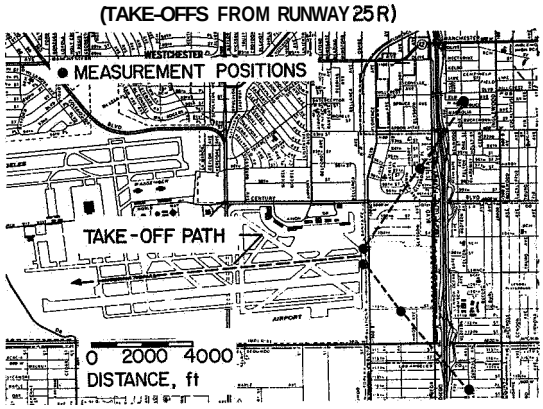

Figure 3

EXAMPLE OF DOWNWIND SOUND PROPAGATION FROM JET AIRCRAFT

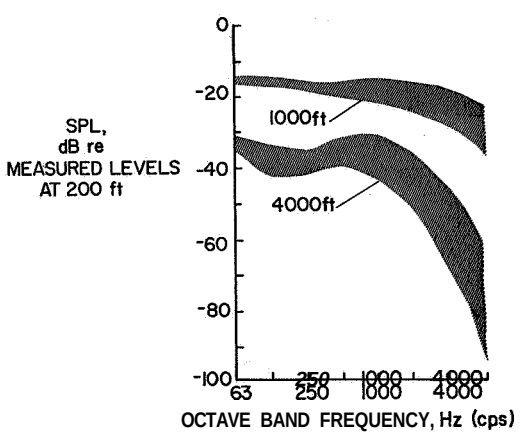

Figure 4

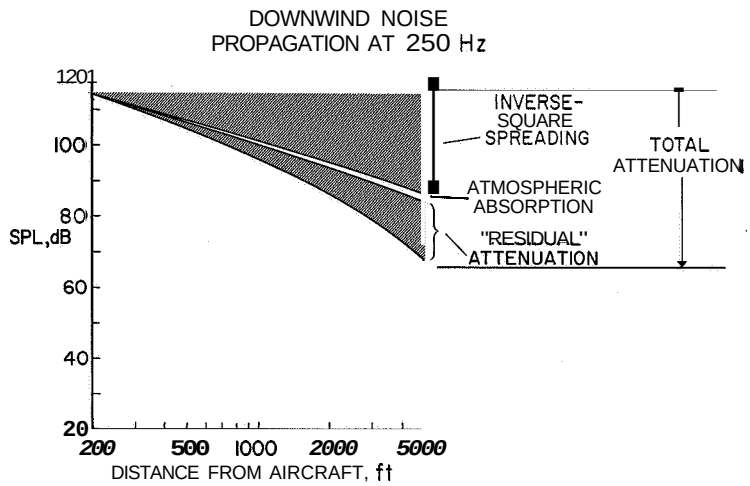

Figure 5

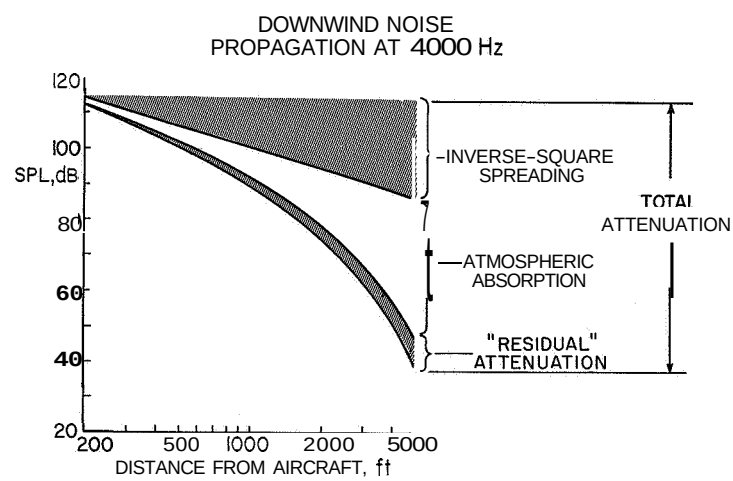

Figure 6

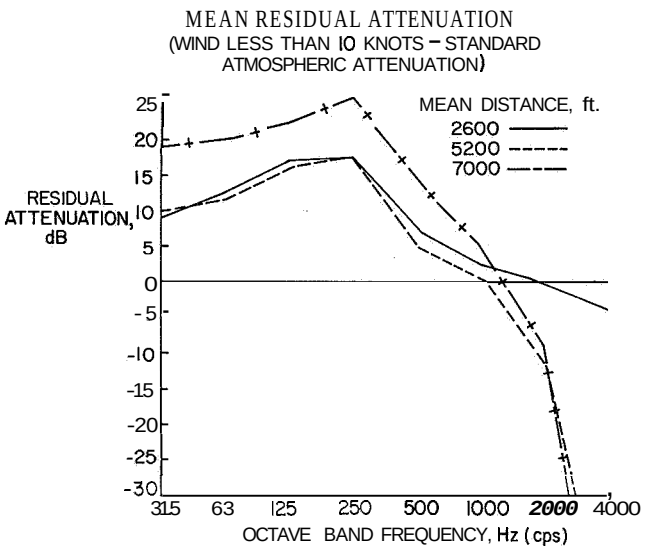

Figure 7

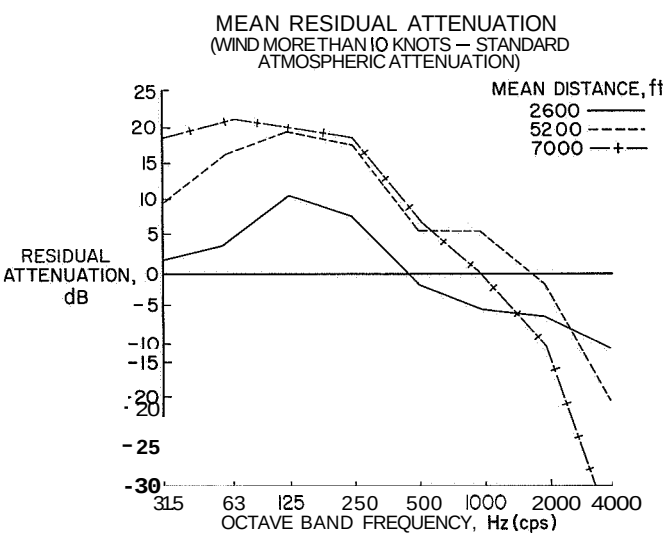

Figure 8

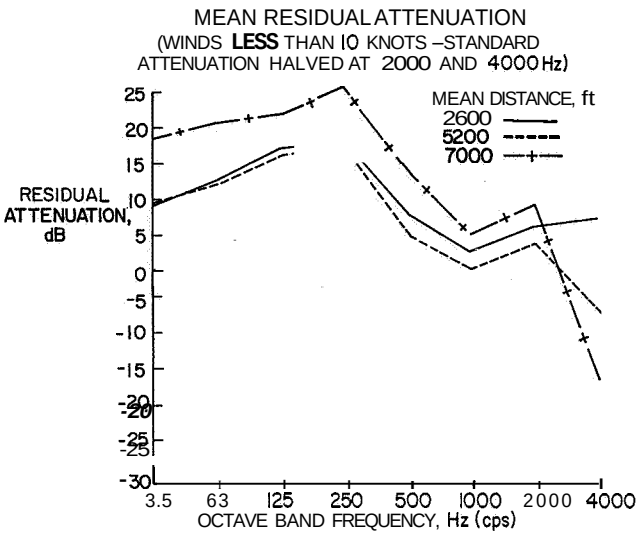

Figure 9

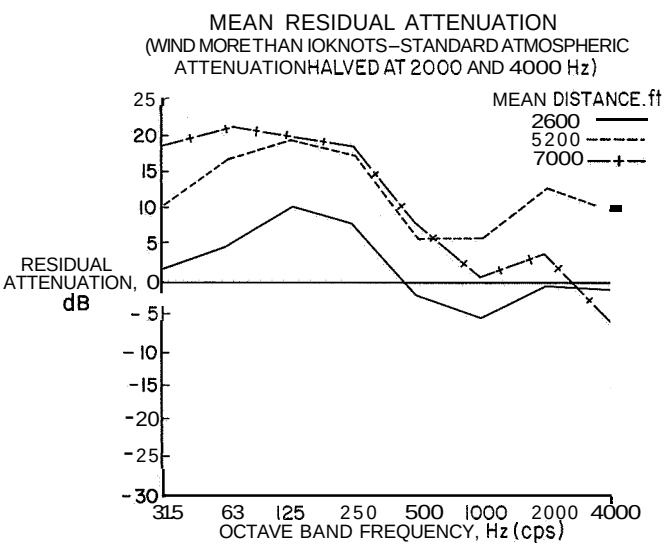

Figure 10

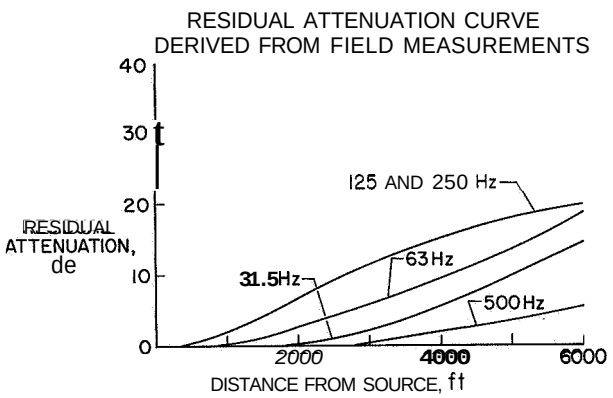
RESIDUAL ATTENUATION CURVE
DERIVED FROM FIELD MEASUREMENTS
40
30
20
10
0
RESIDUAL
ATTENUATION,
de
125 AND 250 Hz
63Hz
31.5Hz
500Hz
2000
4000
6000
DISTANCE FROM SOURCE, ft

Figure 11

31. METHODS OF DETERMINING THE EXCESS ATTENUATION FOR GROUND-TO-GROUND NOISE PROPAGATION

By Stanley H. Guest

NASA George C. Marshall Space Flight Center

and

Bert B. Adams

Lockheed Missiles and Space Company

SUMMARY

Three basic methods of obtaining excess attenuation values for ground-to-ground sound propagation are described for use in various applications. The acquisition of the acoustic data, the selection of usable information, and the influencing meteorological factors are given along with the results. The relative effects of seasonal variation, relative humidity, and temperature are provided in addition to the nonlinearity effects with distance as were observed from the data. The results obtained from this study can be applied to noise control relating to airport/community problems as well as to any other general noise abatement situation concerning sound propagation over the ground surface.

INTRODUCTION

According to the Federal Aviation Administration, the revenue air passenger miles are expected to increase by 250 percent within the next 10 years. (See ref. 1.) It is reasonable to expect that the interference of airplane noise with people will also increase proportionately. It is thus apparent that this ever-growing problem must be given serious study.

Because of the increasing complexity of the physical and psychological problems created by the general and continued use of jet engines by both military and civilian agencies, The Federal Aviation Administration instituted what is known as the Interagency Noise Abatement Program in an attempt to find techniques to alleviate as much as possible for as many people as possible at a cost that is within reason, these acoustical problems adversely affecting our environment. The techniques include a combination of three basic approaches to these problems: (1) modifying the sound source (that is, producing quieter jet engines), (2) optimizing the flight path along which the sound is transmitted, and (3) developing a satisfactory airport/community interface, both physically and psychologically.

The sound source problem will not be handled in this paper, nor will the interfacing be directly discussed.

The consideration of the transmission path and the variables affecting the sound propagation is a complicated task and would directly impact such aspects as airport planning and layout, residential and commercial land zoning, building code criteria, personnel safety and annoyance factors, test procedures for aircraft certification, and many other considerations which require long-term planning and airport/community interface.

To plan for community activities in relation to large noise sources (jet ports), studies are being made of the behavior of sound as it is propagated from its source to a receiver, where both the source and receiver are at ground level. The substance of this paper is, effectively, a study of far-field attenuation of sound, the results of which can be applied to airport "ground operations" from the landing of the aircraft through the "taxi" phase, passenger pick-up, and so forth, until just after take-off. This period of ground operation can be lengthy and contributes largely to the growing problem of aircraft noise.

SYMBOLS

C_A velocity of sound (vector to Athens), m/sec

C_H velocity of sound (vector to Huntsville), m/sec

EA excess attenuation including all attenuation of energy in excess of spherical divergence, dB/unit distance

N integer

$OBSPL_d$ octave band sound pressure level at distance radius R_d from source, dB, re $2 \times 10^{-5} N/m^2$

$OBSPL_j$ octave band sound pressure level at any position j, dB, re $2 \times 10^{-5} N/m^2$

$OBSPL_k$ octave band sound pressure level at any position k, dB, re $2 \times 10^{-5} N/m^2$

$OBSPL_n$ octave band sound pressure level at position n, dB, re $2 \times 10^{-5} N/m^2$

$OBSPL_o$ octave band sound pressure level at a reference position R_o, dB, re $2 \times 10^{-5} N/m^2$

R.H. relative humidity at ground level, percent

R_d distance radius to any microphone more distant than R_o, distance units

R_j	distance radius from sound source to microphone position j, distance units
R_k	distance radius from sound source to microphone position k, distance units
R_n	distance radius to position n, distance units
R_o	distance radius to reference microphone closest to source, distance units
T_G	temperature at ground level, ^oC
W_A	wind velocity toward Athens, m/sec
W_H	wind velocity toward Huntsville, m/sec
μ	mean value
σ	standard deviation
ψ^2	average of squared values

TEST SETUP AND DISCUSSION OF PROBLEM

Because of its large test-stand facilities, where large rocket engines and boosters are static tested under varied weather conditions, the George C. Marshall Space Flight Center has ready-made high-energy sound sources which are ideal for this type of study: the S-IC, booster for the Saturn V space vehicle; the S-IB, booster for the Saturn IB space vehicle; and the F-1 rocket engine, the single-engine element of the S-IC booster. To make extensive studies of the acoustic energy propagation by these sound sources, a Land Acoustical Monitoring System (LAMS) has been permanently installed at the center. Only the installation of this Land Acoustical Monitoring System was necessary to take advantage of the following already existing factors at the Marshall Space Flight Center for acoustic studies: first, the large sound source; second, long data samples to be obtained over an extended test duration; third, a sound source invariant with time or test; fourth, a large number of tests and data measurements; and fifth, extensive meteorological survey information at the actual location of the test. (The Aerospace Environment Division, Aero-Astrodynamics Laboratory, Marshall Space Flight Center, makes systematic studies of meteorological conditions,)

The LAMS system consists of two radial lines of transducers located in two directions from the test stands. (See fig. 1.) The first line of transducers consists of

29 microphones along a 36-km line at an azimuth of approximately 310° (±3°) in the direction of Athens, Alabama, and the second consists of 22 microphones along an 18-km line at an azimuth of approximately 45° (±6°) in the direction of Huntsville, Alabama. The microphones are mounted on telephone poles at 40 feet above the local terrain at a median separation distance of 1.5 km (Athens LAMS) and 0.9 km (Huntsville LAMS). The three static test stands are located in a triangular pattern at a maximum distance of less than 1.5 km apart. Figure 1 also shows the relative positions of the microphones and test stands with the ground elevation along each radial LAMS line. It can be seen that the elevation is relatively constant (±25-foot variations) along the Athens LAMS and along the first 15 km of the Huntsville LAMS. (Only four microphones are placed at higher elevations and they are at the greatest distance from the source.)

The ground cover for the Athens LAMS is estimated to be 80-percent open fields (farms, pastures, grassland) with intermittent trees and hedgerows. The Huntsville LAMS is approximately 60- to 70-percent open country with wooded areas, partly deciduous and partly evergreen. No other quantitative information is currently available concerning the physical makeup of the soil or the impedance characteristics typical of the ground and its cover. For both lines, it can only be estimated that the tree height averages 20 to 30 feet and the grass cover is about 6 inches. No bodies of water intervene.

The acoustic data used in this study were acquired from among 79 tests during the period from June 1965 to January 1967 by using the static tests of the Saturn V booster (214.5 dB sound power level; all sound power levels referenced to 10^{-13} watt), the S-IB booster (204 dB sound power level), and the F-1 rocket engine (204.5 dB sound power level).

DATA ACQUISITION SYSTEM

The data acquisition system, basically designed by Bolt Beranek and Newman, Inc., of Boston, Massachusetts, consisted of 51 permanently located microphones on 40-foot telephone poles. The Chesapeake NM 135 and a modified model of increased sensitivity, along with several Shure microphones, were calibrated before each test by a hand-held calibrator (diaphragm type) producing a single frequency signal (100 Hz). The microphones were again checked, this time remotely, just before static test firing of the engines, by an insert voltage technique. The remote check was made on the assumption that the spectral response characteristics remained flat, after the laboratory calibration, over the frequency range from 1 Hz to 2000 Hz. Remote attenuator settings (5, 10, and 30 dB), available for each microphone, were used when prior prediction of the sound field indicated that radical levels were expected. This prediction was based on the velocity-of-sound profiles containing vector wind, temperature, and humidity factors.

The output from each microphone was amplified and fed to an FM modulator and then to the base station at the George C. Marshall Space Flight Center (MSFC) over landlines. The signal was directly recorded on a 14-track recorder for data processing. The accuracy quoted on the data-acquisition system was ±2 dB for 95-percent confidence level from 1 Hz to 1000 Hz. The background noise was also recorded just before data acquisition to prevent use of any anomalous electrical noise or any interfering physical noise which might be recorded from any of the microphones.

The data reduction from the magnetic tape to a digital form was conducted on an automatic octave band data system. The data were printed on cards for computer use and were also plotted for visual inspection. The time-history record was observed from several transducers and an analysis was made of an acceptable portion of the test data. An averaging time of 50 seconds was used for tests of sufficient duration and an averageing time of 20 seconds for others. (The average test duration was 75 seconds.)

From the statistical considerations, concerning only the conversions from magnetic tape to digital form, the averaging appeared to be quite acceptable. On the assumption of a normal probability distribution, a confidence level of 99.5 percent had less than ±1 dB spread for the 10-Hz center frequency octave band data that were averaged for 20 seconds. The 50-second averaging time yielded less than ±0.6 dB spread for the same confidence level and frequency.

The meteorological data (velocity of sound, wind, temperature, and relative humidity as a function of altitude; 79 600 points of information) used in this study were obtained from the facilities of the Marshall Aero-Astrodynamics Laboratory which are located approximately 2 km from the static test stands. These operations are similar to those of a U.S. weather station in data acquisition, record keeping, and handling of statistics. The equipment facilities and data handling techniques are described in reterences 2 and 3. The atmospheric data were obtained from ground level to an altitude of 20 to 50 km. It has been established from these data that, in general, the effects of refraction of sound waves back to the ground plane for distances of approximately 20 km away from the source depend primarily on the existing conditions (velocity profile) at low altitudes, that is, less than 3 kilometers above the ground. To be safe the velocity of sound profiles and vector winds were observed from ground level to an altitude of 5 km.

The atmospheric conditions for all altitudes were acquired by releasing a radiosonde transducer about 2 minutes before firing time. The radiosonde, tracked by a GMD system, reported position coordinates for determination of winds aloft. The temperature, relative humidity, and position coordinates were reported at 30-second intervals. The wind values, after being smoothed by a seven-point weighted mean technique, were then recorded. The relative humidity was used with the temperature and wind vector information to produce velocity-of-sound profiles as functions of azimuth angle,

The meteorological values given were generally in 150-meter altitude increments. This increment varied slightly because of the rate of change of ascent of the balloon with altitude.

DATA SELECTION AND ANALYSIS

After the data had been reduced to a usable form (that is, octave band spectra as a function of distance from the source and all the supporting data including the atmospheric conditions), it became obvious that not all the data were applicable to defining the attenuation caused by the ground surface and its cover. This fact is due to the refractive properties of the layered atmosphere. For example, the atmospheric medium with its layered structure of warmer or cooler air or with winds aloft can alter the sound pressure levels on the ground about the source by refracting the energy along-paths not common with that of propagation in an isentropic homogeneous medium. The resultant is seen in the form of sound pressure gradients (with distance) that are not related to those normally found with the loss in proportion to the inverse of the distance and the normal attenuation properties. For cases of energy being returned to the ground, where ray concentration is greater than normal, the gradient is considered to be positive. It may be highly positive for cases where ray paths converge, a caustic or a focal zone being produced; or conversely, the gradient may be highly negative, and the energy directed away from the ground plane, again deviating from the normal propagation path considered for a homogeneous isentropic atmosphere. These situations occur in the Marshall data, as they would in any locale where the atmospheric gradients are significant. Thus, to determine the attenuation characteristics associated with the ground plane or the atmospheric media, these extraneous effects of atmospheric conditioning must at least be recognized. Since the quantitative effects of refraction are very difficult to describe analytically, the data for cases where significant atmospheric gradients were present were eliminated. It can only be hoped that the effects of scattering and dispersion due to turbulence will be minimized by the selection of data from tests where wind velocity was relatively low; thus, having many tests, especially for the various field conditions, is necessary for any isolation of the variables involved.

The selection of which tests to use, for cases of nonsignificant refraction conditions, was made on the basis of wind velocity and the velocity-of-sound profile (vector profiles) for each LAMS line. The test data were considered to be acceptable for analysis if the wind speed was less than approximately 5 m/sec (ground level), if the gradient did not exceed 10 m/sec-km (0.010 sec^{-1}) for the gross profile characteristics, and if no additional excessive gradients were observed in the small layer structure of the atmosphere. For example, if the gross characteristic of the velocity-of-sound profile up to 3 km altitude was -5 m/sec-km but had a local additional gradient of ±10 m/sec-km over an

altitude segment of greater than a half kilometer, then that test was not considered as representative of a nonrefractive atmospheric situation. This local additional gradient change of ±10 m/sec-km was adopted as a general rule for data selection after examining the data and the results of acoustic ray-tracing programs and decibel contour plots with the meteorological data as input. The gross characteristics of the velocity-of-sound profiles observed from the data used in this study are given in table I with the wind vectors (and standard deviations) for the Huntsville and Athens LAMS lines at altitude increments of one-half kilometer. The temperature and the relative humidity at ground level are also given by seasonal periods (summer, May to August; fall, September to November; winter, December to February; spring, March to April). By applying these criteria for limiting the use of data acquired under what are considered to be significantly refractive conditions, the potential number of data points representing values for attenuation in the frequency range from 1 Hz to 1000 Hz was reduced. (For the first proposed approach, method I, the data bits were reduced from 943 500 to 61 505. See table II).

ANALYSIS METHODS

Several computer programs were written for the IBM 7094 to perform the calculations and data sorting for different analysis methods. The three approaches used are given in the following sections.

Method I

In the first approach all acoustic data were corrected for background noise level. For those cases in which the data did not exceed the noise floor by at least 3 dB, the data were rejected. For a single test case, and along a specific LAMS line where a common directivity index was assumed (that is, the directivity index at 310° azimuth was considered to be constant within ±3° about the line), the octave band sound pressure level for two microphones was assumed to be given by

$$OBSPL_j - OBSPL_k = 20 \log_{10} \frac{R_k}{R_j} + EA(f)\left(R_k - R_j\right) \qquad (1)$$

where OBSPL values are the octave band sound pressure levels at any microphone j and k; R_j and R_k are the distances corresponding to any two microphones; and EA(f) is the excess attenuation per octave band, given in dB/distance. The excess attenuation, that is, the attenuation due to the air, the ground cover, or any other cause (excluding divergence) for any octave band, is given as

$$EA(f) = \frac{OBSPL_j - OBSPL_k + 20 \log_{10} \frac{R_j}{R_k}}{R_k - Rj} \text{ dB/distance}$$

If it is assumed that the EA per unit distance is independent of the distance from the source and if this comparison is made for each microphone or combination of microphones, $\frac{N(N-1)}{2}$ comparisons per octave band are made where N represents the number of microphones which have provided octave band data for that test. (See fig. 2.)

By multiplying the EA values for any one test by the number of comparisons used from that test, that is, $(EA)_{test} \left[\frac{N(N-1)}{2}\right]_{test}$, summing all such terms for many tests, and dividing by the total $\frac{N(N-1)}{2}$ for all the tests (for a given octave band), a weighted average for the excess attenuation is found.

Method II

The second analytical approach was to acquire the EA values as they were similarly obtained by references 4 and 5, among others. The closest microphone was chosen as the reference point and the EA values were then calculated from ever-increasing distances from the reference. (See fig. 2.)
From

$$OBSPL_o - OBSPL_d = 20 \log_{10} \frac{R_d}{R_o} + EA(f)(R_d - R_o)$$

$$EA(f) = \frac{OBSPL_o - OBSPL_d + 20 \log_{10} \frac{R_o}{R_d}}{R_d - R_o} \text{ dB/distance}$$

where R_o is the radial position of the reference microphone, the closest to the source, and R_d indicates the radial position of the next more distant microphone in sequence.

Method III

A third approach was used also to look at the EA values in piecewise distance increments, not overlapping increments, over the entire measurement range. (See fig. 2.) The equations were basically the same; only the input was arranged differently.

The excess attenuation is expressed as

$$EA(f) = \frac{OBSPL_n - OBSPL_{n+1} + 20 \log_{10} \frac{R_n}{R_{n+1}}}{R_{n+1} - R_n} \text{ dB/distance}$$

where R_n is the radius position of any microphone in a sequence and R_{n+1} is the next adjacent microphone at a greater distance from the source. All microphones were used together with the adjacent one to form a piecewise description of EA along the propagation path. Thus, the EA per unit distance would be observed in small increments at an ever-increasing distance from the source. This approach indicates any nonlinear effects of attenuation and the position or distance range at which they would occur, that is, because of the sound pressure decreasing with increased distances, or could help in determining whether the turbulence effects, the terrain, or even whether the meteorological conditions of refraction are causing the attenuation to appear nonlinear or nonuniform over the measurement field.

Method III provides the most information about the EA characteristics with distance along the transmission path since the only averaging used is over the number of tests involved; whereas the other methods involved averaging over long distances and nonuniform sound pressure level gradients.

RESULTS AND DISCUSSION

The methods of handling the acoustic data are varied and should certainly depend on the objective of the researcher. In the literature several forms of analysis are noted; some are presented as dependent on the distance from the source (refs. 4 to 8), others are given for use with various distance ranges (refs. 4 and 9), in another approach (ref. 10) the excess attenuation is given as a function of the product of the distance and the frequency, and still other presentations are given as independent of distance (refs. 7, 11, and 12).

The results herein were all acquired from the same set of data but analyzed in various ways (methods I, II, and III as described) and presented accordingly for use in application to various problems. In the future it is hoped that the complexity of this problem due to the currently inseparable influence of several variables can be reduced. Also the physical phenomena causing the varied interpretations should be separated and more effectively considered. Much more work is to be done with the Marshall data but this work requires a large amount of computer time on a limited basis and therefore will proceed accordingly.

It is thought that the data acquisition program at Marshall – the large number of measurements from many tests, the detail in the meteorological data, the long sound durations, and long averaging times in conjunction with the stationary high-energy sources – makes these data much more appealing for study than some tests with conditions that are somewhat meagerly described in the literature.

Method I

Results for method I (EA values averaged over all possible combinations of microphones, independent of distance) are presented in this section. The EA values derived from this portion of the analysis represent the average attenuation per season (including ground and propagational medium effects) per unit distance over all possible microphone combinations and thus are independent of the distance from the source.

The averaged EA values, computed for each LAMS line, for various seasons (figs. 3 to 6) do not appear to change significantly to merit consideration of the season as a variable in the application of the EA values. From figure 7, however, there appears to be some physically reasonable order to the EA values across the entire frequency range. The highest values of attenuation were observed in the sequence of fall, summer, winter, and spring over most of the frequency range. Since the layer of ground cover has possibly reached a maximum depth in the fall, that is, dropped leaves, highest weed and crop growth, and so forth, the fall season might be of correct order. Likewise the ground cover growth is standing erect and at near maximum height with leaves still on the trees in the summer and thus possibly implies greater attenuation than is observed with the more barren ground plane of the spring and winter. However, the differences in the values for the four seasons (by chosen date) possibly do not merit concern since the spread of data averages is so small. Reference 5 shows a similar spread of EA values for the seasons. The variation is more exaggerated but the ground conditions are possibly quite different in Leningrad, Russia.

The average value of the excess attenuation from method I, including atmospheric and ground effects (constructive and destructive interference is negligible for the frequency range and the geometry) is indicated in figure 8 with the plot of the excess attenuation values for air. (See ref. 13.) Of notable mention for field data is that the excess attenuation for air (ref. 13) tends to exceed the cumulative effects of classical absorption, the excess attenuation for the air media, the effects of turbulence as a scattering agent, and the absorptive properties of the ground plane and its cover (acting to some degree, on the macroscale, as a layer of sound-absorbing material on a wall) at the higher frequency values of 1000 Hz and above. This comparison, of course, considered the averaged temperature and relative-humidity conditions.

The effect of relative humidity on the EA values did not appear to be significant; however, only three tests were available for use in the low humidity range and thus the standard deviations for data were larger than for the comparisons using larger test samples. Likewise, the effect of temperature as measured in the ground plane did not correlate with the EA variations in any discernible order that was incompatible with the seasonal order.

The attenuation at the lower frequency range is somewhat more pronounced than has been expected since few EA values are found in the literature for acoustic energy below 30 Hz. The attenuations in this frequency range are significantly greater than can be attributed to the molecular absorption phenomenon for the atmosphere. The small increase in the EA values (fig. 8) in the 50-Hz region is not explainable, other than being related to some ground-cover characteristics (showing a similar trend on Athens and Huntsville LAMS lines) or to the prevalent physical characteristics of the atmosphere.

Method II

Method II made use of a reference microphone in connection with all others to provide EA values for a sequence of ever-increasing propagation distances. (See fig. 2). This method effectively smooths some of the nonuniform EA values noted over the propagation path (as found from method III).

The EA values, as obtained from approximately 3200 data bits, are provided in figures 9 and 10 for only the summer season because of a lesser number of tests available for analysis in the other three seasons. These data also indicate that the nonlinearity of EA with distance is more pronounced for less than 25 000 feet from the source. Beyond 35 000 feet the nonlinearity is not noted in the data. From observing the averages of the EA values per season from method I (fig. 7), it is expected that any seasonal effect still should be of minimal concern.

Figure 11 delineates the comparison of the results of other researchers for approximately the same conditions; however, referenced reports presented very meager information on the meteorological or other test conditions. It is noted that there is a spread of the EA values over the entire frequency range. Perhaps the ground conditions were a factor in some of the cases where large differences were observed, but it is also possible that other factors could be responsible for some of the wide variations in results. These factors could include a nonstationary sound source, lack of meteorological data, a small number of measurements, the inclusion of data for extreme atmospheric conditions (winds, velocity profiles, and short test durations and data averaging times), and, in general, other similar deficiencies in complete, applicable, and accurate data acquisition.

Method III

The values of EA, as obtained from piecewise distance increments, are given over the entire measurement range; that is, the EA value between microphones 1 and 2 EA_{12} was plotted at the distance midpoint of that increment and EA23 likewise, until all the microphones were used. For several of the octave bands the general results of method III compared favorably with the results of method II. (See figs. 12 and 13 and compare methods II and III for 500 Hz and 250 Hz.) The other octave band frequency data lacked sufficient statistical accuracy for reporting at this time.

The nonuniformity of the variation of EA values with distance, from method III, indicates that they do not always fall into a more orderly pattern as derived from method II results, since there is extensive inherent averaging with that approach (method II). The nonuniformity of EA with distance is physically due to nonuniformity in the data; that is, the sound pressure levels varied nonuniformly. This variation is due to either actual differences in rates of absorption in each of the increments, effects of refraction in certain local areas (lapse conditions for higher EA values, and rays returning for lower EA values), effects of local winds in certain increments, local terrain effects, or other inhomogeneities in the atmosphere. The EA values from method III, however, tend to be positive in an exaggerated manner when there is even a very local shadow zone. Because of the extreme sensitivity to small sound pressure level changes over small distances, the EA values for method III are not statistically acceptable to merit explicit use in an engineering application to airport noise at this time. Thus these small variations in sound pressure levels distort the average EA values and thus present a problem in acquiring a set of'experimental data from the field corresponding to the theoretical perfect atmosphere and terrain conditions of the laboratory.

This third method would be the most descriptive of the three approaches since it provides the EA values as they exist over each small distance increment and these values are not lost in the averaging process; however, a great number of tests would be required for a statistically acceptable definition of the attenuation features. Thus this method did not produce any usable engineering values even with the relatively large number of tests available.

CONCLUSIONS

In general, the following statements can be made concerning the analyses of the data by the three methods described herein:

1. Method I – All possible microphone combinations – provides excess attenuation EA values that are low because of weighted averaging resulting from the nonlinearity effects.

2. Method I serves basically as an approach for recognizing relative EA effects.

3. The EA values for air (molecular absorption) appear to be high for the frequency range above 1000 Hz or 2000 Hz.

4. Seasonal effects on EA values appear to be small.

5. Variations of relative humidity and temperature (ground values) have little effect on EA values.

6. The meteorological effects have a great influence on computed EA values. Supporting data for tests are mandatory.

7. Methods II and III provide comparable results if ground effects are homogeneous and there are no atmospheric refraction cases.

8. Methods II and III more nearly provide the EA values for general engineering/airport use application, The method used should be compatible with the desired objective.

9. The method used for determining EA information should be selected on the basis of its providing the desired objective for engineering application.

REFERENCES

1. Sperry, W. C.; Powers, J. O.; and Oleson, S. K.: Status of the Aircraft Noise Abatement Program. Sound and Vib., vol. 2, no. 8, Aug. 1968, pp. 8-21.

2. Turner, Robert E.; and Schow, Robert R.: MSFC Atmospheric Sounding Station Semiannual Operation Review. MTP-AERO-62-59, NASA George C. Marshall Space Flight Center, 1962.

3. Turner, Robert E.; and Jendrek, Richard A.: Radiosonde Automatic Data Processing System. NASA TM X-53186, 1964.

4. Parkin, P. H.; and Scholes, W. E.: The Horizontal Propagation of Sound From a Jet Engine Close to the Ground, at Radlett. J. Sound Vib., vol. 1, no. 1, Jan. 1964, pp. 1-13.

5. Parkin, P. H.; and Scholes, W. E.: The Horizontal Propagation of Sound From a Jet Engine Close to the Ground, at Hatfield. J. Sound Vib. vol. 2, no. 4, Oct. 1965, pp. 353-374.

6. Anon.: Method for Calculating the Attenuation of Aircraft Ground to Ground Noise Propagation During Takeoff and Landing. AIR 923, Soc. Automot. Eng., Mar. 1, 1968.

7. Dneprovskaya, I. A.; Iofe, V. K.; and Levitas, F. I.: On the Attenuation of Sound as It Propagates Through the Atmosphere. Sov. Phys. – Acoust., vol. 8, no. 3, Jan.-Mar. 1963, pp. 235-239.

8. Ingard, Uno: A Review of the Influence of Meteorological Conditions on Sound Propagation. J. Acoust. Soc. Amer., vol. 25, no. 3, May 1953, pp. 405-411.

9. Franken, Peter A.; and Bishop, Dwight E.: The Propagation of Sound From Aircraft Ground Operations. NASA CR-767, 1967.

10. Wiener, Francis M.; and Keast, David N.: Experimental Study of the Propagation of Sound Over Ground. J. Acoust. Soc. Amer., vol. 31, no. 6, June 1959, pp. 724-733.

11. Anon.: Acoustical Considerations in the Planning and Operation of Launching and Static Test Facilities for Large Space Vehicles. Phase I. BBN 884 (Contract Nas 8-2403), Bolt, Beranek, and Newman, Inc., Dec. 11, 1961.

12. Benson, R. W.; and Karplus, H. B.: Sound Propagation Near the Earth's Surface as Influenced by Weather Conditions. WADC Tech. Rep. 57-353, Pt. I, U.S. Air Force, Mar. 1958. (Available from DDC as AD 130793.)

13. Harris, Cyril M.: Absorption of Sound in Air Versus Humidity and Temperature. NASA CR-647, 1967.

TABLE I.- METEOROLOGICAL CONDITIONS ASSOCIATED WITH THE ACOUSTIC DATA (LAMS)

(a) Summer

Altitude, m	Wind velocity					
	To Athens			To Huntsville		
	ψ^2	μ	σ	ψ^2	μ	σ
0	5.91	0.50	2.38	3.00	-0.16	1.72
500	12.83	.66	3.52	8.87	-.71	2.88
1000	14.50	.25	3.79	12.05	-.79	3.38
1500	16.75	.08	4.09	19.75	-1.25	4.26
2000	17.20	.12	4.14	26.04	-1.79	4.78
2500	18.75	-.29	4.32	21.45	-2.12	4.11
3000	26.25	-.50	5.09	20.45	-2.04	4.03

Altitude, m	Sound velocity (referenced to ground value)					
	To Athens			To Huntsville		
	ψ^2	μ	σ	ψ^2	μ	σ
0	0	0	0	0	0	0
500	16.42	-3.67	1.72	23.67	-4.38	2.11
1000	19.88	-6.79	1.94	62.50	-7.42	2.73
1500	94.08	-9.33	2.65	120.04	-9.75	4.99
2000	139.33	-11.50	2.66	193.41	-12.83	5.36
2500	196.58	-13.75	2.74	250.08	-15.00	5.00

TABLE I.- METEOROLOGICAL CONDITIONS ASSOCIATED WITH THE ACOUSTIC DATA (LAMS) – Continued

Altitude, m	W_A, m/s	W_H, m/s	C_A, m/s	C_H, m/s	T_G, °C	Relative humidity, percent
0	2	1	0	0	31	87
500	1	3	-3	-1		
1000	-1		-7	-4		
	-3		-10	-7		
2000	-3	0	-13	-9		
2500	-4	0	-16	-12		
3000	-4	0	-19	-15		
S-IB; test 37; June 29, 1966						
0	0		0	0	31	84
500	-2		-3	-3		
1000	-3		-7	-5		
1500	-4		-10	-8		
2000	-3	-3	-11	-11		
2500	-4	-3	-14	-14		
3000	-4	0	-17	-17		
0	-2	-3	0	0	26	78
500	2	-8	-3	-9		
1000	0	-11	-3	-14		
1500	0	-13	-5	-18		
2000	0	-13	-8	-21		
2500	-4	-10	-13	-19		
3000	-7	-9	-17	-19		

TABLE I.- METEOROLOGICAL CONDITIONS ASSOCIATED WITH THE ACOUSTIC DATA (LAMS) – Continued

Altitude, m	W_A, m/s	W_H, m/s	C_A, m/s	C_H, m/s	T_G, °C	Relative humidity, percent
0	3	-2	0	0	28	41
500	4	2	-4	-1		
1000	4	2	-7	-4		
1500	5	0	-9	-9		
2000	6	-2	-10	-12		
2500	5	-3	-13	-16		
3000	3	-4	-17	-19		
F-1; test 30; May 11, 1966						
0	5	1	0	0	26	45
500	7	3	-3	-2		
1000	7	7	-5	-1		
1500	5	11	-6	3		
2000	2	13	-10	4		
2500	3	12	-15	3		
3000	5	12	-19	2		
F-1; test 31; May 18, 1966						
0	-2	3	0	0	27	74
500	-3	4	-5	-3		
1000	-5	6	-9	-4		
1500	-6	6	-12	-5		
2000	-7	5	-15	-8		
2500	-10	2	-19	-13		
3000	-11	-2	-23	-19		

TABLE I.- METEOROLOGICAL CONDITIONS ASSOCIATED WITH THE ACOUSTIC DATA (LAMS) - Continued

(a) Summer - Continued

Altitude, m	W_A, m/s	W_H, m/s	C_A, m/s	C_H, m/s	T_G, °C	Relative humidity, percent
0	-4	3	0	0	29	68
500	-6	2	-6	-6		
1000	-7	2	-9	-8		
1500	-9	0	-13	-11		
2000	-9	0	-16	-15		
2500	-9	-1	-16	-15		
3000	-9	-2	-18	-18		
0	1	-3	0	0	30	43
500	2	-2	-2	2		
1000	4	-3	-4	-7		
1500	3	-5	-8	-11		
2000	2	-5	-11	-14		
2500	2	-5	-13	-16		
3000	4	-4	-13	-16		
0	3	0	0	0	32	32
500	3	-3	-7	-7		
1000	2	-3	-7	-10		
1500	1	-4	-11	-14		
2000	2	-6	-13	-19		
2500	2	-9	-15	-24		
3000	4	-10	-13	-25		

TABLE I.- METEOROLOGICAL CONDITIONS ASSOCIATED WITH THE ACOUSTIC DATA (LAMS) - Continued

(a) Summer - Continued

Altitude, m	W_A, m/s	W_H, m/s	C_A, m/s	C_H, m/s	T_G, °C	Relative humidity, percent
F-1; test 35; June 22, 1966						
0	3	-1	0	0	33	33
500	6	-1	0	-3		
1000	6	-2	-4	-8		
1500	6	-4	-6	-12		
2000	6	-5	-9	-17		
2500	9	-6	-7	-18		
3000	11	-6	-6	-19		
23, 1966						
0	5	0	0	0	32	38
500	7	-2	-1	-5		
1000	6	-1	-5	-7		
1500	7	-2	-7	-11		
2000	6	-3	-11	-15		
2500	6	-2	-11	-13		
3000	6	-1	-12	-15		
0	-1	1	0	0	37	47
500	0	0	-3	-5		
1000	-2	-3	-8	-11		
1500	2	-3	-8	-15		
2000	2	-3	-10	-18		
2500	2	-3	-13	-20		
3000	2	-3	-14	-22		

TABLE I.- METEOROLOGICAL CONDITIONS ASSOCIATED WITH THE ACOUSTIC DATA (LAMS) - Continued

Altitude, m	W_A, m/s	W_H, m/s	C_A, m/s	C_H, m/s	T_G, °C	Relative humidity, percent
0	0	1	0	0	37	46
500	-1	2	-5	-5		
1000	-2	0	-8	-8		
1500	-1	0	-11	-11		
2000	0	0	-13	-13		
2500	0	-1	-15	-15		
3000	0	-2	-18	-18		
0	-2	-2	0	0	35	44
500	-3	-2	-4	-4		
1000	-4	-2	-8	-8		
1500	-4	-2	-11	-11		
2000	-4	-2	-12	-12		
2500	-2	-1	-13	-13		
3000	-2	0	-14	-14		
0	-1	-1	0	0	34	51
500	-5	-5	-7	-7		
1000	-3	-3	-8	-8		
1500	-3	-3	-10	-10		
2000	-3	-3	-12	-12		
2500	-2	-2	-15	-15		
3000	-2	-2	-17	-17		

TABLE I.- METEOROLOGICAL CONDITIONS ASSOCIATED WITH THE ACOUSTIC DATA (LAMS) – Continued

(a) Summer – Continued

Altitude, m	W_A, m/s	W_H, m/s	C_A, m/s	C_H, m/s	T_G, °C	Relative humidity, percent
0	2	0	0	0	34	50
500	3	0	-3	-4		
1000	2	-2	-7	-9		
1500	2	-4	-9	-13		
2000	4	-4	-9	-15		
2500	4	-2	-12	-16		
3000	2	-2	-15	-17		
F-1; test 45; July 13, 1966						
0	-2	0	0	0	40	41
500	-3	0	-7	-6		
1000	-4	0	-11	-8		
1500	-5	1	-15	-10		
2000	-5	-1	-16	-15		
2500	-3	-2	-17	-18		
3000	-3	-2	-19	-20		
0	0	0	0	0	39	43
500	-2	-1	-6	-4		
1000	-4	-1	-10	-7		
1500	-4	0	-14	-10		
2000	-5	-2	-17	-14		
2500	-5	-3	-19	-17		
3000	-4	-3	-21	-20		

TABLE I.- METEOROLOGICAL CONDITIONS ASSOCIATED WITH THE ACOUSTIC DATA (LAMS) - Continued

(a) Summer - Continued

Altitude, m	W_A, m/s	W_H, m/s	C_A, m/s	C_H, m/s	T_G, °C	Relative humidity, percent
F-1; test 47; July 25, 1966						
0	1	0	0	0	34	42
500	2	-1	-2	-6		
1000	2	-1	-5	-8		
1500	2	-2	-7	-12		
2000	4	-4	-8	-16		
2500	5	-3	-9	-17		
3000	4	-1	-9	-15		
F-1; test 48; August 5, 1966						
0	0	0	0	0	34	51
500	0	-1	-2	-6		
1000	2	-1	-5	-8		
1500	3	-3	-7	-12		
2000	2	-3	-8	-16		
2500	1	-1	-9	-17		
3000	0	0	-9	-15		
49; August 9, 1966						
0	0	0	0	0	33	53
500	1	2	-3	-3		
1000	0	2	-6	-6		
1500	-1	4	-11	-6		
2000	-1	5	-14	-8		
2500	-1	3	-15	-11		
3000	-1	1	-16	-15		

TABLE I.- METEOROLOGICAL CONDITIONS ASSOCIATED WITH THE ACOUSTIC DATA (LAMS) – Continued

(a) Summer – Concluded

Altitude, m	W_A, m/s	W_H, m/s	C_A, m/s	C_H, m/s	T_G, °C	Relative humidity, percent
0	-3	-3	0	0	27	39
500	-3	-7	-4	-7		
1000	-2	-5	-6	-9		
1500	0	-3	-6	-9		
2000	0	-1	-7	-7		
2500	-3	-1	-10	-8		
3000	-5	0	-13	-8		
F-1; test 65; June 14, 1967						
0	1	3	0	0	33	34
500	2	0	-4	-6		
1000	1	-2	-8	-10		
1500	1	-3	-11	-14		
2000	2	-3	-12	-17		
2500	3	-5	-14	-21		
3000	4	-7	-14	-25		
F-1; test 68; August 16, 1967						
0	3	-2	0	0	30	35
500	4	0	-2	-1		
1000	5	1	-5	-4		
1500	5	0	-7	-8		
2000	5	-3	-9	-13		
2500	4	-5	-13	-17		
3000	5	-2	-13	-15		
Average					32.16	49.96

TABLE I.- METEOROLOGICAL CONDITIONS ASSOCIATED WITH THE ACOUSTIC DATA (LAMS) – Continued

(b) Fall

Altitude, m	Wind velocity					
	To Athens			To Huntsville		
	ψ^2	μ	σ	ψ^2	μ	σ
0	0.4	-0.40	0.49	0.2	-0.20	0.40
500	10.0	-1.60	2.72	3.80	1.40	1.36
1000	7.4	-1.80	2.03	4.0	1.20	1.60
1500	17.8	-3.00	2.97	2.40	.40	1.50
2000	39.4	-4.60	4.27	9.40	.60	3.00
2500	61.8	-6.60	4.27	11.6	.80	3.31
3000	77.4	-7.40	4.76	27.8	1.40	5.08

Altitude, m	Sound velocity (referenced to ground value)					
				To Huntsville		
	ψ^2	μ	σ	ψ^2	μ	σ
0	0	0	0	0	0	0
500	20.8	-4.0	2.19	6.2	-2.2	1.17
1000	51.4	-7.0	1.55	25.4	-4.6	2.06
1500	94.0	-9.2	3.06	51.8	-6.8	2.36
2000	159.0	-11.8	4.44	57.8	-7.0	2.97
2500	225.8	-14.2	4.92	64.6	-7.8	1.94
3000	309.4	-17.0	4.52	90.4	-8.8	3.60

TABLE I.- METEOROLOGICAL CONDITIONS ASSOCIATED WITH THE ACOUSTIC DATA (LAMS) – Continued

(b) Fall – Continued

Altitude, m	W_A, m/s	W_H, m/s	C_A, m/s	C_H, m/s	T_G, °C	Relative humidity, percent
F-I; test 52; September 13, 1966						
0	-1	1	0	0	29	57
500	-1	2	-4	-3		
1000	-1	1	-6	-7		
1500	0	0	-8	-10		
2000	0	1	-9	-10		
2500	-3	3	-12	-9		
3000	-3	5	-15	-9		
F-I; test 54; October 26, 1966						
0	-1	0	0	0	22	20
500	-3	2	-4	-1		
1000	-3	0	-7	-5		
1500	-3	0	-6	-5		
2000	-1	-1	-6	-8		
2500	-1	-2	-6	-9		
3000	-1	-4	-9	-13		
F-I; test 71; October 19, 1967						
0	0	0	0	0	16	29
500	-6	-1	-8	-4		
1000	-5	-1	-10	-6		
1500	-8	-2	-15	-9		
2000	-12	-4	-19	-10		
2500	-13	-4	-20	-10		
3000	-13	-4	-21	-12		

TABLE I.- METEOROLOGICAL CONDITIONS ASSOCIATED WITH THE ACOUSTIC DATA (LAMS) - Continued

(b) Fall - Concluded

Altitude, m	W_A, m/s	W_H, m/s	C_A, m/s	C_H, m/s	T_G, °C	Relative humidity, percent
0	0	0	0	0	20	16
500	2	3	-2	-1		
1000	1	3	-6	-4		
1500	0	2	-9	-7		
2000	-4	5	-14	-4		
2500	-7	5	-18	-6		
3000	-8	9	-20	-3		
F-I; test 73; November 16, 1967						
0	0	0	0	0	15	16
500	0	1	-2	-2		
1000	-1	3	-6	-1		
1500	-4	2	-8	-2		
2000	-6	2	-11	-3		
2500	-9	2	-15	-5		
3000	-12	1	-20	-7		
Average					20.4	27.4

TABLE I.- METEOROLOGICAL CONDITIONS ASSOCIATED WITH THE ACOUSTIC DATA (LAMS) - Continued

(c) Winter

Altitude m	Wind velocity					
	To Athens			To Huntsville		
	ψ^2	EL	σ	ψ^2	EL	σ
0	2.2	-0.6	1.36	1.8	0.2	1.33
500	10.6	-.6	3.20	17.80	1.4	3.98
1000	29.2	-2.8	4.62	23.60	.4	4.84
1500	67.6	-4.4	6.94	25.80	2.2	4.58
2000	116.4	-6.4	8.68	29.2	4.0	3.63
2500	128.2	-7.4	8.57	45.40	6.2	2.64
3000	147.6	9.2	7.93	63.2	7.6	2.33

Altitude, m	Sound velocity (referenced to ground value)					
	To Athens			To Huntsville		
	ψ^2	μ	σ	ψ^2	EL	σ
0	0	0	0	0	0	0
500	14.0	-2.8	2.48	12.2	-1.8	2.99
1000	63.6	-7.2	3.43	3.8	-5.2	3.31
1500	136.6	-10.2	5.71	31.8	-4.6	3.26
2000	213.8	-12.6	7.42	15.8	-3.0	2.61
2500	293.6	-15.2	7.91	19.8	-2.6	3.61
3000	417.2	-19.2	6.97	32.4	-2.8	4.96

TABLE I.- METEOROLOGICAL CONDITIONS ASSOCIATED WITH THE ACOUSTIC DATA (LAMS) – Continued

Altitude, m	W_A, m/s	W_H, m/s	C_A, m/s	C_H, m/s	T_G, °C	Relative humidity, percent
S-IC; test 16; February 17, 1966						
0	-2	-2	0	0	10	38
500	-2	-4	-4	-7		
1000	-4	-6	-8	-11		
1500	-6	-4	-12	-10		
2000	-8	0	-13	-5		
2500	-8	6	-15	0		
3000	-10	11	-18	-3		
0	-2	2	0	0	13	38
500	-2	7	-4	-1		
1000	-8	7	-12	-2		
1500	-14	6	-19	-3		
2000	-20	6	-25	-4		
2500	-20	6	-29	-7		
3000	-20	5	-31	-9		
0	1	1	0	0	20	40
500	2	2	-1	-1		
1000	1	1	-5	-5		
1500	3	3	-5	-5		
2000	3	3	-5	-5		
2500	2	3	-7	-7		
3000	2	5	-11	-11		

TABLE I.- METEOROLOGICAL CONDITIONS ASSOCIATED WITH THE ACOUSTIC DATA (LAMS) - Continued .

(c) Winter - Concluded

Altitude, m	W_A, m/s	W_H, m/s	C_A, m/s	C_H, m/s	T_G, °C	Relative humidity, percent
S-IB; test 32; January 17, 1966						
0	-1	0	0	0	20	50
500	-5	-2	-6	-3		
1000	-7	-4	-9	-6		
1500	-9	-2	-12	-5		
2000	-10	1	-17	-3		
2500	-13	5	-22	0		
3000	-15	8		2		
S-IB; test 40; November 16, 1966						
0	1	0	0	0	18	60
500	4	4	1	1		
1000	4	4	-2	-2		
1500	4	8	-3	0		
2000	3	10	-5	2		
2500	2	11	-8	1		
3000	-3	9	-14	-2		
F-1; test 24; April 27, 1966						
0	3	0	0	0	27	75
500	3	5	-3	2		
1000	2	8	-7	4		
1500	0	11	-11	4		
2000	-1	12	-13	4		
2500	-2	14	-17	4		
3000	-4	14	-22	0		

TABLE I.- METEOROLOGICAL CONDITIONS ASSOCIATED WITH THE ACOUSTIC DATA (LAMS) - Continued

(d) Spring

Altitude, m	Wind velocity					
	To Athens			To Huntsville		
	ψ^2	μ	σ	ψ^2	μ	σ
0	6.5	0.16	2.54	8.16	1.83	2.19
500	23.3	.00	4.83	44.83	5.83	3.29
1000	16.16	-1.50	3.73	71.5	7.83	3.19
1500	15.83	-2.83	2.80	99.33	9.33	3.50
2000	27.50	-4.50	2.70	113.33	10.0	3.65
2500	52.00	-6.66	2.76	141.0	11.0	4.47
3000	78.0	-8.0	3.74	150.33	11.33	4.69

Altitude, m	Sound velocity (referenced to ground value)					
	To Athens			To Huntsville		
	ψ^2	μ	σ	ψ^2	μ	σ
0	0	0	0	0	0	0
500	18.67	-3.33	2.75	8.17	.83	2.73
1000	63.00	-7.67	2.04	10.50	.16	3.24
1500	129.66	-11.33	1.14	20.50	-1.17	4.38
2000	206.66	-14.33	1.15	26.17	-2.25	4.59
2500	378.00	-19.33	2.08	29.17	-2.83	4.60
3000	520.00	-22.67	2.46	45.00	-5.00	4.47

TABLE I.- METEOROLOGICAL CONDITIONS ASSOCIATED WITH THE ACOUSTIC DATA (LAMS) - Continued

(d) Spring - Continued

Altitude, m	W_A, m/s	W_H, m/s	C_A, m/s	C_H, m/s	T_G, °C	Relative humidity, percent
F-1; test 18; March 18, 1966						
0	1	3	0	0	19	100
500	1	12	3	6		
1000	-2	14	8	5		
1500	-5	16	12	5		
2000	-5	16	15	3		
2500	-7	16	17	3		
3000	-9	17	21	2		
F-1; test 19; March 21, 1966						
0	0	4	0	0	28	43
500	2	4	-2	-2		
1000	0	6	-7	-4		
1500	-2	7	-12	-7		
2000	-5	8	-13	-8		
2500	-7	10	-21	-7		
3000	-7	10	-23	-10		
F-1; test 20; March 21, 1966						
0	3	4	0	0	28	44
500	5	8	0	1		
1000	2	9	-6	-1		
1500	1	9	-10	-4		
2000	-1	10	-16	-6		
2500	-5	11	-21	-6		
3000	-4	13	-21	-6		

TABLE I. - METEOROLOGICAL CONDITIONS ASSOCIATED WITH THE ACOUSTIC DATA (LAMS) – Concluded

Altitude, m	W_A, m/s	W_H, m/s	C_A, m/s	C_H, m/s	T_G, °C	Relative humidity, percent
F-1; test 21; March 29, 1966						
0	-2	-2	0	0	16	25
500	-1	2	-3	0		
1000	-2	4	-6	-1		
1500	-4	5	-10	-1		
2000	-7	4	-14	-4		
2500	-8	2	-18	-7		
3000	-9	2	-21	-9		
0	-4	2	0	0	23	17
500	-10	4	-9	-2		
1000	-9	6	-12	-2		
1500	-7	8	-13	-4		
2000	-8	10	-15	-4		
2500	-11	13	-22	-4		
3000	-15	12	-28	-7		

TABLE II.- NUMBER OF DATA SAMPLES FOR EACH SEASON FOR HUNTSVILLE AND ATHENS LAMS FOR METHOD I

[Total, 61 565 data points]

(a) Huntsville

Season	Number of data samples at a frequency, Hz, of –											
	1	2	4	8	16	32	63	125	250	500	1000	2000
Spring	120	165	395	457	556	497	357	348	311	165	24	1
Summer	795	937	1789	2004	2194	1802	1330	1348	1099	633	160	30
Fall	293	352	632	658	696	537	312	287	215	126	33	2
Winter	467	509	637	670	732	694	605	516	352	205	64	15
Total	1675	1963	3453	3789	4178	3530	2604	2499	1977	1129	281	48

(b) Athens

Season												
	1	2	4	8	16	32	63	125	250	500	1000	2000
Spring	129	192	351	544	627	622	572	525	364	165	33	8
Summer	1109	1552	2593	3056	3227	3058	2687	2496	1881	678	116	7
Fall	180	258	435	511	586	576	525	464	293	146	56	5
Winter	344	357	419	492	551	498	445	342	245	76	38	5
Total	1762	2359	3798	4603	4991	4754	4239	3827	2783	1065	243	25

MICROPHONE LAYOUT FOR LAMS LINES

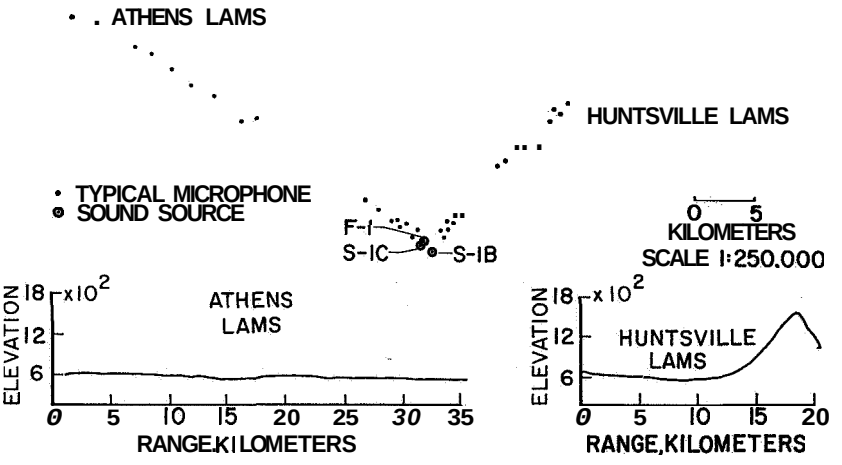

Figure 1

VARIATIONS OF METHODS

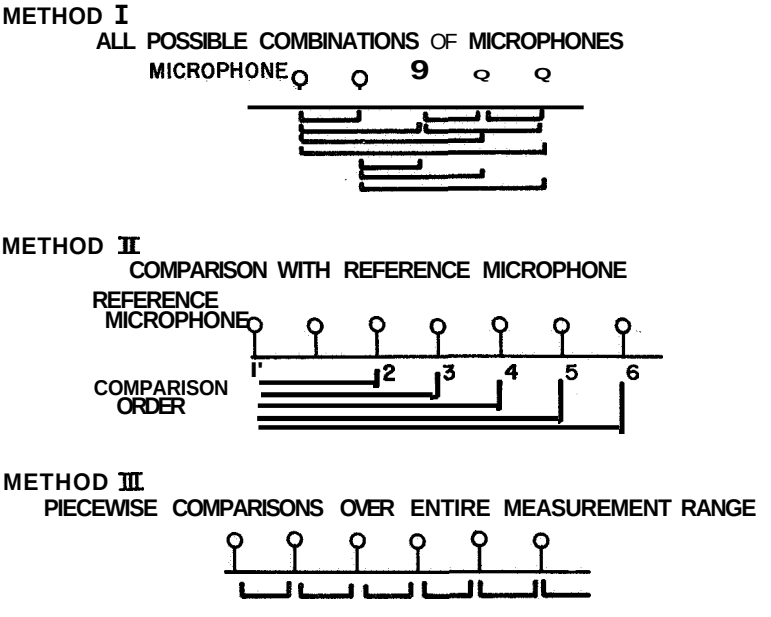

Figure 2

EXCESS ATTENUATION (METHOD I) FOR GROUND-TO-GROUND PROPAGATION FOR FALL SEASON AT MSFC,ALA.

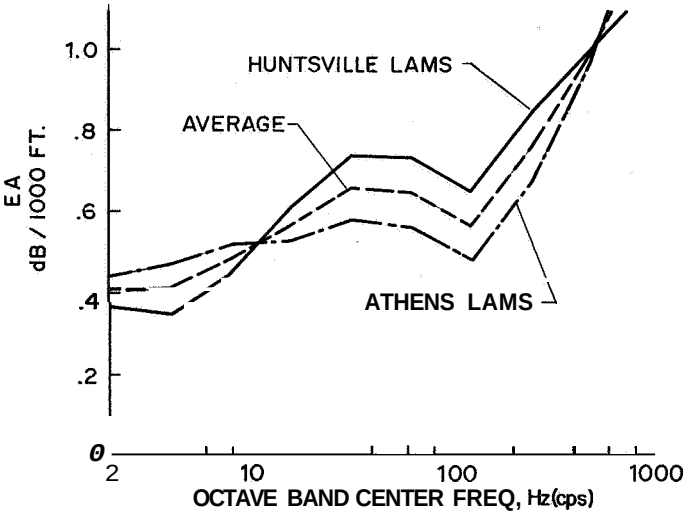

Figure 3

EXCESS ATTENUATION (METHOD I) FOR GROUND-TO-GROUND PROPAGATION FOR SUMMER SEASON AT MSFC,ALA.

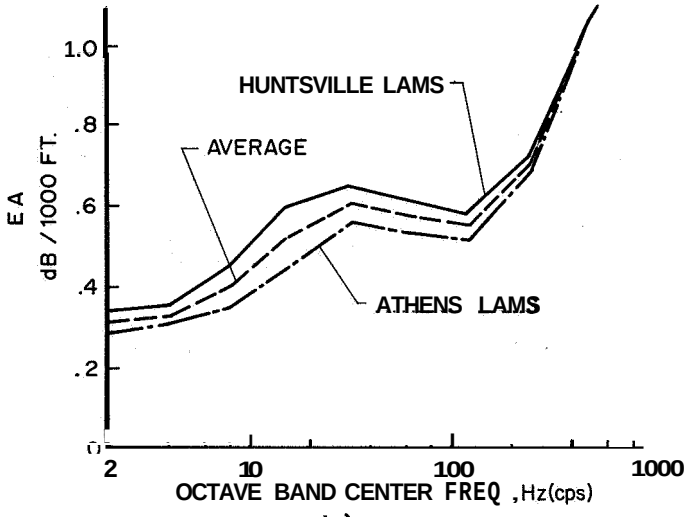

Figure 4

EXCESS ATTENUATION (METHOD I) FOR GROUND – TO-GROUND PROPAGATION FOR WINTER SEASON AT MSFC, ALA.

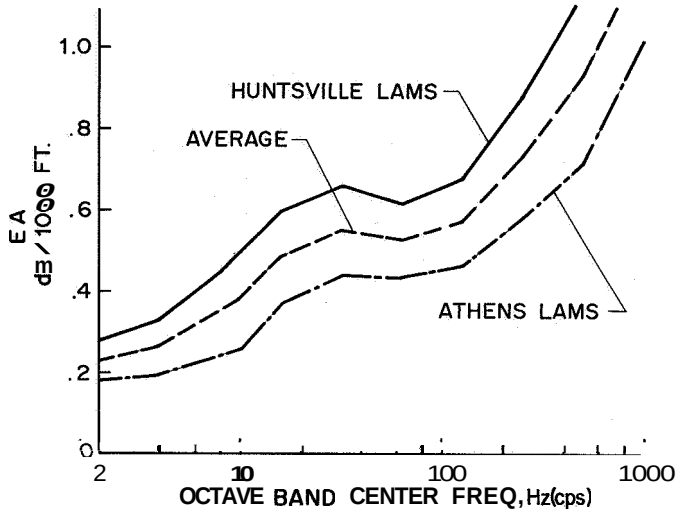

Figure 5

EXCESS ATTENUATION (METHOD I) FOR GROUND – TO-GROUND PROPAGATION FOR SPRING SEASON AT MSFC, ALA.

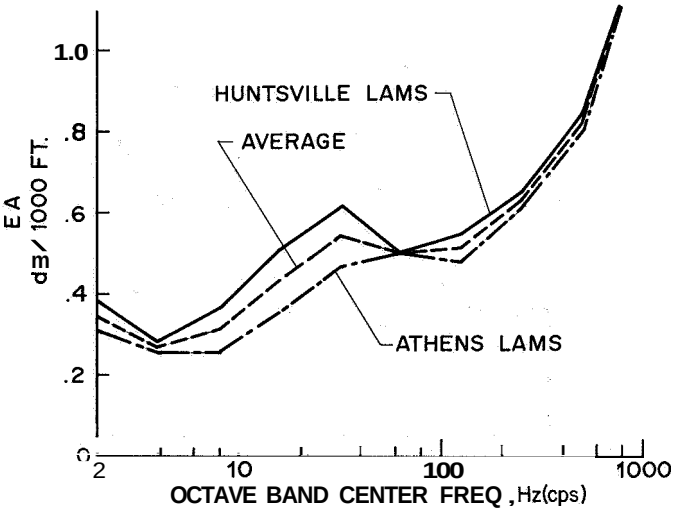

Figure 6

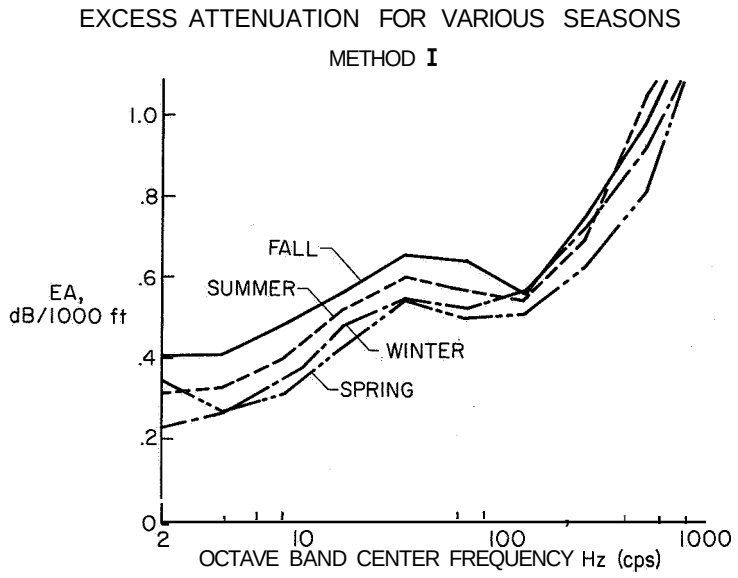

Figure 7

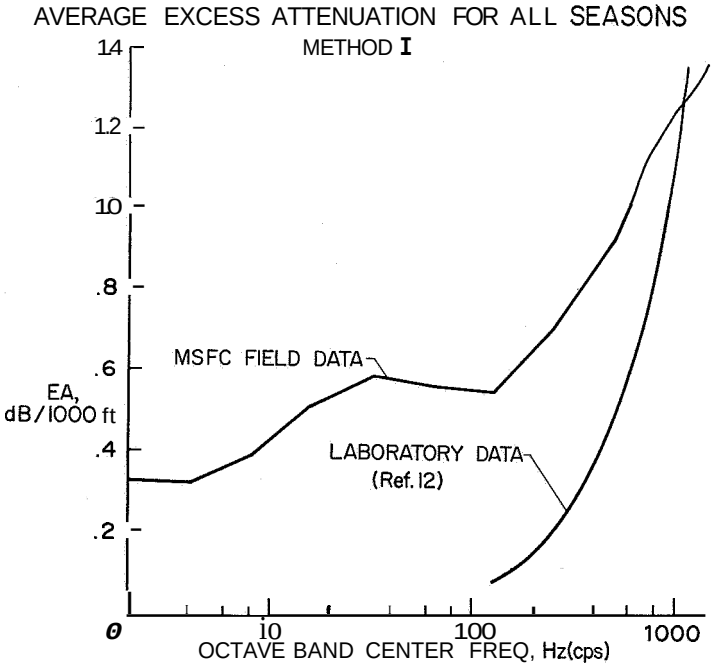

Figure 8

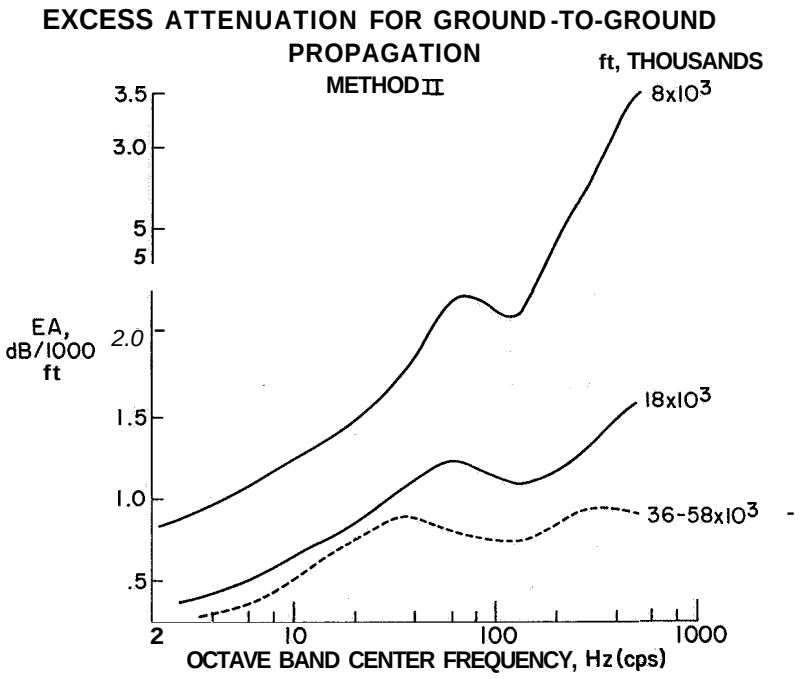

Figure 9

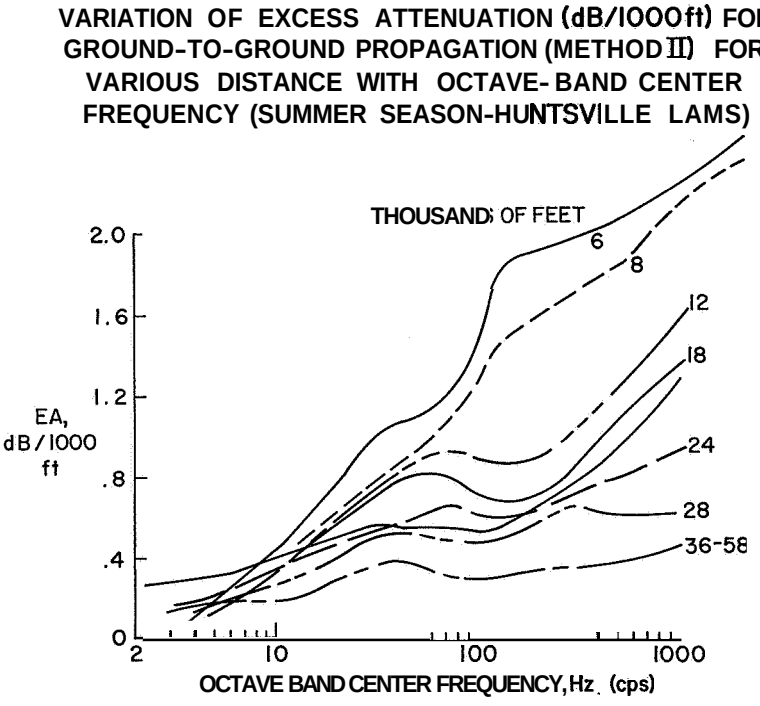

Figure 10

EXCESS ATTENUATION (dB/1000ft) AT A 2-KILOMETER DISTANCE AS A FUNCTION OF OCTAVE-BAND CENTER FREQUENCY, Hz

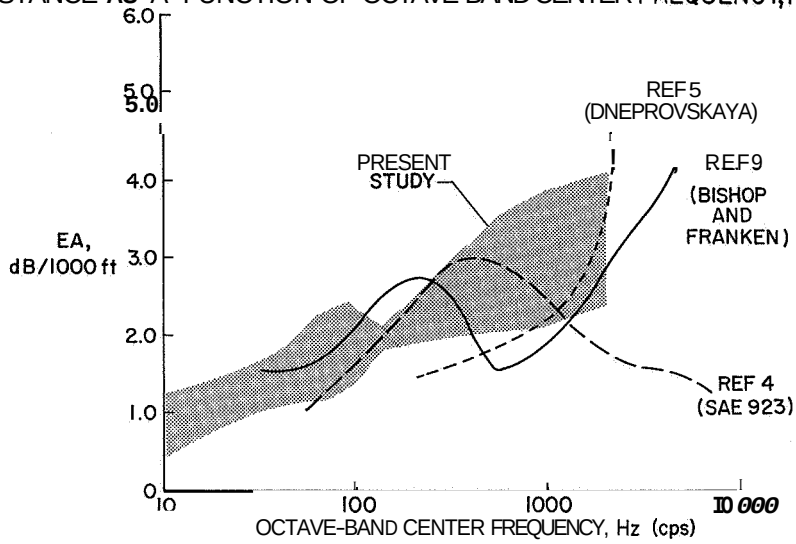

Figure 11

TYPICAL EXCESS ATTENUATION METHODS II AND III; 500 Hz CENTER FREQUENCY BAND

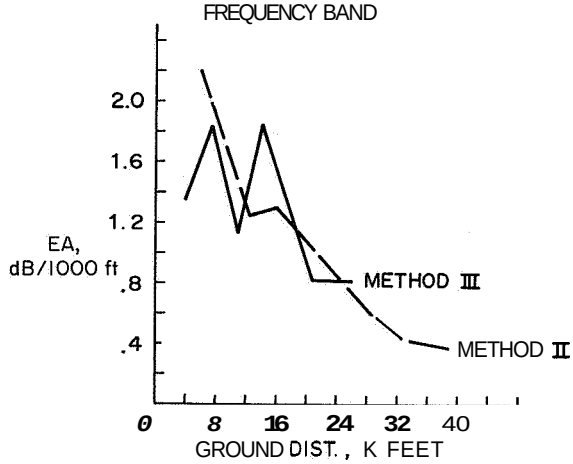

Figure 12

EXCESS ATTENUATION FROM METHODS II AND III
(SUMMER SEASON)
250 Hz CENTER FREQUENCY BAND

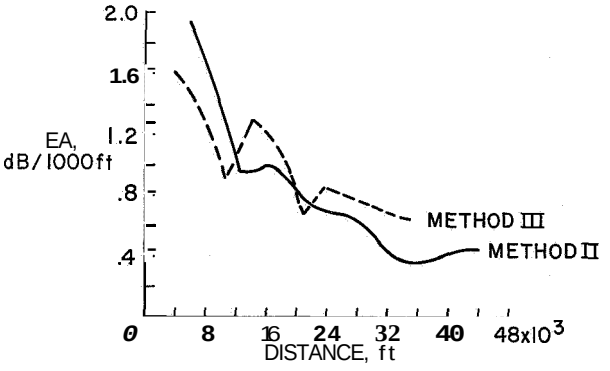

Figure 13

32. EFFECTS OF ATMOSPHERIC REFRACTION ON FAR-FIELD SOUND PROPAGATION

By Orvel E. Smith

NASA George C. Marshall Space Flight Center

32

SUMMARY

Far-field sound intensity levels are calculated by using a theoretical model based on refraction laws. The theoretical model requires a knowledge of the sound-source characteristics and the velocity-of-sound profile. The velocity-of-sound profile is derived from virtual temperature, wind speed, and wind direction, which are either measured or predicted. The necessary simplifying assumptions used in deriving the theoretical model are discussed. The sound intensity level as derived from the theoretical model and empirical measurements from static firings of the Saturn booster are compared. Practical operation techniques used in obtaining atmospheric measurements, atmospheric predictions, and sound-intensity-level calculations for the static firing of large boosters are discussed.

INTRODUCTORY DISCUSSION

Characteristics of Sound Source

In order to indicate the magnitude of the sound generated from several aerospace boosters, a comparison of the estimated total acoustical power level for Jupiter, Saturn I, Saturn V, and a 20-million-pound-thrust booster is presented in figure 1. The values are determined by assuming an exhaust velocity for the engines and by assuming that 1 percent of the jet total power is converted into acoustical power. An increase of only 10 dB for the total acoustical power level of the 1.5-million-pound-thrust engine over that of the 0.15-million-pound-thrust engine is not an impressive increase. However, of greater importance is the fact that as the engine thrust increases, a larger part of the acoustical energy is generated at the lower frequencies. The theoretically derived power levels do not form an estimate of the frequency dependence of the acoustical energy. For this reason experimental values for the acoustical power level are needed. It is known (ref. 1) that the power spectrum of peak acoustical energy for the Jupiter engine shifts by 1 octave toward the lower frequencies of Saturn I. The acoustical energy generated by the Saturn I engine peaks between 10 cps and 100 cps (ref. 1). The lower the frequency, the smaller the acoustical attenuation is for sound propagation through the atmosphere, and thus the greater the possibility is of disturbances to the surrounding communities. Also, the lower the frequencies, the higher the probability becomes that building

structures will be damaged as a result of acoustical energy resonating with the natural frequencies of building structures. The sound directivity of the source is also an important characteristic of the sound source. The study of sound propagation can be approached from three interrelated uisciplines: (1) the characteristic of the sound source; (2) the propagating media; and (3) the response of the receiver.

Inverse Square Law for Sound Propagation

By using the estimated total acoustical power level for the Jupiter, Saturn I, and Saturn V vehicles and the assumptions of the inverse square law for sound propagation, the overall sound pressure level in decibels (dB re: 10^{-13} watt) as a function of distance from the sound source is calculated (see fig. 2). The value of 110 dB has been selected as a critical overall sound pressure level in terms of disturbances to the surrounding community. The radius for the critical sound pressure level, with the assumption of the inverse square law, is 10 km for the Saturn I and 19 km for the Saturn V. Under the assumption of the inverse square law for sound propagation, the prediction would be that every time a Saturn V is static fired at George C. Marshall Space Flight Center (MSFC), an overall sound pressure level equal to or greater than 110 dB would result over the city of Huntsville, Alabama, as well as over a number of surrounding communities (a populated area of approximately 200 000 inhabitants). (See fig. 3.)

The inverse square law assumes a homogeneous medium through which the acoustical energy is propagated; that is, the velocity of sound with respect to altitude and horizontal distance is constant. Although this condition never exists in the real atmosphere, the inverse square law has some theoretical value in understanding certain boundary or limiting conditions for the propagation of sound through the atmosphere and gives a first estimate of the magnitude of the problem for far-field sound intensity levels.

Approaches to Problem of Far-Field Acoustics

In view of the overall sound pressure level as a function of distance from the sound source as estimated by the inverse square law, the question of what can be done to reduce the problem of sound generated by the large engines arises. Three approaches are followed:

(1) Locating the sound source in a remote area (A new static test facility located in a less densely populated area has been developed; the MSFC-Mississippi Test Facility (MTF) located in southern Mississippi has been in operation since early 1966, Static firings of the Saturn V booster (S-IC) and F-1 engines have continued at MSFC in Huntsville, but on a reduced firing schedule.)

(2) Suppressing the sound at the source (The MSFC Test Laboratory has a working sound-suppression model. From this model, sound-suppression techniques can be studied, and the feasibility of engineering a full-scale sound-suppression system can be determined.)

(3) Restricting the operation (This approach consists of three parts; first, the relationship between atmospheric conditions and sound propagation is determined; then, the atmospheric conditions which cause anomalous sound propagation are predicted; and, finally, static tests are restricted to those conditions which will not produce high sound pressure levels in the surrounding communities. This approach is discussed in detail subsequently.)

RAY ACOUSTICS AND SOUND INTENSITY LEVEL

One method that has been used by several investigators (refs. 2 to 4) to study the relationship between atmospheric conditions and sound propagation over long distances is known as ray acoustics or sound ray tracing technique. Essentially, the acoustical equivalence to Snell's refraction law is derived and a system of practical equations developed to obtain the ray patterns. By definition, a ray is a curve whose tangent everywhere points in the direction in which the energy contained in the vibrating element is propagated. The derivation of the acoustical equivalence to Snell's refraction law is not presented herein since the derivation in view of the applications to the acoustic problem at MSFC is presented in detail by Heybey in reference 5 and more recently by Buell in references 6 and 7. Furthermore, these investigators give the necessary analytical expressions for determining the theoretical sound intensity level. The following results on sound attenuation are obtained from reference 6, and the section "Formulation for Geometry of Sound Rays" is a direct quote from that reference.

Sound Attenuation

In reference 6 an analytical description for hemispherical spreading of sound intensity at a distance is expressed as

$$I = \left(\frac{W}{\pi r^2}\right)\exp(-\alpha r) \qquad (1)$$

where W is the sound power, a is the attenuation coefficient, and I is the intensity at a distance r. The effect of the atmosphere on sound attenuation is obtained by an analysis of the factors that influence the attenuation coefficients. For sound in the atmosphere, the attenuation coefficient is divided into three parts:

$$a = \alpha_1 + \alpha_2 + a3 \qquad (2)$$

where α_1 is the classical absorption, α_2 is the intermolecular absorption, and α_3 is the miscellaneous absorption (e.g., attenuation by fog, clouds, dust, and scattering due to small-scale eddies of wind and temperature).

The classical absorption α_1 is made up of four parts:

$$\alpha_1 = \alpha_v + \alpha_c + \alpha_d + \alpha_r \tag{3}$$

where α_v is absorption due to viscosity, α_c is absorption due to conduction heat, α_d is absorption due to molecular diffusion, and α_r is absorption due to radiation of heat.

The attenuation coefficients are discussed in references 8 and 9, but they have been stated here for purposes of completeness and comparison.

Estimates for α_1 and α_2 have been made in reference 6 with the use of perturbation methods for realistic small-scale and large-scale variations in the atmospheric parameters which affect these coefficients.

The root-mean-square variability of the classical attenuation coefficient α_1, at a frequency f of 1 kilocycle and a distance r of 10 km, is given as approximately 0.009 dB for small-scale variations in the atmospheric parameters (variation in the correlation scale parameter of 0.2 km and standard deviation in temperature of 0.3° C) and 0.14 dB for large-scale variations in the atmospheric parameters (standard deviation in temperature of 3.0° C).

The upper limit for the root-mean-square variability of the intermolecular absorption coefficient α_2, at a distance r of 10 km, is given as 0.2 dB for small-scale variations in the atmospheric parameters and 5.0 dB for large-scale variations. Over short time periods, α_2 is negligible, but over long periods where conditions on the entire ray path are subject to change, the variability of α_2 is quite large. The value of α_2 depends on a complicated function of the sound frequency and the water vapor content of the air, whereas α_1 is mainly temperature dependent and related to frequency in a much simpler manner. From these results, it is noted that the variability of α_2 can be much larger than the variability of α_1.

Formulation for Geometry of Sound Rays (Ref. 6)

"The geometry of the sound rays has a pronounced effect on sound intensity estimates. The usual ray tracing methods for an atmosphere consisting of layers that are homogeneous in the horizontal are based on the ray equations

$$\begin{aligned} dx/dt &= c\cos\varphi + u \\ dy/dt &= u \\ dz/dt &= c\sin\varphi \end{aligned} \tag{4}$$

and a variation of Snell's law

$$\frac{c}{\cos\varphi} + u = \frac{c_o}{\cos\varphi_o} + u_o = K \quad \text{(a constant)} \tag{5}$$

where (x,y,z) refer to a "ray point", and
c – speed of sound, u – wind component in the plane of propagation, v – wind component perpendicular to the plane of propagation, φ – elevation angle of the phase normal (from horizontal upward), "o" – reference to initial conditions at the source. It is assumed that c, u, v are functions of the vertical coordinate, z. The plane of propagation is taken as the (x,z) plane. It is readily seen from (5) that if the combination c(z) + u(z) equals the value initially on the right-hand side, the value of φ is zero and the "ray" is horizontal. When such conditions prevail the ray is bent earthwards and a "direct" sound ray returns to earth.

"The ray equations (4) and Snell's law (5) may be solved explicitly for a layered atmosphere if suitable assumptions are made concerning the variations of c(z) and u(z) within the layers. Since c(z) and u(z) are measured at discrete points, the usual assumption is that values of c(z) and u(z) are linear functions of z between these points. A system of equations for calculating the ray paths under these conditions is given by the system of relations

$$\begin{aligned}
r_2 - r_1 &= -R(\sin\psi_2 - \sin\psi_1), \\
\tan\psi_1 &= c_1 \sin\varphi_1/(c_1\cos\varphi_1 + u_1), \\
\tan\psi_2 &= c_2 \sin\varphi_2/(c_2\cos\varphi_2 + u_2), \\
\cos\varphi_1 &= c_1 \cos\varphi_o/\left[c_o - (u_1 - u_o)\cos\varphi_o\right], \\
\cos\varphi_2 &= c_2 \cos\varphi_o/\left[c_o - (u_2 - u_o)\cos\varphi_o\right], \\
1/R &= \left[(c_2 - c_1)\cos\varphi^* - (u_2 - u_1)\right]/c^*(z_2 - z_1), \\
\cos\varphi^* &= (\cos\varphi_1 + \cos\varphi_2)/2, \\
c^* &= (c_1 + c_2)/2.
\end{aligned} \tag{6}$$

In the above, r_2-r_1 is the horizontal distance traveled by the ray in crossing the layer from z_1 to z_2. The subscripts 1 and 2 refer to the bottom and top of this layer, respectively. The total ray path is obtained by adding a string of relations like the first above as the ray passes through successive layers until one is reached in which the ray becomes horizontal. When this occurs the distance traveled is doubled to find the final point where the ray returns to the ground (horizontal). The second and third relations of (6) give the inclination of the ray tangent, ψ, at the bottom and top of the layer. The fourth and fifth relations give the inclination of the phase normal, φ, at the bottom and top of the layer; re-statements of Snell's law, (2). The sixth relation gives the radius of curvature, R, of the ray in the layer. Since the sixth relation is in finite difference form, averaged values

of cos φ^* and c^* are used as given by the last two relations. In the above, the rays are arcs of circles within each discrete layer.

"The distinction between phase normal and ray tangent has been maintained. Inspection of the second and third relations also indicate that ψ and φ differ but little. In the atmosphere $c \geq 330$ msec^{-1} while u is at most of the order of 30 msec^{-1} in the lower few kilometers with which we are concerned. In many ray tracing models this distinction is ignored as trivial. Since the elevation angle of the phase normal, φ, seldom exceeds 20^o or so, ray tracing models frequently use a simplified form of Snell's law, $(c+u)/\cos\varphi = (c_o+u_o)/\cos\varphi_o$. In view of the errors in wind measurement, the difference in the results of using this simplification or the more correct form, (5), appears insignificant.

When the rays are computed, the intensity is estimated from the expression

$$I = I_* \, f \, \exp(-\alpha r) \tag{7}$$

where I_* is the intensity expected from hemispherical spreading, and the final factor is the attenuation as in (1). The new factor, f, is the "focusing factor", which, for rays returning to the ground, is

$$f = r/\left[\tan\psi_o(\partial r/\partial\psi_o)\right]. \tag{8}$$

The focusing factor expresses nothing more than the area of a ray tube compared with its initial area, i.e., the amount of spreading of the rays. (The ray tube is the locus of sound energy flow while the phase normals are normals to the surfaces of constant phase or wave fronts. The presence of wind forces a distinction between these directions.)

"It is readily seen from (8) that if $\partial r/\partial\psi$ should be zero for a returning ray, the intensity from (7) would become infinite. Such a point (or locus of points) is called a focus. The ray tracing method fails to adequately describe the situation at such points and intensity must be estimated by more sophisticated procedures. These zones, under suitable conditions, are locations of unusually high sound intensity."

Velocity-of-Sound Profile

The first essential in applying the sound ray tracing technique is an adequate description of the velocity-of-sound profile. The velocity of sound is given by

$$c = 20.0468T^* + \text{Wind component}$$

where T^* is virtual temperature in ^{o}K and c is the velocity of sound in m/sec. The wind component is longitudinal to the azimuth of interest and is determined from the wind speed and direction.

In the practical ray tracing equations that are used herein, the velocity of sound with respect to height is considered to be linear over a small height increment or layer. The height increment is taken to be approximately 200 meters as determined by data reduction for the velocity of sound from rawinsonde measurements at 1/2-minute increments of balloon elapse time. The velocity of sound with respect to altitude is the only required data for the ray tracing equations. This system of equations simply traces the ray through the atmosphere by computing the segment of path in each succeeding layer. The path of the ray will either continue to transverse the layers or return to the earth's surface, depending on the slopes of the velocity-of-sound profile or vertical gradients. Two fundamental assumptions underlying ray tracing methods are as follows: (1) the change of speed of sound in a wavelength is small compared with the speed of sound (i.e., $\lambda|\nabla c| << c$); and (2) the variation of the properties of the air over a distance of 1 wavelength must be small $\left(\text{i.e., } \lambda|\nabla^2 c| << |\nabla c|\right)$. Here ∇c is the gradient of c and $\nabla^2 c$ is its Laplacian. Buell (ref. 6) gives the interpretation that the speed of sound must change smoothly from place to place. These requirements are equally applicable to the wind vector. To assist in determining how detailed the velocity-of-sound profile should be for ray acoustics to be valid, Buell (ref. 6) has evaluated the inequality

$$H >> \left(\lambda^2 \frac{c_0}{4\pi} \frac{dc}{dz}\right)^{1/3} = H^*$$

For the ray method to be valid, H (the depth of the uniform layer) must be much greater than H*. This inequality relationship is illustrated in figure 4, which is taken from reference 6. In reading from figure 4, for a velocity-of-sound gradient dc/dz of 0.008 sec^{-1} and a wavelength λ of 50 meters, H^* is 200 meters. The depth of the uniform layer H should be much greater than 200 meters for the ray method to be valid. The merits of this relationship were actually experienced. The MSFC Aerospace Environment Division is responsible for all atmospheric measurements, predictions, and related research for MSFC. The MSFC Test Laboratory is responsible for all static firings and thus the far-field acoustic predictions. In seeking ways to improve far-field sound-intensity estimations, atmospheric measurements were furnished to the Test Laboratory at 15-second rawinsonde time increments which correspond to height increments of about 100 meters. A comparison of the derived sound intensity level with measured sound pressure levels shows greater discrepancies in the results than when atmospheric measurements were furnished at 30-second balloon-elapse-time increments or approximately 200-meter height increments.

From ray acoustic calculations, the vertical gradients of the velocity of sound with respect to the ray patterns can be characterized. Five idealized velocity-of-sound profiles are presented in figure 5. The first profile has a single negative gradient. The rays are deflected upward into the atmosphere, and this produces the condition of no rays

returning. The second profile is known as the "zero" gradient. This condition is required for the inverse square law of sound propagation to be valid.

The third profile has a positive gradient followed by a negative gradient. This condition produces ray concentration and, in practice, has been observed to produce near uniformity in the distance between consecutive intercepts of the ray to the plane tangent to the initial velocity of sound. Thus, uniform rays returning could be an alternate description for this condition. Also, this type of profile closely approximates sound intensity levels derived from the inverse square law.

The fourth profile is characterized by a negative gradient, then a positive gradient, followed by a negative gradient. This condition produces ray focusing. The positive gradient must be such that the velocity of sound in this layer exceeds that at the earth's surface or the initial velocity of sound. The fifth profile produces the combination condition of ray concentration and focusing.

The ray path for idealized velocity-of-sound profiles has been computed with the use of a general-purpose analog computer. The resulting ray profiles are shown in figures 6 to 10 to illustrate specific characteristics of the ray profile patterns for the given velocity-of-sound profiles. The velocity-of-sound gradients are comparable to those which could occur in the atmosphere, but they do not necessarily represent the most severe velocity-of-sound gradients. In a calm atmosphere – that is, with no wind and a dry-adiabatic-lapse rate of 10° C per 1000 meters of altitude (a temperature decrease of 10° C per 1000 meters), the resulting velocity-of-sound gradient dc/dz would be $-0.006\ \text{sec}^{-1}$, since a change in temperature of 1° C produces approximately a 0.6-m/sec change in the speed of sound for the usual ranges of atmospheric temperature near the ground. An adiabatic-lapse rate is a very unstable atmosphere and a condition that would not exist over a very thick layer for a long time without the wind blowing. A reasonably large value for wind shear near the ground over a 1000-meter layer is $0.002\ \text{sec}^{-1}$. This value of wind shear first added to and next subtracted from -0.006 gives the values for the velocity-of-sound gradient of $-0.004\ \text{sec}^{-1}$ and $-0.008\ \text{sec}^{-1}$, corresponding to the downwind and upwind directions, respectively. A reasonably large temperature increase with height up to 500 meters is 20° C over the United States Plain states during early morning in winter. With this condition, the wind should be calm. The resulting value for dc/dz would be $0.024\ \text{sec}^{-1}$. Large temperature inversions also occur in the Los Angeles area. Using a lapse rate of one-half that of the dry adiabatic lapse and a wind shear of $0.002\ \text{sec}^{-1}$ over 1000 meters produces values for dc/dz of $-0.001\ \text{sec}^{-1}$ and $0.005\ \text{sec}^{-1}$. The general formula for the velocity-of-sound gradient can be expressed as $\frac{\partial T}{\partial z}\frac{a}{\partial T} - \frac{\partial u}{\partial z}$, where $\partial T/\partial z$ is the vertical temperature gradient taken as negative for temperature decreasing with height and positive (an inversion) for temperature increasing with height, where $\frac{\partial c}{\partial T} = \frac{10}{T^{1/2}}$ is the speed-of-sound gradient with T in $^{\circ}$K and $\partial c/\partial T$

in $m\text{-}sec^{-1}\text{-}{}^{o}K^{-1}$, and where $\partial u/\partial z$ is the wind-component gradient, with (+) indicating the downwind direction and (-) indicating the upwind direction. Thus, for no change in wind direction with respect to height and with a temperature decrease of 5^{o} C per 1000 meters (a common occurrence), any time the wind speed increases by more than 3 m/sec from the ground to a 1000-meter altitude, a velocity-of-sound inversion in the downwind direction will occur; sound rays will return and the sound intensity level from a sound will be propagated in the downwind direction at higher levels than in the upwind direction.

Figure 6 illustrates the increase in the height of the shadow zone (area to the right of and under the rays) as the velocity-of-sound gradient becomes more negative. Figure 7 shows the ray profiles for an initial zero gradient followed by various negative and positive gradients for higher layers. Figure 8 illustrates the effects of the magnitude and height of the velocity-of-sound inversion on the ray profile pattern. Figure 9 portrays the ray profiles for various negative-positive-negative velocity-of-sound gradients, the size of the shadow zone, and the location of the focal zones. Figure 10 shows various combinations of ray focusing and uniform rays returning for the first two layers being positive gradients with different slopes.

The ordinate and abscissa scales in all the analog computer plots (figs. 6 to 23) can be scaled either up or down by dividing the values on the two scales by the same number, and the resulting ray plots would still be valid. For example, the height (ordinate) and horizontal distance (abscissa) could be divided by any factor up to 10. The upper limit of the scaling factor is determined by the required critical thickness as shown in figure 4.

Moving Sound Source

The discussion up to this point has been with respect to sound propagation through the atmosphere for a stationary sound source at the ground. The determination of ray acoustics and sound intensity for a moving sound source such as an aircraft or aerospace vehicle in flight is recognized as being very complex. An analytical formulation of the equations necessary to treat this problem has been established by Buell in reference 10. An effort is presently being made to establish the practical equations necessary to calculate sound intensity for a moving source. In the meantime, some interesting ray patterns from an elevated sound source have been obtained on an analog computer and are presented in figures 11 to 23. These analog computer results simulate a sound source above the ground for various velocity-of-sound profiles. In studying these graphs, the reader is to envision that the resulting ray patterns are from the sound of a vehicle at ignition and in flight or, of particular interest to this conference, from the sound of an aircraft on the ground and during take-off and landing. The ray interference or dynamics

of the ray are missing from the simulation; it must be assumed that the method of simulation freezes the motion of the sound source at the indicated altitudes.

It can be noted in figures 11 and 12 that the negative-gradient profiles show no rays returning to the earth's surface for a sound source located on the ground. One would conclude that there would be no apparent problem (noise nuisance or disturbances) for this condition. If the sound source is located above the ground, the extent that rays return depends on the height of the sound source and the gradient of the velocity-of-sound source.

Figures 13 and 14 illustrate the ray patterns for velocity-of-sound profiles with negative-positive gradients and with the sound source at different heights above the ground. Figures 15 and 16 illustrate the ray patterns for velocity-of-sound profiles with positive-negative gradients and with the sound source at different heights. Figures 17 to 23 are presented to illustrate the ray patterns for various three-layered velocity-of-sound profiles with the sound source at various heights.

Another limitation of ray acoustics should be pointed out; in figure 23 with the sound source located at 1 km, the linear layered model for the velocity-of-sound profile yields a shadow zone to the right of the height at 1 km. At 1 km, the derivative of the velocity of sound is discontinuous. Reference 7 points out that if this "corner" were rounded, the area to the right at 1 km would be completely filled with rays. Furthermore, at this local maximum (corner point) there is an infinite discontinuity in $dr/d\psi_0$ and since this calculation of sound intensity is for returning rays, there is reason to be concerned that estimates are due to the linear layered atmospheric model and have little to do with the sound propagation phenomena. In reference 7 methods are proposed for rounding the corner of the velocity-of-sound profile. The ray location and sound intensity estimates from the linear layered model are compared with those from a parabolic model.

COMPARISON OF CALCULATED AND MEASURED SOUND LEVELS

The ray patterns in themselves do not give an estimate of the sound intensity level to be expected from a given velocity-of-sound profile. Only through experience and the collection of measured sound-pressure-level data can a correlation between the ray patterns and sound intensity level be obtained. However, from theoretical considerations, it can be stated that in those areas where sound rays do return, the sound intensity level may be higher than that predicted by the inverse square law. Conversely, in those areas where no rays return, the sound intensity level will be lower than that predicted by the inverse square law.

Estimates of sound intensity level as a function of distance in all directions from the static test stand (the sound source) must be made for all static firings of large boosters at MSFC and at MSFC-MTF. For this purpose, a number of digital computer programs have been developed during the several years of operations. Only the simplest of these programs will be described and the resulting sound intensity levels compared with measured sound pressure levels from static tests.

The sound intensity level IL is calculated from the expression

$$IL = D + 22 + 10 \log\left(\frac{1}{r}\left|\frac{d\psi_o}{dr}\right| \cot \psi_o\right) \qquad (9)$$

where $D = 10(\log PWL - \log 10) + 130$ and where r is the horizontal distance from the sound source to the incidence of the ray landing on the plane tangent to the earth's surface at the sound source. The terms r and $d\psi_o/dr$ are derived from the velocity-of-sound profile; ψ_o is the angle of the ray leaving the sound source and is incremented at small arbitrary intervals. The overall sound intensity level IL is in units of dB re: 10^{-16} watts/cm^2.

The characteristics of this equation are as follows:

(1) When the increase of the velocity of sound with respect to height is linear, the argument of the logarithm for small angles ψ_o is approximately $1/r^2$. Therefore, under this condition the inverse square law for sound propagation is approximated.

(2) At a focal point the intensity level is undefined, since at a focal point, $dr/d\psi_o$ is zero. $\left(\text{The condition of } \frac{dr}{d\psi_o} = 0 \text{ defines a focal point.}\right)$

(3) When the velocity of sound decreases at all altitudes, no rays return and hence the intensity level is not determinable. Only for the condition of rays returning can the intensity level be calculated.

It is recognized that the obvious extensions to equation (9) are the inclusion of a term for the directivity of the sound source and a term for atmospheric attenuation. The more complete form would appear as

IL = PWL of source + Directivity of Source + Frequency of source

+ Velocity of sound in the propagating media + Attenuation

The first term, the PWL of source, can be determined theoretically, but it should also be determined from measurements for the particular engine or engine cluster. The second term, directivity of source, is dependent on the configuration of the static test and engine characteristics and should be determined from measurements. The third term, frequency of sound source, should be determined from measurements. The fourth term,

velocity of sound in the propagating media, is controlled by the atmospheric conditions. The fifth term, the attenuation of sound through the atmosphere, is probably the least understood and is an area for considerable basic research using carefully controlled sound and atmospheric measurements. The attenuation term should include molecular attenuation as well as dynamic effects of atmospheric turbulence.

The MSFC-Test-Laboratory estimates of the sound pressure level and directivity for the S-IC and F-1 engine are presented in the following table, where direction is with respect to the center axis of the jet:

S-IC (a)			F-1 engine (east-area stand) (b)		
Direction, deg	Sound pressure level, SPL, dB	Xrectivity, dB	Direction, deg	Sound pressure level, SPL, dB	Directivity dB
0	140.0	2.7	0	140.5	4.6
10	140.4	3.1	10	140.5	4.6
20	141.1	3.8	20	141.0	5.1
30	142.1	4.8	30	141.0	5.1
40	142.5	5.2	40	140.0	4.1
50	142.0	4.7	50	140.0	4.1
60	140.3	3.0	60	138.0	2.1
70	137.8	.5	70	135.0	-.9
80	134.9	-2.4	80	133.0	-2.9
90	132.0	-5.3	90	134.0	-1.9
100	129.8	-7.5	100	132.0	-3.9
110	128.2	-9.1	110	130.5	-5.4
120	127.2	-10.1	120	129.5	-6.4
130	126.5	-10.8	130	128.5	-7.4
140	125.6	-11.7	140	127.5	-8.4
150	124.2	-13.1	150	126.0	-9.9
160	122.5	-14.8	160	124.0	-11.9
170	122.3	-15.0	170	122.5	-13.4
180	122.1	-15.2	180	120.5	-15.4

[a]Average power level of 210.9 dB and average sound pressure level of 137.3 dB (based on measurements at distance of 610 meters from source).

[b]Average power level of 203.5 dB and average sound pressure level of 135.9 dB (based on measurements at distance of 305 meters from source).

Figure 24 shows a comparison of the sound intensity level, the inverse-square-law result, and the measured overall sound pressure level for a static firing of Saturn I on February 27, 1963, at 1648 CST. For the azimuth 45° east of north (fig. 24), the sound intensity levels compare favorably with the overall-sound-pressure-level measurements. The sharp rise in the sound-intensity-level curve at a 16-km distance is attributed to a focal point (or focal zone). The sound intensity level is infinite; however, inasmuch as finite yet small increments of ψ_c are used, the computed unsteady levels are unrealistically high in the neighborhood of a focal point. When the sound intensity levels are displayed as in figure 25, the focal areas are characterized by high intensity-level values and large gradients. For figure 25, the sound intensity levels were derived for 36 azimuths and isacoustic lines (lines of constant sound intensity level) were drawn.

These sound-intensity-level estimates are with respect to a flat earth surface. Hills which are high enough to intercept the ray path and local wind and temperature gradients over the hills can conceivably modify the resulting sound intensity level. (Compare the ray profile in fig. 26 with the intensity levels in fig. 24.)

The test results from a static firing of Saturn I on March 13, 1964, at 1633 CST are presented for a 45° azimuth in figure 27. Two focal zones are indicated, one at 13 km and another at 22 km. The sound-intensity-level estimates are within 5 dB of the measured sound pressure levels.

The results from two static firings are presented to illustrate the rapid change over short time periods in the sound ray patterns in area extent, the variability of sound-intensity estimates, and the difficulty in predicting the velocity-of-sound profile. The results from a static firing on October 23, 1964, are shown in figures 28 to 31, and the results from a static firing on November 23, 1964, are presented in figures 32 to 35.

Figure 28 shows the areas in which sound rays returned and the sound intensity levels based on a 12-hour forecast of wind and virtual temperature valid for October 23, 1964, at 1640 CST. This prediction of sound rays and intensity levels can be compared with the results from the rawinsonde measurements presented in figure 30. In addition, intensity levels based on rawinsonde measurements taken at 1539 CST – that is, taken 61 minutes before firing time – are presented in figure 29. The ray pattern based on rawinsonde measurements at firing (fig. 30) can be compared with the ray pattern based on rawinsonde measurements 34 minutes later (fig. 31). Although the change in ray pattern is rather systematic, the sound-intensity-level estimate at a given point varies considerably. The 12-hour prediction (fig. 28) is judged to be very good.

Figures 32 to 35 present the sequence of sound ray patterns and sound intensity levels based on the 12-hour atmospheric prediction valid for November 23, 1964, at 1640 CST (the static firing time) and the results based on rawinsonde measurements

taken at T-45, T-0, and T+36 minutes. A no-change extrapolation of the ray pattern from the rawinsonde measurements for T-45 minutes to a T-0 pattern would have produced poorer results than the original 12-hour forecast. The ray pattern for T+36 minutes is in closer agreement with the 12-hour prediction than the T-0 pattern. No claim is made that the predictions of the velocity-of-sound profile which yield such close agreement in ray patterns are this accurate in general.

The MSFC Test Laboratory has, on occasions, rescheduled static firings on the basis of predicted velocity-of-sound profiles. At present, the entire test operation is based on atmospheric measurements and predictions furnished by the MSFC Aerospace Environment Division, whereas in former times, the acoustical horn was used to augment the expected far-field sound intensity level.

A comparison of the sound intensity level and the sound-pressure-level measurements obtained from a measuring program conducted at the MSFC Missippippi Test Facility in 1962 and 1963 is presented. The sound source was an acoustical horn which at that time had a sound-power-level capability up to 6000 watts. (At MSFC in Huntsville, the acoustical horn had sound-power-level capability up to 178 000 watts.) The atmospheric measurements were obtained from the rawinsonde GMD-1B system. By using these simultaneous measurements of sound pressure levels and atmospheric measurements from which sound intensity levels have been calculated, a comparison is made between the sound intensity level and sound pressure level. The best agreement between the sound pressure level and the sound intensity level within a ±500-meter distance was chosen for this comparison. These data are summarized in figures 36 and 37 for two different atmospheric conditions. In figure 36, a comparison is made between sound intensity level and the measured sound pressure level for the atmospheric conditions which produce uniform rays returning. The standard regression error is 5.2 dB. In figure 37, the intensity levels for all conditions of rays returning, including focal conditions, are compared with the sound-pressure-level measurements. The standard regression error here is 7.1 dB. Contributing to the regression errors are (1) theoretical assumptions for the intensity level calculations, (2) errors in atmospheric and acoustic measurements, and (3) time and space variability of atmospheric parameters. The major criticism of this comparison is the manner in which the best agreement between the sound intensity level and the sound-pressure-level measurements was selected. In view of the influence of small errors in the velocity-of-sound profile on the sound intensity level and short time variations in the wind flow, the comparison made in this manner may not be entirely invalid. Plots were made of the difference between the sound pressure level and the sound intensity level as a function of distance from the sound source, and no apparent correlation with respect to distances from the sound source was noted. Therefore, it is concluded that under similar situations at MTF, practical results from the sound-intensity-level calculations can be used to predict the expected sound pressure

level as a function of distance from the source for the Saturn V and larger vehicle boosters.

Through improved atmospheric measurements and sound-intensity-level programs and with the Saturn booster as the sound source, there have been some improvements in the statistical estimates of the differences between sound intensity level and sound-pressure measurements. However, large improvements cannot be expected because of the inherent variability of the wind and temperature profile from which the velocity-of-sound profile is derived. With the use of realistic interval correlation coefficients to relate the random variability of temperature and the wind vector profile, a Monte Carlo simulation was performed in reference 7 to determine the standard deviations of sound intensity level for ray returns for distances from 5 to 50 km. Three degrees of atmospheric variability were used: (1) small variability (time period less than 1 hour); (2) moderate variability (time period of 4 to 6 hours); and large variability (time period of 8 to 12 hours). Systematic changes in the wind and temperature that might be caused by morning radiation temperature inversion and frontal passages were excluded from this consideration. The modal values of the standard deviations from this simulation, when not less than 20 percent of the rays failed to return, were 2.5 to 5.0 dB for all three variability scales.

STATISTICAL ANALYSIS

Far in advance of actual static tests, sometimes several years in advance, the planning engineers must know the influence of pertinent atmospheric conditions on the facility operations. Two approaches may be used to show the relationship between atmospheric variables and engineering design parameters used in planning a facility. One approach is to take the summarized statistics of atmospheric variables and attempt to derive the influence of these variables on the facility. The monthly mean values of temperature and the wind components and their standard deviations for discrete altitude levels were used in reference 11 to arrive at an estimated frequency at which sound generated from the vehicle would be intensified by quadrant areas. Estimates based on such a procedure should be viewed with caution because the correlations between atmospheric variables with respect to altitude should be considered. Often the required correlation values are not immediately available and must be derived.

It is proposed that a better procedure is to (1) derive the required analytical equations relating the atmospheric variables to the required engineering design parameters, (2) use the individual atmospheric measurements to calculate the engineering parameters for design, and (3) summarize these data in a statistical manner.

This method will not only yield a more efficient estimate of the frequency of the occurrence for the particular parameters of interest, but will often be more economical than computing all the required correlations between the atmospheric variables themselves.

This procedure was followed in constructing figures 38 to 43, which are discussed in the following paragraphs. The ray acoustics and intensity levels were calculated by using the individual rawinsonde measurements taken at MSFC at 1630 CST for January and July of 1962 and 1963. The frequency at which the rays return along each of 36 azimuths was computed.

From figure 38 it can be seen that 100 percent of the rawinsonde measurements for January 1962 and January 1963 at 1630 CST produced rays returning somewhere along the 90° azimuth (east of MSFC); along the 270° azimuth (west of MSFC), only 35 percent of the rawinsonde measurements produced rays returning. Similarly, the frequency of rays returning along the 90° and 270° azimuths for July of 1962 and 1963 at 1630 CST are 60 percent and 18 percent, respectively (see fig. 39). Any time rays returned, the sound pressure level from a static test could be expected to be higher than for the condition of no rays returning. Therefore, charts like these for all months of the year would assist a site planning group in placing the test facility at such a location in the community that the likelihood for disturbances due to anomalous sound propagation resulting from test operations would be a minimum. From a knowledge of the prevailing wind direction over Huntsville up to a 3000-meter altitude, the conclusion that the frequency at which rays returned would be higher toward the east than toward the west could be reached. However, the relative frequency of rays returning for the two directions could not be stated. This information has already been used to advantage by a facility planning group at MSFC in the design and layout of the Saturn V static test stand.

A knowledge of the frequency of rays returning anywhere along an azimuth leaves much to be desired for detailed facility planning. A knowledge of the frequency of rays returning within a given area would be more useful. Since the computations of rays returning were by necessity carried out in a polar coordinate system, unit area is designated by 5-km intervals along (and ±5° on either side of) each of the 36 azimuths. The frequencies at which at least one ray returned within a 5-km interval along each of the 36 azimuths were computed. These frequencies are summarized for January and July in figures 40 and 41. The highest insistence of rays returning is east of the static test stand out to a distance of 10 km. It is noted that Army headquarter buildings and industrial plants are located in the first 5 km east of the static test stand. Between 10 and 20 km east of the test stand is located a recently constructed residential area. The business district of Huntsville is located northeast of the static test stand between 10 and 15 km. Thus it is obvious that an engineering effort should be made to minimize the

sound pressure level produced by the boosters in these directions. During July the pattern of the frequency of rays returning is more circular than that for January. The boundaries of the Redstone Arsenal are approximated by a circle of 10-km radius. Thus, it is observed that there is less than a 25-percent chance that rays will return outside the, arsenal boundaries during July.

Because of the directivity effects, the static test stand should be orientated such that the sound pressure level is minimized east and northeast of the static test stand. This conclusion is valid for the existing community. However, since the construction of the S-IC static test stand, a multimillion dollar jet airport has been built just west of the arsenal boundaries. This poses the problem of predicting the future growth of a community surrounding the static test area.

The question that still must be answered is how frequently will atmospheric conditions be such that anomalous sound propagation will cause disturbances to the outlying community during static tests of the Saturn V or other vehicles yet to be built. By using the theoretical intensity-level equation as described previously, the frequencies at which the intensity levels equal or exceed 110 dB for the condition of rays returning have been calculated. It must be realized that no attenuation factor has been included in these calculations; therefore, the frequencies at which the intensity level exceeds 110 dB will be higher than they should be. Figures 42 and 43 indicate that when rays return, there is a high probability the sound generated by the Saturn V will equal or exceed 110 dB out to distances of 20 km.

It is realized that the available data sample is small for the detailed statistical treatment as presented in figures 38 to 43. The techniques or methods of statistical analysis should prove helpful in determining statistics of acoustical parameters for other locations and related problems. However, the statistical analysis of the acoustical parameters should be performed with the use of individual atmospheric measurements obtained at the specific localities.

OPERATION OF ATMOSPHERIC MEASURING SYSTEM

At MSFC an atmospheric measuring system has been in operation since October 1961. The equipment consists of two GMD-1B units with the capabilities of GMD-2 units. Through a switching mechanism, the GMD-2 can be operated automatically to produce punched cards for azimuth and elevation angles, ratios of temperature and humidity ordinates, and slant range at 5-second intervals of balloon flight time. This latter system is known as the ADP system - that is, the automatic data processing system (ref. 12). Predictions up to 36 hours in advance of static tests are required for the wind speed, direction, and virtual temperature profiles. Weather charts by facsimile and weather

teletype information are received to assist in making these predictions. From 6 hours prior to static test time until actual static test time, rawinsonde measurements are performed at 1- to 2-hour intervals. Until recently, the MSFC Test Laboratory made sound-pressure-level measurements with the use of the acoustical horn as a sound source. If through these measuring techniques and predictions the sound pressure level in the community appears to be too high – that is, equal to or greater than 110 dB, the test conductor cancels the static firing and reschedules the test when the atmospheric conditions are more favorable.

CONCLUDING REMARKS

Many methods can be used to obtain numerical solutions to the differential equations for sound rays. Although there are recognized limitations in ray acoustics, instructive and useful results indicating the effects of atmospheric refraction can be obtained from ray acoustic methods. The several analog computer solutions illustrate the ray paths propagated through a linear layered model of the velocity-of-sound profile and quantitatively give a relative comparison of sound pressure levels that may result from a sound source located on the ground and in the air. Through a systematic study of the propagation of sound through the atmosphere, analytical techniques have been developed for determining the far-field sound intensity level resulting from a sound source located on the ground that compares very favorably with sound pressure levels measured under field-test and operational conditions. The major requirement is the velocity-of-sound profile, which can be obtained from atmospheric measurements of the wind and virtual temperature profiles. Prediction of the sound intensity levels for a test operation requires a forecast of the wind and virtual temperature profiles. A study is in progress to develop sound-intensity estimation techniques for a moving sound source. A satisfactory analytical model for determining far-field sound-intensity estimates for a moving sound source would be most useful in acoustic studies related to aircraft in flight. The statistical methods for ray refraction for particular locations of interest could be useful in planning future airports and land usage near the existing airports.

REFERENCES

1. Dorland, Wade D.: Far-Field Noise Characteristics of Saturn Static Tests. NASA TN D-611, 1961.

2. Cox, Everett F.; Plagge, H. J.; and Reed, J. W.: Meteorology Directs Where Blast Will Strike. Bull. Amer. Meteorol. Soc., vol. 35, no. 3, Mar. 1954, pp. 95-103.

3. Perkins, Beauregard, Jr.; Lorrain, Paul H.; and Townsend, William H.: Forecasting the Focus of Air Blasts Due to Meteorological Conditions in the Lower Atmosphere. Rep. No. 1118, Ballistic Res. Lab., Aberdeen Proving Ground, Oct. 1960.

4. Rothwell, P.: Calculation of Sound Rays in the Atmosphere. J. Acoust. Soc. Amer., vol. 19, no. 1, Jan. 1947, pp. 205-221.

5. Heybey, Willi H.: Theoretical Aspects of Planar Sound Propagation in the Atmosphere. MTP-AERO-62-72, NASA George C. Marshall Space Flight Center, Oct. 23, 1962.

6. Buell, C. Eugene: Variability of Sound Propagation Prediction Due to Atmospheric Variability. NASA CR-61160, Kaman Aircraft Corp., Jan. 1967.

7. Buell, C. Eugene: Comparison of Two Methods for Estimating Sound Intensity. NASA CR-61187, Kaman Nuclear, Jan. 1968.

8. Bishop, Dwight E.; and Franken, Peter A.: Propagation of Sound From Airport Ground Operations. Conference on Progress of NASA Research Relating to Noise Alleviation of Large Subsonic Jet Aircraft, NASA SP-189, 1968. (Paper No. 30 herein.)

9. Guest, Stanley H.; and Adams, Bert B.: Methods of Determining the Excess Attenuation for Ground-to-Ground Noise Propagation. Conference on Progress of NASA Research Relating to Noise Alleviation of Large Subsonic Jet Aircraft, NASA SP-189, 1968. (Paper No. 31 herein.)

10. Buell, C. Eugene: Variability of Sound Propagation Prediction Due to Atmospheric Variability. KN-68-698-4 (Contract No. NAS8-11348), Kaman Nuclear, June 28, 1968.

11. Anon.: Acoustical Considerations in the Planning and Operation of Launching and Static Test Facilities for Large Space Vehicles. Phase I. BBN-884 (Contract NAS8-2403), Bolt, Beranek, and Newman, Inc., Dec. 11, 1961.

12. Turner, R. E.: Radiosonde Data System. Instr. Control Syst., vol. 40, Apr. 1967, pp. 99-100.

ESTIMATED ACOUSTICAL POWER LEVEL FOR SEVERAL AEROSPACE VEHICLES

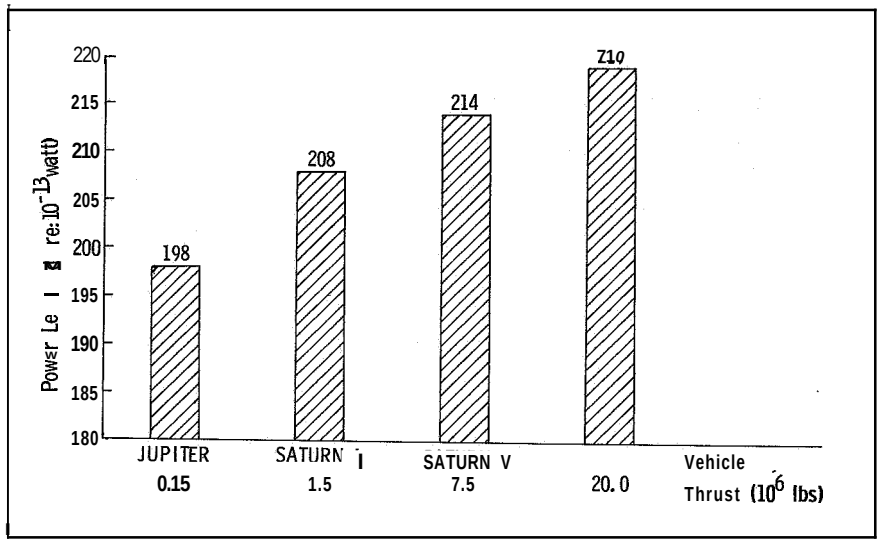

Figure 1

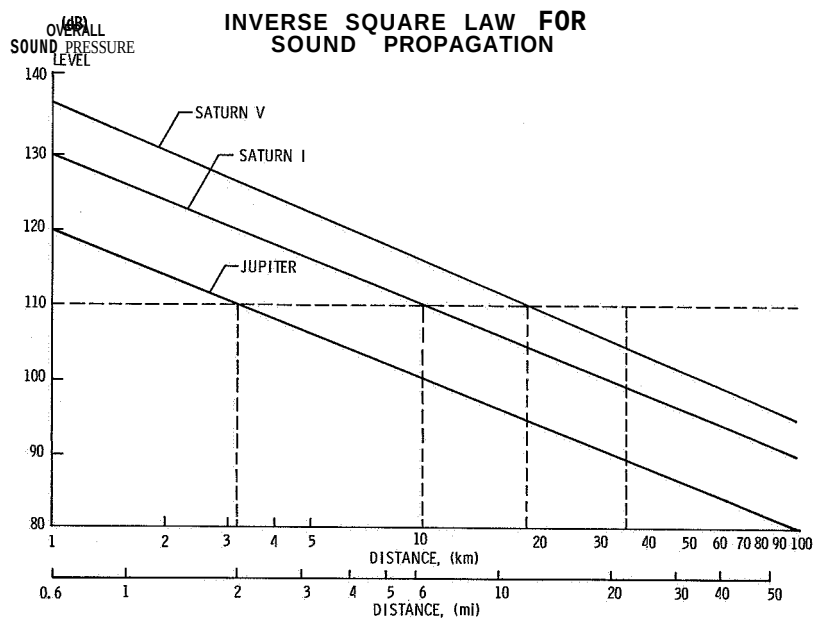

Figure 2

RADII TO CRITICAL SOUND PRESSURE LEVEL (110 dB) FOR SATURN I AND SATURN V USING INVERSE SQUARE LAW

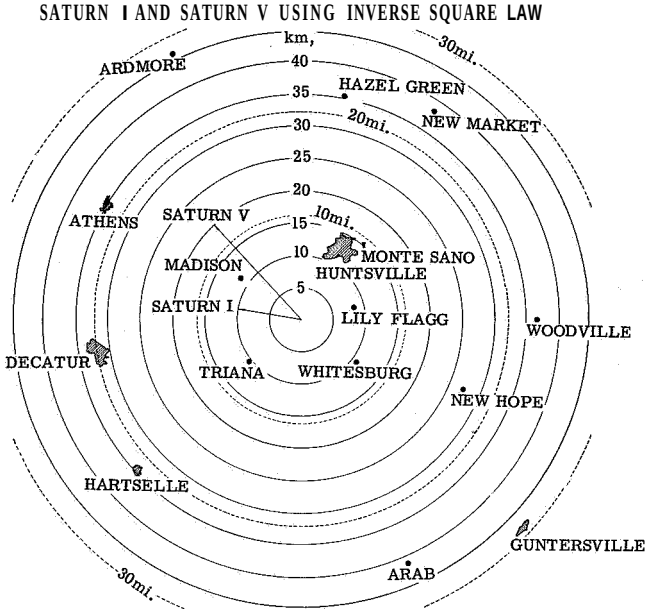

Figure 3

GRAPH OF $H^* = \left(\lambda^2 \frac{c_o}{4\pi} \frac{dc}{dz}\right)^{1/3}$

[λ = WAVELENGTH; c_o = INITIAL SPEED OF SOUND; $\frac{dc}{dz}$ = GRADIENT OF SPEED OF SOUND ABOVE UNIFORM LAYER; f = FREQUENCY]

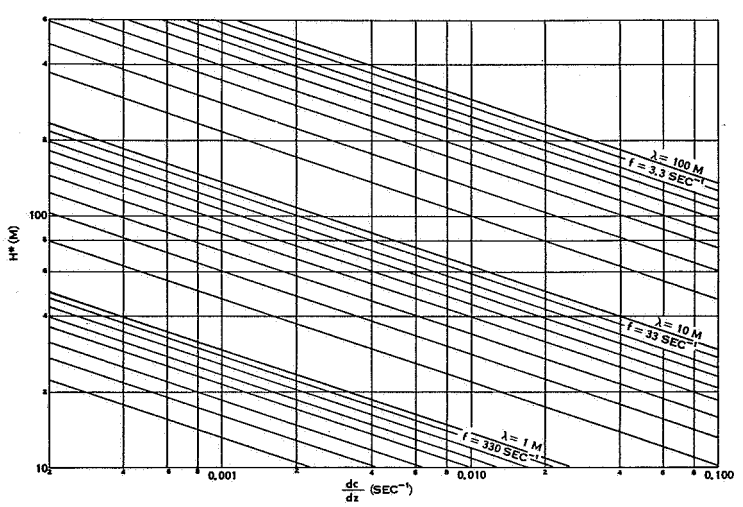

Figure 4

VELOCITY-OF-SOUND **PROFILES** AND RAY PATTERNS

1. 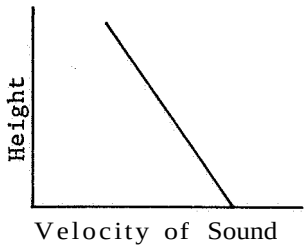

Rays are deflected upward (no rays returning)

2. 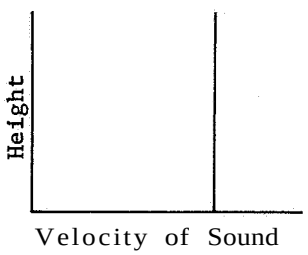

Rays returning uniformly in all directions (Inverse–Square–Law Condition)

3. 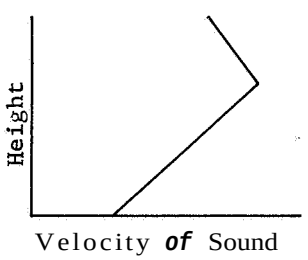

Uniform rays returning (ray concentration)

4. 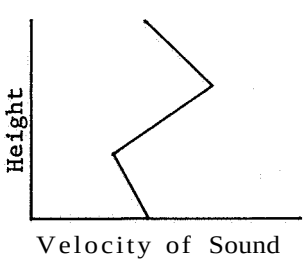

Ray focusing

5. 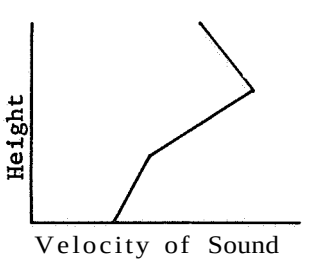

Ray concentration and focusing

Figure 5

ANALOG RAY TRACE SOLUTIONS SHOWING VARIOUS NEGATIVE GRADIENT PROFILES

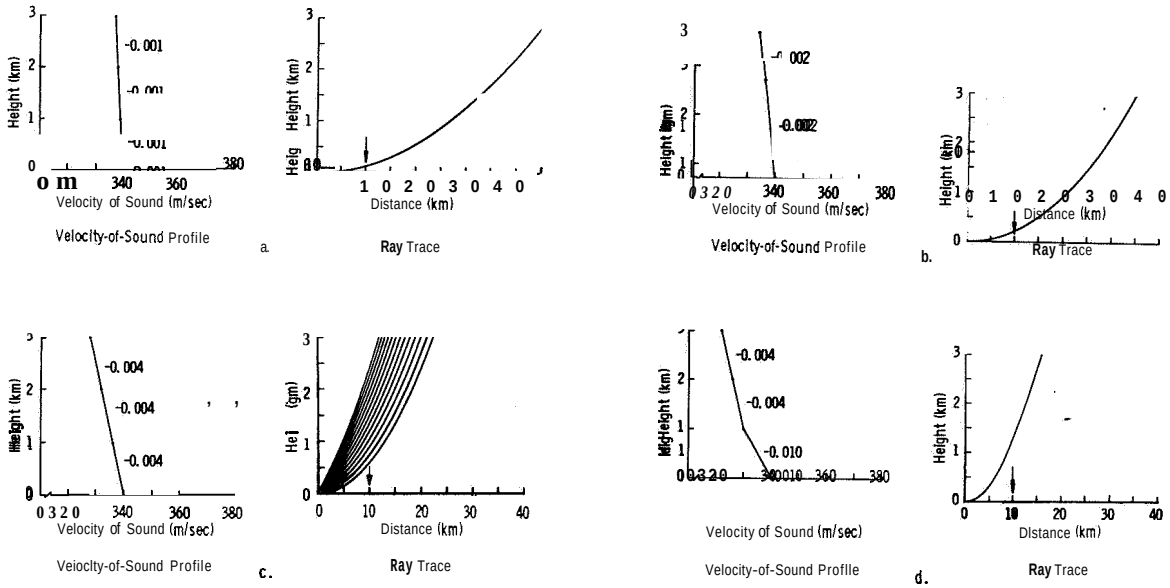

Figure 6

ANALOG RAY TRACE SOLUTIONS SHOWING VARIOUS ZERO-POSITIVE-NEGATIVE AND ZERO-NEGATIVE-POSITIVE GRADIENT PROFILES

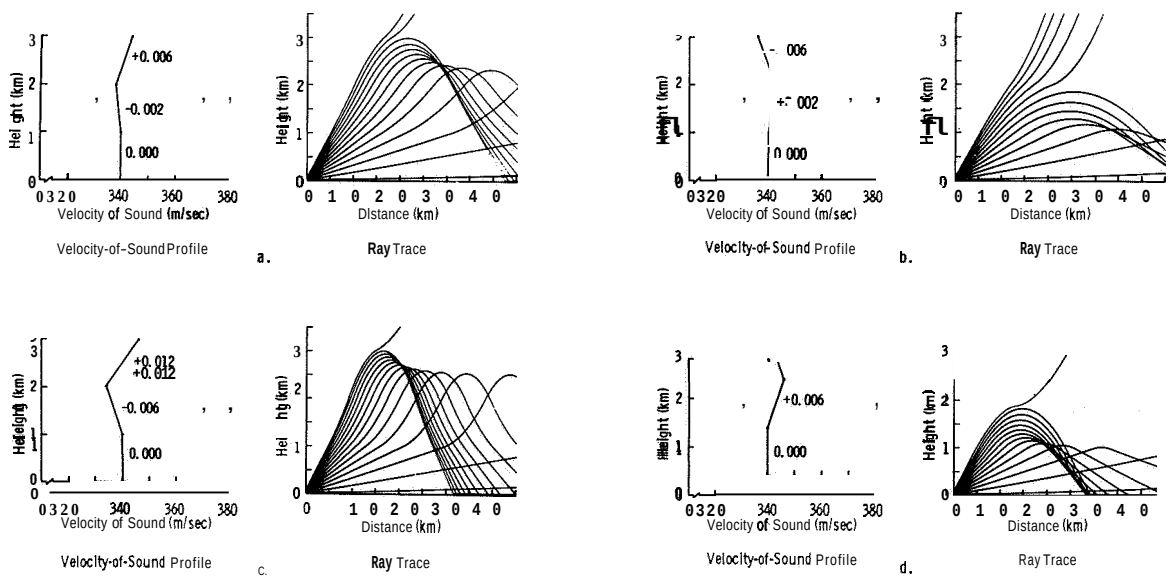

Figure 7

ANALOG RAY TRACE SOLUTIONS SHOWING VARIOUS POSITIVE-NEGATIVE GRADIENT PROFILES

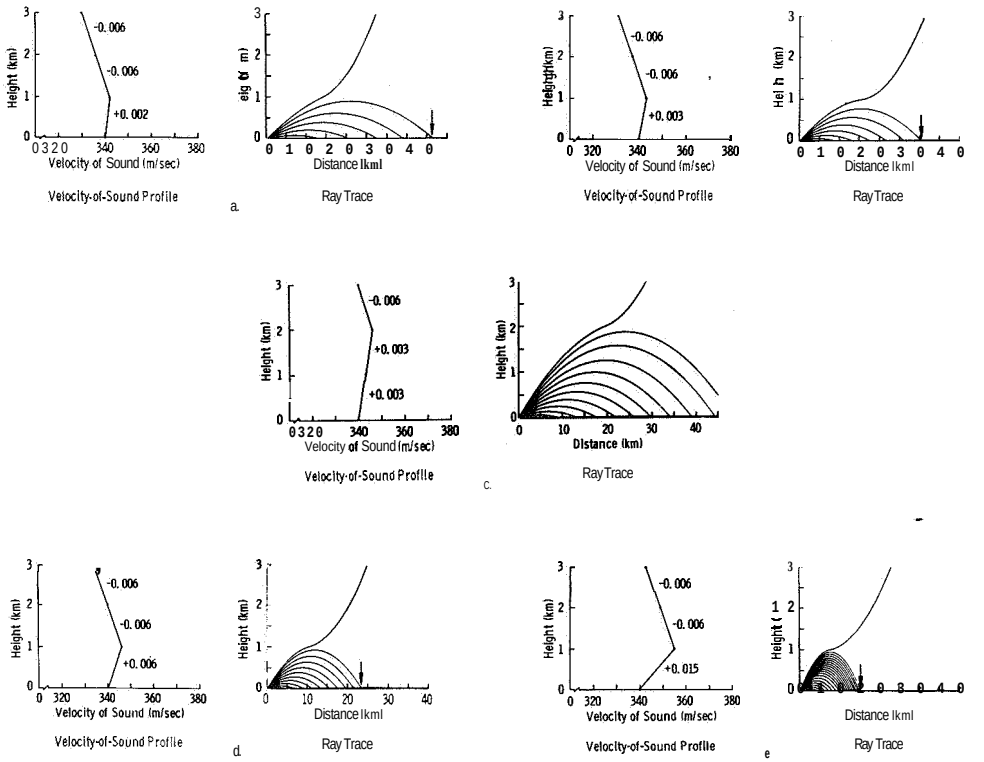

Figure *8*

ANALOG RAY TRACE SOLUTIONS SHOWING VARIOUS NEGATIVE-POSITIVE-NEGATIVE GRADIENT PROFILES

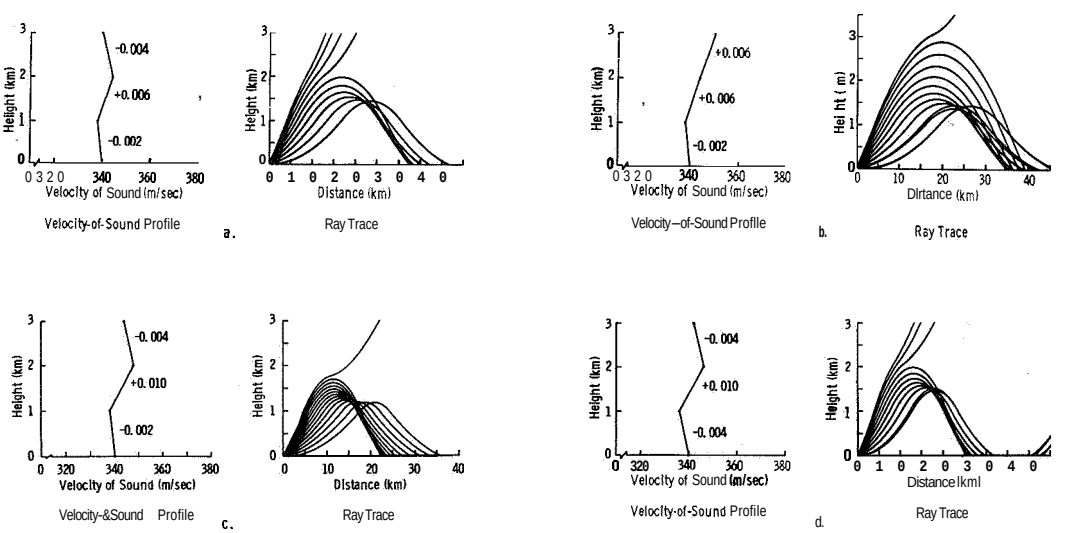

Figure *9*

ANALOG RAY TRACE SOLUTIONS SHOWING VARIOUS POSITIVE-POSITIVE-NEGATIVE GRADIENT PROFILES

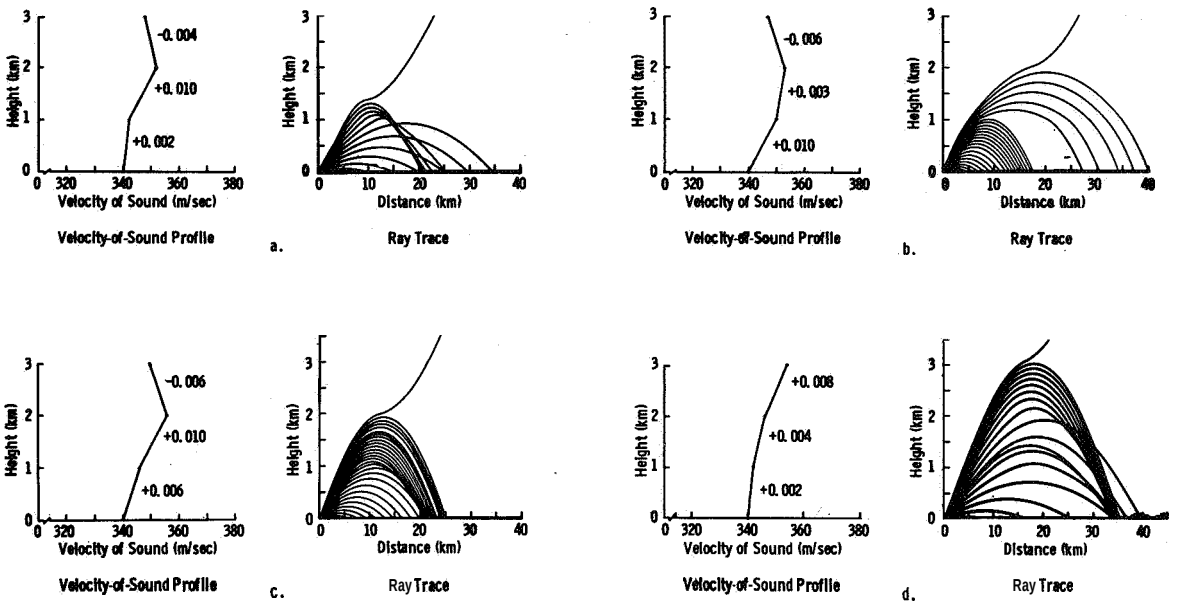

Figure 10

ANALOG RAY TRACE SOLUTIONS FOR SOUND SOURCE AT HEIGHTS OF 0, 1, AND 2 km (STRONG NEGATIVE GRADIENT)

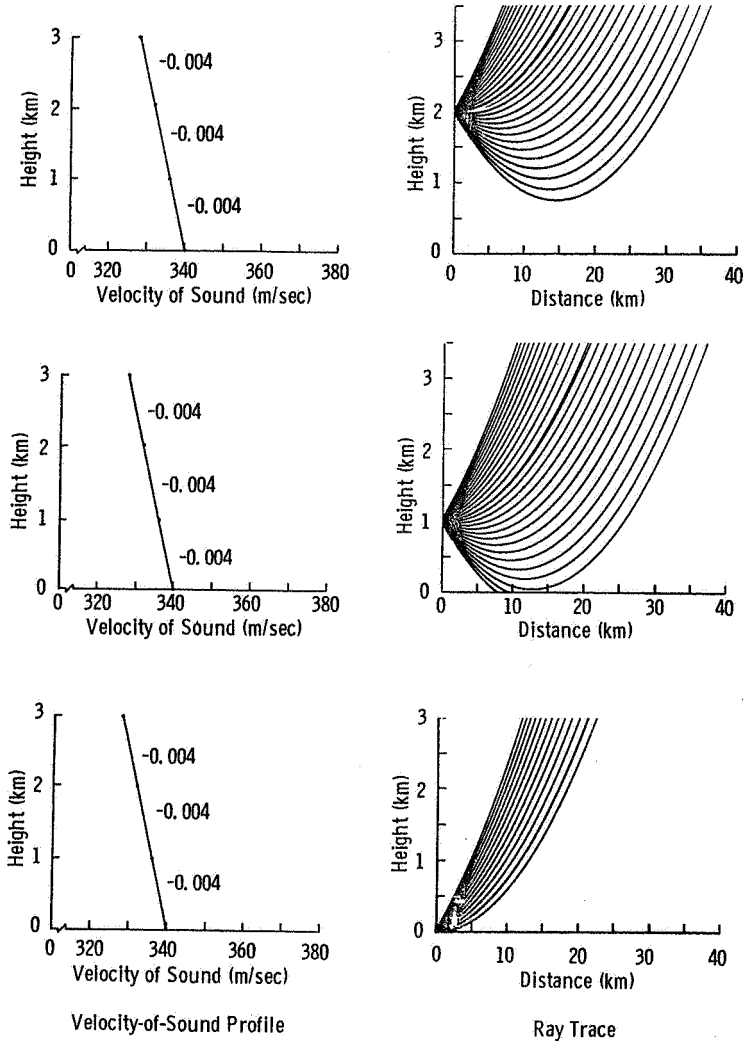

Figure 11

ANALOG RAY TRACE SOLUTIONS FOR SOUND SOURCE AT HEIGHTS OF 0, 1, AND 2 km (NEGATIVE GRADIENT)

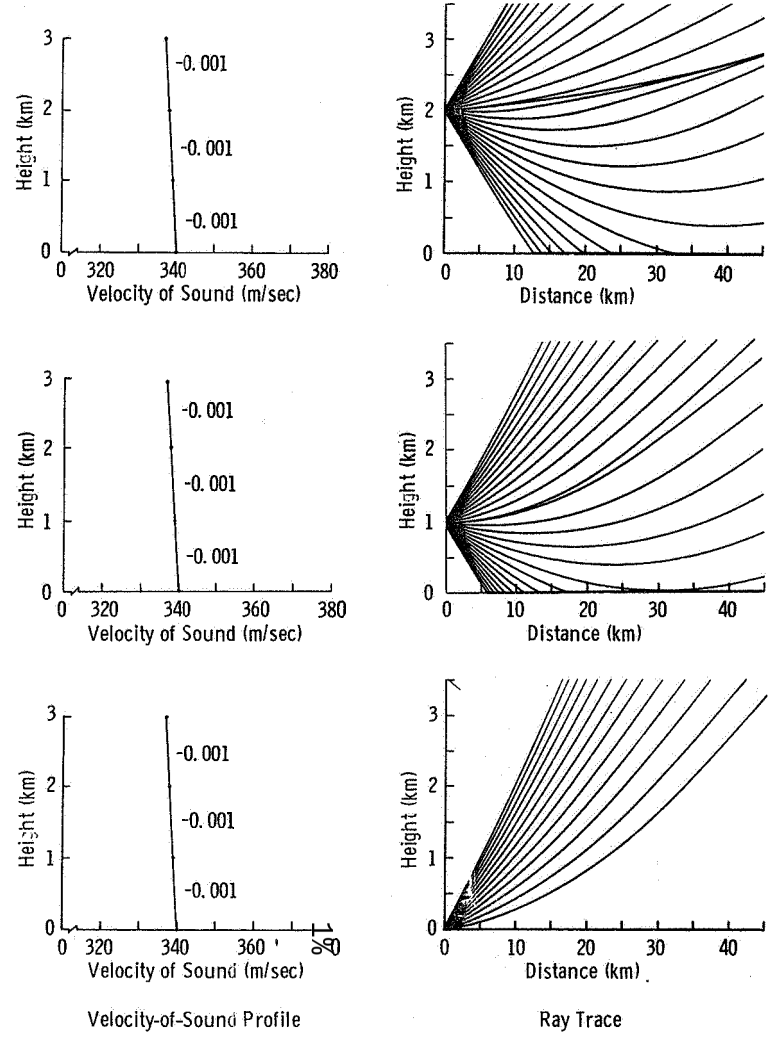

Figure 12

ANALOG RAY TRACE SOLUTIONS FOR SOUND SOURCE AT HEIGHTS OF 0, 1, AND 2 km (STRONG NEGATIVE-POSITIVE GRADIENT)

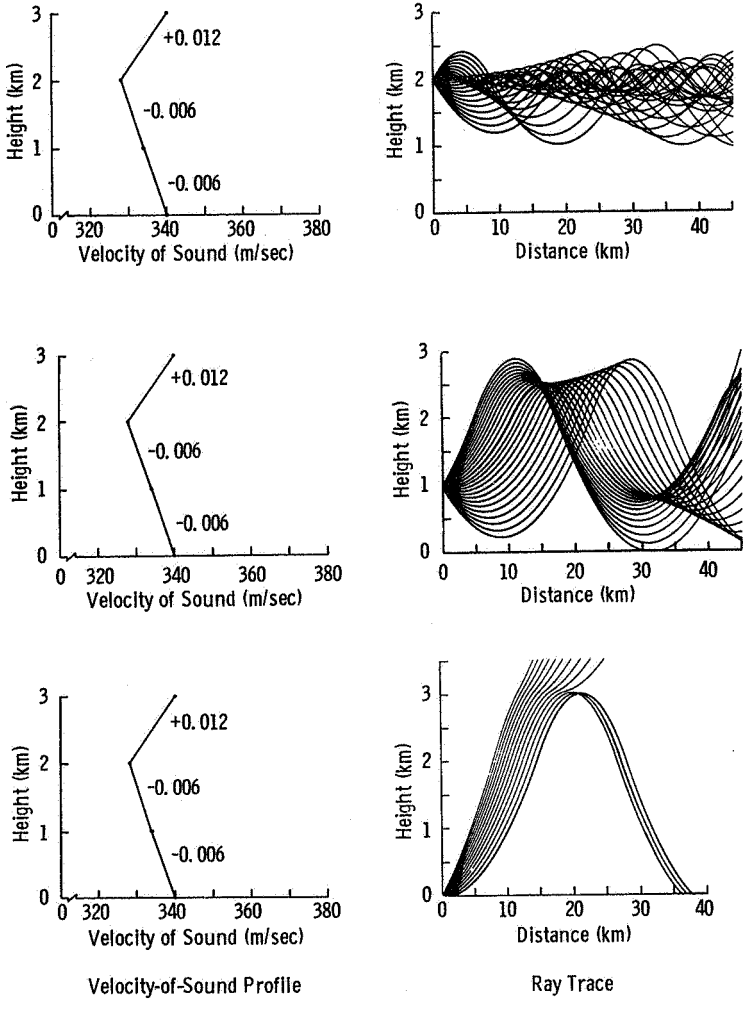

Figure 13

ANALOG RAY TRACE SOLUTIONS FOR SOUND SOURCE AT HEIGHTS OF 0, 1, AND 2 km (NEGATIVE-POSITIVE GRADIENT)

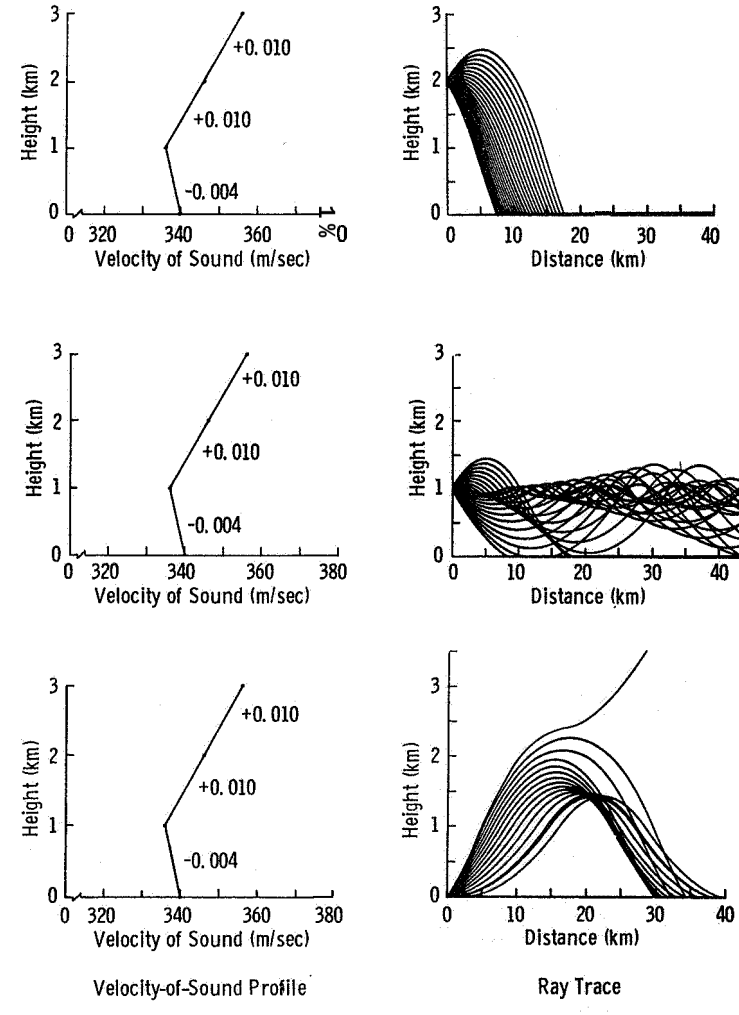

Figure

ANALOG RAY TRACE SOLUTIONS FOR SOUND SOURCE AT HEIGHTS OF 0, 1, AND 2 km (POSITIVE-NEGATIVE GRADIENT)

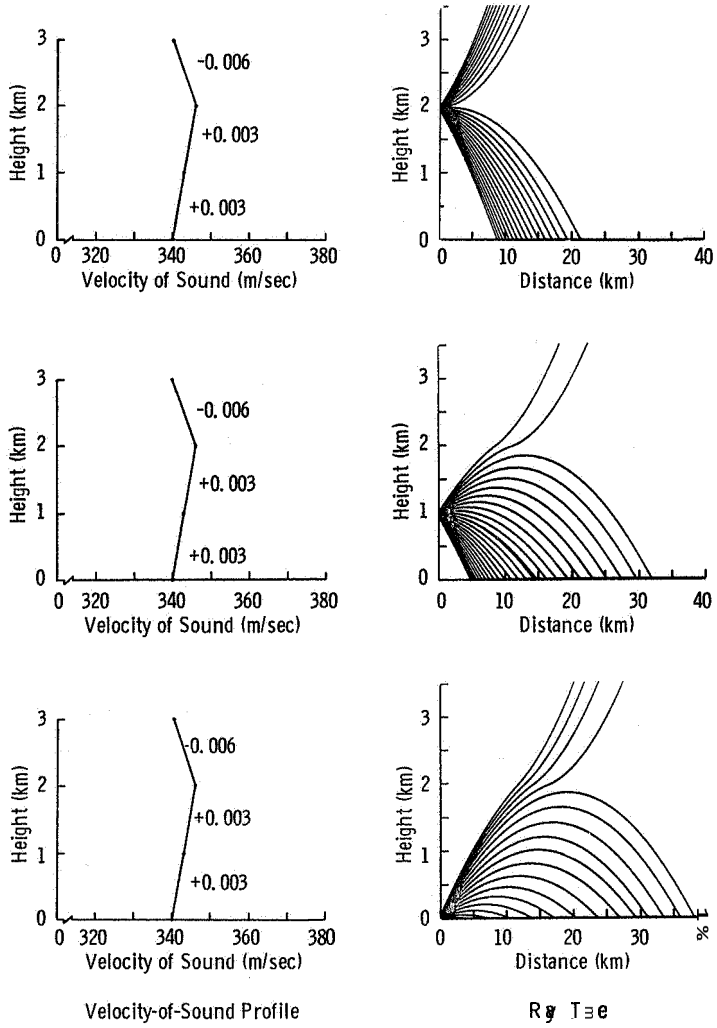

Figure 15

ANALOG RAY TRACE SOLUTIONS FOR SOUND SOURCE AT HEIGHTS OF 0, 1, AND 2 km (STRONG POSITIVE-NEGATIVE GRADIENT)

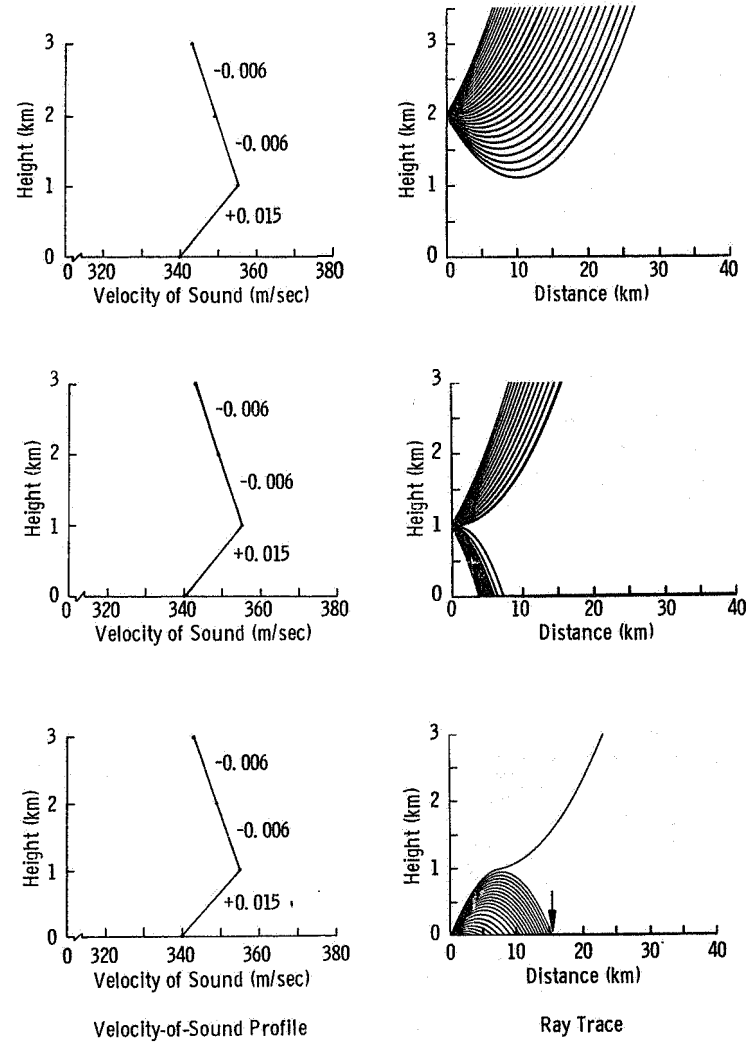

Figure 16

ANALOG RAY TRACE SOLUTIONS FOR SOUND SOURCE AT HEIGHTS OF 0, 1, AND 2 km (NEGATIVE-POSITIVE-NEGATIVE GRADIENT)

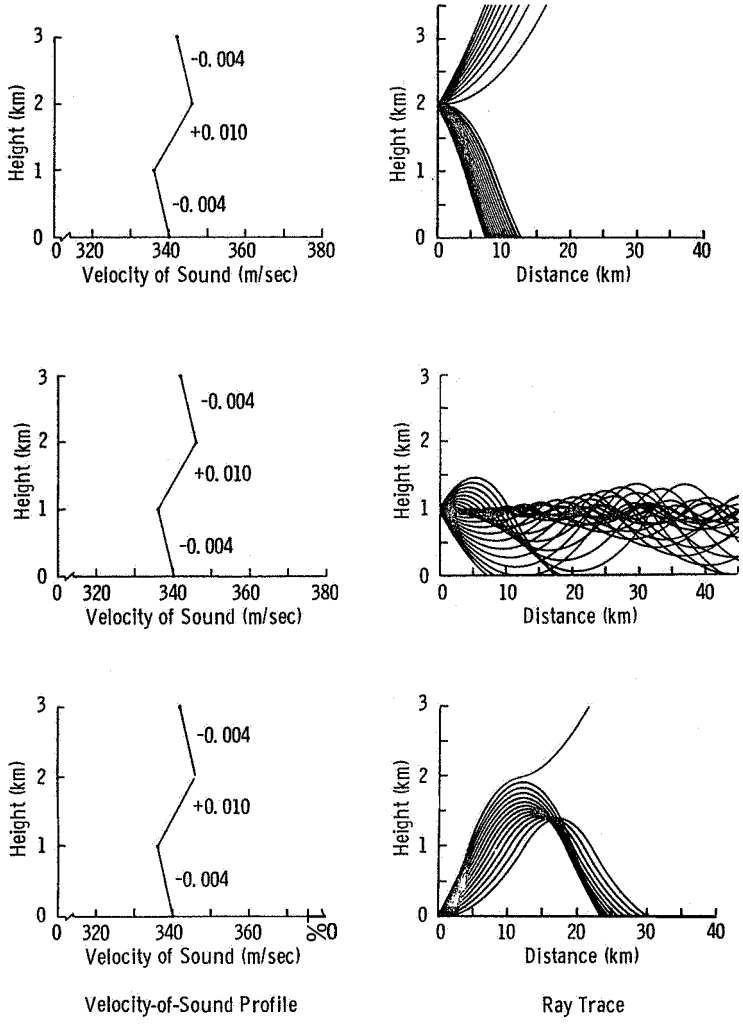

Figure 17

ANALOG RAY TRACE SOLUTIONS FOR SOUND SOURCE AT HEIGHTS OF 0, 1, AND 2 km (STRONG NEGATIVE-NEGATIVE-POSITIVE GRADIENT)

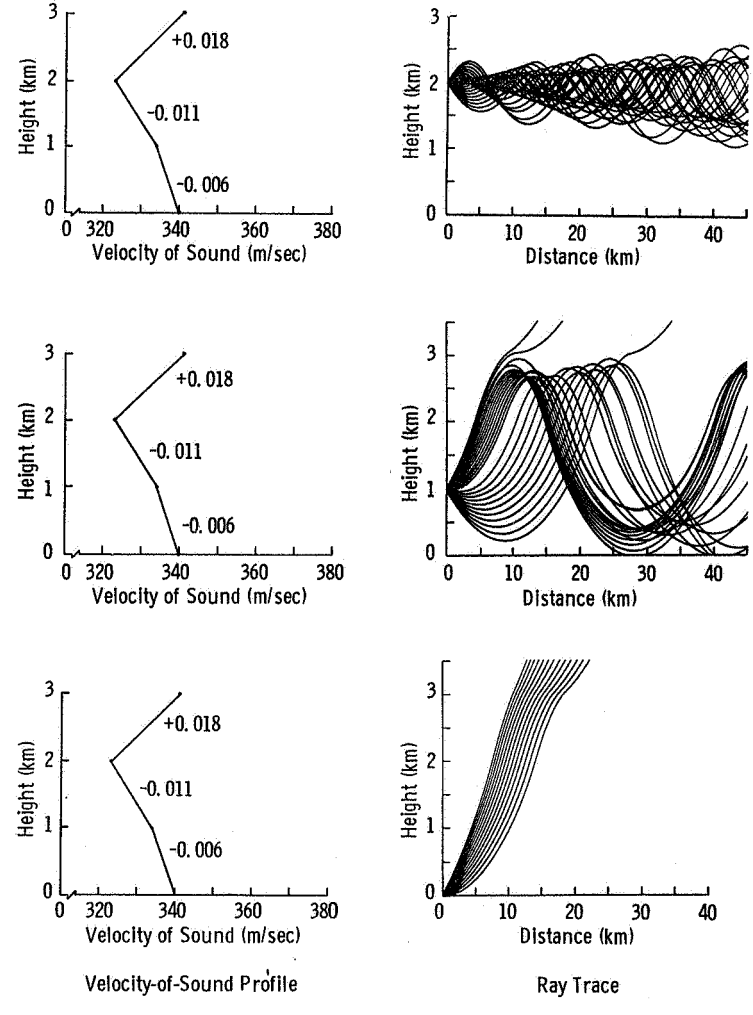

Figure 18

ANALOG RAY TRACE SOLUTIONS FOR SOUND SOURCE AT HEIGHTS OF 0, 1, AND 2 km (ZERO-NEGATIVE-POSITIVE GRADIENT)

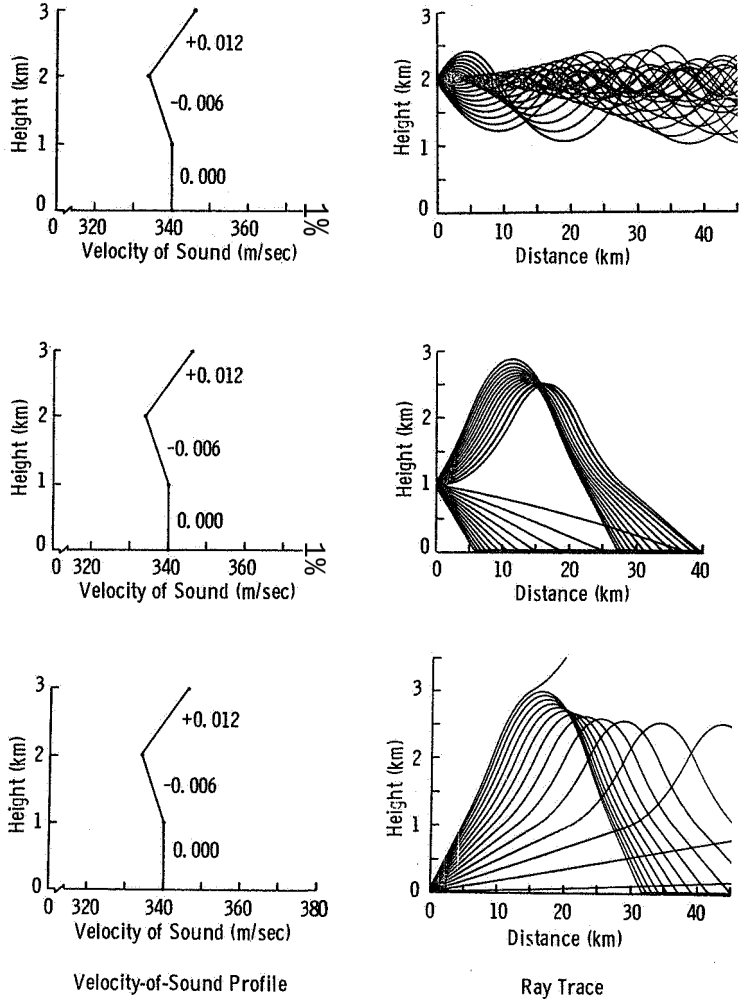

Figure 19

ANALOG RAY TRACE SOLUTIONS FOR SOUND SOURCE AT HEIGHTS OF 0, 1, AND 2 km (ZERO-POSITIVE-NEGATIVE GRADIENT)

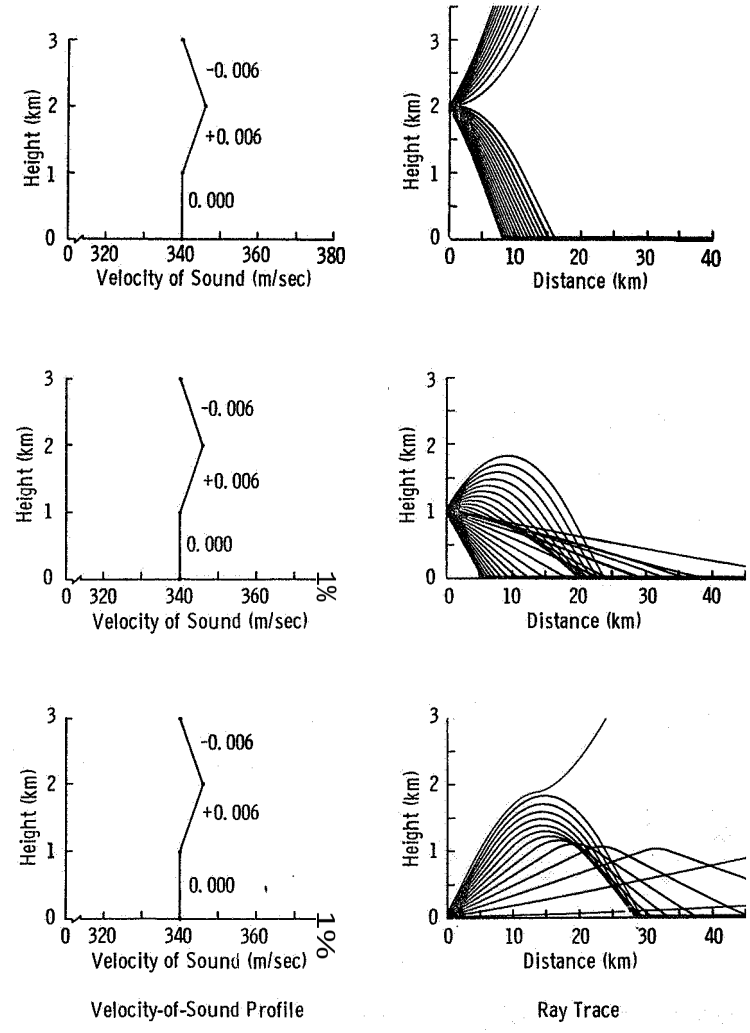

Figure 20

ANALOG RAY TRACE SOLUTIONS FOR SOUND SOURCE AT HEIGHTS OF 0, 1, AND 2 km (POSITIVE-POSITIVE-NEGATIVE GRADIENT)

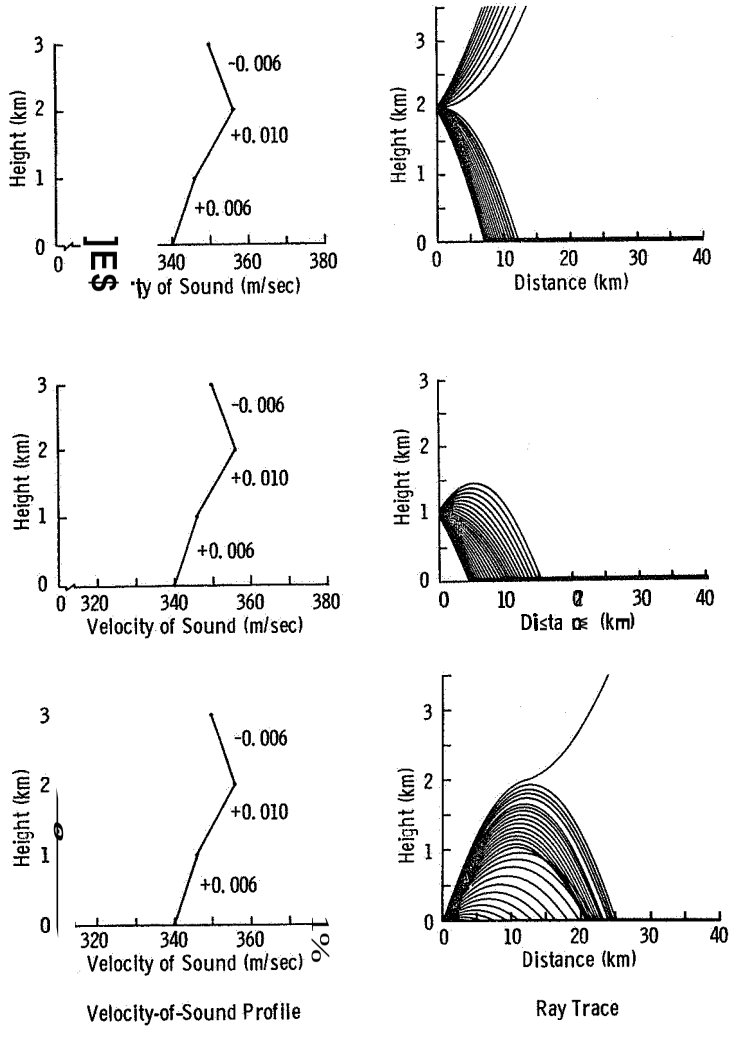

Figure 21

ANALOG RAY TRACE SOLUTIONS FOR SOUND SOURCE AT HEIGHTS OF 0, 1, AND 2 km (STRONG POSITIVE-POSITIVE-NEGATIVE GRADIENT)

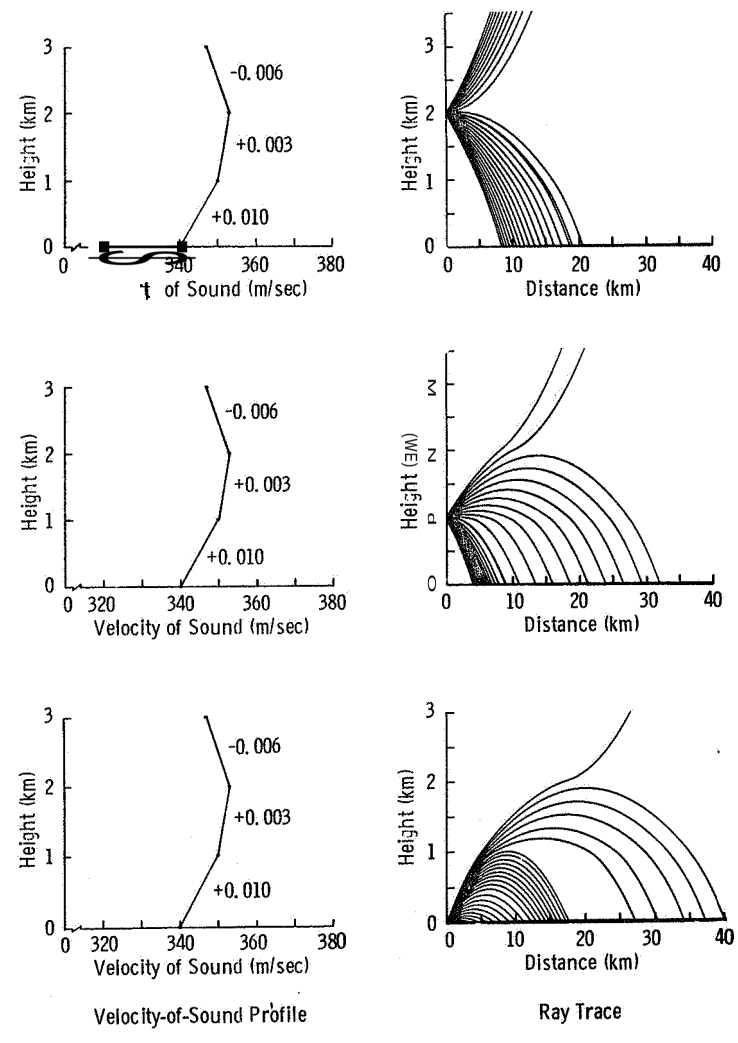

Figure 2

ANALOG RAY TRACE SOLUTIONS
FOR SOUND SOURCE AT HEIGHTS OF 0, 1, AND 2 km
(STRONG POSITIVE-NEGATIVE-POSITIVE GRADIENT)

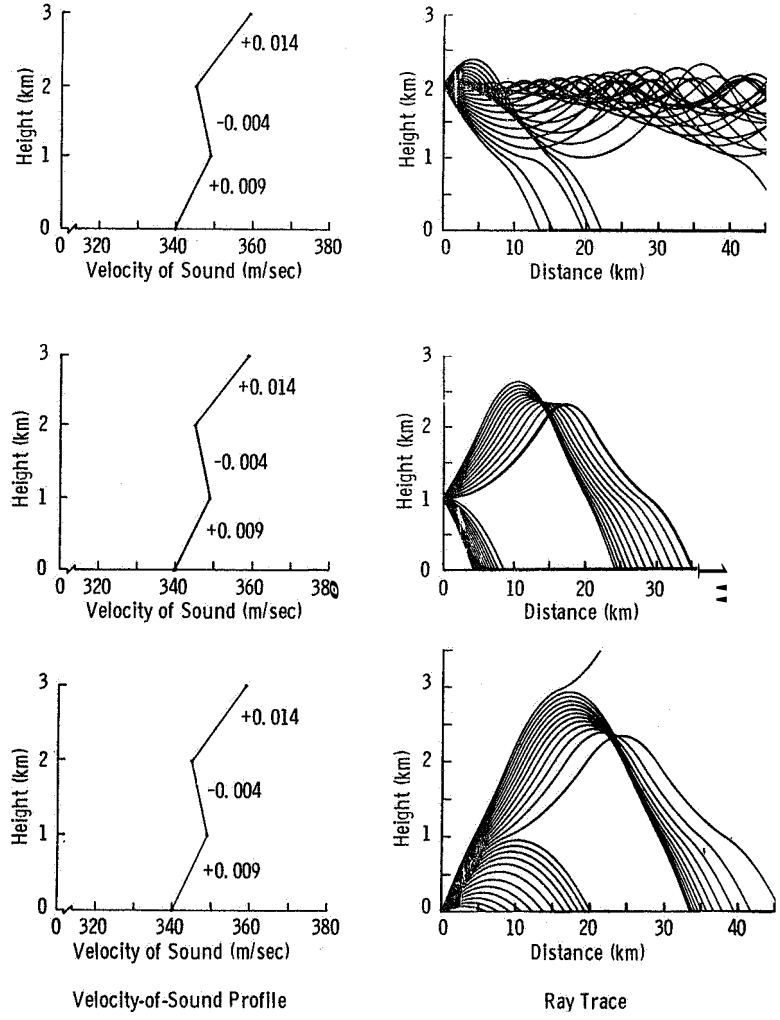

Figure 23

COMPARISON OF SOUND INTENSITY LEVEL WITH MEASURED SOUND PRESSURE LEVEL FOR STATIC TEST, FEBRUARY 27, 1963, 1648 CST, LONG 45° AZIMUTH (HUNTSVILLE, ALABAMA)

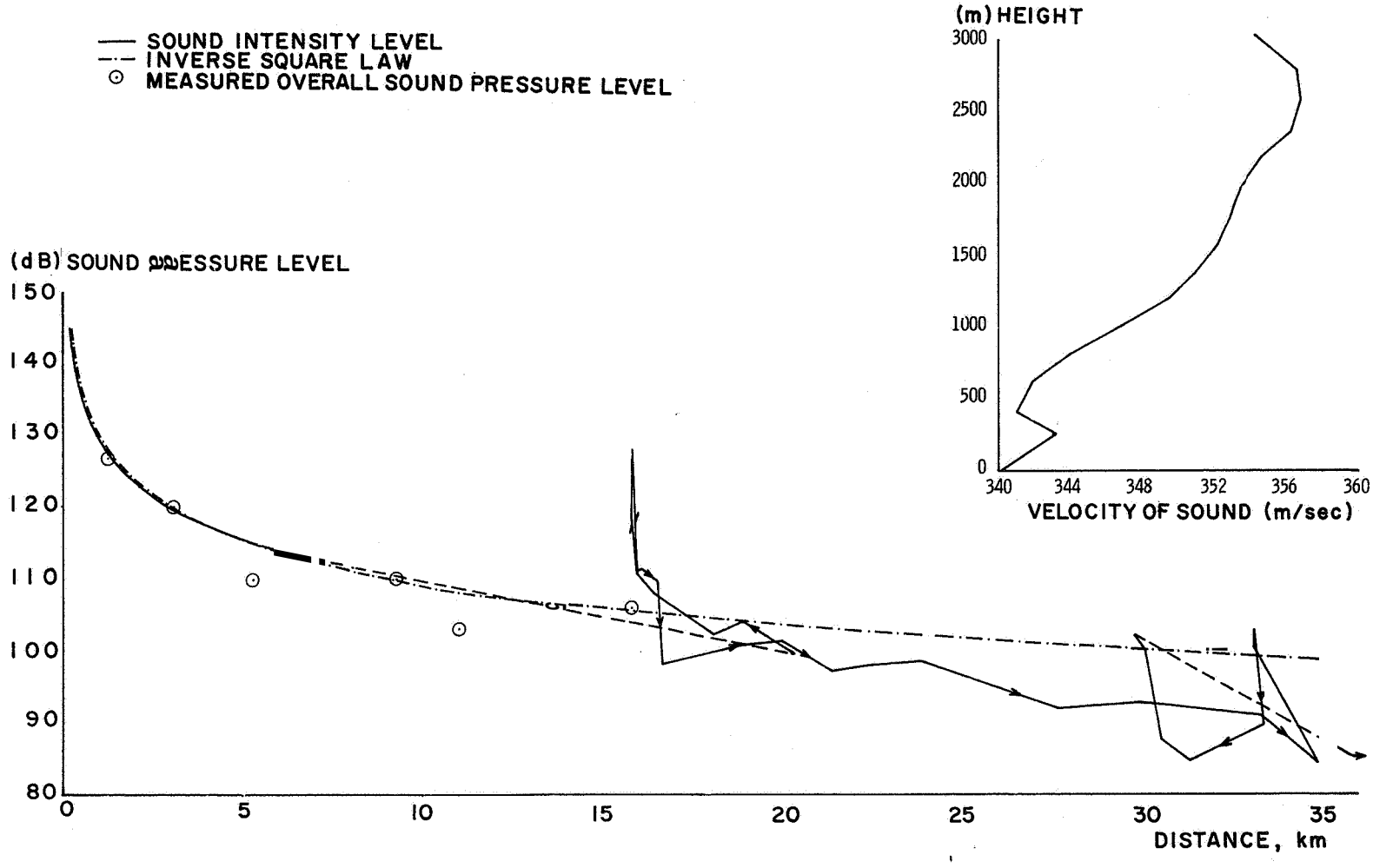

Figure 24

SOUND INTENSITY LEVELS IN VICINITY OF MSFC STATIC TEST FEBRUARY 27, 1963,1648 CST

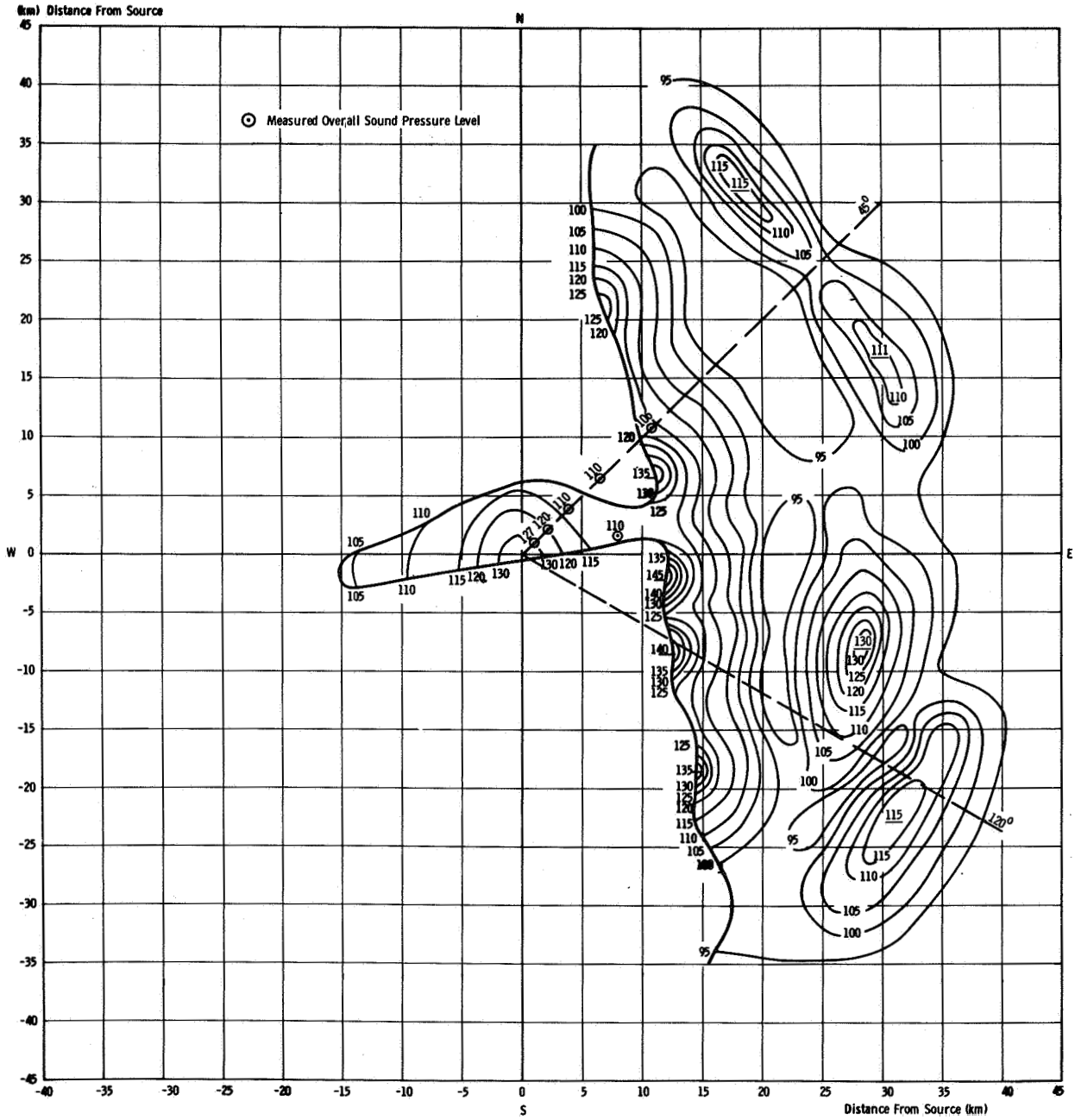

Figure 25

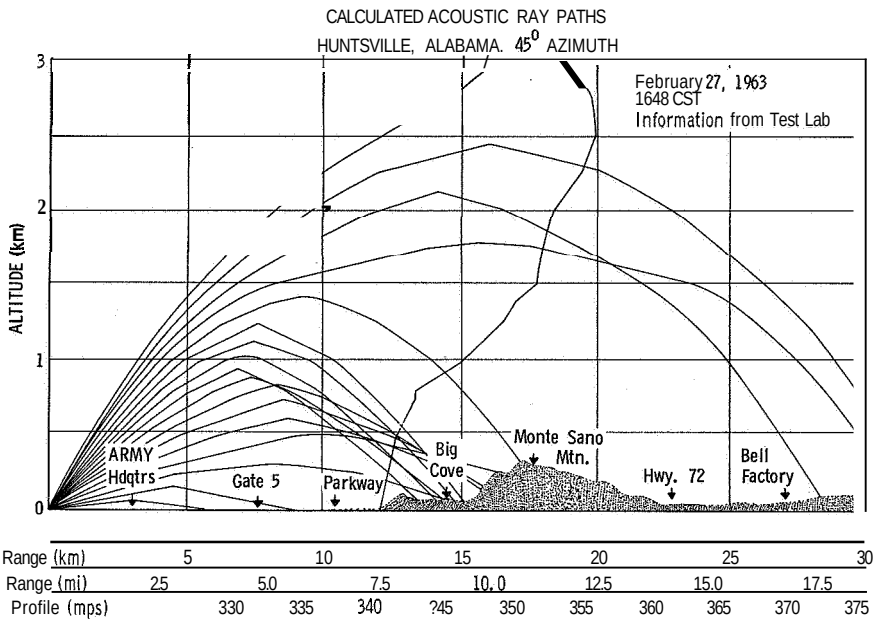

Figure 26

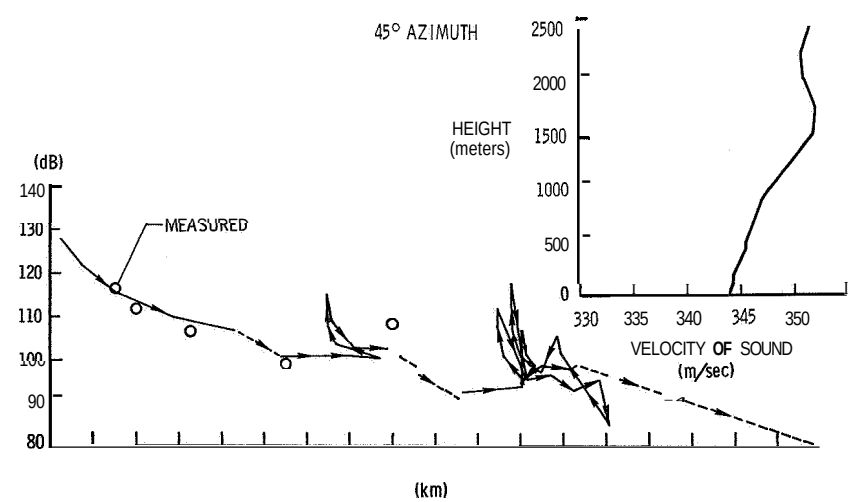

Figure 21

SOUND INTENSITY LEVELS

12-HOUR ATMOSPHERIC PREDICTION

(FOR STATIC FIRING: OCT. 23, 1964, 1640 CST)

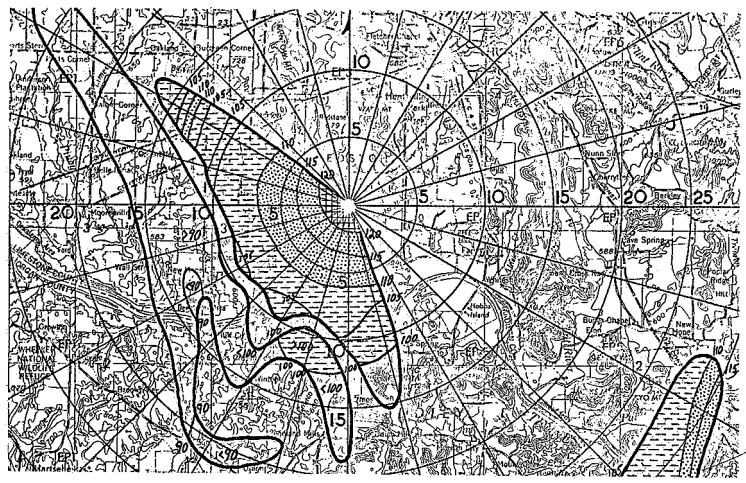

Figure 28

SOUND INTENSITY LEVELS

RAWINSONDE MEASUREMENTS; T-61 MINUTES

(FOR STATIC FIRING: OCT. 23, 1964)

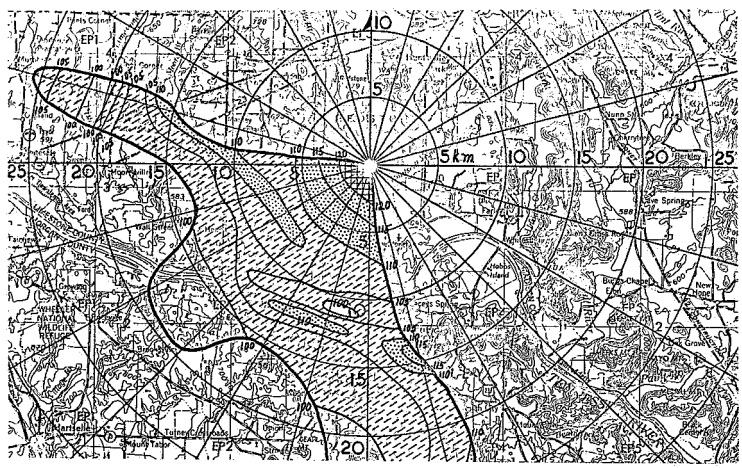

Figure 29

SOUND INTENSITY LEVELS

RAWINSONDE MEASUREMENTS; T-0 MINUTES

(FOR STATIC FIRING: OCT. 23, 1964)

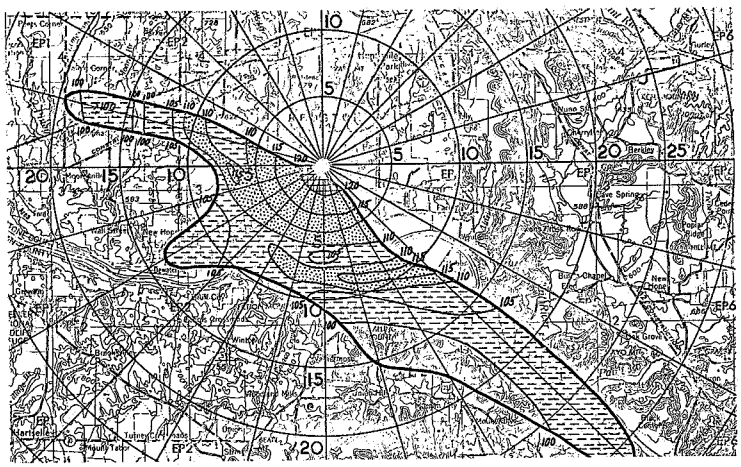

Figure 30

SOUND INTENSITY LEVELS

RAWINSONDE MEASUREMENTS; T+34 MINUTES

(FOR STATIC FIRING: OCT. 23, 1964)

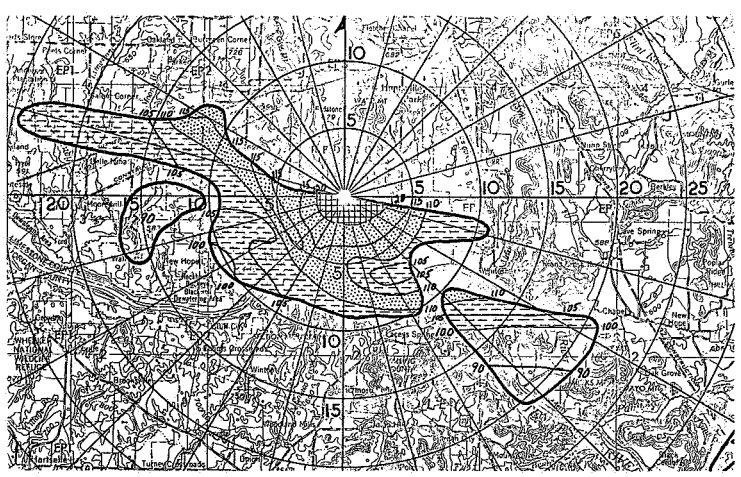

Figure 31

SOUND INTENSITY LEVELS

12-HOUR ATMOSPHERIC PREDICTION

(FOR STATIC FIRING: NOV. 23, 1964, 1640 CST)

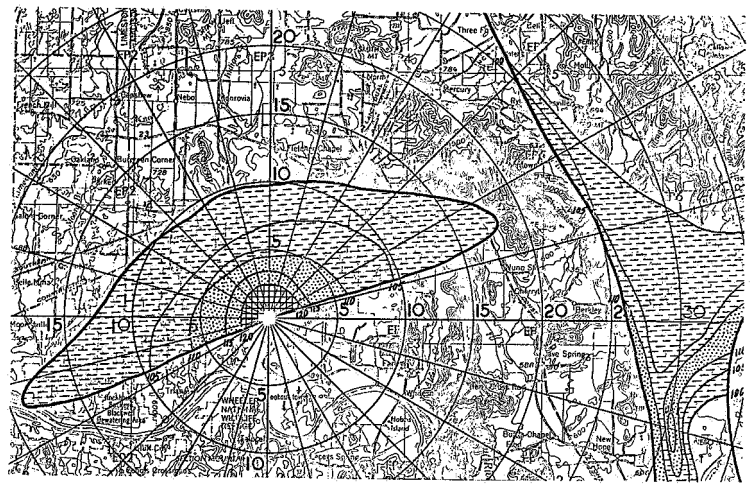

Figure 32

SOUND INTENSITY LEVELS

RAWINSONDE MEASUREMENT: T-45 MINUTES

(FOR STATIC FIRING: NOV. 23, 1964)

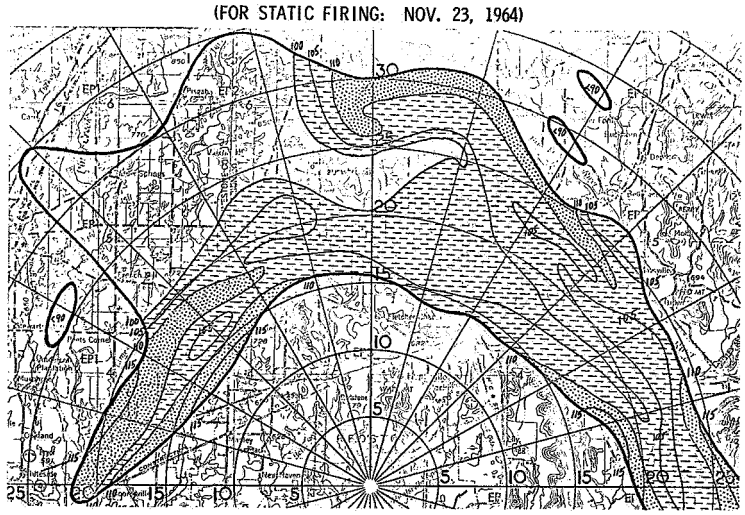

Figure 33

SOUND INTENSITY LEVELS

RAWINSONDE MEASUREMENT; T-0 MINUTES

(FOR STATIC FIRING: NOV. 23. 1964)

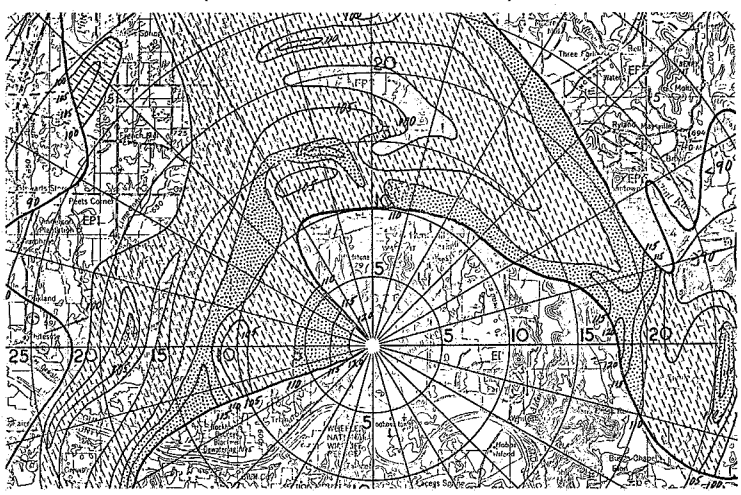

Figure 34

SOUND INTENSITY LEVELS

RAWINSONDE MEASUREMENT; T+36 MINUTES

(FOR STATIC FIRING: NOV. 23, 1964)

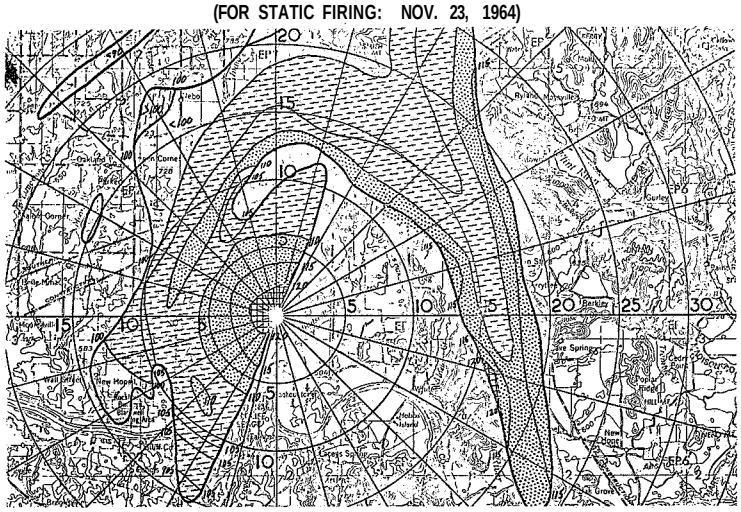

Figure 35

COMPARISON OF SOUND INTENSITY LEVEL AND MEASURED OVERALL SOUND PRESSURE LEVEL FROM ACOUSTICAL HORN FOR CONDITION OF UNIFORM RAYS RETURNING
JANUARY 1963 TO JUNE 1963

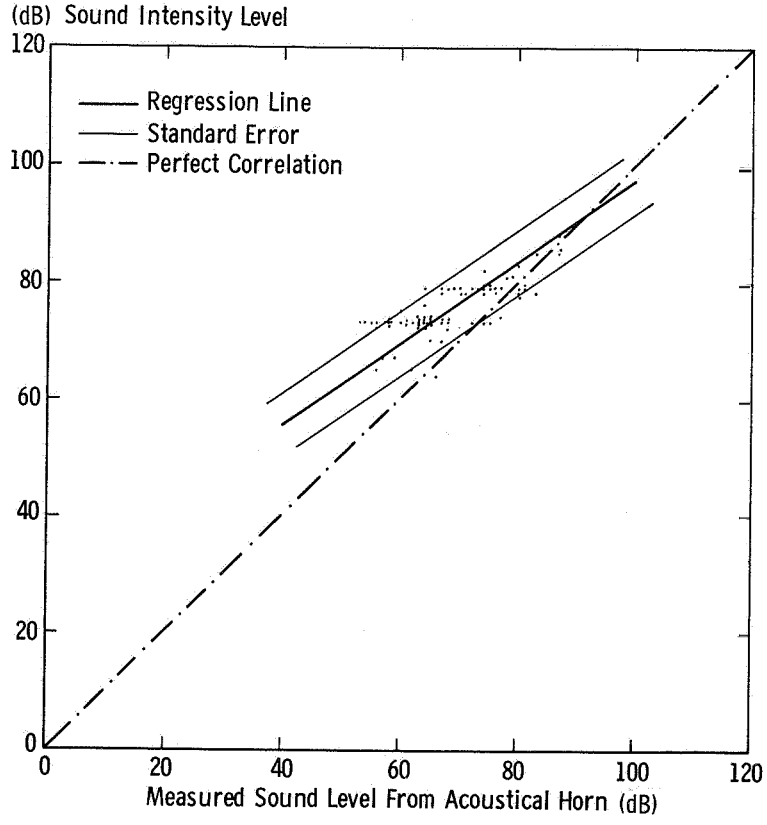

Figure 36

COMPARISON OF SOUND INTENSITY LEVEL FOR ALL CASES (FOCUSING CONDITIONS AND UNIFORM RAYS RETURNING) WITH MEASURED OVERALL SOUND PRESSURE LEVEL FROM ACOUSTICAL HORN
JANUARY 1963 TO JUNE 1963

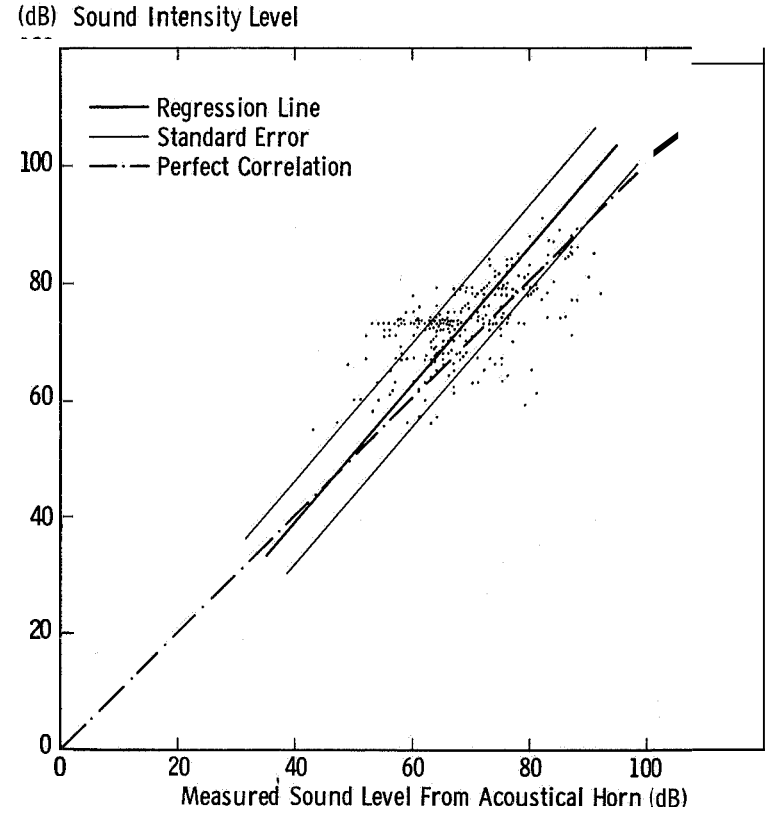

Figure 37

FREQUENCY OF RAYS RETURNING WITH RESPECT TO AZIMUTHS

JANUARY (1962-1963)

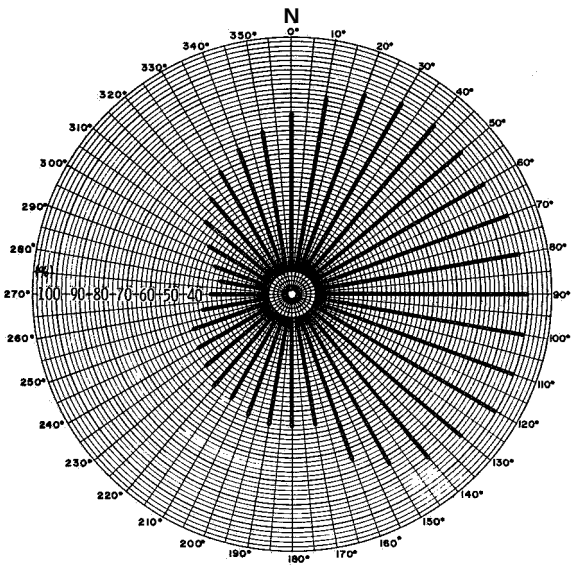

Figure 38

FREQUENCY OF RAYS RETURNING WITH RESPECT TO AZIMUTHS

JULY (1962-1963)

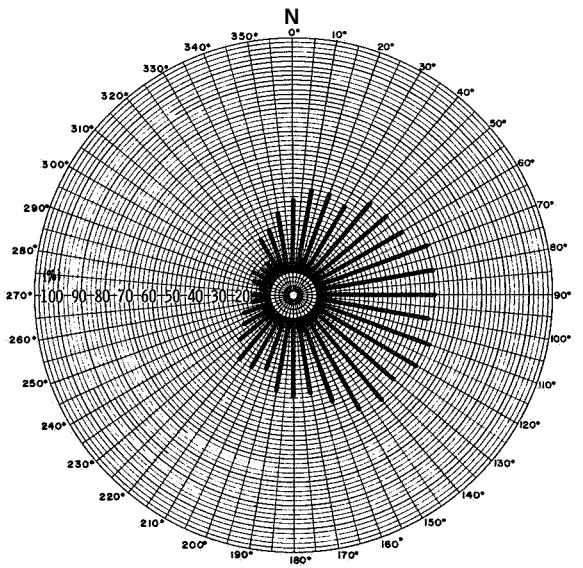

Figure 39

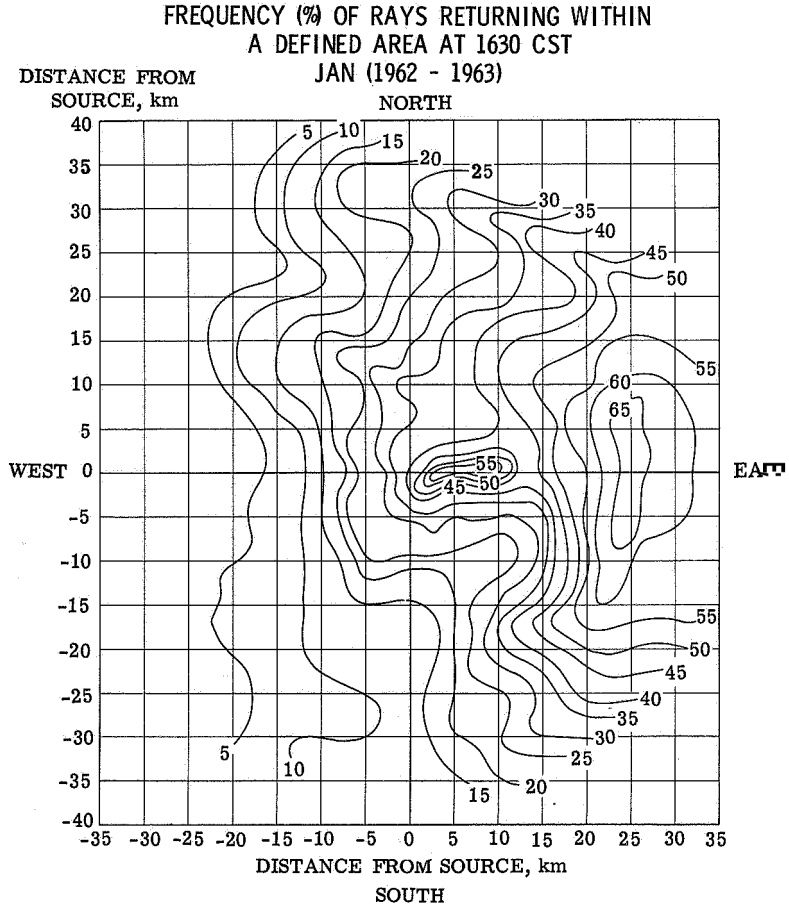

Figure 40

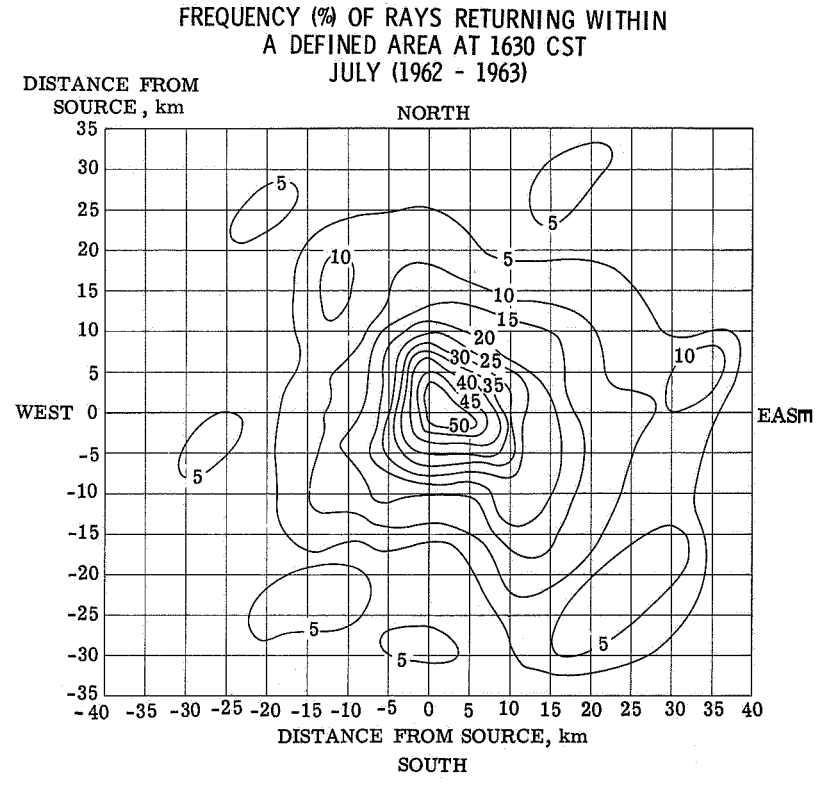

Figure 41

FREQUENCY (%) OF THE RAYS THAT RETURNED AT 1630 CST WHICH PRODUCED SOUND INTENSITY LEVELS $\geq$ 110dB FOR SATURN V

JAN (1962 - 1963)

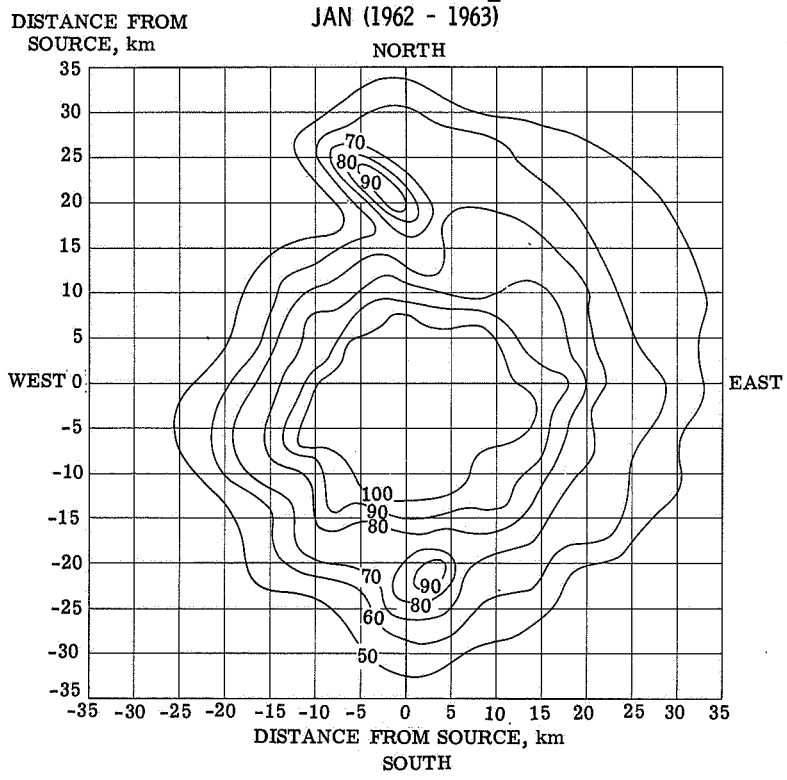

Figure 42

FREQUENCY (%) OF THE RAYS THAT RETURNED AT 1630 CST WHICH PRODUCED SOUND INTENSITY LEVELS $\geq$ 110dB FOR SATURN V

JULY (1962 - 1963)

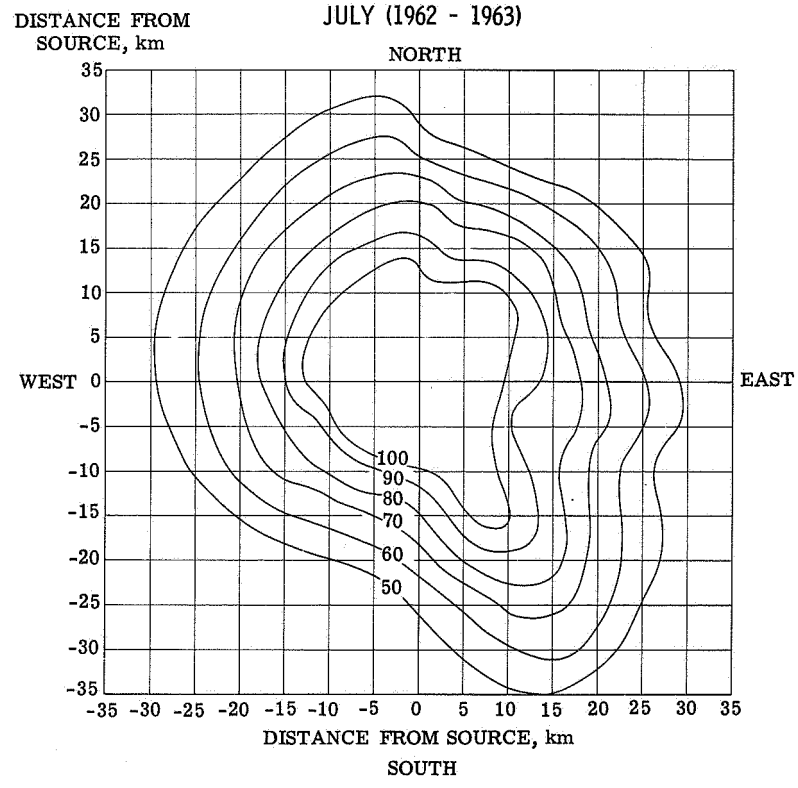

Figure 43

33. SYNTHESIS OF AIRCRAFT NOISE

By Ernest G. Hinterkeuser

The Boeing Company - Vertol Division

SUMMARY

Procedures are described for synthesizing the flyover-noise time histories of an aircraft for both take-off and cruise conditions. Special attention is given to the noise level, spectral and directivity characteristics of the source, and the exposure time and Doppler effects which are related to the speed and distance (altitude) of the aircraft.

A proposed jet powered VTOL aircraft capable of carrying 60 passengers over a 500-mile range is used as an example to illustrate the procedures involved in synthesizing the noise of a proposed aircraft. Some applications of such synthesis studies are cited for subjective studies involving future aircraft or proposed modifications to present aircraft.

INTRODUCTION

The problem of minimizing and controlling the ground noise from aircraft terminal operations is receiving the attention of not only the aircraft manufacturers and operators, but also the public segment of our population centers near aircraft terminals. The individual aircraft sound sources and their treatment are being examined for potential noise-reduction benefits to be gained by appropriate design changes and noise-source acoustical treatments. In consonance with an overall approach to evaluate the potential benefits, the subjective reactions of people to the noise from aircraft need to be predicted beforehand, and if this proves difficult or even impossible analytically, a subjective test program using a panel of listeners is preferred.

Boeing-Vertol has developed and successfully applied a unique method for simulating forward flight effects on aircraft sound sources which are subsequently used in listening tests (ref. 1). The techniques and the jury tests together result in an evaluation of the noise from various designs of aircraft or various operating conditions. The predicted aircraft sounds, which are created electronically on magnetic tape and used in a loudspeaker playback system for aural evaluation, may represent an aircraft in its preliminary design stages. In addition to acoustically evaluating a complete aircraft in its initial design stages, the effects of changes or treatments of propulsion components may be appraised. Furthermore, any changes in aircraft operating procedures which affect the external sound field may be simulated and evaluated by actual listening.

NOISE SIMULATION PROCEDURES

There are several approaches possible in simulating the noise from aircraft operations (fig. 1). If an actual noise recording of the individual component creating the noise or a complete aircraft noise signature is available and it is desired to alter some slight operating characteristic such as applied power, a filter reshaping of the frequency spectrum or a boost in electrical gain to the total noise signal will suffice to create a new sound based on the original recording. A more technically challenging but more versatile approach involves the pure electronic synthesis of sounds using audio-tone oscillators, wave-shape generators, and random-noise generators. There is, however, a limit to the number of subjective aural attributes contributing to a believable sound synthesis if several other mechanical manipulations with these electronic sound sources are omitted. In order to describe such a modified electronic synthesis in-detail, a simulation procedure of a VTOL aircraft noise will be outlined as an example. It should be noted, however, that the general techniques are applicable to many types of aircraft sounds, including those of fixed-wing aircraft, and not to VTOL aircraft noise alone.

The particular aircraft, which is a turbofan-powered jet-lift VTOL, is first examined from its operational considerations and airframe design (fig. 2). The aircraft is designed for the short-haul, city center to city center transport market and its details are derived from the study in reference 2. The aircraft has a 500-nautical-mile range and is sized to carry 60 passengers. The airframe consists of a conventional fuselage with forward-swept wings having pod-buried turbofan lift engines at the tips. During vertical take-off these 10 engines provide upward thrust as do the deflected exhausts of the four cruise powerplants located at the rear of the fuselage. As more cruise-engine deflected exhausts are diverted to the rear of the aircraft, forward speed is attained until sufficient aerodynamic wing lift sustains the aircraft in a conventional manner. The lift engines are then shut down and the aircraft proceeds at cruise altitudes to its destination, where the reverse operational procedure is used for a vertical descent and landing.

Several predominant noise sources emanate from the lift engine. In order to synthesize these sounds, a detailed prediction of the amplitude and frequency content is first necessary. These predictions are based on references 3 to 5. The downward-sloping broadband spectra with increasing frequency (fig. 3) are representative of the lift-engine primary and bypass exhausts. These spectra are electronically generated and combined using shaped broadband random-noise generators. The upward slope in sound pressure level with increasing frequency represents the lift-engine intake noise, on which several pure tones from audio-oscillators are superimposed by electronic mixing to represent inlet whine. The predicted cruise-powerplant noise (fig. 4) is synthesized similarly. All these four primary noise sources (the lift-engine and cruise-powerplant intake and exhaust noises) are recorded simultaneously on separate tracks of a multitrack tape

recorder to represent predicted aircraft noise levels audible to an outdoor observer at a 500-foot distance from the aircraft. These primary, amplitude-time steady sounds then represent the basic noise component library for this particular aircraft from which a composite aircraft noise simulation is derived.

Before the simulation procedure for obtaining the combined total spectrum of an aircraft is described, a particular subjective aspect concerning the natural amplitude fluctuations of noise is noteworthy. The upper portion of figure 5 illustrates the amplitude-time history of an actual jet noise recording. Superimposed on the general rise and decay of the sound envelope representing aircraft approach and recession are random amplitude fluctuations of considerable magnitude caused by wind turbulence, ground reflections, and sound scattering. Although the amplitude rise and decay can be approximated purely electronically by raising and lowering a volume control during a rerecording of a steady-state noise, the amplitude fluctuations cannot be satisfactorily achieved by changes of the electrical volume in small, fluctuating increments. No matter how random the artificially introduced volume fluctuations are, listening to such a record and comparing it with that of an actual jet noise recording reveals the lack of realism still not overcome in this purely electronic approach. (See middle of fig. 5.) For achieving this natural effect, the amplitude-time steady-noise spectra are therefore beamed from a loudspeaker out of doors and rerecorded through a microphone. This method has the desired result of including the natural random-amplitude fluctuations from actual wind noise, sound scattering, and ground reflections. (See lower part of fig. 5.) This latter improved method results in a subjectively superior outdoor aircraft noise simulation as confirmed by critical listening tests.

To achieve the effects of noise directivity, the four basic noise spectra are set to their correct relative volume levels, mixed electronically in the case of aircraft side-line noise, and projected from three separate speakers mounted on top of a vehicle (fig, 6). The cruise-engine inlet noise radiates toward the front of this simulated aircraft; cruise-engine exhaust noise radiates to the rear of the vehicle; and a combination of lift-engine intake and exhaust noise is projected to the side line.

This complex of sound sources is then moved past a stationary microphone which records the total perceived noise (fig. 7). The distance at which the vehicle with its sound sources passes the microphone is dictated by the sound-power generating capacity of the electrical equipment; the amounts of vehicle engine, gear, and tire noises; and ambient sound levels. The geometrical relationship of the moving vehicle position and the stationary microphone recording the total noise is then regulated to simulate the proposed aircraft movements at a 500-foot distance from an outdoor listener. When the vehicle is at position 1, overall noise is low, inlet noise from the front speaker predominates the spectrum, and the aircraft approach noise situation is recorded. As the vehicle

advances to point 2, the noise level is at its peak and consists primarily of sounds from the side-directed speaker. As the vehicle proceeds to position 3, representing a receding aircraft, the overall noise level again falls and the spectrum of the cruise-engine exhaust noise from the rear speaker prevails.

The remaining acoustical feature to be added to the total noise recorded by the field microphone is the Doppler shift. (See lower part of fig. 8.) This effect is obtained in the laboratory by rerecording the final sound obtained in the field on a variable-speed tape recorder. By increasing the playback tape speed during the approach portion of the simulated aircraft noise, the entire spectrum is shifted toward the high-frequency end. This playback speed is smoothly brought back to normal at the peak noise level representing the aircraft overhead position. Without hesitation during this entire playback, the tape speed is then brought to below normal to simulate the lowering infrequency of all the spectra which are heard emanating from a receding aircraft. To compensate for the amplitude-time pattern distortion of the noise envelope which would result from these tape manipulations and to obtain finally a symmetrical flyover time history, it is necessary to distort this pattern prior to this Doppler shift procedure. This may be accomplished in the field by driving the vehicle past the microphone so that the approach noise duration is effectively stretched in time. The vehicle is speeded up to shorten the latter half of the flyover noise duration. (See upper part of fig. 8.)

The simulated aircraft noise now contains all the subjectively important aural characteristics of transient aircraft flyover noise. The aircraft sounds obtained at this stage may be further developed by spectrum shaping and by changes in the amplitude-time characteristic to simulate other distances or even indoor observer positions by reducing the spectral energy by an assumed or measured building sound transmission loss.

CONCLUDING REMARKS

The methods outlined herein have been used at Boeing-Vertol in subjective rating experiments using several different types of aircraft in the take-off and cruise modes. The techniques are also being applied for in-house evaluations of future aircraft designs and for proposed modifications of existing aircraft before hardware is committed to flight testing or production.

REFERENCES

1. Hinterkeuser, Ernest G.; and Sternfeld, Harry, Jr.: Subjective Response to Synthesized Flight Noise Signatures of Several Types of V/STOL Aircraft. NASA CR-1,118, 1968.

2. Fry, Bernard L.; and Zabinsky, Joseph M.: Feasibility of V/STOL Concepts for Short-Haul Transport Aircraft. NASA CR-743, 1967.

3. Sawhill, R. H.: Noise Prediction Methods for Gas Turbine Engines. Doc. No. D6-2269 TN, Boeing Co., 1964.

4. McKaig, M. B.; and Sawhill, R. H.: Procedures for Jet Noise Prediction. Boeing Doc. No. D6-2357 TN, Boeing Co., 1965.

5. O'Keefe, J. V.: PNdB Ground Contour Determination for Jet Aircraft. D6-15082 TN, Boeing Co., 1966.

PROCEDURES FOR AIRCRAFT NOISE SIMULATION

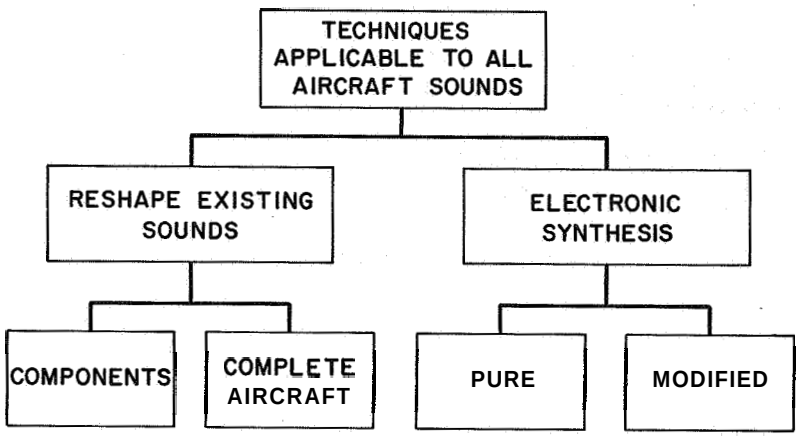

Figure 1

VTOL AIRCRAFT JET LIFT CONFIGURATION

TOTAL THRUST 90,000 POUNDS

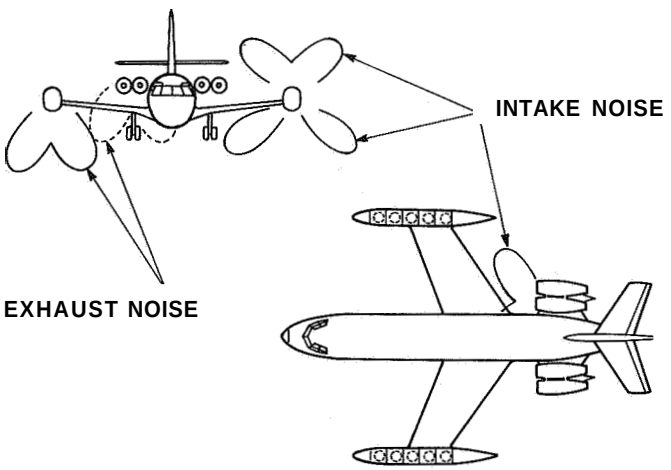

Figure 2

PREDICTED JET LIFT TAKE-OFF SPECTRUM
LIFT POWERPLANT

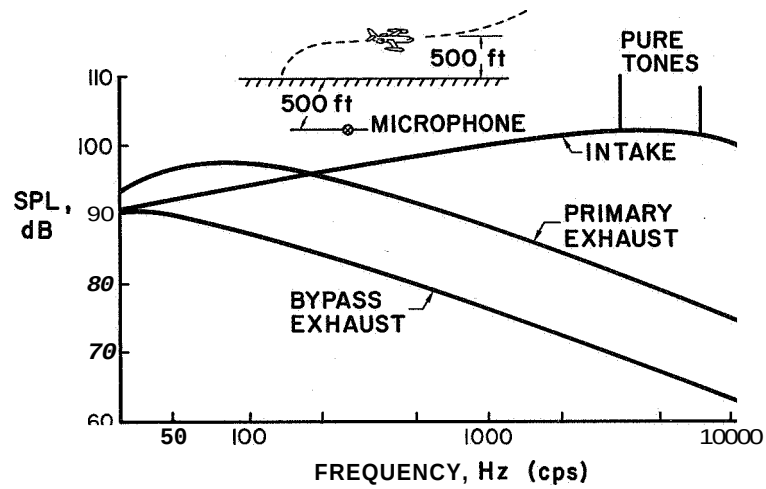

Figure 3

PREDICTED JET LIFT TAKE-OFF SPECTRUM
CRUISE POWERPLANT

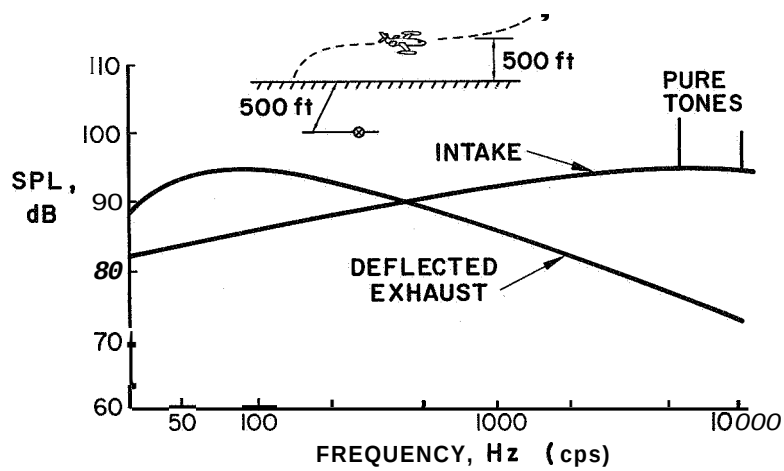

Figure 4

i

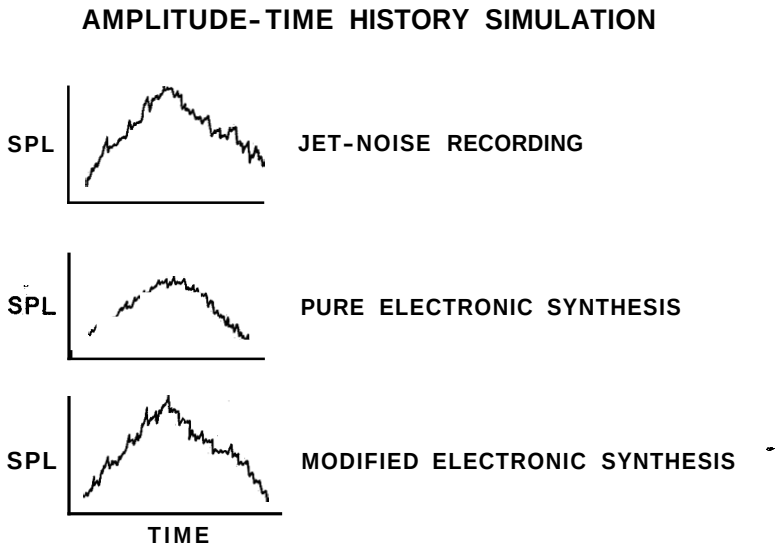

Figure 5

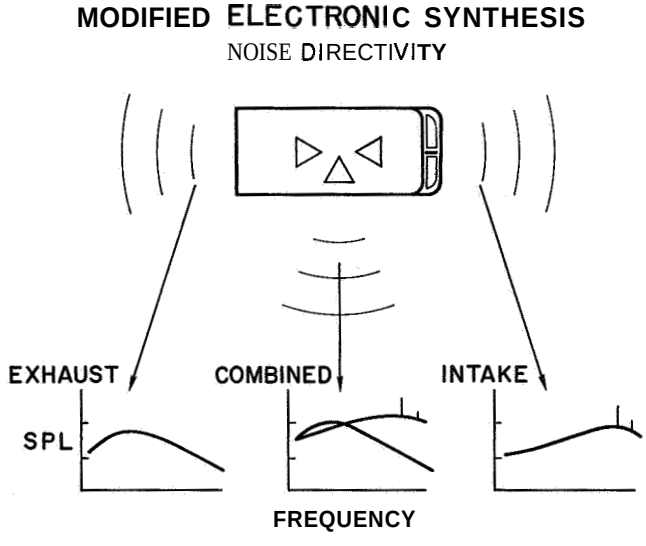

Figure *6*

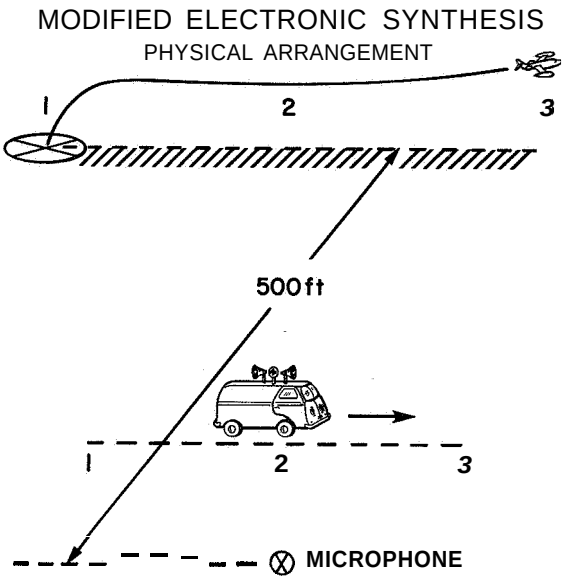

Figure 7

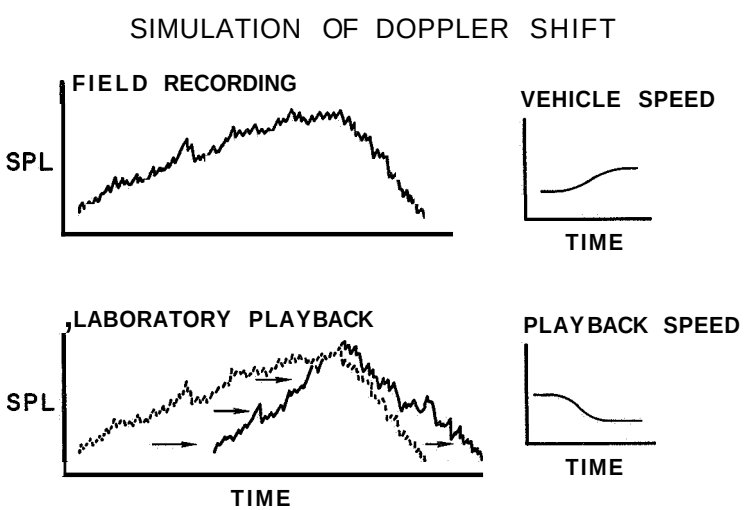

Figure 8

34. PREDICTION OF EFFECTS OF NOISE ON MAN

By Karl D. Kryter

Stanford Research Institute

SUMMARY

The major basic deleterious effects of noise on man are (1) masking of speech, (2) damage to hearing, and (3) perceived noisiness or unwantedness. Present knowledge permits accurate quantitative prediction from spectral measures of a noise and the effects of the noise on the understandability of speech and on temporary and permanent deafness. Methods for the quantitative prediction from spectral measures of noise and the basic effects of noise on perceived noisiness and behavior of people have been developed to the point that standarization of these methods is perhaps possible.

INTRODUCTION

In the standardized terminology of acoustics, "noise" is defined as unwanted sound. However, confusion sometimes results in the use of the word noise as an appellation for unwanted sound because there are two general classes of "unwantedness." In the first category the sound signifies or carries information about the sound's source which the listener has learned to associate with some unpleasantness not due to the physical sound but due to some other attribute of the source. For instance, the sound of the fingernail on the blackboard suggests perhaps an unpleasant feeling in tissues under the fingernail; the sound of an airplane suggests, to some persons, fear that the plane may be falling on their home; a baby's cry causes anguish in a mother; the squeak of a floorboard is frightening because it may indicate the presence of a prowler. In all these examples, it is not the sound as noise that is unwanted (although for other reasons it may also be unwanted), but the information it conveys to the listener. This information is strongly influenced by past experiences of each individual and, in the author's opinion, its effects cannot be quantitatively related to the physical characteristics of the sounds.

In the second category, the unwanted effects of sounds are related to physical characteristics of the sound in ways that are more or less universal and invariant for all people, These effects are both physiological and psychological; the effects are psychological only in the sense that man learns through normal experience of the relations between the characteristics of sounds and their basic perceptual effects. The effects referred to and to be discussed subsequently are (1) the masking of wanted sounds, particularly speech, (2) auditory fatigue, (3) loudness or perhaps some general quality of

bothersomeness or distractiveness, and (4) possibly startle (although, because of man's ability to adapt to repeated stimulations, this effect will vary in time).

These effects presumably are (1) very similar for all people, (2) not dependent on learning nor can they for the most part be "unlearned," and (3) quantitatively related to the physical nature of sounds. Because of these characteristics, they deserve the attention of persons interested or involved in the design of devices that generate sound, in the control of the sound during its transmission, or in the protection of the health and well-being of people exposed to the sound. Indeed, nearly all measurement of sound by acoustical engineers is made for the immediate or ultimate purpose of evaluating the effects of the sound on man.

MASKING OF SOUNDS

It is likely that the most disruptive, harmful, and widespread effect of noise is that of masking or interference with the perception of wanted auditory signals, in particular, speech. It is also an unfortunate fact that this masking effect is something for which there is no adaptation. Masking is primarily to be understood in terms of a competition that takes place in the inner ear or cochlea of man's auditory system for the attention of the receptor cells in the cochlea. These receptor cells respond solely on the basis of physical forces exerted upon them and cannot distinguish between sounds that the listener may want to hear and the sounds he may not want to hear.

Perhaps for present purposes only two particularly important features of masking need be mentioned here:

(a) The so-called spread of masking that occurs from low-frequency sounds upon higher frequency sounds

(b) The audibility of speech in the presence of a masking noise

Spread of Masking

Figure 1, based on reference 1, illustrates the general amount of masking of one pure tone which occurs from the presence of another pure tone. For example, the curve labeled "20 dB" in figure 1 indicates the intensity required of a "probe" tone at frequencies between 80 and 1000 Hz to be just heard in the presence of a steady-state 200-Hz tone at an intensity of 20 dB. In the absence of the 200-Hz masking tone, any tone will be audible when its intensity, as plotted in figure 1, is at zero dB. Thus, the curves in figure 1 represent the increases in intensity required at a given frequency to make a tone audible in the presence of the 200-Hz masking tone.

There are two things to be noted in particular about figure 1: (1) the frequencies above the masking tone or sound are masked to a greater extent than are frequencies below the masking tone, and (2) as the intensity of the masking tone or sound is increased, the degree of upward spread of masking is increased.

Masking of Speech

The masking effects of noise on speech are sufficiently known to permit the preparation of standardized procedures for predicting from these physical measurements of speech and noise the needed masking that will occur and its effects upon the understandability of the speech. This calculation procedure is called the "Articulation Index" and essentially reflects (a) the relation between the speech spectrum and the spectrum of the noise, (b) the variations in intensity of the speech spectrum, and (c) the relative contributions of different segments of the speech spectrum to the understanding of speech. Figure 2, derived from references 2 and 3, illustrates the typical way in which an articulation index (AI) is calculated and the basis for the calculations.

AUDITORY FATIGUE AND DAMAGE TO HEARING

Although masking of speech may be the most bothersome effect from work, sociological, and behavioral points of view, it should not be overlooked that the ear is subject to fatigue and damage as a result of exposure to noise. This damage to hearing tends to occur somewhat slowly and painlessly with continued exposure to noise so that the ear is often permanently damaged before people are aware of what is happening. It is partly for this reason that noise is an occupational health hazard in the military services and in many industries, including, of course, the aviation industry.

As with masking of speech, it is possible to depict certain general relations between noise exposure and auditory fatigue in terms of the spectrum of the noise and the duration of exposures. Figure 3 (from ref. 4) shows a set of so-called equinoxious damage risk contours for exposure to noise. Any point on these curves is presumed to represent the same amount of damage risk to hearing as any other point. For example, a one-third octave band of noise with a center frequency (cf) of 200 Hz, an intensity of 105 dB, and a daily duration of 60 minutes will cause the same amount of auditory fatigue and eventual permanent damage to hearing as a one-third octave band of noise with a center frequency of 3000 Hz, a sound pressure level of 105 dB, and a daily duration of only 3 minutes. The damage risk exposures in figure 3 will, it is believed, cause in no more than 50 percent of the people a permanent threshold shift of no more than 10 dB at 1000 Hz or below, 15 dB at 2000 Hz, and 20 dB at 3000 Hz or above. These permanent threshold shifts will occur only after approximately 10 years of almost daily exposure to the noise conditions depicted. On the basis of present knowledge, such as that illustrated in figure 3, it is

possible to predict with reasonable accuracy the permanent threshold shift or damage to hearing that is likely to occur in given percentages of people for given years of exposure to a wide variety of noises of differing spectral and temporal patterns.

The noise from past and present aircraft is a hazard to hearing only to operational and maintenance personnel working in or close to the aircraft. However, the external noise from aircraft would not have to be increased too much beyond the present levels and/or durations before legitimate claims could be made that some small amount of damage to hearing occurs in some small percentage of the people living in communities near airports.

LOUDNESS AND PERCEIVED NOISINESS

In general, the acceptability of noise to people has been evaluated in terms of its judged subjective annoyance value. Sometimes subjects have been asked to rate the loudness rather that the annoyance or unwantedness of the sounds on the presumption that the response of people to either of these questions would be about the same.

Psychological judgment tests have demonstrated that people will consistently judge among themselves the "unwantedness," "unacceptableness," "objectionableness," or "noisiness" of sounds that vary in spectral content and duration provided that the sounds do not differ significantly in their meaning. The subjects in these tests are asked to consider the terms in quotation marks as being synonymous when making their judgments. This general attribute or quality of sound is designated as "perceived noisiness." It is presumed that, for the judgment of perceived noisiness, the human auditor subconsciously combines the inherent effects of loudness, masking, auditory fatigue, and perhaps distractiveness and startle into a single overall reaction to a sound. It is to be emphasized that the effects the meaning of sounds have upon judgments as to acceptability are specifically excluded from or kept constant for this attribute of perceived noisiness.

The unit of perceived noisiness is called the "noy." A sound that is judged to be subjectively equal in noisiness to an octave band of random noise with a center frequency of 1000 Hz (referred to hereinafter as the standard reference band), a sound pressure level of 40 dB (re 0.0002 microbar), and a duration of 1/2 second is given a value of 1 noy. A sound that is judged to be twice as noisy as a sound of 1 noy has a value of 2 noys, four times as noisy a value of 4 noys, and so forth.

It has been customary to express acoustic and psychoacoustic measurements in terms of a decibel scale. For this reason the noy value of a sound that presumably reflects the magnitude in noisiness as perceived by a person is usually converted to the so-called PNdB scale. This conversion consists of referring to the sound pressure level of the standard band that has the same noy value as a given sound as the PNdB value of

the given sound. For example, noise that has a noy value of 1 has a PNdB value of 40, the sound pressure level of the reference band at 1 noy. The relations between noy and PNdB values, band center frequency, and band sound pressure level for bands of sound of equal bandwidth and the same temporal pattern are shown in figure 4.

Although the noy and PNdB terminology and concepts are analogous to and based upon the sone and phon units used for loudness, some frequency bands of noise are slightly different when one judges loudness than when one judges unwantedness, as is shown by the difference between the 80-noy and 80-sone contours at the top of figure 4. Other differences, perhaps more important, to be found between judgments of loudness and perceived noisiness are described subsequently.

In figure 4, several functional relations are shown that perhaps require further explanation. The noy contours in this figure were obtained by having the subjects or the experimenters adjust the intensity of different frequency bands of noise until they sounded equally noisy or unwanted or unacceptable as a band of noise at 1000 Hz whose intensity was kept constant. For example, a band of noise with a center frequency of 1000 Hz and an intensity of 40 dB is equal subjectively to other frequency bands having the intensities indicated by the 1 noy contour. It is seen that bands of frequencies in the region from 2000 to 5000 Hz are judged to be the most unwanted at a given sound pressure level.

To help quantify the scale of perceived noisiness as the intensity of a sound is increased while the frequency content is kept constant, the number 1 was arbitrarily assigned to the reference or standard band with center frequency of 1000 Hz and set at a sound pressure level of 40 dB (re 0.0002 microbar). Subjects were then asked to adjust the 1000-Hz band until it sounded twice as unwanted as the reference band at an intensity of 40 dB. This intensity was assigned a value of 2 noys, which indicates that subjectively the sound was now twice as unwanted. The different intensities required to obtain additional doublings of the unwantedness were determined. It was found that, on the average, increasing the intensity by 10 dB resulted in a doubling in the subjective noisiness of sounds.

CONCEPTS OF PERCEIVED NOISINESS

Starting with the relations shown in figure 4, or other somewhat similar relations, attempts have been made to build a general set of procedures for calculating from physical measures what is or will be the perceived noisiness to the average person of sounds, regardless of their source and exclusive of their meanings. Indeed, procedures have been developed for estimating the perceived noisiness of (a) single occurrences of sounds of different spectra but of like durations, (b) single occurrences of sounds of different spectra and of like or different durations, and (c) multiple daily occurrences

of sounds of different spectra and of like as well as of different durations. These procedures are described subsequently.

Single Occurrences of Noise That Differ in Spectral Shape, Bandwidth, and Tonal Complexity

In figure 4 it was observed that the perceived noisiness of a sound of a given bandwidth changed as its center frequency was varied. However, noises of common interest are much more complex in their spectral content and bandwidths. The effect of changing the bandwidth of sounds is taken into account in the calculation of the perceived noisiness (PN) or perceived noise level (PNL) in accordance with the following formulas and approximation methods:

$$\text{Perceived noisiness} = \left[\text{Noys (max. band)} + 0.15\left(\sum \text{All bands} - \text{Noys (max. band)}\right)\right]$$

$$\text{Perceived noise level in PNdB} = 40 + 10 \log_2 \text{PN}$$

Approximation methods:

- PNL in dB(N), sound level meter, N weighting network
- PNL in dB(A), sound level meter, A weighting network + 13 dB

These formulas, which were developed by S. S. Stevens (ref. 5) for the calculation of loudness, have been empirically derived and work very well for noises that are of a single temporal pattern and differ only in their general spectral shape and width.

However, it has been found that a sound that consists of a broadband spectrum plus steady-state pure-tone or line spectral components is more unacceptable or noisier than a sound without these components, even though the pressures in the different frequency bands are the same for the two sounds. The tone-to-noise ratio (T/N) can, when the tone and noise are measured separately, be evaluated from one-tenth or narrower to full-octave band levels. When, as is usually the case, the tone and noise are measured together, the presence of pure-tone or line spectral components is identified by the ratio of the tone-plus-noise in a band to the noise in adjacent bands (T + N)/AN. When this ratio is 3.0 dB or greater, it is presumed that significant pure-tone or line spectral components are present.

Figure 5, based on reference 6, illustrates the subjective penalty that is generally found when pure-tone or line spectral components are present. This penalty, which is read from the ordinate, means that the band containing a pure-tone or line spectral component has an apparent subjective intensity equal to the actual measured sound pressure

level in the band in question plus the number of decibels read from the ordinate in the figure. It is seen that the penalty earned by pure-tone or line components depends upon their frequency and the degree to which they exceed the background noise. The results of new tests of the pure-tone penalty are discussed in reference 7.

Single Occurrences of Noises of Differing Temporal Pattern

Although loudness tends to remain constant if the intensity remains constant, the perceived noisiness of a sound increases as the noise is continued in time. To a first approximation it is found that the perceived noisiness of a sound is equal to the integrated, on an energy basis, PNdB values that are found in successive 1/2-second intervals during the occurrence of a noise. For practical purposes, an occurrence of a noise is said to extend between the times the noise is within 10 dB of its maximum level. The formula for calculating the effective perceived noise level (EPNL) of a sound is as follows:

$$\text{Effective perceived noise level in EPNdB} = \left(\sum_{0.5} \log_{10}^{-1} \text{PNdB}/10\right) - 12$$

$$\text{Approximation methods} \begin{cases} \text{EdB(N)} = \left(\sum_{0.5} \log_{10}^{-1} \text{dB(N)}/10\right) - 12 \\ \text{EdB(A)} = \left(\sum 0.5 \log_{10} \text{dB(A)}/10\right) + 1 \end{cases}$$

where 0.5 is 1/2-second interval of time, and -12 is based on a reference duration of 8 seconds. It would appear, on the basis of present data, that the most accurate and general way of measuring or calculating from physical measurements the true unwantedness or noisiness of a sound is to determine tone-corrected PNdB values every 1/2 second during the sound and from these values to calculate their total or effective value. PNdB units that are calculated with tone corrections are usually designated PNdB_t.

Several units have been proposed for measuring or estimating the perceived noisiness of sounds. The most widely used or proposed measurements are summarized in table I. Several additional variations of these basic units are also in use or being evaluated, as are briefly discussed in reference 8.

COMPOSITE NOISE RATING

One prime goal of noise evaluation is to determine the acceptability of a total noise environment present day after day in a given community or neighborhood. Research data collected to date indicate that the equal energy assumption used in calculating the EPNL of a sound apparently works reasonably well for the determination of the reaction of

people to multiple sounds occurring during a day; that is, two sounds of equal EPNL have the same effect as one sound having an EPNL 3.0 dB higher than that of the individual sounds. In addition, it has been found that people react or complain more about noises occurring late at night (presumably because of interference with sleep and perhaps because the environment is, in general, quieter during that period and, therefore, more noise is noticeable). It has been proposed that a 10-dB penalty be placed upon noises that occur at night.

The sum of these ideas - that response to noises occurs on an energy basis and that there is a 10-dB greater sensitivity during the night than the day to noise - has been called the Composite Noise Rating (CNR). K. N. Stevens, A. C. Pietrasanta, and staff members of Bolt Beranek and Newman developed the Composite Noise Rating procedure for the U.S. Air Force (ref. 9). This procedure is used in the Department of Defense Land Use Planning Guide (ref. 10) and is also to be found in various technical reports prepared for the Federal Aviation Administration. The general formulas for *CNR* are as follows:

For noises of equal duration per occurrence but of differing spectra and/or numbers of occurrences,

$$CNR = \overbrace{\text{EPNL} + (10 \log_{10} N) - 12}^{7\text{ a.m.} - 10\text{ p.m.}} \oplus \overbrace{\text{EPNL} + (10 \log_{10} N) - 2}^{10\text{ p.m.} - 7\text{ a.m.}}$$

where N is number of occurrences of sounds and $\oplus$ is addition on $10 \log_{10}$ antilog basis.

For noises of equal or unequal durations per occurrence and of differing spectra and/or numbers of occurrences,

$$\text{CNR} = 10 \log_{10} \left[\overbrace{\sum_{0.5} \left(\log_{10}^{-1} \text{PNdB}_{0.5}/10 \right) - 24}^{7\text{ a.m.} - 10\text{ p.m.}} \right] \oplus \left[\overbrace{\sum_{0.5} \left(\log_{10}^{-1} \text{PNdB}_{0.5}/10 \right) - 14}^{10\text{ p.m.} - 7\text{ a.m.}} \right]$$

Originally, and during use, different units of measurement of the noise other than the EPNL units were used; also, from time to time, various "correction factors" have been applied to the units of noise measurement to account for presumed effects of the socio-economic status of a neighborhood, that is, whether a neighborhood was close to heavy industry, rural, and so forth. There is obviously a need for standardizing the units of measurements and corrections to be used for the calculation of CNR.

As described previously, calculated PNL, EPNL, and CNR are based on the concept of a general reaction to sound that is the conglomerate effect of the attributes of loudness, masking of speech, auditory fatigue, and perhaps distractiveness and startle independently of any meaning the sound may have. It is to be noted that the behavioral reactions of most practical interest are those typically observed after months or years of daily or almost daily exposure to the respective noise environments. In that regard, it is estimated that there is an initial adaptation or familiarization over a period of the first several months of exposure to a given noise environment that reduces reactions to the noise by an amount equivalent to a reduction of about 10 CNR.

Figure 6 summarizes the general relations between CNR and various human reactions to sound. These relations are extrapolated from and consistent with laboratory and field research and actual "real-life" behavior of people in communities. (See ref. 11.) It is presumed that the range in reactions of people to a given noise environment as illustrated in figure 6 is a joint function of (a) individual personality differences, (b) individual and group differences in attitudes toward and abilities in the expression of complaints and other related behavior, and (c) variations in CNR exposure conditions between and in rooms in homes and buildings and areas in a community. Some new data on the problem of noise in communities are presented in references 12 and 13.

Unfortunately, one cannot really know the true EPNL or CNR received by individual people in their homes, or even on the streets in their communities, inasmuch as noise surveys depict only the noise present during some period of time at one point, or at most several points outdoors in a neighborhood. The actual noise in individual rooms and individual yards within that neighborhood must vary tremendously. Nevertheless, it is reasonable to believe that controlling noise in terms of EPNL and CNR must provide the most efficient and adequate criterion for reducing, by purely physical and operational means, the long-term reaction of people to noise in or at their homes and places of work.

CONCLUDING REMARKS

Perhaps the most beneficial and practical applications of effective perceived noise level, and when possible Composite Noise Rating, are not with respect to present-day noises or noise environments but (1) as guides for the design and operation of so-called quiet engines, (2) in the forecasting of noise environments for neighborhoods and communities as new airports, roadways, and industries are developed and used, and (3) as guides for setting acoustical standards for new housing.

REFERENCES

1. Carter, Norman L.; and Kryter, Karl D.: Masking of Pure Tones and Speech. J. Aud. Res., vol. 2, no, 1, Jan. 1962, pp. 66-98.

2. French, N. R.; and Steinberg, J. C.: Factors Governing the Intelligibility of Speech Sounds. J. Acoust. Soc. Amer., vol. 19, no. 1, Jan. 1947, pp. 90-119.

3. Kryter, Karl D.: Methods for the Calculation and Use of the Articulation Index. J. Acoust. Soc. Amer., vol. 34, no. 11, Nov. 1962, pp. 1689-1697.

4. Kryter, K. D.; Ward, W. Dixon; Miller, James D.; and Eldredge, Donald H.: Hazardous Exposure to Intermittent and Steady-State Noise. J. Acoust. Soc. Amer., vol. 39, no, 3, Mar. 1966, pp. 451-464.

5. Stevens, S. S.: Calculation of the Loudness of Complex Noise. J. Acoust. Soc. Amer., vol. 28, no. 5, Sept. 1956, pp. 807-832.

6. Kryter, K. D.: Concepts of Perceived Noisiness, Their Implementation and Application. J. Acoust. Soc. Amer., vol. 43, no. 2, Feb. 1968, pp. 344-361.

7. Pearsons, Karl S.: Assessment of the Validity of Pure Tone Corrections to Perceived Noise Level. Conference on Progress of NASA Research Relating to Noise Alleviation of Large Subsonic Jet Aircraft, NASA SP-189, 1968. (Paper No. 36 herein.)

8. Kryter, Karl D.; Johnson, Paul J.; and Young, James R.: Judgment Tests of Aircraft Noise. Conference on Progress of NASA Research Relating to Noise Alleviation of Large Subsonic Jet Aircraft, NASA SP-189, 1968. (Paper No. 37 herein.)

9. Stevens, Kenneth N.; Pietrasanta, Adone C.; and The Staff of Bolt Beranek and Newman Inc.: Procedures for Estimating Noise Exposure and Resulting Community Reaction From Air Base Operations. WADC Tech. Note 57-10, DDC Doc. No. AD 110705, U.S. Air Force, Apr. 1957.

10. Anon.: Land Use Planning With Respect to Aircraft Noise. AFM 86-5, TM 5-365, NAVDOCKS P-98, U.S. Dep. Defense, Oct. 1, 1964; also issued as a Tech. Rep. by Bolt, Beranek & Newman, Inc. (Available from DDC as AD 615015.)

11. Galloway, W. J.; and Von Gierke, H. E.: Individual and Community Reaction to Aircraft Noise; Present Status and Standardization Efforts. INC/C4/P9, Amer. Stand. Ass., Nov. 1966.

12. Connor, William K.: Community Reactions to Aircraft Noise - Noise Measurements. Conference on Progress of NASA Research Relating to Noise Alleviation of Large Subsonic Jet Aircraft, NASA SP-189, 1968. (Paper No. 40 herein.)

13. Hazard, William R.: Community Reactions to Aircraft Noise – Public Reactions. Conference on Progress of NASA Research Relating to Noise Alleviation of Large Subsonic Jet Aircraft, NASA SP-189, 1968. (Paper No. 41 herein.)

TABLE I.- PROCEDURES THAT HAVE BEEN PROPOSED FOR ESTIMATION OF JUDGED PNL FROM OBJECTIVE **SOUND** MEASUREMENTS

[Within each class of sounds the units of measurement are rank ordered in accordance with relative accuracy with which usually they predict the judged perceived noisiness or unacceptability of sounds. (See ref. 6)]

Class of sound	Sound measurement equipment	
	1/3- **or** full-octave band filters and sound level meter, slow meter action	Sound level meter with frequency-weighting networks, slow meter action
Sounds of same temporal but different spectral patterns:		
Broadband spectra, no pure tones or line spectra	1. Peak PNdB **2. Max.** PNdB	3. dB(N) **4.** dB(A) + **13**
Broadband spectra, with pure tones or line spectra	1. Peak $PNdB_t$ **2. Max.** $PNdB_t$	
Sounds of differing temporal and spectral patterns:		
Broadband spectra, no pure tones or line spectra	1. EPNdB **2.** EEPNdB	3. EdB(N) **4.** EdB(A) + 13 5. EEdB(N) **6.** EEdB(A) + 13
Broadband spectra, with pure tones or line spectra	1. $EPNdB_t$ **2.** $EEPNdB_t$	

THRESHOLD SHIFT DUE TO A 200-HZ MASKING TONE

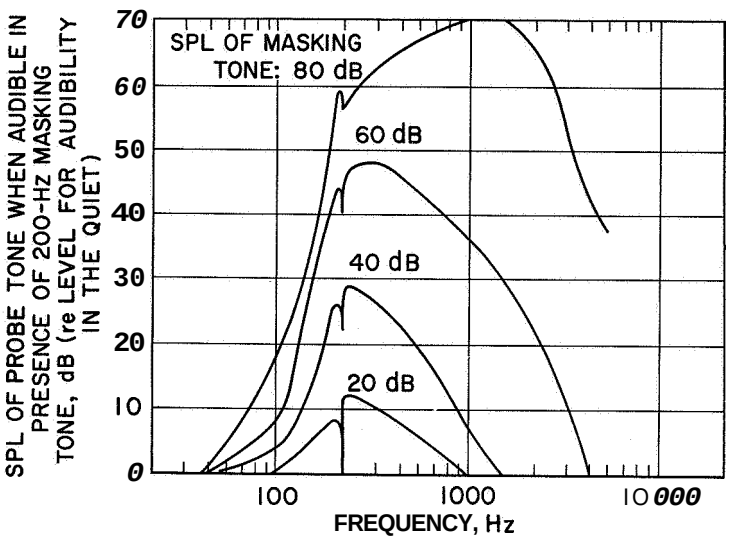

Figure 1

PROCEDURE FOR CALCULATION OF THE ARTICULATION INDEX

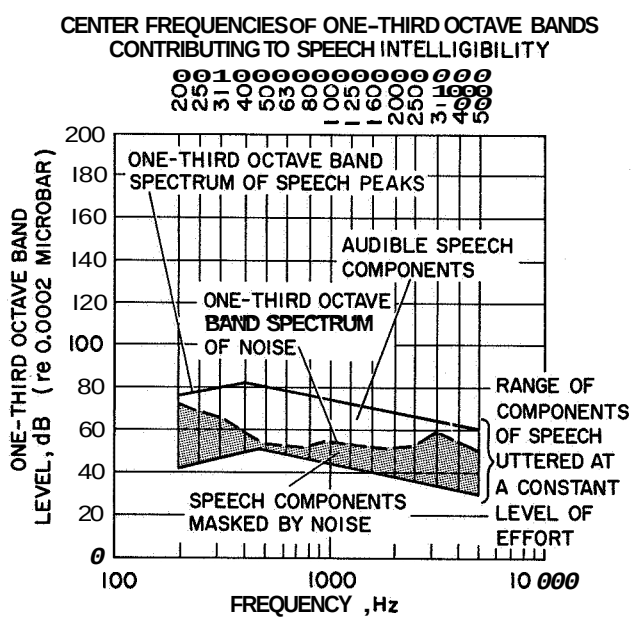

BAND cf, Hz	SPEECH PEAKS MINUS NOISE, dB	WEIGHT	COL 2 X COL 3
2001	4	0.0004	0.0016
250	10	0.0010	0.0100
315	13	0.0010	0.0130
400	24	0.0014	0.0336
500	26	0.0014	0.0364
630	26	0.0020	0.0520
800	24	0.0020	0.0480
1000	21	0.0024	0.0504
1250	18	0.0030	0.0540
1600	18	0.0037	0.0666
2000	15	0.0037	0.0555
2500	15	0.0034	0.0510
3150	6	0.0034	0.0204
4000	8	0.0024	0.0192
5000	12	0.0020	0.0240
		AI = 0.5357	
AI OF 0.54 = 75 % WORDS CORRECT			

Figure 2

EXPOSURES TO BANDS OF NOISE THAT WILL CAUSE ABOUT 10 dB THRESHOLD SHIFT AT 1000 Hz OR BELOW, 15 dB AT 2000 Hz, OR 20dB AT 3000 Hz AND ABOVE

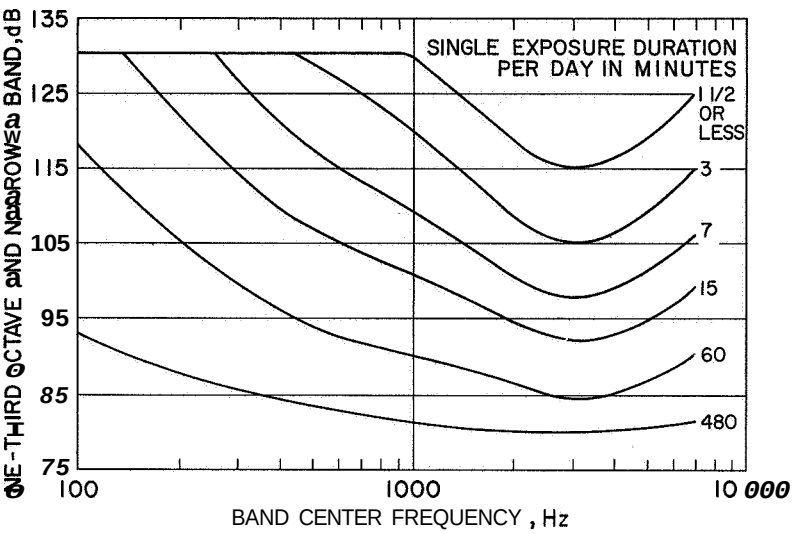

Figure 3

NOISINESS OF BANDS OF SOUND

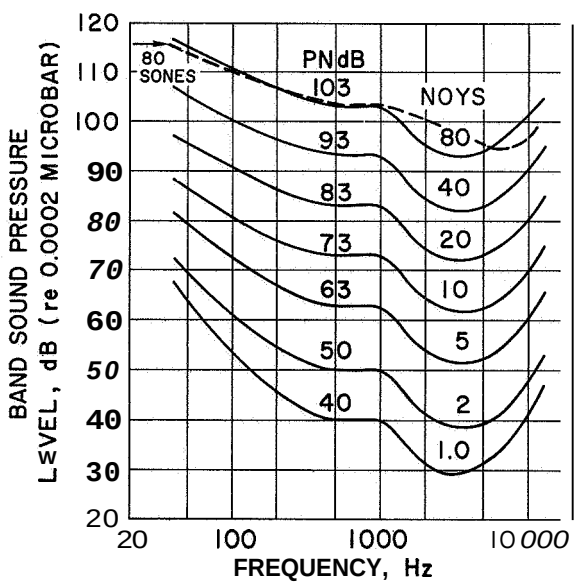

Figure 4

PENALTY FOR PURE TONES OR LINE SPECTRA

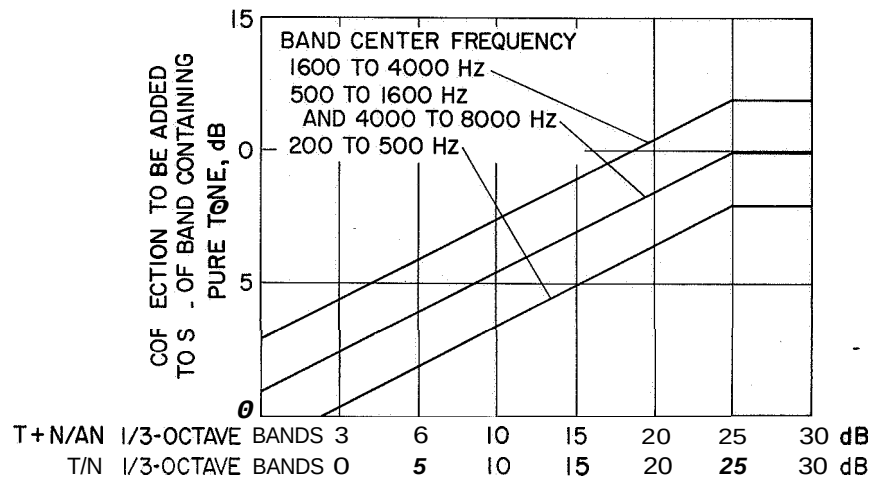

Figure 5

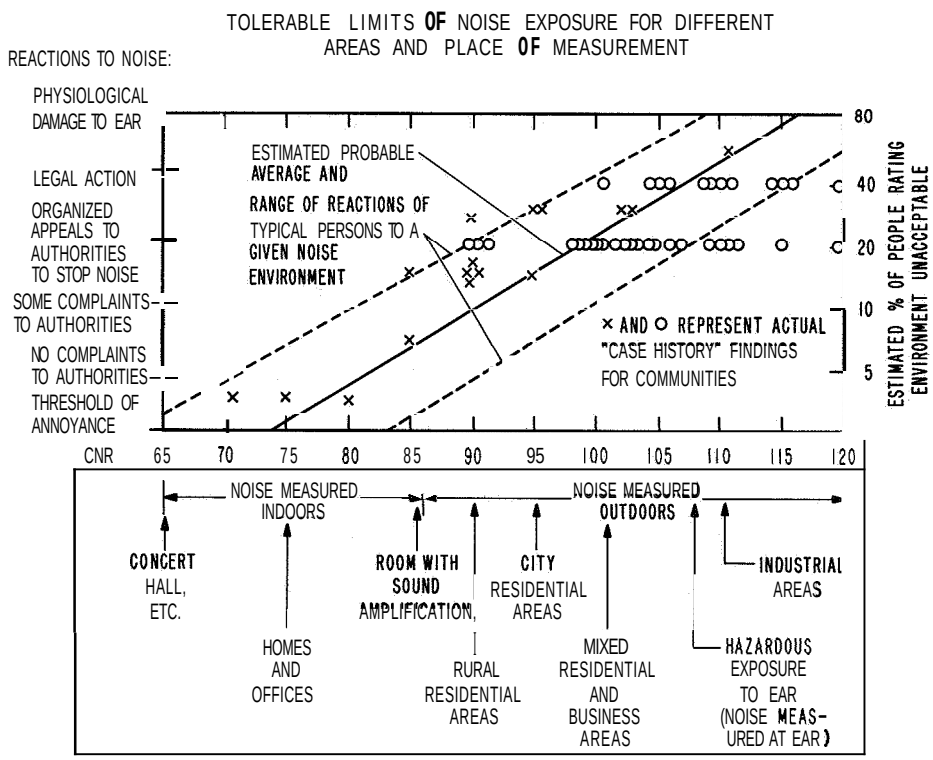

Figure 6

35. STUDIES RELATING THE INDIVIDUAL CHARACTERISTICS OF PEOPLE WITH THEIR RESPONSES TO NOISE

By Richard G. Pearson and Franklin D. Hart

North Carolina State University

SUMMARY

One hundred sixty-six male and female adult subjects varying in age, occupation, educational level, race, and area of residence were exposed to and rated the annoyance of aviation and industrial noise stimuli under two "psychologically different" indoor room environments. This followed assessment of personality and of attitudes toward community, transportation, and noise. Mean annoyance ratings of the subjects exposed to several acoustic stimuli varied considerably despite the fact that the stimuli levels in the test room were held constant at 82 dB (sound pressure). Ratings did not vary with psychological environment but did vary extensively among subjects. Factor analysis of the personality-attitude data resulted in identification of several useful factors for multiple regression prediction of annoyance – for example, noise sensitivity, imperturbable personality, antiaviation and isolationist attitudes, and anxiety.

INTRODUCTION

The noise problem today is recognized to be a complex, multidimensional one. Whether unwanted sound is disturbing to man's composure and activity appears to be a function of a unique, and often unaccountable, subjective reaction. This reaction is unique because it resides within a particular person whose personality, attitudes, and experiences are unlike anyone else's, and it is often unaccountable because for many noise situations scientists find difficulty in isolating and relating the multiplicity of factors which seem to be involved.

Knowledge about many of the relevant factors, both physical and social-psychological, is being enlarged. Yet there does seem to be a lack of knowledge of how many of these factors interact and ultimately relate to the annoyance response. A clearer understanding of the interaction between physical and psychological variables in the noise situation, it seems, would permit prediction, and thus eventual mitigation, of annoyance. The laboratory study described in this paper is a step in this direction. The work represents progress on a program of research (under NASA Grant NGR34-002-055) that involves consideration of the interaction among three variables: noise, the environment of exposure, and the people exposed.

METHOD

Test Facility

An experimental living room test facility was designed which would permit individual exposure to noise stimuli under controlled laboratory conditions. The facility was within a large laboratory and was of typical 2-inch by 4-inch stud and dry wall construction. The exterior and floor were made of 1/2-inch-thick plywood. Contiguous with the living room was the experimenter's control room as shown in the floor plan (fig. 1). A one-way vision mirror was installed for observation by the experimenter of subject activity. Also indicated are the locations of a microphone, used to monitor sound pressure level, and speakers. A couch was positioned in front of and facing the fireplace. Plush chairs, tables, and lamps were positioned around the room. Other furnishings included bric-a-brac, wall accessories, and drapes. The floor was covered wall-to-wall with heavy, commercial-grade sponge-rubber pad and high-density, loop-pile carpet.

In this study testing was conducted under two conditions: (a) the somewhat plush environment just described, hereafter called "Soft," and (b) an austere room with all furnishings, drapes, and carpet removed and hardwood classroom chairs substituted, hereafter called "Hard."

Sound Capability

For sound storage and playback a 1/4-inch, $7\frac{1}{2}$-in./sec, AM magnetic tape system was used. The stereo tape recorder used was chosen for its low background noise and good frequency response in the audio range. Recorder output was sufficient to drive a pair of power amplifiers to their full (50 watt) output rating. Each amplifier served identical speaker systems consisting of a 30-inch low-frequency speaker, a 12-inch midrange speaker and a 3-inch by 9-inch exponential horn. System output was found to be relatively flat (±2 dB) in its working range of 10 Hz to 20 kHz. Sound measurements in the test room were made with a microphone amplifier and 1/2-inch capacitive microphone.

Experimental Materials

For purposes of this experiment a decision was made to work with stimulus sounds (or noises) that were of acknowledged industrial interest and also that were qualitatively different – that is, represented different frequency spectra. Several noise stimuli were recorded, and the following six stimuli were selected as meeting these criteria:

A. Jet airplane flyover

B. Burnishing machine in a factory

C. Tractor-trailer truck changing gears while climbing a hill

D. Helicopter flyover

E. Air (pneumatic chipping) hammer

F. Propeller airplane flyover

Additional preliminary studies had indicated that testing at approximately 82 dB would provide an optimal spread of annoyance response; that is, if testing were conducted at a higher level, say 90 dB, virtually all subjects would find the stimuli so annoying that psychological factors would cease to be a part of the picture. In making a master tape, then, the input level for each sound was adjusted to give a level of 82 dB in the test room.

Other studies in the laboratory led to the development and refinement of an Annoyance Rating Scale (fig. 2). Subjects were allowed to indicate their response anywhere along the continuum (they could check a point between adjectives); therefore, 25 steps were determined to cover effectively the range of responses observed. Meanwhile steps had been taken toward developing an attitude survey, and when it seemed feasible to begin the main effort, attention was then given to the recruitment of subjects.

Subjects

Contact was made by phone and in person with over 30 industries, government offices, and churches in the Raleigh, North Carolina, area to solicit their help in bringing the project to the attention of employees, friends, and others. Initial screening was accomplished over the telephone when a volunteer called. Conditions of the study were described, and subjects were told they would receive $18.00 for participation. No mention was made of the use of noise. Selection of more than one person from a household, drifters, and unemployed persons was avoided. A deliberate attempt was made, as the volunteer list grew, to direct solicitation efforts in the direction of a broad, heterogeneous sample. Complete experimental data were ultimately obtained on 166 subjects who represented 57 different occupations and 47 employers. Distribution of subjects according to age, area of residence, sex, race, education, and income is given in table 1.

Procedure

Test sessions were conducted both afternoons and evenings. Upon reporting, each subject was tested for hearing deficit. Four volunteers were disqualified at this stage on the basis of serious hearing loss. The number in each group varied from 9 to 20. When all subjects had received the audiometric check, the experimenter described the procedures that would be followed that day, emphasized the importance of honest response, and confirmed volunteer status. Psychometric assessment followed, required about 2 hours' time, and involved both a personality test and an attitude survey.

The personality test employed was the Cattell 16 Personality Factor Test (generally called 16 P-F Test) in forms A and B. The test describes those attitudes or characteristics typically noted among individuals. For example, some of the 16 factors are described by such words as the following: reserved, emotionally stable, aggressive, enthusiastic, conscientious, dependent, adaptable, imaginative, shrewd, analytical, and tense. After completing the 16 P-F Test, subjects were given a "Community Social Survey" which included general biographical questions about occupation, education, income, and residence and sampled feelings toward Raleigh, the county area, and certain aviation subjects. The first question to mention the topic of noise was number 19 at the bottom of the second page. Later questions dealt more specifically with history of noise exposure, noise sources, complaints, and feelings regarding degree of sensitivity to noise. Lastly, the survey required subjects to indicate the strength of their agreement or disagreement with 10 statements representing attitudes toward aviation, noise sources, and local government policies in the areas of commerce and taxation.

The final phase of testing on the first day involved an orientation exposure to the noise stimuli in the experimental living room. Here groups were constituted of from 6 to 10 subjects and use of the Annoyance Rating Scale was described. Each of the six noise stimuli described previously was presented four times following a random schedule. Subjects were encouraged to relax and believe that they were spending a casual evening in their living room at home. Each stimulus was presented for 15 seconds after which the subjects were asked to make their rating with care and then sit back and relax during a 45-second interval between sounds. It should be emphasized that this test session was designed to acquaint subjects with procedures in the living room and give them practice in the use of the rating scale. The data to be used to compare the effects of the Soft and Hard room conditions were collected on the second and third test days. Upon returning for these sessions in the living room, subjects made six ratings of each of the six noise stimuli, following the same random schedule each day, but of course under different room conditions. A photograph of subjects being tested in the Soft room is shown as figure 3. An important point to note here is that room acoustic characteristics were taken into account in presenting the noise stimuli. A microphone in the room permitted both room conditions to be equated at the same peak sound pressure level, 82 dB. A further control involved testing half the subjects first in the Soft condition and then in the Hard condition; the other half, in the reverse order.

DISCUSSION OF RESULTS

The first approach in data analysis involved a statistical evaluation (analysis of variance) of the annoyance ratings as made under the two room and six noise conditions.

This evaluation revealed statistically significant differences among average (mean) ratings for the different noise stimuli. The spectra for the noise stimuli with the corresponding mean rating-scale values are shown in figure 4. The highest rating, 19.2, was associated with stimulus E, the pneumatic chipping hammer, characterized by the intermittent burst of raucous, predominantly high-frequency noise. This was significantly more annoying (as determined by the Duncan Multiple Range Test) than stimuli A, the jet airplane flyover, and D, the helicopter flyover. Stimuli C and F, the truck and propeller airplane flyover, tied for the lowest ratings; these were significantly less annoying than stimulus B, the factory noise. Bearing in mind that all sounds were equated for peak sound pressure level, a considerable range of mean annoyance ratings made with the 25-point scale is observed. In terms of scale wording this represents a range of from "very annoying" to "somewhat annoying." This finding was, of course, not unexpected and reemphasizes the often-stated need to take spectral characteristics of the noise source into account in attempts to understand annoyance.

The mean annoyance ratings obtained under the Hard and Soft room conditions, surprisingly, were identical (11.76). A higher rating had been expected in the Hard room, the postulate being that the austere environment would invoke some psychological stress that would summate with noise and lead to a greater degree of annoyance. Although some subjects did respond in this direction, still others responded in a reverse manner. In any event the magnitude of differences overall was small, so that the room condition as such was of little importance in the ratings. What may be of more importance in this context is the task which the subject is performing in a given room environment – for example, the disruption of conversation or television viewing; further study is proposed in this direction. The ratings among the subjects showed a large range – from a low of 1.65 to a high of 22.20 on the 25-point scale. This range of variation indicated that some subjects found the noises extremely annoying, whereas others found them hardly objectionable.

Recognizing then that the major factor determining the varied responses obtained with the ratings was not a physical one but a human one, an analysis was undertaken which focused on the behavioral psychometric data. This analysis involved the technique of factor analysis which is often used in attempts to isolate the major factors that account for relationships among large amounts of descriptive data. The data input included 53 measures obtained in the personality testing and social survey. The factor analysis output listed 18 factors (table 2) which can be taken to describe the subject sample. In this technique, each factor is defined by several items which are related by some common theme or thread – an example is given in table 3 – and it is up to the investigator to give this theme a name. This can be a tedious, arbitrary process and the names chosen are open to debate. With regard to the question mark next to Factor 9 (table 2) it should be

noted that while the major survey item involved here was concerned with aviation employment, it is difficult to argue for a "Proaviation" factor since only 6 of the 166 subjects were so employed.

Implications of the factors as they relate to the annoyance ratings should be noted.[1] It should be interjected that many of the factors are weighted heavily in terms of attitudes and not personality traits. This is important to note since personality traits are relatively permanent characteristics of an individual, whereas attitudes can be dealt with and changed! Factor 1, Noise Sensitivity, is a rather general factor defined by individual attitudes and feelings toward noise – for example, concern about present sources of noise disturbance and about noise in the years ahead. Factor 2, Worldly Exposure, involves income, education, and experience with noise sources and air travel. At one extreme this could, for example, characterize a person who has never flown. It would be interesting to determine at some future date the effect on such a person of exposure to urban commerce, air travel, and noise sources. Factor 5, Antiaviation, was concerned with attitudes toward community air service, use of taxes to support aviation, condemnation of private property for airport expansion, and the possibility of an air crash threatening life and property. One extreme of attitudes in this factor is characterized by opposition to everything related to aviation. Factor 6 involved attitudes toward growth and commerce, generally; therefore it was called an Isolationist factor.

Factor 10, Phobic, is described by statements measuring generalized anxiety toward flying and fear regarding the sound of airplanes overhead. Factor 14, Exposure Experience, is to be distinguished from Factor 2 in that it is concerned with noise exposure at work or home and its effect on one's health. Again, at one extreme this factor would characterize a person who seeks a low-noise work environment and is concerned about noise as a stress affecting his health. Factor 17, Neighborhood Attitude, is described in terms of feelings toward one's neighborhood and its degree of noisiness; and, finally, Factor 18, Complainer, identifies tendencies toward complaining or protesting about noise.

A brief summary of the analysis which focused on the behavioral psychometric data is as follows:

(a) A general noise sensitivity factor was identified as a major one in prediction of an individual's annoyance rating; this implies a need to be concerned with noise as a general problem and not as one specific to aviation.

---

[1] A multiple regression prediction, based on the 18 factors, was made for each of the 12 experimental conditions, that is, 6 rooms by 2 environments.

(b) On the other hand, some of the subjects were identified as having antiaviation attitudes and as reacting more negatively to noise; both industry and government will have to be concerned with such attitudes.

(c) Some fear, anxiety, and health complaints were identified as relating to the annoyance ratings; this may indicate a need for informational campaigns on the part of those who defend the aviation safety record.

Although it was encouraging to find in the sample a few "Imperturbables," one might wonder if this group will decline. One could postulate that noise in a peacetime, affluent, suburban culture would be less welcome.

CONCLUDING REMARKS

Three points concerning human reaction to noise are emphasized: First, the annoyance response is an individual characteristic since it resides within a particular person whose personality, attitudes, and experiences are unlike anyone else's. Second, the response is a complex product of these individual characteristics (including history of exposure to noise) and the noise stimulus characteristics. Third, the response is predictable if the appropriate factors are assessed. The factors identified in this study should be important in this regard, and it is hoped that the approach taken by the authors to the noise problem will be used in future noise alleviation programs.

TABLE 1.- DISTRIBUTION OF SUBJECTS ACCORDING TO CHARACTERISTICS

Age	Number	Residence	Number
20 to 29	68	City proper	67
30 to 39	53	Suburban	86
40 to 49	39	Rural	13
50 to 59	6		
Sex	**Number**	**Race**	**Number**
Male	84	Caucasian	152
Female	82	Negro	14
Education	**Number**	**Family income**	**Number**
Grade school	0	Below $5000	25
Some high school	2	$5000 to $7000	24
High school graduate	37	$7000 to $9000	31
Some college	72	$9000 to $12,000	43
College graduate	48	Over $12,000	43
Graduate degree	7		

TABLE 2.- RESULTS OF FACTOR ANALYSIS

Factor	Name
1	Noise Sensitivity
2	Worldly Exposure
3	Self-Sufficiency
4	High Anxiety
5	Antiaviation
6	Isolationist
7	Pragmatist
8	Passivity
9	Aviation Employment (?)
10	Phobic
11	Residential Area
12	Idealist
13	Conservative
14	Exposure Experience
15	Interference With Routine
16	Imperturbable
17	Neighborhood Attitude
18	Complainer

TABLE 3.- EXAMPLE OF DEFINITION OF ONE FACTOR IN FACTOR ANALYSIS

[Factor 16 (Imperturbable)]

Attitude:

Finds little to criticize about community

Personality traits:

Humble, mild, accommodating
Prudent, serious, sober
Trusting, adaptable
Conscientious, persevering

FLOOR PLAN OF TEST FACILITY

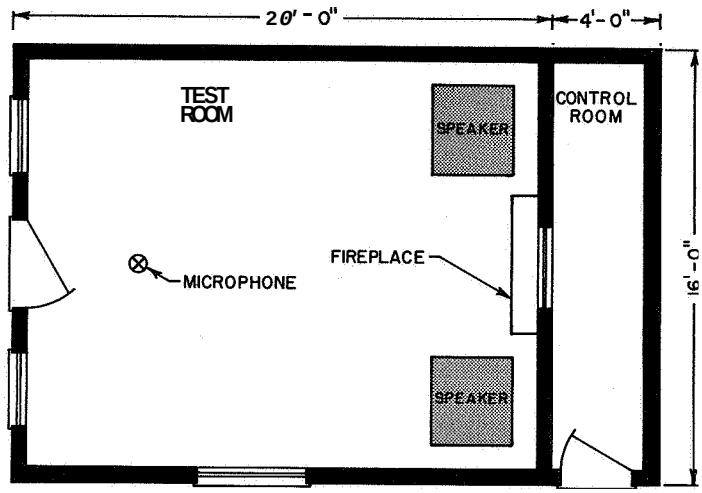

Figure 1

COPY OF ANNOYANCE RATING SCALE

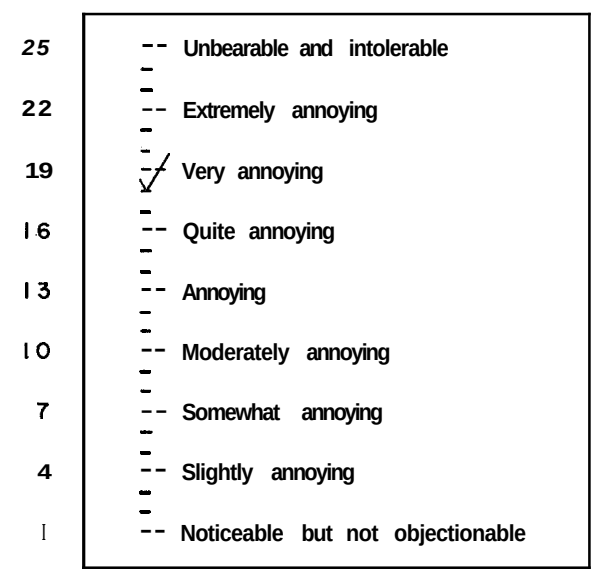

Figure 2

SUBJECTS IN TEST ROOM

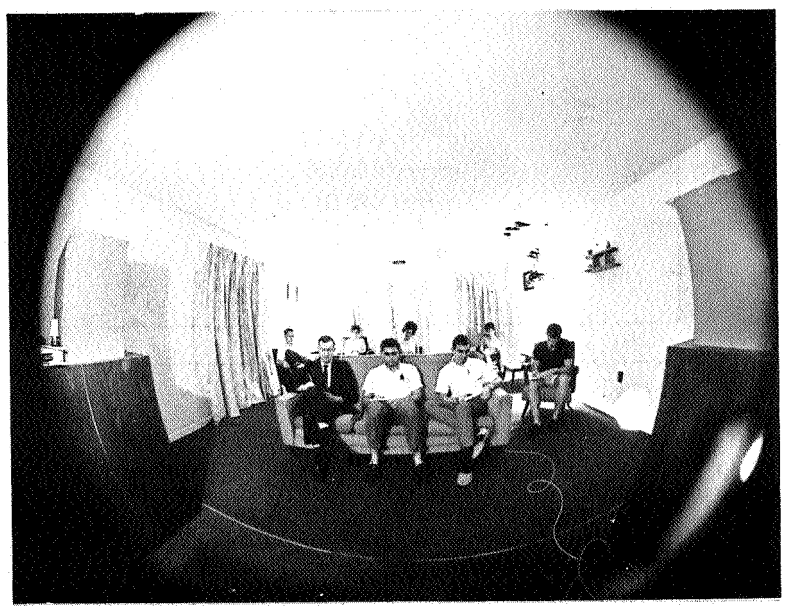

L-68-8584

Figure 3

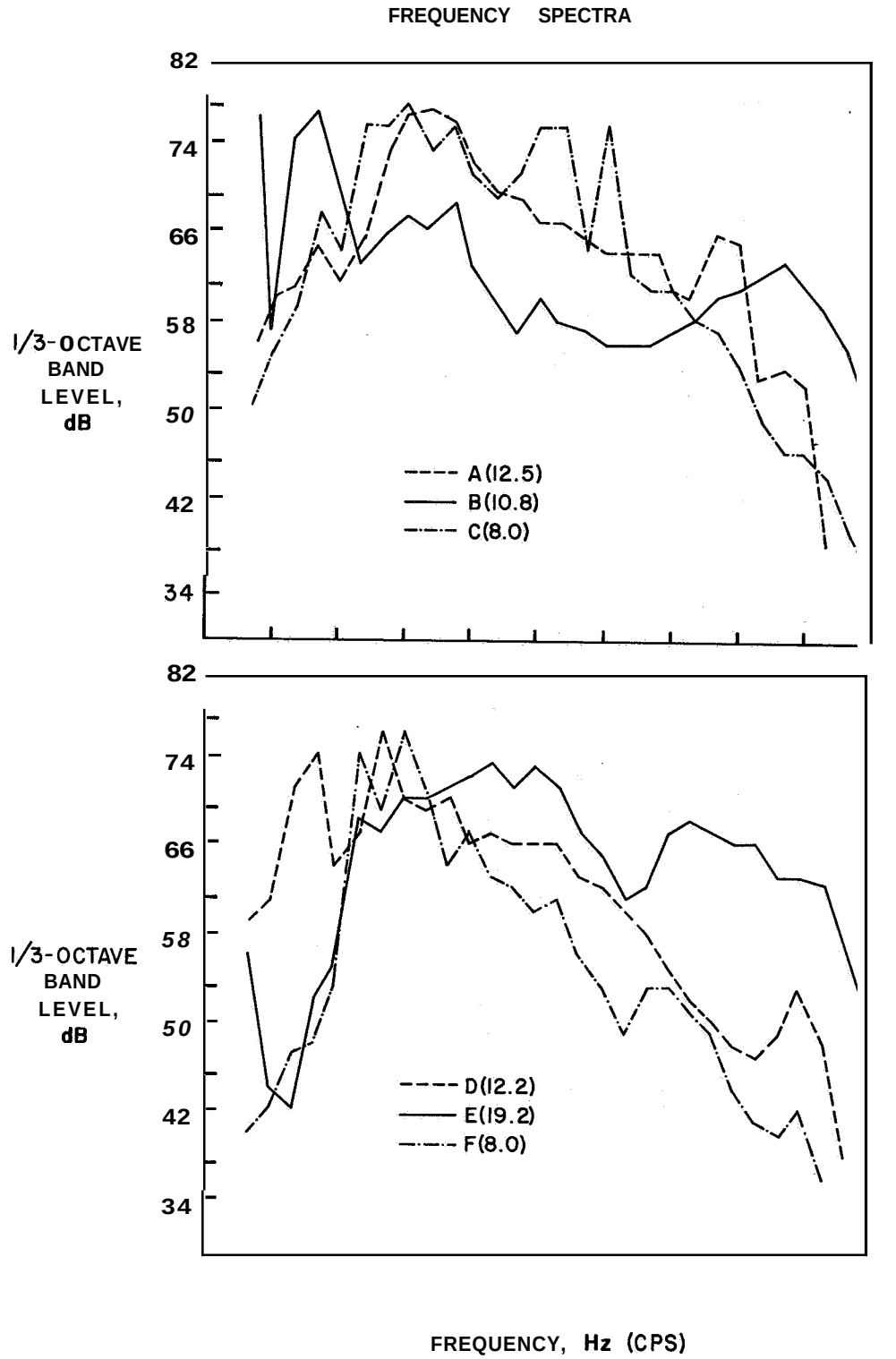
FREQUENCY SPECTRA
82
74
66
58
50
42
34
1/3-OCTAVE BAND LEVEL, dB
A(12.5)
B(10.8)
C(8.0)
82
74
66
58
50
42
34
1/3-OCTAVE BAND LEVEL, dB
D(12.2)
E(19.2)
F(8.0)
FREQUENCY, Hz (CPS)

Figure 4

36. ASSESSMENT OF THE VALIDITY OF PURE TONE CORRECTIONS TO PERCEIVED NOISE LEVEL

By Karl S. Pearsons

Bolt Beranek and Newman, Inc.

SUMMARY

Judgment tests were conducted to determine the validity of pure tone corrections to perceived noise level. Stimuli for these tests included broadband noise with single tones, modulated tones, or multiple tones. These stimuli were presented at a constant duration of 4 seconds. Other stimuli included single tones in broadband noise for durations ranging from 4 to 32 seconds. The results of the judgment tests indicate that the perceived noise level with tone corrections adequately predicts the noisiness of these stimuli. In addition, for those stimuli varying in duration, a duration correction is necessary.

INTRODUCTION

The presence of pure tones or discrete frequencies in aircraft engine noise appears to be an annoyance for the listener. The magnitude of the annoyance, insofar as it affects the assessment of aircraft flyover noise, has been measured by subjective testing.

Some early subjective testing produced pure tone corrections for the perceived noise level calculation procedure to account for the additional noisiness of these discrete frequencies. The initial part of this paper describes these tone corrections. The remainder of the paper deals with the validation of these tone corrections by using various types of pure tone and broadband noise stimuli.

The stimuli used in these validation tests are listed in figure 1. These stimuli were selected to check the adequacy of proposed tone correction methods. As indicated in the figure, they include single tones in broadband noise, modulated tones in broadband noise, and multiple tones in broadband noise. All these stimuli were presented at a constant duration of 4 seconds. Other tests included single tones in broadband noise for durations approximating those of present-day aircraft flyovers (4 to 32 seconds).

Before further details of some of these subjective tests are discussed, the method usually used to describe the tones as they might appear in the presence of broadband noise is noted. Figure 2 shows two representations of some broadband noise along with a single tone at 1000 Hz. The magnitude of the tone is indicated by how much it exceeds the measurement of noise in a 1/3-octave band as shown in the upper curve. This measure is called the tone-to-noise ratio (T/N) as determined in a 1/3-octave band. In the example

shown it is 10 dB. The lower curve is a different representation of the same stimuli using a vertical line for the tone.

When a tone is added to noise and the perceived noise level is calculated in a manner described by Karl D. Kryter (ref. 1), the noisiness of the combination is underestimated by the perceived noise level calculation. In other words, some sort of a correction is necessary to account for the presence of the pure tone.

TONE CORRECTION

In the development of the pure tone corrections and in the subsequent judgment tests, groups of college students were employed as subjects. In general, the tests were conducted in an anechoic chamber with one to four subjects. All subjects were screened audiometrically prior to the judgment tests. For these tests the subjects were presented with 4-second octave bands of noise both with and without pure tones. By using the method of paired comparisons, the subjects were asked to judge which of two sounds was the more annoying or objectionable. The levels at which 50 percent of the subjects stated that one of the pairs was noisier or more objectionable than the other were selected as the levels of equal noisiness. For these judged levels of equality, the corrections were determined by noting the amount that the octave band of noise without the tone needed to be increased to be equal to the octave band of noise with the tone. These judgments were determined for various frequencies and tone-to-noise ratios and resulted in the set of corrections depicted in figure 3. Notice that as the tone-to-noise ratio is increased, the correction increases; likewise, as the frequency is increased to about 4000 Hz, the tone correction also increases. For a given frequency and tone-to-noise ratio, the amount of correction necessary is determined from the graph. This correction is added to the 1/3-octave band level prior to calculation of perceived noise level. In this way, if more than one tone is present, more than one correction can be added.

VALIDATION TESTS

Single Tones

As mentioned before, the development of these corrections utilized octave bands of noise. Since most aircraft flyovers produce broadband noise, it was important to determine whether the corrections did indeed work for tones in broadband noise. Therefore, additional judgment tests using the conditions and techniques described were conducted. Figure 4 shows what happens in a typical judgment test comparing broadband noise with the same broadband noise with a tone inserted. The broadband noise alone is called the standard and the broadband noise with the tone, the comparison. After a typical judgment where the subjects have stated that the two are approximately equal in noisiness, perceived

noise levels (PNL) are calculated for both the standard and the comparison. Note that the perceived noise level of 95 PNdB for the standard is quite a bit higher than the 85 PNdB calculated for the comparison. The two measures may be compared by noting the difference or the level of comparison relative to the level of the standard. In this first case, for perceived noise level alone, the difference is -10 PNdB; in other words, the comparison measured 10 PNdB below the level of the standard at the judged equal noisiness point. If the measure being employed is a good one, the difference is close to zero. Then the results can be said to be in good agreement with the judgment data.

When the pure tone correction is added, the perceived noise level for the standard does not change since there is no pure tone. However, the pure tone correction for the comparison, in this case, has the net effect of adding about 10 PNdB to the perceived noise level; thus, the perceived noise level (PNL) of the comparison is made equal to that of the standard.

A summary of results in terms of comparison minus standard level is shown in figure 5. Each point represents the results for 20 subjects. A group of data taken at various tone frequencies for perceived noise level alone is shown as a measure. Compared with this measure are the results using perceived noise level with the tone correction as a measure. By looking at the median lines, it can be seen that the perceived noise level with the tone correction agrees much more closely with the judgment results (that is, the comparison minus the standard is nearer zero) than do the results with perceived noise level without the pure tone corrections. The various points on the figure indicate different spectrum shapes of broadband noise that were used in the test. The spread of the points provides an indication of the repeatability that the group had when both the same and different shapes of broadband noise are used. Standard deviations for the data at various frequencies vary from 1.5 to 2.5 PNdB. It may be concluded then that for single steady tones in broadband noise, the pure tone correction seems to work well.

Modulated Tones

However, in aircraft flyover noise the tones are not as steady and also there may be more than one of them. First look at the problems of nonsteady-state tones. For the sample shown in figure 4 of a single tone in broadband noise, the tone is amplitude modulated. This procedure was followed for a series of tests to investigate the effects of amplitude modulating a tone in broadband noise. Judgment tests were conducted in which the modulated tones in broadband noise were compared with the broadband noise alone.

Figure 6 shows the results of the tests in a manner similar to that shown in figure 5. The level of the comparison is again plotted against the level of the standard. The rate of modulation or the envelope of the sketch in the upper portion of the figure is shown on the abscissa, that is, no modulation, 5 Hz, etc. The various coded points indicated the

frequency (500 or 2000 Hz) of the tone that was modulated. Again, the results are shown for perceived noise level without the pure tone corrections and also the results for pure tone with the tone corrections.

In most cases, the results with the tone corrections are in much closer agreement with the judgment data than those results without the tone corrections. The one case where the results are not in particularly good agreement is for the low-rate amplitude-modulation case. This difference may be due to the large annoying beats associated with signals of this type.

In figure 7 are the results for the frequency-modulated tones. In this case, the tone is modulated in frequency at various rates. Again, the perceived noise levels with tone corrections are in closer agreement with the judgment data than those results for perceived noise level without tone corrections.

Multiple Tones

Investigations have also been conducted for the case where more than one tone is present in the stimulus. Both harmonically and inharmonically related tones were employed. The stimuli for these tests consisted of either two- or five-tone complexes in broadband noise. Samples of some of the stimuli that were used are shown in figure 8. The two-tone complexes are shown at the top of the figure and the five-tone complexes are shown at the bottom. The frequency and range of the two-tone and five-tone stimuli are given in the following table:

Frequency of lowest tone, Hz (cps)	Range, octaves
250	1/10, 1/3, 1, 4/3, 2
500	
1000	
2000	
4000	

The range refers to the difference in frequency between the highest and lowest component in the tone complex. For the samples shown, the lowest tone was always 1000 Hz. As shown in the table, frequencies of 250, 500, 2000, and 4000 Hz were also tested. Both the harmonically related tones, that is, the 1- and 2-octave ranges and the inharmonically related, the 1/10-, 1/3-, and 4/3-octave ranges, were used to determine whether any difference existed between the two cases. Actually, there was very little difference in the judgment results for the various ranges, at least from the 1/10-octave range to the 2-octave range. Therefore, the results of the various ranges were averaged and the

averages are plotted in figure 9 according to the frequency of the lowest pure tone components. Again, results are shown for perceived noise level without tone correction for both the two-tone and five-tone complexes. Also shown are the perceived noise levels with tone corrections. Again, as in previous figures the results with the tone corrections are in much closer agreement with the judgment data than are those without the tone corrections. Also, as indicated in figure 9, there does not appear to be an appreciable difference between the two-tone or the five-tone complexes.

A 16-tone complex was also tested, as shown in figures 9 and 10. This sample is somewhat similar to the so-called "buzz tones" present in high bypass ratio turbofan engines. The results of this test are shown on the right-hand side of figure 9. Again, the perceived noise levels with tone corrections are in much closer agreement with the judgment results; that is, they lie closer to the zero line than do the perceived noise levels alone. Note that for the perceived noise level alone in this case, the estimates were as much as 10 dB too low, whereas with the tone correction the estimate was only about 2 dB high.

The tests described up to this point have all been conducted at a constant duration; however, some aircraft flyovers are much longer in duration than others, and certainly are longer than the 4-second samples employed in these tests.

Since there was a possibility that the duration effect might interact with the pure tone effect, some additional tests have been conducted to see whether these tone and duration effects can be accounted for by present duration and tone correction techniques. Before the details of the tests are presented, the ideas behind the present duration correction will be discussed. Figure 11 shows two simulations of aircraft flyovers plotted with sound pressure level as a function of time. The time history on the right is twice as long as the time pattern on the left if measurements are made at the 10-dB-down points. It has been shown from subjective tests that in order for the two signals to be judged equally noisy, the level of the longer duration sound must be decreased by 3 dB. This relationship or tradeoff seems to hold up fairly well over the range from 4 seconds to 64 seconds as measured at the points 10 dB down from the maximum level.

In the tests that were used to generate this kind of relationship, both the standard and the comparison were of similar spectral shape. The only thing that was varied was the duration of the signal itself. To learn more of any possible interaction between tone and duration parameters, stimuli were employed such as those shown in figure 12. As shown in this figure, the standard was a noise alone for a given duration (12 seconds) and the comparison was a combination of tone and noise of a different duration. The other parameter that was varied was a tone-to-noise ratio or the amount that the tone exceeded the noise in a 1/3-octave band. The results of these tests are shown in figure 13. Here are shown as a function of tone-to-noise ratio and duration the judgment data determined both for perceived noise level with and without tone and duration corrections. The

results for the perceived noise level alone are shown as open symbols connected by dashed lines on the figure, whereas the results for the perceived noise level with tone and duration corrections are shown as closed symbols bounded by a shaded area. Note that the shaded area is in much closer agreement with the zero line; that is, it agrees closer with the judgment results than the line connected points do. This condition is especially true for the longer durations where, without the corrections, errors of as much as 13 dB occur. Separate plots of the perceived noise level with just the duration correction and also with just the tone correction were also made but the combination of both tone and duration corrections provides the best agreement with the judgment results.

Other tests were also conducted by using stimuli with different time patterns. Both tone and noise were employed with the duration of the tone differing from the duration of the noise. Also, the time at which the tone peaked was different from the time that the noise reached its peak. Without going into the details of the results, it is sufficient to say that varying the duration of the tone provided little change in the judgment results compared with those results where the duration of the tone was comparable with the duration of the noise. Also, the time at which the tone peak occurred did not seem to affect greatly the judgment results. If tone and duration corrections are applied to PNL for all these cases, the agreement with the judgment data is better than that for PNL alone. It should be mentioned that the tone and duration corrections that have been described here are not unique. There are others available that may do as good a job. Some of these other techniques are discussed in reference 2.

CONCLUDING REMARKS

From the results of the investigations described in this paper, several conclusions can be drawn. The main conclusion is that the perceived noise level with a tone correction predicts the noisiness of broadband noise stimuli containing single, modulated, and multiple tones for the stimuli employed in the judgment tests. Also, for complex stimuli varying in both tone content and duration, a duration correction is also necessary for optimum prediction of noisiness. All the questions with regard to discrete frequency components in aircraft engine noise however have not been answered. An attempt has been made rather to provide a better understanding of the state of the art with regard to subjective testing of tones in noise. It should be mentioned that the tone and duration corrections that have been described here are not unique. There are others available that may do as good a job.

REFERENCES

1. Kryter, Karl **D.:** Prediction of Effects of Noise on Man. Conference on Progress of NASA Research Relating to Noise Alleviation of Large Subsonic Jet Aircraft, **NASA** SP-189, 1968. (Paper No. **34** herein.)

2. Kryter, Karl **D.;** Johnson, P. J.; and Young, J. R.: Judgment Tests of Aircraft Noise. Conference on Progress of NASA Research Relating to Noise Alleviation of Large Subsonic Jet Aircraft, NASA SP-189, 1968. (Paper No. **37** herein.)

TEST STIMULI

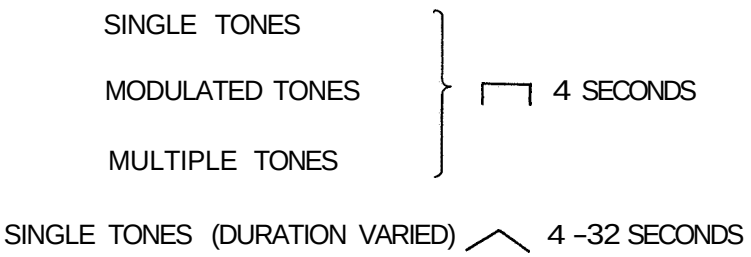

Figure 1

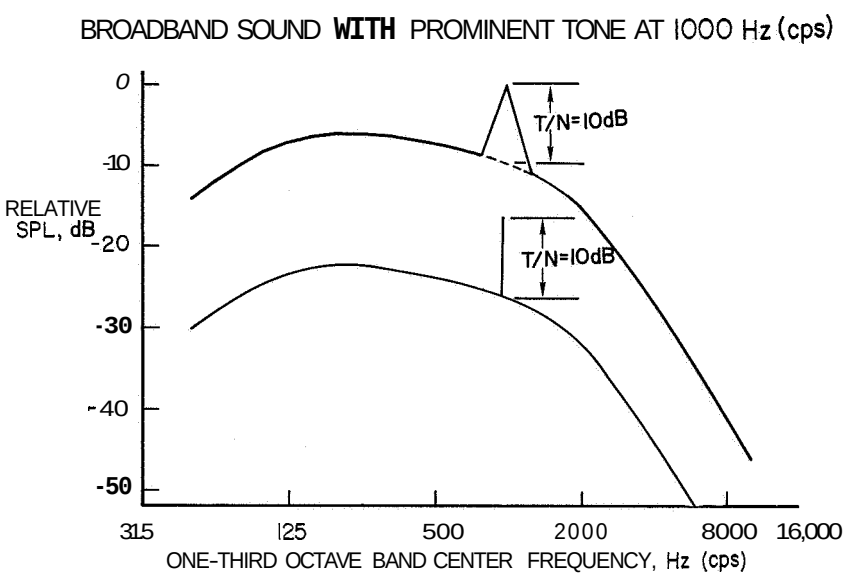

Figure 2

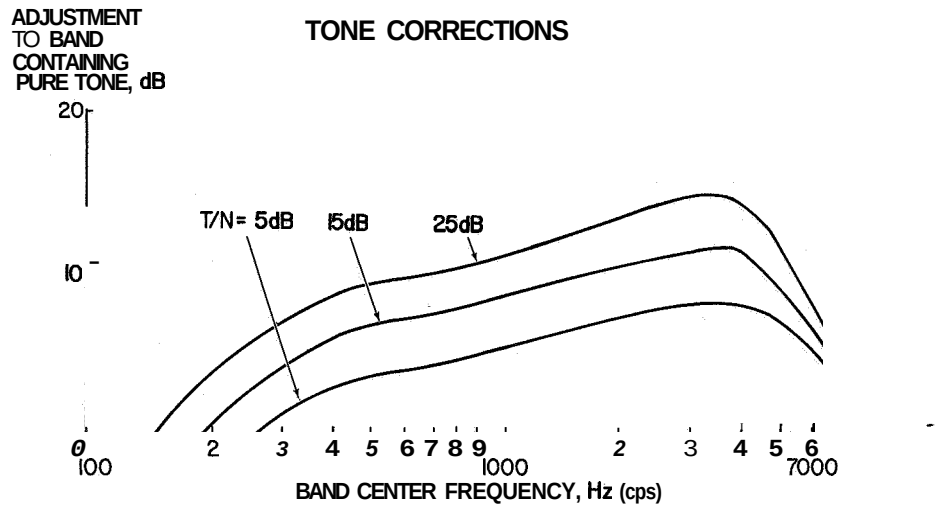

Figure 3

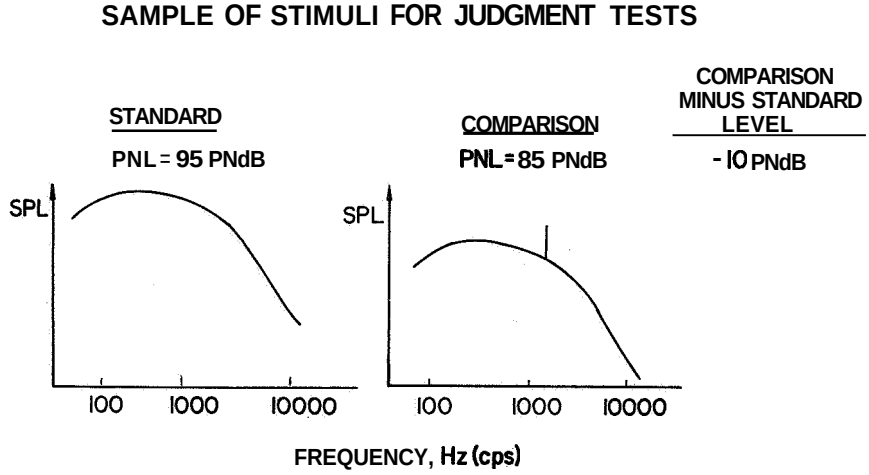

Figure 4

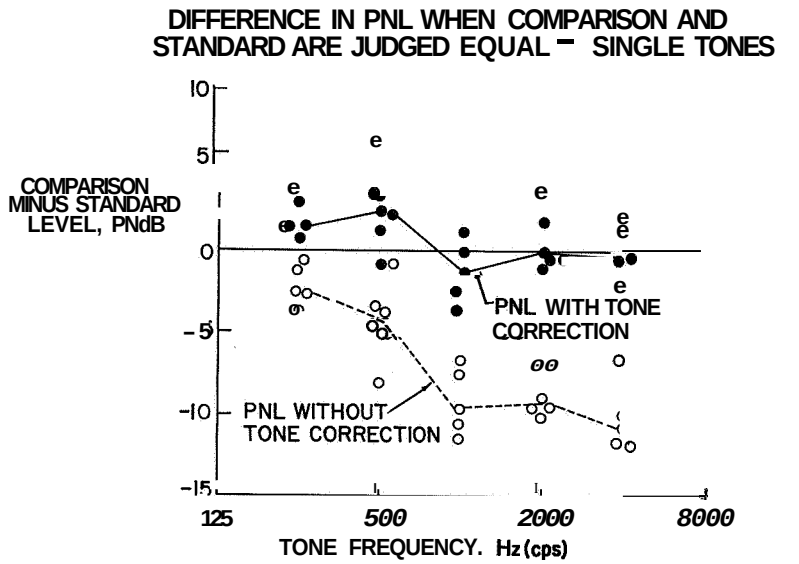

Figure 5

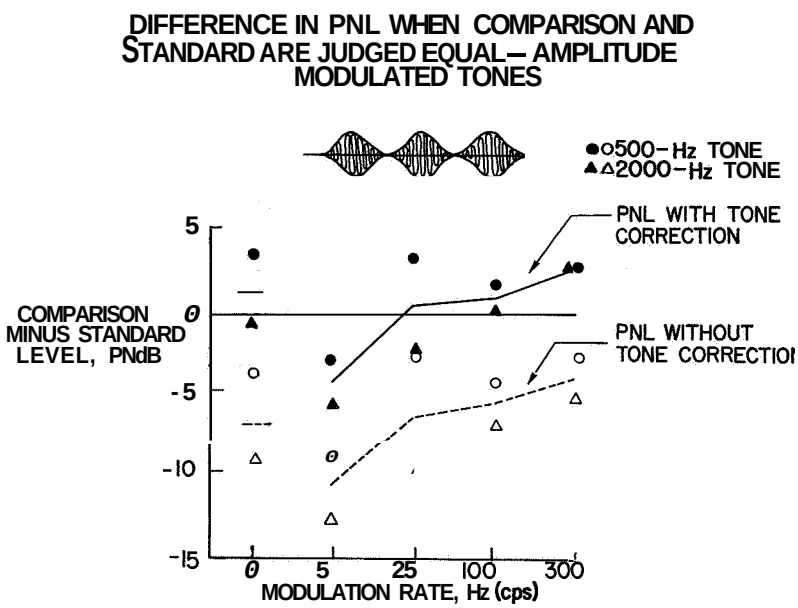

Figure 6

DIFFERENCE IN PNL WHEN COMPARISON AND STANDARD AREJUDGED EQUAL— FREQUENCY MODULATEDTONES

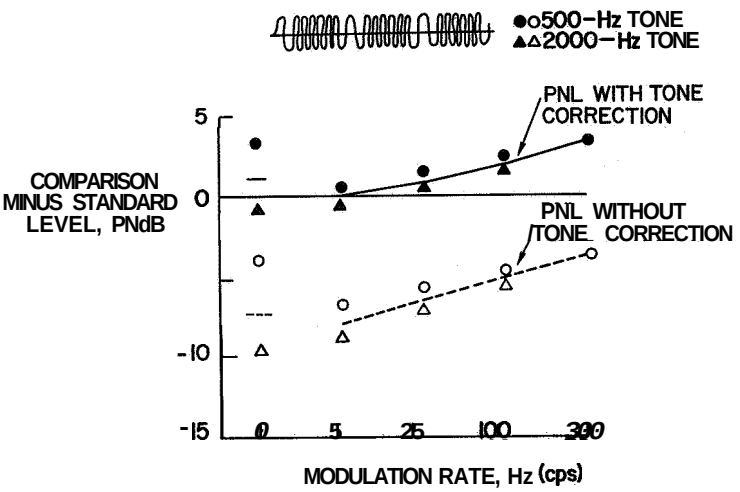

Figure 7

SAMPLE OF COMPARISON STIMULI USING 2—AND 5—TONE COMPLEXES

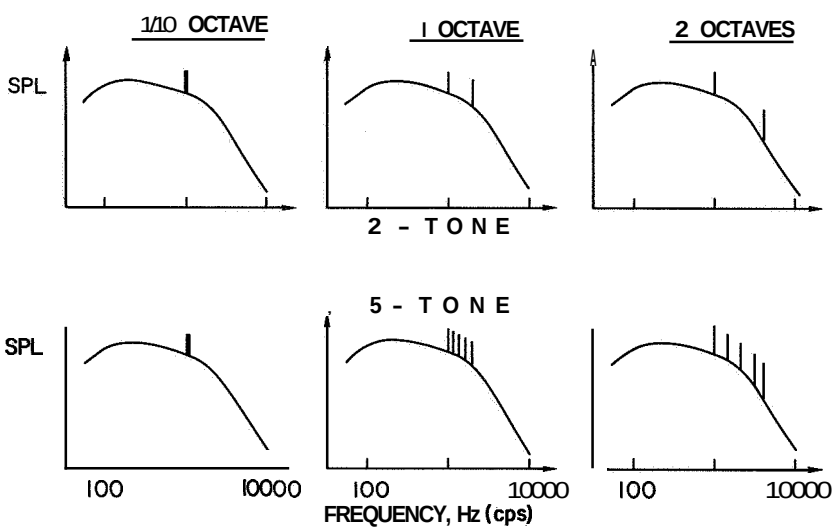

Figure 8

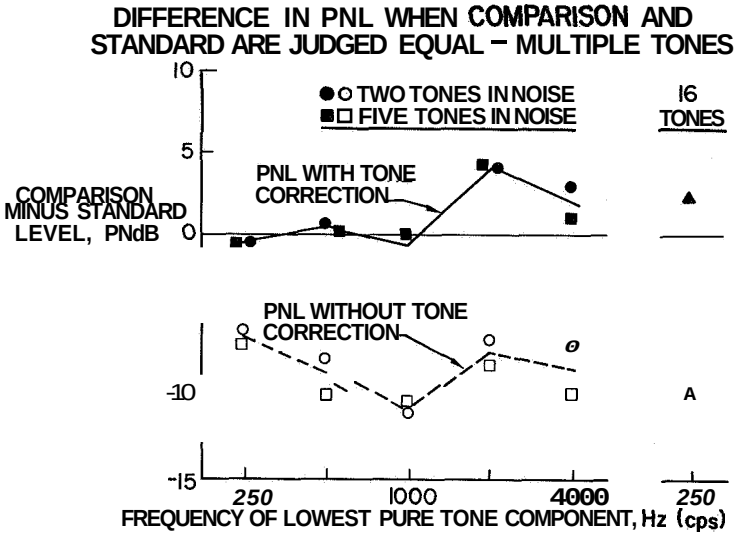

Figure 9

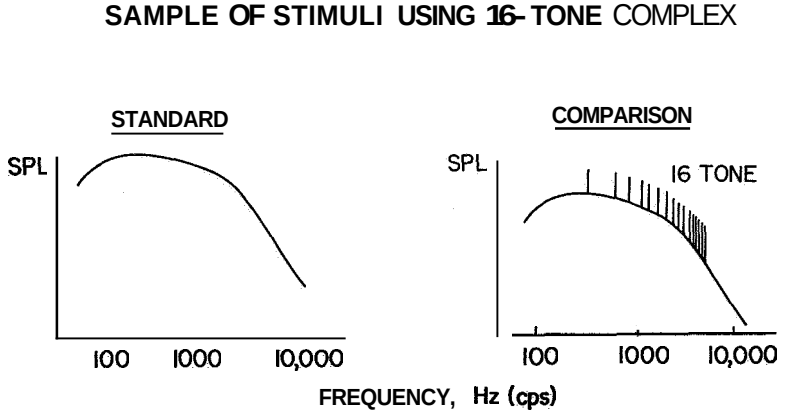

Figure 10

DURATION EFFECT

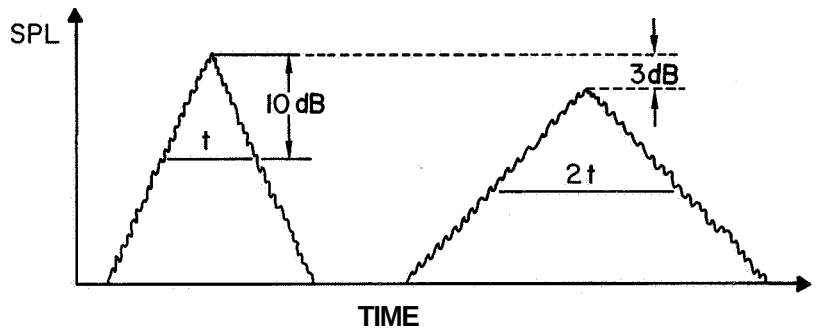

Figure 11

SAMPLE OF STIMULI FOR VARIABLE-DURATION TEST

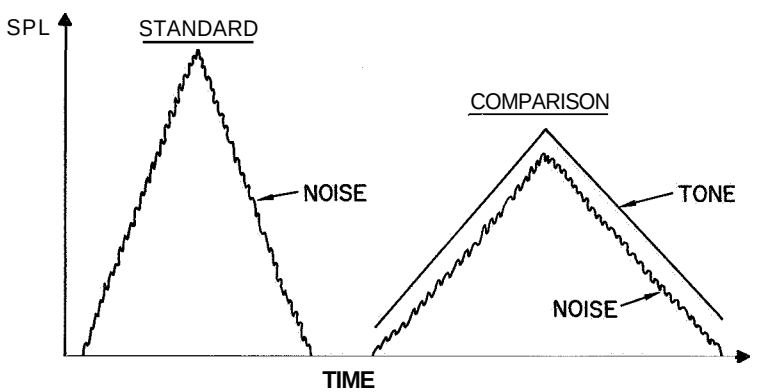

Figure 12

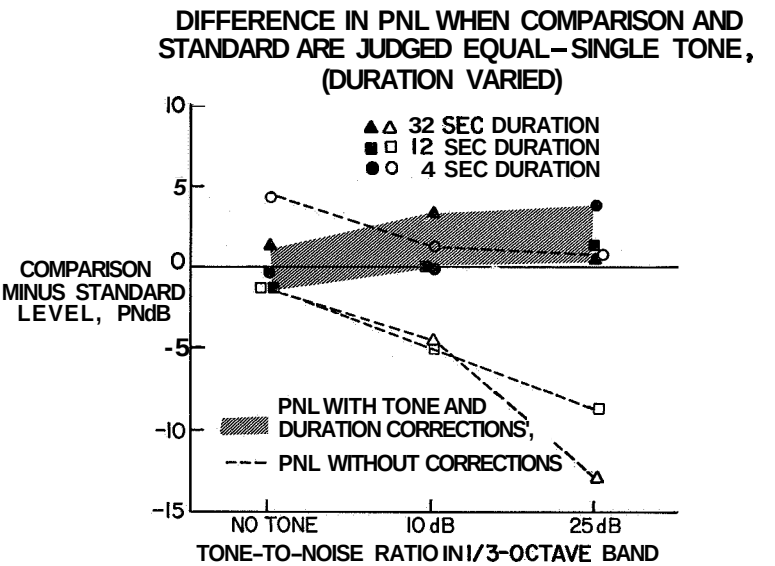
DIFFERENCE IN PNL WHEN COMPARISON AND STANDARD ARE JUDGED EQUAL–SINGLE TONE, (DURATION VARIED)
▲△ 32 SEC DURATION
■□ 12 SEC DURATION
●○ 4 SEC DURATION
COMPARISON MINUS STANDARD LEVEL, PNdB
10
5
0
-5
-10
-15
PNL WITH TONE AND DURATION CORRECTIONS,
PNL WITHOUT CORRECTIONS
NO TONE
10 dB
25 dB
TONE-TO-NOISE RATIO IN 1/3-OCTAVE BAND

Figure 13

37. JUDGMENT TESTS OF AIRCRAFT NOISE

By Karl D. Kryter, Paul J. Johnson,
and James R. Young

Stanford Research Institute

SUMMARY

Psychological tests were conducted to determine the ability of various physical units to predict the judged perceived noisiness of the sounds from a variety of aircraft operating under landing and take-off power. The best agreement between objective measures and subjective judgments of the noisiness or unacceptability of aircraft noise of all types is generally found by calculating the tone-corrected effective perceived noise level in EPNdB$_t$ from 1/3-octave band spectra taken every 1/2 second during the noise cycle. When low-frequency aircraft noise is compared with high-frequency aircraft noise, a systematic overestimation of the perceived noisiness of the lower frequency noise is obtained by the various PNdB units.

INTRODUCTION

Over the past 20 to 30 years, research has led to the development of a number of ways of measuring noise that purport to be correlated with the measurement or response of man's auditory system to noise. These methods run the gamut from simple peak sound-level meter readings to weightings of 1/3-octave band spectra taken every 1/2 second during the duration of a noise occurrence. Although the measurement procedures vary, the purpose and goal of making these measurements is to estimate or predict how unwanted, unacceptable, or noisy the sounds being measured are perceived to be by people.

Most of the psychological tests concerned with establishing the relationships between perceived noisiness and the physical aspects of aircraft noise have been conducted in the laboratory with recordings of the noise; relatively small groups of subjects and often a restricted variety of aircraft noises were used. The present tests were designed to permit as valid an examination as possible of the ability to predict from physical measurements the judged acceptability to people of a wide variety of actual aircraft noise when heard in or outside typical homes. In addition, a number of ancillary questions related to the generation and propagation of the noise and the reaction of house structures to the noise were to be investigated. These tests were recently conducted at the NASA Wallops Station.

The present report is concerned primarily with the relation between the psychological judgment of people outdoors and physical measurements made from recordings of the noise from microphones located outdoors. Measurements of house vibrations at Wallops

Station are reported in reference 1. Additional technical reports by the National Aeronautics and Space Administration and Stanford Research Institute on various aspects of the studies will be prepared later as further analyses of the data are completed.

PROCEDURE

A frame house, a brick-veneer house, and a large yard near one of the houses, all located in a residential area of Wallops Station, were chosen as the test sites. The subjects were adults, primarily housewives, selected from communities in the local area. Figure 1 is a photograph of some of the subjects as seated for the tests. The subjects were tested with an audiometer and all were found to have normal hearing (±15 dB from audiometric zero). The subjects were paid and given careful instructions prior to and during the tests as to the importance of the tests and the nature of the task they were to perform.

The fundamental task of the subjects was to mark on an answer sheet which of two aircraft sounds presented to them in a brief period of time they considered to be the least acceptable, assuming these noises were heard in or near their home 20 to 30 times per day. The subjects also rated each noise on a scale ranging from completely acceptable to completely unacceptable.

Because of the very large number of aircraft tested, it was not possible to pair, for the judgments, each aircraft noise with every other aircraft noise. Instead, two of the aircraft were chosen to provide a reference, or standard, noise, and this noise was paired with the noise from each of the other aircraft when operating under landing and take-off power. The reference, or standard, aircraft chosen were the turbojet 880 and the 1049G (Super Constellation), a propeller-driven aircraft with reciprocating engines (recip-prop).

The aircraft were flown so that about 5 minutes elapsed between pairs of noises, and usually 1 minute elapsed between each member of a pair. The altitude for the operational conditions for each aircraft was carefully monitored and controlled for all flights. An attempt was made to operate the reference aircraft at an altitude that would be reasonable for that aircraft at about 2 to 3 miles from an airport. Figure 2 is a schematic illustration of the flight paths followed by aircraft for the tests. Table I summarizes the aircraft tested and number of overflights made per aircraft.

Physical Measurements

Tape recordings made of the aircraft noises reaching the ground were played through 1/3-octave band filters. Each filter output was passed through an envelope detector, smoothed, and sampled every 1/2 second. These samples were digitized and stored on magnetic tape and were used for subsequent calculation of the following units:

(1) Max dB(A), dB(B), dB(C), dB(N)

(2) Max phons (Stevens), PNdB, $PNdB_{t_1}$, and $PNdB_{t_2}$

(3) Peak phons (Stevens), PNdB, $PNdB_{t_1}$, and $PNdB_{t_2}$

(4) E (effective) dB(A), dB(N), PNdB, $PNdB_{t_1}$, and $PNdB_{t_2}$

(5) EE (estimated effective) PNdB, $PNdB_{t_1}$, and $PNdB_{t_2}$

References 2 and 3 give a detailed description of these units. These units of noise measurement appear at the present time to be the best available units for the evaluation of the perceived noisiness of the sound from aircraft. An additional method is that of calculating loudness levels, in phons, by the 1/3-octave band method of Zwicker (ref. 4). It is planned to obtain max phons (Zwicker) for these aircraft noises for their inclusion in the final report of the tests conducted at Wallops Station.

One-third—octave band spectra present outdoors when the overall sound pressure level (SPL) was at max dB(C) are shown in figure 3 for representative flights for each of the aircraft tested.

Psychological Measurements

The paired-comparison tests which are believed to provide the most essential psychological data from this study are scored and interpreted as follows:

Step 1.- The percent of listeners in a group (for this report a group of 33 people) who preferred the reference aircraft noise when it appeared first in a given pair and when it appeared second in the same pair are averaged.

Step 2.- The percent obtained in step 1 is plotted against the level, measured by a given physical unit, of the comparison aircraft noise. Inasmuch as the level of the comparison noise was systematically varied, the percent of people, in general, who preferred the reference noise increased as the level of the comparison noise increased. An attempt was made to have the comparison noise vary over a range that caused the percent of people preferring the reference aircraft noise to change from near zero percent to near 100 percent. Sample plots of the data are shown in figure 4.

Step 3.- On each function, such as those shown in figure 4, a perpendicular is dropped to the abscissa from the point where the 50-percent line crosses the curve drawn through the data points.

Step 4.- The value obtained in step 3 is taken as the level, for the given unit of measurement, required for the comparison noise if and when it is to be perceived as equal to the reference aircraft noise in unacceptability or noisiness.

Step 5.- The difference, if any, between the reference and comparison noises when judged to be equal is taken as the index of the ability of each of the physical units to properly measure or indicate the perceived noisiness of each pair of sounds.

RESULTS AND DISCUSSION

Table 11 presents a summary of averaged data obtained when the noise from jet aircraft was judged against that from other jet aircraft or from turboprop aircraft, reciprop aircraft, or helicopters. Two equally important indicators that show the accuracy with which an objective measure predicts the subjective judgment data are shown in table 11 and are described as follows:

(1) The average of the differences between an objective measure for the reference and comparison aircraft noise when they are judged to be equally noisy. If the physical units were perfectly correlated with the psychological data, the average of the differences would be zero for each pair; that is, when the aircraft noises were judged to be equal, they would be measured physically as being equal.

(2) The range of the differences between an objective measure for the reference and comparison aircraft noise when they are judged to be equally noisy. It is important that an objective measure be reasonably accurate with respect to the most common or most prevalent aircraft noises evaluated. This accuracy is reflected in the average of the differences between the objective measures of any two noises judged to be subjectively equal.

Two particular conclusions can be drawn from table II. First, the average differences for the better units are significantly smaller when the comparison and reference noises are both high-frequency jet noises than when one of the noises is a low-frequency propeller-aircraft noise. These differences are about 1.5 dB when the comparison and reference noises are both high-frequency jet noises and about 3.0 dB when one is a low-frequency propeller-aircraft noise. Appropriate modifications to procedures for measuring noise in the lower frequency bands should reduce the differences between the physical measures and judged noisiness and thereby provide an effective perceived noise level that would predict, with an average accuracy of about 1.0 dB, judgments of the noisiness or unacceptability of aircraft noise regardless of its source, spectral complexity, and, within limits, duration. Second, when all types of aircraft noises and both the average differences and the total range of differences between the values for the references and comparison noises are considered, the most accurate units of measurement are usually $EPNdB_t$.

The relative accuracy of the various objective measures is illustrated in table III, which shows how each unit ranks with regard to the average of the average differences and the range of differences. A unit with the rank of one would have the best agreement with the subjective judgments.

Two other recent studies (see refs. 5 and **6)** have been made of subjective judgments of aircraft noise in which all, or nearly all, of the objective measures used in the present study were evaluated. Table IV shows that EPNdB has the highest rank in each of the studies. It should be pointed out, however, that the practical significance between some of the differences in these measures, an amount equivalent to less than 1.0 dB in level in some cases, is perhaps questionable.

CONCLUSIONS

The following conclusions are based on the results from judgment tests of aircraft noise:

1. The best agreement between objective measures and subjective judgments of the noisiness or unacceptability of aircraft noise of all types is generally found by calculating the tone-corrected effective perceived noise level in $EPNdB_t$ from 1/3-octave band spectra taken every 1/2 second during the noise cycle.

2. When aircraft noise containing its energy predominately in the lower frequencies is compared with predominately high-frequency aircraft noise, a systematic overestimation by about **3.0** dB of the perceived noisiness of the lower frequency noise is obtained by the various PNdB units.

REFERENCES

1. Mayes, William H.; Findley, Donald S.; and Carden, Huey D.: House Vibrations Significant for Indoor Subjective Response. Conference on Progress of NASA Research Relating to Noise Alleviation of Large Subsonic Jet Aircraft, NASA SP-189, 1968. (Paper No. 39 herein.)

2. Kryter, K. D.: Concepts of Perceived Noisiness, Their Implementation and Application. J. Acoust. Soc. Amer., vol. 43, no. 2, Feb. 1968, pp. 344-361.

3. Stevens, S. S.: Procedure for Calculating Loudness: Mark VI. J. Acoust. Soc. Amer., vol. 33, no. 11, Nov. 1961, pp. 1577-1585.

4. Zwicker, E.: A Graphic Method of Determining Loudness and Loudness Level From the "Third-Octave" Level Diagram. Frequenz, vol. 13, no. 8, Aug. 1959, pp. 234-238.

5. Hecker, Michael H. L.; and Kryter, Karl D.: Comparisons Between Subjective Ratings of Aircraft Noise and Various Objective Measures. Tech. Rep. NO-68-33, FAA, Apr. 1968.

6. Kryter, K. D.; Johnson, P. J.; and Young, J. R.: Psychological Experiments on Sonic Booms. Annex B of Sonic Boom Experiments at Edwards Air Force Base, NSBEO-1-67 (Contract AF 49(638)-1758), CFST1, U.S. Dep. Com., July 28, 1967.

TABLE I.- NUMBER OF OVERFLIGHTS FOR JUDGMENT TESTS

[Total of 189 pairs]

Reference aircraft:	
Turbojet. 880	132
Recip-prop, 1049G	80
Comparison aircraft:	
Turbofan (front). 727	22
Turbofan (front). C-141A	22
Turbofan (aft). 990	28
Turbojet. 720	20
Turbojet. 1329 Jet Star	18
Turbojet (afterburner). F-106	12
Turboprop (STOL). CV-7A	16
Turboshaft (helicopter). 204B	20
Turboshaft (helicopter). CH-47	8

TABLE II.- COMPARISON OF OBJECTIVE MEASURES AND SUBJECTIVE JUDGMENTS

Aircraft noise	Indicator of accuracy	Best units					
		EPNdB	EdB(N)	$EPNdB_{t_1}$	Peak $PNdB_{t_1}$	Max dB(B)	Max dB(C)
Jet vs jet	Average difference	1.2	1.4	1.5	2.9	2.0	2.1
	Range of differences	4.5	4.5	7.5	11.0	5.5	7.5
Jet vs turboprop, reeip-prop, or helicopter	Average difference	2.4	2.5	3.5	5.6	7.0	7.9
	Range of differences	9.0	8.0	10.0	17.0	20.0	25.0

Aircraft noise	Indicator of accuracy	Best units			Worst units		
		EPNdB EdB(N)	$EPNdB_{t_1}$ $EPNdB_{t_2}$	EEPNdB	Peak $PNdB_{t_1}$	Max dB(B)	Max dB(C)
Grand average for all aircraft	Average difference	1.7	2.2	2.8	4.0	4.1	4.6
	Range of differences	8.5	10.3	11.0	19.0	20.0	25.0

TABLE III.- RELATIVE ACCURACY WITH WHICH OBJECTIVE MEASURES PREDICT JUDGMENT DATA OBTAINED AT WALLOPS STATION

[20 units used]

Unit name	Rank	Unit name	Rank
EPNdB	1	Max phons	8
EdB(N)	1	Max dB(A)	8
$EPNdB_{t_1}$	2	Max $PNdB_{t_2}$	9
$EPNdB_{t_2}$	2	Max PNdB	9
EEPNdB	3	Max dB(N)	9
EdB(A)	4	Peak $PNdB_{t_2}$	10
$EEPNdB_{t_1}$	5	Max $PNdB_{t_1}$	11
$EEPNdB_{t_2}$	6	Peak $PNdB_{t_1}$	12
Peak phons	7	Max dB(B)	13
Peak PNdB	8	Max dB(C)	14

TABLE IV.- BEST AND WORST PREDICTORS OF JUDGMENTS OF AIRCRAFT NOISE

Predictors	Edwards AFB field tests (ref. 5)	FAA laboratory tests (ref. 6)	NASA field tests
Best	$EPNdB_{t_1}$ $EEPNdB_{t_1}$ EEPNdB	$EPNdB_{t_2}$ EPNdB Max dB(N)	EPNdB, EdB(N) $EPNdB_{t_1}$, $EPNdB_{t_2}$ EEPNdB
Worst	Max dB(A) Max dB(C) Max dB(B)	Peak $PNdB_{t_1}$ Max $PNdB_{t_1}$ Max dB(C)	Peak $PNdB_{t_1}$ Max dB(B) Max dB(C)

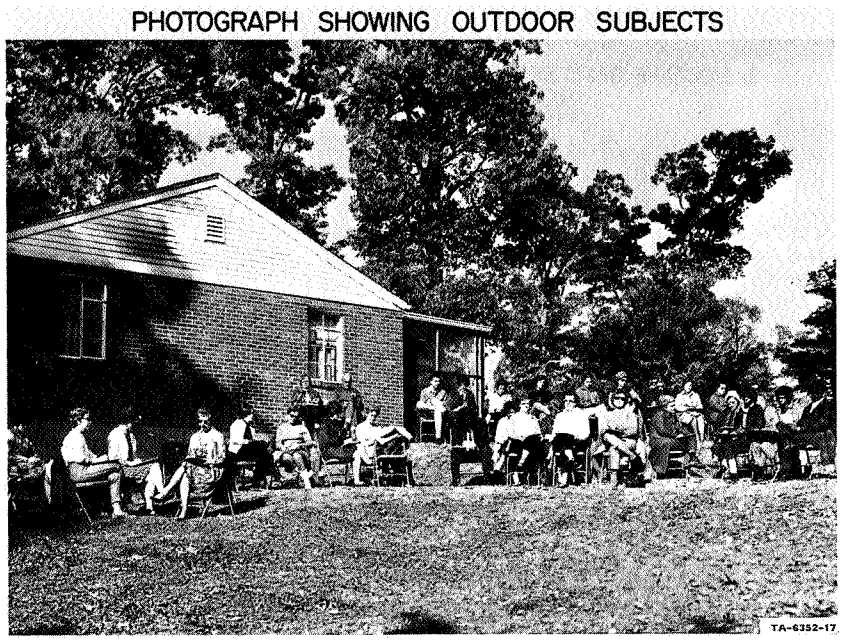

Figure 1 L-68-8585

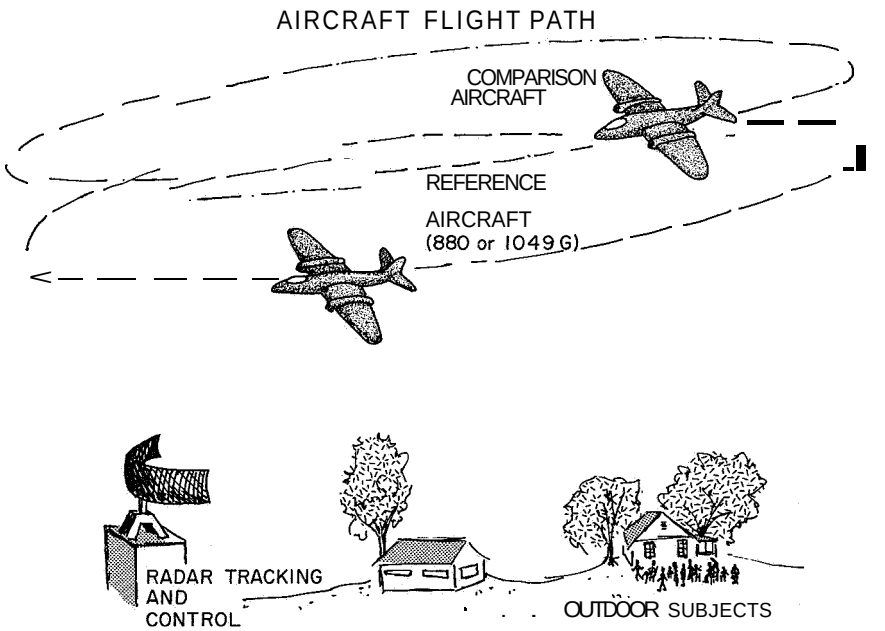

Figure 2

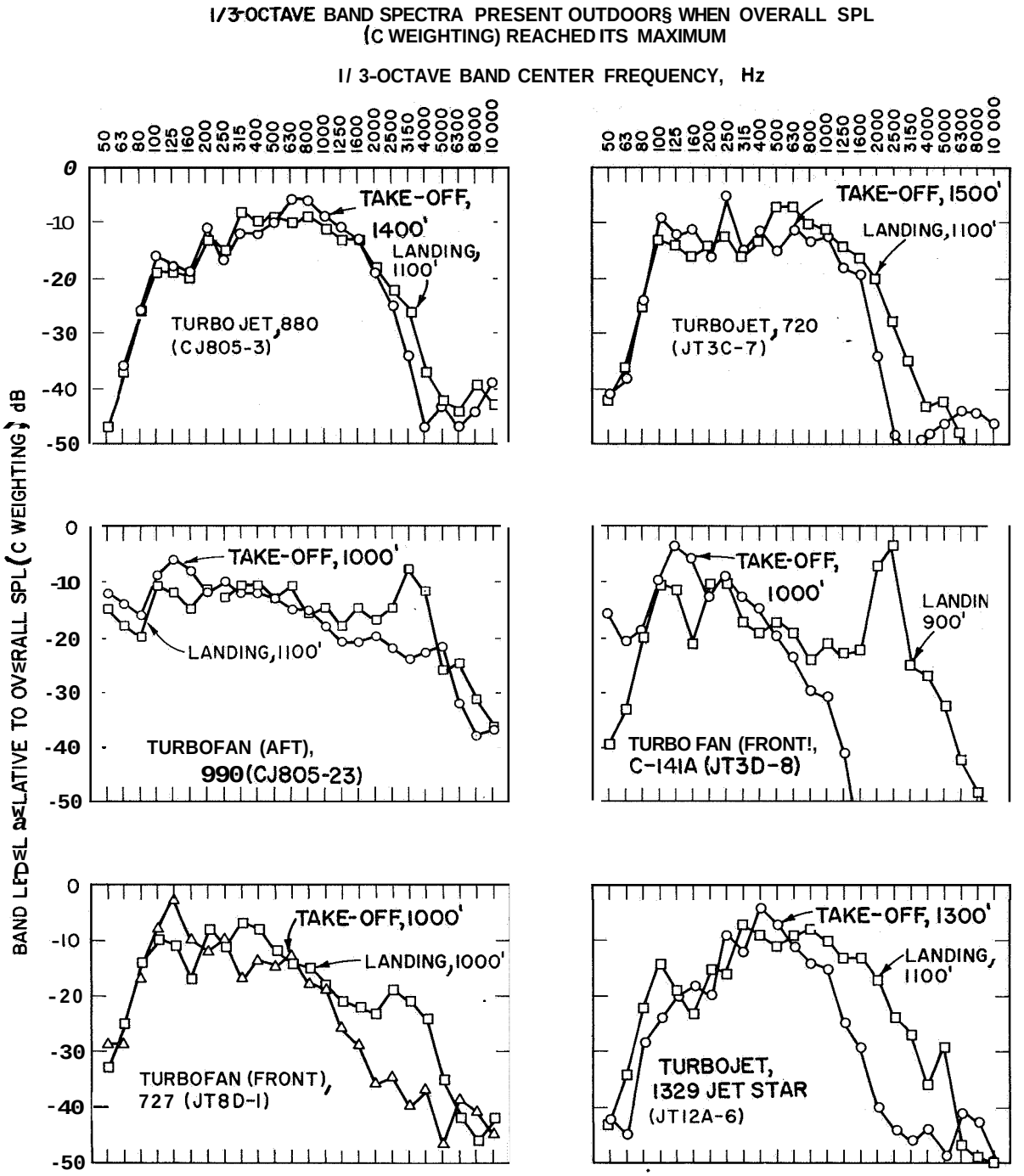
1/3-OCTAVE BAND SPECTRA PRESENT OUTDOORS WHEN OVERALL SPL (C WEIGHTING) REACHED ITS MAXIMUM
1/ 3-OCTAVE BAND CENTER FREQUENCY, Hz
50 63 80 100 125 160 200 250 315 400 500 630 800 1000 1250 1600 2000 2500 3150 4000 5000 6300 8000 10 000
BAND LEVEL RELATIVE TO OVERALL SPL (C WEIGHTING), dB
0 -10 -20 -30 -40 -50
TAKE-OFF, 1400'
LANDING, 1100'
TURBOJET, 880 (CJ805-3)
TAKE-OFF, 1500'
LANDING, 1100'
TURBOJET, 720 (JT3C-7)
TAKE-OFF, 1000'
LANDING, 1100'
TURBOFAN (AFT), 990 (CJ805-23)
TAKE-OFF, 1000'
LANDIN 900'
TURBO FAN (FRONT!, C-141A (JT3D-8)
TAKE-OFF, 1000'
LANDING, 1000'
TURBOFAN (FRONT), 727 (JT8D-1)
TAKE-OFF, 1300'
LANDING, 1100'
TURBOJET, 1329 JET STAR (JT12A-6)

Figure 3(a)

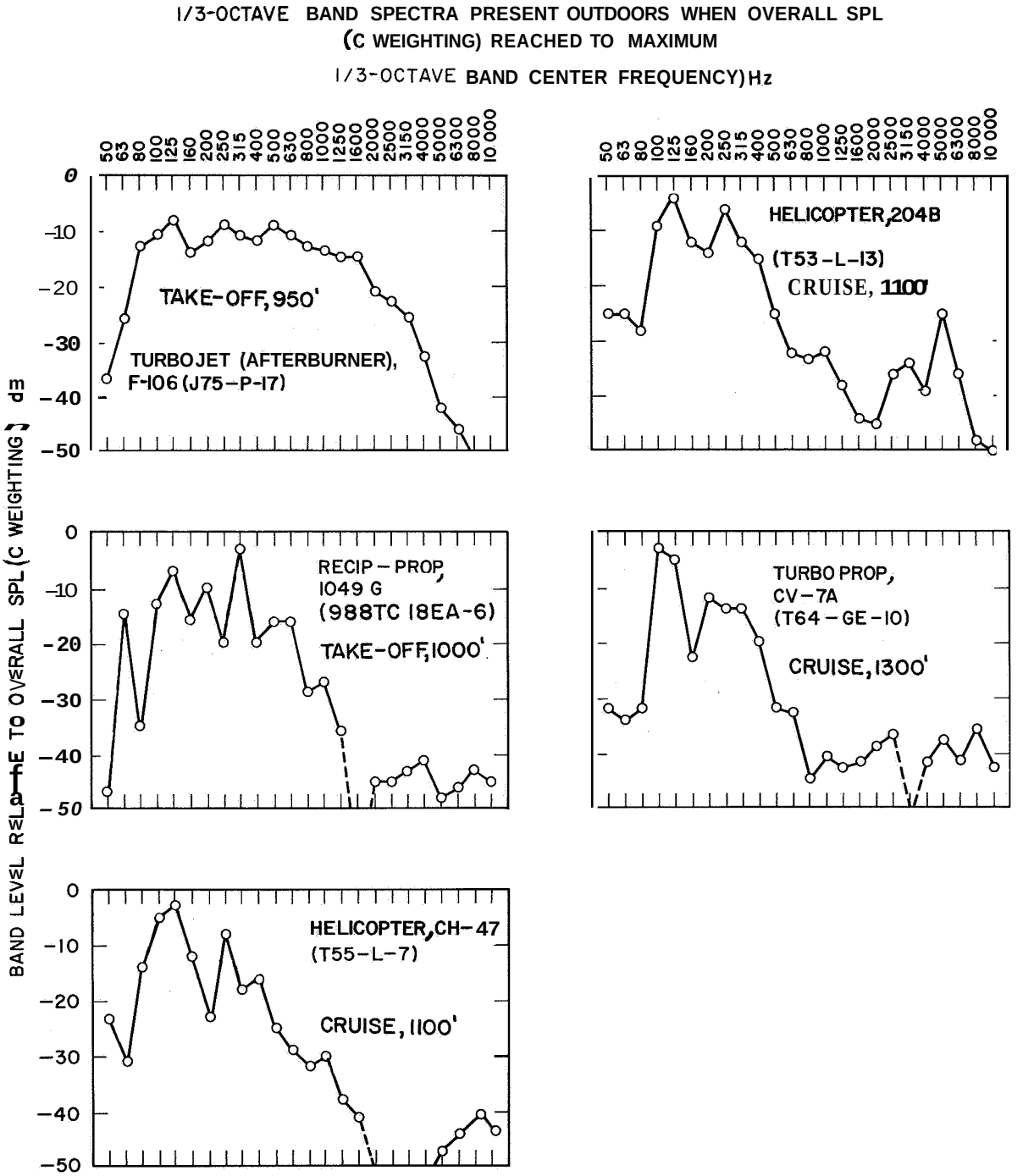
1/3-OCTAVE BAND SPECTRA PRESENT OUTDOORS WHEN OVERALL SPL
(C WEIGHTING) REACHED TO MAXIMUM
1/3-OCTAVE BAND CENTER FREQUENCY) Hz
50 63 80 100 125 160 200 250 315 400 500 630 800 1000 1250 1600 2000 2500 3150 4000 5000 6300 8000 10 000
0
-10
-20
-30
-40
-50
BAND LEVEL RELATIVE TO OVERALL SPL (C WEIGHTING) dB
TAKE-OFF, 950'
TURBOJET (AFTERBURNER),
F-106 (J75-P-17)
HELICOPTER, 204B
(T53-L-13)
CRUISE, 1100'
RECIP-PROP,
1049 G
(988TC 18EA-6)
TAKE-OFF, 1000'
TURBO PROP,
CV-7A
(T64-GE-10)
CRUISE, 1300'
HELICOPTER, CH-47
(T55-L-7)
CRUISE, 1100'

Figure 3(b)

EXAMPLES OF PAIRED–COMPARISON JUDGMENTS OF SUBSONIC NOISE BY OUTDOOR LISTENERS AT WALLOPS STATION

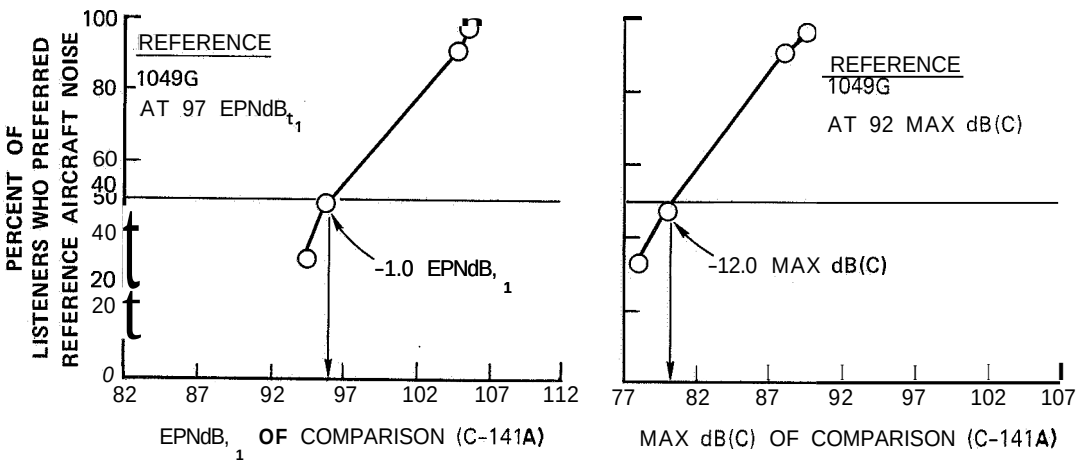

Figure 4

38. PERCEIVED SOUND AND THE FREQUENCY RESPONSE CHARACTERISTICS OF THE HUMAN AUDITORY SYSTEM

By Jess H. Jones

NASA George C. Marshall Space Flight Center

SUMMARY

A simple model of the human auditory system is presented from a dynamic response point of view – that is, input-output. The output of a human auditory system, which is defined as the perceived sound, is determined by multiplying the input acoustic stimulus by the square of the complex frequency response function of the auditory system. It is shown that, in terms of this model, the inverse equal noisiness (or equal loudness) contours are in effect the transfer function for the human auditory system. Perceived sound estimates obtained through the use of this model are presented and it is shown that these estimates agree with judgment test results as well as or better than the predictions obtained by presently accepted methods.

Arguments are presented which show that the results obtained through the use of this approach for input sound pressure level values in excess of 60 dB (re: 0.00002 N/m^2) can be considered valid. The further implication is that for input sound pressure levels above this value, the human auditory system can be considered to function as a linear system.

The so-called critical bandwidth phenomenon is also interpreted within the framework of the proposed model; however, the resulting critical bandwidths are greater than the presently accepted values. In the frequency region near the peak in the response curve, this model clearly predicts that the perceived sound level will decrease instead of increase for bandwidths greater than the critical band.

INTRODUCTION

When an auditory system is exposed to an acoustical stimulus, the resultant quantity is normally referred to as the "perceived noise." In the past, the magnitude of this perceived noise has been specified in several different ways. The approach by Stevens in references 1 and 2 provides a measure of this magnitude or loudness in terms of units of loudness called sones or its logarithmic equivalent is the loudness level in phons. Zwicker and Feldtkeller (ref. 3) and Zwicker (ref. 4) also present a measure of this loudness in phons. Kryter (ref. 5) and Kryter and Pearsons (ref. 6) present a similar approach in which they choose to describe the magnitude of the perceived noise as noisiness, where the unit of noisiness is called noys, and its logarithmic equivalent is the perceived noise level in PNdB.

The concepts presented in this paper provide yet another approach to the elusive problem of estimating the magnitude of the perceived noise. The ideas contained herein are being presented with the hope that these concepts will provide a simpler interpretation of the phenomena of perceived noise. In the author's opinion, it is necessary to introduce additional descriptive terms, in order to adequately discuss the magnitude of perceived noise associated with these new concepts. Instead of the output of an auditory system being referred to as perceived noise, it will be hereafter referred to as "perceived sound." The unit of perceived sound is called "perceived pressure" and its logarithmic equivalent is the "perceived sound level" in dB(J). These terms are defined in the text.

Perceived sound can be qualitatively described in many different ways. It can be described by the characteristics of loudness, noisiness, annoyance, distraction, discomfort, or any other desired quality. These so-called qualities of perceived sound are very subjective in nature and, consequently, are very difficult to determine. When a person is asked to judge the perceived sound in terms of one of its desired qualities, the reaction or, more specifically, the response of that individual is dependent upon that quality which he is being asked to judge. This is to be expected and is in fact borne out by the results of tests concerning perceived sounds of equal loudness and equal noisiness. These studies have revealed that subjects responded differently when asked to judge sounds of equal loudness, as compared with sounds of equal noisiness. Persons, therefore, seemed to respond differently to the various qualities which can be ascribed to the perceived sound. This difference may be due to the fact that the individuals are not sure just what it is they are trying to judge, or the differences may, in fact, be real. At any rate, loudness (or noisiness, etc.) is then a psychological term which is used to describe the magnitude of an auditory sensation.

The concepts introduced in this discussion can be applied to any desired quality of perceived sound, but in order to compare predictions with measured results, the subsequent equations are developed with the quality of noisiness in mind. If the response characteristics for a different quality are desired, mentally substitute that desired quality for noisiness.

SYMBOLS

BSPL	band sound pressure level
f	frequency
Af	frequency bandwidth
f_L	lower limit of band

f_U	upper limit of band
f_c	geometric mean center frequency of band
f_p	peak frequency
$\|H(f)\|^2$	frequency response function
$\|H(f_c)\|^2$	relative auditory frequency response function
$\overline{J^2}(f)/Hz$	mean squared perceived pressure per unit bandwidth
$\overline{J^2_{\Delta f}}(f_c)$	perceived mean squared pressure in band
K,k_p	perceived constants
N,i	integers
OASPL	overall sound pressure level
OBPSL	octave band perceived sound level, dB(J)
OBSPL	octave band sound pressure level of input, dB
P_o	standard acoustic reference pressure, **0.00002** N/m^2
$\overline{P^2}(f)/Hz$	mean squared pressure per unit bandwidth
$\overline{P^2_{\Delta f}}(f_c)$	mean squared pressure in the band
PSL	perceived sound level
$S_I(f)$	power spectral density of input acoustic stimulus, $\overline{P^2}(f)/Hz$
$S_p(f)$	perceived spectral density of output, $\overline{J^2}(f)/Hz$
SPL_i	sound pressure level of input stimulus
s_p	perceived sound (mean squared value of perceived pressure)

STATE OF THE ART

When an attempt is made to determine the state of the art with regard to the definition, measurement, and calculation of perceived sound, the complexity and seemingly orderly progression of events is immediately evident. No doubt, one of the more recent studies to be examined would be that of Kryter (ref. 7), and then works of both Pearsons and Kryter (refs. 5, 6, 8, 9, and 10), Stevens (refs. 1 and 2), Mintz and Tyzzer (ref. 11), Beranek, Marshall, Cudworth, and Peterson (ref. 12), Churcher and King (ref. 13), and Fletcher and Munson (ref. 14). These studies do not represent the total effort of all workers in this area, but they have a more direct bearing on the topic of this paper. From these few basic studies, the total scope of this problem area is immediately apparent.

It is not the intent here to elaborate to any extent on what has been done in the past; those associated with this field are well aware of these facts. However, because the major discussion herein is concerned with the calculation of perceived sound, it may be well to mention the progression of events which have led to the presently accepted calculation schemes.

Those who have been faced with the necessity of computing the perceived sound of a given noise spectrum are well aware of the tedious and extremely time-consuming methods which have been devised. These techniques owe their origin, in reality, to the early pioneering work of Fletcher and Munson (ref. 14). One of the first attempts to calculate perceived sound (referred to as loudness at that time) was made by Gates (Discussion, ref. 13), who proposed that the total loudness of a complex sound could be found by a direct summation of the loudness units representing the spectrum of a complex sound. This technique was later elaboarated upon by Beranek, Marshall, Cudworth, and Peterson (ref. 12) and Mintz and Tyzzer (ref. 11). Stevens (refs. 1 and 2), however, found later that, if the total loudness was obtained through a summation of loudness units, this indicated loudness would exceed the actual loudness of the total noise by a factor of more than 2. Consequently, Stevens devised a summation procedure that was empirically derived from a series of tests which tended to weight the total loudness of a complex noise spectrum to the maximum loudness unit of that noise spectrum. This technique, which seemed to be successful in predicting the results of judgment tests, is in the form of a numerical calculation scheme. The unit of loudness used by Stevens is called sones, and its logarithmic equivalent is the loudness level in phons. Zwicker and Feldtkeller (ref. 3) and Zwicker (ref. 4) devised a procedure which is similar to that used by Stevens but is handicapped somewhat because it is in the form of a graphical calculation scheme.

Kryter (ref. 5) and then Kryter and Pearsons (ref. 6) devised a procedure almost exactly paralleling that of Stevens; the only exception is that this technique is derived for noisiness and Stevens' technique is intended to be used for loudness evaluation. Kryter's procedure is a numerical calculation scheme; that is, the scheme is based on experimental data presented in tabular form and the computations are performed with the aid of an empirical weighting equation. The unit of noisiness is called noys and its logarithmic equivalent is perceived noise level in PNdB.

All these calculation schemes are somewhat awkward to use and difficult to relate to a valid physical interpretation of the perceived quality of sound. It is also difficult, though not impossible (ref. 15), to build an instrument so that a direct measure of the perceived sound can be made.

The intent of this discussion is to put forth several ideas in order to simplify the calculation procedure for estimating the magnitude of perceived sound and present a simple model for describing the human auditory system. Doing so will place the calculation scheme on a firm physical basis. As a result of this simplified approach, it is shown that an instrument can easily be built so that a direct on-line measure of the magnitude of the perceived sound can be made. There is no need to discuss the obviously far-reaching benefit of an instrument of this nature.

In this paper, an attempt is made to show that this simplified procedure provides estimates which agree with the results of judgment tests as well as or better than the presently accepted methods. Additionally, it is not limited by complex sounds containing strong pure tone components or high level narrow-band energy. Furthermore, it is shown that this approach provides a better insight into the physical aspects of the human auditory system.

PERCEIVED SOUND MODEL

The basic intent of this discussion is to depart somewhat from present ideas and procedures. .Some may consider this departure as radical or reverting to concepts that have long since been abandoned, but it is believed that this departure is warranted in view of the simplicity and physical insight which can be achieved by the use of this very basic and simple method.

The proposal here is to consider the human auditory system from a dynamic response point of view – that is, input-output; this is illustrated in figure 1 as an input altered by the appropriate response function and the output.

The input implies any type of acoustic stimulus – that is, broad-band noise, narrow-band noise, pure tones, multiple tones, and so forth. By the use of certain assumptions concerning the statistical characteristics between tones in a multitone configuration or between tones and bands of noise, this input can be made to apply to any combination of tones and/or bands of noise. For the purpose of this analysis, it is assumed that tones in a multitone configuration and tones in bands of noise are statistically unrelated; therefore, the mean squared pressures will be added directly.

The human auditory system consists of the ear and its associated physical hearing mechanisms, the nerve system, the brain, and any other elements, both psychological and physical, which would have any possible effect upon the total hearing process. This auditory system can be represented by a transfer function which will in turn operate in a systematic manner upon the input in order to transform it into the perceived sound. The auditory system is, by its very nature, a dynamic system and, because of this, it will have definite frequency response characteristics. These response characteristics will also vary from individual to individual; therefore, if the perceived sound that is representative of an average or typical listener is to be predicted, the response characteristics of the typical or average human auditory system will have to be used.

The output is the perceived sound, and the unit of perceived sound is called a perceived pressure. It is emphasized that this unit of perceived sound is not the same as the unit of noisiness (noy) and the unit of loudness (sone) which have been used in the past. The perceived pressure is directly related to the input sound pressure. By defining it in this fashion, a direct relationship can be established to relate noisiness to a physical quantity. The logarithmic equivalent of the perceived pressure is the perceived sound level in dB(J). The dB(J) is written in this manner to indicate that the output was obtained with a J weighting function. This is analogous to the notation used when presenting results obtained with the A, B, or C weighting scales presently in use. The perceived sound level in dB(J) is defined as follows:

$$PSL \equiv 20 \log_{10}\left\{\sqrt{s_p}/P_o\right\} \tag{1}$$

The perceived sound level can, therefore, be directly related to the input sound pressure level.

Another obvious benefit of defining perceived sound in this fashion is that it is now possible to discuss such things as a perceived spectrum or a spectral distribution of the perceived sound. Equation (1) can be extremely useful in determining what portion of the spectrum is having the most influence on the total perceived sound. Furthermore, the perceived spectrum can be presented as an octave band, a one-third octave band, a spectral density, or in any other desired form. These quantities are defined as follows:

$$\text{Band perceived sound level} \equiv 20 \log_{10} \left\{ \frac{\sqrt{\overline{J^2_{\Delta f}(f_c)}}}{P_o} \right\} \tag{2}$$

If Af is equal to an octave band, equation (2) would become the octave band perceived sound level, and so forth.

The perceived spectral density of output is

$$S_p(f) \equiv \overline{J^2}(f) \Big/ \text{Hz} \tag{3}$$

This definition is analogous to the power spectral density of the input acoustic stimulus.

The overall perceived sound or, more specifically, the perceived sound can then be defined as follows:

$$s_p \equiv \int_0^\infty S_p(f)\, df = \int_0^\infty \overline{J^2}(f) \Big/ \text{Hz}\, df \tag{4}$$

These definitions are consistent with presently accepted terminology except they are now being related to the unit of perceived sound.

If the human auditory system is considered a constant parameter linear system, then the input and output (fig. 1) can be related as follows (ref. 16):

$$|H(f)|^2 S_I(f) = S_p(f) \qquad (0 \leq f < \infty) \tag{5}$$

It might be argued that the auditory system cannot be considered as a linear system, and in view of the present interpretation of perceived sound which normally expresses loudness in sones or noisiness in noys, this seems to be true. However, in light of the concepts which are being presented in this discussion, it can and will be shown that, within given amplitude ranges of the input stimulus, the auditory system can indeed be represented by a linear system.

Accepting the concept of a linear system for the present time, the characteristics of $|H(f)|^2$ will now be defined. If $S_I(f)$ and $S_p(f)$ are known, the characteristic definition would be complete. Upon close examination, it is easily seen that this is indeed the case. The quantity $S_I(f)$ can readily be measured, but although this cannot be done with $S_p(f)$, an individual can be asked to judge (perceive) with reasonable accuracy a constant noisiness function. The perceived values of constant noisiness are the equal noisiness (or equal loudness) contours which presently exist. From these equal noisiness curves, $|H(f)|^2$ can be determined.

First assume that the equal noisiness curves were obtained by judging the noisiness of bands of noise. (See **ref.** 6.) Equation (5) can then be written as

$$\int_{f_L}^{f_U} |H(f)|^2 S_I(f)\, df = \int_{f_L}^{f_U} S_p(f)\, df \tag{6}$$

where f_U and f_L are the upper and lower limits of any arbitrary band. These upper and lower limits could also be made to apply to any desired band of interest – that is, octave band, one-third octave band, and so forth.

If $|H(f)|^2$ is assumed constant over the frequency band of interest, equation (6) can be written as

$$|H(f)|^2 \int_{f_L}^{f_U} S_I(f)\, df = \int_{f_L}^{f_U} S_p(f)\, df \tag{7}$$

If a person is judging a constant noisiness, then $\int_{f_L}^{f_U} S_p(f)\, df$ is constant; also, the integral in the left-hand side of the equation is actually the mean squared pressure in the band. From this, then, equation (7) becomes

$$\overline{P^2_{\Delta f}}(f_c) \left|H(f_c)\right|^2 = k_p \tag{8}$$

Converting equation (8) to the band sound pressure level in dB yields

$$BSPL(f_c) + 10 \log_{10} \left\{ \left|H(f_c)\right|^2 \right\} = K \tag{9}$$

Equation (9) states that as one proceeds from one band to the next throughout the whole audio range, the sound pressure level in each band must change in such a fashion that K remains a constant; this is by definition the concept of the equal noisiness curves. The only restriction is that the response function is assumed to be constant over the band of interest.

It is desirable to define a relative frequency response function. Therefore, this function will be defined such that $\left|H(f_c)\right|^2$ is unity when the sound pressure level of a band of noise or a pure tone centered at 1000 Hz equals K. From this definition, equation (9) becomes

$$10 \log_{10} \left\{ \left|H(f_c)\right|^2 \right\} = BSPL(f_c = 1000 \text{ Hz}) - BSPL(f_c) \tag{10}$$

where $|H(f_c)|^2$ is the relative auditory frequency response function and

$$10 \log_{10}\left\{|H(f_c)|^2\right\}$$

is the relative response in dB.

Equation (10) is the relationship that was used to obtain the relative auditory response function for a typical or average human auditory system. It can be seen from the derivation of the relationship that the term $BSPL(f_c)$ is, in reality, the equal noisiness curves and $BSPL(f_c=1000\ Hz)$ is the equal noisiness value at the center band frequency of 1000 Hz.

HUMAN AUDITORY RESPONSE FUNCTION

The method of Kryter and Pearsons (refs. 6 and 17) seems to give results which appear to be in better agreement with the results of judgment tests than any of the other existing techniques; therefore, the concept of PNdB seems to have gained general acceptance. For this reason, the relative auditory response function is determined from the data of Kryter and Pearsons.

If the input stimulus is restricted to levels which are greater than 60 dB (re: 0.00002 N/m^2), then, with the aid of the equal noisiness values presented in reference 17 and equation (10), the relative response functions can be determined. The results of this operation are presented in figure 2. The scatter band represented by the shaded region in figure 2 is the total scatter in the response function for this extreme range in sound pressure level. In view of the extreme variability which normally occurs in judgment tests which are used to arrive at the equal noisiness curves, this scatter band can be considered negligible. The average of this scatter is presented in figure 3, and it is this response function which has been used to obtain most of the results presented in this paper.

Examination of figure 2 indicates that the relative response function is independent of the amplitude of the input stimulus. From this, it can be concluded that the auditory system functions as a linear system for input sound pressure levels in excess of approximately 60 dB. This conclusion can also be drawn from the existing procedure for calculating perceived noise without resorting to the concepts presented herein and is clearly illustrated in figure 4. The perceived noise level in PNdB has been computed (ref. 17) for nine different spectrum shapes (fig. 4(b)) for various input levels of each spectrum. If attention is restricted to levels in excess of approximately 60 dB for the input stimulus, it is seen that, for a 10-dB increase in input (for a given spectrum), the perceived noise level increased by 10 PNdB. This in itself implies some sort of linear or one-to-one

correspondence. Clearly, for levels below 60 dB and for low frequency energy spectra, the relationship is no longer linear. Furthermore, the family of curves presented in figure 4(b) merely reflects the influence of the frequency response characteristics of the human auditory system on these various input spectra.

APPLICATION OF THE PERCEIVED SOUND LEVEL

Now that the frequency response function of the auditory system has been determined, it is possible to compute the perceived sound level. This computation is easily done with the aid of equation (1) and the frequency response function of figure 3.

This proposed method is not restricted in the sense that it has to be applied to a given type of input format – that is, octave band form, one-third octave band form, and so forth – but works equally well with any type of input format since the response function is independent of bandwidth.

Inasmuch as the relative response function was defined such that the input stimulus was equal to the perceived level at a frequency of 1000 Hz, equation (1) can now be written in terms of this relative response function as

$$\mathrm{OBPSL}(f_c) = \mathrm{OBSPL}(f_c) + 10 \log_{10} \left\{ \left| H(f_c) \right|^2 \right\} \tag{11}$$

in units of dB(J). The only restriction on equation (11) is that the relative frequency response function is assumed to be constant within the octave band.

The point that should be emphasized now is the ease and simplicity by which the perceived sound level is determined. There is no need to have a weighting function which is related to the amplitude of the input stimulus as is presently in use with the noy or sone scales; this simplifies immensely the calculation procedure. The application of the proposed method is analogous to the procedure that would be used to correct acoustic test data because of the nonuniform frequency response characteristics used to acquire the data.

It is a simple matter to construct an electronic instrument to measure directly the perceived sound level. This is analogous to the A, B, or C weighting scales presently in use. It will be shown that predicted subjective responses obtained with the aid of the response curve in figure 3 agree with judged responses as well as or better than estimates obtained by using any of the presently accepted loudness or noisiness prediction methods. Furthermore, it will be shown that, by slight modification of the response curve in figure 3, even better agreements between predicted and judged results can be obtained.

Before the comparison of results is introduced, it is important to discuss the relative significance of the absolute magnitude of the perceived sound level predicted by the proposed method in comparison with that predicted by other methods. It is almost meaningless to compare the absolute values resulting from these methods because of the way in which the reference for the loudness level and perceived noise level was arbitrarily defined and also because of the difference in the weighting characteristics between the proposed method and these other methods – that is, the methods of Kryter, Stevens, and Zwicker. It might be argued that the reference of the proposed method is just as arbitrary. Indeed, this may be true but, because of the manner in which this reference was defined, it is believed that more physical meaning can be placed on these results. In any event, in order to avoid this problem, the absolute magnitudes are not compared directly, but instead each is compared with its own standard (difference from the standard); then these differences are compared. This is the conventional procedure.

In order to provide an indication of the difference between the values obtained by the proposed method and those obtained by other methods (Kryter's in particular), the spectra of figure 4(a) were recomputed with the aid of the proposed method. These results are presented in figure 5. In comparing the results of figures 4 and 5, as well as other comparisons presented later in this paper, it is seen that the perceived sound level (PSL) estimates (numerical values) are always less than the perceived noise level (PNL) estimates (numerical values). The amount they differ depends upon the breadth of the energy of a given input sound spectrum as well as the location, in frequency, of the predominant energy. In general, it seems that the broader the energy distribution and the lower the peak frequency of this energy, the greater the difference between the PSL and the PNL. For the type III spectra of figure 4(a), this difference is about 6.5. For spectra narrower than type I (spectra 1 to 4 of fig. 6), this difference is about 3.

EVALUATION OF THE PROPOSED METHOD

Now that the frequency response function has been developed, the ability of the response function of figure 3 to predict the results of judgment tests will be determined. Insofar as this response function has been developed from a noisiness point of view, comparison is restricted to those judgment tests in which the subjects were asked to judge noisiness. In doing so, only the results of tests performed by Kryter (ref. 5), Kryter and Pearsons (ref. 6), and Little (ref. 18) will be used.

Comparison With Bands of Noise Without Tones

Kryter and Pearsons (ref. 6) performed a very comprehensive test series in which subjects were asked to adjust the level of the comparison stimulus of nine widely different spectra (fig. 6) until each was just as acceptable (noisy) to them as the standard spectrum.

The levels of these spectra have been adjusted so that they correspond to the average result of the judgment tests for which each of the comparison stimuli was as acceptable as the standard stimulus. Table 1 compares the predictions of various assessment methods, both electronic and other prediction methods. Table 1 shows that the proposed method and the method of Kryter seem to have better agreement with the results of the judgment tests when comparing the average differences from the standard. For an ideal method, these differences should be zero – in fact, the method should predict the same value for each of the judged spectra – this can be used as a gage to determine the superiority of one method over another.

A more detailed account, delineating the difference from the standard for each of the individual comparison spectra, is presented in table 2. Another equally valid gage is the ability of a prediction method to "rank," in the order of noisiness or loudness whichever the case may be, any given input spectra.

Hereafter, to simplify the discussion of the results, only comparisons between the proposed method and that of Kryter are made. In reality, the techniques of Kryter, Stevens, and Zwicker are essentially from the same mold; therefore, conclusions drawn concerning the method of Kryter can, in general, be applied to those of Stevens and Zwicker.

The other means of determining the adequacy of a given prediction method, as mentioned previously, is its ability to rank any given input spectra. The input spectra cannot be ranked according to the predicted magnitude of noisiness presented in table 1 because obviously they should all be the same value. The variations which are presented merely indicate the inadequacies of the methods and provide some measure of the prediction accuracy. The rank therefore has to be determined by different means.

One means of determining the rank is to readjust all the results of the judgment tests (i.e., the spectra presented in fig. 6) to a constant overall sound pressure level value. By doing this, the spectrum which had to be increased the most to obtain the selected overall value would be judged the "noisiest" and the spectrum which was changed by the smallest amount would be judged the "least noisy." This then provides valid results based on judgment tests from which the predictions, determined from the readjusted values, can be compared.

The judgment tests of Kryter and Pearsons (ref. 6) were determined in this fashion, and the results are presented in table 3. From this table, both techniques are seen to rank the input spectra about equally as well; however, both techniques seem to rank spectrum 6 noiser than it should be. In light of this present approach and after examining the input spectra in figure 6, a slight change in the high frequency portion (approximately 5000 Hz) of the frequency response function (fig. 3) could easily shift spectrum 6 into its proper order without affecting the ranking of the other spectra.

From an earlier study by Kryter (ref. 5), an additional comparison between predicted and judgment results can be made. In this study the subjects were asked to judge, by the method of paired comparison, the noisiness of six different types of aircraft spectra. The results of this comparison are presented in tables 4, 5, and 6. The PNdB values were determined by using the noy curves of reference 17. These tables show that both methods, again, are equally as effective in predicting the results of judgment tests. The predictions in the order of noisiness are better for these judged results than they were in the previous comparison.

It seems appropriate at this time to question the methods which various investigators have used in the past to obtain the "average results" of their judgment tests. Stevens (ref. 19), in discussing this problem, is of a similar opinion that too little attention is paid to the method used in averaging the data. Because of the large variations in the results, which seem to be inherent in most judgment tests, different averaging methods could introduce a rather significant bias. The subjective bias which is already present in the data is bad enough, but this problem is being compounded because of this so-called "averaging bias."

The common method of averaging the results is to obtain the arithmetic average of the decibels. When viewed from an energy standpoint, this operation is actually obtaining the geometric mean value of the mean squared sound pressures of the input stimulus. In other words,

$$\sum_{i=1}^{N} \frac{SPL_i}{N} = 10 \log_{10} \left\{ \frac{1}{P_0^2} \left(\overline{P_1^2}\, \overline{P_2^2} \cdots \overline{P_N^2} \right)^{1/N} \right\}$$

The proposed method for estimating noisiness returns the calculation procedure to an energy basis; consequently, it implies that the judgment results should be averaged by using the mean squared pressures of the input stimulus. This operation, therefore, results in the arithmetic mean of the mean squared pressures; that is,

$$\overline{P^2} = \sum_{i=1}^{N} \frac{\overline{P_i^2}}{N}$$

If the arithmetic mean of the mean squared pressures is compared with the geometric mean, it can be shown that

$$\sum_{i=1}^{N} \frac{\overline{P_i^2}}{N} \geq \left(\overline{P_1^2}\, \overline{P_2^2} \cdots \overline{P_N^2} \right)^{1/N}$$

Because of the extreme variability which is present in most judgment test data, the decibel values obtained from the arithmetic means are, in general, usually greater than the numerical average of the decibels (geometric mean). The amount by which one exceeds the other is a function of the range of values to be averaged, as well as the distribution of the values within this range.

Another method commonly used (ref. 19) is as follows: The decibel values to be averaged are first converted to their equivalent sone values, then the arithmetic mean of these sones is computed, and finally this averaged value is converted back to its equivalent decibel value. This is the analogous procedure that would be followed for obtaining the average based upon the mean squared pressures. But because the weighting of the amplitude of the input stimulus by sones in comparison with that by mean squared pressures is drastically different, the resulting average will not be the same. Averaging by the use of sones will, in general, result in a value which will fall between the values obtained by the first two methods cited.

Take a typical judgment test result and determine the average with the aid of these three different methods. Assume that the values to be averaged are those given by judged results of spectrum 4 of figure 16 in reference 6. The corresponding averages are

Average of the decibels	80.0 dB
Average of the mean squared pressures	83.3 dB
Average of the sones	81.2 dB

These differences may not seem to be significant at first glance, but it must be emphasized that this is introducing an artificial bias into the subjective response; furthermore, it makes valid comparisons of the results of different investigators exceedingly difficult if not impossible. This "error" is comparable in magnitude to the time error which has been observed; that is, the error in judging the second sound in a given pair as being noisier than the first, even though they are both the same amplitude.

There is yet another means of determining the average results of judgment tests. This average is obtained by plotting a curve of the percentage of people judging the comparison stimulus to be potentially noisier than the standard against the amplitude of the comparison stimulus. The point at which the 50-percent line crosses this curve is then the sound pressure level that is required for that comparison stimulus to be perceived as noisy as the standard. The question being raised here is, "How is this average related to the three other methods previously discussed?"

Having touched briefly on the fact that the weighting of the amplitude of the input stimulus by sones (or noys) and the weighting of the amplitude of the input stimulus by mean squared pressures are drastically different from each other, the consequences are examined. First of all, it is well known that, if the input sound pressure level changes

by a factor of 10 dB, the mean squared pressure changes by a factor of 10, but the noy (or sone) value would change by a factor of only 2. It can be seen from this that the noy (or sone) scales put a great amount of emphasis upon the lower sound pressure levels of a given spectrum. If these noisiness units (or loudness units) are summed to arrive at a total noisiness (or loudness) value, the result would be proportionately greater than the sum of the mean squared pressures; this is believed to be the reason why it has been proven that the total noisiness (or loudness) cannot be obtained through a direct summation. Stevens (ref. 1) first recognized this fact and subsequently derived an empirical relationship for summing these noisiness (or loudness) units. The results of this study indicate that this summing procedure, even though "seemingly correct" values are achieved through its use, still merely reflects the improper weighting characteristics of the input stimulus and, furthermore, that the so-called "bandwidth effect" – that is, the variation of coefficients for different types of data analysis – is also a manifestation of the same improper weighting. This bandwidth effect implies that the noisiness (or loudness) is dependent upon how the data are reduced, but this implication is not realistic. This study concludes that, if the proper weighting is used – that is, that which is proportional to the mean squared pressure – the total perceived level can be obtained through a direct summation.

Now the perceived noise level and the perceived sound level are computed for the judgment test results of Kryter and Pearsons (ref. 6), but, instead of using the average of the decibels as before, the average computed by the arithmetic mean of the mean squared pressures is used. These results, presented in the same manner as before, are given in tables 7, 8, and 9, and the average difference from the standard is considerably less than before. The order of the predicted rank remains the same, but the ranking from the judgment test results have changed. This also indicates the necessity of averaging the results properly (by mean squared values). Averaging the results in this manner has improved the agreement between methods.

Comparison of Bands of Noise With Tones

Figure 7 presents the results of a study of a pure tone immersed in a band of noise performed by Kryter and Pearsons (ref. 6). The indicated tone-band combination of each comparison stimulus was judged by the method of paired comparison to be as noisy as the standard band of noise without a pure tone. The band of noise was from 3680 to 7500 Hz and the center of frequency was computed to be 5280 Hz. Tables 10 and 11 compare these judged results with the predicted results of the proposed method and the method of Kryter with the pure tone correction applied (ref. 9). It can be seen from these results that the proposed method is satisfactory. Generally it is not considered important where the

pure tone is situated in a given band of noise. This study, however, reveals that the perceived level is critically dependent upon the location of the pure tone in the band of noise; this is particularly true in those frequency regions where the frequency response function is changing rapidly with frequency. (See fig, 3.) If the frequency response function is flat within the band of noise, the location of the pure tone within the band of noise is not important.

In 1961 Little (ref. 18) made a study in which 65 subjects were asked to judge the relative annoyance of two different types of present-day jet-engine sound spectra. One of these spectra had several high-amplitude narrow-band spikes. (See fig. 4 of ref. 18.) The proposed method was applied to these judged spectra and the results compiled. (See fig. 8.) Figure 8 presents the frequency distribution of energy that the average or typical human would perceive. These perceived spectra were judged to be equally noisy; therefore, the total energy associated with these spectra should be equal. It can be seen that the overall levels differ by approximately 1.5 dB(J). This again is considered to be a very good comparison especially for these types of spectra.

REVISED RELATIVE AUDITORY RESPONSE FUNCTION

The frequency response function presented in figure 3 was derived exclusively from existing data. This response function does a good job of predicting the results of judgment tests; however, it seems to be still lacking in certain respects. As mentioned previously, slight modifications in this response function can be made to achieve better agreement with judged results. Through "trial and error," a modified auditory response function was obtained. (See fig. 9.) This response function was applied to the judgment test of reference 6, and the results tabulated in tables 12, 13, and 14.

Table 12 compares the absolute magnitudes of the predictions of the proposed method and the Kryter method. The spectra presented in table 12 were all judged to be equally noisy; therefore, an ideal assessment method should indicate the same value for each spectrum. As can be seen, the average difference is small – that is, -0.6 for the Kryter method and -0.9 for the proposed method; for these types of spectra, such small values are considered to be very good.

Table 13 presents the individual differences from the standard. Table 14 presents the rank, in the order of noisiness, of each of the input spectra given in table 12. The purpose of this exercise is to verify that the prediction technique is able to select the spectra that would be perceived to be the noisiest from a variety of input stimuli which all have the same total energy content; that is, the physical overall mean squared pressure is constant for all input spectra. The rank was determined in the same manner as before. It can be seen that the proposed method was successful in selecting the noisiest

spectrum, whereas the Kryter approach ranked the noisiest spectrum (spectrum 3) fourth in the order of noisiness.

The other spectra, with the exception of 6, seem to be ranked in their approximate order.

INTERPRETATION OF THE CRITICAL BAND PHENOMENON

It is of interest to determine how much insight the proposed model can present in the interpretation of the "critical band phenomenon." These so-called "critical bands" can be determined very easily with the aid of the proposed model, and although the results do not agree with the presently accepted bandwidths (refs. 20 and 21), the similarities are amazing.

In light of the proposed method, the critical bandwidth can be explained in the following manner. Consider, for example, a pure tone acoustic stimulus (fig. 10) consisting of a two-tone complex with the two tones symmetrically centered about a center frequency f_c and separated in frequency by Δf. By using this as the input stimulus, the magnitude of perceived noisiness or loudness can be determined with the aid of the proposed method. In computing the perceived sound level, the center frequency was held constant and the bandwidth Δf was varied. By using the modified frequency response function in figure 9, the perceived sound level is computed with the given stimulus positioned at several center frequencies. These results are presented in figure 10, which shows that, for a given center frequency, as the bandwidth is initially increased, the perceived sound level remains constant until a "critical bandwidth" is reached. Beyond this critical bandwidth, the perceived level will change. Depending upon the center frequency, the perceived level will either increase or decrease. The change in the perceived sound is sometimes rather sudden (see f_c = 500 Hz and f_c = 10 000 Hz), and sometimes is very gradual (see f_c = 160 Hz). This effect is also a function of the center frequency of the input stimulus.

This critical band phenomenon can be interpreted as follows. As the bandwidth is increased, the upper frequency tone will be perceived to be noisier and the lower frequency tone will decrease in noisiness. These two effects tend to offset one another; thereby, approximately a constant total perceived noisiness is maintained until a critical bandwidth is reached where the upper frequency tone will become the controlling factor and the perceived sound level will increase. The upper frequency tone is the controlling one for center frequencies f_c below the peak frequency in the response function, that is, ≈3200 Hz; the lower frequency tone will control the perceived level for center frequencies above 3200 Hz. As expected from this model, with the center frequency at the peak in the response curve and with bandwidths greater than the critical band, the perceived level will decrease instead of increase. (See f_c = 2250 Hz and f_c = 3700 Hz in fig. 10.) It

is not known whether this effect has been observed before. Also, for Δf much greater than the critical bandwidth, the perceived levels will also begin to decrease. (For example, see f_c = 10 000 Hz.)

The critical bandwidth is critically dependent upon the rate of change of the response function with frequency, that is, $d\left\{|H(f)|^2\right\}/df$. Slight variations in the response function will produce significantly different results. This fact could account for the difference between the results obtained from the proposed model and the presently accepted values of the critical band. To illustrate these differences, the critical bands determined theoretically by the proposed method, with the aid of the modified response function of figure 9, are compared (fig. 11) with those experimentally determined by Zwicker, Flottorp, and Stevens (ref. 20) and Zwicker (ref. 21).

The most prominent features in these theoretically computed critical bandwidths are the large mid frequency bulge (between 200 and 1000 Hz) and the sharp "apparent" discontinuity in the frequencyregion on either side of the peak in the frequency response function. The low frequency bulge is due to the "flattening out" of the response function in the 200 to 1000 Hz range and, consequently, a steeper slope in the response function would greatly affect the critical band values in this frequency range.

The apparent discontinuity is due, in part, to a relatively flat portion of the response function in the range from 2700 to 3500 Hz and also to the slope of the response function in the frequency region on either side of peak in the response curve. A more peaked function and/or a function with a greater slope would greatly affect the theoretically determined bandwidths in this region. It must be remembered that the frequency response function presented herein was obtained by applying a smooth function to only nine data points within the frequency range from 50 to 12 000 Hz, and, furthermore, the equal noisiness curves were obtained with relatively large bandwidth signals; this would cause the validity of the assumption that $|H(f)|^2$ is constant within the band to be questioned. The frequency resolution is therefore very poor for this type of analysis. The proposed model suggests that the equal noisiness function (or loudness, etc.) should be determined with smaller bandwidths of the input acoustic stimulus at more closely spaced center frequencies within the audio range of interest. This would allow the frequency response function of the human auditory system to be determined with greater frequency resolution and accuracy.

CONCLUDING REMARKS

A model of the human auditory system was proposed to function as a simple input–output system. For a system of this type, the output (defined as the perceived sound) can be determined by multiplying the input acoustic stimulus by the square of the

complex frequency response function of the human auditory system. The results obtained through the use of this model are in agreement with results obtained in recent judgment tests. The small variability which is present in the predicted results (approximately 5 dB(J)) is considered to be insignificant in view of the extremely large variability which is inherent in most judgment test results (usually 10 to 20 dB).

The results of these studies suggest the following comments:

1. The human auditory system may be considered to function as a simple input-output linear system (at least for input sound pressure levels in excess of approximately 60 dB).

2. The results of the perceived sound which are obtained through the use of this model agree with judgment test results as well as or better than estimates obtained by the presently accepted methods.

3. A simple instrument may be built to obtain a direct on-line measure of the perceived sound as well as the spectral distribution of the perceived sound.

4. The proposed model provides an alternative interpretation of the critical bandwidth phenomenon.

5. The proposed model provides new insight into the operational aspects of the human auditory system.

6. The proposed model may eliminate the cumbersome and complicated procedures now used to compute the perceived sound.

REFERENCES

1. Stevens, S. S.: Calculation of the Loudness of Complex Noise. J. Acoust. Soc. Amer., vol. 28, no. 5, Sept. 1956, pp. 807-832.

2. Stevens, S. S.: Procedure for Calculating Loudness: Mark VI. J. Acoust. Soc. Amer., vol. 33, no. 11, Nov. 1961, pp. 1577-1585.

3. Zwicker, E.; and Feldtkeller, R.: Über die Lautstärke von Gleichfdrmigen Geräuschen. Acustica, vol. 5, no. 6, 1955, pp. 303-316.

4. Zwicker, E.: Uber psychologische und methodische Grundlagen der Lautheit. Akust. Beih., Heft 1, 1958, pp. 237-258.

5. Kryter, Karl D.: Scaling Human Reactions to the Sound From Aircraft. J. Acoust. Soc. Amer., vol. 31, no. 11, Nov. 1959, pp. 1415-1429.

6. Kryter, Karl D.; and Pearsons, Karl S.: Some Effects of Spectral Content and Duration on Perceived Noise Level. NASA TN D-1873, 1963.

7. Kryter, Karl D.: Evaluation of Psychological Reactions of People to Aircraft Noise. Alleviation of Jet Aircraft Noise Near Airports, Office Sci. Technol., Mar. 1966, pp. 13-27.

8. Pearsons, Karl S.; and Kryter, Karl D.: Laboratory Studies of Subjective Reactions to Sonic Booms. NASA CR-187, 1965.

9. Kryter, K. D.; and Pearsons, K. S.: Judged Noisiness of a Band of Random Noise Containing an Audible Pure Tone. J. Acoust. Soc. Amer., vol. 38, no. 1, July 1965, pp. 106-112.

10. Kryter, Karl D.: Review of Research and Methods for Measuring the Loudness and Noisiness of Complex Sounds. NASA CR-422, 1966.

11. Mintz, F.; and Tyzzer, F. G.: A Loudness Chart for Octave-Band Data on Complex Sounds. J. Acoust. Soc. Amer., vol. 24, no. 1, Jan. 1952, pp. 80-82.

12. Beranek, L. L.; Marshall, J. L.; Cudworth, A. L.; and Peterson, A. P. G.: Calculation and Measurement of the Loudness of Sounds. J. Acoust. Soc. Amer., vol. 23, no. 3, May 1951, pp. 261-269.

13. Churcher, B. G.; and King. A. J.: Performance of Noise Meters in Terms of the Primary Standard. J. Inst. Elec. Eng. (London), vol. 81, July 1937, pp. 57-90.

14. Fletcher, Harvey; and Munson, W. A.: Loudness, Its Definition, Measurement and Calculation. J. Acoust. Soc. Amer., vol. V, no. 2, Oct. 1933, pp. 82-108.

15. Anon.: Loudness Analyzer Model 8051A – A Powerful New Instrument for Noise Abatement Studies. Tech. Data, Hewlett Packard, Aug. 15, 1967.

16. Crandall, Stephen H.: Statistical Properties of Response to Random Vibration. Random Vibration, Stephen H. Crandall, ed., Technol. Press, M.I.T., and John Wiley & Sons, Inc., c.1958, pp. 77-90.

17. Kryter, K. D.; and Pearsons, K. S.: Modification of Noy Tables. J. Acoust. Soc. Amer. (Lett. to Ed.), vol. 36, no. 2, Feb. 1964, pp. 394-397.

18. Little, John W.: Human Response to Jet Engine Noises. Noise Contr. Shock Vib., vol. 7, no. 3, May-June 1961, pp. 11-13.

19. Stevens, S. S.: The Measurement of Loudness. J. Acoust. Soc. Amer., vol. 27, no. 5, Sept. 1955, pp. 815-829.

20. Zwicker, E.; Flottorp, G.; and Stevens, S. S.: Critical Band Width in Loudness Summation. J. Acoust. Soc. Amer., vol. 29, no. 5, May 1957, pp. 548-557.

21. Zwicker, E.: Subdivision of the Audible Frequency Range Into Critical Bands (Frequenzgruppen). J. Acoust. Soc. Amer. (Lett. to Ed.), vol. 33, no. 2, Feb. 1961, p. 248.

TABLE 1.- COMPARISON OF ASSESSMENT METHODS FOR NOISES JUDGED TO BE EQUALLY NOISY (ACCEPTABLE)

[An ideal assessment method should indicate same value for each indicated spectrum.
(From Kryter and Pearsons, ref. 6)]

Spectrum / Assessment method	1	2	3	4	5	6	7	8	9	Range	Average difference from standard
	Noise 150-30 Hz	Standard Noise 300-120 Hz	Noise 400-480 Hz	Noise 4800–10 000 Hz	Noise 150-4800 Hz "flat"	Noise 150–4800 Hz +6 dB/Oct slope	Noise 150–4800 Hz –12 dB/Oct slope	Diese engine	707-120B landing turbofan with hushkit		
Overall "flat", dB	92.0	90.0	80.5	80.0	80.5	83.0	84.5	81.0	80.0	12.0	-6.5
A scale, dB	82.0	90.0	19.0	14.5	19.5	81.0	80.5	79.0	80.0	15.5	-10.4
B scale, dB	90.5	90.0	18.5	15.0	19.5	81.0	83.0	84.5	80.0	15.5	-8.5
C scale, dB	92.0	90.0	19.5	16.5	80.0	81.5	84.5	81.0	80.0	15.5	–1.4
Stevens (averagea), phons	89.7	93.5	87.3	90.5	91.5	92.3	88.0	88.8	90.0	6.2	–3.8
Zwicker[b] 1/3-octave band, phons	92.5	91.0	87.0	89.0	95.5	96.5	95.5	95.0	95.5	10.0	-3.7
Kryter (averagea), PNdB	92.8	94.3	91.8	89.5	92.0	95.8	90.3	90.5	93.0	6.3	-2.3
Proposed, dB(J)	89.5	91.0	88.9	86.6	87.0	92.2	84.0	84.6	87.3	8.2	-3.4

[a] Average of octave and 1/3-octave band values.

[b] Calculated by E. Zwicker.

TABLE 2.- DIFFERENCE FROM STANDARD (COMPARISON MINUS STANDARD)

Spectra (from table 1	Prediction method	
	Kryter, PNdB (a)	Proposed, dB(J) (a)
	b94.3	b91.0
1	-1.5	-1.5
2	0	0
3	-2.5	-2.1
4	-4.8	-4.4
5	-2.3	-4.0
6	+1.5	+1.2
7	-4.0	-1.0
8	-3.8	-6.4
9	-1.3	-3.1
Average difference from standard	-2.3	-3.4

[a] + indicates overestimation;
- indicates underestimation.

[b] Level of standard.

TABLE 3.- RANK (ORDER OF NOISINESS) OF PERCEIVED SPECTRA

[Input spectra readjusted to constant OASPL value]

Rank of perceived spectra	Prediction method		Rank from judgment test (a)
	Kryter (a)	Proposed (a)	
Noisiest	9	6	4,9
	6	3	---
	6	9	3,5
	5	4	---
to	3		
	4	5	6
	7	7	8
	2	8	2
Least noisy	8 1	1	1

[a] Numbers refer to spectra in table 1.

TABLE 4.- COMPARISON OF ASSESSMENT METHODS FOR NOISES TO BE JUDGED EQUALLY NOISY

[An ideal assessment method should indicate same value for each indicated spectrum. (From Kryter, ref. 5)]

Indoor spectrum / Assessment method		B' Caravelle	C' Comet	D' 707-09	E' 707-15A	F' 707-22	Range	Average difference from standard
Kryter (octave band[b]), PNdB	94.0	89.8	88.2	90.0	86.6	89.7	7.4	-5.1
Proposed, dB(J)	87.8	82.6	81.5	82.9	80.0	82.9	7.8	-5.8

[a]Super-Constellation.

[b]Computed by using revised noy curves from Kryter and Pearsons (ref. 17).

TABLE 5.- DIFFERENCE FROM STANDARD (COMPARISON MINUS STANDARD)

Spectra (from table 4)	Prediction method: Kryter, PNdB (a)	Prediction method: Proposed, dB(J) (a)
	[b]94.0	[b]87.8
A	0	0
B	-4.2	-5.2
C	-5.8	-6.3
D	-4.0	-4.9
E	-7.4	-7.8
F	-4.3	-4.9
Average difference from standard	-5.1	-5.8

a - indicates underestimation.

b Level of standard.

TABLE 6.- RANK (ORDER OF NOISINESS) OF PERCEIVED SPECTRA

[Input spectra readjusted to constant OASPL value]

Rank of perceived spectra	Prediction method: Kryter (a)	Prediction method: Proposed (a)	Rank from judgment test (a)
Noisiest	D,F	F	E,F
	---	D	---
to	E	E	D
	C	C	C
	B	B	B
Least noisy	A	A	A

TABLE 7.- COMPARISON OF ASSESSMENT METHODS FOR NOISES JUDGED TO BE EQUALLY NOISY (ACCEPTABLE)

[An ideal assessment method should indicate same value for each indicated spectrum. Average judged results obtained through average of mean squared pressures. (From Kryter and Pearsons, ref. 6)]

Spectrum / Assessment method	1	2	3	4	5	6	7	8	9	Range	Average difference from standard
	Noise 150-300 Hz	Standard Noise 600-1200 Hz	Noise 2400-4800 Hz	Noise 4800-10000 Hz	Noise 150-480 Hz "flat"	Noise 150-4800 Hz +6 dB/Oct slope	Noise 150-4800 Hz -12 dB/Oct slope	Diesel engine	707-120B landing turbofan with hushkit		
Kryter (averagea), PNdB	94.3	94.3	92.7	92.8	93.3	97.2	91.3	92.7	95.7	4.5	-0.6
Proposed, dB(J)	91.0	91.0	89.8	89.9	88.3	93.6	85.0	86.8	90.0	6.0	-1.7

[a]Average of the octave and 1/3-octave band values.

TABLE 8.- DIFFERENCE FROM STANDARD (COMPARISON MINUS STANDARD)

Spectra from table 7)	Prediction method	
	Kryter, PNdB (a)	Proposed, dB(J) (a)
	[b]94.3	[b]91.0
1	0	0
2	0	0
3	-1.6	-1.2
4	-1.5	-1.1
5	-1.0	-2.7
6	+2.9	+2.6
7	-3.0	-6.0
8	-1.6	-4.2
9	+1.4	-1.0
Average difference from standard	-0.6	-1.7

[a] + indicates overestimation;
- indicates underestimation.

[b]Level of standard.

TABLE 9.- RANK (ORDER OF NOISINESS) OF PERCEIVED SPECTRA

[Input spectra readjusted to constant OASPL value]

Rank of perceived spectra	Prediction method		Rank from judgment test (a)
	Kryter, (a)	Proposed, (a)	
Noisiest	9	6	3
	6	3	5
	5	9	9
	3	4	4
to	4	5	6
	7	2	7
	2	7	8
	8	8	2
Least noisy	1	1	1

[a]Numbers refer to spectra in table 7.

TABLE 10.- COMPARISON OF ASSESSMENT METHODS FOR STIMULUS TO BE JUDGED EQUALLY NOISY

[Ideal method should indicate same value for each indicated stimulus. (From Kryter and Pearsons, fig. 8 of ref. 6)]

Stimulus	Prediction method	
	Kryter, PNdB	Proposed, dB(J)
S	90.5	89.5
C-1	92.5	90.5
C-2	88.0	88.7
C-3	84.0	87.5

TABLE 11.- DIFFERENCE FROM STANDARD (COMPARISON MINUS STANDARD)

Stimulus	Prediction method	
	Kryter, PNdB (a)	Proposed, dB(J) (a)
	[b]90.5	[b]89.5
S	0	0
C-1	+2.0	+1.0
C-2	-2.5	-0.8
C-3	-6.5	-2.0
Average difference from standard	-2.3	-0.6

TABLE 12.- COMPARISON OF ASSESSMENT METHODS FOR NOISES JUDGED TO BE EQUALLY NOISY (ACCEPTABLE)

[An ideal assessment method should indicate same value for each indicated spectrum. Average test values were obtained through the average of the mean squared pressures and by applying the response function of fig. 9. (From Kryter and Pearsons, ref. 6)]

Spectrum / Assessment method	1	2	3	4	5	6	7	8	9	Range	Average difference from standard
	Noise 150–300 Hz	Standard Noise 600–1200 Hz	Noise 2400–4800 Hz	Noise 4800–10 000 Hz	Noise 150–4800 Hz "flat"	Noise 150–4800 Hz +6 dB/Oct. slope	Noise 150–4800 Hz –12 dB/Oct. slope	Diesel engine	707–120B turbofan hushkit		
Kryter (averagea), PNdB	94.3	94.3	92.7	92.8	93.3	97.2	91.3	92.7	95.7	4.5	–0.6
Proposed, dB(J)	91.0	90.1	89.5	87.7	88.9	93.5	85.0	87.0	91.3	8.5	–0.9

TABLE 13.- DIFFERENCE FROM STANDARD (COMPARISON MINUS STANDARD)

Spectra (from table 12)	Prediction method	
	Kryter, PNdB (a)	Proposed, dB(J) (a)
	b94.3	b90.1
1	0.0	+0.9
2	0.0	0.0
3	–1.6	–0.6
4	–1.5	–2.4
5	–1.0	–1.2
6	+2.9	+3.4
7	–3.0	–5.1
8	–1.6	–3.1
9	+1.4	+1.2
Average difference from standard	–0.6	–0.9

TABLE 14.- RANK (ORDER OF NOISINESS) OF PERCEIVED SPECTRA

[Input spectra adjusted to constant OASPL value]

Rank of perceived spectra	Prediction method		Rank from judgment test (a)
	Kryter (a)	Proposed (a)	
Noisiest	9	3	3
	6	6	5
	5	9	9
	3	5	4
to	4	4	6
	7	2	7
	2	7	8
	8	8	2
Least noisy	1	1	1

[a]Numbers refer to spectra in table 12.

INPUT-OUTPUT CONCEPT OF HUMAN AUDITORY SYSTEM

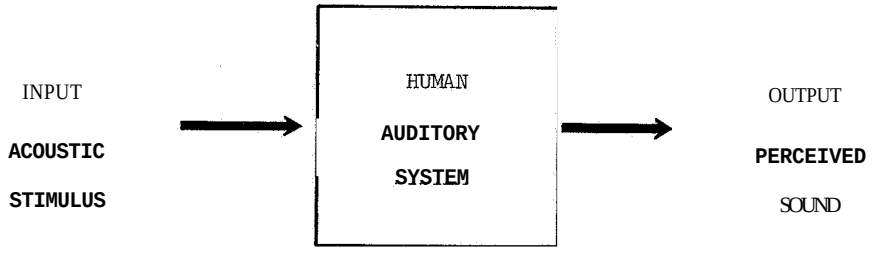

Figure 1

SCATTER BAND OF RELATIVE RESPONSE FUNCTION

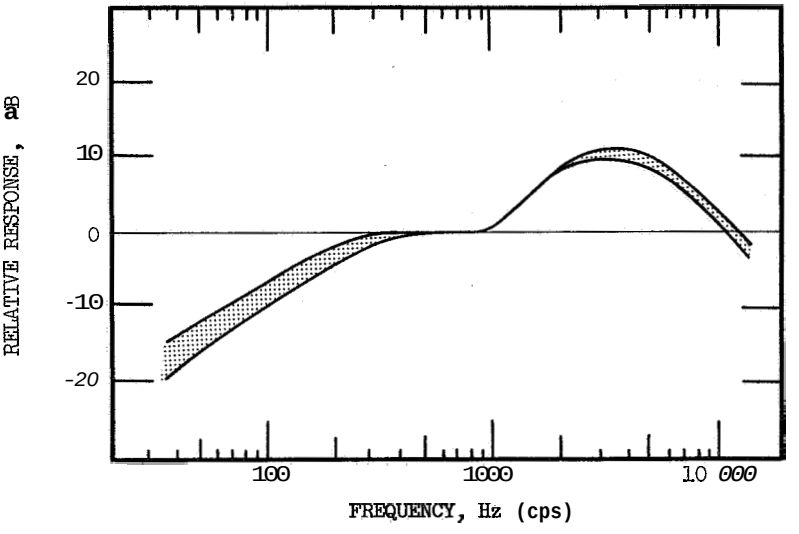

Figure 2

TYPICAL OR AVERAGE HUMAN AUDITORY RESPONSE FUNCTION (AVERAGE OF SCATTER BAND IN FIG. 2)

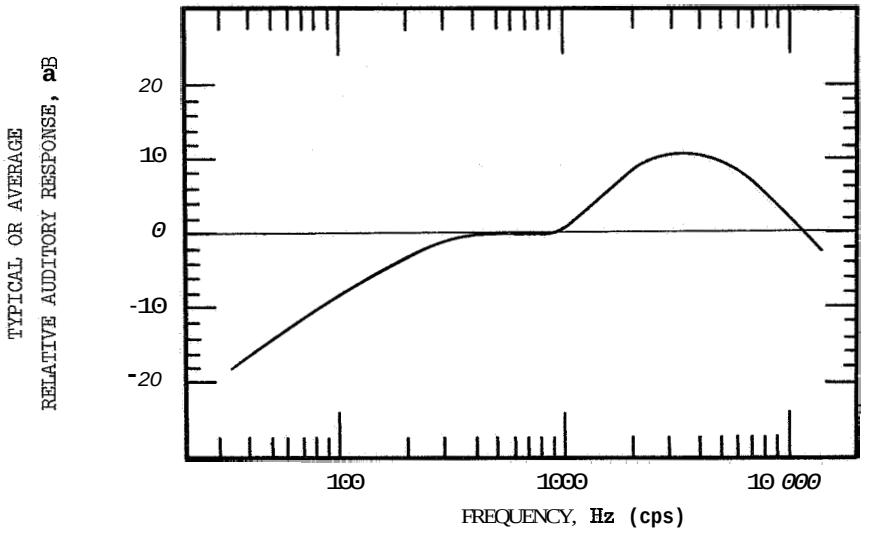

Figure 3

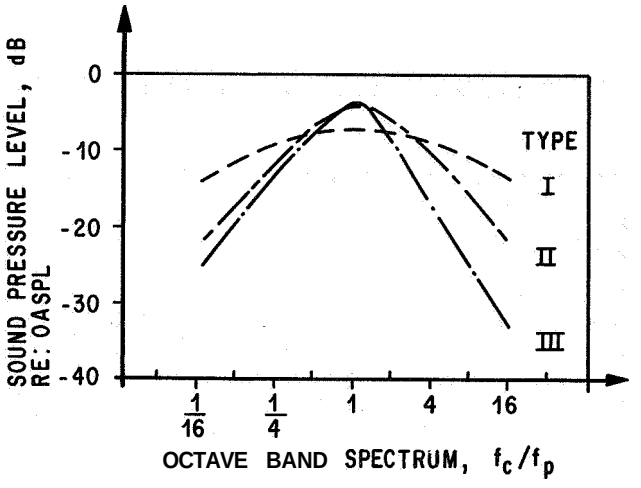
SOUND PRESSURE LEVEL, dB
RE: OASPL
0
-10
-20
-30
-40
TYPE
I
II
III
1/16
1/4
1
4
16
OCTAVE BAND SPECTRUM, f_c/f_p

(a)

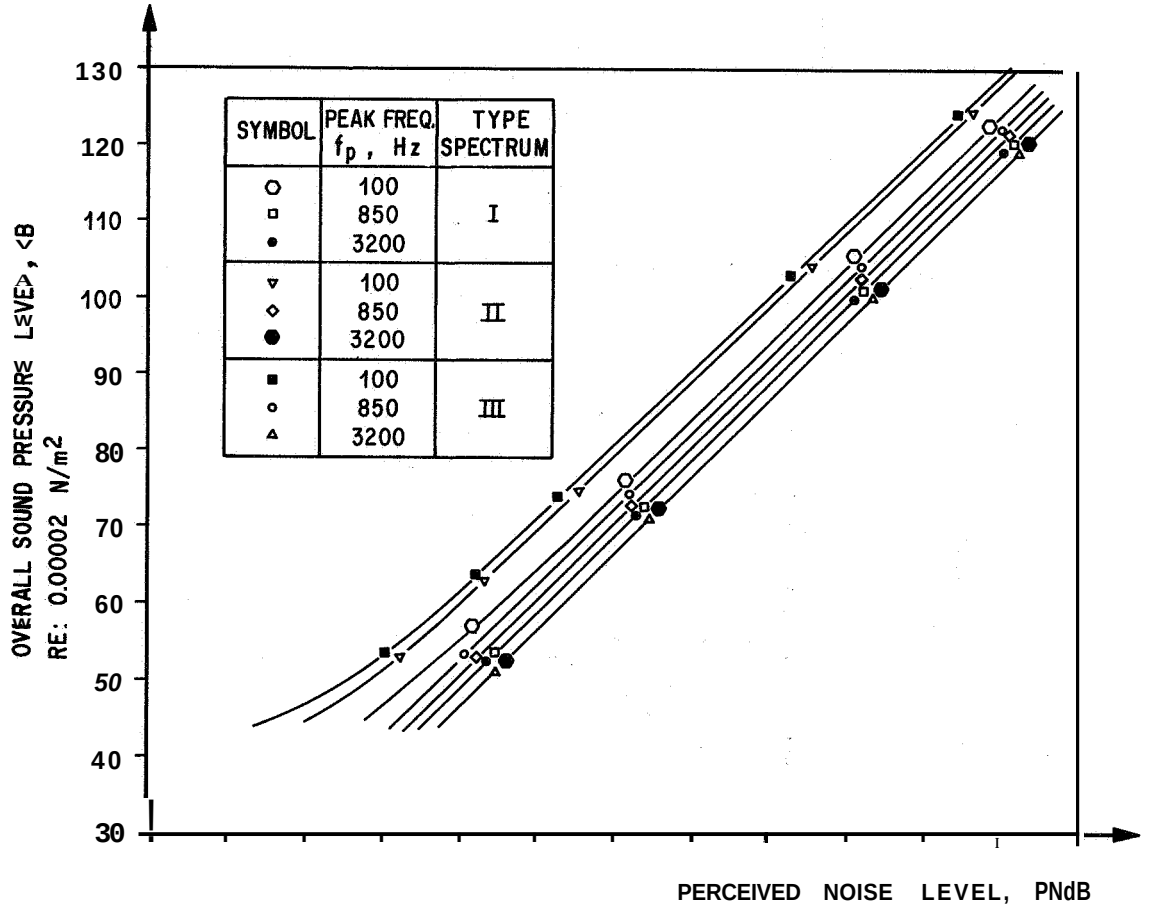
SYMBOL
PEAK FREQ. f_p, Hz
TYPE SPECTRUM
100
850
3200
I
100
850
3200
II
100
850
3200
III
OVERALL SOUND PRESSURE LEVEL, dB
RE: 0.00002 N/m2
130
120
110
100
90
80
70
60
50
40
30
PERCEIVED NOISE LEVEL, PNdB

(b)

Figure 4

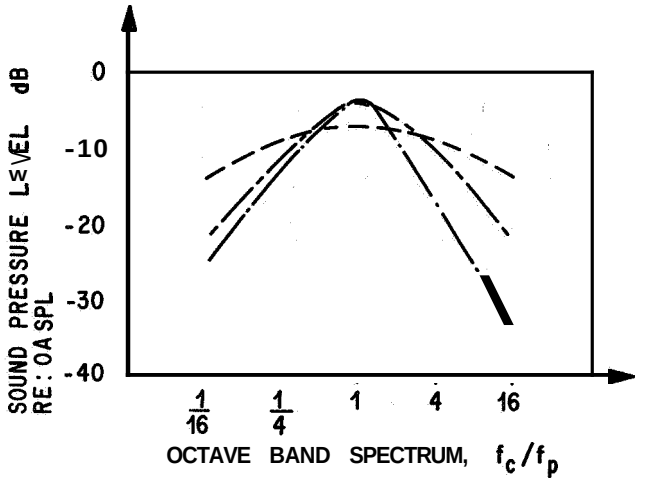
SOUND PRESSURE LEVEL dB
RE: OA SPL
0
-10
-20
-30
-40
1/16
1/4
1
4
16
OCTAVE BAND SPECTRUM, f_c/f_p

(a)

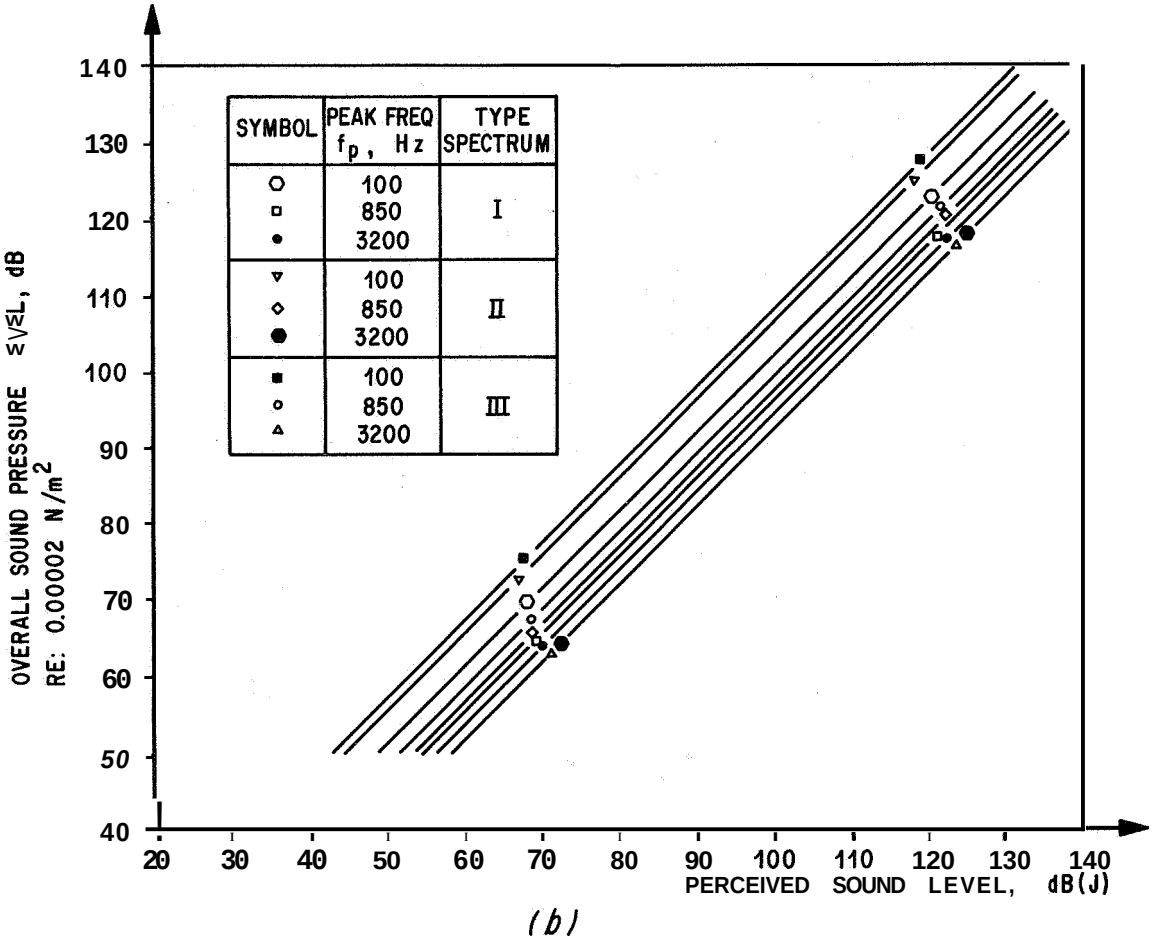
SYMBOL
PEAK FREQ f_p, Hz
TYPE SPECTRUM
100
850
3200
I
II
III
OVERALL SOUND PRESSURE LEVEL, dB
RE: 0.00002 N/m^2
140
130
120
110
100
90
80
70
60
50
40
20
30
40
50
60
70
80
90
100
110
120
130
140
PERCEIVED SOUND LEVEL, dB(J)

(b)

Figure 5

SPECTRA USED IN JUDGMENT TEST
(DATA FROM KRYTER AND PEARSONS, REF. 6)

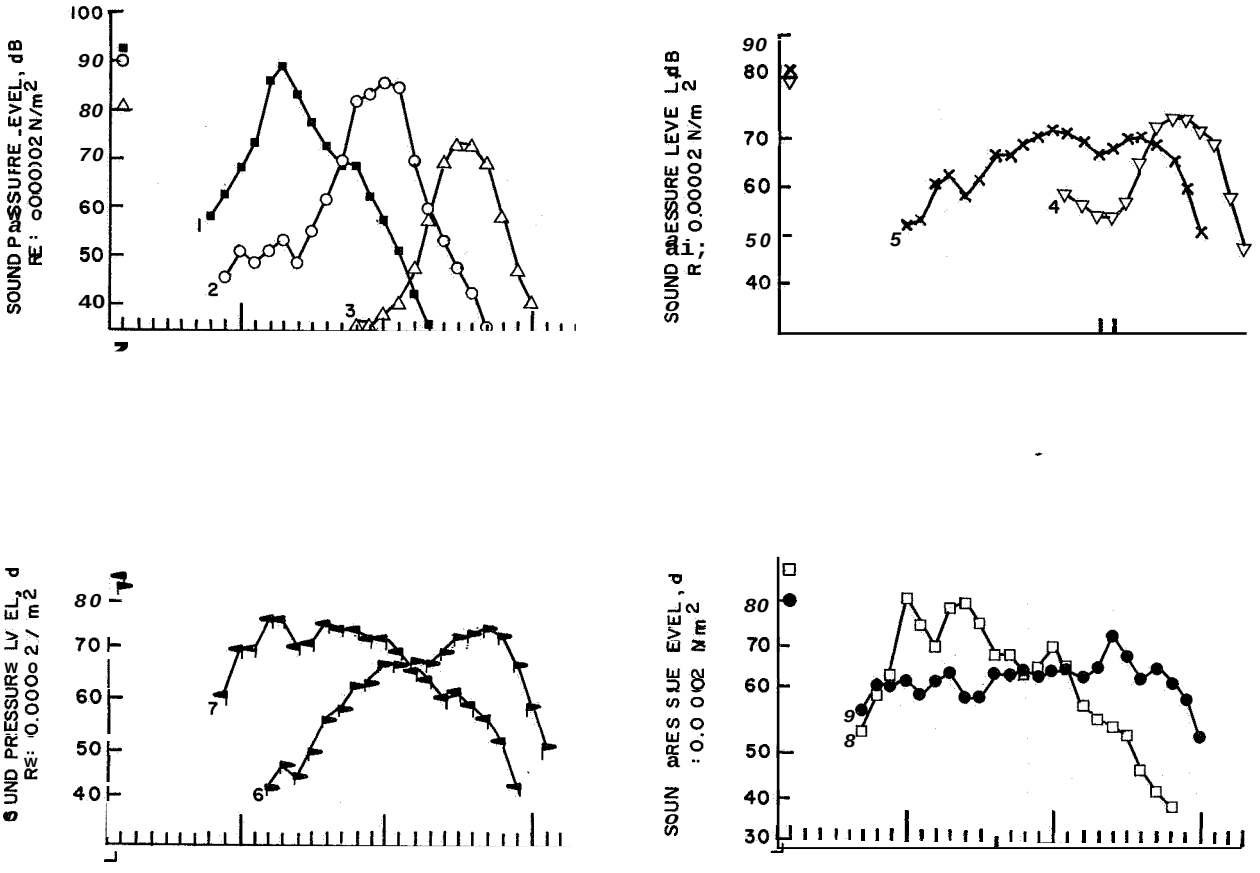

RESULTS OF JUDGMENT TEST FOR COMBINATION OF PURE TONE IN BAND OF NOISE
(DATA FROM KRYTER AND PEARSONS, REF. 6)

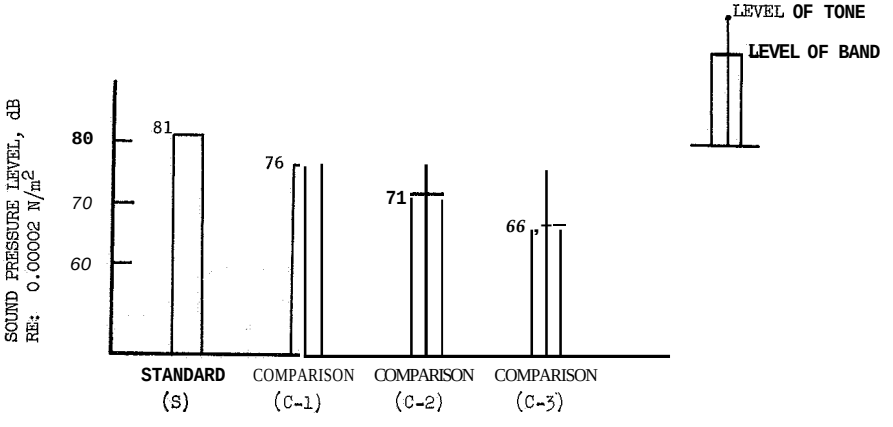

Figure 7

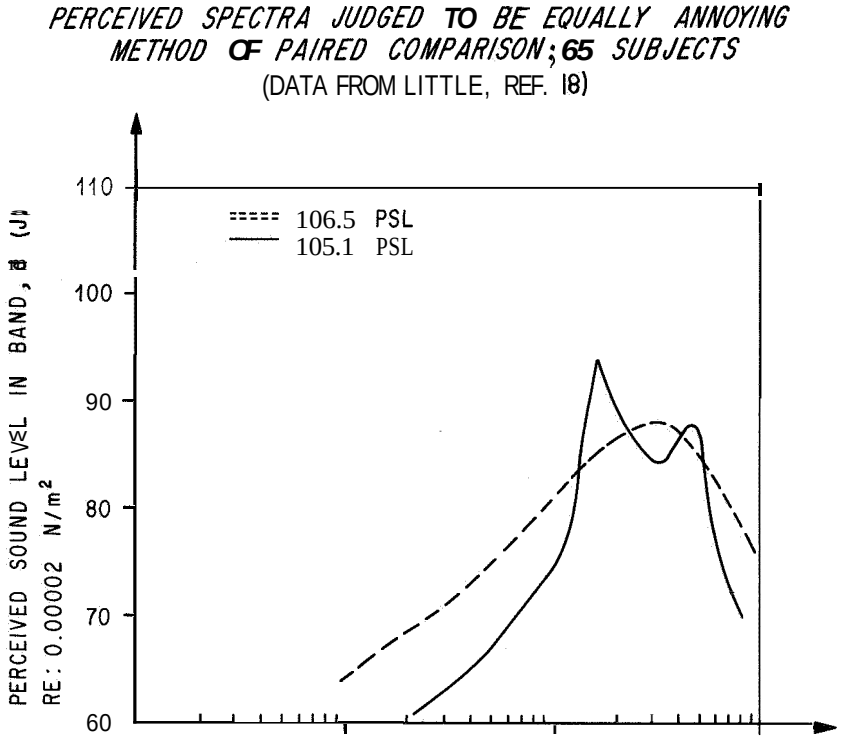

Figure 8

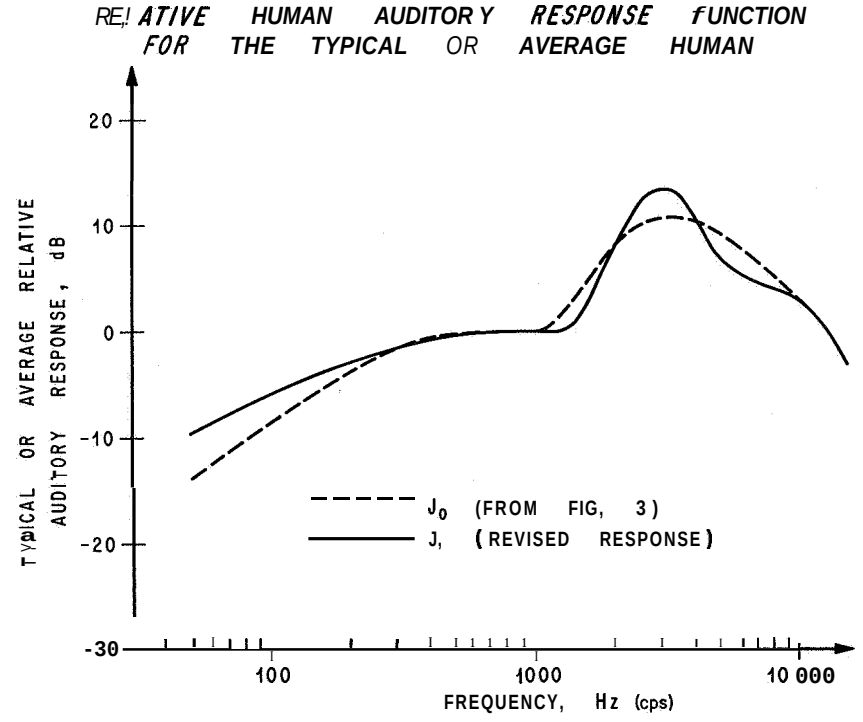

Figure 9

DEPENDENCE Of PERCEIVED **SOUND** *ON THE SPACING Of TONES IN A TWO-TONE COMPLEX FOR VARIOUS CENTER FREQUENCIES*

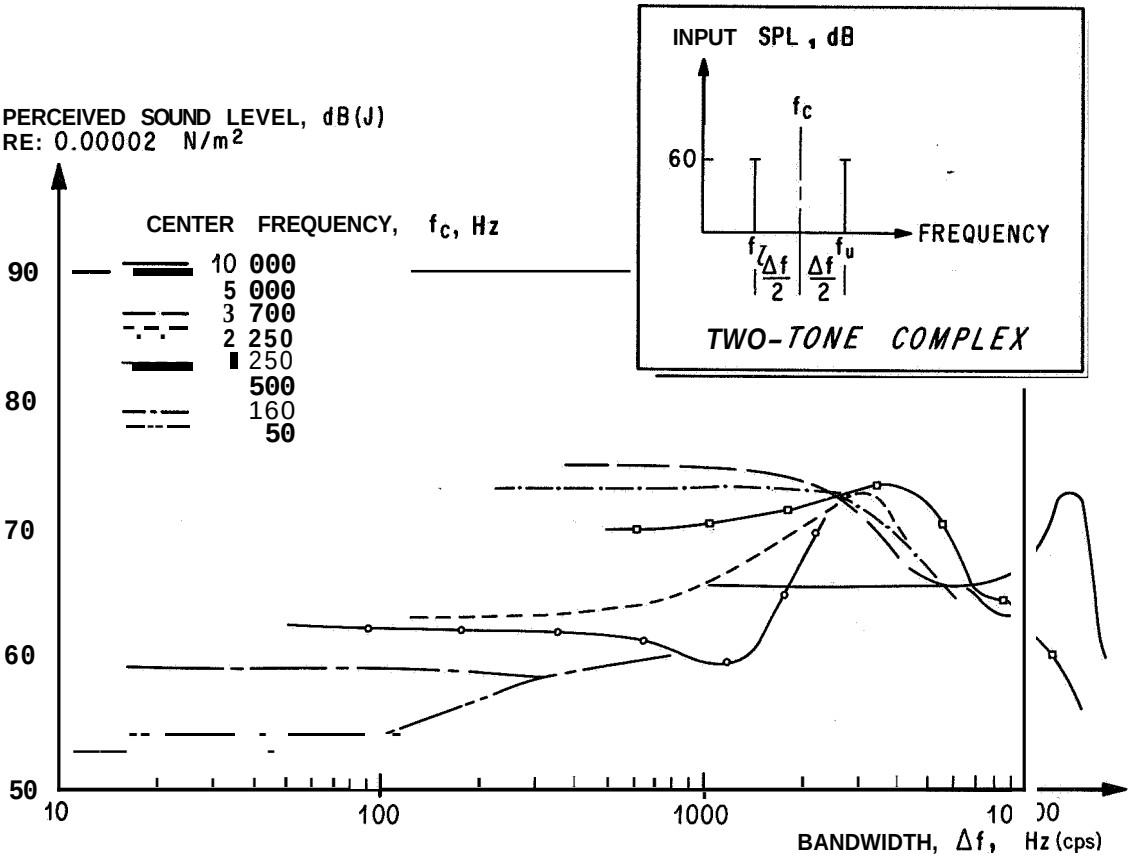

Figure 10

CRITICAL BANDWIDTH PRESENTED AS A FUNCTION OF CENTER FREQUENCY OF BAND

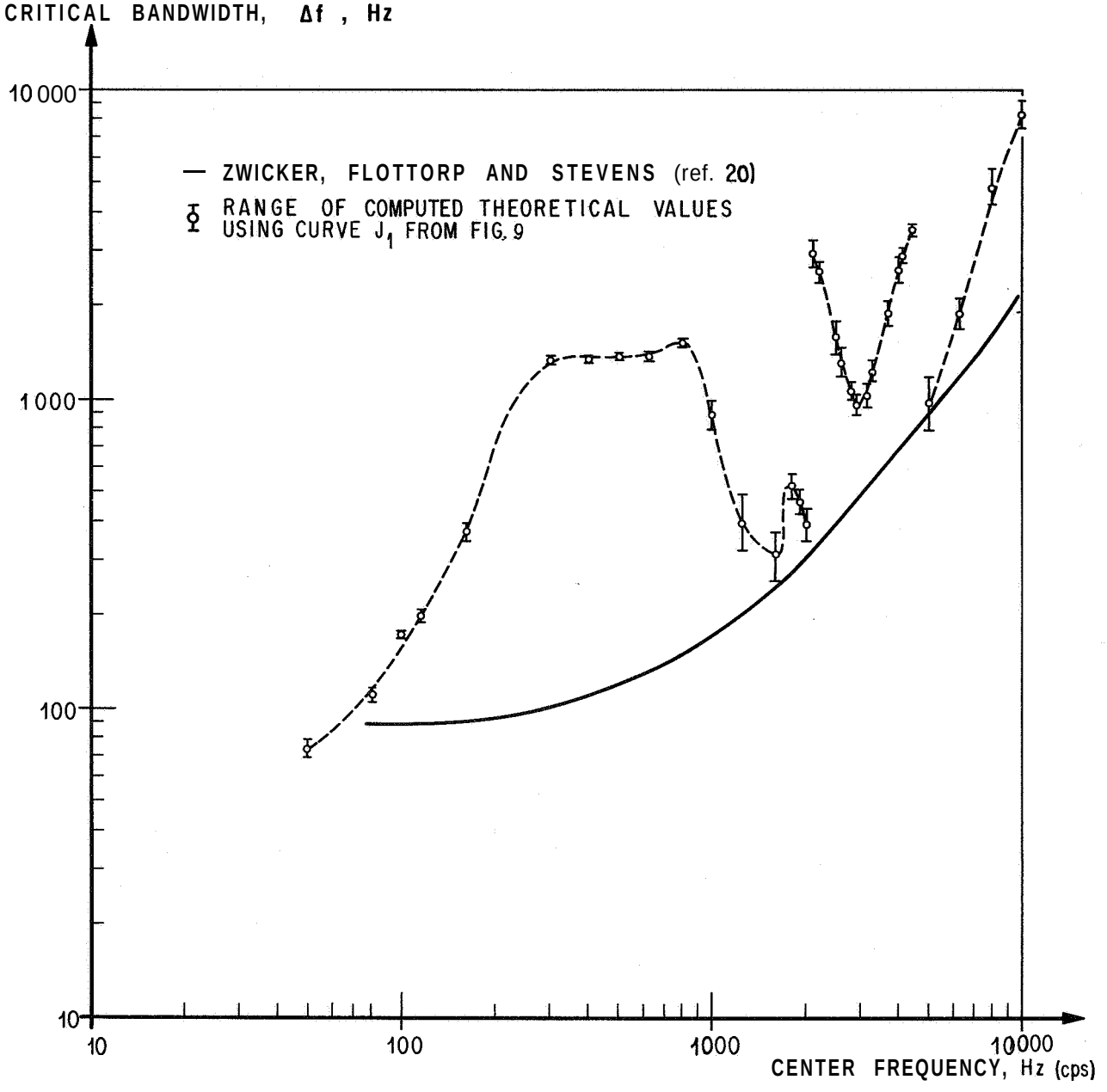

Figure 11

39. HOUSE VIBRATIONS SIGNIFICANT FOR INDOOR SUBJECTIVE RESPONSE

By William H. Mayes, Donald S. Findley,
and Huey D. Carden

NASA Langley Research Center

SUMMARY

An aircraft flyover is observed by a person inside a house in three ways: the acoustic transmission through the structure, the vibrations of the structure, and the noise radiated by decorative objects in contact with the structure. The average house structure provides from about 10 to 25 dB of noise reduction in the frequency range of 30 to 3000 Hz. The house vibration responses at the lower frequencies are associated with the framing members, whereas the vibration responses at the higher frequencies are associated with the window and wall panels. The indoor noise and vibration levels due to aircraft flyovers are of the same order of magnitude as those associated with rail and road traffic and normal household activities.

INTRODUCTION

One aspect of the aircraft noise problem involves people inside houses. The dynamic response of the house structure is important because it affects both the noise and vibration stimuli of the observers inside the house. The nature of the noise-induced house-structure response problem is illustrated schematically in figure 1. The aircraft noise excitation is evident to a person inside the house by means of three different phenomena. He hears the noise transmitted through the building walls; he can sense directly the vibrations of the various components of the house such as walls and ceilings; and he can hear the radiated noise from objects such as shelves, dishes, and ornaments, set in motion by the vibration of the walls with which they are in contact.

A programed overflight was conducted to study these phenomena at the NASA Wallops Station. Vibration response and noise transmission characteristics of two houses were investigated. The purpose of this paper is to discuss the results from this study for each of the three phenomena for aircraft noise excitation and to compare the associated responses with those from other noise sources.

EXPERIMENTAL STUDIES

Two of the houses used in aircraft noise reduction studies are shown in figure 2. One house was of brick-veneer construction with a concrete-slab foundation and steel casement windows; the other was of aluminum-siding construction with a cinder-block foundation and double-hung windows. Both houses were one-story six-room structures and had asphalt-shingle roofs with interior construction of sheet rock with plaster.

The houses were fully furnished and during test operations all windows and external doors were closed. Data were obtained for 10 different aircraft during flyovers at simulated landing approach and climbout thrust conditions at various altitudes.

Noise Reduction

An example of the manner in which the inside noise is related to the outside noise for the aluminum-siding house is shown in figure 3. One-third octave band spectra are plotted for measurement locations both inside and outside the house. These particular spectra are for a turbofan aircraft in the landing approach condition, It is obvious that the two spectra differ in several respects and that these differences result from the influences of the structure. A dominant feature of each spectrum, however, is a strong peak at about 2000 Hz. These peaks are associated with discrete-frequency noise from the fan sections of the engines. The differences between these two spectra indicated by the hatched region represent the noise reductions supplied by the structure at various frequencies. Noise reduction is plotted as a function of frequency in figure 4.

Noise reductions due to the house are seen to vary considerably with frequency. These variations with frequency are believed to be associated with the vibrational characteristics of the structure which are discussed subsequently in more detail. The average noise reduction increases generally as a function of frequency and varies from about 5 dB at the lower frequencies to about 20 dB at the higher frequencies, for this particular house.

A summary of the noise reduction data from this and other studies is included in figure 5. The range of noise reductions obtained in the present study is represented by the data between the solid curves. Similar data recorded in houses on the East Coast, the West Coast, and the Gulf Coast by other investigators (refs. 1 and 2) are included for comparison and are represented by the area between the dashed curves. The data of the present study overlap those of the previous studies; this suggests that the noise reduction characteristics of the test houses of figure 2 were roughly similar to those of houses in other regions of the country. The average noise reduction for all houses considered varies from about 10 dB to 25 dB in the frequency range of 30 to 3000 Hz.

The noise reduction of a house is believed to be a function of several variables such as type of construction, size and style, furnishings, windows and doors, workmanship, condition of materials, and age. Each of these may under certain circumstances be significant. In spite of the existence of many differences between houses, there also exist many similarities in dynamic behavior because of the common usage of standard size components such as beams, rafters, wall panels, and windows,

Vibration Responses

A series of experiments has been conducted to define the dynamic response characteristics of house components and to evaluate their responses to aircraft noise. One of the experiments involved the use of a mechanical shaker, as illustrated in the sketch of figure 6, to excite the structure with a sinusoidally varying load at a point on the wall for the purpose of defining its dynamic response characteristics. During these experiments the input force was varied both in frequency and in magnitude to study various response modes of the structure. The associated acceleration responses as functions of the input force are shown in figure 6 for one of these response modes at a frequency of 100 Hz. Acceleration response increases in a linear manner as the input force increases. Similar results were obtained for a range of response modes and for several different measurement locations.

During forced vibration tests, about a 2-pound force from the shaker resulted in vibrations over a large portion of the house which were of the same order of magnitude as those observed during aircraft flyovers. These results suggest that over the range of interest for aircraft-induced vibrations, the house structures behave essentially in a linear manner.

An example of the types of data obtained for a constant force input of a shaker as a function of frequency for the aluminum-siding house is shown in figure 7. Several response peaks can be seen in the acceleration spectrum of figure 7. Probe transducer surveys have made possible the definition of the mode shapes associated with many of these frequencies. Mode shapes for four vibration modes associated with the peaks labeled A, B, C, and D in figure 7 are shown in figure 8. The vibration modes of the building below approximately 100 Hz were associated mainly with the framing members such as wall studs and floor joists. Similar low-frequency response spectra have been obtained for many different houses. This similar response may be expected since houses are customarily built with standard size framing members.

No attempt was made to define in detail the mode shapes for the high-frequency portion of the spectrum of figure 7; such high-frequency modes involved mainly the window and wall panels. This general result for many houses is probably associated also with the use of standard size window and wall panels in house construction.

From a subjective reaction standpoint, high-frequency noise transmitted through the structure can be important; therefore, modifications to a house structure to attenuate high-frequency noise would involve considerations of the window and wall panels. Another source of high-frequency noise is the vibration and rattle of ornaments and fixtures attached to or in contact with a wall; this is a result of low-frequency wall motions. When the wall motions reach a given amplitude, such objects will vibrate at frequencies higher than the wall frequencies and in a range readily observable as rattles.

Noise-Induced Rattle

A specific example of a rattle situation involving wall mounted plaques is illustrated in figure 9. Wall acceleration level as a function of frequency is given for two types of excitation. The solid curve with hatching represents a rattle boundary established by tests with the use of a mechanical shaker, illustrated in the sketch. For wall accelerations exceeding those of the boundary at the frequencies indicated, the plaques will rattle in an annoying manner. Shown for comparison is an acceleration spectrum measured at the same instrument location for an aircraft flyover. The aircraft-noise-induced accelerations exceeded those of the rattle boundary and the plaques rattled. Such a rattle situation is a classical example of nonlinear dynamic responses where the excitation of a structure by one frequency results in responses at a different frequency.

COMPARISON OF VIBRATION AND NOISE LEVELS FROM AIRCRAFT AND OTHER SOURCES

A comparison of the wall vibration levels of houses due to aircraft noise with vibrations as a result of other common events is given in figure 10. The bars indicate the ranges of wall acceleration level for each of the events listed. Also indicated, as a matter of interest, are the vibration levels associated with perception and onset of annoyance from experience with continuously operating rotating machinery (ref. 3). Comparable perception and annoyance levels for flyover noise-induced transients have not yet been defined. The aircraft-noise-induced vibrations are of the same order of magnitude as those associated with rail and road traffic and normal household activities; acceleration levels associated with loud hi-fi operations are the most severe to which house structures are exposed.

Similar results are presented in figure 11 for the indoor noise levels associated with the same events of figure 10. The sound pressure levels from all these events exceed normal speech levels; hence, occasional speech interference would be encountered. The highest sound pressure levels were associated with loud hi-fi operations.

CONCLUDING REMARKS

An aircraft flyover is observed by a person inside a house in three ways: the acoustic transmission through the structure, the vibrations of the structure, and the noise radiated by decorative objects in contact with the structure. The average house structure provides from about 10 to 25 dB of noise reduction in the frequency range of 30 to 3000 Hz. The house vibration responses at the lower frequencies are associated with the framing members, whereas the vibration responses at the higher frequencies are associated with the window and wall panels. The indoor noise and vibration levels due to aircraft flyovers are of the same order of magnitude as those associated with rail and road traffic and normal household activities.

REFERENCES

1. Anon.: Methods for Improving the Noise Insulation of Houses With Respect to Aircraft Noise. Rep. 1387 (Contract FH-941), Bolt Beranek and Newman Inc., Nov. 1966.
2. Bishop, Dwight E.: Reduction of Aircraft Noise Measured in Several School, Motel, and Residential Rooms. J. Acoust. Soc. Amer., vol. 39, no. 5, May 1966, pp. 907-913.
3. Rathbone, Thomas C.: Human Sensitivity to Product Vibration. Prod. Eng., vol. 34, Aug. 5, 1963, pp. 73-77.

NATURE OF THE PROBLEM

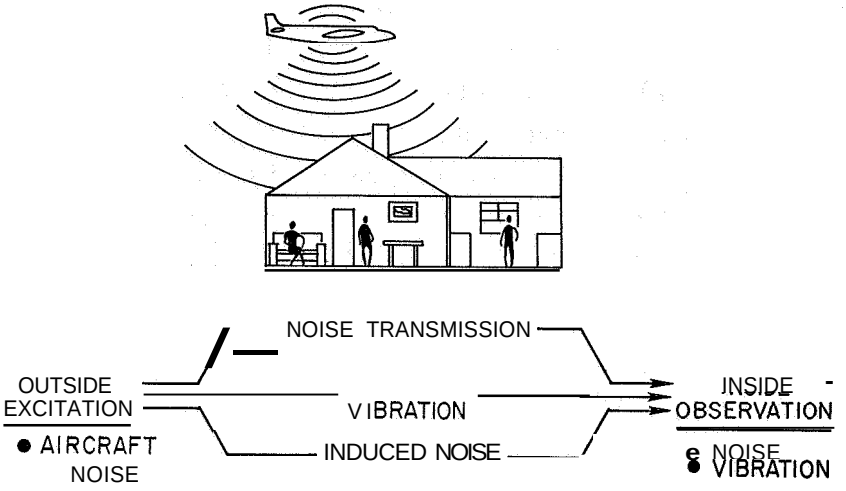

Figure 1

TEST HOUSES

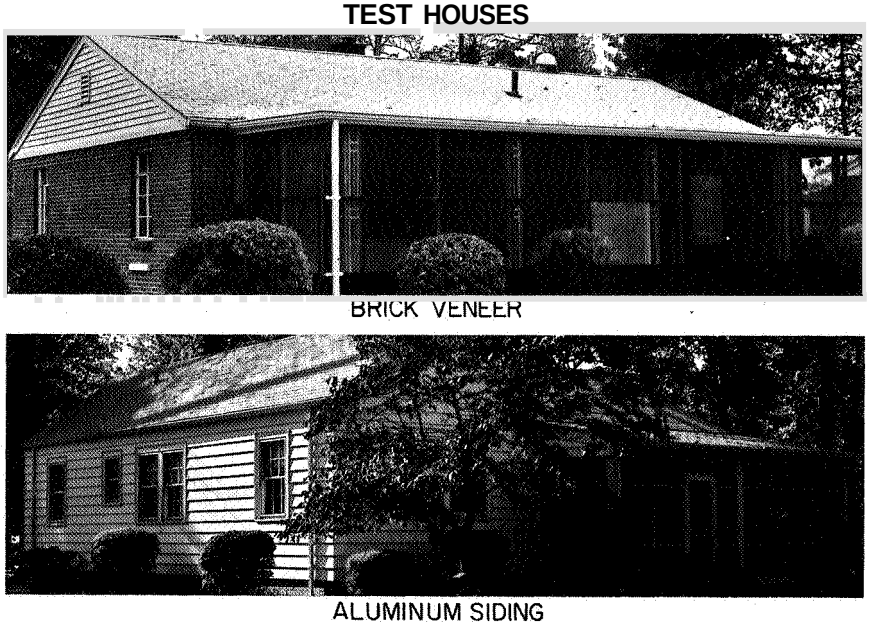

L-68-8586

Figure 2

EXAMPLE OF AIRCRAFT NOISE SPECTRA

ALUMINUM SIDING

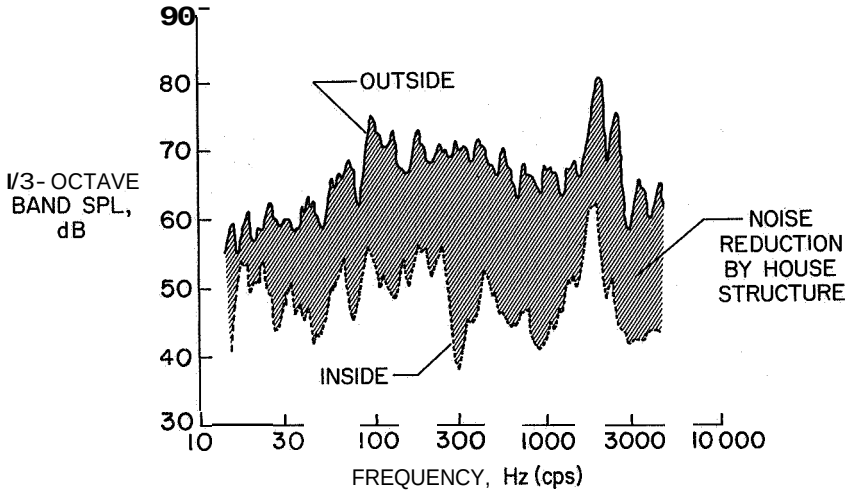

Figure 3

NOISE REDUCTION BY HOUSE STRUCTURE

ALUMINUM SIDING

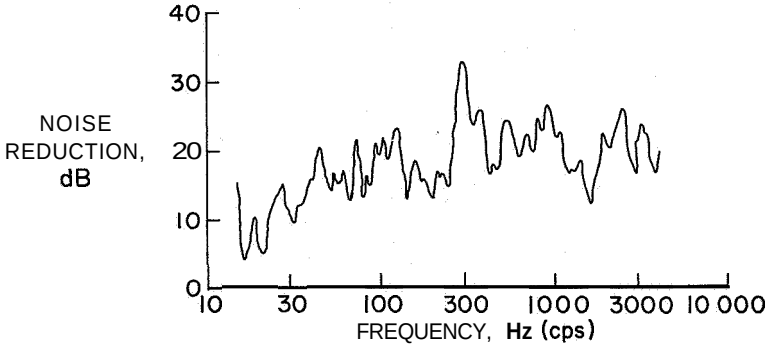

Figure 4

SUMMARY OF NOISE REDUCTION BY HOUSE STRUCTURES

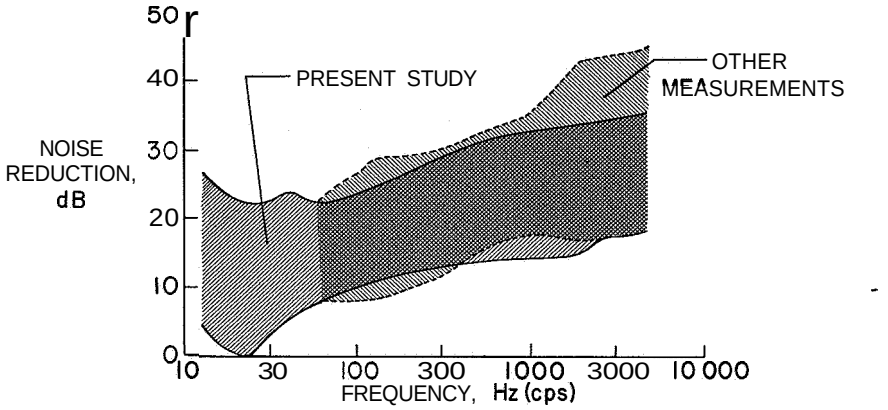

Figure 5

WALL ACCELERATION RESPONSES

MECHANICAL EXCITATION; FREQUENCY□100 Hz

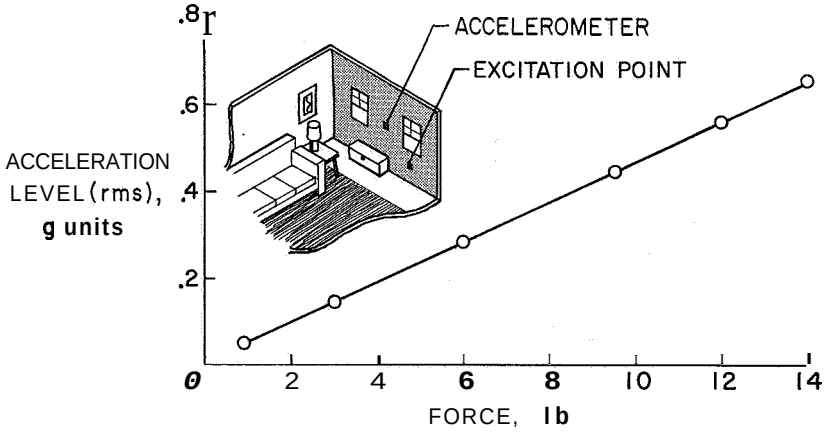

Figure 6

WALL ACCELERATION RESPONSES

MECHANICAL EXCITATION FORCE = 1.5 lb

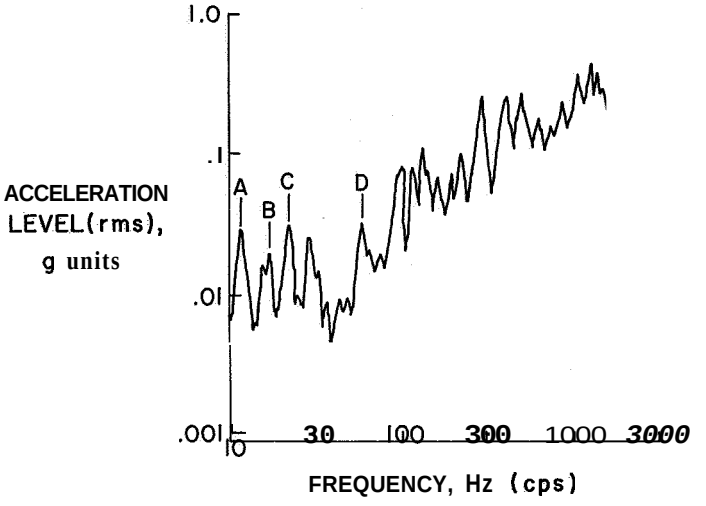

Figure 7

WALL-VIBRATION MODE SHAPES

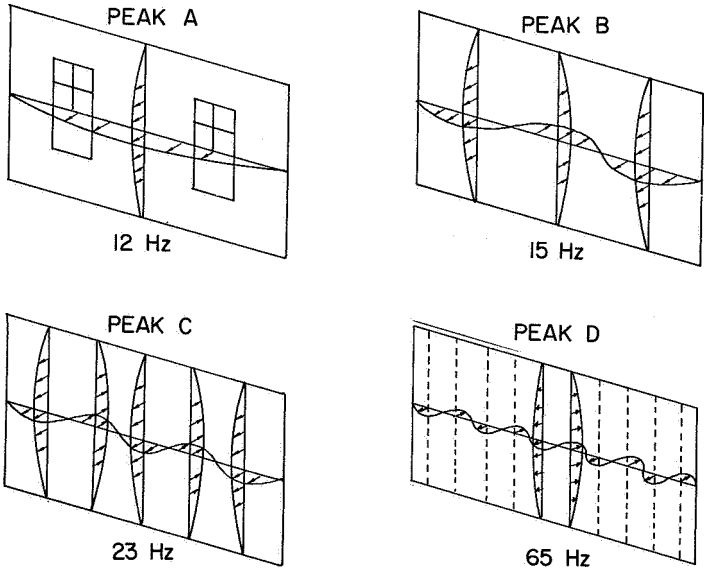

Figure 8

EXAMPLE **OF** RATTLE

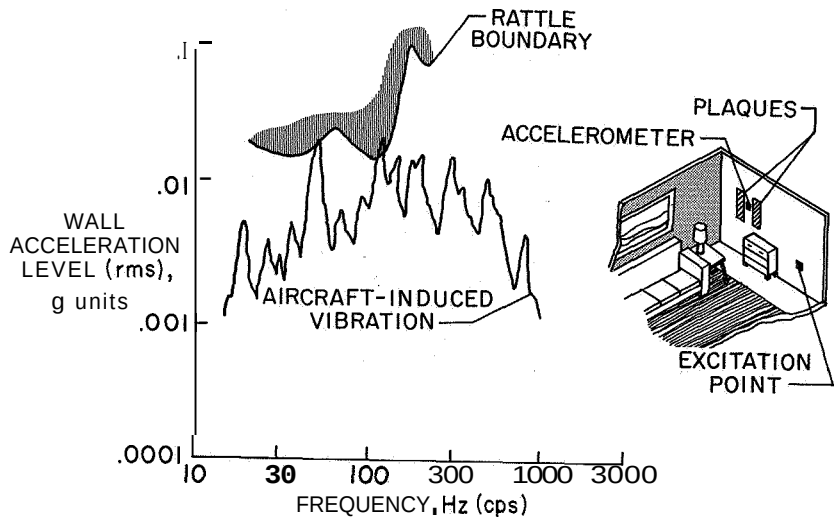

Figure 9

MEASURED INDOOR VIBRATION LEVELS

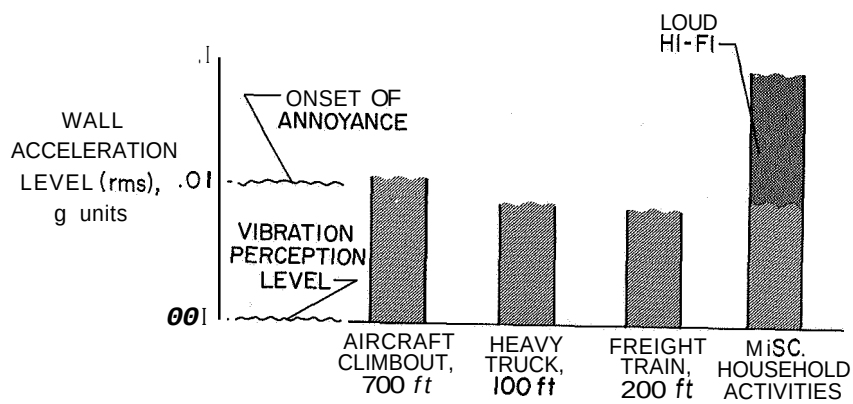

Figure 10

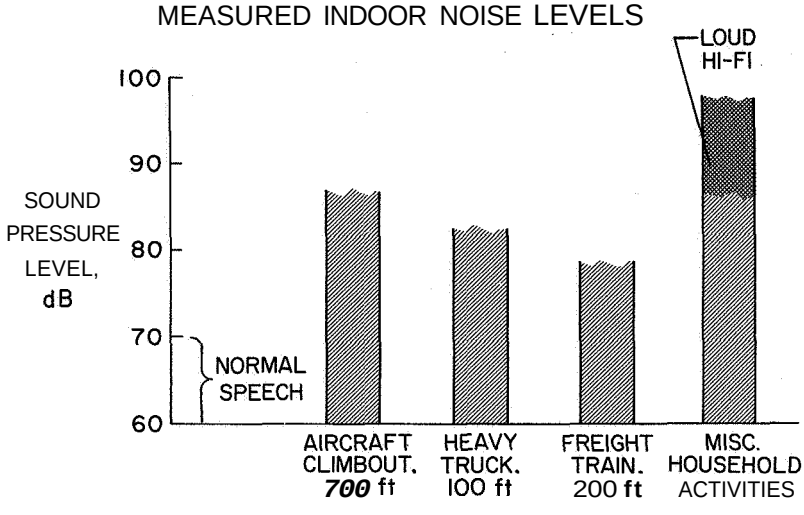
MEASURED INDOOR NOISE LEVELS
LOUD HI-FI
100
90
80
70
60
SOUND PRESSURE LEVEL, dB
NORMAL SPEECH
AIRCRAFT CLIMBOUT, 700 ft
HEAVY TRUCK, 100 ft
FREIGHT TRAIN, 200 ft
MISC. HOUSEHOLD ACTIVITIES

Figure 11

40. COMMUNITY REACTIONS TO AIRCRAFT NOISE

NOISE MEASUREMENTS

By William K. Connor

TRACOR, Inc.

SUMMARY

Aircraft noise measurements were made in communities exposed in varying degrees to the noise of flight operations from major airports. The primary purpose of these measurements was to define the noise exposure for a 3-month period in areas for which social data were also obtained by means of interviews. The acoustical and social data are being used in a study of community reaction to aircraft noise. Further data must be taken before an extensive analysis is performed. A secondary purpose of the noise measurement program was to evaluate, in a community context, noise level estimates obtained from the guide "Land Use Planning With Respect to Aircraft Noise." A comparison of measured noise levels with the estimates revealed no inconsistencies in 85 percent of the cases examined, and the discrepancy was in no case greater than 10 PNdB. The noise data also afforded a comparison of several acoustical parameters which are used as measures of aircraft noise. For such community data, there was a standard deviation of 3 units or less between any two parameters, except for certain pairs including speech interference level.

INTRODUCTION

This paper and reference 1 describe a current program of research concerning community reaction to aircraft noise (under Contract NASw-1549). Although procedures for computing psychophysical parameters of aircraft noise are well developed (ref. 2), there as yet exists no methodology capable of accurately predicting the reaction of individuals or groups to a given noise exposure. Annoyance resulting from aircraft noise has been known to vary from one person or community to another under identical exposure conditions. The social and psychological factors which may account for such variations are the central focus of this study.

The paper at hand deals with the aircraft noise exposure data related to this study. The social data and analysis are discussed in the coordinate paper by Hazard (ref. 1).

DISCUSSION

Survey Program

The plan of research requires that both social and acoustical data be taken around several major commercial airports located in cities of the United States. The areas in which such data were acquired were confined to within a 12-mile radius of the airport in question. A further delineation of survey areas was made by using a sampling plan which selected a balanced cross section of the population from the standpoint of socioeconomic and noise exposure variables.

The actual sample ultimately consisted of from 11 to 22 census tracts in each city. Many of these census tracts were situated more or less on a line extended from the ends of principal runways. The noise exposure in such tracts tended to be due-largely to aircraft flyovers associated with the particular runway. In other sample areas located within 3 miles of the airport, noise exposure was due to a combination of flyovers, other flight operations, and ground operations. The sample tracts were surveyed by both social and acoustical scientists, but not necessarily at the same time.

The program is comprised of two active phases of approximately 1 year each. In the first phase, four cities were surveyed in the summer of 1967. In the second phase, not yet begun, data will be obtained in three more cities. Only a preliminary analysis has been made of the data now available. A comprehensive analysis culminating in major conclusions can be performed only after the survey data from all seven cities are available.

Exposure to Aircraft Noise

Requirements for acoustical data.- The primary function of the acoustical measurements is to define the aircraft noise exposure for each of the sample areas for a period of at least 3 months immediately prior to the social survey. This minimum period was agreed upon in consultation with other scientists active in the general field of human reaction to noise. It was also agreed that the best formulation of long-term aircraft noise exposure was in terms of PNdB with corrections for discrete frequency components, This formulation requires that the acoustical data be analyzed by using bands no wider than 1/3 octave and that the noise be sampled at least once per second in real time. A secondary purpose of the field measurements is to obtain some validation of the aircraft noise level contours in the guide "Land Use Planning With Respect to Aircraft Noise" (ref. 3), hereinafter referred to as "Land Use Planning." The fundamental question to be answered is, "How do noise levels predicted on the basis of the guide compare with levels measured in various communities?" Obviously, the usefulness of the guide is contingent upon the answer to this question.

Data acquisition.- The acoustical data requirements entailed tape recording of aircraft noise at the various survey sample areas in each city. The recording systems incorporated automatic electrical calibration after each noise recording and a 48-interval time-of-day encoded signal. Both calibration and time signals were recorded on the data tapes. The recording site, apparent aircraft operations (when visible), and general observations were logged and keyed to the data tape reels. An additional feature of the recording systems was an automatic monitor and control unit whereby recording was initiated when the A-weighted sound pressure level (SPL) exceeded a preset value. A member of the measurement team was in attendance at all times, however.

Data processing.- The large amount of recorded acoustical data necessitated automatic analysis. An analog/digital system built for this purpose is shown in block-diagram form in figure 1. The system output, in digital tape form, consists of SPL's in each of twenty-four 1/3-octave bands (as well as A-weighted (ref. 4) and N-weighted (ref: 5) SPL's) for each second of analog data tape, together with appropriate identification and index markers. These data were further processed with a series of routines on the UNIVAC 1108 computer to produce a second set of digital tapes which contained the values of a number of psychophysical parameters (perceived noise levels in PNdB (refs. 6 and 7), with and without corrections for discrete frequency components; loudness level in phons (ref. 8); speech interference levels; etc.), again for 1-second sampling intervals. These tapes also included values of peak levels, durations of various parameters above given thresholds, and other pertinent information.

Determination of noise exposure.- It was impossible for several reasons to sample aircraft noise continuously in each survey tract over the entire 3-month period of interest. Therefore, the procedure shown in block form in figure 2 was used in the process of computing long-term noise exposure. Noise data were taken in as many tracts as possible under known airport operating conditions. These conditions included the type of operation of heavy aircraft (landing or take-off) as well as the runway usage during each noise-recording period.

Hourly wind data for the 3 months of interest, together with information from the airport control-tower staff concerning local runway-assignment practices as related to wind conditions, were processed with a simple computer routine to determine runway usage over the 3-month period. This usage factor was multiplied by the airport operations count (a function of time of day) to obtain the number and type of heavy-aircraft operations utilizing each runway according to time of day, averaged over the 3-month period. An additional weighting factor related to flight path made it possible to obtain the average number of operations passing over or near each sample tract.

The average number of operations and the maximum PNL occurring during each particular type of operation were combined into the following noise exposure index for use in the preliminary analysis of the combined social and acoustical data:

$$\text{Exposure index} = \text{PNL} + A \log_{10}\left(N_{day} + BN_{night}\right)$$

where

PNL — maximum measured flyover perceived noise level, energy-averaged for all observed flyovers of a particular type

N_{day}, N_{night} — number of daytime, nighttime flyovers of the particular type

A,B — constants

This index is a general case of the composite noise rating (CNR) formulation (ref. 3), which has had considerable use. A value (or set of values) was assigned to each sample tract which was surveyed in the field study. (In actuality, one further step was involved in determining the noise exposure values: The indices for all aircraft operation types affecting each tract were combined on an energy-addition basis.)

For some tracts, noise data could not be obtained in the field for all operating conditions. However, it was usually possible in these cases to use data taken at a site symmetrically opposite the airport. These data were applicable to the subject tract when the direction of aircraft operations was reversed. If no field noise data whatsoever could be obtained, noise contours for the most prevalent aircraft types taken from "Land Use Planning" were used to estimate maximum flyover levels.

Results of Preliminary Analysis

Aircraft operations data.- A plot of the aircraft operations count as a function of time of day for each of the four airports studied thus far is shown in figure 3. Although the airports varied considerably in size, the daily pattern of operations was remarkably uniform from one to another. This pattern may be partially attributed to public travel requirements. It is also noteworthy that nighttime operations, which are known to produce considerable annoyance and complaints, represent only a small fraction of the total number.

Noise level data.- The aircraft noise recorded at the various survey sites, after the processing described previously, was analyzed to find the maximum PNL value for each flyover. The results were plotted for each of 73 original data tape reels in the form of a distribution. Two such distributions are shown in figures 4 and 5. Each distribution applies to a single survey site and usually to a particular known mode of operation of

the airport. Corrections for discrete frequency noise components were not included in these PNL values, in order to make possible a direct comparison with the uncorrected PNL's of the "Land Use Planning" contours. The energy averages of these distributions were used in computing the noise exposure indices for the various survey tracts according to the formula given in a foregoing section.

An interesting aspect of the PNL distributions is the variation in their shape from one survey tract to another. In some (fig. 4), there is a highly peaked distribution, which indicates a predominance of aircraft noise from a single type of operation (and aircraft). In others (fig. 5), there is a quite broad distribution, which perhaps indicates contributions from aircraft operations on more than one runway as well as variations in aircraft, flight procedure, trajectory, and so forth. The procedure of energy averaging, although consistent with accepted practice, places the greatest emphasis upon the highest observed PNL values in these distributions. In consequence, essentially no effect is attributed to flyover noise much below the highest level. It would seem that a number of flyovers with maximums of 90 PNdB are significant in terms of human annoyance even if an equal number attained 100 PNdB. Therefore, further analysis of the data will include formulations for correlation with annoyance measures derived from the social data which give greater weight to the less noisy flyovers above a certain threshold level.

For each of the PNL distributions, estimates of the noise maximums were made by using the "Land Use Planning" contours for civil aircraft ranging from four-engine piston and turboprop aircraft to four-engine jet aircraft. These estimates were based upon the operations proximal to the recording site under the prevailing wind conditions. The range of these estimates is shown above the plots of figures 4 and 5 for comparison. A positive indication of inconsistency between the predicted and the measured levels is for the latter to exceed the former significantly. (The reverse situation may mean only that the noisier aircraft or operations are not represented.) Such an indication was present in 11 of the 73 distributions. The maximum difference between the highest predicted and the highest measured levels was 10 PNdB. It may be concluded that the "Land Use Planning" contours afford a reasonably good estimate of aircraft noise levels provided that vagaries of local operation are known and taken into account.

Comparison of noise parameters.- The format of the analyzed, computer-processed acoustical data made possible a ready comparison of several noise parameters associated with effects on humans. Similar comparisons have been made (refs. 9, 10, and 11), but not for so large a mass of data (about 4730 flyovers) or for acoustical data so well-distributed over a wide range of community exposure conditions. Some of the parameters to be compared herein are defined for the present purpose as follows:

PNdB1 maximum flyover PNdB value computed (with pure tone corrections) from 1/3-octave band data sampled once per second

PNdB2 PNdBl without pure tone corrections

PNdB3 PNdB value computed (without pure tone corrections) from maximum flyover levels occurring in each 1/3-octave band (not necessarily simultaneously), sampled once per second (ref. 12)

PHONS maximum flyover value of loudness level computed according to Stevens' Mark VI method (ref. 8)

dBN maximum flyover SPL weighted according to inverse of 40-noy contour (ref. 5); zero reference at 1 kHz

dBA maximum flyover A-weighted SPL (ref. 4)

SIL maximum flyover speech interference level (arithmetic average of SPL's in the 1-kHz, 2-kHz, and 4-kHz octave bands)

The numerical differences between the values of every pair of these parameters were analyzed for approximately 4730 recorded flyovers. The results are shown in matrix form in the following table:

	PNdB2	PNdB3	PHONS	dBN	dBA	SIL
PNdB1	2.6/1.4*	1.2/1.5	4.1/2.6	9.7/2.6	14.2/3.0	25.0/2.8
PNdB2	-------	-1.4/1.0	1.5/1.7	7.1/1.8	11.6/2.2	22.4/2.9
PNdB3	-------	--------	2.9/1.8	8.4/1.9	13.0/2.4	23.8/3.1
PHONS	-------	--------	------	5.5/1.8	10.1/2.0	20.8/3.8
dBN	-------	--------	------	------	4.6/2.1	15.3/3.9
dBA	-------	--------	------	------	-------	10.8/3.8

*Average for all flyovers of (value in left-hand column minus value of row parameter)/standard deviation.

The usefulness of each noise measure as applied to community-wide aircraft noise is apparent from the data of the table. It can be seen that the three PNdB-type measures correlate with one another quite well; the spread is no larger than that normally encountered in the data of psychophysical comparisons of such noise. The various measures in

the table are in order of descending correlation with PNdB1, the most recent and sophisticated form. The two weighted-SPL measures, with standard deviations with respect to PNdBl of 2.6 and 3.0 units, should certainly be adequate for most aircraft noise measurements. PNdBl should be used for limited classes of data and for aircraft-certification purposes, however. The SIL's can hardly be expected to correlate well with perceived noise levels, but it is also of interest to see if they can be approximated by dBA or dBN. Unfortunately, a reasonable approximation cannot be made, although this does not necessarily mean that dBA is not a useful speech interference measure itself. Indeed it has been shown that, for some types of noise at least, dBA is fully as good a measure as the SIL as computed for the present comparison. (See ref. 13.)

CONCLUDING REMARKS

In the first phase of this study, now complete, a large mass of acoustical data was acquired. These data were used to derive a noise exposure index for the preliminary analysis of the social data and also for secondary evaluations. Following the anticipated second phase of the study, the complete acoustical data will be further analyzed to test the relative power of several different formulations of noise exposure in predicting community reaction.

REFERENCES

1. Hazard, William R.: Community Reactions to Aircraft Noise – Public Reactions. Conference on Progress of NASA Research Relating to Noise Alleviation of Large Subsonic Jet Aircraft, NASA SP-189, 1968. (Paper No. 41 herein.)

2. Kryter, K. D.: Concepts of Perceived Noisiness, Their Implementation and Application. J. Acoust. Soc. Amer., vol. 43, no. 2, Feb. 1968, pp. 344-361.

3. Anon.: Land Use Planning With Respect to Aircraft Noise. AFM 86-5, TM 5-365, NAVDOCKS P-98, U.S. Dep. Defense, Oct. 1, 1964. (Available from DDC as AD 615015.)

4. Anon.: American Standard Specification for General-Purpose Sound Level Meters. S1.4-1961, Amer. Stand. Ass., Inc., Jan. 9, 1961.

5. Kryter, K. D.; and Pearsons, K. S.: Modification of Noy Tables. J. Acoust. Soc. Amer. (Lett. to Ed.), vol. 36, no. 2, Feb. 1964, pp. 394-397.

6. Kryter, Karl D.: Scaling Human Reactions to the Sound From Aircraft. J. Acoust. Soc. Amer., vol. 31, no. 11, Nov. 1959, pp. 1415-1429.

7. Kryter, Karl D; and Pearsons, Karl S.: Some Effects of Spectral Content and Duration on Perceived Noise Level. J. Acoust. Soc. Amer., vol. 35, no. 6, June 1963, pp. 866-883.

8. Stevens, S. S.: Procedure for Calculating Loudness: Mark VI. J. Acoust. Soc. Amer., vol. 33, no. 11, Nov. 1961, pp. 1577-1585.

9. Bishop, Dwight E.: Descriptions of Flyover Noise Signals Produced by Various Jet Transport Aircraft. Tech. Rep. DS-67-18, FAA, Aug. 1967.

10. Robinson, D. W.; Bowsher, J. M.; and Copeland, W. C.: On Judging the Noise From Aircraft in Flight. Acustica, vol. 13, no. 5, 1963, pp. 324-336.

11. Bishop, Dwight E.: Frequency Spectrum and Time Duration Descriptions of Aircraft Flyover Noise Signals. Tech. Rep. DS-67-6, FAA, May 1967.

12. Anon.: Procedure for Describing Aircraft Noise Around an Airport. Recommendation R 507, 1st ed., Int. Organ. Stand., Oct. 1966.

13. Klumpp, R. G.; and Webster, J. C.: Physical Measurements of Equally Speech-Interfering Navy Noises. J. Acoust. Soc. Amer., vol. 35, no. 9, Sept. 1963, pp. 1328-1338.

BLOCK DIAGRAM OF ACOUSTICAL DATA-PROCESSING SYSTEM

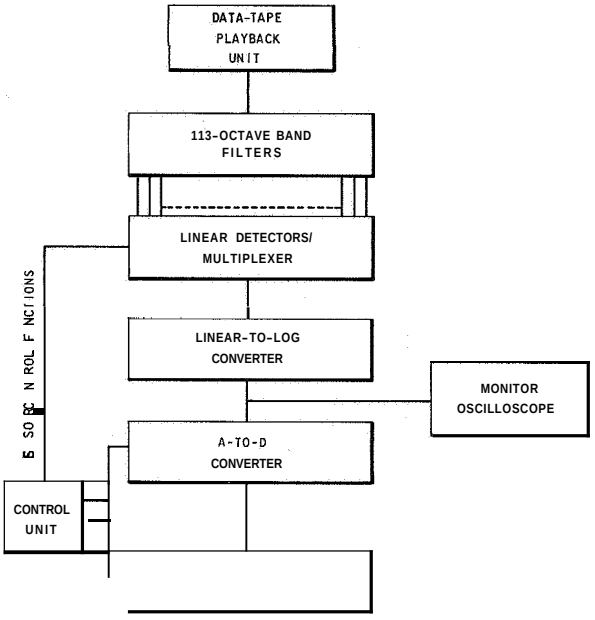

Figure 1

PROCEDURE FOR COMPUTING HOURLY NOISE EXPOSURE IN A GIVEN SURVEY TRACT

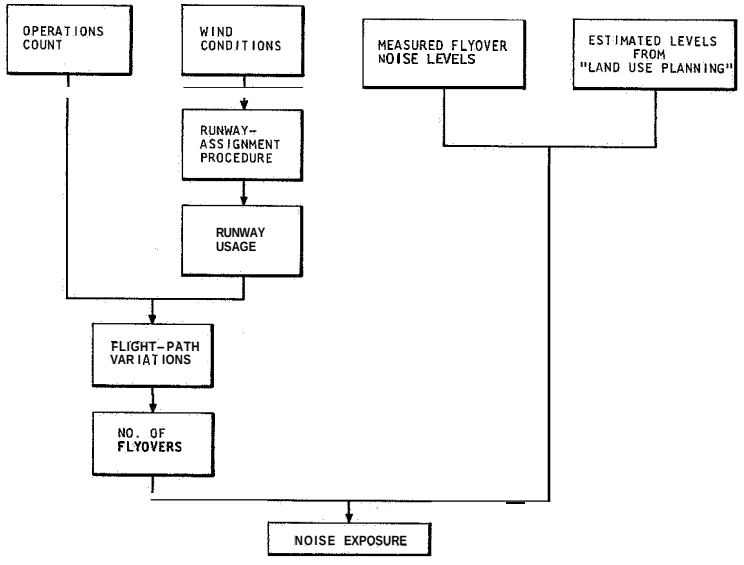

Figure 2

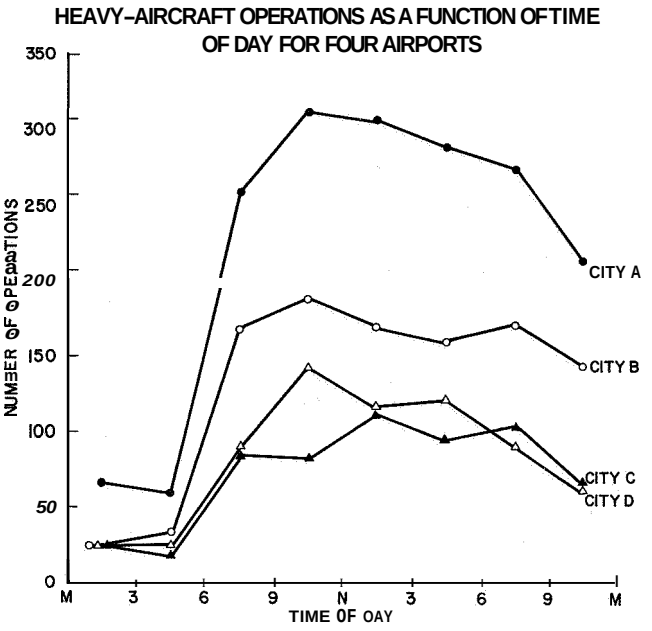

Figure 3

DISTRIBUTION OF MEASURED PNL'S - SITE A

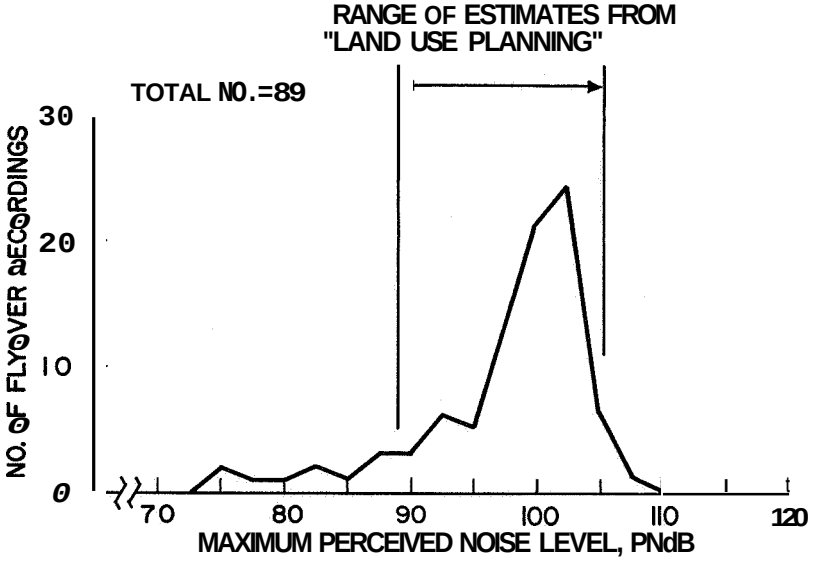

Figure 4

DISTRIBUTION OF MEASURED PNL'S - SITE B

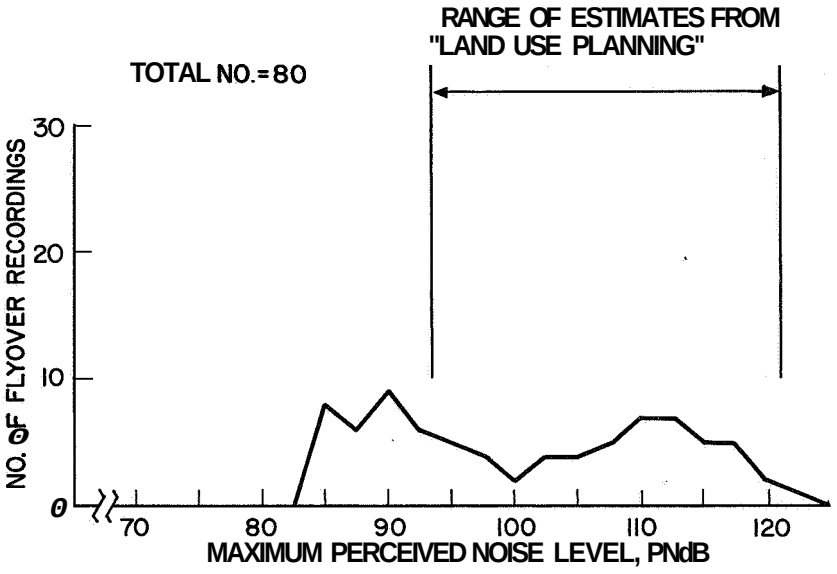

Figure 5

41. COMMUNITY REACTIONS TO AIRCRAFT NOISE

PUBLIC REACTIONS

By William R. Hazard
TRACOR, Inc.

SUMMARY

In summary, the greater the noise exposure, the greater is the annoyance in a direct linear ratio for only about half the population survey. Aircraft noise exposure culminated in complaint behavior for a small but statistically significant proportion of this group. For the other half of the sample, the evidence is that annoyance does not have a simple monotonic relationship to noise exposure. Mediating factors operate so that as exposure increases beyond about 90 PNdB, there is not a corresponding increase in annoyance. Six primary and seven secondary mediating factors are identified. Further examination of these and other influences will be determined in future research.

INTRODUCTION

A question which can properly be asked of the finding that a given composite noise exposure and annoyance are correlated can be put this way: Does aircraft noise exposure really lead to profound and direct annoyance, or are there factors other than exposure itself that "trigger" annoyance reactions? The presence of social and psychological influences has been known, in a general sense, since the first pilot studies of community reactions to aircraft noise, but their precise definition and the extent of their explanatory power is at present unknown. A central part of the study for NASA (under Contract NASw-1549) was devoted to answering the question, "What conditions, if any, exist to make the connection between aircraft noise exposure and annoyance more or less pronounced?"

SCOPE OF RESEARCH

To answer this question, it was decided to conduct interviews with persons living near seven of our nation's largest international airports. In the first phase of the research, hour-long interviews were obtained in 4212 households within a 12-mile radius of four major cities: two in the Midwest, one in the Southwest, and one on the West Coast. The interviews and noise measurements by acoustical scientists were obtained in the late summer of 1967. In the second phase, not yet underway, the research is scheduled to be carried out in three Eastern cities.

The total research program encompasses an active data gathering and data reduction period of 2 years, in which two types of data are taken in the field. A noise measuring team obtains physical measurements of noise in sectors of the community where social scientists are also working. These noise measurements are presented in reference 1.

SAMPLING PLAN

The general location of the data gathering near the airports is indicated in figure 1. In all social surveys, careful consideration must be given to the selection of persons to be interviewed who are representative of a total population or universe of well-defined characteristics. The concern in this study was to ensure that interviewees were representative of the total population of persons exposed to relatively high levels of aircraft noise near major airports.

The modified probability sampling plan shown in figure 1 is technically what is called a "three-stage-judgment, stratified probability sample," but for convenience it is labeled "Thunderbird", since the noise measurement data and interviews were collected in scattered areas roughly circumscribed by the boundaries of an Indian "thunderbird" design emanating from the ends of the most often used runways at the various airports, supplementary data being gathered in all areas immediately adjacent to the airport sites. The sampling plan ensured that data would be gathered under flight paths up to 12 miles from the end of the runways, and that representative areas overflown by approach and landing patterns would be included.

The blocks in which noise measurements were made coincided with areas where interviewers were working, whenever possible. These scattered sampling points were selected so that the widest possible range of income classes was represented in the different noise exposure areas. Blocks were numbered within these areas, and interviewing was conducted in the chosen blocks by a rotation procedure. Interviewers were given addresses to call upon, the number depending upon the quota of interviews needed within each block or census tract. The choice of the homes in which data were gathered was not left to the interviewer to determine; the selection was prearranged according to the sampling plan. In order to study the relationship between noise exposure and psychological or social reactions, it was necessary to assign to each household a noise exposure number. Therefore, noise measurements were made in each census tract during a 2- to 3-week period concurrent with interviewing.

DEFINITION OF ANNOYANCE

The first index of reactions to aircraft noise was a replication of a measure developed by the National Opinion Research Center for their studies of reactions to noise from

U.S. Air Force Bases in 1952 and 1955 to 1957. This index was the first of six ways of measuring annoyances that were explored before it was decided to settle on a composite index based primarily on attitudinal reactions to disturbance of daily activities. The initial disturbance measure was constructed in this manner: Respondents that were bothered by aircraft noise and who freely volunteered, first without prompting and later with prompting, were asked to identify the kinds of daily activities that were disturbed by the noise and to indicate how bothered they were. Answers were scored according to the scale in a little device called an "opinion thermometer." (See fig. 2.)

A person who answered "not at all" to disturbance of sleep, for example, chose a score of one; if he was "extremely disturbed," he chose a score of 5. Intermediate points on the scale, of course, referred to intermediate degrees of sleep disturbance, according to the respondent's own estimation. Responses from the 4212 persons interviewed were approximately normally distributed, with a modal position of three-on the scale. A total of 4153 persons – 98.6 percent of the total sample – reported one or more disturbances of daily activities by aircraft noise and, correspondingly, at least some degree of bother. A total of 76 percent of the sample – 3188 persons – had an average position of three or higher on the opinion thermometer scale.

Percentages of persons in the total sample who reported "extreme bother," that is, who reported a No. 5 response for disturbed activities are shown in table I. The most disturbed activity is television or radio reception; next is interruption of face-to-face conversation.

The disturbance index termed annoyance *(G)* was made up by simply adding the opinion thermometer scores for each activity disturbed. Each respondent was then eligible for a disturbance score of from 1 to 45, depending on his distribution of responses. The mean for this distribution was 24. Less than 2 percent of the sampled population had a score of zero.

The final summary annoyance measure was constructed by weighting and adding to this disturbance index the respondents' scores from other variables such as past annoyance with airplane noise, perception of neighbors being annoyed by the noise, and perception of airplane noise being a city-wide problem.

In an analysis of the interrelationships of these variables within the annoyance dimension, a Varimax factor analysis revealed the factor "loadings," which can be thought of as equivalent to within-class correlation coefficients between each item and the cluster of items that make up the annoyance dimension. See table 11. On the basis of standardized weights, also determined by Varimax rotation, a new summary criterion measure, annoyance (R), was constructed, with a range of from 1 to 15.

Varimax factor weights were used to describe the relative influence of each item on the composite annoyance (R) scale, which consists of the highly intercorrelated annoyance-type responses being discussed. The summary annoyance (R) scale was thus constructed as follows:

$$\text{Annoyance (R)} = 0.1900(V6) + 0.2088(V3) + 0.2473(V1) + 0.2494(V2)$$

The simple product-moment correlation between exposure and annoyance (R) for the four-city sample is a rather low 0.35. However, in the presence of other conditions this correlation is increased to 0.65. By projecting the multiple correlation coefficient to population parameters, it is estimated that nearly all the persons in high exposure zones are annoyed under certain conditions. These specifying conditions will now be discussed.

PREDICTORS OF ANNOYANCE

With this clarification of the operational meaning of annoyance, the question of the relative influence of aircraft noise exposure itself can be considered in comparison with other relevant variables in predicting annoyance reactions. For the sample as a whole in the four Phase I cities, aircraft noise exposure accounted for nearly 6 percent of the variance in annoyance. This result means that a significant portion of annoyance can be traced to noise exposure itself. In addition, however, high noise exposure accompanied by certain other conditions explains nearly half of the variance in annoyance scores – a total of 45 percent. Of these conditions, six are important in that they account for an accumulated total of one-third of the variation in annoyance reactions:

(1) Awareness of aircraft between midnight and 6 a.m., particularly between the hours of midnight and 3 a.m.

(2) High exposure, generally above the 90 PNdB level

(3) Respondent sensitivity to noise in general

(4) Underlying awareness of marked increases in the frequency of jet traffic for the past 5 years

(5) Unwillingness to adapt to additional increases in aircraft noise

(6) Having a past history of complaints to public officials about neighborhood inconveniences.

The analysis demonstrates that these predictors are independent, that is, are not significantly correlated among themselves for the range of noise exposure studied. It is possible, therefore, to estimate the contribution that each one makes to mean annoyance levels for the populations under study. It should be kept in mind that these

predictors are valid for the combined sample of the four Phase I cities but may not be universally applicable. Greater confidence in the ordering of these specifying conditions at the conclusion of the study will follow analysis of the Phase II data.

The average annoyance levels are more than doubled when aircraft are heard during the sleeping hours between midnight and 6 a.m. These levels are increased by two-thirds under high average aircraft noise exposure and are increased by about one-third when high general noise sensitivity is present. The other factors – perception of increases in the frequency of jet traffic, unwillingness to adapt to increased aircraft noise, and having a past complaint history – lead to slight but notable increases in annoyance.

To pinpoint these and other effects more precisely, a multiple regression analysis was conducted in which weights for each predictor variable were computed. In their simplest sense, these weights measure changes in mean annoyance scores in terms of standard deviation units of each predictor variable. This procedure assures the same variability of the predictors so that they can be directly compared in terms of their joint power in predicting differences on the annoyance (R) scale. In other words, the weights determine the slope of the regression of mean annoyance scores, shown as y in figure 3, for values of each predictor variable, expressed as x. Each person in this scattergram is a dot, the position of which represents his score on two variables – for example, his annoyance score along the ordinate or y-axis of the figure and his aircraft noise exposure score along the abscissa. The regression line is drawn through the mid-point or mean of the distribution of annoyance scores for each category of noise exposure.

The degree of slope of the line tells immediately whether there is an increase in average annoyance as noise exposure increases. As indicated earlier, there would be a slight rise in the line if only noise exposure was considered in attempting to predict annoyance. The line rises, however, if not only noise exposure but also social-psychological factors, the most important of which are nighttime noise exposure and high sensitivity to noise, are taken into account.

The equation used for determining the slope of the regression line and the standardized weighting factors for the variables discussed are shown in table III. The predictor variables are listed along the left side of this table, and their standardized weights are shown as the beta regression coefficient b*.

The purpose of a multiple regression analysis such as this analysis is to predict a particular value or score for a person having a certain combination of characteristics; that is, to know how well all predictor variables acting together explain differences in the criterion measure. Thus, the amount of variation around mean annoyance levels is in part accounted for by the contribution of each predictor variable. The difference in mean

annoyance levels not accounted for by these coefficients is an unexplained variation, that is, the error term in the regression equation. The research problem is to find the best set of variables to reduce error in predicting mean annoyance scores for different groups and different cities under study. Forty-five percent of the differences in mean annoyance levels with the primary set of predictors are accounted for, and the results are highly significant, at the 0.9999 confidence level.

SECONDARY PREDICTORS OF ANNOYANCE

Early in the analysis, it was discovered that the best set of predictors of annoyance in one exposure zone was not necessarily the best set in other zones and that some conditions of annoyance have greater general applicability than others since they appear to be independent of degree of exposure to aircraft noise, whereas other conditions appear to be either a function of exposure or tend to mediate the relationship between exposure and annoyance. Thus, certain predictors are important in high noise exposure areas and are unimportant in low exposure zones.

For the purposes of this paper, table IV presents a summary typology of these predictors of annoyance within five mutually exclusive noise exposure classes. Here, as before, the larger the magnitude of the regression coefficient, the greater the reduction of error in predicting annoyance. This classification shows that persons living in high exposure ranges who scale high in annoyance are generally in high income brackets, were not aware of the extent of airport-related noise when they moved into the neighborhood, are generally dissatisfied with their neighborhood environments, and are aware of neighbors moving away because of the noise.

Persons living in moderate exposure ranges who show high annoyance tend to be women who are at home during most hours of the week and believe they cannot accept further increases in aircraft noise exposure, but believe that the airport industry is important to the economy of the city.

Persons living in low noise exposure ranges who are high in annoyance tend to be young adult males who are exposed to aircraft traffic mostly during the weekends, who occupy high occupational positions, have stable residence histories, and believe that neighbors have been influenced to leave because of aircraft noise.

Persons in all exposure ranges who say they are annoyed perceive a steady increase in the volume of air traffic over their neighborhoods and have a history of complaining to public officials about one problem or another. Thus, persons who appear to be the most annoyed know how and to whom to complain, and this knowledge appears to increase their apprehension about real or imagined noise exposure.

CONCLUDING REMARKS

For the sample as a whole and across all exposure ranges, the predictors of annoyance with the greatest general applicability are, in their order of importance·

(1) Aware of aircraft between midnight and 6 a.m.

(2) Live in high aircraft exposure areas

(3) Have high noise susceptibility

(4) Perceive a steady increase in the amount of air traffic

(5) Argue that they would be unable to adapt to increased exposure

(6) Have knowledge of how to complain effectively.

Secondary factors which explain additional variation in annoyance scores in some localities include

(1) Living from 3 to 6 miles from the airport

(2) High occupational status, high income, and expensive residence

(3) Having fear of aircraft crashing in the neightborhood

(4) Long-time residency in the neighborhood

(5) Knowledge of neighbors who have moved away due to aircraft noise

(6) Generally positive attitudes toward the aircraft industry

(7) Belief that the airport is important to the economy of the city.

Thus, with a knowledge of aircraft noise exposure and knowledge of the distribution of certain sociopsychological characteristics in any given locality, the probable degree of annoyance can be predicted provided, of course, that the four cities studied are representative of high aircraft exposure areas. The reliability of these predictors can be established in Phase II of the research when the addition of more cities to the study allows between-city comparisons.

REFERENCE

1. Connor, William K.: Community Reactions to Aircraft Noise – Noise Measurements. Conference on Progress of NASA Research Relating to Noise Alleviation of Large Subsonic Jet Aircraft, NASA SP-189, 1968. (Paper No. 40 herein.)

TABLE I.- PERCENT HIGHLY BOTHERED BY ACTIVITIES DISTURBED

Activity	Percent highly bothered
TV/radio reception	**20.6**
Conversation	**14.5**
Telephone	**13.8**
Relaxing outside	**12.5**
Relaxing inside	**10.7**
Listening to records/tapes	**9.1**
Sleeping	**7.7**
Reading	**6.3**
Eating	**3.5**

TABLE 11.- PRINCIPAL FACTOR IN VARIMAX FACTOR ANALYSIS

V	Variable	Loading	Standardized weights
1	Neighbors annoyed	**0.8004**	**0.2473**
2	Annoyance (G)	.7843	.2494
3	City–wide annoyance	.6158	.2088
4	Complaint potential	.5759	.1883
5	Noise adaptability	-.5241	-.1683
6	Past annoyance	.5014	.1900
7	Perceives air traffic increase	.4554	.1258
8	Noise induced mobility	.4387	.1178

TABLE III.- PREDICTORS OF ANNOYANCE BY MULTIPLE **LINEAR** REGRESSION

$$\bar{Y} = a + b_1x_1 + b_2x_2 + b_3x_3 + b_4x_4 + b_5x_5 + b_6x_6 + b_7x_7 + \text{Error}$$

where

a $\bar{Y}$ intercept of the regression line

Error = Residual sum of squares (variance around the regression line that cannot be accounted for by the relationship of predictor variables and annoyance)

b^* standardized regression coefficients

Variable (x)		Regression coefficient, b^*
$\bar{Y}$	Index of annoyance	
x_1	Level of perception of aircraft between midnight and 3 a.m.	0.243
x_2	Summary index of aircraft noise exposure	.239
x_3	Frequency of perceived flyovers	.207
x_4	Index of complaint potential	.201
x_5	Index of adaptability to noise	.168
x_6	Noise sensitivity	.165
x_7	Level of perception of aircraft between 3 a.m. and 6 a.m.	.131

TABLE IV.- PREDICTORS OF ANNOYANCE (R) BY AIRCRAFT NOISE

Exposure class	Annoyance predictors (x) that are independent of degree of aircraft noise exposure	Regression coefficient, b^*	Predictors (x) that mediate relationship between noise exposure and annoyance	Regression coefficient, b^*
Very high exposure range	Perceives increase in air traffic	0.174	High house cost	0.527
	High individual complaint potential	.170	Positive attitude toward aircraft industry	.383
			Fear of airline crashes	.344
			Home ownership	.311
			Low neighborhood satisfaction	.154
			No prior awareness of airplane noise	.153
			High income	.131
			Low paranoia	.118
High exposure range	High individual complaint potential	0.166	Unable to adapt to increased airplane noise	0.195
	Perceives increase in air traffic	.159	Know of neighbors moving away due to noise	.185
Moderately high exposure range	Perceives increase in air traffic	0.292	Unable to adapt to increase in air traffic	0.242
	High individual complaint potential	.230	Sees airport as important to city	.166
			Positive attitude toward aircraft industry	.154
Moderate exposure range	High individual complaint potential	0.165	See airport as important to city	0.171
	Perceives increase in air traffic	.161	Female	.160
Low exposure range	High individual complaint potential	0.302	Positive attitude toward aircraft industry	0.334
	Perceives increase in air traffic	.263	Male	.298
			Low residential mobility	.213
			No prior awareness of aircraft noise	.153
			High occupational position	.148
			No family connection with aircraft industry	.137
			Fear of airplane crashes	.133
			Young adult age range	.130
			Know of neighbors moving away due to noise	.130

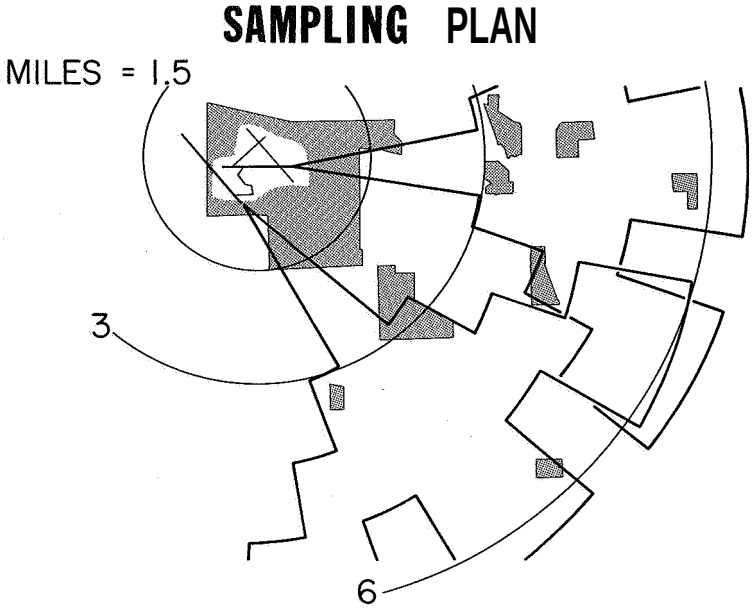

Figure 1

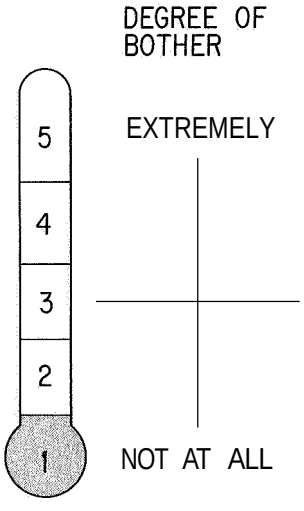

Figure 2

REGRESSION OF y ON x

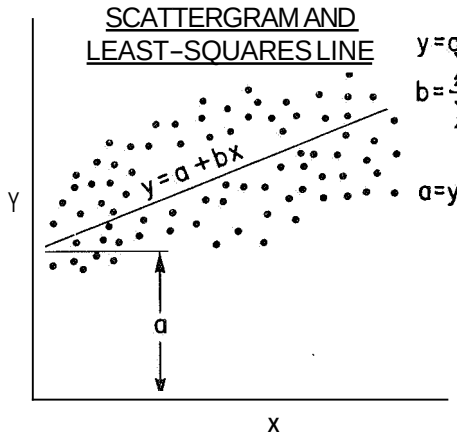

$y = a + bx$ where

$b = \frac{\sum xy}{\sum x^2}$ (Regression coefficient that determines slope of regression line)

$a = y - bx$ (y-Intercept of regression line)

Figure 3

LIST OF ATTENDEES

ACKLEY, James M.	Stresskin Products Company
AHLERS, Edward B.	IIT Research Institute
AHRENS, Donald J.	Cessna Aircraft Company
AIKEN, William S., Jr.	NASA Headquarters
ALEXANDER, William T.	U.S. Army Aviation Materiel Laboratories
ALLEN, Lewis H.	Pan American World Airways, Inc.
ANDERSEN, Wilbur Lee	The Garrett Corporation
ATHERTON, Harper	Air Transport Association of America
AUDETTE, Richard R.	General Electric Company
AVERBUCH, Aaron	University of Illinois
BAALS, Donald D.	NASA Langley Research Center
BALLENTINE, John R.	Lockheed Georgia Research Laboratory
BARLOW, William H.	Hughes Tool Company
BARTEL, H. W.	Lockheed-Georgia Company
BAUMAN, Joseph	NASA Wallops Station
BAXTER, Paul J.	Wright-Patterson Air Force Base
BECKER, William B.	Air Transport Association of America
BELCHER, Peter M.	North American Rockwell Corporation
BENHAM, Robert B.	Naval Air Propulsion Test Center, Naval Base, Philadelphia
BENNETT, S. H.	Huyck Metals Company
BENSON, Robert W.	Robert W. Benson and Assoc., Inc.
BERENDT, Raymond D.	National Bureau of Standards
BERGIN, Harrison D.	Town-Village Aircraft Safety & Noise Abatement Committee, Lawrence, N.Y.
BERMAN, Robert	Federal Aviation Administration
BIES, David A.	Bolt Beranek and Newman, Inc.
BIRD, William	Air Canada
BISHOP, Dwight E.	Bolt Beranek and Newman, Inc.
BLACKSTOCK, D. T.	University of Rochester
BORSKY, Paul N.	Columbia University
BOSWINKLE, Robert W., Jr.	NASA Langley Research Center
BREER, Robert A.	AVCO Aerostructures Division
BRISTOL, Carl W.	Pratt & Whitney Aircraft Division
BROOKS, George W.	NASA Langley Research Center
BROUN, Richard H.	Department of Housing and Urban Development

BROWN, Richard F.	Trans World Airlines, Inc.
BRUNELLE, Vernon C.	Air Line Pilots Association
BURTON, William	Westinghouse Electric Corporation
CALE, David B.	U.S. Army Aviation Materiel Laboratories
CARDEN, Huey D.	NASA Langley Research Center
CARHART, N. A.	McDonnell Douglas Corporation
CARROLL, E. A.	Trans World Airlines, Inc.
CARSON, William	Langley Air Force Base
CAWTHORN, Jimmy M.	NASA Langley Research Center
CHAMBERS, Glenn R.	Langley Air Force Base
CHENG, David H.	City College of New York
CHESTNUTT, David	NASA Langley Research Cent-er
CLEVELAND, W. L.	Dade County Port Authority, Miami International Airport
CLOSE, W. H.	Office of Noise Abatement, Department of Transportation
COFER, Wesley R., Jr.	Cofer & Jordan, Hampton Planning Commission
COLE, John N.	Wright-Patterson Air Force Base
COLLINS, Walter V.	Los Angeles Sound Abatement Coordinating Committee
CONNOR, Andrew B.	NASA Langley Research Center
CONNOR, Neil A.	Federal Housing Administration, Department of Housing and Urban Development
CONNOR, William K.	TRACOR, Inc.
COOK, Richard K.	ESSA Research Laboratories of U.S. Department of Commerce
COOK, Woodrow L.	NASA Ames Research Center
COOPER, George E.	NASA Ames Research Center
COPELAND, Robert	Brunswick Corporation
COPELAND, W. Latham	NASA Langley Research Center
CORRIGAN, Leo A.	Allison Division
CORTRIGHT, Edgar M.	NASA Langley Research Center
COX, C. R.	Bell Helicopter Company
COXON, John S.	McDonnell Douglas Corporation
COYKENDALL, Richard E.	United Air Lines
CRIGLER, John L.	NASA Langley Research Center
CULLEN, John K.	Pan American World Airways, Inc.

DAVIES, Ralph L.	The Boeing Company
DAVIS, J. T.	Delta Air Lines
DINGELDEIN, Richard C.	NASA Langley Research Center
DOAK, P. E.	University of Southampton
DONELY, Philip	NASA Langley Research Center
DOSANJH, Darshan S.	Syracuse University
DRAKELEY, George T.	The Boeing Company
DRALEY, Eugene C.	NASA Langley Research Center
DUBERG, John E	NASA Langley Research Center
DUNMORE, J.	AVCO Corporation
DUTTON, Benson L.	U.S. Office of Education, Department of Health, Education, and Welfare
EDGE, Philip M., Jr.	NASA Langley Research Center
EICHELMAN, E.	U.S. Army Mobility Equipment Research and Development Center, Fort Belvoir, Va.
EISENHART, Robert D.	The Boeing Company'
ELLIS, Loren	United Air Lines
ENGELBRECHT, Alfred E.	North American Rockwell Corporation
ERICKSON, Arnold R.	Huyck Metals Company
ERZBERGER, Heinz	NASA Ames Research Center
FARRELL, James H.	Conesco Division of Flow Corporation
FARRIS, Edsel S.	The Boeing Company
FAVRE, Harrison B.	McDonnell Douglas Corporation
FAYE, Alan E., Jr.	NASA Ames Research Center
FEDER, Ernest	Pratt & Whitney Aircraft Division
FEDZIUK, Henry A.	NASA Langley Research Center
FEILER, Charles E.	NASA Lewis Research Center
FERRILL, R. S.	Lockheed-Georgia Company
FINDLEY, Donald S.	NASA Langley Research Center
FISHER, James I.	Huyck Metals Company
FOLEY, William M.	Research Laboratories, United Aircraft Corporation
FOSTER, Charles R.	Office of Noise Abatement, Department of Transportation
FRENCH, C. T.	P. R. Mallory Company
FRICKE, Werner	Bell Aerosystems Company
GACH, Martin	Federal Aviation Administration
GARBELL, Esther F.	Garbell Research Foundation

GARBELL, Maurice A.	Garbell Research Foundation
GARRICK, I. Edward	NASA Langley Research Center
GELDER, Thomas F.	NASA Lewis Research Center
GERSHON, I. J.	Wright-Patterson Air Force Base
GESSOW, Alfred	NADA Headquarters
GETLINE, Gordon L.	General Dynamics Corporation
GIBSON, J. S.	Lockheed-Georgia Company
GOODFRIEND, Lewis S.	Goodfriend-Ostergaard Associates
GORDON, Colin G.	Bolt Beranek and Newman, Inc.
GORDON, D. K.	McDonnell Douglas Corporation
GRAEF, J. D.	American Airlines, Inc.
GRAY, Alan	General Electric Company
GRAY, Larry	The Garrett Corporation
GREEN, James S.	General Dynamics Corporation
GREGORY, Edward M.	NASA Langley Research Center
GUEST, Stanley H.	NASA George C. Marshall Space Flight Center
GUTTMANN, Karl H.	Department of the Navy
HANSON, Carl M.	McDonnell Douglas Corporation
HARPER, Charles W.	NASA Headquarters
HARPER, W. L.	Trans World Airlines, Inc.
HARRIS, T. Aubrey	Consultant
HART, Franklin D.	North Carolina State University
HART, R. K., Sr.	Pan American World Airways, Inc.
HAVILAND, John K.	University of Virginia, Virginia Associated Research Center
HAZARD, William R.	TRACOR, Inc.
HELDENFELS, Richard R.	NASA Langley Research Center
HELLER, Hanno H.	Bolt Beranek and Newman, Inc.
HENDERSON, Herbert R.	NASA Langley Research Center
HERRON, William R.	National Bureau of Standards
HIGGINS, Charles C.	The Boeing Company
HILTON, David A.	NASA Langley Research Center
HPNTERKEUSER, Ernest	The Boeing Company – Vertol Division
HINTON, Lloyd	National Aircraft Noise Abatement Council
HIRSH, Ira J.	Central Institute for the Deaf
HODGES, Beverly W.	The Boeing Company
HOLL, Raymond	British Embassy
HOLMES, H. Rolland	Lockheed Aircraft Corporation

HOOVER, Isaac H.	Office of Noise Abatement, Department of Transportation
HUBBARD, Harvey H.	NASA Langley Research Center
HUNTER, George P.	Federal Aviation Administration
JOHNSON, Elven A.	Andrews Air Force Base
JOHNSTON, Gordon	Research Laboratories, United Aircraft Corporation
JONES, Jess H.	NASA George C. Marshall Space Flight Center
JONES, Walton L.	NASA Headquarters
KADLEC, Paul W.	Eastern Airlines, Inc.
KAMPS, Edwin C.	Rohr Corporation
KARLSON, John E.	Karlson Research and Manufacturing Company
KATZOFF, Samuel	NASA Langley Research Center
KESTER, J. D.	Pratt & Whitney Aircraft Division
KENYON, George C.	NASA Ames Research Center
KING, Robert J.	Sikorsky Aircraft
KIRBY, Robert H.	NASA Langley Research Center
KORNHABER, Bernard R.	Brunswick Corporation
KORYCINSKI, Peter F.	NASA Langley Research Center
KRAMER, James J.	NASA Lewis Research Center
KRAUSE, Fritz R.	NASA George C. Marshall Space Flight Center
KRYGER, Ronald	Industrial Acoustics Company, Inc.
KRYTER, Karl D.	Stanford Research Institute
LAUGHLIN, L. Eugene	The Boeing Company
LEE, Robert	General Electric Company
LEWIS, James H.	National Transportation Safety Board, Department of Transportation
LICHTMAN, Eugene A.	Department of the Navy
LOFTIN, Laurence K., Jr.	NASA Langley Research Center
LOTT, Merrill A.	Federal Aviation Administration
LOVING, Donald L.	NASA Langley Research Center
LOWRY, John G.	NASA Langley Research Center
LOWSON, Martin V.	Wyle Laboratories
LUKAS, Jerome S.	Stanford Research Institute

MACE, William D.	NASA Langley Research Center
MANGIAROTTY, R. A.	The Boeing Company
MANI, Ramani	General Electric Company
MARSH, Alan H.	McDonnell Douglas Corporation
MARTENSON, A. J.	General Electric Company
MARTIN, Dennis 3.	NASA Langley Research Center
MARTIN, George C.	The Boeing Company
MASSEY, J. W.	The Garrett Corporation
MATTSON, Axel T.	NASA Langley Research Center
MAURER, Otto F.	Wright-Patterson Air Force Base
MAYES, William H.	NASA Langley Research Center
McALLISTER, George T.	U.S. Army Aviation Materiel Laboratories
McATEE, John C.	Wright-Patterson Air Force-Base
McBRIDE, Joseph F.	NASA Lewis Research Center
McCORMICK, Ralph B.	The Boeing Company
McGARVEY, Joseph H.	U.S. Army Aviation Materiel Laboratories
McGOWAN, William A,	NASA Headquarters
McIVER, Dale	Office of Congressman Fraser
McLEOD, Norman J.	NASA Flight Research Center
McNAIR, Robert	Westinghouse Electric Corporation
McPIKE, A. L.	McDonnell Douglas Corporation
MEANY, Robert C.	United Air Lines
MERKIN, Allan	NASA Headquarters
METZGER, Frederick B.	Hamilton Standard Division
MILLER, Douglas S.	The Boeing Company
MILLMAN, V.	Rohr Corporation
MONTEGANI, Francis J.	NASA Lewis Research Center
MOORE, R. E.	Lear Jet Industries, Inc.
MORGAN, William R.	General Electric Company
MOTSINGER, R. E.	General Electric Company
NAVARRO, Roger L.	NASA Wallops Station
NELSON, Clifford H.	NASA Langley Research Center
NEVIUS, Harold E.	General Dynamics Corporation
NICHOLS, Mark R.	NASA Langley Research Center
NORDSTROM, Donald C.	The Boeing Company
NORRIS, L. R.	Headquarters, U.S. Air Force
NORTON, Harry T., Jr.	NASA Langley Research Center

O'BREIN, Philip R., Jr.	Langley Air Force Base
O'BRIEN, Thomas J.	Federal Aviation Administration
ODELL, Albert H.	Port of New York Authority
OLCOTT, Jack	Aeronautical Research Associates of Princeton, Inc.
OLESON, Stanley K.	Federal Aviation Administration
OLIVIER, David	Brunswick Corporation
OPENCHOWSKI, A. K.	Rohr Corporation
ORELUP, M. J.	Allison Division
OSCAR, K.	U.S. Army Mobility Equipment Research and Development Center, Fort Belvoir, Va.
OSMUN, W. G.	Air Transport Association of America
PARKER, James	Biotechnology, Inc.
PARROTT, Tony L.	NASA Langley Research Center
PAULLIN, Robert L.	Office of Noise Abatement, Department of Transportation
PEARSON, Richard G.	North Carolina State University
PEARSONS, Karl S.	Bolt Beranek and Newman, Inc.
PENDLEY, Robert E.	McDonnell Douglas Corporation
PENNELL, Maynard L.	The Boeing Company
PIERPONT, William G.	Beech Aircraft Corporation
PLUMBLEE, Harry E., Jr.	Lockheed Georgia Research Laboratory
POTTER, Richard C.	Wyle Laboratories
POWER, Joseph K.	Federal Aviation Administration
POWERS, John O.	Federal Aviation Administration
PROCHNIK, Martin	Department of Interior
QUIGLEY, Hervey C.	NASA Ames Research Center
RANNELLS, John	Department of Transportation
REETHOF, Gerhard	Pennsylvania State University
REINHART, W. A.	The Boeing Company
REKOS, Nelson F.	NASA Headquarters
RIBNER, H. S.	University of Toronto
ROBERTSON, Jack E.	Wyle Laboratories
ROGERS, James	Grumman Aircraft Engineering Corporation
ROSE, Gary B.	Pan American World Airways, Inc.
ROSE, Justus F., Jr.	Wright-Patterson Air Force Base
ROSSILION, John	Brunswick Corporation
RUCKER, Carl E.	NASA Langley Research Center

RUGER, Charles	General Applied Science Laboratories, Inc.
RUNYAN, Harry L.	NASA Langley Research Center
RUSSELL, R. E.	The Boeing Company
SALLEE, G. P.	American Airlines, Inc.
SANDERS, Newell D.	NASA Lewis Research Center
SANDS, Johnny M.	Federal Aviation Administration
SCHOTT, G. J.	The Boeing Company
SCOTT, C. W.	McDonnell Douglas Corporation
SEVIK, Maurice	Pennsylvania State University
SHAHADY, P. A.	Wright-Patterson Air Force Base
SHELLY, John J.	Aviation Development Council
SHEPANEK, Raymond A.	Federal Aviation Administration
SHERIDAN, Hugo G.	Department of the Navy
SIGG, Emil	Flight Safety Foundation
SLOSARIK, S. E.	Union Carbide Corporation
SLUTSKY, Simon	New York University
SMITH, E. B.	General Electric Company
SMITH, Orvel E.	NASA George C. Marshall Space Flight Center
SNODGRASS, J. C., Jr.	Aerospace Industries Association of America, Inc.
SNOW, N. J.	Rohr Corporation
SODERMAN, Paul T.	U.S. Army Aeronautical Research Lab.
SOULE, Hartley A.	Consultant
SPARKS, Cecil R.	Southwest Research Institute
SPARKS, John H.	Andrews Air Force Base
SPERRY, William C.	Federal Aviation Administration
SPICE, B. J.	Vought Aeronautics Division
STAHR, R. Scott	Eastern Airlines, Inc.
STRUNCK, James E.	Assistant Corporation Counsel, Law Department, City of Chicago
SUMMERFIELD, Martin	Princeton University
SUN, Cedric	Aircraft Porous Media, Inc.
SURPRENANT, Norman	Brunswick Corporation
SWANSON, Andrew G.	NASA Langley Research Center
TAMASY, John	The Garrett Corporation
TAYLOR, John P.	National Academy of Science
TAYLOR, Willard L.	Civil Aeronautics Board
TEDRICK, Richard N.	The Garrett Corporation

THIELMAN, R. F.	Rohr Corporation
THOMPSON, Floyd L.	NASA Headquarters
THOMPSON, J. R.	Lockheed-California Company
TORKELSON, D. W.	The Boeing Company
TURSIC, R. J.	Allison Division
TYLER, John M.	Pratt & Whitney Aircraft Division
TYSON, T. J.	Dynamic Science Division of Marshall Industries
URQUHART, G. R.	Rohr Corporation
VOCE, J. D.	Rolls-Royce Limited
VON GIERKE, Henning E.	Wright-Patterson Air Force Base
WAFFORD, John H.	Wright-Patterson Air Force Base
WAKELING, D. J. N.	British Overseas Airways Corporation
WALKER, Curtis L.	Allison Division
WALLACE, R. E.	The Boeing Company
WANG, Chiao J.	Office of the Secretary of Defense, Advanced Research Projects Agency
WATSON, H. A., Jr.	McDonnell Douglas Corporation
WATTER, Michael	Institute for Defense Analyses
WEBBER, Christopher J.	Rolls-Royce Limited
WEISS, William	Grumman Aircraft Engineering Corporation
WELLS, R. J.	General Electric Company
WENTZ, Daniel S., II	NASA Langley Research Center
WEST, William L.	Langley Air Force Base
WEXLER, Gerald	Industrial Acoustics Company, Inc.
WHITCOMB, Milton A.	National Academy of Science
WHITE, John W.	U.S. Army Aviation Materiel Laboratories
WHITE, R.	Allison Division
WHITTEN, Raymond	NASA Headquarters
WICK, Bradford H.	NASA Ames Research Center
WIDNALL, Sheila	Massachusetts Institute of Technology
WILCOX, John R.	American Airlines, Inc.
WILLIAMS, Carl E.	Naval Aerospace Medical Institute
WILSON, Lennox N.	IIT Research Institute
WIRT, L. S.	Lockheed-California Company
WOODALL, James F.	Federal Aviation Administration
WOOTTEN, E. John	B & K Instruments, Inc.
WRIGHT, Lyle A.	McDonnell Douglas Corporation
WYSZPOLSKI, Eugene F.	NASA Headquarters

YAFFEE, Michael L. — **Aviation Week & Space Technology**

ZORUMSKI, William E. — **NASA Langley Research Center**

ZWIEBACK, Edgar L. — **McDonnell Douglas Corporation**